

TECHNISCHE UNIVERSITÄT MÜNCHEN

WACKER-Lehrstuhl für Makromolekulare Chemie

**Expansion of Rare Earth Metal-Mediated Group  
Transfer Polymerization to New Monomers**

Stephan Salzinger

Vollständiger Abdruck der von der Fakultät für Chemie der Technischen Universität  
München zur Erlangung des akademischen Grades eines

**Doktors der Naturwissenschaften**

genehmigten Dissertation.

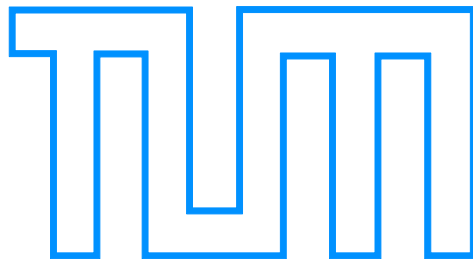
Vorsitzender: Univ.-Prof. Dr. Ulrich K. Heiz

Prüfer der Dissertation:

1. Univ.-Prof. Dr. Dr. h.c. Bernhard Rieger
2. Univ.-Prof. Dr. Kai-Olaf Hinrichsen
3. Priv.-Doz. Dr. Wolfgang Eisenreich

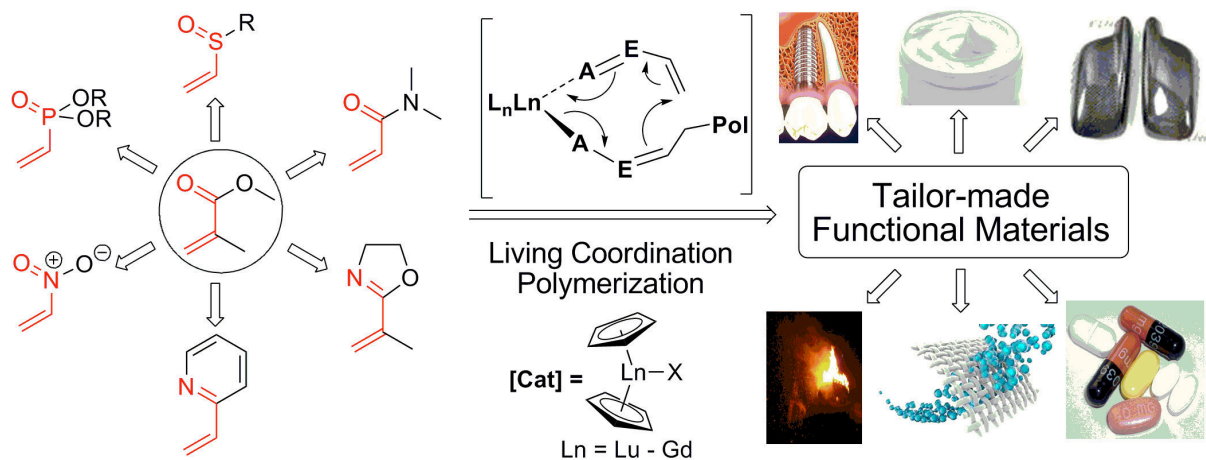
Die Dissertation wurde am 11.06.2013 bei der Technischen Universität München eingereicht  
und durch die Fakultät für Chemie am 23.09.2013 angenommen.





# Expansion of Rare Earth Metal-Mediated Group Transfer Polymerization to New Monomers

Erweiterung der Seltenerdmetall-medierte  
Gruppentransferpolymerisation auf neue Monomere



Dissertation

Zur Erlangung des akademischen Grades eines  
Doktors der Naturwissenschaften

vorgelegt von

Stephan Salzinger

Garching bei München, Juni 2013



*„Die intensive Beschäftigung mit dem Text meiner Dissertation [...] bekräftig[t] mich in der Überzeugung, dass meine Dissertation kein Plagiat ist.“*

- Annette Schavan, Bundesministerin für Bildung und Forschung, 2013

Für  
Jessica, „my hard headed woman“,  
Lena Mae,  
meine Eltern  
und alle, die mich während meines Studiums unterstützten.

Die vorliegende Arbeit entstand in der Zeit von September 2010 bis April 2013 am WACKER-Lehrstuhl für Makromolekulare Chemie unter der Betreuung von Prof. Dr. Dr. h.c. Bernhard Rieger.



Mein besonderer Dank gilt meinem Doktorvater *Prof. Dr. Dr. h.c. Bernhard Rieger* für die herzliche Aufnahme in den Arbeitskreis und dafür, dass er es mir ermöglicht hat, mich so umfassend und eingehend mit der faszinierenden Chemie der Seltenerd-medierten Gruppentransferpolymerisation zu beschäftigen. Weiterhin möchte ich mich bei ihm für sein Interesse an meiner Arbeit, für das in mich gesetzte Vertrauen, unsere ausführlichen fachlichen Diskussionen, seine zahlreichen guten Anregungen und Ratschläge sowie für die Freiheiten, die ich während meiner ganzen Promotion genießen durfte, bedanken.

*Dr. Carsten Troll* gebührt mein Dank für die hervorragende Organisation des Lehrstuhls und seine Ratschläge bei Fragen und Problemen jeglicher Art. Darüber hinaus möchte ich ihm für seine immerwährende Unterstützung sowie dafür danken, dass er mir in jeder Hinsicht den Rücken freigehalten hat.

Zu großem Dank verpflichtet bin ich meinen Laborkollegen: *Dr. Manuel Winkenstette* für ausgezeichnete fachliche Diskussionen, die Einführung in die metallorganische Chemie und seine aufmunternde Art. *Sandra Hochwarter* danke ich für ihr Verständnis für die andauernde Überfüllung des Labors mit meinen Studenten sowie für unsere vielen tollen Gespräche bei Kaffee oder Zigarette. *Dipl.-Ing. Andreas Eisele* danke ich für viele gute Ratschläge, auch abseits der Chemie. *Dipl.-Ing. Markus Hammann* danke ich für sein positives und freundliches Wesen, für seine bedingungslose Hilfestellung bei Problemen aller Art und für das Korrekturlesen dieser Arbeit. Ihnen allen möchte ich darüber hinaus für das hervorragende Arbeitsklima im Labor, für ihre Unterstützung während meiner gesamten Promotion und insbesondere für ihre Freundschaft danken. Ohne Euch wäre mein Weg sicher um einiges schwerer gewesen.

*Dr. Uwe B. Seemann* danke ich für seine umfangreiche Hilfestellung insbesondere zu Beginn meiner Arbeit, für die Einführung in die Lichtstreuung und in die Chemie der Poly(vinylphosphonat)e und allen voran für seine Freundschaft.

Großer Dank gebührt meinem Freund und Kollegen *Dr. Ning Zhang* für die fruchtbare Zusammenarbeit auf dem Gebiet der Seltenerd-medierten Gruppentransferpolymerisation, für unsere fachlichen Diskussionen, seine Herzlichkeit und Offenheit. Ning, ich wünsche dir alles Gute für deine Familie und deinen neuen Arbeitskreis!

Besonderen Dank schulde ich insbesondere meinem langjährigen Mitarbeiter und Masterand *Benedikt S. Soller* für seine engagierte Mitarbeit, seinen kreativen wissenschaftlichen Input, für viele tolle Gespräche bei einem Feierabendbier und für das Mitbetreuen meiner Studenten. Benedikt, auch dir wünsche ich alles Gute! Ich hoffe, du erhältst die Gelegenheit, dich in deiner Promotion weiter diesem Thema, das dich so begeistert, widmen zu können.

Darüber hinaus gilt mein Dank allen Studenten, die mich während meiner Promotion mit ihrer Arbeit unterstützt haben: *Ekatarina Kralina, Markus Grandl, Felix Flegiel, Andreas Hilger, Dimitri Starkov, Maria Haslböck, Felix S. Geitner, Missy S. Liu, Bruno Jacobi, Sabrina Mahnel, Qingqi Zhao, Marlene Schmid* und *Fabian Linsenmann*. Vielen Dank für euren ungebremsten Einsatz, die stete Verbesserung der Aktivitätsmessungen und für die tolle Zusammenarbeit.

*Prof. Dr. Rainer Jordan* danke ich für seine Unterstützung auf dem Gebiet der SI-GTP, für seine Ratschläge, seine Offenheit und für die anregenden und netten Gespräche am Rande von Konferenzen. Für die Ermöglichung meines Kurzaufenthalts an der King Abdullah University for Science and Technology und für die Bereitstellung seiner Dissertation möchte ich *Prof. Dr. Jörg Eppinger* danken. Seine Arbeit war für mich ein entscheidender Einstieg in die Chemie der seltenen Erden. *Prof. Dr.-Ing. Oscar Nuyken* danke ich für viele aufschlussreiche Gespräche und seine Anekdoten im Kaffeezimmer.

Besonderer Dank gebührt *Dr. Sergej Vagin* für viele fruchtbare Diskussionen in allen Bereichen meiner Arbeit; sie waren stets eine wichtige Anregung für mich. *Dr. Carly Anderson* danke ich für ihre stete Hilfe bei der Verbesserung meiner wissenschaftlichen Ausdrucksweise im Englischen. *Dr. Alexander Schöbel* danke ich für viele wissenschaftliche Diskussionen insbesondere zu Beginn dieser Arbeit. *Dr. Christian Anger, Frank Deubel* und *Andriy Plikhta* gebührt mein Dank für die fruchtbare Zusammenarbeit und für viele schöne Stunden in unserem Kaffeezimmer. *Frank Deubel* sei darüber hinaus für seinen unendlichen Fundus an schlechten Witzen und für seinen zweifelhaften Humor gedankt. Großer Dank geht auch an meinen Kollegen *Victor Bretzler* für seine Freundschaft und für sein offenes Ohr. *Dominik Lanzinger* danke ich für die gemeinsamen Diskussionen über metallorganische Chemie sowie für unsere erfolgreiche Untersuchung der Flammseigenschaften von Poly(vinylphosphonat)en.



*Dr. Eberhardt Herdtweck* gilt mein Dank für die kompetente Röntgenkristallstrukturanalyse. Mein Dank geht auch an das Team für Elementaranalyse des Anorganisch-chemischen Instituts der TUM, insbesondere an *Ulrike Ammari* für ihre stete Hilfe.

Dem Dank verpflichtet bin ich weiterhin dem immerwährend engagiertem Team unseres Lehrstuhlsekretariats: *Annette Bauer*, *Sabine Saul-Hubrich* und *Gabriele Uruk*. Ihre Arbeit war mir eine große Unterstützung!

Des Weiteren gilt mein Dank dem gesamten WACKER-Lehrstuhl für Makromolekulare Chemie für die Unterstützung, für viele nützliche Ratschläge zur Problemlösung und nicht zuletzt für das hervorragende Arbeitsklima am Lehrstuhl. Vielen Dank für die schöne Zeit, die ich hier am Lehrstuhl verbringen durfte!

Zu großem Dank verpflichtet bin ich meinen Eltern, *Josef* und *Sieglinde Salzinger*, für ihre immerwährende Unterstützung während meines gesamten Studiums sowie meinem Bruder, *Michael Salzinger*, für zahlreiche gute Ratschläge, und dafür, dass sie alle immer an mich geglaubt haben.

Last, but not least, geht mein ganz großer Dank an meine Frau *Jessica L. Smith-Salzinger* für ihre Liebe, ihr großes Verständnis und ihre liebevolle bedingungslose Unterstützung während dieser Arbeit und meines gesamten Studiums. Ohne dich hätte diese Arbeit nicht in dieser Form entstehen können und mein Weg wäre um ein vieles schwerer gewesen.



## List of Abbreviations

2IF	2- <i>iso</i> -propenylfurane	
2IMI	2- <i>iso</i> -propenyl-2-methylimidazole	
2IT	2- <i>iso</i> -propenylthiophene	
2VP	2-vinylpyridine	
$\alpha$	arbitrary position constant in the Kelen-Tüdös method	
$\alpha$	polarizability	
$\alpha$	empirical form factor in the Mark-Kuhn-Sakurada-Houwink equation	
$A^\ddagger$	pre-exponential factor in the Arrhenius equation	
$A_2$	second virial coefficient	
Ac	Acetyl	
AFM	atomic force microscopy	
AIBN	azo- <i>iso</i> -butyronitrile	
Alk	alkyl	
Ar	aryl	
ATRP	atom transfer radical polymerization	
$\beta$ MMBL	$\alpha$ -methylene- $\beta$ -methyl- $\gamma$ -butyrolactone	
B	base	
bdsa	<i>bis</i> (dimethylsilyl)amide	
btsa	<i>bis</i> (trimethylsilyl)amide	
Bu	butyl	
$\gamma$ MMBL	$\alpha$ -methylene- $\gamma$ -methyl- $\gamma$ -butyrolactone	
$c$	mass concentration	[g/L]
C or conv	conversion	
CA	contact angle	
Cat	catalyst	
Cat*	active catalyst	
Cp	cyclopentadienyl	
Cp*	1,2,3,4,5-pentamethylcyclopentadienyl	
$\delta$	chemical shift	
$\Delta E^\ddagger$	Arrhenius activation energy	[J/mol]
$\Delta G^\ddagger$	Gibbs free activation enthalpy	[J/mol]

## List of Abbreviations

---

$\Delta H^\ddagger$	activation enthalpy	[J/mol]
$\Delta S^\ddagger$	activation entropy	[J/Kmol]
D	donor	
Da = g/mol	Dalton	
DAVP	dialkyl vinylphosphonate	
DAVPO	dialkylvinylphosphineoxide	
DBVPO	di- <i>n</i> -butylvinylphosphineoxide	
DCM	dichloromethane	
DEEP	diethyl ethylphosphonate	
DEVF	diethyl vinylphosphonate	
DEMVP	diethyl 1-methylvinylphosphonate	
DMAA	<i>N,N</i> -dimethyl acrylamide	
DMF	<i>N,N</i> -dimethyl formamide	
DMMA	<i>N,N</i> -dimethyl methacrylamide	
DMSO	dimethyl sulfoxide	
DIVP	di- <i>iso</i> -propyl vinylphosphonate	
DPVP	di- <i>n</i> -propyl vinylphosphonate	
DPVPO	diphenylvinylphosphineoxide	
DSC	differential scanning calometry	
E	field intensity	[N/C]
EDX	energy dispersive X-ray spectroscopy	
EGDM	ethylene glycol dimethacrylate	
eq	equivalent	
ESI	electrospray ionization	
Et	ethyl	
EtOx	2-ethyl-2-oxazoline	
EVS	ethyl vinylsulfonate	
FCS	fetal calf serum	
FFF	field-flow fractionation	
GPC	gel permeation chromatography	
GTP	group transfer polymerization	
$h = 6.63 \times 10^{-34} \text{ m}^2 \text{ kg s}^{-1}$	Planck constant	
HD-PE	high density poly(ethylene)	
I	initiator	

## List of Abbreviations

---

I*	active initiator	
$I^*$	initiator efficiency	
$I^*_t$	initiator efficiency at a given reaction time t	
init per or Init. period	initiation period	
$I_s$	intensity of scattered light	
<i>iPr</i>	<i>iso</i> -propyl	
IPO <sub>x</sub>	2- <i>iso</i> -propylene-2-oxazoline	
IR	infrared	
k	rate constant	
k	arbitrary constant in the Zimm plot	
$k^\ddagger$	universal rate constant for a transition state	
K	optical constant	
$K^\ddagger$	equilibrium constant between reactants and transition state	
$k_B = 1.38 \times 10^{-23} \text{ m}^2 \text{ kg s}^{-2}$	Boltzmann constant	
$K_v$	empirical parameter in the Kuhn-Mark-Sakurada-Houwink equation	
$\lambda$	wavelength	[m]
L	anionic ligand	
L	distance from scattering center to detector	
LCROP	living cationic ring opening polymerization	
LCST	lower critical solution temperature	
LD-PE	low density poly(ethylene)	
LLD-PE	linear low density poly(ethylene)	
Ln	rare earth metal	
M	molar mass	[g/mol]
MA	methyl acrylate	
MALDI	matrix-assisted laser desorption ionization	
MALS	multi angle (laser) light scattering	
MBL	$\alpha$ -methylene- $\gamma$ -butyrolactone	
Me	methyl	
$M_{\text{exp}}$ or $M_{\text{th}}$	expected molecular weight according to a living-type polymerization mechanism	[g/mol]
MMA	methyl methacrylate	
$M_{\text{Mon}}$	monomer molar mass	[g/mol]

## List of Abbreviations

---

$\overline{M}_n$ or $M_n$	number-averaged molecular weight	[g/mol]
Mon	monomer	
Ms	mesyl = methanesulfonyl	
MS	mass spectrometry	
Mt	megatons	
MVK	methyl vinyl ketone	
MVSN	methyl vinyl sulfone	
MVSO	methyl vinyl sulfoxide	
$\overline{M}_w$ or $M_w$	weight-averaged molecular weight	[g/mol]
$\overline{M}_z$	z-averaged molecular weight	[g/mol]
$\eta$	dynamic viscosity	[Pa s]
$[\eta]$	intrinsic viscosity	[Pa s]
n	molar amount	[mol]
n	index of refraction	
$N_A = 6.02 \times 10^{23} \text{ mol}^{-1}$	Avogadro constant	
NE	nitroethylene	
NMR	nuclear magnetic resonance	
NP	2-nitropropylene	
p	number of collisions in the Arrhenius equation	
P*	reactive chain end	
P( $\theta$ )	scattering function	
P2VP	poly(2-vinylpyridine)	
PBS	phosphate buffered saline	
PDAVP	poly(dialkyl vinylphosphonate)	
PDEAM	poly( <i>N,N</i> -diethyl acrylamide)	
PDEVPP	poly(diethyl vinylphosphonate)	
PDI	polydispersity index	
PDIVP	poly(di- <i>iso</i> -propyl vinylphosphonate)	
PDMVP	poly(dimethyl vinylphosphonate)	
PDPVP	poly(di- <i>n</i> -propyl vinylphosphonate)	
PE	poly(ethylene)	
PEG	poly(ethylene glycol)	
PEGDM	poly(ethylene glycol dimethacrylate)	
PET	poly(ethylene terephthalate)	

## List of Abbreviations

---

Ph	phenyl	
PIPOx	poly(2- <i>iso</i> -propenyl-2-oxazoline)	
pK <sub>a</sub>	Brønsted acidity	
PNIPAM	poly( <i>N-iso</i> -propyl acrylamide)	
PMMA	poly(methyl methacrylate)	
ppm	parts per million	
PP	poly(propylene)	
PS	poly(styrene)	
PUR	poly(urethane)	
PVC	poly(vinyl chloride)	
PVPA	poly(vinylphosphonic acid)	
$\langle r_g^2 \rangle$	mean square radius of gyration	[m <sup>2</sup> ]
r	rate	
r	copolymerization parameter	
$R = 8.31 \text{ J mol}^{-1} \text{ K}^{-1}$	universal gas constant	
R( $\theta$ )	Rayleigh ratio	[1/m]
RDS	rate determining step	
RE	rare earth	
REM-GTP	rare earth metal-mediated group transfer polymerization	
R <sub>ex</sub> ( $\theta$ )	excess Rayleigh ratio	[1/m]
RI	refractive index	
r <sub>p</sub>	propagation rate	
S	stoichiometric ratio	
SAM	self-assembled monolayer	
SANS	small angle neutron scattering	
SAXS	small angle X-ray scattering	
SEC	size exclusion chromatography	
SI	surface-initiated	
SI-ATRP	surface-initiated atom transfer radical polymerization	
SI-GTP	surface-initiated group transfer polymerization	
SIPGP or SI-PGP	self-initiated photografting and photopolymerization	
SKA-GTP	silyl ketene acetal-mediated group transfer polymerization	
SLS	static light scattering	
$\theta$	scattering angle	

## List of Abbreviations

---

T	temperature	[°C, K]
TBAB	tetrabutyl ammonium bromide	
TBAF	tetrabutyl ammonium fluoride	
<i>t</i> Bu	<i>tert</i> -butyl	
TGA	thermogravimetric analysis	
thf	tetrahydrofuran (ligand)	
THF	tetrahydrofuran (solvent)	
TMS	trimethylsilyl	
TMSPM	3-(trimethoxysilyl)propyl methacrylate	
ToF	time of flight	
TOF	turnover frequency	[s <sup>-1</sup> ]
TON	turnover number	
UCST	upper critical solution temperature	
UV	ultraviolet	
V	scattering volume	[m <sup>3</sup> ]
V <sub>H</sub>	hydrodynamic volume	[m <sup>3</sup> ]
Vis	visible	
VPA	vinylphosphonic acid	
V <sub>R</sub>	retention volume	[m <sup>3</sup> ]
w%	weight percent	
X	(pseudo)halogen	
X	initiating ligand	
X	molar feed fraction	
$\overline{X}_n$	number-averaged degree of polymerization	
XPS	X-ray photoelectron spectroscopy	
Z	probability of collisions to lead to a subsequent reaction in the Arrhenius equation	



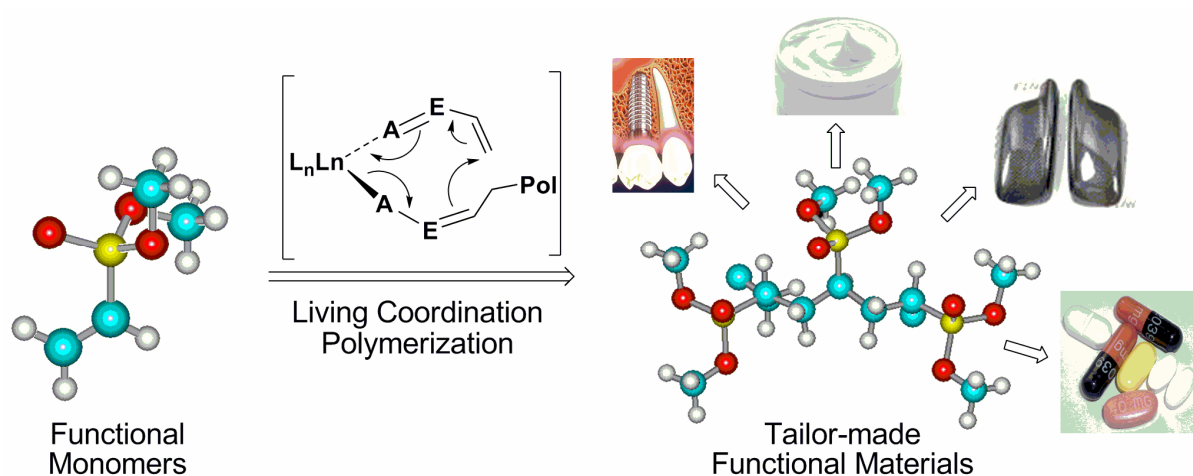
## Table of Contents

<b>1 RARE EARTH METAL-MEDIATED GROUP TRANSFER POLYMERIZATION AS A VERSATILE TOOL FOR THE PRODUCTION OF FUNCTIONAL MATERIALS .....</b>	<b>1</b>
<b>2 THEORETICAL BACKGROUND .....</b>	<b>9</b>
2.1 SYNTHETIC ROUTES TOWARDS RARE EARTH METAL COMPLEXES .....	11
2.1.1 Salt Metathesis Route .....	12
2.1.2 Precursor Route .....	14
2.2 PRINCIPLES OF POLYMERIZATION .....	19
2.2.1 Classification of Polymerization Methods .....	19
2.2.2 Kinetics of Living Coordination Polymerizations .....	22
2.2.3 Chain-growth Copolymerizations .....	24
2.3 THE TRANSITION STATE MODEL FOR THE DETERMINATION OF ACTIVATION ENTHALPY AND ENTROPY .....	27
2.4 DETERMINATION OF MOLECULAR WEIGHT AND MOLECULAR WEIGHT DISTRIBUTION ...	29
2.4.1 Absolute Methods for the Determination of the Molecular Weight .....	29
2.4.2 Static Light Scattering .....	31
2.4.3 Determination of the Molecular Weight Distribution .....	35
2.4.4 Gel Permeation Chromatography (GPC) .....	37
2.4.5 Gel Permeation Chromatography Multi Angle Light Scattering (GPC-MALS) ...	38
2.5 THERMOSENSITIVE BEHAVIOR OF POLYMERS .....	40
2.6 REFERENCES .....	43
<b>3 EXPANSION OF RARE EARTH METAL-MEDIATED GROUP TRANSFER POLYMERIZATION TO NEW MONOMERS .....</b>	<b>47</b>
<b>4 RARE EARTH METAL-MEDIATED GROUP TRANSFER POLYMERIZATION OF VINYLPHOSPHONATES .....</b>	<b>53</b>
<b>5 POLY(VINYLPHOSPHONATE)S SYNTHESIZED BY TRIVALENT CYCLOPENTADIENYL LANTHANIDE-INDUCED GROUP TRANSFER POLYMERIZATION .....</b>	<b>77</b>

<b>6</b>	<b>SURFACE-INITIATED GROUP TRANSFER POLYMERIZATION MEDIATED BY RARE EARTH METAL CATALYSTS .....</b>	<b>97</b>
<b>7</b>	<b>POLY(VINYLPHOSPHONATE)S WITH WIDELY TUNEABLE LCST: A PROMISING ALTERNATIVE TO CONVENTIONAL THERMORESPONSIVE POLYMERS .....</b>	<b>113</b>
<b>8</b>	<b>RARE EARTH METAL-MEDIATED GROUP TRANSFER POLYMERIZATION: FROM DEFINED POLYMER MICROSTRUCTURES TO HIGH PRECISION NANO-SCALED OBJECTS .....</b>	<b>139</b>
<b>9</b>	<b>MECHANISTIC STUDIES ON INITIATION AND PROPAGATION OF RARE EARTH METAL-MEDIATED GROUP TRANSFER POLYMERIZATION OF VINYLPHOSPHONATES .....</b>	<b>157</b>
<b>10</b>	<b>C–H BOND ACTIVATION BY <math>\sigma</math>-BOND METATHESIS AS A VERSATILE ROUTE TOWARDS HIGHLY EFFICIENT INITIATORS FOR RARE EARTH METAL-MEDIATED GROUP TRANSFER POLYMERIZATION .....</b>	<b>199</b>
<b>11</b>	<b>APPLICATION OF RARE EARTH METAL-MEDIATED GROUP TRANSFER POLYMERIZATION TO NEW MONOMER CLASSES .....</b>	<b>211</b>
<b>12</b>	<b>CONCLUSION AND OUTLOOK .....</b>	<b>221</b>
<b>13</b>	<b>ZUSAMMENFASSUNG UND AUSBLICK .....</b>	<b>233</b>
<b>14</b>	<b>APPENDIX .....</b>	<b>245</b>

## CHAPTER 1:

# RARE EARTH METAL-MEDIATED GROUP TRANSFER POLYMERIZATION AS A VERSATILE TOOL FOR THE PRODUCTION OF FUNCTIONAL MATERIALS



*“Chemistry is moving to both make the molecules but also to make them by design to have a function. What people are really interested in is the function. Making a molecule – that’s terrific. But what you really want is a molecule that does something.”*

- George Whitesides, 2012



Within the last decades, synthetic polymer-based materials have gained an indisputable dominance for an enormous range of applications and, nowadays, their use is by no means limited to packaging materials. On the contrary, synthetic polymers are fundamental basis for the comfort and the requests of our modern consumer-based society, satisfying essential needs such as mobility, the quality of living, health care and electronic devices. Moreover, they are an indispensable factor in securing our future energy supply by the development of efficient concepts for energy production from renewable sources, for the storage of this produced energy and its conversion. Accordingly, without polymeric materials, our modern society is hard to imagine.

The increasing importance of synthetic polymer-based materials is hereby not only owed to their enormous versatility and their nearly limitless possibilities for the production of new materials, but also to a variety of other advantages in comparison to classic raw materials such as wood, glass, ceramics, or metals. Synthetic polymers commonly exhibit a lower density, resistance to corrosion and chemicals can be tailored, and their production is possible in high automation and number at comparatively lower temperatures and energy consumption. These advantages and their versatility lead to an enormous increase per annum of polymer production and since the end of the 1980s the production of polymeric materials exceeds, by volume, crude steel production.<sup>[1,2]</sup> Civilization quantum leaps are commonly accompanied by the use of new materials, accordingly, using the classic definition to divide history by the predominantly used raw material, we have therefore entered the age of polymers.

Since the first industrial production of synthetic polymers more than 100 years ago, a vast knowledge of polymer-based materials and polymerizable substances has been developed. Yet, opposed to predictions in the 1980s, nowadays, still more than 60% of the world polymer sales volume is ascribed to a few so-called commodity materials based on a small number of common monomers as an inexpensive feedstock.<sup>[3]</sup> Accordingly, almost 50% of the European polymer production 2011 are allotted to poly(ethylene) (PE) and poly(propylene) (PP) (Figure 1.1).<sup>[1]</sup> A further quarter of the production is covered by the commodity materials poly(vinyl chloride) (PVC), poly(ethylene terephthalate) (PET) and poly(styrene) (PS).<sup>[1]</sup> These materials still prevail not only according to the readily available monomers and their low production costs, but also as a result of the continuous improvement of their properties by the development of suitable catalysts and additives.

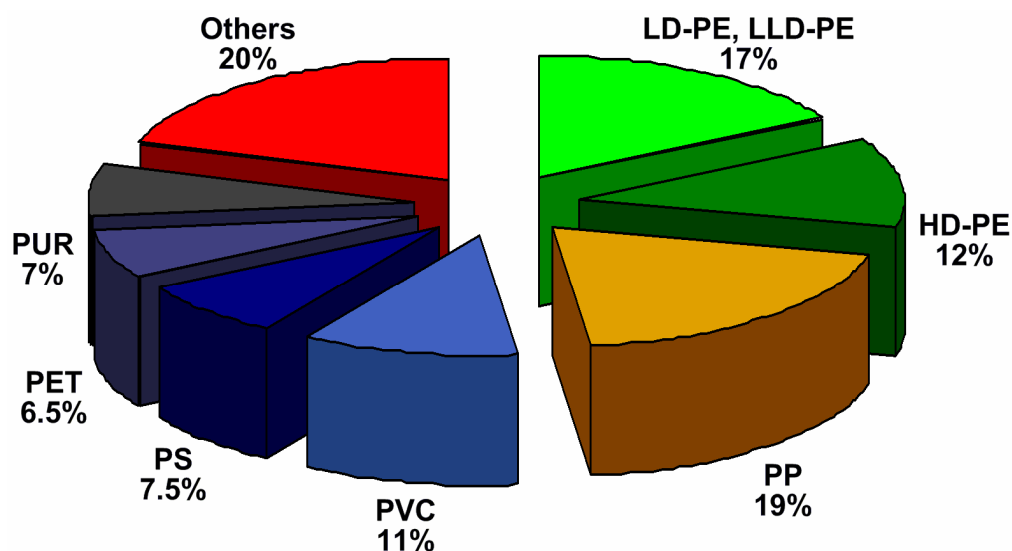


Figure 1.1: Polymer production of EU-27, Norway and Switzerland 2011 (total: 47 Mt).<sup>[1]</sup>

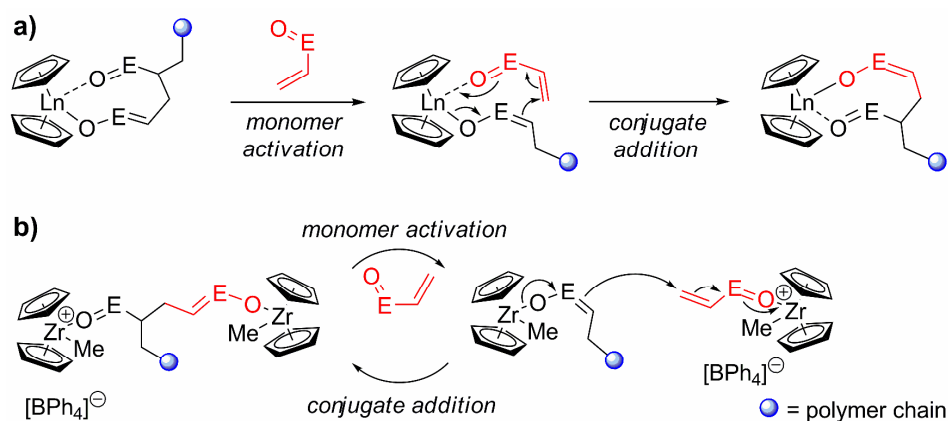
Particularly, the tremendous development of PE and PP is a consequence of Ziegler's discovery in 1953 that  $\text{TiCl}_3$  in combination with aluminium alkyls can polymerize ethylene.<sup>[4]</sup> Only one year later, 1954, using the same type of catalyst, Natta succeeded in the first formation of high-molecular weight PP.<sup>[5]</sup> Until then, polymerization of  $\alpha$ -olefins such as propylene was not possible due to the formation of stable allylic radicals in radical polymerization processes. Furthermore, by coordination of the transition metal polymerization catalyst at the active chain end, for the first time, precise control of the polymer tacticity could be tailored.

Today, a variety of coordination polymerization types has been described, being amongst the most important methods for polymer synthesis. A vast number of catalysts have been presented and alteration of metal center and ligand sphere allows precise adjustment of structure, tacticity, molar mass and dispersity of the obtained polymer product. As the properties of polymer-based materials generally depend strongly on these parameters, the use of polymerization catalysis enables precise control of the material properties. As a consequence, the discovery of coordination polymerizations largely contributed to a better understanding of the basic structure-property relationship of polymeric materials. For their groundbreaking invention with the following tremendous development of the so-called migratory-insertion polymerization, and the enormous impact it had shown on chemical industry and material science, Ziegler and Natta were awarded with the Nobel Prize in Chemistry in 1963. Nowadays, except for low density poly(ethylene) (LD-PE), PE and PP are exclusively produced by catalytic coordination polymerization.

Especially in regard to the current economic situation under the pressure of the American economic stagnation and the Euro crisis, chemical industry is actively searching for new growth fields, requiring further development of polymer-based materials. Although some of the requirements may be met by cost-efficient modification of established materials, not for all applications a simple optimization of conventional polymers will be sufficient. Accordingly, even though the majority of produced polymeric materials is based on only a few commodity polymers, this need for new materials with designed properties has driven polymer research in recent years. The necessity of such specialty polymers ranges from high-performance materials for aerospace applications and medical chemistry to new energy technologies (*e.g.* proton conducting membranes in fuel cells or bulk heterojunction solar cells).<sup>[6-14]</sup>

Of these designed materials, polymers comprising heteroatoms have attracted great interest during the last decades and are increasingly becoming a focus of research activities. The number of available functionalities tailored by the introduction of heteroatoms is vast and, in combination with macromolecular organization and self-assembly principles, a wide range of new functional materials is accessible. In order to precisely adjust the properties of these functional materials, a straight-forward approach *via* coordination polymerization of functional monomers seems most promising, as it allows for an exact control of the polymer microstructure and ensures, in contrast to post-polymerization modifications, a high density of functionalization. For this purpose, suitable polymerization methods need to be tolerant to the usually polar nature of the respective monomers.

Coordinative-anionic addition polymerization, also referred to as transition metal-mediated group transfer polymerization, represents a well-established route for the coordination polymerization of polar-modified olefins, *i.e.* (meth)acrylic monomers. It has been first described in 1992 in two independent *JACS* communications by Yasuda *et al.*<sup>[15]</sup> using neutral lanthanidocenes (*e.g.*  $[\text{Cp}^*_2\text{SmH}]_2$ ) and by Collins and Ward<sup>[16]</sup> using a two-component catalyst group 4 metallocene system. The reaction proceeds in both cases *via* repeated conjugate addition involving either one or two coordinating metal complexes (Scheme 1.1).<sup>[15-20]</sup> The works of Collins, Ward, and Yasuda *et al.* indicate the start of a paradigm shift in early transition metal polymerization catalysis of polar, heteroatom-functionalized vinyl monomers. Instead of protection of the functional group and introduction of high steric constraints at the active site – to ensure monomer–metal coordination *via* the double bond following a migratory-insertion polymerization mechanism – the metal center remains easily accessible and the coordination occurs *via* the heteroatom.<sup>[20]</sup>



**Scheme 1.1: Proposed monometallic (a) and bimetallic (b) propagation mechanism for coordinative-anionic polymerization of Michael acceptor-type monomers; E = C(OR), C(NR<sub>2</sub>), P(OR)<sub>2</sub>.**

Rare earth metal-based catalysts are of particular interest, as they facilitate the polymerization of a broad variety of monomers following different polymerization mechanisms, *i.e.* (meth)acrylate group transfer polymerization, olefin, diene and (syndiospecific) styrene migratory-insertion polymerization as well as ring-opening polymerization of lactones, lactides, cyclic ethers, and carbonates.<sup>[17-19,21]</sup> Using a one-directional mechanistic crossover, these different polymerization methods can be combined in a living fashion, further increasing the versatility of organo-rare earth metal compounds for the synthesis of functional high value polymers.<sup>[20]</sup>

Rare earth metal-mediated group transfer polymerization (REM-GTP) combines the advantages of living ionic and coordination polymerizations, making it a promising and versatile tool for the synthesis of designed functional materials. Intensive research on REM-GTP has been carried out over the past two decades, optimizing reaction conditions, initiator efficiency, and control over stereoregularity, on the use of different metals, as well as on their implementation to a variety of monomers, for example, different (meth)acrylates and (meth)acrylamides.<sup>[17-20]</sup> As the polymerization of these monomers is also possible *via* other methods and as their stereospecific polymerization does not lead to a substantial improvement of the material properties, despite its advantages and potential, the interest in REM-GTP has decreased over the past years.

Nonetheless, in principle, REM-GTP is not restricted to (meth)acrylic monomers. Recent publications have shown the suitability of REM-GTP to a variety of other monomer classes, particularly poly(vinylphosphonate)s, a material class which is not satisfactorily accessible *via* other polymerization methods.<sup>[22,23]</sup> Requirement to the monomers suitable for REM-GTP is a Michael acceptor-type behavior with S-cis position of the double bonds and a pronounced  $\pi$ -overlap (Figure 1.2).



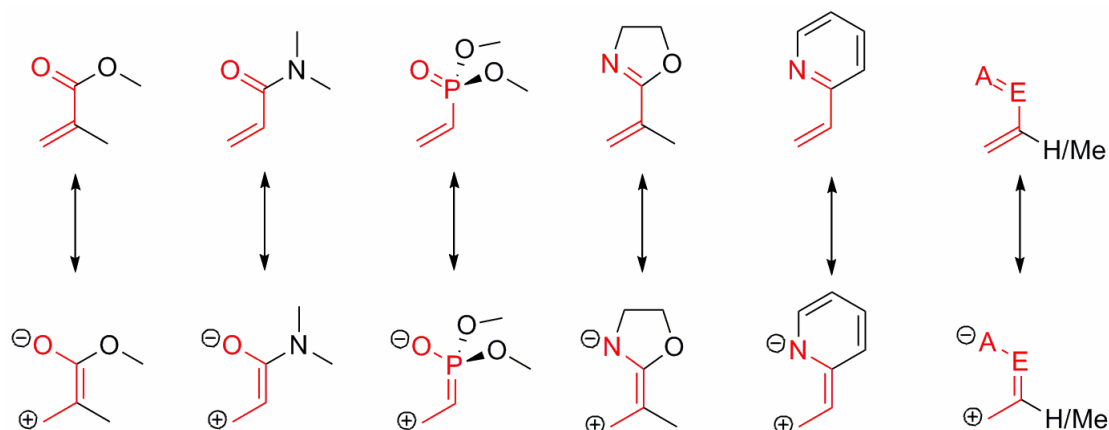


**Figure 1.2: Example monomers suitable for REM-GTP: methyl methacrylate (MMA), *N,N*-dimethyl acrylamide (DMAA), dimethyl vinylphosphonate (DMVP), 2-*iso*-propylene-2-oxazoline (IPOx), 2-vinylpyridine (2VP) and the general structure of suitable Michael acceptor-type monomers (from left to right).**

Initial investigations on rare earth metal-mediated vinylphosphonate polymerization have proven the livingness of polymerization and suggest a GTP mechanism taking place,<sup>[23]</sup> however, other typical characteristics of REM-GTP, *e.g.* the efficient initiation by strongly basic carbanion initiators or the rare earth cation size-reactivity relationship, were found to be strongly altered for its application to vinylphosphonates.<sup>[23,24]</sup> Accordingly, in order to expand the applicability of REM-GTP to the above mentioned scope of monomers, a deeper understanding of the underlying initiation and propagation mechanism is necessary.

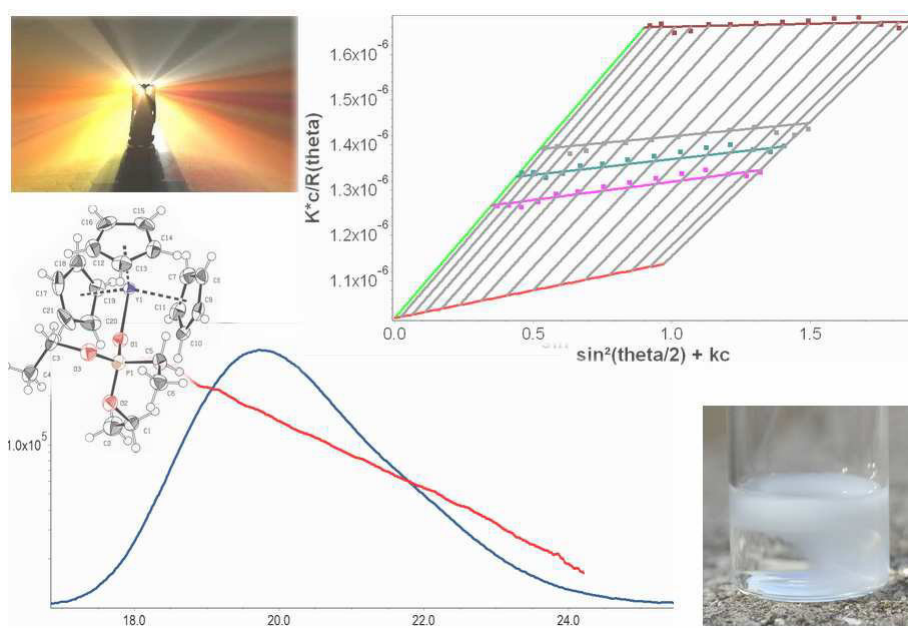
Therefore, it was a major scope of this thesis to conduct detailed mechanistic studies in order to verify the origin of unexpected monomer polymerization behavior and to allow a prediction of this behavior for other monomers of interest. On basis of the mechanistic conclusions drawn, a systematic improvement of the applied catalysts should be performed, both regarding their initiator efficiency and activity. Particularly, this includes the investigation of versatile complex synthesis routes in order to allow an easy and sophisticated modification of the catalyst properties. Developing a deeper understanding of the monomer polymerization behavior, the catalyst applicability should be widened, therefore broadening the scope of REM-GTP onto the vast variety of Michael acceptor-type monomers. To further increase the versatility of REM-GTP, on basis of initiation mechanism studies, control of chain end functionalization should be enabled, particularly leading towards the development of a surface-initiated group transfer polymerization (SI-GTP) mediated by rare earth metal catalysts.

## References

- [1] PlasticsEurope, Facts about Plastics, [www.plasticseurope.org](http://www.plasticseurope.org) (01/2012).
- [2] Worldsteel Association, Crude Steel Production, [www.worldsteel.org](http://www.worldsteel.org) (01/2012).
- [3] B. Rieger, in *Skriptum zur Vorlesung Makromolekulare Chemie II*, Technische Universität München, April **2009**.
- [4] K. Ziegler, E. Holzkamp, H. Breil, H. Martin, *Angew. Chemie* **1955**, 67, 541.
- [5] G. Natta, *Angew. Chemie* **1955**, 67, 393.
- [6] N. Yousfi-Steiner, P. Mocotéguy, D. Candusso, D. Hissel, *J. Power Sources* **2009**, 194, 130.
- [7] S. J. Peighambardoust, S. Rowshanzamir, M. Amjadi, *Int.J. Hydrogen Energy* **2010**, 35, 9349.
- [8] Y. Wan, K. S. Chen, J. Mishler, S. C. Cho, X. C. Adroher, *Appl. Energy* **2011**, 88, 981.
- [9] S. Günes, H. Neugebauer, N. S. Sariciftci, *Chem. Rev.* **2007**, 107, 1324.
- [10] Y.-J. Cheng, S.-H. Yang, C.-S. Hsu, *Chem. Rev.* **2009**, 109, 5868.
- [11] B. C. Thompson, J. M. J. Fréchet, *Angew. Chem. Int. Ed.* **2008**, 47, 58.
- [12] G. Denner, M. C. Scharber, C. J. Brabec, *Adv. Mater.* **2009**, 21, 1323.
- [13] C. J. Brabec, S. Gowrisanker, J. J. M. Halls, D. Laird, S. Jia, S. P. Williams, *Adv. Mater.* **2010**, 22, 3839.
- [14] P. M. Beaujuge, J. M. J. Fréchet, *J. Am. Chem. Soc.* **2011**, 133, 20009.
- [15] H. Yasuda, H. Yamamoto, K. Yokota, S. Miyake, A. Nakamura, *J. Am. Chem. Soc.* **1992**, 114, 4908.
- [16] S. Collins, S. G. Ward, *J. Am. Chem. Soc.* **1992**, 114, 5460.
- [17] H. Yasuda, E. Ihara, *Adv. Polym. Sci.* **1997**, 133, 53.
- [18] H. Yasuda, *Prog. Polym. Sci.* **2000**, 25, 573.
- [19] L. S. Boffa, B. M. Novak, *Chem. Rev.* **2000**, 100, 1479.
- [20] E. Y.-X. Chen, *Chem. Rev.* **2009**, 109, 5157.
- [21] J. Gromada, J.-F. Carpentier, A. Mortreux, *Chem. Rev.* **2004**, 248, 397.
- [22] G. W. Rabe, H. Komber, L. Häußler, K. Kreger, G. Lattermann, *Macromolecules* **2010**, 43, 1178.
- [23] U. B. Seemann, J. E. Dengler, B. Rieger, *Angew. Chem. Int. Ed.* **2010**, 49, 3489.
- [24] U. B. Seemann, *Ph.D. Thesis*, Technische Universität München, Garching bei München, October **2010**.

## CHAPTER 2:

## THEORETICAL BACKGROUND



*“Try to learn something about everything and everything about something.”*

- Thomas Henry Huxley (1825-1895)



In this chapter, an introduction will be given to principles of polymerization as well as to synthetic and analytical methods which are of importance to the results presented in this work. This includes a brief overview of the synthesis of rare earth metal complexes, the classification and definition of polymerization types and a short account on the thermosensitive behavior of polymer solutions. An introduction to the polymerization kinetics of living coordination polymerizations, the kinetic analysis of activation enthalpy and entropy according to the transition state model, as well as a brief outline on absolute analytical methods for the determination of the molecular weight of polymers will be presented. A detailed overview of vinylphosphonate polymerization as well as an introduction to rare earth metal-mediated group transfer polymerization (REM-GTP) will be given in chapter 4.

### 2.1 Synthetic Routes towards Rare Earth Metal Complexes

Within the past two decades, rare earth metal complexes have become an increasing focus of both academic and industrial research according to their versatile use as homogeneous catalysts for a vast variety of polymerizations and related catalytic transformations. Large efforts have been directed especially towards their utilization as a catalyst or initiator for coordination-addition or migratory-insertion polymerization of polar and non-polar olefins and for living anionic ring-opening polymerization of lactones and lactides,<sup>[1-5]</sup> as well as to their application as catalysts for olefin hydrogenation, hydrosilylation, hydroboration and alkyne dimerization.<sup>[6-10]</sup> These application-driven research efforts were accompanied by a tremendous development of efficient and versatile synthetic strategies for the synthesis of rare earth metal complexes within the last 20 years. Particularly, the development of synthetic routes *via* homoleptic  $\sigma$ -bonded amide and alkyl precursor complexes has been an essential basis for the growing importance of rare earth metal-based catalysts.<sup>[9,10]</sup>

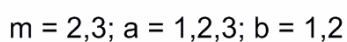
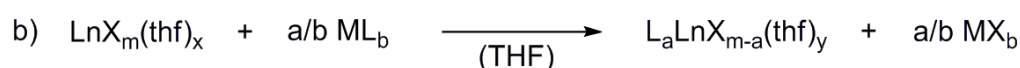
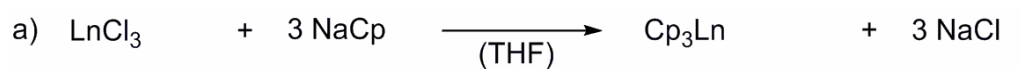
According to the significant interest in rare earth metal complexes and their extreme sensitivity to oxygen and moisture, a variety of different synthetic strategies has been developed since the middle of the last century. It is surprising however, that until the end of the 1990ies, the salt metathesis route following the original synthesis protocol reported by Wilkinson in 1954 has been the only well-studied and well-established synthetic route.<sup>[9,11,12]</sup> The synthesis of divalent rare earth metallocenes from the corresponding metals in liquid

ammonia with cyclopentadienes according to E. O. Fischer,<sup>[13-16]</sup> as well as transmetallation (e.g. with mercury or thallium complexes)<sup>[17-19]</sup> and a synthetic route *via*  $\text{Ln}(\text{C}_6\text{F}_5)_2$ <sup>[20]</sup> are limited to those lanthanides, which form sufficiently stable divalent cations.<sup>[9]</sup> Desilylation as well as destannylation fail in case of *ansa*-lanthanidocenes<sup>[21-23]</sup> and the direct reduction of the ligand by the rare earth metal is restricted to a limited number of systems.<sup>[9,24,25]</sup>

Within the last 20 years, more attention has been drawn to precursor routes, particularly *via* homoleptic  $\sigma$ -bonded amide and alkyl precursors.<sup>[9-11,26]</sup> To date, the only well-established methods for the synthesis of rare earth metal complexes are the salt metathesis and the precursor route, which will be both presented in more detail in the following. The present work exclusively used rare earth metallocenes, hence, the different synthetic approaches are compared for the synthesis of these systems. However, most statements can be transferred directly also for the synthesis of half sandwich or non-metallocene-based rare earth metal complexes.

### 2.1.1 Salt Metathesis Route

In the original synthesis protocol by Birmingham and Wilkinson, trivalent rare earth metal cyclopentadienides  $\text{Cp}_3\text{Ln}$  were synthesized from the anhydrous rare earth metal chlorides and sodium cyclopentadienide ( $\text{NaCp}$ ) in tetrahydrofuran (THF) solution (Scheme 2.1a).<sup>[12,27]</sup> Within the continuous development of the salt metathesis route, various ligand salts ( $\text{ML}_b$ ) have been reacted with different rare earth metal salts  $\text{LnX}_m$  (often in form of thf adducts) in order to form a variety of rare earth metal complexes of the general structure  $\text{L}_a\text{LnX}_{m-a}(\text{thf})_y$  (Scheme 2.1b).<sup>[9]</sup>



**Scheme 2.1:** Synthesis of rare earth metal complexes according to the salt metathesis route; a) original synthesis protocol according to Birmingham and Wilkinson<sup>[12,27]</sup> and b) its further development.<sup>[9]</sup>

This synthetic route is fast and requires a minimum of reaction steps at the rare earth metal center. However, despite the versatility of applied reagents, some intrinsic limitations of this method could not be solved. Whereas this synthetic procedure is well suited for non-bridged cyclopentadienyl complexes, it is restricted to a small number of *ansa*-cyclopentadienyl ligands and often fails for the synthesis of indenyl- and fluorenyl-based systems,<sup>[9,28,29]</sup> presumably due to the small thermodynamic driving force between educts and products as a result of the small electronegativity difference between the mainly applied alkali metals and the rare earth metal center. Especially in case of trivalent rare earth metal complexes, this synthetic route often suffers from the contamination of the product with alkali salts and solvent molecules by ate complex formation (Figure 2.1).<sup>[9,11,26,30]</sup> Consequently, the salt metathesis route is encumbered by lengthy and tedious purification procedures often resulting in low product yields.<sup>[11,26,30]</sup>

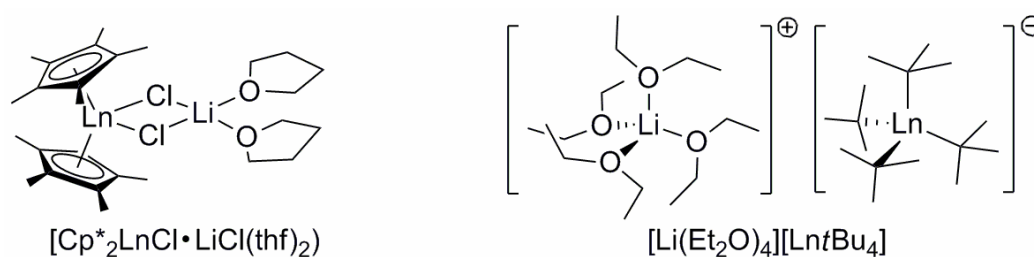


**Figure 2.1:** Examples for ate complexation at rare earth metal complexes.<sup>[10]</sup>

Especially in case of *ansa*-rare earth metallocenes (and also for a variety of other chelating ligands), this synthetic route proves to be very inefficient.<sup>[9,28,29]</sup> This may be attributed to the instability of the used dialkali salts of the applied ligands (at the often necessary elevated reaction temperatures) as well as the possible formation of multimetallic complexes and clusters by bridging *via* the used chelating ligands or  $\mu$ -halogen bridges (Figure 2.2).<sup>[9]</sup> According to theoretical calculations, the formation of multinuclear complexes *via* ligand bridges is often energetically favored over chelating structures if the coordination sphere is saturated with halogen atoms.<sup>[31]</sup>

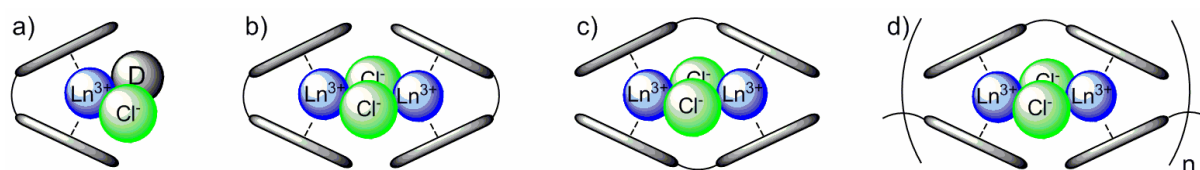
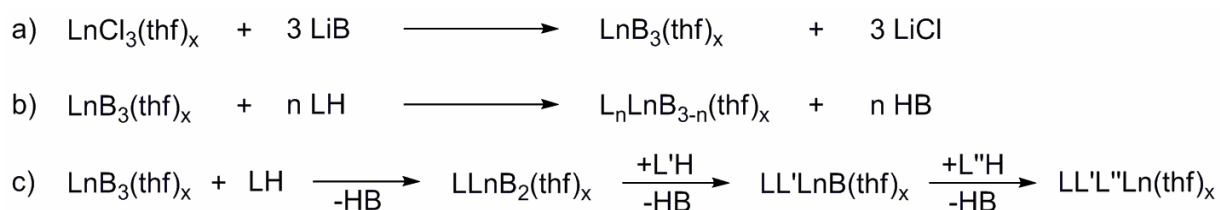


**Figure 2.2:** Competitive formation of monometallic species a) and multimetallic clusters b) - d).

Despite the simplicity of the salt metathesis route and the few reaction steps involved, its strong disadvantages, especially for the formation of more complex coordination spheres, limit its utilization to the synthesis of a very restricted variety of structures. Consequently, the development of the precursor route has been an indispensable improvement of the synthetic methodology towards rare earth metal complexes.

### 2.1.2 Precursor Route

The precursor route for rare earth metal complex synthesis involves the formation of reactive precursor complexes of the general structure  $\text{LnB}_3(\text{donor})_x$  and  $\text{LnB}_2(\text{donor})_x$  for tri- and divalent rare earth metal centers, respectively. B represents a strongly basic  $\sigma$ -donor ligand and the coordination sphere of the precursor complex is saturated by a variable amount of coordinated neutral donor molecules, *e.g.* solvent molecules such as THF. There are different possibilities for the formation of these precursors, in case of trivalent metal centers however, most commonly they are formed *via* salt metathesis from the rare earth metal chloride THF adduct  $\text{LnCl}_3(\text{thf})_x$  and the lithium salt of the base LiB (Scheme 2.2a).<sup>[9,10]</sup> Suitable bases B ensure that the resulting precursor complex is well-soluble in non-polar solvents and inhibit the formation of ate complexes, allowing a simple and complete separation of the formed alkali halogenide. The precursors are transformed into the desired complexes by simple deprotonation of the ligands under formation of HB (Scheme 2.2b), which is commonly a volatile compound and can thus be removed easily *in vacuo*.<sup>[9,10]</sup> This approach allows a consecutive introduction of different ligands and thus opens the access to complex coordination spheres (Scheme 2.2c).<sup>[10]</sup>



**Scheme 2.2: Synthesis of trivalent rare earth metal complexes *via* the precursor route: a) formation of the precursor complex, b) introduction of the ligand sphere by protonolysis of B, c) possibility for the consecutive introduction of different ligands (x = 0-3.5).**

This synthetic approach has been first applied to rare earth metals in the late 1980ies, when the amide route, which has previously been successfully introduced to group 4



chemistry,<sup>[32-37]</sup> was transferred to rare earth metal systems.<sup>[38-40]</sup> Over the past two decades, a large variety of different bases has been presented. Most common are amide and alkyl species, but also the use of phosphides<sup>[41,42]</sup> and a variety of other carbon-based bases, *e.g.* phenyl and alkynide,<sup>[10]</sup> has been reported.

The established amide route for group 4 metal complex synthesis commonly utilizes strongly basic dialkylamides, *e.g.* dimethyl- or diisopropylamide.<sup>[9,26]</sup> The application of these dialkylamides towards rare earth metal precursors leads to the formation of oligomeric species or polymeric networks resulting in poor solubility, decreased reactivity and frustrating characterization.<sup>[9,10]</sup> The agglomeration of monometallic species is a result of both steric and electronic factors and may be attributed to the high basicity of the amides (*e.g.*  $pK_a(\text{HNiPr}_2) = 36.0$ <sup>[43]</sup>) as well as to a sterical undersaturation at the rare earth metal center.<sup>[9]</sup> High basicity (*i.e.* reactivity) also facilitates the formation of ate complexes.<sup>[9,10]</sup>

According to their lower basicity and better steric shielding of the metal center, the use of silylamides instead of dialkylamides gives access to discrete monometallic precursors.<sup>[9]</sup> The first described  $\text{Ln}(\text{btsa})_3$  precursors ( $\text{btsa} = \text{bis}(\text{trimethylsilyl})\text{amide}$ ,  $\text{N}(\text{SiMe}_3)_2$ ,  $pK_a(\text{HN}(\text{SiMe}_3)_2) = 25.8$ <sup>[44]</sup>) however, suffer from the enormous steric demand of the *btsa* ligand resulting in a low reactivity of the precursor complex, particularly with sterically hindered CH-acidic compounds such as indenyl and fluorenyl ligands.<sup>[9,11]</sup> Accordingly, the use of  $\text{Ln}(\text{btsa})_3$  precursors gives rather poor yields and is limited to less sterically demanding substrates.<sup>[9]</sup>

Strong improvement could be made in the second half of the 90ies by the use of the less bulky *bdsa* ligand ( $\text{bdsa} = \text{bis}(\text{dimethylsilyl})\text{amide}$ ,  $\text{N}(\text{SiMe}_2\text{H})_2$ ,  $pK_a(\text{HN}(\text{SiMe}_2\text{H})_2) = 22.8$ <sup>[9,26]</sup>) yielding stable precursor complexes of the structure  $\text{Ln}(\text{bdsa})_3(\text{thf})_x$  over the whole size range of the rare earth metals (with  $x = 1$  for Sc, and  $x = 2$  for all other rare earth metals).<sup>[9,11,26]</sup> The enhanced flexibility of these precursors in comparison to their *btsa* analogues, and the possibility of THF dissociation ensures ligand approach and proton transfer.<sup>[11]</sup> According to the convenient synthesis protocol of this extended silylamide route<sup>[9,11,26]</sup> and the pronounced stability of the *bdsa* precursor complexes, both in solid state and solution, complex synthesis *via* the  $\text{Ln}(\text{bdsa})_3(\text{thf})_x$  precursor was chosen as a major synthetic route for this work.

However, the extended silylamide route also suffers from both kinetic and thermodynamic limitations. Thermodynamically, the low basicity of the *bdsa* ligand leads to strong restrictions concerning the spectrum of suitable protic substrates, *e.g.* deprotonation of amide-containing constrained geometry or fluorenyl-based ligand systems is not possible.<sup>[9,26]</sup> Kinetically, steric repulsion hinders the reaction between a variety of substrates and the

$\text{Ln}(\text{bdsa})_3(\text{thf})$  reaction intermediate.<sup>[9,26]</sup> Accordingly, the extended silylamide route is more versatile than the original *btsa*-silylamide route, but still limited. Additionally, the present Si–H bonds do not only stabilize the rare earth metal center by agostic interactions, but can also facilitate side reactions. Formed complexes of the general structure  $\text{L}_2\text{Ln}(\text{bdsa})$  tend to decompose by Si-H activation over the course of several weeks if not completely purified.<sup>[9]</sup> Within the frame of this work, hydrosilylation reactions were observed between the Si-H group and ketones or aldehydes, therefore inhibiting the synthesis of the corresponding enolic initiators *via* the extended silylamide route.

According to the limitations of the extended silylamide route, the use of the more reactive alkyl precursors was evaluated as a second precursor route within this framework. In analogy to the amine elimination route, also in the alkyl precursor route, the silyl-substituted derivatives  $\text{CH}_2\text{SiMe}_3$ ,  $\text{CH}(\text{SiMe}_3)_2$  and  $\text{C}(\text{SiMe}_3)_3$  are the most applied alkyl ligands in rare earth metal chemistry and will be discussed briefly in the following.<sup>[10]</sup> Within the last two decades, a large variety of other precursors with  $\sigma$ -bonded carbon-based ligands has been described. For a detailed overview on synthesis, structure and properties of homoleptic rare earth metal precursors containing Ln–C  $\sigma$ -bonds, the reader is directed to a recent review from Zimmermann and Anwander.<sup>[10]</sup>

The particular importance of silyl-substituted ligands in rare earth metal chemistry can be largely ascribed to the remarkable stability of the resulting complexes. This stability can be mainly explained by two considerations: first,  $\beta$ -hydride elimination is an important decomposition pathway in rare earth metal chemistry; in case of trimethylsilyl-substituted derivatives, ligand degradation reactions are impeded by the absence of  $\beta$ -hydrogen atoms.<sup>[10]</sup> Second, the strong stabilizing effect of the silyl substituents is ascribed to the stabilization of the respective anion by  $(p \rightarrow d)_\pi$  or  $(p \rightarrow \sigma^*)$  interaction with the silicon atom.<sup>[10,45-47]</sup>

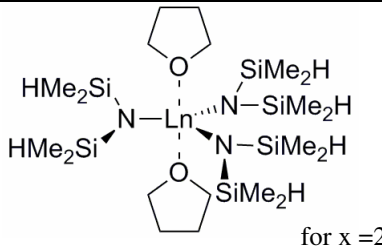
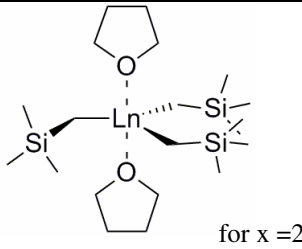
Within the series of trimethylsilyl-substituted methyl ligands, the extremely bulky *tris*(trimethylsilyl)methyl  $\text{C}(\text{SiMe}_3)_3$  is used only for divalent lanthanide precursors.<sup>[10]</sup> According to its enormous steric demand, it efficiently suppresses ate complexation for the large divalent lanthanide cations.<sup>[10]</sup> *Bis*(trimethylsilyl)methyl  $\text{CH}(\text{SiMe}_3)_2$  is a suitable ligand for both divalent and trivalent rare earth metal precursors. According to its insufficient steric and electronic saturation of the large divalent metal centers, its use is hereby limited to the smallest Yb(II) metal center.<sup>[10]</sup> On the contrary, the  $\text{CH}(\text{SiMe}_3)_2$  precursors of trivalent rare earth metals are accessible over the whole cation size range.<sup>[10,48-52]</sup> Depending on the synthesis conditions, the precursors can be obtained either as solvent adducts or, in analogy to the similar-sized *btsa* ligand, also solvent-free. However, the synthesis is hampered by readily

occurring ate complexation, particularly in presence of donor solvents.<sup>[10]</sup> This unwanted reaction can be avoided by synthesis starting from  $\text{Ln}(\text{OAr}^{\text{tBu}})_3$  instead of the rare earth metal chloride.<sup>[48]</sup> According to their “alkyl-only” character, solvent-free  $\text{Ln}(\text{CH}(\text{SiMe}_3)_2)_3$  precursors have found large attention, as salt or solvent coordination at the product complexes is precluded.<sup>[10]</sup> As a major drawback of the trivalent bis(trimethylsilyl)methyl precursors, the protonolysis reaction with protic substrates is usually kinetically controlled and strongly sensitive to the applied reaction conditions and the steric demand of the reactants.<sup>[10]</sup> Hence, in analogy to the btsa precursors, their use is limited for the middle-sized and large trivalent rare earth cations and sterically less demanding ligands only.<sup>[9,10]</sup>

Already described as early as 1973 by Lappert and Pearce,<sup>[53]</sup> the application of homoleptic (trimethylsilyl)methyl rare earth metal complexes  $\text{Ln}(\text{CH}_2\text{SiMe}_3)(\text{thf})_x$  ( $x = 2-3$ ) as a synthesis precursor has undergone a tremendous development in the last decade.<sup>[10]</sup> Today, these precursor complexes are amongst the most widely used starting materials in organo-rare earth metal chemistry.<sup>[10]</sup> Commonly synthesized from  $\text{LiCH}_2\text{SiMe}_3$  and  $\text{LnCl}_3(\text{thf})_x$ , often in hexane suspension,<sup>[54,55]</sup> these precursors can be obtained only for small and middle-sized rare earth metals, with Sm marking the upper cation size limit.<sup>[10]</sup> The insufficient steric shielding of the metal center by the  $\text{CH}_2\text{SiMe}_3$  ligand results in donor molecule (commonly THF) coordination, and as a major drawback of this precursor route, in thermal instability of these precursor complexes, both in solid state and in solution.<sup>[10,56]</sup> This instability increases for larger metal centers and decomposition leads to insoluble oily products under the formation of  $\text{SiMe}_4$ .<sup>[56]</sup> As another disadvantage of this alkyl precursor route, readily occurring ate complexation can lead to products which are of only limited use as synthesis precursors.<sup>[10]</sup> Despite the aforementioned drawbacks (cation size restriction, thermal instability, and ate complex formation),  $\text{Ln}(\text{CH}_2\text{SiMe}_3)(\text{thf})_x$  is amongst the most widely used precursors as it opens the access to complex ligand spheres *via* consecutive protonolysis of the  $\text{CH}_2\text{SiMe}_3$  ligands, and as it displays high reactivity according to both the good accessibility of the metal center and the high basicity of the  $\text{CH}_2\text{SiMe}_3$  group (the  $\text{pK}_a$ -value of  $\text{SiMe}_4$  has not been exactly determined, but is estimated from gas phase acidities to be in the range of similar hydrocarbyl proligands, *i.e.*  $\text{pK}_a(\text{SiMe}_4) > 40$ <sup>[10,57-60]</sup>), thus being applicable to a broad scope of protic substrates.<sup>[10]</sup> Additionally, remaining  $\text{CH}_2\text{SiMe}_3$  groups can initiate a variety of catalytic transformations, which is a strong advantage especially in comparison to the less reactive bdsa ligand.<sup>[9,10]</sup> Consequently, an exchange of one  $\text{CH}_2\text{SiMe}_3$  group by suitable initiators is often unnecessary.

As both  $\text{Ln}(\text{bdsa})_3(\text{thf})_x$  and  $\text{Ln}(\text{CH}_2\text{SiMe}_3)(\text{thf})_x$  were used as synthesis precursors within the scope of this work, a detailed comparison of these two precursor routes is summarized in Table 2.1.

Table 2.1: Comparison of the extended silylamide route and the  $\text{CH}_2\text{SiMe}_3$  precursor route.

$\text{Ln}(\text{bdsa})_3(\text{thf})_x$ (x = 1,2)	$\text{Ln}(\text{CH}_2\text{SiMe}_3)(\text{thf})_x$ (x = 2,3)
<i>Precursor Structure</i>	<i>Precursor Structure</i>
 <p style="text-align: center;">for x = 2</p>	 <p style="text-align: center;">for x = 2</p>
<i>Advantages</i>	<i>Disadvantages</i>
<ul style="list-style-type: none"> <li>• No cation size limit</li> <li>• Stable in solid state and solution</li> <li>• Storage possible</li> <li>• Rarely occurring ate complexation at precursor and target structures</li> </ul>	<ul style="list-style-type: none"> <li>• Sm as upper cation size limit</li> <li>• Thermally instable in solid state and solution</li> <li>• Storage not possible</li> <li>• Readily occurring ate complexation at precursor and target structures</li> </ul>
<i>Disadvantages</i>	<i>Advantages</i>
<ul style="list-style-type: none"> <li>• <math>\text{pK}_a(\text{HN}(\text{SiMe}_2\text{H})_2) = 22.8</math></li> <li>• Thermodynamic limitation for protonolysis (low <math>\text{pK}_a</math>) restricts substrate range</li> <li>• Kinetic limitation for protonolysis by steric repulsion</li> <li>• Low reactivity of bdsa as initiator for catalytic transformations</li> <li>• Reactive Si-H bonds can lead to side reactions</li> </ul>	<ul style="list-style-type: none"> <li>• <math>\text{pK}_a(\text{SiMe}_4) &gt; 40</math></li> <li>• No (negligible) thermodynamic limitation for protonolysis (high <math>\text{pK}_a</math>) allows reaction with a broad range of substrates</li> <li>• No (negligible) kinetic limitation for protonolysis by steric repulsion</li> <li>• High reactivity of <math>\text{CH}_2\text{SiMe}_3</math> as initiator for catalytic transformations</li> <li>• No reactive Si-H bonds present</li> </ul>

## 2.2 Principles of Polymerization

### 2.2.1 Classification of Polymerization Methods

The classification of polymerizations can follow a broad variety of different criteria. The most common classifications hereby regard<sup>[61]</sup>

- the origin of the polymers (synthetic or natural),
- the chemical structure of the polymerizable moiety of the monomer (*e.g.* vinyl-group or ring-opening polymerizations),
- the existence or non-existence of low-molecular weight condensation byproducts (original classification of polymerizations according to Carothers 1929),<sup>[62]</sup>
- the type of initiation (*e.g.* thermal, photochemical),
- the nature of the active species (*e.g.* radical, cationic, anionic),
- the mechanism (*e.g.* in case of coordination polymerizations into migratory-insertion or coordination-addition polymerization),
- the livingness of the polymerization and
- the reaction conditions (*e.g.* in bulk, suspension, emulsion).

However, the most important criterion for the classification of polymerization reactions is the process of polymer formation. Hereby, polymerization methods are classified into two major classes: chain-growth and step-growth polymerizations. For chain-growth polymerizations, the polymer formation occurs only *via* addition of monomer units to a growing polymer chain end; for step-growth polymerizations, formed polymer chains can react with either a monomer or another polymer.<sup>[61]</sup> Combining this criterion with Carothers' criterion of the existence or non-existence of low-molecular weight byproducts yields the four basic types of polymerization (according to IUPAC)<sup>[61,62]</sup>:

- polyaddition (step-growth without formation of byproducts, *e.g.* poly(urethane) formation),
- polycondensation (step-growth with formation of byproducts, *e.g.* synthesis of Nylon 6.6),
- chain polymerization (chain-growth without formation of byproducts, *e.g.* living ionic polymerizations, coordination polymerizations) and
- the very seldom condensative chain polymerization (chain-growth with formation of byproducts).

In case of chain-growth polymerizations, a further differentiation is made between living- and non-living-type polymerizations. According to Swarc, ideal living polymerizations are defined as chain-growth polymerizations for which no termination or chain transfer reactions occur and for which the rate constant of the initiation reaction is much higher than the rate constant of the propagation reaction.<sup>[63,64]</sup> As a consequence, the apparent reaction rate is not influenced by initiation and termination reactions and the concentration of active chain ends remains constant throughout the whole polymerization. Accordingly, the molecular weight of the formed polymer is determined only by the monomer-to-initiator ratio and the obtained molecular weight distribution is very narrow, following a Poisson-type distribution.<sup>[61,65]</sup> The reaction kinetics of living polymerizations will be discussed in more detail in chapter 2.3.

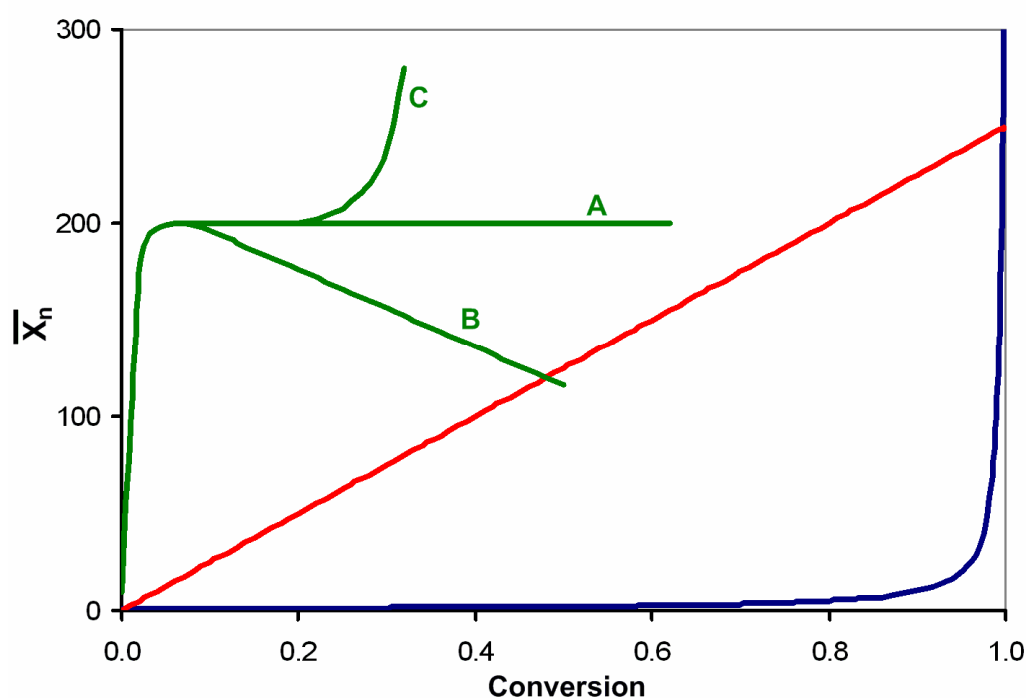


**Figure 2.3: Number-averaged degree of polymerization as a function of the conversion of functional (polymerizable) groups for different polymerization types: (blue) step-growth polymerization with ideal stoichiometry ( $S = 1$ ), (red) living chain-growth polymerization with  $[Mon]_0/[I]_0 = 250$  and (green) non-living chain growth polymerization with the ratio of propagation to termination rate unaffected (A), decreasing (B) or increasing (C) for higher conversions.**

Each of these polymerization types shows a characteristic relationship between the obtained number-averaged degree of polymerization and the conversion of functional (polymerizable) groups (Figure 2.3).<sup>[61]</sup> The stepwise growth of polyaddition and polycondensation reactions leads to low degrees of polymerization up to high conversions, at which the molecular weight then increases drastically. Hence, high molecular weight polymers may only be obtained for

very high monomer conversions, and only, if the right stoichiometry between the reaction partners is used. The relationship between molecular weight, stoichiometry and conversion is described in the Carothers' equation<sup>[61]</sup>

$$\overline{X}_n = \frac{S+1}{2S \times (1-C) + 1 - S} \quad (2.1)$$

using the conversion  $C$  and the initial stoichiometric ratio of the reaction partners  $S = n_{A,0}/n_{B,0}$ , thus allowing a precise prediction of the molecular weight obtained by certain reaction conditions.

For living chain-growth polymerizations, due to the fast initiation and the absence of termination reactions, a linear increase of the number-averaged degree of polymerization upon monomer conversion is observed.<sup>[61]</sup> For non-living chain-growth polymerizations, the relationship between molecular weight and conversion is dependent on the effect of the monomer concentration and the viscosity on propagation and termination rates. Accordingly, depending on the applied reaction conditions, the molecular weight can be unaffected by the conversion (*e.g.* if both rates are not affected), it can increase (if the termination rate is slowed down, *e.g.* due to an increase of the reaction mixture viscosity during free radical polymerizations) or decrease for higher conversions (*e.g.* if the propagation rate follows first order kinetics in monomer concentration whereas the termination reaction is not affected by this concentration). As the relationship between the degree of polymerization and the conversion is characteristic for different polymerization classes, the determination of this relationship allows an identification of the occurring polymerization mechanism.

For all polymerization classes, the polymer formation can be facilitated by a catalyst. A catalyst is defined to remain unchanged, *i.e.* to not be converted, during the course of a reaction. Consequently, catalytic polymerizations are defined by exhibiting turn over numbers, TONs, for both monomer conversion *and* polymer chain production, *i.e.* a polymerization catalyst must produce more than one polymer chain.<sup>[5]</sup> Therefore, living polymerizations are *per se* not catalytic. In case of living coordination polymerizations, *e.g.* rare earth metal-mediated GTP, for which the chain-growth *is* catalyzed by a coordinated metal complex (which thus serves as both initiator *and* catalyst), this leads to a terminology conflict. To overcome this, according to previous literature, the term “catalyst” is used within the frame of this work only concerning the catalyzed monomer addition.<sup>[5]</sup> In general, a differentiation should be made between *catalyzed* (with a catalyst having a TON for monomer conversion only) and *catalytic* polymerizations.

### 2.2.2 Kinetics of Living Coordination Polymerizations

Chain-growth polymerizations initiated by coordination and metal oxide initiators are called coordination polymerizations and are usually ionic in nature.<sup>[66]</sup> The chain-growth is thereby mediated by a (metal) catalyst coordinated at the growing chain end. Also for these coordination polymerizations, both living (*e.g.* coordination-addition polymerization or living ring-opening polymerizations) and non-living (*e.g.* migratory-insertion polymerization of olefins using classical Ziegler-Natta catalysts) forms exist.

For ideal living polymerizations, the apparent rate is not influenced by initiation or termination reactions. The propagation (apparent) rate  $r_p$  of classical ionic (non-coordinative) polymerizations commonly follows a bimolecular reaction between a reactive chain end  $P^*$  and a monomer  $Mon$ . The rate law for the propagation reaction therefore reads<sup>[61]</sup>

$$r_p = [Mon] \times \sum_r (k_{p,r} [P^*]_r). \quad (2.2)$$

For the kinetic analysis of polymerizations, it is commonly assumed, that the reactivity of the growing polymer chain is not influenced by its molecular weight.<sup>[61]</sup> This condition is often already fulfilled for very low degrees of polymerization.<sup>[61]</sup> Furthermore, the concentration of growing chain ends is equal (or proportional in case of multifunctional initiators) to the concentration of used initiator  $[I]_0$ . However, in case of non-ideal living polymerizations, initiators may be deactivated by impurities or by radical recombination. This initial deactivation is commonly addressed by the determination of the initiator efficiency  $I^*$ , which does not change throughout the reaction if the initiation rate is much higher than the propagation rate. These considerations allow a simplification of the rate law to

$$r_p = k_p [P^*] [Mon] = k_p [I^*] [Mon] \quad (2.3)$$

with

$$[I^*] = [I]_0 \times I^* \quad (2.4)$$

and

$$[Mon] = [Mon]_0 \times (1-C). \quad (2.5)$$

According to the linear relationship between number-averaged molecular weight and monomer conversion for living polymerizations, the initiator efficiency  $I^*$  is calculated from



the initial monomer-to-initiator ratio  $[\text{Mon}]_0/[\text{I}]_0$ , the conversion  $C$ , the monomer molar mass  $M_{\text{Mon}}$  and the number-averaged molecular weight of the formed polymers  $\overline{M}_n$  following

$$I^* = M_{\text{Mon}} \times ([\text{Mon}]_0/[\text{I}]_0) \times C/\overline{M}_n. \quad (2.6)$$

It should be noted, that the calculation of the initiator efficiency from the molecular weight of the formed polymers is only valid in the absence of termination reactions.

In contrast to classical (non-coordinative) polymerizations, the propagation of coordination polymerizations can involve either one or two catalyst molecules. In case of metal catalysts, these are called mono- and bimetallic polymerizations. For some types of catalysts, both mechanisms can also occur simultaneously. Additionally, the corresponding rate determining step (RDS) can be independent of the monomer concentration, *i.e.* if the RDS is not the coordination of a monomer at the catalyst. Hence, in case of coordination polymerizations, the reaction orders of monomer and catalyst cannot be presumed and thus have to be determined. Therefore, the general rate law for coordination polymerizations reads

$$r_p = k_p[\text{Cat}]^m[\text{Mon}]^n. \quad (2.7)$$

Nevertheless, in case of living coordination polymerizations, the determination of the initiator efficiency according to equation 2.6 (substituting  $[\text{I}]_0$  by the initial catalyst concentration  $[\text{Cat}]_0$ ) allows access to the active catalyst concentration  $[\text{Cat}^*]$ . This is a major advantage in comparison to non-living coordination polymerizations, for which the determination of the number of active sites is a common problem, thus inhibiting a validation of the actual catalytic activity of each active site (*i.e.* the determination of turnover frequency, TOF, and number, TON). The corresponding rate law for living coordination polymerizations thus reads

$$r_p = k_p[\text{Cat}^*]^m[\text{Mon}]^n. \quad (2.8)$$

Importantly, for bimetallic living propagation reactions, the initiator efficiency never raises above 50%, as two catalysts/initiators are necessary for chain growth of one polymer chain.<sup>[5]</sup> However, this effect may also be observed for monometallic propagation reactions, for which two metal complexes are forming a bifunctional initiator, *e.g.* for redox initiation of MMA polymerization by divalent lanthanide initiators.<sup>[5,67]</sup>

### 2.2.3 Chain-growth Copolymerization

In chain-growth polymerizations, polymers which contain units of two or more different monomers are called copolymers. They can be formed by either sequential, *i.e.* block or graft copolymerization or simultaneous, *i.e.* statistical, random or alternating copolymerization of the comonomers.<sup>[66]</sup> Chain copolymerizations are of both large commercial and academic interest as they allow for the synthesis of an almost unlimited number of different tailor-made products with specific functionality.<sup>[66]</sup> Especially simultaneous copolymerizations are of great importance for the understanding of the influence of the chemical structure on monomer and chain end reactivity, thus giving mechanistic insights into the occurring propagation mechanism.<sup>[66]</sup>

The reactivity of the monomers in copolymerizations cannot simply be determined from their homopolymerization rates, as some monomers are more reactive in copolymerization, whereas other monomers are less reactive.<sup>[66]</sup> Intriguingly, this feature often allows the study of copolymerization rates to provide a deeper insight into the underlying polymerization mechanism than the corresponding homopolymerizations. For the determination of the copolymerization parameters, the chemical reactivity of the propagating chain is commonly assumed to depend only on the identity of the monomer at the growing end and independent of the chain composition preceding the last monomer unit.<sup>[66,68-71]</sup> This is referred to as the *first-order Markov* or *terminal model* of copolymerization.<sup>[66]</sup> There has been developed a number of more powerful, but also more complicated models, *e.g.* the *penultimate model* considering the last two monomer units of the propagating chain or models including monomer complex formation and depropagation reactions, however, in most cases, the terminal model sufficiently describes a copolymerization.<sup>[66,68-71]</sup>

In the terminal model for the copolymerization of two comonomers, it can be differed between four different propagation reactions



between the reactive chain ends  $\text{Mon}_1^*$  and  $\text{Mon}_2^*$  and the comonomers  $\text{Mon}_1$  and  $\text{Mon}_2$  with the corresponding rate constants  $k_{11}$ ,  $k_{12}$ ,  $k_{21}$  and  $k_{22}$ . The corresponding conversion rates of both monomers read

$$-d[\text{Mon}_1]/dt = k_{11}[\text{Mon}_1^*][\text{Mon}_1] + k_{21}[\text{Mon}_2^*][\text{Mon}_1] \quad (2.13)$$

$$-d[\text{Mon}_2]/dt = k_{12}[\text{Mon}_1^*][\text{Mon}_2] + k_{22}[\text{Mon}_2^*][\text{Mon}_2]. \quad (2.14)$$

Dividing equation 2.13 by 2.14 yields the ratio of the rates of comonomer addition to the propagating chains, *i.e.* the *instantaneous copolymer composition*<sup>[66]</sup>

$$\frac{d[\text{Mon}_1]}{d[\text{Mon}_2]} = \frac{k_{11}[\text{Mon}_1^*][\text{Mon}_1] + k_{21}[\text{Mon}_2^*][\text{Mon}_1]}{k_{12}[\text{Mon}_1^*][\text{Mon}_2] + k_{22}[\text{Mon}_2^*][\text{Mon}_2]} \quad (2.15)$$

In order to remove the unknown concentrations of the reactive chain ends  $[\text{Mon}_1^*]$  and  $[\text{Mon}_2^*]$ , a steady state is assumed for both concentrations, *i.e.* the rates of the interconversion reactions 2.10 and 2.11 have to be equal.<sup>[66]</sup> Combining this assumption with the use of the monomer reactivity ratios  $r_1$  and  $r_2$  (also: copolymerization parameters), which are defined as

$$r_1 = k_{11}/k_{12} \quad (2.16)$$

$$r_2 = k_{22}/k_{21} \quad (2.17)$$

yields the copolymerization equation

$$\frac{d[\text{Mon}_1]}{d[\text{Mon}_2]} = \frac{[\text{Mon}_1](r_1[\text{Mon}_1] + [\text{Mon}_2])}{[\text{Mon}_2]( [\text{Mon}_1] + r_2[\text{Mon}_2])} \quad (2.18)$$

The copolymerization parameters  $r_1$  and  $r_2$  show characteristic values for the different types of copolymerizations. So-called *ideal* copolymerizations are characterized by  $r_1 r_2 = 1$ , with  $r_1 = r_2 = 1$  termed *random* or *Bernoullian* copolymerization, *alternating* copolymerizations by  $r_1 r_2 = 0$  and copolymerizations with a tendency to form *block* or block-like copolymer structures by  $r_1 > 1$  and  $r_2 > 1$ .<sup>[66]</sup>

Most experimental evaluations of the copolymerization parameters use a linearization of the copolymerization equation in  $r_1$  and  $r_2$ .<sup>[66]</sup> Mayo and Lewis<sup>[69]</sup> rearranged the copolymerization equation to

$$r_2 = \frac{[\text{Mon}_1]}{[\text{Mon}_2]} \left[ \frac{d[\text{Mon}_2]}{d[\text{Mon}_1]} \left\{ 1 + \frac{r_1[\text{Mon}_1]}{[\text{Mon}_2]} \right\} - 1 \right]. \quad (2.19)$$

$r_2$  is plotted for various assumed values of  $r_1$ , with each experiment giving a straight line. The intersection of the straight lines yields the best values of  $r_1$  and  $r_2$ .<sup>[66]</sup> A more straight-forward approach was presented by Fineman and Ross, who rearranged equation 2.18 to

$$\frac{[\text{Mon}_1]}{[\text{Mon}_2]} \frac{d[\text{Mon}_2]}{d[\text{Mon}_1]} \left( \frac{d[\text{Mon}_1]}{d[\text{Mon}_2]} - 1 \right) = \left( \frac{[\text{Mon}_1]}{[\text{Mon}_2]} \right)^2 \frac{d[\text{Mon}_2]}{d[\text{Mon}_1]} \times r_1 - r_2 \quad (2.20)$$

for the determination of  $r_1$  and

$$\frac{[\text{Mon}_2]}{[\text{Mon}_1]} \left( \frac{d[\text{Mon}_1]}{d[\text{Mon}_2]} - 1 \right) = \left( \frac{[\text{Mon}_2]}{[\text{Mon}_1]} \right)^2 \frac{d[\text{Mon}_1]}{d[\text{Mon}_2]} \times (-r_2) + r_1 \quad (2.21)$$

for the determination of  $r_2$  (the slope of the corresponding linear plots gives statistically more significant values than the y-intercept).<sup>[66,72]</sup> The experimental data points are unequally weighed by both the Mayo-Lewis and the Fineman-Ross method, with high mol fractions having the greatest effect on the obtained monomer reactivity ratios.<sup>[66]</sup> In case of the Fineman-Ross method, calculation of the copolymerization parameters from the y-intercept instead of the slope gives a higher weighing of the data points with low mol fractions. Kelen and Tüdös addressed this problem by introducing an arbitrary position constant  $\alpha$  giving all data points equal weight.<sup>[73]</sup> The linearization according to Kelen and Tüdös reads

$$\frac{\frac{[\text{Mon}_1]}{[\text{Mon}_2]} \frac{d[\text{Mon}_2]}{d[\text{Mon}_1]} \left( \frac{d[\text{Mon}_1]}{d[\text{Mon}_2]} - 1 \right)}{\alpha + \left( \frac{[\text{Mon}_1]}{[\text{Mon}_2]} \right)^2 \frac{d[\text{Mon}_2]}{d[\text{Mon}_1]}} = \left( r_1 + \frac{r_2}{\alpha} \right) \frac{\left( \frac{[\text{Mon}_1]}{[\text{Mon}_2]} \right)^2 \frac{d[\text{Mon}_2]}{d[\text{Mon}_1]}}{\alpha + \left( \frac{[\text{Mon}_1]}{[\text{Mon}_2]} \right)^2 \frac{d[\text{Mon}_2]}{d[\text{Mon}_1]}} - \frac{r_2}{\alpha} \quad (2.22)$$

using  $\alpha = (F_m F_M)^{1/2}$  with  $F_m$  and  $F_M$  corresponding to minimum and maximum values of

$$F = \left( \frac{[\text{Mon}_1]}{[\text{Mon}_2]} \right)^2 \frac{d[\text{Mon}_2]}{d[\text{Mon}_1]} \quad (2.23)$$

In many cases, the instantaneous copolymer composition, *i.e.* the ratio of comonomer conversion rates, is not directly accessible. Then, even if the conversion is held as low as possible, the differential form of the copolymerization equation suffers from limitations which arise from the necessity to isolate the copolymer sample or, if the copolymer composition is measured by a change of the comonomer feed ratio, from the necessity to have a significantly measurable change in the feed composition.<sup>[66]</sup> Thus, an integral approach, for which the experimental results for the change in copolymer or feed composition with conversion are fitted to an integrated form of the copolymerization equation, provides a method yielding more reliable values for the copolymerization parameters  $r_1$  and  $r_2$ .<sup>[66]</sup> However, this involves a largely increased experimental and computational effort.

## 2.3 The Transition State Model for the Determination of Activation Enthalpy and Entropy

There are two major theories to describe the temperature-dependence of the reaction rate constant. The *collision model* according to Arrhenius describes a dependence of the rate constant on the pre-exponential factor  $A^\ddagger$ , the product of the number of collisions  $p$  and the probability of collisions to lead to a subsequent reaction  $Z$ , and the Boltzmann factor  $\exp(-\Delta E^\ddagger/RT)$ , which gives a measure for the number of molecules having sufficient energy to react<sup>[61]</sup>:

$$k = A^\ddagger \times \exp(-\Delta E^\ddagger/RT) = pZ \times \exp(-\Delta E^\ddagger/RT) \quad (2.24)$$

$\Delta E^\ddagger$  is called the apparent or Arrhenius activation energy. Strictly speaking, the Arrhenius equation can only be applied to gas phase reactions.<sup>[74]</sup> In all cases for which the simple *collision model* is not sufficient, *e.g.* condensed or mixed phase reactions, the Eyring equation, a *transition state model*, can be used.<sup>[61,74]</sup> According to this model, for a bimolecular reaction with the rate law

$$r = k[A][B], \quad (2.25)$$

the reaction is proceeding over an instable transition state  $AB^\ddagger$  as the potential energy maximum. This transition state can react to product C or back to the starting materials A and B:



The transition state model uses two basic principles<sup>[74]</sup>:

- There is a thermodynamic equilibrium between the transition state and the reactants at the top of the energy barrier.
- The rate of the chemical reaction is proportional to the concentration of the particles in the transition state.

According to the equilibrium (steady state) approximation between A and B and the transition state  $AB^\ddagger$ , the following rate law can be derived from equation 2.26:

$$r = k^\ddagger[AB^\ddagger] = k^\ddagger K^\ddagger[A][B] \quad (2.27)$$

with the universal rate constant for a transition state  $k^\ddagger$ .<sup>[61,74]</sup>  $k^\ddagger$  is directly proportional to the frequency of the vibrational mode responsible for converting the activated complex to the product<sup>[74]</sup> and can be calculated following

$$k^\ddagger = k_B T/h. \quad (2.28)$$

From equations 2.25, 2.27 and 2.28 and the van't Hoff reaction isotherm  $\Delta G^\ddagger = -RT \times \ln K^\ddagger$  with the Gibbs free activation enthalpy  $\Delta G^\ddagger$ , the overall reaction rate constant  $k$  can be described by<sup>[61,74]</sup>

$$k = (k_B T/h) \times K^\ddagger = (k_B T/h) \times \exp(-\Delta G^\ddagger/RT). \quad (2.29)$$

Using the Gibbs-Helmholtz equation

$$\Delta G^\ddagger = \Delta H^\ddagger - T\Delta S^\ddagger, \quad (2.30)$$

equation 2.29 is transformed into the **Eyring equation**

$$k = (k_B T/h) \times \exp(\Delta S^\ddagger/R) \times \exp(-\Delta H^\ddagger/RT) \quad (2.31)$$

with its linear form

$$\ln(k/T) = -\Delta H^\ddagger/R \times 1/T + \Delta S^\ddagger/R + \ln(k_B/T). \quad (2.32)$$

Plotting  $\ln(k/T)$  against  $1/T$  yields the activation enthalpy  $\Delta H^\ddagger$  and entropy  $\Delta S^\ddagger$  of the rate determining step (RDS) from the slope and the y-intercept of the linear fit curve, respectively. Activation enthalpies  $\Delta H^\ddagger$  are typically in the range of 20 to 150 kJ/mol, with higher activation enthalpies resulting in slower rates.<sup>[74]</sup> Intriguingly, the activation entropy  $\Delta S^\ddagger$  allows mechanistic conclusions, as it is a measure for the change of translational, rotational and vibrational degrees of freedom in the RDS.<sup>[74]</sup> Thus, it gives insight into the relative extent of order and steric constraints in ground and transition state and allows a differentiation between associative (negative  $\Delta S^\ddagger$ ) or dissociative (positive  $\Delta S^\ddagger$ ) mechanisms (*e.g.*  $S_N1$ - or  $S_N2$ -type reactions).

## 2.4 Determination of Molecular Weight and Molecular Weight Distribution

### 2.4.1 Absolute Methods for Molecular Weight Determination

Among the vast variety of methods which have been developed for the determination of the molecular weight of polymers (and particles), there is only a limited number of so-called absolute methods. Absolute determinations require all parameters to be determined from 1<sup>st</sup> principles, *i.e.* no assumptions are made of molecular models or conformation and no reference to standards (no calibration) is necessary. Absolute methods are often very expensive, both in time and equipment.<sup>[61]</sup> Hence, in preparative laboratories, simple relative methods, which are calibrated to reference systems, are preferred. In basic research however, where the correlation between molecular structure and physical properties has to be elucidated, the use of absolute methods is often inevitable, especially if new materials are synthesized, for which no adequate reference system is available.<sup>[61]</sup>

Generally, depending on the underlying physical principles, methods for the determination of the molecular weight yield different molecular weight averages for polydisperse samples (the determination of the molecular weight distribution will be described in chapter 2.4.3). Hereby, physical methods which measure systems in their thermodynamic equilibrium commonly yield simple averages of the molecular weight.<sup>[61]</sup> The three most important of these are the number-averaged molecular weight

$$\overline{M}_n = \frac{\sum_i n_i M_i}{\sum_i n_i} = \frac{\sum_i c_i}{\sum_i c_i M_i^{-1}}, \quad (2.33)$$

with absolute values obtained from methods, for which the quantity to be measured is only dependent on the mass concentration of the molecules  $c_i$ , but at the same time independent from their molecular weight  $M_i$ , such as cryoscopy as well as vapor pressure or membrane osmometry, the weight-averaged molecular weight

$$\overline{M}_w = \frac{\sum_i n_i M_i^2}{\sum_i n_i M_i} = \frac{\sum_i c_i M_i}{\sum_i c_i}, \quad (2.34)$$

with absolute values yielded by methods, for which the quantity to be measured is dependent on both the mass concentration of molecules  $c_i$  and their molecular weight  $M_i$ , *i.e.* static light scattering (SLS) and small angle X-ray and neutron scattering (SAXS and SANS, respectively), and the z-averaged molecular weight

$$\overline{M}_z = \frac{\sum_i n_i M_i^3}{\sum_i n_i M_i^2}, \quad (2.35)$$

with its absolute values determined from the sedimentation equilibrium, *e.g.* by ultracentrifugation.<sup>[61]</sup>

Besides the above mentioned, there are two other common methods, which allow an absolute determination of the molecular weight under certain conditions, *i.e.* end group analysis, *e.g.* *via* titration or NMR spectroscopy, and mass spectrometry. End group analysis yields the number-averaged molecular weight, is restricted to polymers with a known constitution and only gives reliable values up to rather low molecular weights, with the maximum being dependent on the applied analytical technique.<sup>[61]</sup> Mass spectrometry yields both the molecular weight and its distribution (*vide infra*) and it is the only method which determines reduced molecular weights.<sup>[61]</sup> However, it is commonly assumed that ionization and detection (thus signal intensity) is independent of the chain length. This condition is not met in many cases, especially for molecular weights above 10 kDa. Additionally, for some polymer types, degradation by chain scission is observed during mass spectrometric analysis, again, with a larger effect for higher molecular weight fractions.<sup>[61]</sup> These effects result in an underestimation of both the molecular weight average and the polydispersity by mass spectrometry and limit its accurate use to low molecular weight materials.

Commonly, methods yielding the number-averaged molecular weight, *e.g.* vapor pressure osmometry, are more precise in case of lower molecular weight samples, whereas methods yielding the weight-averaged molecular weight, *e.g.* static light scattering, give better results for higher molecular weight samples. The development of high energy lasers has led to a tremendous improvement of light scattering methods, as with these light sources, the signal-to-noise ratio of light scattering experiments could be largely increased.<sup>[75]</sup> As a consequence, the introduction of laser light scattering could compensate for the low scattering intensity of lower molecular weight samples, thus allowing molecular weight determination for particles/polymers down to a molecular weight of several hundred Da.<sup>[61]</sup> According to the resulting suitability of laser light scattering for the absolute analysis of the molecular weight over the range of several magnitudes (from  $10^{2-3}$  up to at least  $10^7$  Da), this method was chosen in the present work for the determination of the molecular weight of the new polymer types obtained by rare earth metal-mediated GTP, particularly poly(vinylphosphonate)s. Therefore, a brief introduction to the principles of static light scattering will be presented in the following chapter.



### 2.4.2 Static Light Scattering

Light scattering is an everyday phenomenon, *e.g.* the blue sky, the red sunset or the visibility of dust particles in a light beam are a result of scattered light. As an electromagnetic wave, light causes charges to polarize when it interacts with matter. The formed oscillating charges radiate light with a frequency equal (Rayleigh scattering) or different to the incident light source (Raman scattering). The intensity of this scattered light  $I_S$  is dependent on the matter's polarizability  $\alpha$ , which is directly related to its index of refraction  $n$ <sup>[75]</sup>:

$$I_S \propto \alpha \approx n^2 - 1 \quad (2.36)$$

For solutes, the polarizability is expressed as the specific refractive index increment,  $(dn/dc)$ <sup>[75]</sup>:

$$I_S \propto (dn/dc)^2 \quad (2.37)$$

In polymers and particles, the single scattering centers move in alignment (in phase), thus the intensity of the light scattered by a particle  $I_{S,P}$  is proportional to the square sum of the absolute values of the field intensity  $E_i$  of the light scattered by each scattering center  $i$ <sup>[75]</sup>:

$$I_{S,P} \propto |\sum_i E_i|^2 \quad (2.38)$$

The overall scattering intensity is then calculated as the sum of the square absolute values of the field intensity  $E_j$  of the light scattered by each particle  $j$ :

$$I_S = \sum_j I_{S,P,j} \propto \sum_j |E_j|^2 \quad (2.39)$$

Accordingly, large particles exhibit a higher scattering intensity than a number of smaller particles with the same overall mass, *e.g.* two particles, each having half the molecular weight of a larger particle, together scatter light with only half intensity than the large particle. Consequently,  $I_S$  is determined by the polarizability, the molar mass of the particles  $M$  and the particle mass concentration  $c$ :

$$I_S \propto \alpha \times cM \quad (2.40)$$

For particles with a diameter larger than  $\lambda/20$  with  $\lambda = \lambda_0/n$ , the vacuum wavelength of the incident light  $\lambda_0$  and the index of refraction  $n$ , intramolecular interference leads to a reduction

of the scattering intensity as the scattering angle increases.<sup>[75,76]</sup> The intensity of the scattered light therefore reads

$$I_s(\theta) \propto \alpha \times cM \times P(\theta) \quad (2.41)$$

with the form factor or scattering function  $P(\theta)$ , which is determined by the mean square radius of gyration  $\langle r_g^2 \rangle$  of the particle.<sup>[75]</sup> It should be noted that  $P(0^\circ) = 1$ . The dependency of the intensity of the scattered light on the particle mass concentration, its molecular weight and the scattering angle  $\theta$  is visualized in Figure 2.4.

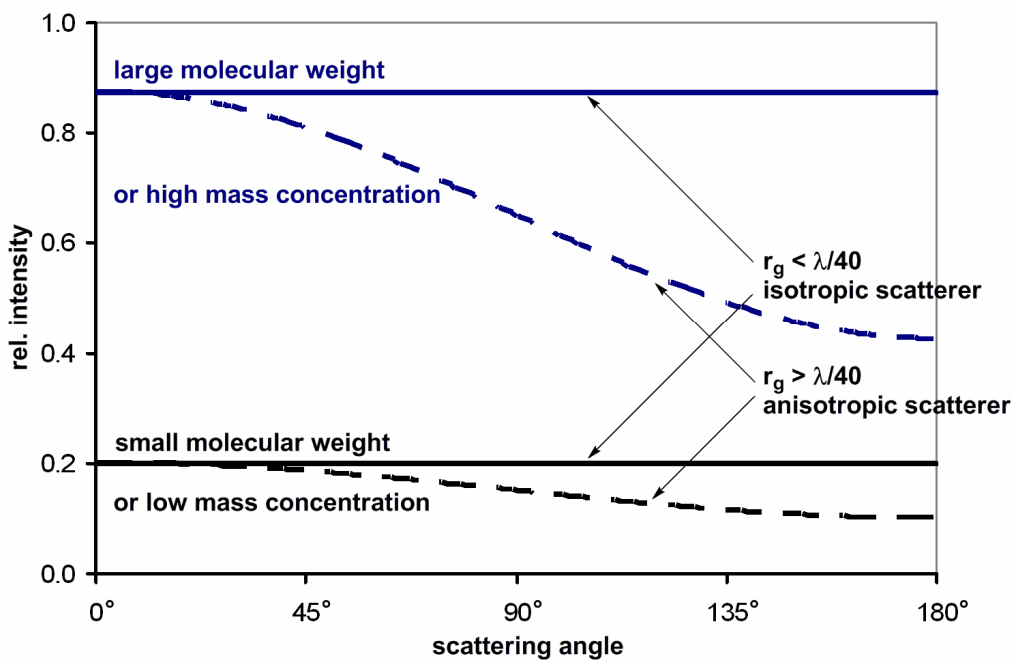


**Figure 2.4: Dependency of the scattering intensity on particle mass concentration and molecular weight and its angular dependency for isotropic and anisotropic scatterers.**

As the intensity of scattered light is furthermore dependent on the intensity of the incident light  $I_0$ , the detection volume  $V$  and the distance  $L$  from the scattering center to the detector, light scattering experiments measure the so-called Rayleigh ratio

$$R(\theta) = \frac{I_s(\theta)}{I_0} \times \frac{L^2}{V} \quad (2.42)$$

with the intensity of scattered light  $I_s(\theta)$  at the angle  $\theta$ . For the assumption of an infinitely diluted gas ( $c \rightarrow 0$ ),  $R(\theta)$  can be derived as

$$R(\theta) = K \times cM \times P(\theta) \quad (2.43)$$

with the optical constant

$$K = 4\pi^2 n_0^2 (dn/dc)^2 N_A^{-1} \lambda_0^{-1} \quad (2.44)$$

with the refractive index of the medium (solvent, vacuum)  $n_0$  and the Avogadro constant  $N_A$  (for an exact derivation of this equation, see Ref. [76]). For a polydisperse sample and  $\theta \rightarrow 0^\circ$ , the overall Rayleigh ratio reads

$$R(0^\circ) = \sum_i R_i(0^\circ) = K \times \sum_i c_i M_i = K \times c \overline{M_w}, \quad (2.45)$$

*i.e.* as light scattering is dependent on both particle mass concentration and particle molecular weight, it provides the weight-averaged molecular weight of the sample.

For solutions, the measured Rayleigh ratio is equal to the sum of the Rayleigh ratio of the solvent and the so-called excess Rayleigh ratio  $R_{ex}(\theta)$  caused by the solute. Taking into regard the (now non-zero) concentration of the solute, from the excess Rayleigh ratio, the weight-averaged molecular weight of the solute can be determined according to the Zimm formalism of the Rayleigh-Debye-Gans light scattering model for dilute polymer solutions<sup>[75,76]</sup>

$$\frac{Kc}{R(\theta)} = \frac{1}{M_w P(\theta)} + 2A_2 c + 3A_3 c^2 + \dots \approx \frac{1}{M_w P(\theta)} + 2A_2 c \quad (2.46)$$

with the second virial coefficient  $A_2$  as a measure of solvent-solute interaction (with  $A_2 > 0$  corresponding to a good solvent for the sample).

For equation 2.46, there are three limits of interest: the low concentration limit ( $c \rightarrow 0$ )

$$\frac{Kc}{R(\theta)} = \frac{1}{M_w} \times \frac{1}{P(\theta)}, \quad (2.47)$$

yielding the mean square radius of gyration  $\langle r_g^2 \rangle$  from  $P(\theta)$ , the low angle limit ( $\theta \rightarrow 0$ )

$$\frac{Kc}{R(0^\circ C)} = \frac{1}{M_w} + A_2 c, \quad (2.48)$$

yielding the second virial coefficient  $A_2$ , and the low concentration and low angle limit ( $c \rightarrow 0, \theta \rightarrow 0$ )

$$\frac{Kc}{R(0^\circ C)} = \frac{1}{M_w}, \quad (2.49)$$

yielding the weight-averaged molecular weight.<sup>[75]</sup> The extrapolation on  $c \rightarrow 0$  and  $\theta \rightarrow 0$  is usually performed in so-called Zimm plots, for which  $[Kc/R(\theta)]$  is plotted against  $[\sin^2(\theta/2) + kc]$  (Figure 2.5).<sup>[76]</sup> The constant  $k$  is arbitrary and is used to put  $\sin^2(\theta/2)$  and  $kc$  in the same numerical range. The final results are independent of this factor.<sup>[76]</sup>

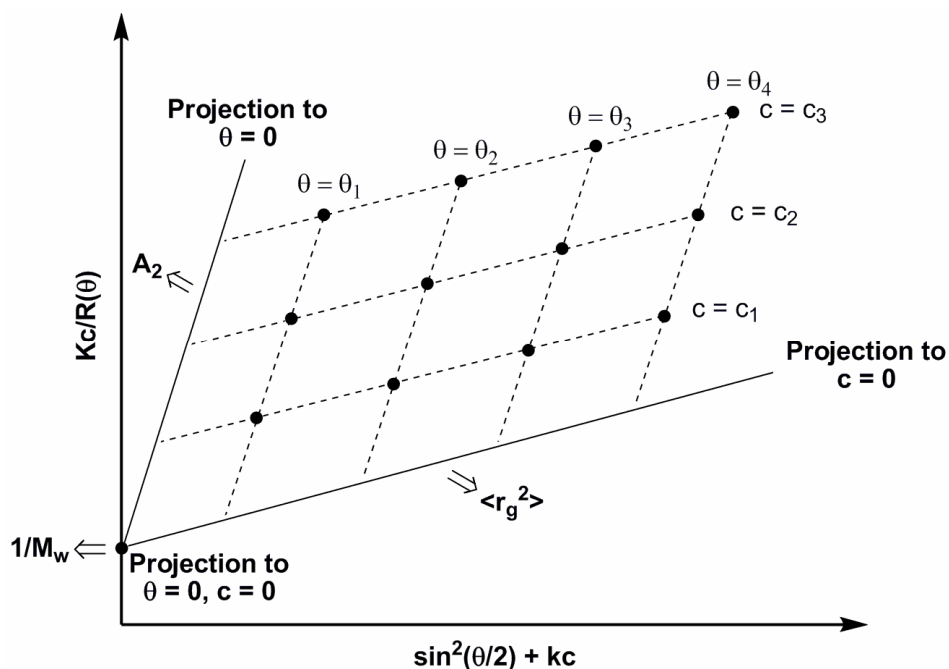


Figure 2.5: Zimm plot extrapolation to  $c \rightarrow 0$  and  $\theta \rightarrow 0$  for the determination of  $A_2$ ,  $\langle r_g^2 \rangle$  and  $\overline{M}_w$ .

All parameters used in equations 2.47-2.49 are physical and apparatus constants or can be measured from 1<sup>st</sup> principles. As no assumptions of molecular models or conformation are necessary to derive these equations, multi angle static (laser) light scattering (MALS) presents a powerful and versatile absolute method for the determination of the weight-averaged molecular weight. In many cases however, knowledge of the number-averaged molecular weight and the polydispersity is necessary, *e.g.* in the analysis of living-type polymerizations such as REM-GTP. In order to obtain number-averaged molecular weight and polydispersity of a sample, static light scattering can be combined with a separation method, which allows the separation of the sample according to molecular weight or size (as a function of the molecular weight for a homogeneously constituted sample), *i.e.* with a method for the determination of the molecular weight distribution.

### 2.4.3 Determination of the Molecular Weight Distribution

According to the statistic principles of polymerizations, synthetic polymers are commonly not molecularly uniform, *i.e.* they consist of polymer chains with different degrees of polymerization and therefore exhibit a molecular weight distribution. The width of this distribution can be characterized by the ratio of different molecular weight averages, and is most commonly expressed by the polydispersity index<sup>[61]</sup>

$$\text{PDI} = \frac{\overline{M}_w}{\overline{M}_n}. \quad (2.50)$$

This polydispersity index can be determined from two separate (absolute) analytical methods, *e.g.* from the weight-averaged molecular weight as derived from static light scattering and the number-averaged molecular weight from vapor pressure osmometry. Nevertheless, methods which fractionate the polymer sample according to the molecular weight of the polymer chains access the actual molecular weight distribution and therefore provide much more information, *e.g.* on the polymerization mechanism (for different distribution functions, see Ref. [61]).

For the determination of the molecular weight distribution, a large variety of different techniques has been presented, *e.g.* ultracentrifugation, mass spectrometry, dynamic light scattering, preparative precipitation fractionation, the determination according to a variety of viscoelastic properties as well as size exclusion chromatography (SEC) and field-flow fractionation (FFF).<sup>[61]</sup> Again, it can be differed between absolute and relative methods. The only methods for the determination of the molecular weight distribution which are *per se* absolute, are ultracentrifugation and mass spectrometry,<sup>[61]</sup> with the latter being limited for its accurate use to low molecular weight samples only (*vide supra*).

All other methods require calibration by known molar mass standards, unless they are combined with methods for the absolute determination of the molecular weight of each fraction *i* instead of a simple determination of the mass of each fraction. In contrast to equations 2.33-2.35, which can only be applied for molecular uniform fractions, the molecular weight averages of the sample are then calculated according to<sup>[61]</sup>

$$\overline{M}_n = \frac{\sum_i n_i \overline{M}_{n,i}}{\sum_i n_i} = \frac{\sum_i c_i}{\sum_i c_i \overline{M}_{n,i}^{-1}} \quad (2.51)$$

$$\overline{M}_w = \frac{\sum_i n_i \overline{M_{n,i}} \overline{M_{w,i}}}{\sum_i n_i \overline{M_{n,i}}} = \frac{\sum_i c_i \overline{M_{w,i}}}{\sum_i c_i}, \quad (2.52)$$

*i.e.* knowledge of both number-averaged and weight-averaged molecular weights of all fractions  $i$  is necessary. If only one average is determined and equations 2.33 and 2.34 are incorrectly applied for molecularly non-uniform fractions, the PDI is underestimated and determined molar masses are often incorrect, *i.e.* if  $M_i = \overline{M_{n,i}}$  is used,  $\overline{M}_w$  is underestimated, and, if  $M_i = \overline{M_{w,i}}$  is used,  $\overline{M}_n$  is overestimated.<sup>[61]</sup>

For separation methods, which access a quasi-continuous molecular weight distribution, *i.e.* achieving good separation and determining very small molecular weight intervals, the single fractions can be assumed as molecularly uniform, *i.e.* equations 2.33 and 2.34 can be applied and only one type of molar mass detection is necessary, *e.g. via* a (multi angle) light scattering detector. The only common techniques yielding a quasi-continuous molecular weight distribution are size exclusion chromatography (SEC) and field-flow fractionation (FFF).

FFF is a type of liquid chromatography which does not use a stationary phase. Instead, the separation takes place in a laminar flow and is caused by an applied cross flow through a membrane perpendicular to the laminar flow.<sup>[75]</sup> Depending on their size, particles can diffuse against the cross flow, resulting in a faster elution for smaller particles as a consequence of the higher laminar flow rate in greater distance to the membrane. As both laminar and cross flow can be adjusted, FFF provides a wide separation range and is a suitable method when column chromatography fails due to sample adsorption and degradation or a limitation of the exclusion limit.<sup>[75]</sup>

SEC is a type of liquid chromatography using a solid porous material with a relatively narrow pore size distribution or a gel as the stationary phase.<sup>[61]</sup> For the analysis of synthetic polymers, the latter is often referred to as gel permeation chromatography (GPC). In SEC, the sample does not adsorb on the stationary phase, instead, separation occurs corresponding to the particle size. The mechanism of separation is not fully understood, however, it is believed that large particles are excluded from the pores resulting in a smaller elution volume compared to small particles for which these pores are accessible.<sup>[61]</sup> According to its versatility and experimental simplicity, GPC was the method of choice for the separation of the new polymer types obtained by rare earth metal-mediated GTP, particularly poly(vinylphosphonate)s. Therefore, a brief introduction to the principles of GPC will be presented in the following chapter.

#### 2.4.4 Gel Permeation Chromatography (GPC)

GPC is a type of SEC using a gel as the stationary phase. For the separation of biopolymers, this type of chromatography is also termed gel filtration.<sup>[61]</sup> GPC allows the separation of a polymer mixture according to the hydrodynamic volume of the corresponding particles, *i.e.* particles with a large volume elute first. According to the pore size distribution of the stationary phase, GPC exhibits an upper and a lower exclusion limit.<sup>[61]</sup> As separation is a result of particle exclusion from the pores (*vide supra*), only molecules with a hydrodynamic diameter within in the range of the pore size distribution can be separated. In case of organic solvents, cross-linked polystyrene is commonly used as the stationary phase, in aqueous systems, cellulose and cross-linked dextrans or poly(acrylamide)s.<sup>[61]</sup> Generally, the eluent should exhibit similar solubility parameters<sup>[76]</sup> than the stationary phase in order to avoid distribution effects and to ensure good separation.<sup>[61]</sup>

Commonly, the mass concentration of the sample in the eluate is measured time- or volume-resolved *via* a concentration detector such as an RI, UV-VIS or IR detector. The width of the elution curve is a measure for the molecular weight distribution, nevertheless, as a result of axial dispersion, also molecularly uniform samples such as proteins show an elution curve instead of a sharp elution peak.<sup>[61]</sup> Accordingly, for samples with narrow polydispersity (PDI below 1.05), if not combined with a molecular weight detector, GPC gives very unreliable values for the PDI.

In order to obtain the molecular weight of a sample from the retention time or volume, a rather simple calibration can be performed with reference standards within the exclusion limits.<sup>[61]</sup> Synthetic polymers are usually non-rigid and often exhibit a random coil conformation; their hydrodynamic volume strongly depends on the swelling behavior as determined by the solvent and the polymer architecture, *e.g.* linear *vs* branched. Therefore, a simple calibration to reference molar mass standards is restricted to cases, for which retention volumes were measured with the same column and solvent at the same temperature, and limited to the determination of the molecular weight of polymers with the same constitution and configuration as the reference system.<sup>[61]</sup>

As an alternative, it is better to perform a calibration for the relationship between retention volume  $V_R$  and hydrodynamic volume  $V_H$  of the particles. As a measure for  $V_H$ , the product of the intrinsic viscosity  $[\eta]$  and the molecular weight of the particle  $M$  can be used, as the intrinsic viscosity, a measure for the solutes contribution to the viscosity  $\eta$  of a solution, is defined as<sup>[61]</sup>

$$[\eta] = \frac{5}{2} \frac{V_H N_A}{M}. \quad (2.53)$$

Calibration with standards of known molecular weight using the empirical Grubisic-Remppe-Benoit equation

$$V_R = A - B \times \lg([\eta] \overline{M_w}) \quad (2.54)$$

is known as the *universal calibration*.<sup>[61]</sup> For the determination of  $[\eta]$ , GPC needs to be coupled with a concentration detector and a viscometer. In order to apply the universal calibration for the determination of the molecular weight of polymer types which have not been used for calibration, the empirical parameters  $K_v$  and  $\alpha$  in the Kuhn-Mark-Sakurada-Houwink equation<sup>[61]</sup>

$$[\eta] = K_v M^\alpha \quad (2.55)$$

have to be known for the sample. Hereby,  $\alpha$  is a measure for the particle form and  $K_v$  is mainly dependent on the swelling behavior of the sample within the used solvent. As equation 2.54 is an empirical approach and requires calibration with standards, and as assumptions are made on particle conformation and swelling behavior in form of the parameters  $K_v$  and  $\alpha$ , the universal calibration is a relative method for the determination of the molecular weight and the molecular weight distribution, even if it is often referred to as absolute. In contrast to viscosimetry, static light scattering is an absolute method for the determination of the molecular weight, and, in combination with gel permeation chromatography, also allows an absolute determination of the molecular weight distribution.

#### 2.4.5 Gel Permeation Chromatography Multi Angle Light Scattering (GPC-MALS)

Coupling a multi angle static (laser) light scattering (MALS) detector with a GPC setup yields the excess Rayleigh ratio  $R_{ex}$  for every eluate data increment  $i$ . As  $R_{ex}$  is dependent on both concentration and molecular weight of the particles, the MALS detector needs to be combined with a concentration detector, *e.g.* an RI or UV-VIS detector, which determines the concentration of the solute for every data increment.<sup>[75]</sup> Instead of Zimm plots, which are used to determine the second virial coefficient  $A_2$ , the  $z$ -averaged mean square radius  $\langle r_g^2 \rangle_z$  and the weight-averaged molecular weight of the sample  $\overline{M_w}$  from light scattering measurements



at different angles and concentrations, online static light scattering measurements are evaluated for every data increment using Debye Plots.<sup>[75]</sup> For the latter, the angular variation of  $R_{ex}$  is measured for only one low concentration, consequently, only the weight-averaged molecular weight and mean square radius of each data increment  $\overline{M_{w,i}}$  and  $\langle r_g^2 \rangle_{z,i}$  are yielded. Commonly, up to a particle radius of 100 nm, the Zimm formalism according to equation 2.46 is used for this evaluation (for larger particles, a variety of other formalisms can be used).<sup>[75]</sup> According to the very low concentrations of the solute in the GPC eluate, in most cases,  $A_2$  can be assumed as 0. If this is not the case,  $A_2$  can be determined from Zimm plots and the term  $A_2c$  is considered in the Debye plot of each data increment.<sup>[75]</sup>

From the excess Rayleigh ratio, its angular dependency and the concentration of each data increment  $R_{ex,i}(\theta)$  and  $c_i$ , the weight-averaged molecular weight and the z-averaged mean square radius of the sample  $\overline{M_w}$  and  $\langle r_g^2 \rangle_z$  can be calculated according to

$$\overline{M_w} = \frac{\sum_i c_i \overline{M_{w,i}}}{\sum_i c_i} \quad (2.56)$$

$$\langle r_g^2 \rangle_z = \frac{\sum_i \langle r_g^2 \rangle_i c_i \overline{M_{w,i}}}{\sum_i c_i \overline{M_{w,i}}} \quad (2.57)$$

If GPC yields good separation, according to the small interval of each data increment, each fraction can be assumed as (nearly) molecularly uniform, *i.e.*  $M_i = \overline{M_{w,i}}$ , and using equations 2.33 and 2.50, absolute values for the number-averaged molecular weight  $\overline{M_n}$  and the polydispersity index PDI can be obtained. However, as good separation needs to be assumed, it should be noted that obtained values are generally more accurate for  $\overline{M_w}$  than for  $\overline{M_n}$ .

Nevertheless, in case of good separation, the PDI values yielded for narrow-disperse systems are more precise than those obtained by conventional GPC, as the actual molecular weight is determined for each data increment and thus, axial dispersion does not affect the results. Additionally, from the determined radius of gyration (above 10 nm), information on branching and conformation of polymer samples can be extracted. Further advantages of the GPC-MALS technique are its insensitivity to changes of the flow rate, solvent and other chromatography conditions.<sup>[75]</sup>

## 2.5 Thermosensitive Behavior of Polymers

Materials that drastically change their chemical or physical properties upon minor changes of environmental parameters, *e.g.* temperature, pH, incidence of light or in an electrical or magnetic field, are so-called stimuli-responsive. According to their versatile utilization, *e.g.* as functional components for drug delivery,<sup>[77-79]</sup> data storage<sup>[80]</sup> or in sensor applications,<sup>[81-83]</sup> there has been vast interest in the development of stimuli-responsive polymer systems. This can be attributed to the possibility to synthesize designed materials, which adjust their chemical and physical properties along with their environment.

Thermally-dependent solubility is hereby one of the most studied fields, especially for polymeric materials. Hereby, two cases have to be considered: the *lower critical solution temperature* (LCST) represents the temperature below which a mixture is a one-phase system for all possible compositions; the *upper critical solution temperature* (UCST) accordingly the temperature above which a one-phase system is present (Figure 2.6).<sup>[84]</sup> In view of that, polymer solutions are termed to show so-called LCST or UCST behavior. The phase transition temperature at a given composition is hereby referred to as the *cloud point*, *i.e.* the lowest cloud point in the phase diagram represents the LCST, the highest the UCST.

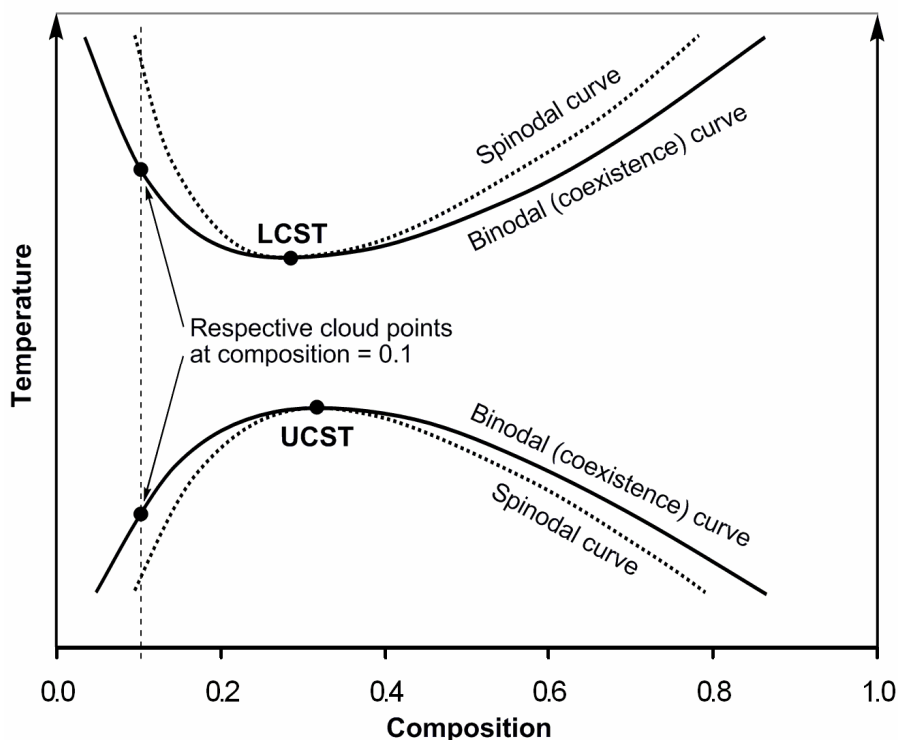


**Figure 2.6:** Phase diagram (Temperature vs Composition) with definition of LCST, UCST and cloud point.

The UCST finds large importance in petrochemistry, *e.g.* wax components of diesel fuel precipitate below a certain temperature thus clogging fuel filters. Also in case of polymers, the solubility in organic solvents commonly increases upon heating the solution, *i.e.* the solution can exhibit a UCST.<sup>[85]</sup> An LCST is typically observed for aqueous solutions of non-ionic tensides such as poly(ethylene glycol) (PEG) or poly(*N*-*iso*-propyl acrylamide) (PNIPAM). The different behavior of these non-ionic tensides in organic and aqueous solution is a result of the present hydrophobic/hydrophilic and hydrogen bond interactions between the polymer chains and water in aqueous solution.<sup>[86]</sup> Generally, the behavior of a polymer chain in a given medium is a result of the interplay of polymer-polymer, polymer-solvent and solvent-solvent interactions.<sup>[86,87]</sup> In the case of aqueous solutions, the solvent-solvent interaction is particularly strong as indicated by its partially ordered structure,<sup>[88-94]</sup> and the solubility of polymer chains results from the energy gain by hydrogen bonding of the hydrophilic moieties with water molecules.<sup>[87,94]</sup> The existent prearrangement of the water molecules requires their reorientation also around nonpolar regions of the polymer chains, being unable to hydrogen bond with them.<sup>[87]</sup> This phenomenon, known as the hydrophobic effect,<sup>[88,90]</sup> results in a decreased entropy upon mixing (negative  $\Delta S$ ).<sup>[87]</sup> At higher temperatures, the entropy term dominates the exothermic mixing enthalpy, causing the water molecules bonding by hydrogen bonds to detach from the polymer, allowing associative contacts between the newly exposed hydrophobic monomer units.<sup>[87,95]</sup> As a consequence, the polymer chains, which adopt an extended coil conformation below the cloud point, collapse and aggregate upon heating. This is referred to as a coil-globule transition mechanism.<sup>[87]</sup> As characteristics of this type of thermal response, the cloud point is unaffected by the solutes concentration over a broad concentration range and the transition upon heating is strongly endothermic. As an alternative thermal response, polymer solutions can also undergo a liquid-liquid phase separation, for which the cloud point shows a pronounced dependency on the polymer concentration.<sup>[96]</sup>

In both cases, the phase transition is commonly completely reversible and the transition temperature can be dependent on the degree of polymerization, the polydispersity, the polymer architecture (linear, branched, *etc.*) and a variety of environmental parameters, *e.g.* pressure, pH or the salt content of the solution.<sup>[97-100]</sup> According to the influence of the molecular weight on their thermo-responsive behavior, thermosensitive polymers are classified into three types: for Type I polymers, the LCST occurs at lower concentrations with increasing polymer molar mass, for Type II polymers, the LCST is insensitive to the weight-averaged molecular weight and Type III polymers display non-monotonous behavior.<sup>[86,101,102]</sup>

Another distinction among polymers with LCST behavior is the presence of hydrogen bond donors and acceptors. Polymers exhibiting both donor and acceptor functionalities, such as PNIPAM, often show a pronounced transition hysteresis,<sup>[103]</sup> which is commonly addressed to the formation of polymer-polymer inter- and intramolecular hydrogen bonds in the collapsed state delaying the hydration of the polymer chain during cooling.<sup>[104]</sup> Furthermore, the presence of hydrogen bond donors can increase the interaction of the polymer chains with blood proteins, hampering the application of these materials in the biomedical field by potentially causing an immunoresponse.<sup>[86,105]</sup>

Since the first report on the LCST behavior of PNIPAM in 1967 by Scarpa *et al.*,<sup>[106]</sup> a vast variety of polymers exhibiting thermo-responsive behavior in aqueous solution has been presented. Besides a variety of poly(*N,N*-dialkyl acrylamides)<sup>[107-109]</sup> and PEG, the gold standard for biomedical applications,<sup>[86]</sup> large interest has been directed particularly towards poly((alkylamino) methacrylate),<sup>[110]</sup> poly(vinyl alkyl ether)s,<sup>[111]</sup> poly(*N*-vinylcaprolactam),<sup>[112]</sup> and poly(2-oxazoline)s.<sup>[86,113,114]</sup>

For the modification of the LCST of these homopolymers, copolymerization of monomers with different hydrophilicity is widely adopted, however, often resulting in gradient copolymers, which tend to assemble into complex nanostructures<sup>[115]</sup> or micelles and therefore exhibit a prolonged or irreversible phase transition.<sup>[96,114-117]</sup> As a consequence, further development of alternative thermoresponsive polymers, which combine biocompatibility, thermoresponsiveness with little dependency on environmental parameters, a reversible phase transition without hysteresis, and the possibility to synthesize random instead of gradient copolymers, is of substantial importance.

## 2.6 References

- [1] H. Yasuda, E. Ihara, *Adv. Polym. Sci.* **1997**, *133*, 53.
- [2] H. Yasuda, *Prog. Polym. Sci.* **2000**, *25*, 573.
- [3] L. S. Boffa, B. M. Novak, *Chem. Rev.* **2000**, *100*, 1479.
- [4] J. Gromada, J.-F. Carpentier, A. Mortreux, *Chem. Rev.* **2004**, *248*, 397.
- [5] E. Y.-X. Chen, *Chem. Rev.* **2009**, *109*, 5157.
- [6] G. A. Molander, *Chemtracts-Org. Chem.* **1998**, *11*, 237.
- [7] R. Anwander, *Rare Earth Metals in Homogeneous Catalysis*, in *Applied Homogeneous Catalysis with Organometallic Compounds* (Eds.: B. Cornils, W. A. Herrmann), VCH Publishers, Weinheim **1999**, 866.
- [8] G. A. Molander, E. C. Dowdy, *Top. Organomet. Chem.* **1999**, *2*, 119.
- [9] J. Eppinger, *Ph.D. Thesis*, Technische Universität München, Garching bei München, April **1999**.
- [10] M. Zimmermann, R. Anwander, *Chem. Rev.* **2010**, *110*, 6194.
- [11] W. A. Herrmann, J. Eppinger, M. Spiegler, O. Runte, R. Anwander, *Organometallics* **1997**, *16*, 1813.
- [12] G. Wilkinson, J. M. Birmingham, *J. Am. Chem. Soc.* **1954**, *76*, 6210.
- [13] E. O. Fischer, H. Fischer, *Angew. Chem.* **1964**, *76*, 52; *Angew. Chem. Int. Ed.* **1964**, *3*, 132.
- [14] E. O. Fischer, H. Fischer, *J. Organomet. Chem.* **1965**, *3*, 181.
- [15] F. Calderazzo, R. Pappalardo, S. Losi, *J. Inorg. Nucl. Chem.* **1966**, *28*, 987.
- [16] J. Jubb, S. Gambarotta, *J. Am. Chem. Soc.* **1994**, *116*, 4477.
- [17] G. B. Deacon, P. I. MacKinnon, T. W. Hambley, J. C. Taylor, *J. Organomet. Chem.* **1983**, *259*, 91.
- [18] G. B. Deacon, A. J. Kloplick, T. D. Tuong, *Aust. J. Chem.* **1984**, *37*, 517.
- [19] G. B. Deacon, C. M. Forsyth, R. H. Newnham, T. D. Tuong, *Aust. J. Chem.* **1987**, *40*, 895.
- [20] G. B. Deacon, *Aust. J. Chem.* **1992**, *45*, 567.
- [21] A. Gulino, *Organometallics* **1988**, *7*, 2360.
- [22] W. J. Evans, T. J. Demig, J. W. Ziller, *Organometallics*, **1989**, *8*, 1581.
- [23] W. P. Kretschmer, J. H. Teuben, S. I. Troyanov, *Angew. Chem.* **1998**, *110*, 92; *Angew. Chem., Int. Ed.* **1998**, *37*, 88.
- [24] P. L. Watson, J. F. Whitney, R. L. Harlow, *Inorg. Chem.* **1981**, *20*, 3271.
- [25] A. Recknagel, F. T. Edelmann, *Angew. Chem.* **1991**, *103*, 720; *Angew. Chem. Int. Ed.* **1991**, *30*, 693.
- [26] J. Eppinger, M. Spiegler, W. Hieringer, W. A. Herrmann, R. Anwander, *J. Am. Chem. Soc.* **2000**, *122*, 3080.
- [27] J. M. Birmingham, G. Wilkinson, *J. Am. Chem. Soc.* **1956**, *78*, 42.

- [28] R. D. Fischer, J. Guan, *J. Organomet. Chem.* **1996**, 532, 147.
- [29] H. Schumann, J. A. Meese-Marktscheffel, L. Esser, *Chem. Rev.* **1995**, 95, 865.
- [30] M. D. Haar, C. L. Stern, T. J. Marks, *Organometallics* **1996**, 15, 1765.
- [31] T. Akhnoukh, J. Müller, K. Quiao, X. F. Li, R. D. Fischer, *J. Organomet. Chem.* **1991**, 408, 47.
- [32] G. M. Diamond, S. Rodewald, R. F. Jordan, *Organometallics* **1995**, 14, 5.
- [33] G. M. Diamond, R. F. Jordan, J. L. Petersen, *Organometallics* **1996**, 15, 4030.
- [34] G. M. Diamond, R. F. Jordan, J. L. Petersen, *Organometallics* **1996**, 15, 4038.
- [35] G. M. Diamond, R. F. Jordan, J. L. Petersen, *Organometallics* **1996**, 15, 4045.
- [36] G. M. Diamond, R. F. Jordan, J. L. Petersen, *J. Am. Chem. Soc.* **1996**, 118, 8024.
- [37] Vogel, A.; Priermeier, T.; Herrmann, W. A. *J. Organomet. Chem.* **1997**, 527, 297.
- [38] M. Booji, N. H. Kiers, H. J. Heeres, J. H. Teuben, *J. Organomet. Chem.* **1989**, 264, 79.
- [39] S. D. Stults, R. A. Andersen, A. Zalkin, *Organometallics* **1990**, 9, 115.
- [40] S. D. Stults, R. A. Andersen, A. Zalkin, *Organometallics* **1990**, 9, 1623.
- [41] G. W. Rabe, J. W. Ziller, *Inorg. Chem.* **1995**, 34, 5378.
- [42] G. W. Rabe, J. Riede, A. Schier, *Chem. Commun.* **1995**, 577.
- [43] A. Streitwieser, E. Juaristi, L. L. Nebenzahl, in *Comprehensive carbanion chemistry, Part A* (Eds.: E. Buncl, T. Durst), Elsevier-North Holland: Amsterdam, **1980**, 323.
- [44] R. R. Fraser, T. S. Mansour, S. Savard, *J. Org. Chem.* **1985**, 50, 3232.
- [45] C. Eaborn, R. Eidenschink, P. M. Jackson, D. R. M. Walton, *J. Organomet. Chem.* **1975**, 101, C40.
- [46] P. v. R. Schleyer, T. Clark, A. J. Kos, G. W. Spitznagel, C. Rohde, D. Arad, K. N. Houk, N. G. Rondan, *J. Am. Chem. Soc.* **1984**, 106, 6467.
- [47] E. A. Brinkman, S. Berger, J. I. Brauman, *J. Am. Chem. Soc.* **1994**, 116, 8304.
- [48] P. B. Hitchcock, M. F. Lappert, R. G. Smith, R. A. Bartlett, P. P. Power, *J. Chem. Soc., Chem. Commun.* **1988**, 1007.
- [49] C. J. Schaverien, A. G. Orpen, *Inorg. Chem.* **1991**, 30, 4968.
- [50] A. G. Avent, C. F. Caro, P. B. Hitchcock, M. F. Lappert, Z. Li, X.-H. Wei, *Dalton Trans.* **2004**, 1567.
- [51] C. Guttenberger, H.-D. Amberger, *J. Organomet. Chem.* **1997**, 545, 601.
- [52] H. Reddmann, C. Guttenberger, H.-D. Amberger, *J. Organomet. Chem.* **2000**, 602, 65.
- [53] M. F. Lappert, R. Pearce, *J. Chem. Soc., Chem. Commun.* **1973**, 126.
- [54] K. C. Hultsch, P. Voth, K. Beckerle, T. P. Spaniol, J. Okuda, *Organometallics* **2000**, 19, 228.
- [55] S. Arndt, P. Voth, T. P. Spaniol, J. Okuda, *Organometallics* **2000**, 19, 4690.
- [56] H. Schumann, D. M. M. Freckmann, S. Dechert, *Z. Anorg. Allg. Chem.* **2002**, 628, 2422.
- [57] D. M. Wetzal, J. I. Brauman, *J. Am. Chem. Soc.* **1988**, 110, 8333.
- [58] E. A. Brinkman, S. Berger, J. I. Brauman, *J. Am. Chem. Soc.* **1994**, 116, 8304.

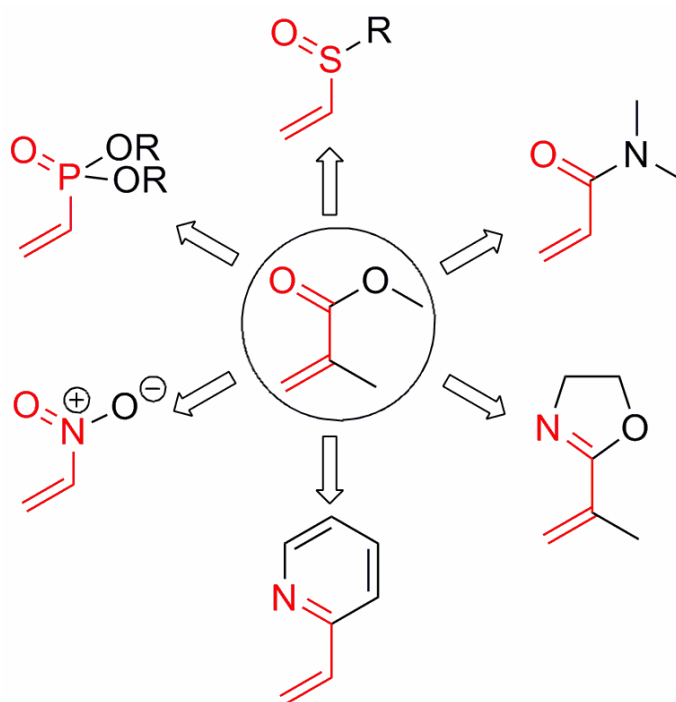
- [59] B. Römer, G. G. Gatev, M. Zhong, J. I. Brauman, *J. Am. Chem. Soc.* **1998**, *120*, 2919.
- [60] Y. Fu, L. Liu, R. Q. Li, R. Liu, Q. X. Guo, *J. Am. Chem. Soc.* **2004**, *126*, 814.
- [61] H.-G. Elias, in *Makromoleküle, Band 1: Chemische Struktur und Synthesen*, Wiley-VCH Verlag GmbH, Weinheim **1999**.
- [62] W. H. Carothers, *J. Am. Chem. Soc.* **1929**, *51*, 2548.
- [63] M. Swarc, *Nature* **1956**, *178*, 1168.
- [64] M. Swarc, *J. Am. Chem. Soc.* **1956**, *78*, 2656.
- [65] P. J. Flory, *J. Am. Chem. Soc.* **1940**, *62*, 1561.
- [66] G. Odian, in *Principles of Polymerization*, John Wiley & Sons, Inc., New York **2004**.
- [67] L. S. Boffa, B. M. Novak, *Macromolecules* **1994**, *27*, 6993.
- [68] T. Alfrey, G. Goldfinger, *J. Chem. Phys.* **1944**, *12*, 115, 205, 332.
- [69] F. R. Mayo, F. M. Lewis, *J. Am. Chem. Soc.* **1944**, *66*, 1594.
- [70] F. T. Wall, *J. Am. Chem. Soc.* **1944**, *66*, 2050.
- [71] C. Walling, in *Free Radicals in Solution*, Wiley, New York **1957**.
- [72] M. Fineman, S. D. Ross, *J. Polym. Sci.* **1950**, *5*, 269.
- [73] T. Kelen, F. Tüdös, *J. Macromol. Sci. Chem.* **1975**, *A9*, 1.
- [74] P. Keusch, in *Eyring Equation*, from [http://www.uni-regensburg.de/Fakultaeten/nat\\_Fak\\_IV/Organische\\_Chemie/Didaktik/Keusch/eyr-e.htm](http://www.uni-regensburg.de/Fakultaeten/nat_Fak_IV/Organische_Chemie/Didaktik/Keusch/eyr-e.htm) (02/2013).
- [75] Wyatt Technology Europe GmbH, *Light Scattering University, LSU Course Manual*, **2010**.
- [76] H.-G. Elias, in *Makromoleküle, Band 2: Physikalische Strukturen und Eigenschaften*, Wiley-VCH Verlag GmbH, Weinheim **2001**.
- [77] K.A. Yoon, D. J. Burgess, *J. Pharm. Pharmacol.* **1997**, *49*, 478.
- [78] M. J. Lawrence, S. M. Lawrence, D. J. Barlow, *J. Pharm. Pharmacol.* **1997**, *49*, 594.
- [79] Z. Sideratou, D. Tsiourvas, C. M. Paleos, *Langmuir* **1999**, *16*, 1766.
- [80] Y. Kawata, *Appl. Phys. Lett.* **2006**, *88*, 123113.
- [81] M. Ahlheim, M. L. Hallensleben, *Die Makromol. Chem.* **1992**, *193*, 779.
- [82] Y. Li, *Appl. Phys. Lett.* **1999**, *74*, 2233.
- [83] M. Ishihara, K. Nakanishi, K. Ono, M. Sato, M. Kikuchi, Y. Saito, H. Yura, T. Matsui, H. Hattori, M. Uenoyama, A. Kurita, *Biomaterials* **2002**, *23*, 833.
- [84] IUPAC, *Kompendium der chemischen Terminologie* **2009**.
- [85] R. Koningsveld, W. H. Stockmayer, E. Nies, in *Polymer Phase-Diagrams. A Textbook*. Oxford University Press, Oxford, New York **2001**.
- [86] O. Sedlacek, B. D. Monnery, S. K. Filippov, R. Hoogenboom, M. Hruby, *Macromol. Rapid Commun.* **2012**, *33*, 1648.
- [87] H. G. Schild, *Prog. Polym. Sci.* **1992**, *17*, 163.
- [88] C. Tanford, in *The Hydrophobic Effect*, J. Wiley and Sons, Inc., New York **1973**.
- [89] P. Molyneux, in *Water, A Comprehensive Treatise* (Ed.: F. Franks), Plenum, New York **1975**.

- [90] A. Ben-Naim, in *Hydrophobic Interactions*, Plenum Press, New York **1980**.
- [91] I. D. Robb, in *Chemistry and Technology of Water-Soluble Polymers* (Ed.: C. A. Finch), Plenum, New York **1981**.
- [92] P. Molyneux, in *Water-Soluble Polymers: Properties and Behavior*, CRC Press, Boca Raton, Florida **1983**.
- [93] F. Franks, D. Eagland, *CRC Crit. Rev. Biochem.* **1985**, *4*, 165.
- [94] J. A. Walker, C. A. Vause, *Sci. Am.* **1987**, *253*, 98.
- [95] B. Widom, B. Bhimalapuram, K. Koga, *Phys. Chem. Chem. Phys.* **2003**, *5*, 3085.
- [96] H. Ajiro, Y. Takahashi, M. Akashi, *Macromolecules* **2012**, *45*, 2668.
- [97] S. Carter, B. Hunt, S. Rimmer, *Macromolecules* **2005**, *38*, 4595.
- [98] S. Rimmer, S. Carter, R. Rutkaite, J. W. Haycock, L. Swanson, *Soft Matter* **2007**, *3*, 971.
- [99] Z. M. O. Rzaev, S. Dincer, E. Piskin, *Prog. Polym. Sci.* **2007**, *32*, 534.
- [100] S. Aoshima, S. Kanaoka, *Adv. Polym. Sci.* **2008**, *210*, 169.
- [101] F. Meeussen, E. Nies, H. Berghmans, S. Verbrugghe, E. Goethals, F. Du Prez, *Polymer* **2000**, *41*, 8597.
- [102] K. Van Durme, S. Verbrugghe, F. E. Du Prez, B. Van Mele, *Macromolecules* **2004**, *37*, 1054.
- [103] X. Wang, X. Qiu, C. Wu, *Macromolecules* **1998**, *31*, 2972.
- [104] H. Cheng, L. Shen, C. Wu, *Macromolecules* **2006**, *39*, 2325.
- [105] R. G. Chapman, E. Ostuni, S. Takayama, R. E. Holmlin, L. Yan, G. M. Whitesides, *J. Am. Chem. Soc.* **2000**, *122*, 8303.
- [106] J. S. Scarpa, O. D. Mueller, I. M. Klotz, *J. Am. Chem. Soc.* **1967**, *89*, 6024.
- [107] K. Zhou, Y. Lu, J. Li, L. Shen, G. Zhang, Z. Xie, C. Wu, *Macromolecules* **2008**, *41*, 8927.
- [108] Y. Cao, N. Zhao, K. Wu, X. X. Zhu, *Langmuir* **2009**, *25*, 1699.
- [109] V. Aseyev, H. Tenhu, F. M. Winnik, *Adv. Polym. Sci.* **2011**, *242*, 29.
- [110] S. H. Yuk, S. H. Cho, S. H. Lee, *Macromolecules* **1997**, *30*, 6856.
- [111] Y. Maeda, *Langmuir* **2001**, *17*, 1737.
- [112] C. de las Heras Alarcón, S. Pennadam, C. Alexander, *Chem. Soc. Rev.* **2005**, *34*, 276.
- [113] N. Zhang, S. Huber, A. Schulz, R. Luxenhofer, R. Jordan, *Macromolecules* **2009**, *42*, 2215.
- [114] S. Salzinger, S. Huber, S. Jaksch, P. Busch, R. Jordan, C. M. Papadakis, *Colloid Polym. Sci.* **2012**, *290*, 385.
- [115] A. Blanz, N. J. Warren, A. L. Lewis, S. P. Armes, A. J. Ryan, *Soft Matter* **2011**, *7*, 6399.
- [116] H. M. L. Lambermont Thijs, R. Hoogenboom, C. A. Fustin, C. Bomal D'Haese, J. F. Gohy, U. S. Schubert, *J. Polym. Sci., Part A: Polym. Chem.* **2009**, *47*, 515.
- [117] L. T. T. Trinh, H. M. L. Lambermont-Thijs, U. S. Schubert, R. Hoogenboom, A. L. Kjøniksen, *Macromolecules* **2012**, *45*, 4337.



## CHAPTER 3:

# EXPANSION OF RARE EARTH METAL-MEDIATED GROUP TRANSFER POLYMERIZATION TO NEW MONOMERS



*“The true delight is in the finding out rather than in the knowing.”*

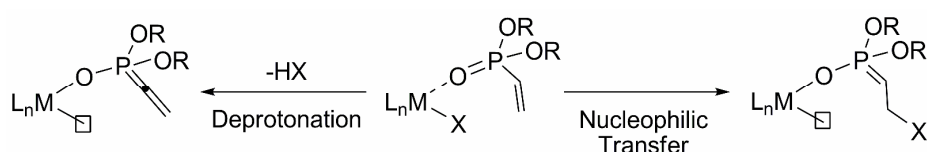
- Isaac Asimov (1919-1992)



The majority of produced polymeric materials is based on a few commodity polymers only; however, the need for new materials with designed properties has been a main driving force in recent polymer research. Coordination polymerization of functional monomers enables a precise adjustment of the polymer structure and thus of the material properties, making this approach a very promising option for the production of tailor-made functional materials. Hereby, organo-rare earth metal compounds facilitate the polymerization of a broad variety of monomers following different polymerization mechanisms, which can be combined in a living fashion, making these catalysts versatile tools for the synthesis of functional high value polymers.<sup>[1-5]</sup>

Rare earth metal-mediated group transfer polymerization (REM-GTP) of polar-modified olefins combines the advantages of living ionic and coordination polymerizations and is thus predestined for the synthesis of designed functional materials. However, according to the restricted utilization for (meth)acrylic monomers only, the interest in REM-GTP has continuously decreased in the first decade of the 21<sup>st</sup> century. Nevertheless, recent publications have shown the suitability of REM-GTP to a variety of other monomer classes, particularly poly(vinylphosphonate)s, a material class which is not satisfactorily accessible *via* other polymerization methods.<sup>[6-8]</sup>

Initial investigations on rare earth metal-mediated vinylphosphonate polymerization have proven the livingness of polymerization and suggest a GTP mechanism taking place.<sup>[7]</sup> Especially concerning the initiation mechanism, typical characteristics of (meth)acrylate REM-GTP were found to be strongly altered for its application to vinylphosphonates. In view of that, complexes with low initiator efficiency and activity for MMA polymerization, *i.e.* Cp<sub>2</sub>LnCl or Cp<sub>3</sub>Ln, were found to exhibit largely increased efficacy for dialkyl vinylphosphonate (DAVP) polymerization.<sup>[7,8]</sup> On the contrary, traditionally used strongly basic carbanion initiators, *e.g.* methyl complexes, did exhibit decreased initiator efficiency with first investigations pointing towards an unusual initiation through deprotonation of coordinated DAVP.<sup>[8]</sup> Accordingly, initiation of REM-GTP was proposed to commonly follow two different types of initiation, either *via* nucleophilic transfer to or *via* deprotonation of a coordinated monomer (Scheme 3.1).



**Scheme 3.1: Possible initiation reactions for rare earth metal-mediated vinylphosphonate polymerizations.**

In case of coordinative-anionic polymerizations, it is well-established that the metal center has to remain easily accessible in order to ensure high activities.<sup>[4]</sup> The initial studies on vinylphosphonate REM-GTP question the general applicability of this concept, as only the sterically more crowded complexes of the small, late lanthanides were able to polymerize vinylphosphonates.<sup>[8]</sup> Accordingly, also a deeper understanding of the factors influencing the propagation rate of REM-GTP is necessary. However, kinetic analysis of vinylphosphonate REM-GTP was found to be hampered by a very fast propagation with a comparatively slow initiation. In view of that, both the synthesis of catalysts exhibiting lower activity and faster initiation, as well as a (differential) method for the kinetic analysis of living polymerizations with comparable initiation and propagation rates needed to be developed.

In summary, in order to expand the efficient utilization of REM-GTP towards a broader scope of monomers, a deeper understanding of the underlying initiation and propagation mechanism is inevitable. Therefore, it was a major scope of this thesis to conduct detailed mechanistic studies in order to verify the origin of unexpected monomer polymerization behavior and to allow a prediction of this behavior for other monomers of interest. On this basis, the range of applicable monomers should be broadened to a variety of polar functionalities which have not yet been tested for REM-GTP. This includes functionalities which undergo metal-*N*- or metal-*S*-coordination (instead of metal-*O*) such as pyridine, thiophene, imidazole and oxazoline as well as nitrogen-, sulfur- and phosphorus-centered moieties (Figure 3.1). Monomers suitable for REM-GTP need to show Michael acceptor-type behavior and a sufficient  $\pi$ -overlap of the double bonds in an *S*-cis conformation.<sup>[4]</sup> Based on the mechanistic studies<sup>[4]</sup> carried out on vinylphosphonate polymerization, for monomers found non-polymerizable by means of REM-GTP, an evaluation should be performed whether limitations occur according to an unfeasible initiation or propagation or as a result of readily occurring termination reactions (*e.g.* as observed for methyl acrylate<sup>[9,10]</sup>).

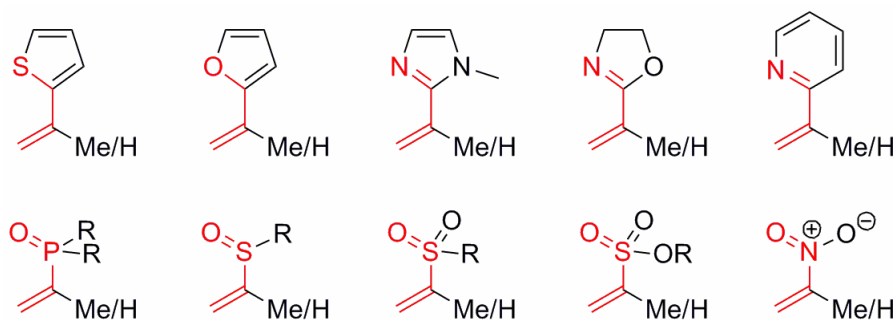
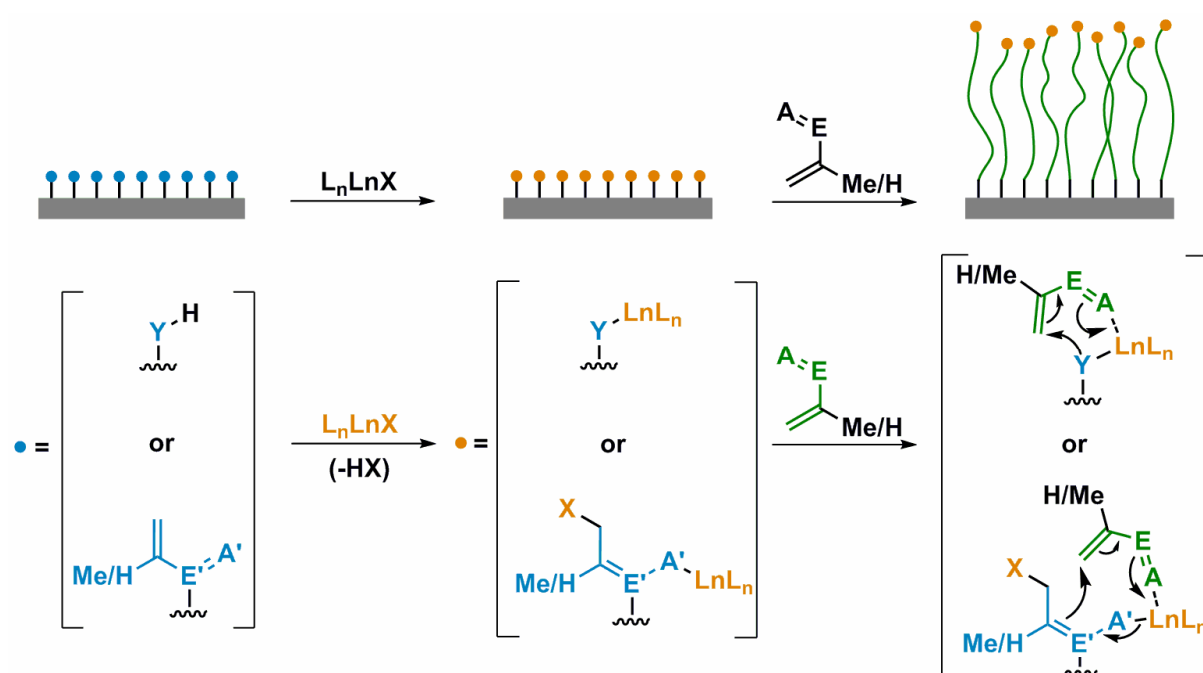


**Figure 3.1: Structures of functional monomers with potential suitability for REM-GTP.**

On basis of the knowledge developed by the use of new monomer classes and the mechanistic conclusions drawn, a systematic improvement of the applied catalysts should be performed, both regarding their initiator efficiency and activity. Particularly, this includes the development of new, preferably enolic initiators with versatile applicability to a broad range of monomer classes, ensuring an efficient initiation also for  $\alpha$ -acidic monomers such as vinylphosphonates. In view of that, investigation of versatile complex synthesis routes in order to allow an easy and sophisticated modification of the catalyst properties is required. As another prerequisite, the newly developed initiators should enable a versatile end group functionalization, particularly leading towards the development of a surface-initiated group transfer polymerization (SI-GTP) mediated by rare earth metal catalysts (Scheme 3.2). A sophisticated SI-GTP should permit the perfect decoration of surfaces with stable, covalently bound coatings of specific functionality.



**Scheme 3.2:** Possible route for the development of a surface-initiated group transfer polymerization (SI-GTP) *via* prior rare earth metal catalyst immobilization and subsequent polymerization of Michael acceptor-type monomers.

Polymer-analogous transformations of the introduced new functionalities, *e.g.* saponification of poly(vinylphosphonate)s to poly(vinylphosphonic acid) (PVPA), opens the access to an even broader scope of functional materials accessible by REM-GTP and should therefore be evaluated. Furthermore, the properties of these new materials, *e.g.* the flame retardant effect

of poly(vinylphosphonate)s or the previously described thermosensitivity of aqueous poly(diethyl vinylphosphonate) (PDEVVP) solutions,<sup>[8,11]</sup> should be studied in detail.

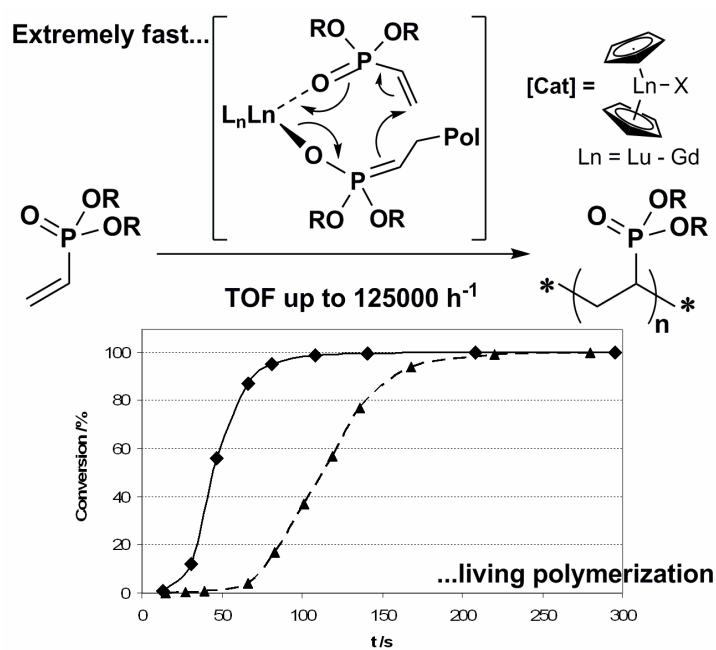
In summary, the main scope of this thesis is to develop a deeper mechanistic understanding of REM-GTP in order to enable an expansion of REM-GTP onto the vast variety of Michael-acceptor-type monomers. In combination with macromolecular organization and self-assembly principles, an expanded REM-GTP should open the access to a wide range of new functional materials. The establishment of a surface-initiated REM-GTP would allow the decoration of surfaces with high-value functional materials in form of dense and stable, covalently bound coatings.

## References

- [1] H. Yasuda, E. Ihara, *Adv. Polym. Sci.* **1997**, *133*, 53.
- [2] H. Yasuda, *Prog. Polym. Sci.* **2000**, *25*, 573.
- [3] L. S. Boffa, B. M. Novak, *Chem. Rev.* **2000**, *100*, 1479.
- [4] E. Y.-X. Chen, *Chem. Rev.* **2009**, *109*, 5157.
- [5] J. Gromada, J.-F. Carpentier, A. Mortreux, *Chem. Rev.* **2004**, *248*, 397.
- [6] G. W. Rabe, H. Komber, L. Häussler, K. Kreger, G. Lattermann, *Macromolecules* **2010**, *43*, 1178.
- [7] U. B. Seemann, J. E. Dengler, B. Rieger, *Angew. Chem. Int. Ed.* **2010**, *49*, 3489.
- [8] U. B. Seemann, *Ph.D. Thesis*, Technische Universität München, Garching bei München, October **2010**.
- [9] E. Ihara, M. Morimoto, H. Yasuda, *Macromolecules* **1995**, *28*, 7886.
- [10] W. R. Mariott, A. Rodriguez-Delgado, E. Y.-X. Chen, *Macromolecules* **2006**, *39*, 1318.
- [11] S. Salzinger, *Master Thesis*, Technische Universität München, Garching bei München, July **2010**.

## CHAPTER 4:

# RARE EARTH METAL-MEDIATED GROUP TRANSFER POLYMERIZATION OF VINYLPHOSPHONATES



*“Science does not advance by piling up information –  
it organizes information and compresses it.”*

- Herbert Alexander Simon (1916-2001)





**Status:** Published online: July 10, 2012  
**Journal:** Macromolecular Rapid Communications  
Issue 33, 1327-1345  
**Publisher:** Wiley VCH  
**Article type:** Review  
**DOI:** 10.1002/marc.201200278  
**Authors:** Stephan Salzinger, Bernhard Rieger

**Content:**

This chapter presents the progress in rare earth metal-mediated group transfer polymerization of vinylphosphonates, which has been made at the beginning of and prior to this work. Particularly, this includes a detailed overview of previous work on vinylphosphonate polymerization by radical and classical anionic methods, a short introduction to REM-GTP, a summary of initial vinylphosphonate REM-GTP investigations between 2007 and 2010 as well as the presentation of early stage catalyst optimization and of a surface-initiated group transfer polymerization, which have both been developed at the beginning of this work and will be described in more detail in chapters 5 and 6.

The main scope of this chapter is to highlight the large potential of rare earth metal-mediated vinylphosphonate polymerization and to show its advantages in comparison to radical and classical anionic approaches. In particular, late lanthanide metallocenes proved to be efficient initiators and highly active catalyst for vinylphosphonate polymerization, yielding polymers of defined molecular weight and low polydispersity. Evidence will be presented for a living-type polymerization character and a GTP mechanism taking place. A summary on methods for the conversion of poly(vinylphosphonate)s to poly(vinylphosphonic acid) will be shown, which open the access to well-defined high molecular weight PVPA with narrow chain length distribution.

## JOHN WILEY AND SONS LICENSE TERMS AND CONDITIONS

Jun 01, 2013

This is a License Agreement between Stephan Salzinger ("You") and John Wiley and Sons ("John Wiley and Sons") provided by Copyright Clearance Center ("CCC"). The license consists of your order details, the terms and conditions provided by John Wiley and Sons, and the payment terms and conditions.

**All payments must be made in full to CCC. For payment instructions, please see information listed at the bottom of this form.**

License Number	3160190431384
License date	Jun 01, 2013
Licensed content publisher	John Wiley and Sons
Licensed content publication	Macromolecular Rapid Communications
Licensed content title	Rare Earth Metal-Mediated Group Transfer Polymerization of Vinylphosphonates
Licensed copyright line	Copyright © 2012 WILEY-VCH Verlag GmbH & Co. KGaA, Weinheim
Licensed content author	Stephan Salzinger, Bernhard Rieger
Licensed content date	Jul 10, 2012
Start page	1327
End page	1345
Type of use	Dissertation/Thesis
Requestor type	Author of this Wiley article
Format	Print and electronic
Portion	Full article
Will you be translating?	No
Total	0.00 USD
Terms and Conditions	

### TERMS AND CONDITIONS

This copyrighted material is owned by or exclusively licensed to John Wiley & Sons, Inc. or one of its group companies (each a "Wiley Company") or a society for whom a Wiley Company has exclusive publishing rights in relation to a particular journal (collectively "WILEY"). By clicking "accept" in connection with completing this licensing transaction, you agree that the following terms and conditions apply to this transaction (along with the billing and payment terms and conditions established by the Copyright Clearance Center Inc., ("CCC's Billing and Payment terms and conditions"), at the time that you opened your RightsLink account (these are available at any time at <http://myaccount.copyright.com>).

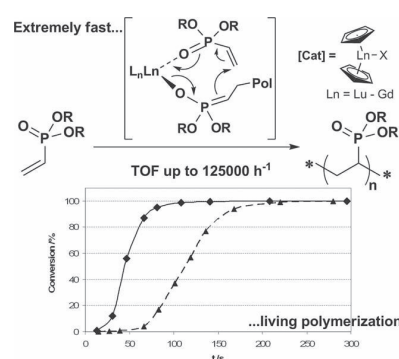
#### Terms and Conditions

1. The materials you have requested permission to reproduce (the "Materials") are protected by copyright.

# Rare Earth Metal-Mediated Group Transfer Polymerization of Vinylphosphonates

Stephan Salzinger, Bernhard Rieger\*

Recent studies have shown that poly(vinylphosphonate)s are readily accessible by rare earth metal-mediated group transfer polymerization (GTP). This article highlights the progress in this new field and advantages of GTP in comparison to classical anionic and radical polymerization approaches. Late lanthanide metallocenes proved to be efficient initiators and highly active catalysts for vinylphosphonate polymerization yielding polymers of precise molecular weight and low polydispersity. Using this method, our group has developed a surface-initiated GTP to prepare poly(vinylphosphonate) brushes. In combination with different ester cleavage strategies, rare earth metal-mediated GTP is an efficient way to create well-defined high-molecular-weight poly(vinylphosphonic acid).



## List of Abbreviations

bdsa, *bis*(dimethylsilyl)amide,  $N(\text{SiHMe}_2)_2$ ; btsa, *bis*(trimethylsilyl)amide,  $N(\text{SiMe}_3)_2$ ; DEMVP, diethyl 1-methylvinylphosphonate; DEVP, diethyl vinylphosphonate; DIVP, diisopropyl vinylphosphonate; DMAA, *N,N*-dimethyl acrylamide; DMVP, dimethyl vinylphosphonate; DPE, 1,1-diphenylethylene; DPVP, di-*n*-propyl vinylphosphonate; EGDM, ethylene glycol dimethacrylate; GTP, group transfer polymerization;  $I^*$ , initiator efficiency; MALS, multi angle (static) light scattering; MMA, methyl methacrylate; PDI, polydispersity index; SAM, self-assembled monolayer; SI-GTP, surface-initiated group transfer polymerization; SIPGP, self-initiated photografting and photopolymerization; SKA-GTP, silyl ketene acetal-initiated group transfer polymerization; TMSPM, 3-(trimethoxysilyl)propyl methacrylate; VPA, vinylphosphonic acid.

M.Sc. S. Salzinger, Prof. B. Rieger  
WACKER-Lehrstuhl für Makromolekulare Chemie,  
Technische Universität München, Lichtenbergstraße 4,  
85748 Garching, Germany  
E-mail: rieger@tum.de

## 1. Introduction

Within the last decades, polymeric materials have gained an indisputable dominance for an enormous range of applications and, nowadays, their use is by no means limited to packaging materials. Due to their broad spectrum of properties, synthetic polymers increasingly substitute classic raw materials such as wood, glass, ceramics, or metals and owing to their nearly limitless possibilities even open new fields of applications. Thus, without polymeric materials, our modern society is hard to imagine. Their versatility leads to an enormous increase per annum of polymer production and since the end of the 1980s the production of polymeric materials exceeds, by volume, crude steel production.<sup>[1]</sup> Using the classic definition to divide history by the predominantly used raw material, we have therefore entered the age of polymers.

Even though the majority of produced polymeric materials are based on only a few commodity polymers, the need for new materials with designed properties has driven polymer research in recent years. The necessity of such specialty polymers ranges from high-performance materials for aerospace applications and medical

chemistry to new energy technologies (e.g., proton-conducting membranes in fuel cells or bulk heterojunction solar cells).<sup>[2]</sup>

Of these designed materials, polymers comprising heteroatoms have attracted great interest during the last decades and are increasingly becoming a focus of research activities. The number of available functionalities tailored by the introduction of heteroatoms is vast and, in combination with macromolecular organization and self-assembly principles, a wide range of new functional materials are accessible.

Phosphorus-containing polymers, especially those comprising phosphonate moieties, are particularly attractive due to their halogen-free flame retardant and proton-conducting properties as well as their commercial application as binders in dental or bone concrete.<sup>[3]</sup> Because of the biocompatibility and low toxicity of these polymers, much attention has recently been directed toward their use in biomedical fields, with applications as diverse as non-fouling coatings, tissue engineering, drug delivery systems, and cell proliferation surfaces.<sup>[4]</sup>

Within this class of phosphorus-containing polymers, poly(vinylphosphonic acid) (PVPA) and its derivatives (Figure 1) have been intensively studied. However, a well-controlled polymerization of vinylphosphonates is hard to establish, as radical and anionic synthesis routes often only lead to incomplete conversion of the monomers and provide materials with low molecular weights. Recently, our group reported that poly(vinylphosphonate)s with high molar mass and low polydispersity can be efficiently prepared in the presence of rare earth metal-containing catalysts following a group transfer polymerization (GTP) mechanism.<sup>[5]</sup>

This article highlights the progress in rare earth metal-mediated GTP of vinylphosphonates and shows advantages of this method in comparison to classical anionic and radical vinylphosphonate polymerizations. It provides insight into early stage catalyst optimization and presents a new possibility for surface modification—surface-initiated group-transfer polymerization (SI-GTP). A short introduction to vinylphosphonate polymerization and rare earth metal-mediated GTP will be given. The latter is also referred to as coordinative-anionic addition- or repeated conjugate addition polymerization. To avoid

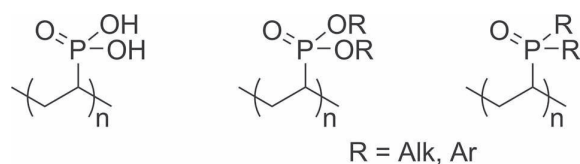


**Figure 1.** Structure of poly(vinylphosphonic acid) (PVPA) (left) and its derivatives, poly(vinylphosphonate) (center) and poly(vinylphosphonoxide) (right).



**Stephan Salzinger** studied chemistry at the Technische Universität München and received his M.Sc. in 2010. In 2009, he carried out research on self-assembling peptide nanotubes under the guidance of M. Amorín and J.R. Granja at the Universidad de Santiago de Compostela. In his master's thesis in the group of B. Rieger, he focussed on stereoregularity and mechanism of vinylphosphonate polymerization. His Ph.D. is concerned with the rare earth metal-mediated group transfer polymerization of hetero-atom functionalized vinylic monomers, for which he received a scholarship from the Fonds der Chemischen Industrie.



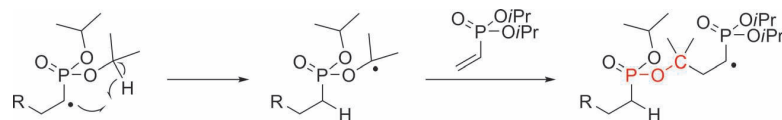
**Bernhard Rieger** studied chemistry at the Ludwig-Maximilians-Universität München (LMU) and received his Ph.D. in 1988. After research at the University of Massachusetts at Amherst and in the plastics laboratory of BASF SE, he received his Habilitation in 1995 at the University of Tübingen. In 1996, he became Professor at the Department Materials and Catalysis at the University of Ulm. Since 2006, he has been Professor at the TUM at the WACKER-Chair of Macromolecular Chemistry and director of the Institute of Silicon Chemistry. He has received a teaching award from the Federal State of Baden-Württemberg and the Philip-Morris Award.

confusion, polymerizations initiated by Grignard reagents, alkali- or aluminum organyls will be referred to as classical anionic polymerization.<sup>[6]</sup>

## 2. Radical and Classical Anionic Vinylphosphonate Polymerization

For clarity, the scope of this article is to show the advantages of rare earth metal-mediated GTP of vinylphosphonates in comparison to classic anionic or radical approaches; for a detailed overview on both synthesis and application of PVPA and its derivatives, for example, poly(vinylphosphonate)s, the reader is directed towards a recent review by Macarie and Iliu.<sup>[4d]</sup>

Preparative routes for the synthesis of vinylphosphonates have been known since the late 1940s, with the first radical polymerization experiments reported shortly after. However, these polymerizations were either unsuccessful or afforded insufficiently characterized, oligomeric materials.<sup>[7]</sup> Later attempts confirmed independently the poor polymerizability of vinylphosphonates by radical means, which failed to yield high-molecular-weight polymers,

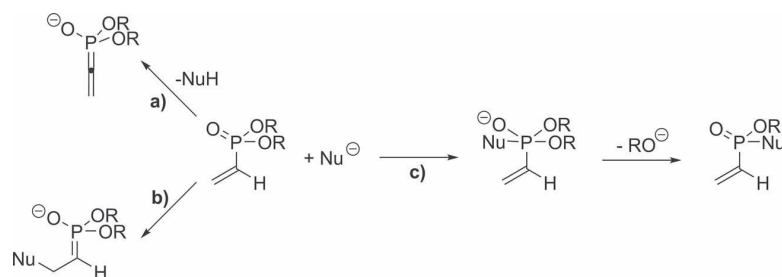


**Scheme 1.** Intramolecular hydrogen transfer from the backbone to the side chain with formation of thermally labile P–O–C bonds during radical polymerization of diisopropyl vinylphosphonate (DIVP) (R = polymer chain).

produced many side products and exhibited incomplete conversion of the monomer.<sup>[8]</sup> In 2008, Hirano and co-workers achieved quantitative conversion of dimethyl vinylphosphonate (DMVP) in bulk with dicumyl peroxide at 130 °C, however, only low-molecular-weight polymers ( $\bar{M}_n < 3.5 \text{ kg mol}^{-1}$ ) were afforded.<sup>[9]</sup>

ESI MS end-group analysis of vinylphosphonate oligomers, synthesized radically with different initiators, revealed that the initiation proceeds via chain transfer from initiator to monomer (hydrogen abstraction).<sup>[10]</sup> The underlying stability of the activated monomer radical and the readily occurring radical abstraction of the  $\alpha$ -CH and side chain protons lead to rapid transfer reactions dominating the chain growth.<sup>[10,11]</sup> The intramolecular hydrogen transfer from side group protons to the backbone radical leads to thermally labile P–O–C bonds in the main chain (Scheme 1), the cleavage of which inhibits the formation of higher-molecular-weight polymers as observed by ESI MS analysis.<sup>[10]</sup> The reaction of initiator radicals with, as well as transfer reactions to the side chains may lead to a local increase of the radical concentration along the polymer chain. This facilitates recombination reactions, explaining the slow rate and the low observed yields of both free and controlled radical vinylphosphonate polymerization.<sup>[4d,11]</sup>

An exception to these poor polymerization results is the synthesis of PVPA, which can be obtained either by free-radical polymerization of vinylphosphonic acid dichloride and its subsequent hydrolysis or directly from vinylphosphonic acid. Therefore, this is the only product, which has commercial applications, for example as binders in



**Scheme 2.** Possible reactions of a vinylphosphonate with a nucleophile: a) abstraction of the acidic  $\alpha$ -CH, b) nucleophilic addition at the double bond, c) nucleophilic addition at the phosphorus and subsequent elimination of an alkoxy group.

bone and dental concrete.<sup>[3m–n,4d,11]</sup> However, the products obtained are very ill defined, with low-to-moderate molecular weight ( $< 62 \text{ kg mol}^{-1}$ ), irregular chain structure, and broad polydispersities.<sup>[3e,4d,8c]</sup>

Anionic polymerizations of vinylphosphonic esters are generally more successful than any method involving radicals,

but are still by no means trivial. First attempts in the early 1960s, using lithium and aluminium alkyls as initiators only provided oligomeric materials.<sup>[7f]</sup> Some improvements were made in the 1970s, however, obtaining poorly characterized polymeric material.<sup>[12]</sup> After these very few publications, the topic was then abandoned for many years until in 1988 Gopalkrishnan reported on successfully performed anionic polymerizations of vinylphosphonates.<sup>[13]</sup> This work was disregarded until 2008, when Parvole and Jannasch grafted poly(diethyl vinylphosphonate) (PDEVVP) onto polysulfones by activation with butyllithium and 1,1-diphenylethylene (DPE) and tested the resulting copolymers for their application as highly proton conducting membranes for fuel cells.<sup>[3g]</sup>

The usage of DPE as coinitiator proved to be essential, as demonstrated by poor polymerization results in the works of Leute and Bingöl in 2007 (without usage of DPE). While Bingöl stated that anionic polymerization of vinylphosphonic esters was impossible, Leute could isolate oligomeric materials, obtaining best results by polymerization in toluene using *n*- or *sec*-BuLi as initiator.<sup>[3e,11]</sup> Similar to the results of radical polymerizations, an initiation by abstraction of the acidic  $\alpha$ -CH was observed to be competing with an initiation by nucleophilic addition to the double bond (Scheme 2a and b).<sup>[11]</sup>

In 2009, Jannasch and co-workers reported a method to produce polystyrene-poly(diethyl vinylphosphonate) (PS-PDEVVP) block copolymers by sequential anionic polymerization of styrene and DEVVP.<sup>[3j]</sup> Again, DPE was used to reduce the reactivity and nucleophilicity of the polystyrene-macroinitiator anion before the second monomer was added. Without DPE, neither copolymerization with styrene nor efficient homopolymerization of DEVVP was possible.<sup>[3j]</sup> In the same year, Meyer and co-workers independently made identical observations for the polymerization of dimethyl and diisopropyl vinylphosphonate.<sup>[3j]</sup>

These results are in line with the general reactivity of DPE, which is commonly used as a coinitiator for anionic (meth)acrylate polymerizations.<sup>[14]</sup> Jannasch and co-workers conclude that DPE suppresses a nucleophilic attack



■ Scheme 3. Structural and electronic similarity of vinylphosphonates and (meth)acrylates.

of the initiator at the phosphorus atom of DEVP, which would result in a substitution reaction and therefore lead to either chain transfer or termination (Scheme 2c).<sup>[3j]</sup> The higher stability of the DPE anion may also inhibit deprotonation of the acidic  $\alpha$ -CH as observed by Leute.<sup>[11]</sup> An addition of DPE is not necessary if the initiating species is not reactive enough to undergo the described side reactions, as observed by Jannasch and co-workers in 2010 for a benzyllithium-macroinitiator during a study for grafting PDEVp onto poly(phenylene oxide).<sup>[3k]</sup>

Despite this recent success, classical anionic polymerization of vinylphosphonates still faces substantial limitations. To date, using this method, no polymers with a molecular weight ( $\bar{M}_n$ ) above  $100 \text{ kg mol}^{-1}$  have been synthesized and the obtained poly(vinylphosphonate)s show a broad molecular weight distribution, even if polymerization is carried out at  $-78 \text{ }^\circ\text{C}$ .<sup>[3j,15]</sup> The broad polydispersity may be attributed to a rather slow initiation, as even after 4 h reaction time at room temperature, the BuLi-DPE initiator complex was found to be co-existing with the growing homopolymer.<sup>[3j]</sup>

At temperatures higher than  $-78 \text{ }^\circ\text{C}$ , a well-controlled polymerization is not possible and either oligomers or polymeric materials with an even broader molecular weight distribution are obtained ( $\text{PDI} > 3$ ).<sup>[11,15]</sup> The rate of polymerization was not exactly determined, but, as indicated by long reaction times until full monomer conversion, this must be quite low. This may be attributed to a resonance stabilization of the anionic chain end by the phosphonate moiety, decreasing the chain end reactivity.<sup>[11]</sup>

Furthermore, the control of stereoregularity using classical anionic polymerization techniques is limited and only possible at very low temperatures. Only minor success was achieved by Kawauchi et al. raising the isotacticity to 67% *meso*-dyads by *t*-BuLi-initiated polymerization

of DMVP at  $-78 \text{ }^\circ\text{C}$ , in comparison to 59% *meso*-dyads for PDMVP obtained by free-radical polymerization.<sup>[15,16]</sup>

However, control of polymer tacticity is essential for optimizing mechanical properties, controlling phase separation in copolymers and polymer blends or other material properties such as proton conductivity.<sup>[3j]</sup> In the case of PVPA, this proton conductivity may be affected by association of the phosphonic acid moieties via hydrogen bonds or anhydride formation at elevated temperatures, which in turn depend on chain tacticity and molecular weight.<sup>[3j]</sup> In order to investigate these influences and optimize the material properties, the synthesis of PVPA and poly(vinylphosphonate)s of defined molecular weight, narrow polydispersity, and tuneable tacticity is required. Thus, further development of suitable polymerization techniques for vinylphosphonates is necessary.

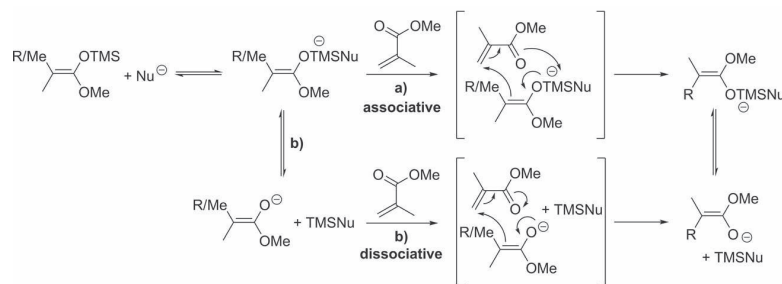
Motivated by this necessity, our group investigated the suitability of rare earth metal compounds for a catalytic polymerization of vinylphosphonate esters. Our research was inspired by the structural and electronic similarity of vinylphosphonates to (meth)acrylates (Scheme 3), for which a rare earth metal-mediated GTP is well established, combining high activity and control of polymer tacticity with a living-type polymerization.<sup>[6]</sup>

### 3. Rare Earth Metal-Mediated GTP

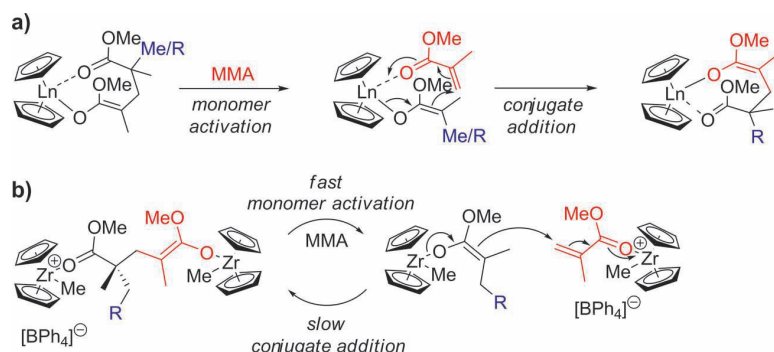
At this point, a brief introduction to GTP will be given, considering mechanisms, presenting selected catalyst systems and clarifying the terminology of catalyst versus initiator. For a detailed overview of both silyl ketene acetal-initiated GTP (SKA-GTP) and transition metal-mediated, coordinative-anionic addition polymerizations, i.e., transition metal-mediated GTPs, numerous comprehensive reviews can be recommended.<sup>[6,17]</sup>

In the mid 1970s, DuPont investigated classical anionic polymerization of methacrylates at  $-80 \text{ }^\circ\text{C}$ , but due to the high cost of refrigeration the project was abandoned.<sup>[17d,18]</sup>

Searching for an alternative process operable at higher temperatures, DuPont started that the development of a trimethylsilyl ketene acetal-initiated polymerization catalyzed by nucleophilic anions.<sup>[17d,19]</sup> At the time, it was proposed that the trimethylsilyl group was transferring to a monomer as it was adding to the growing polymer chain end (Scheme 4a), and therefore the new process was named GTP.<sup>[19]</sup> Although based on the evidence available this associative mechanism is very



■ Scheme 4. a) Associative and b) dissociative mechanism of silyl ketene acetal-mediated group transfer polymerization (SKA-GTP) of MMA (R = polymer chain).



**Scheme 5.** a) Monometallic and b) bimetallic chain propagation for transition metal-mediated group transfer polymerization (R = polymer chain).

unlikely, the name GTP proceeded to be used in chemical literature.<sup>[17d]</sup> The probably occurring dissociative mechanism shows that silyl ketene acetal-mediated GTP can also be understood as a particular form of anionic polymerization (Scheme 4b).<sup>[17d,20]</sup>

In 1992, two independent communications reported on living polymerizations of acrylic monomers using transition metal initiators: the neutral samarocene  $[\text{Cp}^*_2\text{SmH}]_2$  presented by Yasuda et al. as well as a two-component Group 4 metallocene system reported by Collins and Ward.<sup>[21]</sup> The reaction proceeds in both cases via repeated conjugate addition involving either one or two coordinating metal complexes (Scheme 5a and b).<sup>[6,17e–h,21]</sup> This type of polymerization is known as coordinative-anionic addition polymerization and due to its similarity to SKA-GTP, it is also referred to as transition metal-mediated GTP.

The initiation of this type of polymerization usually occurs via transfer of a nucleophilic ligand from the metal complex to a coordinated monomer (this is not the case for divalent lanthanide complexes, where redox initiation takes place).<sup>[6]</sup> As the metal complex also activates the monomers and therefore catalyzes the propagation reaction,

it serves both as an initiator and as a catalyst (in contrast to SKA-GTP, where a nucleophile is added as a catalyst).<sup>[6,17d]</sup> However, catalytic polymerizations are defined by exhibiting turn over numbers, TONs, for both monomer conversion and polymer chain production, that means, a polymerization catalyst must produce more than one polymer chain.<sup>[6]</sup> Therefore, living polymerizations, for example, GTP, are per se not catalytic. To overcome this terminology conflict, according to previous literature, this article uses the term “catalyst” only concerning the catalyzed monomer addition.<sup>[6]</sup>

The works of Collins, Ward, and Yasuda et al. indicate the start of a paradigm shift in early transition metal polymerization catalysis of polar, heteroatom-functionalized vinyl monomers. Instead of protection of the functional group and introduction of high steric constraints at the active site — to ensure monomer–metal coordination via the double bond following a migratory insertion polymerization mechanism — the metal center remains easily accessible and the coordination occurs via the heteroatom.<sup>[6,21]</sup>

Rare earth metal-mediated GTP follows a monometallic propagation mechanism via an eight-membered ring intermediate, through which the catalyst is transferred to the functional group of the added monomer (Scheme 5a).<sup>[6,17e–h]</sup> Hereby, the catalyst both stabilizes the growing chain end and activates the coordinated monomer. Catalysis by Group 4-based compounds either follows this monometallic or a bimetallic mechanism, for which alternating one metal center bears the growing chain end, while the other activates the monomer (Scheme 5b).<sup>[6]</sup> The stabilization of the growing chain end and activation of the monomer decrease side reactions such as chain transfer or termination, allowing a well-controlled polymerization even at higher temperatures. For these reasons, coordinative-anionic addition polymerization can

provide much higher activity in comparison to other living polymerizations and simultaneously yield well-defined materials with narrow polydispersity.<sup>[6]</sup>

The coordination of the catalyst on the growing chain end allows stereospecific polymerization and activity optimization by variation of the metal center and the catalyst ligand sphere.<sup>[6,17e–h]</sup> The number of described catalyst systems is extremely large, some explicit catalysts for stereospecific rare earth metal-mediated GTP of MMA are summarized in Figure 2.<sup>[6]</sup> Besides GTP, rare earth metal complexes are widely used

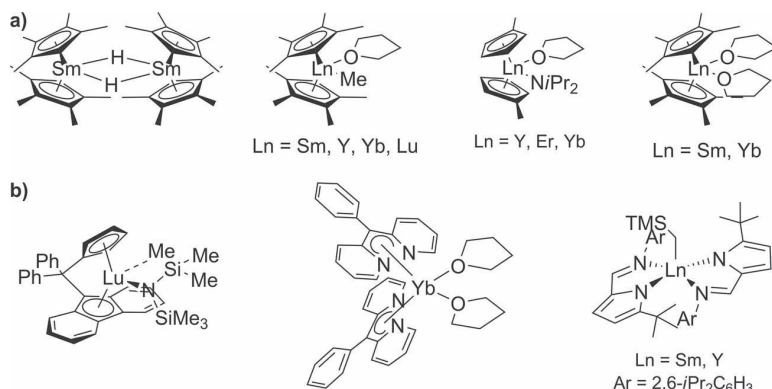


**Figure 2.** Selected catalysts for a) syndio- and b) isospecific rare earth metal-mediated group transfer polymerization of MMA.

for olefin, diene, and (syndiospecific) styrene migratory-insertion polymerizations as well as for living ring-opening polymerizations of lactones, lactides, cyclic ethers, and carbonates.<sup>[17e–h,22]</sup> Using a one-directional mechanistic crossover, these different polymerization methods can be combined in a living fashion, further increasing the versatility of organo-rare earth metal compounds for the synthesis of functional high value polymers.<sup>[6]</sup>

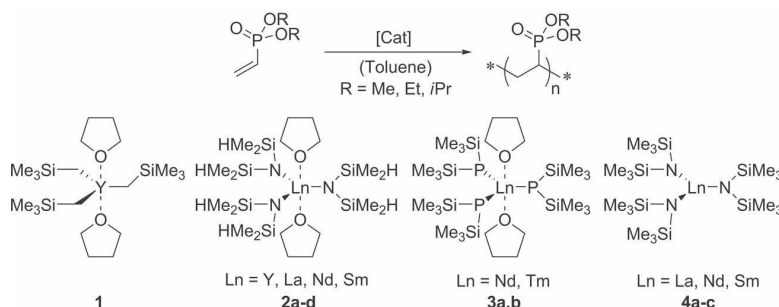
The sensitivity of Group 3 and Group 4 complexes to water and other protic impurities is the major disadvantage of this type of polymerization. However, classical anionic and early transition metal migratory insertion polymerizations face the same limitations.

On both SKA- as well as transition metal-mediated GTP, intensive research has been carried out over the past decades, optimizing reaction conditions, initiator efficiency, and control over stereoregularity, on the use of different metals, as well as on their implementation to a broad variety of monomers, for example, different (meth)acrylates and (meth)acrylamides.<sup>[6,17]</sup> However, Hertler showed in 1991, that SKA-GTP of vinylphosphonates is not possible, and subsequent SKA-GTP of MMA and DEVP lead to end-capping of PMMA chains by exactly one phosphonate monomer.<sup>[23]</sup> To date, there are no reports on successfully performed coordinative-anionic addition polymerizations of vinylphosphonates applying any other metals than rare earth elements.

## 4. Rare Earth Metal-Mediated GTP of Vinylphosphonates

### 4.1. First Examination of Rare Earth Metal Complexes for Vinylphosphonate Polymerization

In 2007, our group reported on catalytic polymerizations of dialkyl vinylphosphonates (alkyl = methyl, isopropyl) using rare earth metal complexes comprising monodentate  $\sigma$ -donor ligands (Scheme 6, complex **1**, **2a–d**).<sup>[11,24]</sup> Hereby, the diisopropyl monomer could only be oligomerized, while polymerization of the dimethyl monomer was limited by the poor solubility of poly(dimethyl vinylphosphonate) (PDMVP) in suitable solvents, such as THF or toluene, which inhibited the formation of higher molecular weight polymers. Using the hardly active  $Y(bdsa)_3(THF)_2$  complex (**2a**), exchange of the THF ligands by DMVP was observed. <sup>1</sup>H and <sup>31</sup>P NMR spectroscopic data revealed that both DMVP ligands coordinate in the *trans* position via

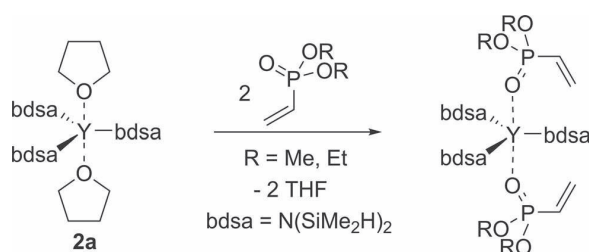


**Scheme 6.** First rare earth metal complexes for catalytic polymerization of vinylphosphonates by Leute (**1**), Dengler (**1**, **2a–d**) and Rabe et al. (**1**, **2a–d**, **3a**, **3b**, **4a–c**).

the oxygen atom of the phosphonate moiety, not via the double bond (Scheme 7).<sup>[24]</sup> Therefore, a GTP mechanism was proposed to take place.<sup>[11,24]</sup>

In a later study, the same type of complexes (Scheme 6) was used for the synthesis of PDEV, which is significantly more soluble in toluene and THF than PDMVP.<sup>[25]</sup> Using the readily available *tris*(alkyl) compound  $Y(CH_2SiMe_3)_3(THF)_2$  (**1**), as well as the *tris*(phosphanide) complexes  $Ln(P(SiMe_3)_2)_3(THF)_2$  ( $Ln = Nd, Tm$ ; **3a**, **3b**), only DEVP oligomers could be obtained in form of viscous oils. The *tris*(amides)  $Ln(btsa)_3$  ( $Ln = La, Nd, Sm$ ; **4a–c**), in contrast, were found to yield solid, colorless materials; however, all these catalysts lead to incomplete conversion of the monomer.<sup>[25]</sup>

Reducing the steric demand of the amide by using the *bdsa*- instead of the very bulky *btsa*-ligand ( $Ln(bdsa)_3(THF)_2$ ,  $Ln = La, Nd, Sm$ ; **2b–d**), PDEV could be obtained in more than 80% yield in toluene solution.<sup>[25]</sup> Careful NMR spectroscopic microstructure analysis revealed that, using the corresponding Sm and Nd complexes (**2c** and **2d**), poly(vinylphosphonate)s with unprecedented isotacticity were obtained ( $m = 95%$ ,  $mm = 79%$ ).<sup>[25]</sup> This evidence for a strong coordination of the phosphonate at the rare earth metal complex



**Scheme 7.** Exchange of THF at  $Y(bdsa)_3(THF)_2$  by addition of dimethyl or diethyl vinylphosphonate (DMVP or DEVP, respectively) as observed by <sup>1</sup>H and <sup>31</sup>P NMR spectroscopic measurements.



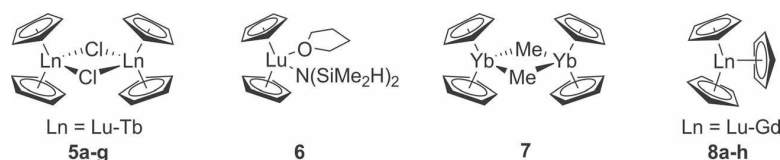


**Figure 3.** Lanthanide metallocenes applied for rare earth metal-mediated group transfer polymerization of vinylphosphonates.

indicates that polymerization does not follow a classical anionic-, but rather a coordinative-anionic (i.e., a GTP) mechanism. Similarly to our results, Y(bdsa)<sub>3</sub>(THF)<sub>2</sub> (**2a**) was found to not initiate DEVP polymerization, but to form Y(bdsa)<sub>3</sub>(DEVP)<sub>2</sub>, as confirmed by <sup>1</sup>H and <sup>31</sup>P NMR spectroscopies (Scheme 7). However, single-crystalline material for structural analysis could not be obtained.<sup>[25]</sup>

These findings have shown that rare earth metal complexes are principally feasible for poly(vinylphosphonate) synthesis, allowing polymerization in a stereospecific manner.<sup>[11,24,25]</sup> Fairly high molecular weights can be achieved, if the right combination of rare earth cation and ancillary ligands is used. However, the activity of complexes with monodentate  $\sigma$ -donor ligands is still quite low, and the observed polydispersities are very broad (PDI > 3), indicating either a non-uniform, that is, slow, initiation or an initiation by more than one of the  $\sigma$ -donor ligands.<sup>[11,24,25]</sup> It could not be shown if polymerization with the described catalysts proceeds in a living fashion, which is an essential observation to support the assumption of a GTP mechanism.

Our group carried out further investigations on the variation of rare earth cation and coordination sphere to optimize both initiator efficiency as well as the activity of the applied complexes and to prove whether rare earth metal-mediated polymerization of vinylphosphonates exhibits a living character or not.

#### 4.2. Vinylphosphonate Polymerizations catalyzed by Late Lanthanide Metallocenes

In 2010, we reported on the first use of late lanthanide metallocenes for vinylphosphonate polymerization (Figure 3).<sup>[5a,26]</sup> We initially tested a series of *bis*(cyclopentadienyl) chloride complexes for polymerization of diethyl vinylphosphonate and obtained polymers with high molecular weight ( $\bar{M}_w$ ) up to 1000 kg mol<sup>-1</sup> (Table 1).<sup>[26]</sup> Complete conversion was achieved at room temperature within 1 h for metals in the series Lu-Er (**5a-d**), with a distinct initiation period and subsequent fast polymerization, showing increasing rate of conversion with decreasing radius of the metal center (Figure 4a).<sup>[5a,26]</sup> These findings are in contrast to methyl methacrylate (MMA) polymerization, for which *bis*(cyclopentadienyl) rare earth metal chloride complexes display only very limited activity (TOF up to 7 h<sup>-1</sup>).<sup>[6,27]</sup>

However, the obtained molecular weights were not consistent with the initial monomer to catalyst ratio, as expected for a living-type polymerization.<sup>[5a,26]</sup> In fact, the molecular weights observed were much higher, indicating low initiator efficiency (Table 1). Yet, for the first time, poly(vinylphosphonate)s with

high molecular weight (above 100 kg mol<sup>-1</sup>) and narrow molecular weight distribution (PDI = 1.10–1.30) could be obtained, as observed by absolute determination via GPC-MALS.<sup>[26]</sup>

By raising the polymerization temperature to 70 °C, complete monomer conversion within 1 h could also be achieved for the earlier lanthanides Ho, Dy, and Tb. Furthermore, the corresponding initiator efficiencies are significantly higher than for polymerizations conducted at room temperature (Table 1).<sup>[26]</sup> A more detailed study using the Cp<sub>2</sub>YbCl complex (**5b**) revealed that the initiation can be significantly accelerated by higher polymerization temperature, but surprisingly, the molecular weight of the product was not affected by the initial monomer to catalyst ratio (Table 2).<sup>[5a]</sup> Similar results were obtained for the amido complex Cp<sub>2</sub>Lu(bdsa)(THF) (**6**) (Table 2, Entries 10–12).<sup>[26]</sup>

**Table 1.** Polymerization of DEVP with Cp<sub>2</sub>LnCl (toluene, monomer-to-catalyst ratio: 200).

Entry	Element	T <sub>p</sub> <sup>a)</sup> [ °C ]	$\bar{M}_w$ <sup>b)</sup> [ kg mol <sup>-1</sup> ]	$\bar{M}_n$ <sup>b)</sup> [ kg mol <sup>-1</sup> ]	PDI <sup>b)</sup>	I <sup>†c)</sup> [%]	Yield <sup>d)</sup> [%]
1	Lu	30	1000	930	1.10	3.5	93
2	Yb	30	1000	830	1.20	4.0	98
3	Tm	30	890	810	1.10	4.0	85
4	Er	30	590	460	1.30	7.1	92
5	Ho	30	840	700	1.20	<sup>-e)</sup>	43
6	Dy	30	780	670	1.20	<sup>-e)</sup>	49
7	Lu	70	470	380	1.25	8.6	99
8	Yb	70	480	370	1.30	8.9	90
9	Tm	70	400	335	1.20	9.8	98
10	Er	70	470	390	1.20	8.4	96
11	Ho	70	375	300	1.25	10.9	93
12	Dy	70	310	210	1.45	15.6	99
13	Tb	70	155	105	1.50	31.2	84

<sup>a)</sup>Polymerization temperature; <sup>b)</sup>determined by GPC-MALS; <sup>c)</sup>I<sup>†</sup> =  $M_{exp}/M_n$ , I<sup>†</sup> = initiator efficiency,  $M_{exp}$  = expected molecular weight, based on living polymerization calculation; <sup>d)</sup>determined by weighing of the components; <sup>e)</sup>not calculated due to incomplete conversion.

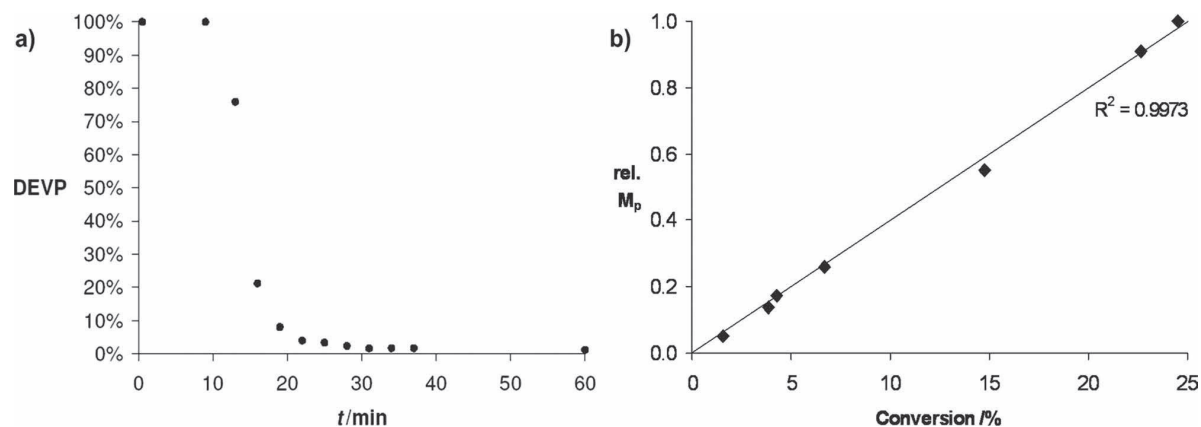


**Figure 4.** a) Monomer conversion for polymerization of DEVP with  $Cp_2YbCl$  (**5b**) at 30 °C in  $C_6D_6$ , as observed by  $^1H$  NMR spectroscopy, exhibiting a distinct initiation period of approx. 10 min; b) linear growth of the relative peak molecular weight upon monomer conversion for polymerization of DEVP with  $Cp_2YbMe$  (**7**) at -10 °C in toluene, as observed by  $^{31}P$  NMR spectroscopy and GPC.

The combination of the observed latency time with the strong dependence of the temperature on the obtained degree of polymerization gives evidence for a slow initiation process. This conclusion is supported by an observed increase of polydispersity during the polymerization and is in accordance with expectation due to the strong bonding of the chloride or amide ligand at the rare earth metal center.<sup>[26]</sup> An increase of the polymerization temperature facilitates the cleavage of these bonds accelerating the rate of initiation. The independence of the obtained molecular

weight on the initial monomer to catalyst ratio and the underlying increase of the initiator efficiency are in good agreement with the assumption of a slow initiation, as the longer reaction times necessary for full monomer conversion allow more catalyst molecules to be activated.

Despite this slow initiation, the fast polymerization rate leads to the formation of polymers with low polydispersity, yet in accordance with the observed low initiator efficiencies. As a consequence of this, with both the chloro- and the amido-metallocenes, it was impossible to perform reliable kinetic studies in order to prove a living-type polymerization. For this purpose, a catalytic system with a faster and simultaneous initiation is required.

In view of this requirement, polymerizations were performed with the *bis*(cyclopentadienyl) methyl species [i.e.,  $Cp_2YbMe$  (**7**)], yielding polymers with molecular weights which corresponded significantly better to the initial monomer to catalyst ratio (Table 3).<sup>[5a,26]</sup> Again, the initiator efficiency was found to be strongly dependent on the polymerization temperature, reaching near complete

**Table 2.** Influence of temperature and monomer-to-catalyst ratio on the obtained molecular weight for polymerization of DEVP in toluene.

Entry	Catalyst	$T_p$ <sup>a)</sup> [ °C ]	Monomer <sup>b)</sup>	$\bar{M}_w$ <sup>c)</sup> [ kg mol <sup>-1</sup> ]	Yield <sup>d)</sup> [ % ]
1	5b	30	50	1010 <sup>d)</sup>	98
2	5b	30	100	865 <sup>d)</sup>	99
3	5b	30	200	983 <sup>d)</sup>	94
4	5b	30	400	1280 <sup>d)</sup>	97
5	5b	-18	200	–	0
6	5b	0	200	1230 <sup>d)</sup>	98
7	5b	50	200	545 <sup>d)</sup>	91
8	5b	70	200	364 <sup>d)</sup>	75
9	5b	90	200	201 <sup>d)</sup>	58
10	6	30	200	779 <sup>e)</sup>	86
11	6	30	400	785 <sup>e)</sup>	88
12	6	70	200	432 <sup>e)</sup>	74

<sup>a)</sup>Polymerization temperature; <sup>b)</sup>monomer-to-catalyst ratio; <sup>c)</sup>determined by weighing of the components; <sup>d)</sup>determined by static light scattering in batch, using Zimm plots; <sup>e)</sup>determined by GPC-MALS.

**Table 3.** Polymerization of DEVP with  $Cp_2YbMe$  in toluene.

Entry	$T_p$ <sup>a)</sup> [ °C ]	Monomer <sup>b)</sup>	$\bar{M}_w$ <sup>c)</sup> [ kg mol <sup>-1</sup> ]	$\bar{M}_n$ <sup>c)</sup> [ kg mol <sup>-1</sup> ]	PDI <sup>c)</sup>	$f$ <sup>d)</sup> [ % ]	Yield <sup>e)</sup> [ % ]
1	-10	200	109	84	1.3	39	87
2	30	200	88	75	1.2	44	92
3	30	400	118	92	1.2	71	96
4	70	200	47	38	1.3	86	88

<sup>a)</sup>Polymerization temperature; <sup>b)</sup>monomer-to-catalyst ratio; <sup>c)</sup>determined by GPC-MALS; <sup>d)</sup> $f = M_{exp}/\bar{M}_n$ ,  $f$  = initiator efficiency,  $M_{exp}$  = expected molecular weight, based on living polymerization calculation; <sup>e)</sup>determined by weighing of the components.

catalyst activation at 70 °C ( $I^* = 86\%$ , Table 3, Entry 4).<sup>[26]</sup> Performing polymerization of DEVP at -10 °C using **7**, linear growth of the relative peak molecular weight  $M_p$  upon monomer conversion could be observed (Figure 4b), as determined by GPC and <sup>31</sup>P NMR spectroscopy, thus giving critical evidence for the hypothesis of a living-type polymerization, that is, a rare earth metal-mediated GTP.<sup>[5a]</sup>

Besides DEVP, other simple dialkyl vinylphosphonate monomers were tested for polymerization with late lanthanide metallocenes, for example, DMVP and diisopropyl vinylphosphonate.<sup>[26]</sup> Both monomers can be polymerized using rare earth metal complexes as initiators. Specifically DMVP showed high conversion rates, however, as described above, the limiting factor is the low solubility of the resulting polymer in solvents suitable for this polymerization technique. PDMVP precipitates almost immediately after formation from toluene (or THF) solution with a molecular weight ( $\bar{M}_w$ ) below 50 kg mol<sup>-1</sup> (determined by static light scattering, using Zimm Plots).<sup>[3j,5b]</sup>

Polymerization of DIVP was found to proceed slower than with DMVP or DEVP, but produces materials with high molecular weights, which correspond better to the initial monomer to catalyst ratio (Table 4).<sup>[26]</sup> This may be explained by the higher steric demand of the side chains, hindering coordination at the active site, and therefore decreasing the rate of polymerization (in contrast to the rate of initiation, which is proposed to be only slightly affected).<sup>[26]</sup> Contrary to DEVP polymerization, in case of DIVP, the lutetium species was the only *bis*(cyclopentadienyl) chloro complex for which a polymeric product could be isolated after several hours of polymerization time.<sup>[26]</sup> Quantitative precipitation of the polymer with hexane was impossible due to the increased solubility of PDIVP in nonpolar solvents leading to the observed low yields, generally between 30% and 60%.<sup>[5b,26]</sup>

Polymerization of diethyl 1-methylvinylphosphonate (DEMVP) was not feasible with the applied rare earth

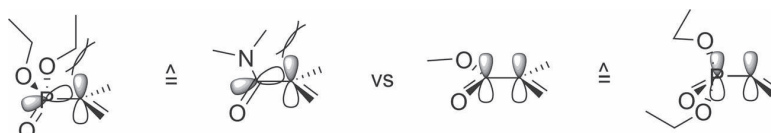


**Figure 5.** Torsion of the C–C or C–P single bond by steric repulsion disturbing the planarity of the Michael system for diethyl 1-methylvinylphosphonate (DEMVP), *N,N*-dimethyl acrylamide (DMAA); in comparison to methyl methacrylate (MMA) and diethyl vinylphosphonate (DEVP) (from left to right).

metal catalysts.<sup>[24,25,26]</sup> Mass spectrometric analysis revealed that not even oligomers were formed.<sup>[26]</sup> It was proposed that the steric repulsion DEMVP at the active site may either totally hinder coordination or lead to a conformational change in the DEMVP moiety disturbing the  $\pi$ -overlap between the P=O and the C=C double bond.<sup>[26,28]</sup> Similar observations were made for different methacrylamides, that is, those for which the steric repulsion of the  $\alpha$ -methyl with the *N*-alkyl groups leads to a torsion of the C–C single bond thereby disturbing the molecules planarity (such as *N,N*-dimethyl methacrylamide (DMAA), Figure 5).<sup>[6,29]</sup>

### 4.3. Copolymerization of Vinylphosphonates with Methyl Methacrylate

To provide further evidence for a living-type polymerization and to support the hypothesis of a rare earth metal-mediated GTP mechanism, copolymerization studies were conducted with a monomer that is acknowledged to undergo polymerization in a GTP fashion. For this purpose, a series of polymerizations of diethyl vinylphosphonate and MMA was performed using the rapidly initiating Cp<sub>2</sub>YbMe complex **7**.<sup>[5a,26]</sup> As described above, previous attempts of copolymerization of these monomers lead only to end-capping of a PMMA chain by a single vinylphosphonate.<sup>[23]</sup>

In our studies, we first investigated the formation of block copolymers via sequential addition of the two monomers. If DEVP was used as the first monomer, a subsequent polymerization of MMA was impossible and the obtained polymer product was found to be PDEVP homopolymer.<sup>[26]</sup> This was ascribed to the strong binding of phosphonates to the rare earth metal center inhibiting the coordination of an acrylic monomer at the active site. In contrast, it was possible to obtain MMA–DEVP copolymers in nearly quantitative yield by sequential monomer addition if MMA was used as the starting monomer (Table 5).<sup>[5a,26]</sup> Similar observations were made previously for coordinative-anionic block copolymerization of MMA and DMAA by an isoelectronic group 4 metallocenium cation, showing that the addition sequence is critical for two monomers with different binding strength to the metal center.<sup>[30]</sup>

The formation of block copolymers was verified by GPC and GPC-MALS analysis of both the initially formed

**Table 4.** Polymerization of DIVP (toluene, monomer-to-catalyst ratio: 200, 30 °C).

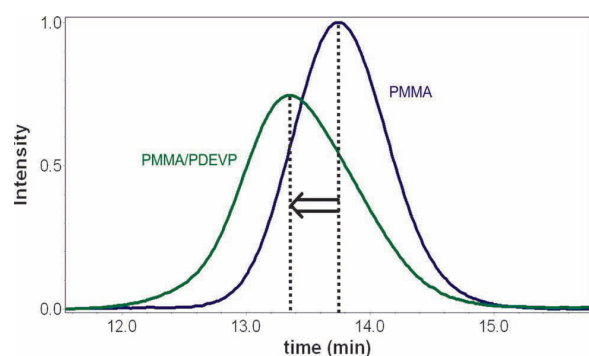
Entry	Catalyst	$\bar{M}_w^a$ [kg mol <sup>-1</sup> ]	$\bar{M}_n^a$ [kg mol <sup>-1</sup> ]	PDI <sup>a</sup>	$I^*^b$ [%]	Yield <sup>c</sup> [%]
1	5a	350	220	1.6	17	43
2	6	80	73	1.1	49	47
3	7	89	84	1.1	46	37

<sup>a</sup>determined by GPC-MALS; <sup>b</sup> $I^* = M_{exp}/\bar{M}_n$ ,  $I^*$  = initiator efficiency,  $M_{exp}$  = expected molecular weight, based on living polymerization calculation; <sup>c</sup>determined by weighing of the components.

■ Table 5. Sequential copolymerization of MMA and DEVP with  $\text{Cp}_2\text{YbMe}$  (toluene, 30 °C).

Entry	MMA <sup>a)</sup>	DEVP <sup>b)</sup>	$\overline{M}_w^c)$ [kg mol <sup>-1</sup> ]	$\overline{M}_n^c)$ [kg mol <sup>-1</sup> ]	PDI <sup>c)</sup>	$I^e)$ [%]	MMA/ DEVP <sup>e)</sup>	Yield <sup>f)</sup> [%]
1	100	–	14	12	1.1	83	–	98
2	100	100	24	22	1.2	120	1.15:1	94
3	100	–	15	13	1.2	77	–	97
4	200	200	60	52	1.1	82	n.d. <sup>g)</sup>	96
5	200	–	23	20	1.1	100	–	99
6	200	100	44	42	1.1	87	2.1:1	98
7	400	–	53	27	2.0	148	–	99
8	400	400	150	98	1.5	108	n.d. <sup>g)</sup>	99

<sup>a)</sup>MMA-to-catalyst ratio; <sup>b)</sup>DEVP-to-catalyst ratio; <sup>c)</sup>determined by GPC-MALS; <sup>d)</sup> $I^e = M_{\text{exp}}/\overline{M}_n$ ,  $I^e$  = initiator efficiency,  $M_{\text{exp}}$  = expected molecular weight, based on living polymerization calculation; <sup>e)</sup>MMA/DEVP ratio in polymer product, determined by <sup>1</sup>H NMR spectroscopy; <sup>f)</sup>determined by weighing of the components; <sup>g)</sup>not determined.



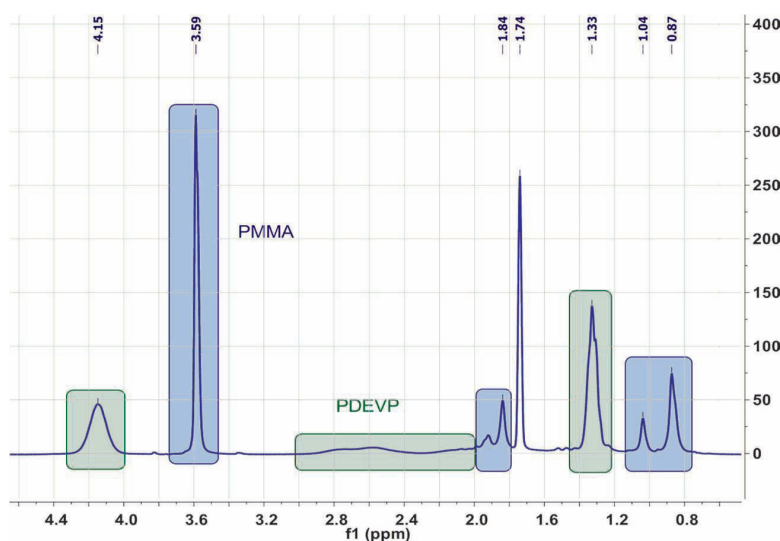
■ Figure 6. GPC elograms for the initial PMMA<sub>200</sub> block (blue) and the corresponding P(MMA<sub>200</sub>-*b*-DEVP<sub>100</sub>) copolymer (green).

PMMA block as well as of the copolymer (Figure 6). The products were found to exhibit narrow polydispersities, with molecular weights being in good agreement with the initial monomer to catalyst ratio (indicating high initiator efficiency).<sup>[26]</sup> An increase of the molecular weight after addition of the second monomer was evident and the crossover to the second monomer (or respectively the initiator efficiency of the (catalyst-bound) PMMA block for DEVP polymerization) was found to be nearly quantitative, as the copolymer analysis revealed monomodal molecular weight distributions (Figure 6).<sup>[26]</sup> The occasional observation of trace amounts of homo-PMMA (which is observed as a minor shoulder on the GPC elution peak) may be attributed to termination during

addition of the second monomer by the residual water in the hygroscopic DEVP (even after drying with calcium hydride, subsequent distillation, and storage under argon atmosphere).

In order to prove the homogeneity of the polymer product, aqueous extraction experiments were carried out with the P(MMA<sub>100</sub>-*b*-DEVP<sub>100</sub>) copolymer, as it showed appreciable solubility in water.<sup>[5a,26]</sup> The aqueous fraction, the residue as well as the initial product showed the same composition, being in good agreement with the initial comonomer ratio, as observed by <sup>1</sup>H NMR spectroscopy (Table 5, Figure 7).<sup>[26]</sup>

A statistical copolymerization by simultaneous addition of MMA and DEVP to the catalyst solution could not be achieved. Similar to the results of DEVP–MMA sequential



■ Figure 7. <sup>1</sup>H NMR spectrum of the aqueous extract of P(MMA<sub>100</sub>-*b*-DEVP<sub>100</sub>) in THF-d<sub>8</sub>, showing characteristic signals corresponding to both PMMA (blue) and PDEVP (green).

copolymerizations, only the formation of PDEVF homopolymers could be observed. Neither incorporation of MMA nor the simultaneous formation of PMMA homopolymers occurred.<sup>[26]</sup> Again, this was attributed to the strong coordination of the vinylphosphonate, and thus of the growing PDEVF chain at the rare earth metal.

It was previously proven that in case of early transition metals, mechanistic crossover is only possible in one direction from coordination-insertion (i.e. migratory insertion) to coordination-addition (i.e. coordinative-anionic) polymerization and not vice versa.<sup>[6]</sup> As rare earth metal-mediated polymerization of MMA is known to proceed in a coordinative-anionic fashion, these results demonstrate that rare earth metal-mediated vinylphosphonate polymerization cannot follow an insertion polymerization mechanism.<sup>[6,17e-h]</sup>

As detailed above, previous NMR spectroscopic studies have shown coordination of vinylphosphonates at rare earth cations via the oxygen of the phosphonate moiety.<sup>[24,25]</sup> The conducted copolymerization studies provide evidence for the pronounced strength of this interaction. In combination with the possibility of stereoregular polymerization, these observations strongly support the hypothesis of a coordinative-anionic, i.e., a group transfer polymerization of vinylphosphonates. In addition, these copolymerization studies have shown that it is possible to form block copolymer structures with a complete crossover from MMA to DEVF (without formation of PDEVF homopolymer), giving further proof for the living character of rare earth metal-mediated vinylphosphonate polymerization.

#### 4.4. Easily Accessible Cp<sub>3</sub>Ln as an Efficient Initiator and Highly Active Catalyst

Synthesis of the described chloro- or amido-metallocenes (**5a-g**, **6**) is facile; however, they were found to exhibit only a slow and non-uniform initiation, leading to low initiator efficiencies, particularly for monomers with a fast polymerization reaction, such as DEVF. The corresponding methyl complexes, in contrast, show a faster and more simultaneous initiation, but are challenging to synthesize and in many cases, were found not to be stable for a prolonged time, especially in solution.<sup>[31]</sup> *Tris*(cyclopentadienyl) rare earth metal complexes (Cp<sub>3</sub>Ln), on the other hand, are easily accessible in high yields in a one-step reaction from the corresponding trivalent rare earth metal chlorides and cyclopentadienyl sodium (NaCp), and are structurally characterized for most of the rare earth metals (Ln: Ce-Lu).<sup>[32]</sup> However, these complexes have not been intensively studied as initiators for rare earth metal-mediated polymerizations.

Recently, we reported on the use of such *tris*(cyclopentadienyl) lanthanide complexes for vinylphosphonate polymerization, allowing a precise control

of molecular weight and molecular weight distribution of the polymer product.<sup>[5b]</sup> In the case of late lanthanides, a fast and simultaneous initiation was observed, as indicated by high initiator efficiencies and remarkably narrow polydispersities (Table 6 and 7). Thus, also for polymerization of DEVF with Cp<sub>3</sub>Lu (**8a**) at -10 °C, a linear growth of the molecular weight with conversion could be observed, as detected by <sup>31</sup>P NMR spectroscopy and GPC-MALS, proving the living character of polymerization with Cp<sub>3</sub>Ln complexes.<sup>[5b]</sup>

The initiation for these unusual catalysts was found to proceed by transfer of the cyclopentadienyl ligand to a coordinated monomer, as observed by ESI and MALDI-ToF MS analysis of produced dialkyl vinylphosphonate (alkyl = methyl, ethyl, isopropyl) oligomers, leading to a new and interesting chain-end functionalization.<sup>[5b]</sup> The possibility of this transfer was attributed to the rather small ionic radii of late trivalent rare earth metals and the steric demand of the cyclopentadienyl ligands. In such sterically crowded Cp<sub>3</sub>Ln complexes, it is unlikely that all three Cp ligands are bound to the metal center in a η<sup>5</sup>-fashion, as underlined by previous X-ray diffraction studies, which have shown that Cp<sub>3</sub>Lu (**8a**) is a polymeric material in the solid state, in which single Cp rings form η<sup>1</sup>(3)-Cp bridges between individual Cp<sub>2</sub>Lu moieties by η<sup>1</sup>-metal Cp bonding.<sup>[33]</sup>

Phosphonates, which are known to be strongly coordinating, two electron donating species, were believed to strengthen the η<sup>1</sup>(-σ)-character of the metal-Cp bond, thus allowing a nucleophilic transfer to a coordinated monomer (Scheme 8).<sup>[5b]</sup> This conclusion is supported by studies from Evans and co-workers with sterically crowded *tris*(pentamethylcyclopentadienyl) lanthanide complexes (Cp<sup>\*</sup><sub>3</sub>Ln, Ln = La, Ce, Pr, Nd, Sm), for which an equilibrium between η<sup>5</sup>- and η<sup>1</sup>-Cp<sup>\*</sup> metal bonding was observed.<sup>[34]</sup>

The larger metal radii of lighter rare earth metals result in sterically less crowded trivalent cyclopentadienyl complexes. This leads to a higher η<sup>5</sup>-character of the metal-Cp bond and therefore a lower nucleophilicity of the Cp<sup>-</sup> anion is expected, disfavoring its transfer to a monomer. Indeed, the initiator efficiency was found to be strongly decreasing for lighter rare earth metals, for example, for polymerization of DEVF at 30 °C from 58%–77% to 8%–24% in the series Lu to Dy (Table 6, Entries 1–3, 16–18).<sup>[5b]</sup> With Tb and the corresponding lighter metals, it was impossible to isolate polymeric material under these conditions.

Similarly to our previous results, owing to the longer reaction times until full monomer conversion, an increase of the monomer to catalyst ratio generally improved the efficiency of initiation [e.g., from 39% to 66% for Yb (Table 6, Entries 4–6)].<sup>[5b]</sup> By raising the reaction temperature to 70 °C, it was also possible to initiate the polymerization of DEVF with earlier lanthanides (Tb, Gd), but with

■ Table 6. Polymerization of DEVP with Cp<sub>3</sub>Ln (toluene, 30 °C).

Entry	Element	Monomer <sup>a)</sup>	Reaction time [h]	$\overline{M}_w$ <sup>b)</sup> [kg mol <sup>-1</sup> ]	$\overline{M}_n$ <sup>b)</sup> [kg mol <sup>-1</sup> ]	PDI <sup>b)</sup>	$I^*$ <sup>c)</sup> [%]	Yield <sup>d)</sup> [%]
1	Lu	200	1	60	57	1.05	58	88
2	Lu	400	1	110	100	1.10	66	99
3	Lu	800	1	210	170	1.26	77	99
4	Yb	200	1	93	83	1.12	39	94
5	Yb	400	1	140	120	1.16	55	93
6	Yb	800	1	230	200	1.15	66	97
7	Tm	200	1	120	100	1.22	33	89
8	Tm	400	1	200	170	1.20	38	93
9	Tm	800	1	230	190	1.16	69	96
10	Er	200	1	180	135	1.36	24	86
11	Er	400	1	260	210	1.25	31	95
12	Er	800	1	380	290	1.34	45	97
13	Ho	200	3	310	240	1.31	14	85
14	Ho	400	3	450	335	1.34	19	85
15	Ho	800	3	640	480	1.34	27	87
16	Dy	200	5	490	400	1.24	8	94
17	Dy	400	5	570	430	1.33	15	96
18	Dy	800	5	710	550	1.31	24	95

<sup>a)</sup>Monomer-to-catalyst ratio; <sup>b)</sup>determined by GPC-MALS; <sup>c)</sup> $I^* = M_{\text{exp}}/\overline{M}_n$ ,  $I^*$  = initiator efficiency,  $M_{\text{exp}}$  = expected molecular weight, based on living polymerization calculation; <sup>d)</sup>determined by weighing of the components.

low polymer yields. In addition, the efficiency of the slower initiating, lighter lanthanide complexes could be enhanced by higher polymerization temperatures, whereas this efficiency was not strongly affected for the fast-initiating, heavy lanthanides.<sup>[5b]</sup>

Cp<sub>3</sub>Ln-initiated polymerization of the sterically more demanding DIVP preceded more slowly, affording polymers, which molecular weight corresponds better to the initial monomer to catalyst ratio (Table 7).<sup>[5b]</sup> In this case, the higher initiator efficiency was attributed to both the slower chain growth (due to the stronger steric hindrance for the coordination of a DIVP monomer) and the absence

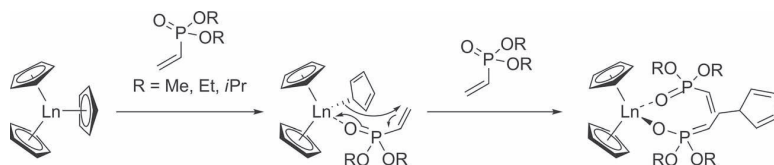
of an initiation period, which is observable for polymerization of DEVP (Figure 8).<sup>[5b]</sup> This initiation period was found to be considerably lengthened through the series Lu to Dy, that is, for increasing metal radius (Table 8). Thus, it was concluded that higher steric constraints (by a sterically more demanding monomer or a smaller rare earth metal) facilitate the nucleophilic transfer of a cyclopentadienyl ligand by destabilizing the reaction intermediate shown in Scheme 8.<sup>[5b]</sup>

Consequently, the initiator efficiency of tris(cyclopentadienyl) lanthanide complexes is strongly affected by the steric demand of the monomer and by

■ Table 7. Polymerization of DIVP with Cp<sub>3</sub>Ln (toluene, 30 °C, monomer-to-catalyst ratio: 200).

Entry	Element	Reaction time [h]	$\overline{M}_w$ <sup>a)</sup> [kg mol <sup>-1</sup> ]	$\overline{M}_n$ <sup>a)</sup> [kg mol <sup>-1</sup> ]	PDI <sup>a)</sup>	$I^*$ <sup>b)</sup> [%]	Yield <sup>c)</sup> [%]
1	Lu	1	39	38	1.03	100	52
2	Yb	1	57	56	1.02	69	53
3	Tm	1	79	76	1.04	51	58
4	Er	3	83	79	1.05	48	28
5	Ho	5	92	86	1.07	44	37

<sup>a)</sup>Determined by GPC-MALS; <sup>b)</sup> $I^* = M_{\text{exp}}/\overline{M}_n$ ,  $I^*$  = initiator efficiency,  $M_{\text{exp}}$  = expected molecular weight, based on living polymerization calculation; <sup>c)</sup>determined by weighing of the components.



**Scheme 8.** Initiation of  $Cp_3Ln$ -induced group transfer polymerization of vinylphosphonates.

metallocenes ( $Cp_2LnX$ ), coordinative-anionic polymerization of vinylphosphonates with high catalytic activity can only be achieved by using late lanthanides. In addition, late lanthanide tris(cyclopentadienyl) complexes proved to be efficient initiators for vinylphosphonate GTP.<sup>[5b]</sup>

the radius (and therefore also the Lewis acidity) of the metal center. In order to investigate the influence of these parameters on the catalytic activity of the different  $Cp_3Ln$  complexes, further polymerizations at 30 °C were carried out with both DEVP and DIVP. The activity was determined by taking aliquots, which were quenched with deuterated methanol and subsequently analyzed by  $^{31}P$  NMR spectroscopy, revealing extremely high activities (TOF up to 125 000  $h^{-1}$ ) and quantitative monomer conversion within a couple of seconds for late lanthanides (Figure 8, Table 8).<sup>[5b]</sup>

In order to determine whether the varying catalytic activities could only originate from different initiator efficiencies, a normalized catalytic activity that only considers active complexes was calculated by dividing the TOF by  $f^*$  (Table 8). This way, it could be shown that the catalytic activity strongly decreases for the earlier (larger) lanthanides. Moving from one metal to its lighter homologue, the normalized catalytic activity was found to drop by an approximate factor of 2.5 to 3.5 for DEVP or of 1.5 to 2 for DIVP, respectively.<sup>[5b]</sup> Moreover, it was observed, that the stronger steric hindrance for coordination of DIVP at the active site leads to a strong decrease (by approximately a factor of 10) in catalytic activity in comparison to DEVP.<sup>[5b]</sup>

As the normalized turnover frequency is independent of the initiator efficiency and initiation mechanism, these results have shown that in case of all lanthanide

## 5. Surface-Initiated GTP

The modification of surfaces with polymer layers to provide protection and/or a specific functionality is widely used and has a large commercial interest. On basis of our studies on rare earth metal-mediated polymerization of vinylphosphonates, our group recently developed a surface-initiated group transfer polymerization (SI-GTP), which allows the covalent modification of solids with dense poly(vinylphosphonate) brushes.<sup>[55]</sup> These stable coatings are particularly interesting for applications in the biomedical field, such as non-fouling coatings or cell proliferation surfaces.

Polymer coatings can be prepared by a variety of different techniques, including the application of polymer solutions or melts (e.g., spraying, spin coating), the chemical grafting of polymers onto the surface, or direct polymerization of monomers on the substrate. For mechanical and chemical stability of polymer coatings, it is beneficial if the polymer layer is covalently bound to the surface. This may be achieved by using the latter two approaches, which are also referred to as “grafting to” and “grafting from” processes. Hereby, the polymerization of monomers onto the surface (i.e. surface-initiated polymerization) allows access to higher grafting densities, that is, higher number of polymer chains per surface area covalently bound to the surface.

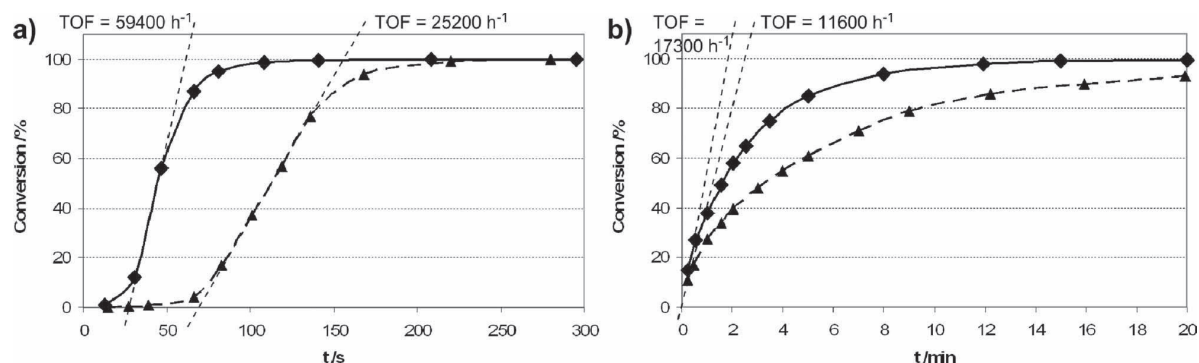


**Figure 8.** Determination of the catalytic activity of a)  $Cp_3Yb$  (**8b**, diamond, plain, TOF = 59 400  $h^{-1}$ ) and  $Cp_3Tm$  (**8c**, triangles, dashed, TOF = 25 200  $h^{-1}$ ) for polymerization of DEVP, and b)  $Cp_3Lu$  (**8a**, diamond, plain, TOF = 17 300  $h^{-1}$ ) and  $Cp_3Yb$  (**8b**, triangles, dashed, TOF = 17 300  $h^{-1}$ ) for polymerization of DIVP.

■ Table 8. Catalytic activity of Cp<sub>3</sub>Ln for vinylphosphonate polymerization of (toluene, 30 °C, monomer-to-catalyst ratio: 600).

Entry	Element	Monomer	Reaction time	Conv. <sup>a)</sup> [%]	Initiation period <sup>b)</sup>	$\bar{M}_n$ <sup>c)</sup> [kg mol <sup>-1</sup> ]	$I^*$ <sup>d)</sup> [%]	TOF <sup>a)</sup> [h <sup>-1</sup> ]	TOF/ $I^*$ [h <sup>-1</sup> ]
1	Lu	DEVP	5 min	100	–	210	47	>125 000	>265 000
2	Lu	DIVP	30 min	100	–	128	89	17 300	19 400
3	Yb	DEVP	10 min	100	20 s	310	32	59 400	185 000
4	Yb	DIVP	62 min	99	–	153	75	11 600	15 400
5	Tm	DEVP	10 min	100	60 s	280	35	25 200	72 000
6	Tm	DIVP	60 min	94	–	179	60	5700	9500
7	Er	DEVP	32 min	100	6 min	530	19	5200	28 000
8	Er	DIVP	3 h	92	–	188	56	2000	3600
9	Ho	DEVP	2 h	99.5	30 min	670	15	1200	8000
10	Ho	DIVP	5 h	49	–	336	17	500	2900
11	Dy	DEVP	5 h	85	100 min	710	12	270	2300

<sup>a)</sup>Conversion, determined by <sup>31</sup>P NMR spectroscopic measurement; <sup>b)</sup>reaction time until 3% conversion is reached; <sup>c)</sup>determined by GPC-MALS; <sup>d)</sup> $I^* = M_{\text{exp}}/(\bar{M}_n \times \text{Conv})$ ,  $I^*$  = initiator efficiency,  $M_{\text{exp}}$  = expected molecular weight, based on living polymerization calculation.

If the grafting density is sufficiently high, polymer brushes are formed, in which most of the polymer chains are arranged perpendicular to the surface, resulting in thick and uniform polymer layers. Therefore, polymer brushes are probably one of the most efficient techniques to achieve stable and homogeneous coatings.<sup>[36]</sup> Polymer brushes can be synthesized using almost all available polymerization methods, including ionic, free/controlled radical, ring-opening metathesis, photochemical and electrochemical polymerization.<sup>[37]</sup> However, as detailed previously, polymerization of vinylphosphonates by radical and anionic approaches only usually affords low yields and degrees of polymerization. Consequently, there are no reports on poly(vinylphosphonate) brushes synthesized by these methods.

Motivated by the idea of providing a method for the production of poly(vinylphosphonate) brushes, our group has recently developed an SI-GTP.<sup>[35]</sup> Our synthetic strategy was inspired by our previous work on MMA-DEVP block copolymerization with Cp<sub>2</sub>YbMe (**7**), for which we observed a fast and efficient crossover from the growing, catalyst-bound PMMA chain to vinylphosphonate polymerization.<sup>[5a,26]</sup> This was in good agreement with previous GTP studies, where enolate initiators (such as the growing PMMA chain) were found to undergo an efficient initiation, which is crucial for a surface-initiated polymerization to obtain a homogeneous growth of the polymer layer and thus uniform coverage of the surface.<sup>[6]</sup>

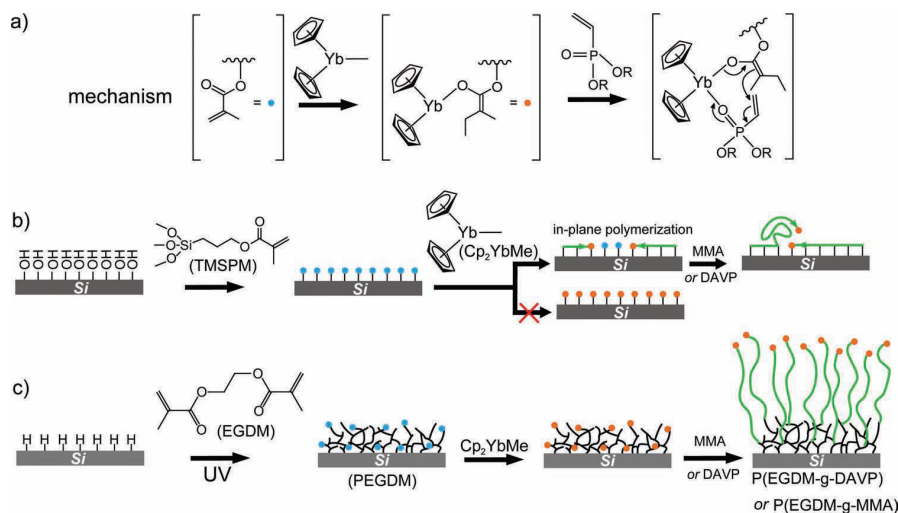
We therefore modified silicon surfaces with methacrylate functionalities, either via a self-assembled monolayer of 3-(trimethoxysilyl)propyl methacrylate (TMSPM) or via a poly(ethylene glycol dimethacrylate) (PEGDM)

film with a branched-network morphology (prepared by self-initiated photografting and photopolymerization (SIPGP) on hydrogen-terminated silicon surfaces, for details and mechanism of SIPGP, see ref. 38), thus forming a binding layer.<sup>[35]</sup> Both functionalized surfaces were treated with toluene solution of **7**, so the catalyst can react with the binding layer in order to be immobilized on the surface, leading to the formation of a highly efficient enolate initiating species (Scheme 9). After the addition of dialkyl vinylphosphonate (alkyl = methyl, ethyl, *n*-propyl), this enolate initiator is transferred to a coordinated vinylphosphonate, thus forming the covalent bond between the surface and the growing polymer chain (Scheme 9a).<sup>[35]</sup>

Initially, we synthesized PDEVP brushes on self-assembled monolayers of TMSPM on silicon wafers, prepared by the silanization of TMSPM on the oxidized silicon wafer. After the successive binding of the catalyst, that means, the reaction of *bis*(cyclopentadienyl) methyl ytterbium (Cp<sub>2</sub>YbMe) with the methacrylate groups via methyl transfer (Scheme 9a) and subsequent polymerization of DEVP, only very low and non-uniform coverage of the surface was observed by AFM measurements and confirmed by XPS.<sup>[35]</sup>

The low surface coverage was attributed to a slow catalyst binding onto the densely packed SAM and to the pre-organization of the surface-bound methacrylates, facilitating their homopolymerization during catalyst impregnation (via in-plane GTP of the MMA moieties, Scheme 9b).<sup>[35]</sup> Such polymerization strongly reduces the number of catalyst binding sites on the surface, decreasing the grafting density for a subsequent SI-GTP. The interplay of the steric hindrance of the catalyst binding onto the





**Scheme 9.** a) Formation of enolate initiating species during catalyst impregnation by reaction of Cp<sub>2</sub>YbMe with surface-bound methacrylates and subsequent initiation of SI-GTP; b) in-plane polymerization of catalyst binding sites leads to inhomogeneous coverage after SI-GTP on a TMSPM monolayer; c) a crosslinked PEGDM network with embedded, but isolated methacrylate moieties leads to high catalyst loading and thus to an efficient SI-GTP.

surface and the polymerization rate of the pre-organized methacrylate monolayer was proposed to determine the amount of surface-bound catalyst and thus the efficiency of the SI-GTP.<sup>[35]</sup>

In comparison to the TMSPM SAM, owing to the much higher thickness, a PEGDM network can provide a higher methacrylate group density per surface area. Moreover, the potential isolation of the preserved methacrylate groups in the rigid network was proposed to reduce the possibility of the polymerization of these functionalities during catalyst impregnation (Scheme 9c). Indeed, the formation of thick and uniform poly(vinylphosphonate) brushes could be observed within a few minutes after addition of vinylphosphonate to the impregnated surface.<sup>[35]</sup>

The formation of these brushes was confirmed by XPS and IR measurements, the latter exhibiting the characteristic P=O and P–O stretching modes at 1228 cm<sup>-1</sup> and 1027/1052 cm<sup>-1</sup>, respectively (Figure 9).<sup>[35]</sup> AFM measurements revealed that the polymer brush layer thickness shows an almost constant growth rate of 26.5 nm min<sup>-1</sup> for DEVP SI-GTP (Figure 10).<sup>[35]</sup> This rapid and constant growth is in agreement with the living character of a GTP. The AFM results, in combination with XPS measurements, could also prove the homogeneity of the polymer brush.<sup>[35]</sup>

The successful modification of the substrate with the poly(vinylphosphonate) brush could be further confirmed via contact angle measurements. The static water contact angle was found to be strongly dependent on the nature of poly(dialkyl vinylphosphonate) side chains; 17 ± 3° for the hydrophilic PDMVP, 76 ± 2° for the hydrophobic PDPVP.<sup>[35]</sup> It could be shown that the thermoresponsive behavior of PDEV, exhibiting a lower critical solution temperature between 40 and 46 °C, was well preserved after anchoring to the substrate, as the static water contact angle increased from 44 ± 2° at room temperature to 66 ± 2° at 50 °C.<sup>[5b,35]</sup>

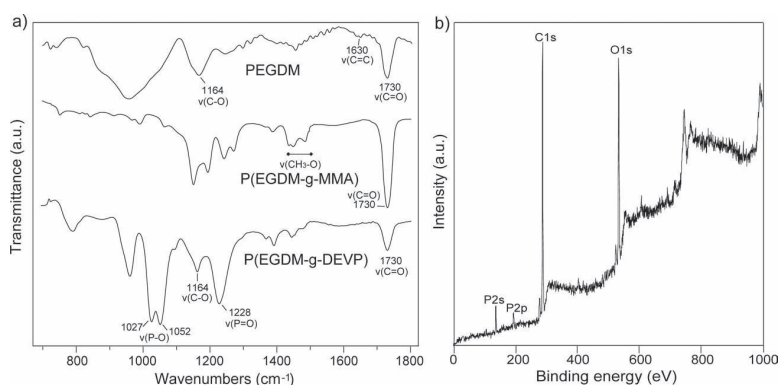


**Figure 9.** a) IR spectra of a poly(ethyleneglycol dimethacrylate) [PEGDM] network, poly(ethyleneglycol dimethacrylate-*graft*-methyl methacrylate) [P(EGDM-*g*-MMA)], and poly(ethyleneglycol dimethacrylate-*graft*-diethyl vinylphosphonate) [P(EGDM-*g*-DEVP)] brushes on silicon; b) XPS spectrum of a [P(EGDM-*g*-DEVP)] brush on silicon.

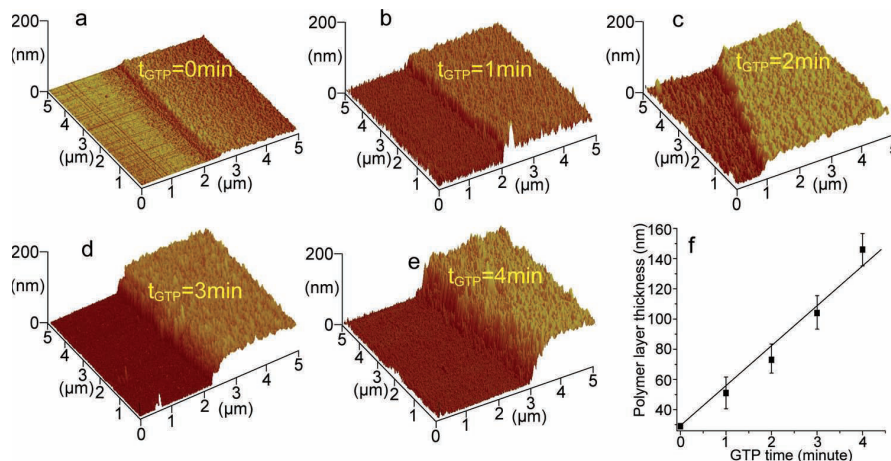
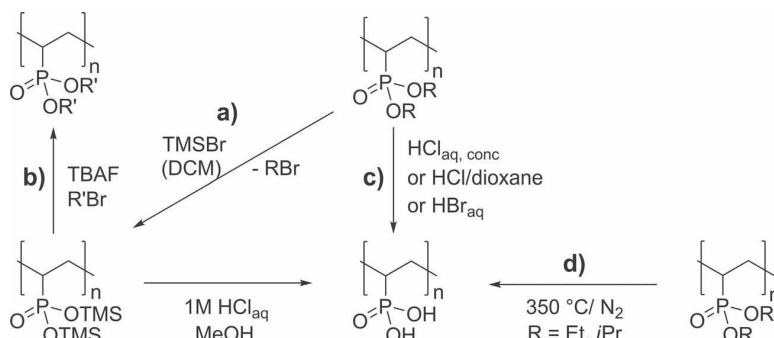


**Figure 10.** Three-dimensional representation of AFM scans of a PEGDM film on a silicon wafer and polymer brushes after SI-GTP of DEVP; a) SI-GTP of EGDM for 30 min gives a PEGDM film with a thickness of  $29 \pm 6$  nm; b)-e) SI-GTP of DEVP on the same substrate after 1, 2, 3, and 4 min results in  $51 \pm 11$ ,  $73 \pm 9$ ,  $104 \pm 11$ , and  $146 \pm 12$  nm thick polymer brush layers, respectively; f) P(EGDM-g-DEVP) layer thickness as a function of SI-GTP time.

Besides poly(vinylphosphonate) brushes, the current method was found to be applicable also to (meth)acrylate monomers, for example, poly(methyl methacrylate) (PMMA) brushes could be synthesized accordingly on PEGDM-modified silicon substrates. Uniform and thick PMMA brushes (ca. 300 nm) were prepared within 5 min at room temperature. The successful synthesis of PMMA brushes on PEGDM films was confirmed by IR (Figure 9a).<sup>[35]</sup>

SI-GTP is thus far the only method for the preparation of thick and uniform, covalent poly(vinylphosphonate) coatings. As PDEVP was demonstrated to maintain its thermoresponsive properties when anchored to the surface, SI-GTP offers a possibility for the synthesis of thermoswitchable coatings, being of great interest as bacterial, protein, peptide, and cell adhesion mediators and first candidates for the study of biomineralization in confined geometries.<sup>[39]</sup> Alongside different ester cleavage strategies, this method also provides an efficient procedure for the synthesis of PVPA brushes.<sup>[35]</sup> Moreover, SI-GTP proved to be experimentally facile, can be performed at room temperature and polymer layer thicknesses up to 300 nm can be achieved within a polymerization time of a few minutes. The versatility of SI-GTP is further underlined by the fact that it is applicable to various other monomers, which can be polymerized by the GTP-technique (e.g. MMA) thus making SI-GTP an interesting alternative to SI-ATRP.<sup>[35]</sup>



**Scheme 10.** Polymer analogous transesterification of poly(vinylphosphonate)s (a, b), chemical (c), and thermal (d) hydrolysis to poly(vinylphosphonic acid).

high-molecular-weight polymers, a mild method to cleave the alkyl groups is required. Recently, Meyer and co-workers presented such hydrolysis under mild conditions by treatment with trimethylsilyl bromide in refluxing dichloromethane.<sup>[3j]</sup>

High conversion rates were observed in the case of both PDMVP and PDEV; however, it was impossible to achieve complete cleavage of the ester side groups for high-molecular-weight PDIVP, probably due to a stronger steric hindrance for cleavage of the isopropyl group and to a higher boiling point of the side product 2-bromopropane, which therefore cannot be removed from the equilibrium.<sup>[5b]</sup>

In our studies, we found that this reaction proceeds in a two-step fashion by transesterification and subsequent hydrolysis, similar to the previously described hydrolysis of monomeric phosphonic esters with trimethylsilyl chloride.<sup>[5b,41]</sup> The intermediate poly(*bis*(trimethylsilyl) vinylphosphonate) could be isolated (Scheme 10a), but proved to be very sensitive to hydrolysis. Direct transformation of this intermediate to other ester functionalities [e.g., poly(*dibenzyl* vinylphosphonate)] by treatment with TBAF and the corresponding bromide (e.g., benzyl bromide) could be established (Scheme 10b).<sup>[5b]</sup>

## 6.2. Thermal Treatment

TGA measurements revealed a two-step thermal decomposition process for poly(*dialkyl* vinylphosphonate)s (alkyl = methyl, ethyl, *iso*-propyl).<sup>[5b,25,42]</sup> In all cases, the second decomposition step occurs at the same temperature range (460–520 °C). In combination with TGA MS measurements, these results indicate degradation of the polymer backbone.<sup>[5b,25]</sup> Depending on the nature of the ester side groups, poly(vinylphosphonate)s were found to differ in the first decomposition step. While for PDIVP, a sharp transition is observed at lower temperatures (245–270 °C) relative to PDEV (280–340 °C), for PDMVP a broader transition at higher temperatures (300–420 °C) is observed.<sup>[5b]</sup> For the latter, partial backbone degradation occurs already during the first decomposition step, as observed by TGA MS studies.<sup>[5b]</sup>

TGA MS as well as TGA FTIR studies indicate that for PDEV and PDIVP, the first decomposition is due to ester side group cleavage via an elimination reaction (with the formation of ethylene and propylene, respectively).<sup>[4d,5b,25]</sup> According to these results, we realized the quantitative synthesis of PVPA by thermal treatment for 30 min at 350 °C in nitrogen atmosphere of both PDEV and PDIVP (Scheme 10d).<sup>[5b]</sup> Full cleavage of the ester side chains was observed by <sup>1</sup>H NMR spectroscopy and further confirmed by elemental analysis. Degradation of the polymer backbone could not be observed.<sup>[5b]</sup> Hence, this method provides a possibility of converting poly(vinylphosphonate)s to PVPA in an economic and clean fashion, without the use of solvents or reagents.

## 7. Conclusion

Due to their versatility, polymers increasingly substitute classic raw materials and are thus indispensable for our modern society. In the last decades, the need for new materials with specifically designed and tailored properties is one of the major driving forces in polymer research. Polymers containing phosphonate moieties, particularly PVPA and its derivatives, have attracted great interest due to a potentially wide range of applications. However, synthesis of poly(vinylphosphonate)s is hard to establish; radical methods generally lead to slow monomer conversion and only polymers with low molecular weight may be obtained. Classical anionic polymerizations of vinylphosphonate esters are more successful, however, conversion rates are low, the synthesis is complicated by readily occurring side reactions, the obtained products exhibit a broad molecular weight distribution and stereospecific polymerization is very limited.

Rare earth metal-mediated GTP combines the suppression of side reactions, high activity, and control of polymer tacticity with a living-type polymerization. This method was applied to the polymerization of vinylphosphonates, demonstrating that rare earth metal complexes are principally feasible for poly(vinylphosphonate) synthesis and that late lanthanide metallocenes exhibit extremely high activity (TOF up to 125 000 h<sup>-1</sup>). The easily accessible *tris*(cyclopentadienyl) lanthanide complexes proved to be efficient initiators, leading to a new and interesting chain end functionalization. Using this type of catalysts, a strong dependency of the metal center on the catalytic activity was observed; the smaller the metal center (i.e. the higher the Lewis acidity), the higher the normalized catalytic activity TOF/*I*<sup>\*</sup>. Consequently, Cp<sub>2</sub>LnX-initiated GTP of vinylphosphonates with high catalytic activity can only be achieved by using late lanthanide complexes. It was shown that rare earth metal complexes principally allow vinylphosphonate polymerization in a stereospecific manner. However, a more detailed study on the effects of the coordination sphere and the rare earth metal center is required.

For DEV and DIVP, this polymerization leads to well-defined polymers with low PDI and a molecular weight close to the initial monomer to catalyst ratio even at elevated temperatures (30–70 °C). Due to the low solubility of PDMVP in suitable solvents, a well-controlled rare earth metal-mediated GTP of DMVP has not been thus far reported. Due to high polymerization activity and facile conversion by both mild hydrolysis or thermal treatment, PDEV was proposed as the ideal precursor for well-defined high-molecular-weight PVPA with narrow chain length distribution.

In our studies, we reported evidence for the living polymerization character and a GTP mechanism taking

place. A living-type polymerization could be proven by observation of a linear growth of the molecular weight upon conversion and by the possibility to produce block copolymers by subsequent polymerization of MMA and DEVP without the formation of PDEVP homopolymer. The possibility of stereospecific polymerization, the complete crossover in copolymerizations from MMA to vinylphosphonate, and thus the evidence for a strong coordination of vinylphosphonates via the phosphonate moiety, in combination with the strong dependency of the reaction rate on the rare earth cation, provide strong evidence for a coordinative-anionic, i.e. a group transfer polymerization.

On basis of our copolymerization studies, the first instance of an SI-GTP has been demonstrated, allowing the first synthesis of poly(vinylphosphonate) brushes. SI-GTP is experimentally facile, can be performed at room temperature and polymer layer thicknesses up to 300 nm can be achieved within a polymerization time of a few minutes. The versatility of SI-GTP is further underlined by the fact that it is applicable to various other monomers, which can be polymerized by the GTP-technique, for example, MMA.

**Acknowledgements:** The authors thank Dr. Ning Zhang, Dr. Sergej Vagin, and Dr. Carly Anderson for valuable discussions. S.S. is grateful for a generous scholarship from the Fonds der Chemischen Industrie.

Received: April 20, 2012; Published online: July 10, 2012; DOI: 10.1002/marc.201200278

**Keywords:** catalysis; group transfer polymerization; poly(vinylphosphonate)s; rare earth metals; surface-initiated polymerization

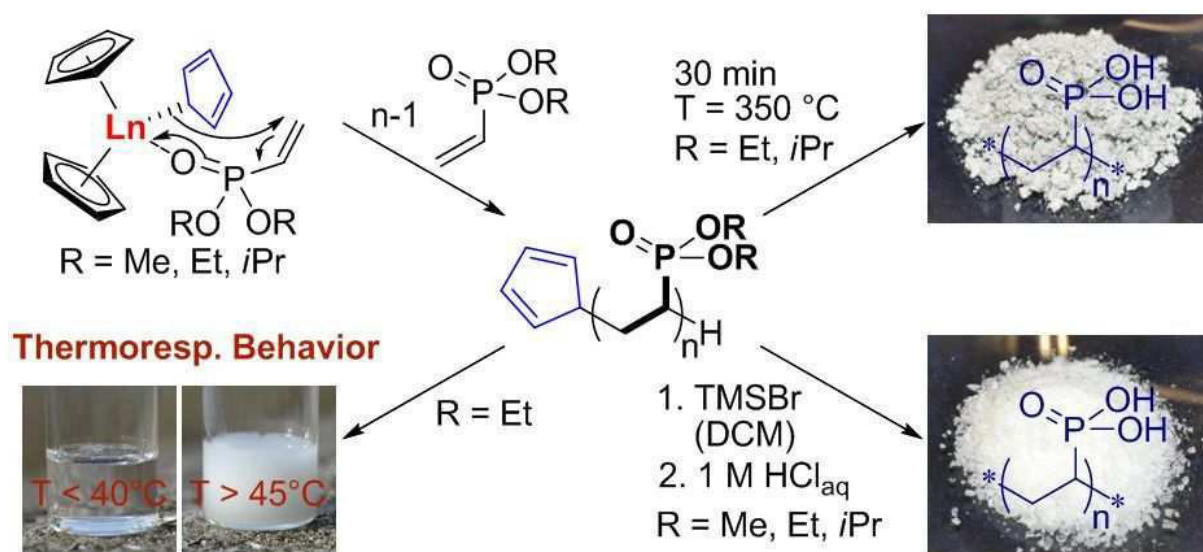
- [1] PlasticsEurope, Facts about Plastics, [www.plasticseurope.org](http://www.plasticseurope.org) (01/2012); Worldsteel Association, Crude Steel Production, [www.worldsteel.org](http://www.worldsteel.org) (01/2012).
- [2] a) S. J. Peighambaroust, S. Rowshanzamir, M. Amjadi, *Int. J. Hydrogen Energy* **2010**, *35*, 9349; b) Y. Wang, K. S. Chen, J. Mishler, S. C. Cho, X. C. Adroher, *Appl. Energy* **2011**, *88*, 981; c) N. Yousfi-Steiner, P. Mocotéguy, D. Candusso, D. Hissel, *J. Power Sources* **2009**, *194*, 130; d) S. Günes, H. Neugebauer, N. S. Sariciftci, *Chem. Rev.* **2007**, *107*, 1324; e) Y.-J. Cheng, S.-H. Yang, C.-S. Hsu, *Chem. Rev.* **2009**, *109*, 5868; f) B. C. Thompson, J. M. J. Fréchet, *Angew. Chem. Int. Ed.* **2008**, *47*, 58; g) G. Denner, M. C. Scharber, C. J. Brabec, *Adv. Mater.* **2009**, *21*, 1323; h) C. J. Brabec, S. Gowrisanker, J. J. M. Halls, D. Laird, S. Jia, S. P. Williams, *Adv. Mater.* **2010**, *22*, 3839; i) P. M. Beaujuge, J. M. J. Fréchet, *J. Am. Chem. Soc.* **2011**, *133*, 20009.
- [3] a) J. R. Ebdon, D. Price, B. J. Hunt, P. Joseph, F. Gao, G. J. Milnes, L. K. Cunliffe, *Polym. Degrad. Stab.* **2000**, *69*, 267; b) D. Price, K. Pyrah, T. R. Hull, G. J. Milnes, J. R. Ebdon, B. J. Hunt, P. Joseph, C. S. Konkel, *Polym. Degrad. Stab.* **2001**, *74*, 441; c) D. Price, K. Pyrah, T. R. Hull, G. J. Milnes, J. R. Ebdon, B. J. Hunt, P. Joseph, *Polym. Degrad. Stab.* **2002**, *77*, 227; d) T. Bock, H. Möhwald, R. Mühlhaupt, *Macromol. Chem. Phys.* **2007**, *208*, 1324; e) B. Bingöl, *Ph.D. Thesis*, Johannes-Gutenberg Universität Mainz, **2007**; f) H. Steininger, M. Schuster, K. D. Kreuer, A. Kaltbeitzel, B. Bingöl, W. H. Meyer, S. Schauff, G. Brunklaus, J. Maier, H. W. Spiess, *Phys. Chem. Chem. Phys.* **2007**, *9*, 1764; g) J. Parvole, P. Jannasch, *Macromolecules* **2008**, *41*, 3893; h) D. Markova, A. Kumar, M. Klapper, K. Müllen, *Polymer* **2009**, *50*, 3411; i) R. Perrin, M. Elomaa, P. Jannasch, *Macromolecules* **2009**, *42*, 5146; j) T. Wagner, A. Manhart, N. Deniz, A. Kaltbeitzel, M. Wagner, G. Brunklaus, W. H. Meyer, *Macromol. Chem. Phys.* **2009**, *210*, 1903; k) M. Ingratta, M. Elomaa, P. Jannasch, *Polym. Chem.* **2010**, *1*, 739; l) V. Atanasov, J. Kerres, *Macromolecules* **2011**, *44*, 6416; m) Y. E. Greish, P.W. Brown, *Biomaterials* **2001**, *22*, 807; n) J. Ellis, A. D. Wilson, *Dent. Mater.* **1992**, *8*, 79.
- [4] a) R. A. Gemeinhart, C. M. Bare, R. T. Haasch, E. J. Gemeinhart, *J. Biomed. Mater. Res., Part A* **2006**, *78A*, 433; b) J. H. Seo, R. Matsuno, M. Takai, K. Ishihara, *Biomaterials* **2009**, *30*, 5330; c) T. Goda, R. Matsuno, T. Konno, M. Takai, K. Ishihara, *J. Biomed. Mater. Res., Part B* **2009**, *89B*, 184; d) L. Macarie, G. Iliu, *Prog. Polym. Sci.* **2010**, *35*, 1078; e) R. Georgieva, R. Tsevi, K. Kossev, R. Kusheva, M. Balgijiska, R. Petrova, V. Tenchova, I. Gitsov, K. Troev, *J. Med. Chem.* **2002**, *45*, 5797; f) S. Monge, B. Camicioni, A. Grailot, J. Robin, *Biomacromolecules* **2011**, *12*, 1973.
- [5] a) U. B. Seemann, J. E. Dengler, B. Rieger, *Angew. Chem. Int. Ed.* **2010**, *49*, 3489; b) S. Salzinger, U. B. Seemann, A. Plikhta, B. Rieger, *Macromolecules* **2011**, *44*, 5920.
- [6] E. Y.-X. Chen, *Chem. Rev.* **2009**, *109*, 5157.
- [7] a) A. H. Ford-Moore, J. H. Williams, *J. Chem. Soc.* **1947**, 1465; b) G. M. Kosolapoff, *J. Am. Chem. Soc.* **1948**, *70*, 1971; c) C. L. Arcus, R. J. S. Matthews, *J. Chem. Soc.* **1956**, 4607; d) R. M. Pike, R. A. Cohen, *J. Polym. Sci.* **1960**, *44*, 531; e) G. S. Kolesnikov, E. F. Rodionova, S. E. Fedorova, L. A. Gavrikova, *Vysokomol. Soedin.* **1960**, *2*, 1432; f) M. H. Bride, W. A. W. Cummings, W. J. Pickles, *Appl. Chem.* **1961**, *11*, 352; g) B. J. Muray, *J. Polym. Sci., Part C* **1967**, *16*, 1869.
- [8] a) Y. A. Levin, A. A. Breus, B. E. Ivanov, *Dokl. Akad. Nauk SSSR.* **1977**, *236*, 287; b) S. Jin, K. E. Gonsalves, *Macromolecules* **1998**, *31*, 1010; c) B. Bingöl, W. H. Meyer, M. Wagner, G. Wegner, *Macromol. Rapid Commun.* **2006**, *27*, 1719.
- [9] T. Sato, M. Hasegawa, M. Seno, T. Hirano, *J. Appl. Polym. Sci.* **2008**, *109*, 3746.
- [10] B. Bingöl, G. Hart-Smith, C. Barner-Kowollik, G. Wegner, *Macromolecules* **2008**, *41*, 1634.
- [11] M. Leute, *Ph.D. Thesis*, Universität Ulm, **2007**.
- [12] a) O. A. Bragina, E. F. Grechkin, *Vysokomol. Soedin. Ser. B* **1971**, *13*, 710; b) V. I. Gusev, V. F. Sopin, R. M. Minigulov, *Khim. Vysokomol. Soedin. Neftekhim.* **1973**, *95*; c) Y. A. Levin, I. P. Gozman, L. K. Gazizova, Y. I. Khristoforova, T. A. Yagfarova, V. A. Bylev, B. E. Ivanov, *Vysokomol. Soedin., Ser. A* **1974**, *16*, 71.
- [13] S. Gopalkrishnan, *Ph.D. Thesis*, Rutgers the State University of New Jersey, New Brunswick **1988**.
- [14] R. P. Quirk, T. Yoo, Y. Lee, J. Kim, B. Lee, *Adv. Polym. Sci.* **2000**, *153*, 69.
- [15] T. Kawauchi, M. Ohara, M. Udo, M. Kawauchi, T. Takeichi, *J. Polym. Sci., Part A* **2010**, *48*, 1677.
- [16] H. Komber, V. Steinert, B. Voit, *Macromolecules* **2008**, *41*, 2119.
- [17] a) G. C. Eastmond, O. W. Webster, *Group Transfer Polymerization*, in *New Methods of Polymer Synthesis*, (Ed: J. R. Ebdon), Blackie, London, England **1991**; b) W. R. Hertler, *Group*

- Transfer Polymerization*, in *Silicon in Polymer Synthesis*, (Ed: H. R. Kricheldorf), Springer, Berlin, Germany **1996**;
- c) W. R. Hertler, *Group Transfer Polymerization for controlled polymer architecture*, in *Macromolecular Design of Polymeric Materials*, (Eds: K. Hatada, T. Kitayama, O. Vogl), Marcel Dekker, New York, NY, USA **1997**; d) O. W. Webster, *Adv. Polym. Sci.* **2004**, *167*, 1; e) H. Yasuda, H. Tamai, *Prog. Polym. Sci.* **1993**, *18*, 1097; f) H. Yasuda, E. Ihara, *Adv. Polym. Sci.* **1997**, *133*, 53; g) H. Yasuda, *Prog. Polym. Sci.* **2000**, *25*, 573; h) L. S. Boffa, B. M. Novak, *Chem. Rev.* **2000**, *100*, 1479.
- [18] B. C. Anderson, G. D. Andrews, P. Arthur, H. W. Jacobson, L. R. Melby, A. J. Playtis, W. H. Sharkey, *Macromolecules* **1984**, *14*, 1599.
- [19] O. W. Webster, W. R. Hertler, D. Y. Sogah, W. B. Farnham, T. V. RajanBabu, *J. Am. Chem. Soc.* **1983**, *105*, 5706.
- [20] R. P. Quirk, J.-S. Kim, *J. Phy. Org. Chem.* **1995**, *8*, 242.
- [21] a) H. Yasuda, H. Yamamoto, K. Yokota, S. Miyake, A. Nakamura, *J. Am. Chem. Soc.* **1992**, *114*, 4908; b) S. Collins, S. G. Ward, *J. Am. Chem. Soc.* **1992**, *114*, 5460.
- [22] J. Gromada, J.-F. Carpentier, A. Mortreux, *Chem. Rev.* **2004**, *248*, 397.
- [23] W. R. Hertler, *J. Polym. Sci., Part A* **1991**, *29*, 869.
- [24] J. Dengler, *Diploma Thesis*, Technische Universität München, Garching bei München, August **2007**.
- [25] G. W. Rabe, H. Komber, L. Häussler, K. Kreger, G. Lattermann, *Macromolecules* **2010**, *43*, 1178.
- [26] U. B. Seemann, *Ph.D. Thesis*, Technische Universität München, Garching bei München, October **2010**.
- [27] Y. Qian, M. D. Bala, M. Yousaf, H. Zhang, J. Huang, J. Sun, C. Liang, *J. Organomet. Chem.* **2002**, *188*, 1.
- [28] S. Salzinger, *Master Thesis*, Technische Universität München, Garching bei München, July **2010**.
- [29] G. M. Miyake, L. Caporaso, L. Cavallo, E. Y.-X. Chen, *Macromolecules* **2009**, *42*, 1462.
- [30] W. R. Mariott, E. Y.-X. Chen, *Macromolecules* **2005**, *38*, 6822.
- [31] a) H. Schumann, W. Genthe, N. Bruncks, J. Pickardt, *Organometallics* **1982**, *1*, 1194; b) P. L. Watson, *J. Chem. Soc., Chem. Commun.* **1983**, 276; c) W. J. Evans, R. Dominguez, T. P. Hanusa, *Organometallics* **1986**, *5*, 263.
- [32] J. M. Birmingham, G. Wilkinson, *J. Am. Chem. Soc.* **1956**, *78*, 42.
- [33] S. H. Eggers, H. Schultze, J. Kopf, R. D. Fischer, *Angew. Chem. Int. Ed.* **1986**, *98*, 631.
- [34] a) W. J. Evans, J. M. Perotti, S. A. Kozimor, T. M. Champagne, B. L. Davis, G. W. Nyce, C. H. Fujimoto, R. D. Clark, M. A. Johnston, J. W. Ziller, *Organometallics* **2005**, *24*, 3916; b) T. J. Mueller, G. W. Nyce, W. J. Evans, *Organometallics* **2011**, *30*, 1231.
- [35] N. Zhang, S. Salzinger, F. Deubel, R. Jordan, B. Rieger, *J. Am. Chem. Soc.* **2012**, *134*, 7333.
- [36] a) R. C. Advincula, W. J. Brittain, K. C. Caster, J. Rühle, *Polymer Brushes*, Wiley-VCH, Weinheim, Germany **2004**; b) R. Jordan, *Surface-initiated Polymerization I&II* Springer-Verlag, Berlin **2006**.
- [37] a) R. Jordan, A. Ulman, *J. Am. Chem. Soc.* **1998**, *120*, 243; b) R. Jordan, A. Ulman, J. F. Kang, M. H. Rafailovich, J. Sokolov, *J. Am. Chem. Soc.* **1999**, *121*, 1016; c) O. Prucker, J. Rühle, *Langmuir* **1998**, *14*, 6893; d) R. Barbey, L. Lavanant, D. Paripovic, N. Schuwer, C. Sugnaux, S. Tugulu, H. A. Klok, *Chem. Rev.* **2009**, *109*, 5437; e) M. Husemann, D. Mecerreyes, C. J. Hawker, J. L. Hedrick, R. Shah, N. L. Abbott, *Angew. Chem. Int. Ed.* **1999**, *38*, 647; f) M. Ulbricht, H. Yang, *Chem. Mater.* **2005**, *17*, 2622; g) M. C. R. Tria, C. D. T. Grande, R. R. Ponnampati, R. C. Advincula, *Biomacromolecules* **2010**, *11*, 3422.
- [38] a) M. Steenackers, S. Q. Lud, M. Niedermeier, P. Bruno, D. M. Gruen, P. Feulner, M. Stutzmann, J. A. Garrido, R. Jordan, *J. Am. Chem. Soc.* **2007**, *129*, 15655; b) N. Zhang, M. Steenackers, R. Luxenhofer, R. Jordan, *Macromolecules* **2009**, *42*, 5345; c) M. Steenackers, A. Küller, S. Stoycheva, M. Grunze, R. Jordan, *Langmuir* **2009**, *25*, 2225; d) T. Chen, I. Amin, R. Jordan, *Chem. Soc. Rev.* **2012**, *41*, 3280.
- [39] S. Tugulu, M. Harms, M. Fricke, D. Volkmer, H. A. Klok, *Angew. Chem. Int. Ed.* **2006**, *45*, 7458.
- [40] a) M. Hartmann, U.-C. Hipler, H. Carlsohn, *Acta Polymerica* **1980**, *31*, 165; b) Q. Wu, R. A. Weiss, *J. Polym. Sci., Part B* **2004**, *42*, 3628; c) Q. Wu, R. A. Weiss, *Polymer* **2007**, *48*, 7558.
- [41] R. Rabinowitz, *J. Org. Chem.* **1963**, *28*, 2975.
- [42] N. Inagaki, K. Goto, K. Katsura, *Polymer* **1975**, *16*, 641.



## CHAPTER 5:

# POLY(VINYLPHOSPHONATE)S SYNTHESIZED BY TRIVALENT CYCLOPENTADIENYL LANTHANIDE-INDUCED GROUP TRANSFER POLYMERIZATION



*„Lanthanons...These elements perplex us in our rearches [sic], baffle us in our speculations, and haunt us in our very dreams. They stretch like an unknown sea before us – mocking, mystifying and murmuring strange relevations and possibilities.”*

- Sir William Crookes (1832-1919)





**Status:** Published online: July 06, 2011  
**Journal:** Macromolecules  
Issue 44, 5920-5927  
**Publisher:** ACS Publications  
**Article type:** Article  
**DOI:** 10.1021/ma200752d  
**Authors:** Stephan Salzinger, Uwe B. Seemann, Andriy Plikhta,  
Bernhard Rieger

**Content:**

This chapter reports on the use of *tris*(cyclopentadienyl)lanthanide complexes ( $\text{Cp}_3\text{Ln}$ , Ln = Gd to Lu) for the polymerization of dialkyl vinylphosphonates (alkyl = methyl, ethyl, *iso*-propyl) yielding polymers of precise molecular weight and low polydispersity. It presents a new form of initiation for REM-GTP which occurs *via* a cyclopentadienyl transfer to a coordinated monomer, induced by steric crowding of the intermediate  $\text{Cp}_3\text{Ln}(\text{DAVP})$ . A strong dependency of the initiator efficiency and the catalytic activity of the applied complexes on the size of the metal center has been observed. Accordingly, the activity of applied complexes can be precisely adjusted by the use of different rare earth metal centers and  $\text{Cp}_2\text{LnX}$ -initiated vinylphosphonate polymerization with high catalytic activity can only be achieved by using late lanthanide complexes.

Additionally, mild methods for the transformation of PDAVP to PVPA by both thermal treatment and acidic hydrolysis will be presented. The so far unreported LCST of poly(diethyl vinylphosphonate) in aqueous solution has been evaluated and was found to be close to the physiological range, and the correlation between the molecular weight and this temperature has been determined.



# RightsLink®

[Home](#)
[Create Account](#)
[Help](#)


**ACS Publications**  
High quality. High impact.

**Title:** Poly(vinylphosphonate)s Synthesized by Trivalent Cyclopentadienyl Lanthanide-Induced Group Transfer Polymerization

**Author:** Stephan Salzinger, Uwe B. Seemann, Andriy Plikhta, and Bernhard Rieger

**Publication:** Macromolecules

**Publisher:** American Chemical Society

**Date:** Aug 1, 2011

Copyright © 2011, American Chemical Society

User ID

  
 Password

[Enable Auto Login](#)  
  
[Forgot Password/User ID?](#)  
**If you're a copyright.com user**, you can login to RightsLink using your copyright.com credentials. Already a **RightsLink user** or want to [learn more?](#)

### PERMISSION/LICENSE IS GRANTED FOR YOUR ORDER AT NO CHARGE

This type of permission/license, instead of the standard Terms & Conditions, is sent to you because no fee is being charged for your order. Please note the following:

- Permission is granted for your request in both print and electronic formats, and translations.
- If figures and/or tables were requested, they may be adapted or used in part.
- Please print this page for your records and send a copy of it to your publisher/graduate school.
- Appropriate credit for the requested material should be given as follows: "Reprinted (adapted) with permission from (COMPLETE REFERENCE CITATION). Copyright (YEAR) American Chemical Society." Insert appropriate information in place of the capitalized words.
- One-time permission is granted only for the use specified in your request. No additional uses are granted (such as derivative works or other editions). For any other uses, please submit a new request.



Copyright © 2013 [Copyright Clearance Center, Inc.](#) All Rights Reserved. [Privacy statement.](#) Comments? We would like to hear from you. E-mail us at [customercare@copyright.com](mailto:customercare@copyright.com)

Reprinted with Permission from Salzinger, S; Seemann, U. B.; Plikhta, A.; Rieger, B. *Macromolecules* **2011**, *44*, 5920. Copyright 2011 American Chemical Society.

## Poly(vinylphosphonate)s Synthesized by Trivalent Cyclopentadienyl Lanthanide-Induced Group Transfer Polymerization

Stephan Salzinger, Uwe B. Seemann, Andriy Plikhta, and Bernhard Rieger\*

WACKER Lehrstuhl für Makromolekulare Chemie, Technische Universität München, Lichtenbergstrasse 4, 85748 Garching bei München, Germany

**S** Supporting Information

**ABSTRACT:** Recent studies have shown that diethyl vinylphosphonate can be converted into high-molecular-weight polymers by rare earth metal-initiated group transfer polymerization. Here we report on the use of tris(cyclopentadienyl)lanthanide complexes ( $Cp_3Ln$ ,  $Ln = Gd$  to  $Lu$ ) for the polymerization of dialkyl vinylphosphonates (alkyl: methyl, ethyl, isopropyl) yielding polymers with precise molecular weight and low polydispersity. Additionally, the thermosensitive behavior of poly(diethyl vinylphosphonate) was characterized, and methods for a conversion of the obtained high-molecular-weight poly(vinylphosphonate)s ( $M_n > 250 \text{ kg mol}^{-1}$ ) to poly(vinylphosphonic acid) by both thermal treatment and a mild hydrolysis were established. A series of independently performed reactions showed high activities and initiator efficiencies for the  $Cp_3Ln$  complexes for the homopolymerization of the applied monomers. Poly(vinylphosphonate)s of high molecular weight with a previously unknown low polydispersity index ( $PDI < 1.05$ ) have been determined by GPC-MALS (multiangle light scattering) methods. The reaction shows a linear  $M_w$  vs consumption plot, thus proving a living type polymerization. The initiation of the reaction has been investigated by end-group analysis with MALDI-ToF and ESI mass spectrometric analysis. A new and interesting chain-end functionalization of the achieved polymers has been detected over the course of the MS analytical studies. The so far unreported LCST (lower critical solution temperature) of poly(diethyl vinylphosphonate) in water has been evaluated, and the correlation between the molecular weight of the material with this temperature has been determined.

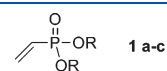


### INTRODUCTION

Poly(vinylphosphonate)s, as well as their derivatives, may be used as binders in dental or bone concrete, in new energy technologies as proton conducting membranes, as halogen-free flame retardants or as antifouling agents on metal surfaces.<sup>1</sup> Polymerization reactions of this type of monomer have first been studied in the 1960s and 1970s, with reports of low molecular weights and yields, mostly achieved by radical and anionic approaches.<sup>2</sup> Only few publications over the last years report on high-molecular-weight poly(vinylphosphonate)s, with even fewer reports on the free acid.<sup>3</sup> A few years ago we reported on successfully performed catalytic polymerizations using rare-earth metal complexes comprising  $\sigma$ -donor ligands.<sup>3c</sup> Later on, initial investigations on the microstructure of poly(diethyl vinylphosphonate) (PDEVVP) were published using the same type of catalytic compounds.<sup>3e</sup> Nevertheless, mechanistic details as well as an absolute characterization of the molecular weight of the PDEVVPs were missing. Recently, we reported on the first use of bis(cyclopentadienyl)ytterbium complexes ( $Cp_2YbCl$  and  $Cp_2YbMe$ ) for the polymerization of diethyl vinylphosphonate (DEVVP, **1b**).<sup>4</sup> This work has demonstrated the first instance of block copolymer production with methyl methacrylate (MMA). The reaction proceeds in a living fashion and appears to be a

group transfer polymerization (GTP), which is already well-known for acrylic monomers.<sup>5</sup>

Nevertheless, the molecular weight of the resulting homopolymers was not consistent with the initial monomer to catalyst ratio, indicating low initiator efficiencies and the use of dialkyl vinylphosphonates other than the diethyl species are still not known. Herein we describe the first use of tris(cyclopentadienyl)lanthanide complexes for the polymerization of dimethyl vinylphosphonate (DMVP, **1a**), diethyl vinylphosphonate (DEVVP, **1b**), and diisopropyl vinylphosphonate (DIVP, **1c**), and we provide pathways for the conversion of high-molecular-weight poly(vinylphosphonate)s to the corresponding poly(vinylphosphonic acid) by both thermal treatment and hydrolysis under mild conditions.



R: Me (**a**), Et (**b**), *i*Pr (**c**).

**Figure 1.** Dimethyl vinylphosphonate (DMVP, **1a**), diethyl vinylphosphonate (DEVVP, **1b**), and diisopropyl vinylphosphonate (DIVP, **1c**).

**Received:** March 31, 2011

**Revised:** June 17, 2011

**Published:** July 06, 2011

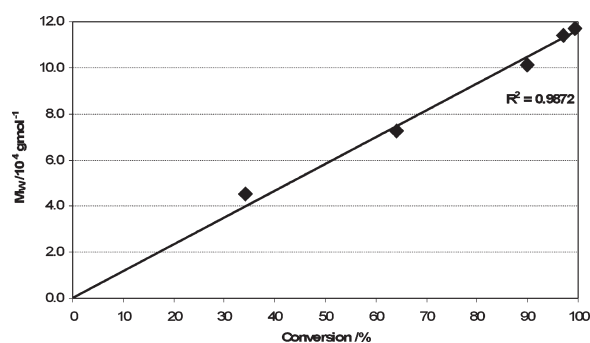
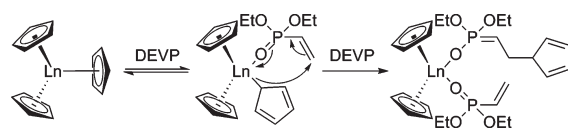


Figure 2. Linear growth of PDEVp molecular weight with conversion ( $\text{Cp}_3\text{Lu}$ , toluene,  $-10\text{ }^\circ\text{C}$ ).

### Scheme 1. Initiation of the $\text{Cp}_3\text{Ln}$ -Induced Polymerization of Vinylphosphonates with the Example Monomer DEVp



## RESULTS AND DISCUSSION

### $\text{Cp}_3\text{Ln}$ Complexes for Vinylphosphonate Polymerization.

The here-presented work is focused on the use of trivalent cyclopentadienyl lanthanide complexes ( $\text{Cp}_3\text{Ln}$ ) for the homopolymerization of various dialkyl vinylphosphonates, allowing a precise control of molecular weight and molecular weight distribution of the polymer product. In addition, these complexes are structurally characterized for most of the rare-earth metals ( $\text{Ln}$ : Ce–Lu),<sup>6</sup> and their synthesis is easier than the previously applied monochloro- or monomethyl complexes ( $\text{Cp}_2\text{YbX}$ , X = Cl, Me),<sup>4</sup> affording even better yields. Initial kinetic studies using  $\text{Cp}_3\text{Lu}$  and DEVp have been performed at  $-10\text{ }^\circ\text{C}$  by taking aliquots during the reaction. A linear growth of the molecular weight with conversion, as detected by  $^{31}\text{P}$  NMR spectroscopy, can be observed which proves the living character of the polymerization reaction supporting further our hypothesis of a GTP mechanism<sup>4</sup> (Figure 2).

In order to understand the initiation process, oligomers have been produced by using a 5 to 1 ratio of DEVp to catalyst in toluene solution and were subsequently analyzed by ESI MS. For all peaks, the molar mass of the corresponding oligomers was found to be  $n \times M_{\text{DEVp}} + 66\text{ g mol}^{-1}$  (Figure S1 and Table S1). The remaining  $66\text{ g mol}^{-1}$  corresponds to a cyclopentadienyl group, which initiated chain growth and a proton from the termination reaction during methanolic work-up. Thus, a transfer of the coordinated ligand to a monomer in the initial step is evident. This type of initiation could also be observed for the polymerization of DMVP and DIVP and was further confirmed by MALDI-ToF MS (exemplarily shown in Figure S2 and Table S2).

Because of the small ionic radii of late trivalent rare earth metals and the steric demand of the ligands, it is therefore unlikely that all three Cp ligands are bound to the metal center in a  $\eta^5$  fashion. This is underlined by previous X-ray diffraction studies which have

Table 1. Polymerization of DEVp ( $\text{Cp}_3\text{Ln}$ , Toluene,  $30\text{ }^\circ\text{C}$ )

entry	$\text{Cp}_3\text{Ln}$	monomer <sup>d</sup>	reaction time/h	$M_w/\text{kDa}$	$M_n/\text{kDa}$	$I^{*b}/\text{PDI}$	yield <sup>c</sup> /%	yield <sup>c</sup> /%
1	Lu	200	1	60	57	1.05	58	88
2	Lu	400	1	110	100	1.10	66	99
3	Lu	800	1	210	170	1.26	77	99
4	Yb	200	1	93	83	1.12	39	94
5	Yb	400	1	140	120	1.16	55	93
6	Yb	800	1	230	200	1.15	66	97
7	Tm	200	1	120	100	1.22	33	89
8	Tm	400	1	200	170	1.20	38	93
9	Tm	800	1	230	190	1.16	69	96
10	Er	200	1	180	135	1.36	24	86
11	Er	400	1	260	210	1.25	31	95
12	Er	800	1	380	290	1.34	45	97
13	Ho	200	3	310	240	1.31	14	85
14	Ho	400	3	450	335	1.34	19	85
15	Ho	800	3	640	480	1.34	27	87
16	Dy	200	5	490	400	1.24	8	94
17	Dy	400	5	570	430	1.33	15	96
18	Dy	800	5	710	550	1.31	24	95

<sup>a</sup> Monomer-to-catalyst ratio. <sup>b</sup>  $I^* = M_{\text{exp}}/M_n$ ,  $I^*$  = initiator efficiency,  $M_{\text{exp}}$  = expected molecular weight, based on living polymerization calculation. <sup>c</sup> Determined by weighing of the components.

shown that  $\text{Cp}_3\text{Lu}$  is a polymeric material in the solid state.<sup>7</sup> In this structure single Cp rings form bridges between the individual  $\text{Cp}_2\text{Lu}$  moieties by  $\eta^1$ -metal–Cp bonding.

By using phosphonates, which are known to be strongly coordinating, two electron-donating species, the  $\eta^1$ -( $\sigma$ )-character of the metal–Cp bond is strengthened, thus allowing a nucleophilic transfer to a coordinated monomer. An additional phosphonate is now able to bind to the vacant coordination site (Scheme 1). The polymerization reaction then proceeds via repeated conjugate addition of a coordinated monomer to the growing chain end.

The investigations of Evans et al. on sterically crowded tris-(pentamethylcyclopentadienyl)lanthanide complexes ( $\text{Cp}^*_3\text{Ln}$ , Ln = La, Ce, Pr, Nd, Sm) and the therein described equilibrium between  $\eta^5$ - and  $\eta^1$ - $\text{Cp}^*$  metal bonding further support the assumption of an initiation by nucleophilic transfer of a cyclopentadienyl ligand.<sup>8</sup>

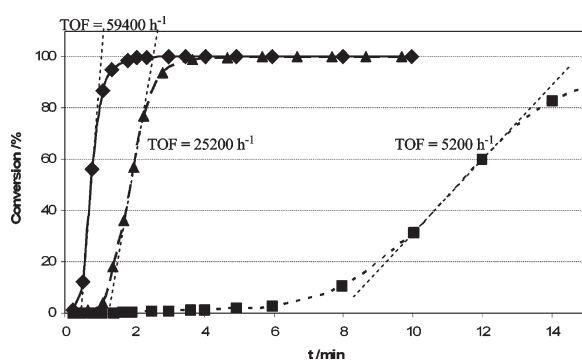
The larger metal radii of lighter rare earth metals result in sterically less crowded trivalent cyclopentadienyl complexes. This leads to a higher  $\eta^5$  character of the metal–Cp bond and should lower the nucleophilicity of the Cp anion, therefore disfavoring its transfer to a monomer. This is confirmed by the use of metal centers with different ionic radii. At  $30\text{ }^\circ\text{C}$  the polymerization of DEVp in toluene is possible when complexes of the heavier rare earth metals are used, showing high polymer yields and low PDI (below 1.4) for all centers between Lu and Dy (Table 1). With Tb and the corresponding lighter metals it was not possible to isolate polymeric material under these conditions.

With decreasing ionic radius the expected molecular weight ( $M_{\text{exp}}$ ) fits better to the determined values. This dependence on the radius is a further evidence for the transfer theory as the lower nucleophilicity of the Cp ligand for early lanthanides leads to lower initiator efficiencies  $I^*$  (higher  $M_n/M_{\text{exp}}$ , observed decrease of  $I^*$  from Lu to Dy: 58–77% (entries 1–3) to 8–24% (entries

**Table 2.** Polymerizations of DIVP ( $\text{Cp}_3\text{Ln}$ , Toluene, 30 °C, Monomer-to-Catalyst Ratio: 200)

$\text{Cp}_3\text{Ln}$	reaction time/h	$M_w/\text{kDa}$	$M_n/\text{kDa}$	PDI	$I^*/\%$	yield <sup>b</sup> /%
Lu	1	39	38	1.03	100	52
Yb	1	57	56	1.02	69	53
Tm	1	79	76	1.04	51	58
Er	3	83	79	1.05	48	28
Ho	5	92	86	1.07	44	37

<sup>a</sup>  $I^* = M_{\text{exp}}/M_n$ ,  $I^*$  = initiator efficiency,  $M_{\text{exp}}$  = expected molecular weight, based on living polymerization calculation. <sup>b</sup> Determined by weighing of the components.

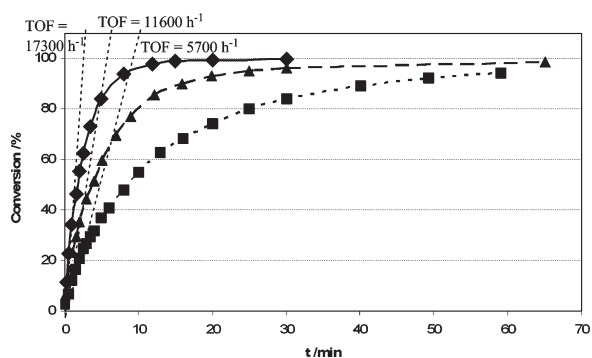
**Figure 3.** Determination of the catalytic activity of  $\text{Cp}_3\text{Yb}$  (diamond, plain,  $\text{TOF} = 59\,400\text{ h}^{-1}$ ),  $\text{Cp}_3\text{Tm}$  (triangles, long dashed,  $\text{TOF} = 25\,200\text{ h}^{-1}$ ), and  $\text{Cp}_3\text{Er}$  (squares, short dashed,  $\text{TOF} = 5\,200\text{ h}^{-1}$ ) for the polymerization of DEVP (monomer-to-catalyst ratio: 600).

16–18)). An increase of the monomer-to-catalyst ratio generally improves the efficiency of this starting process (e.g., from 39% to 66% for Yb (entries 4–6)). This is in good agreement with the expectation as longer reaction times are necessary for full monomer conversion, thus allowing more catalyst molecules to initiate the polymerization.

By increasing the reaction temperature to 70 °C, it was possible to initiate the polymerization also with earlier lanthanides (Tb, Gd), but with low yields (Table S3). In addition, the resulting molecular weights ( $M_n$ ) for the lighter lanthanides correspond slightly better to the calculated values ( $M_{\text{exp}}$ ) for living polymerizations (higher  $I^*$ ).

Besides DEVP, there are other simple dialkyl vinylphosphonate monomers available, e.g., dimethyl vinylphosphonate (DMVP) and diisopropyl vinylphosphonate (DIVP). Both can be polymerized using  $\text{Cp}_3\text{Ln}$  complexes as initiators. Specifically, DMVP showed high reactivity; however, the limiting factor is the low solubility of the resulting polymer in solvents suitable for this polymerization. Formed PDMVP precipitates almost immediately from toluene (or THF<sup>3d</sup>) solution with a molecular weight ( $M_w$ ) below 50 kDa (determined by static light scattering, using Zimm plots). Because of adsorption on the column material, GPC separation, in order to gather information about PDI and  $M_n$ , was not possible.

On the other hand, the polymerization of DIVP proceeds slower than with DMVP or DEVP but produces materials with high molecular weight which corresponds better to the initial monomer-to-catalyst ratio. The higher initiator efficiency can be

**Figure 4.** Determination of the catalytic activity of  $\text{Cp}_3\text{Lu}$  (diamond, plain,  $\text{TOF} = 17\,300\text{ h}^{-1}$ ),  $\text{Cp}_3\text{Yb}$  (triangles, long dashed,  $\text{TOF} = 11\,600\text{ h}^{-1}$ ), and  $\text{Cp}_3\text{Tm}$  (squares, short dashed,  $\text{TOF} = 5\,700\text{ h}^{-1}$ ) for the polymerization of DIVP (monomer-to-catalyst ratio: 600).**Table 3.** Catalytic Activity of  $\text{Cp}_3\text{Ln}$  Complexes for the Polymerization of DEVP (Monomer-to-Catalyst Ratio: 600)

$\text{Cp}_3\text{Ln}$	reaction time	conv <sup>a</sup> /%	init per <sup>b</sup>	$M_n/\text{kDa}$	$I^c/\%$	$\text{TOF}^d/\text{h}^{-1}$	$\text{TOF}/I^e/\text{h}^{-1}$
Lu	5 min	100		210	47	>125000	>265000
Yb	10 min	100	20 s	310	32	59400	185000
Tm	10 min	100	60 s	280	35	25200	72000
Er	32 min	100	6 min	530	19	5200	28000
Ho	2 h	99.5	30 min	670	15	1200	8000
Dy	5 h	85	100 min	710	12	270	2300

<sup>a</sup> Determined by  $^{31}\text{P}$  NMR spectroscopic measurement. <sup>b</sup> Init per: initiation period, reaction time until 3% conversion is reached. <sup>c</sup>  $I^* = M_{\text{exp}}/(M_n \times \text{conv})$ ,  $I^*$  = initiator efficiency,  $M_{\text{exp}}$  = expected molecular weight, based on living polymerization calculation.

attributed to both the slower chain growth (due to the stronger steric hindrance for the coordination of a DIVP monomer) and a shortening/absence of an initiation period which is observable for DEVP (see determination of catalytic activity). Therefore, the rate of the initiation is faster than for the chain growth, affording remarkably narrow PDIs (below 1.1) for all experiments (Table 2). A quantitative precipitation of the polymer with hexane was not possible due to the increased solubility of PDIVP in nonpolar solvents leading to the observed low yields, generally between 30% and 60%.

**Determination of the Catalytic Activity.** The above results indicate clearly that the initiator efficiency is strongly affected by the radius (and therefore also the Lewis acidity) of the metal center. In order to investigate the influence of these parameters on the catalytic activity of the different  $\text{Cp}_3\text{Ln}$  complexes, further polymerizations at 30 °C were carried out with both DEVP and DIVP. The activity was thereby determined by taking aliquots which are quenched with deuterated methanol and subsequently analyzed by  $^{31}\text{P}$  NMR spectroscopy.

The turnover frequency (TOF) was defined as the maximum slope of the conversion vs reaction time plot (Figures 3 and 4). In order to determine whether the varying catalytic activities could only originate from different initiator efficiencies, the polymer contained in the remaining reaction mixture (after taking aliquots) was isolated and the molecular weight

**Table 4. Catalytic Activity of  $Cp_3Ln$  Complexes for the Polymerization of DIVP (Monomer-to-Catalyst Ratio: 600)**

$Cp_3Ln$	reaction time	conv <sup>a</sup> /%	$M_n$ /kDa	$I^{sp}$ /%	TOF <sup>a</sup> /h <sup>-1</sup>	TOF/ $I^*$ /h <sup>-1</sup>
Lu	30 min	100	128	89	17300	19400
Yb	65 min	99	153	75	11600	15400
Tm	60 min	94	179	60	5700	9500
Er	3 h	92	188	56	2000	3600
Ho	5 h	49	336	17	500	2900

<sup>a</sup> Determined by <sup>31</sup>P NMR spectroscopic measurement. <sup>b</sup>  $I^* = M_{exp}/(M_n \times conv)$ ,  $I^*$  = initiator efficiency,  $M_{exp}$  = expected molecular weight, based on living polymerization calculation.

analyzed by GPC-MALS in order to determine the initiator efficiency  $I^*$ . By dividing the TOF by  $I^*$ , a normalized catalytic activity can be calculated which only considers active complexes (Tables 3 and 4).

For the polymerization of DEVP an initiation period is observed (Figure 3 and Figure S3), which is considerably lengthened through the series Lu to Dy and results also in decreasing initiator efficiencies. This decrease is in good agreement with the results detailed above. Different absolute values for  $I^*$  can be attributed to different catalyst and monomer concentrations (see Experimental Section).

The measurements clearly show that not only the initiator efficiency but also the (normalized) catalytic activity strongly decreases for earlier lanthanides (Table 3). The normalized catalytic activity therefore changes by an approximate factor of 2.5–3.5 moving from one metal to its lighter homologue.

For DIVP an initiation period as it is observed for DEVP does not occur (Figure 4 and Figure S4). This can be attributed to the stronger steric demand of DIVP facilitating the nucleophilic transfer of a cyclopentadienyl ligand by destabilizing the intermediate shown in Scheme 1. The stronger steric hindrance also leads to a strong decrease (by approximately a factor of 10) in catalytic activity in comparison to DEVP (Table 4). Both facts explain the observed higher initiator efficiency and lower PDI for the polymerization of DIVP.

Moving from one metal to its lighter homologue, the normalized catalytic activity decreases by a factor 1.5–2, showing that the influence of the metal radii on the catalytic activity is smaller for DIVP than it is for DEVP. Taking into consideration that the steric hindrance influencing the rate of chain propagation, in comparison to DEVP, is stronger for the late (small) lanthanides, this observation is in good agreement with the expectation.

As the normalized turnover frequency is independent of the initiator efficiency and initiation mechanism, these results clearly show that in case of all lanthanide metallocenes ( $Cp_2LnX$ ) coordinative anionic polymerization of vinylphosphonates with high catalytic activity can only be achieved by using late lanthanides. Even if a more uniform start of polymerization can be established by a different initiation, the catalytic activity of earlier lanthanides would still be very limited.

**Solubility and Thermo-responsive Behavior of Poly(vinylphosphonate)s.** Poly(vinylphosphonate)s show a differing solubility behavior depending on the nature of the ester side chain. While PDMVP is soluble in water, it displays very limited solubility in common organic solvents, thus affording precipitation of the material soon after starting polymerization. This inhibits the formation of high-molecular-weight polymers. PDIVP, on the other hand, shows high solubility in many solvents leading to a

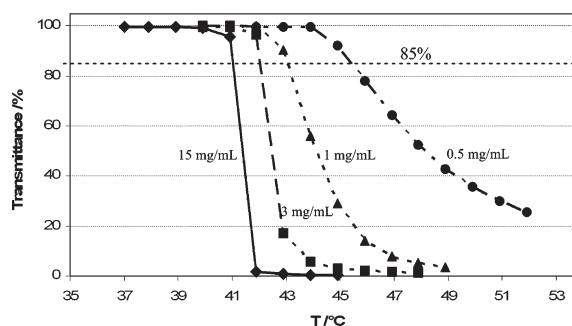


**Figure 5.** Change of transmittance at  $\lambda = 550$  nm for PDEVP with  $160$   $kg\ mol^{-1}$  at different concentrations:  $15$   $mg\ mL^{-1}$  (diamonds, plain),  $3$   $mg\ mL^{-1}$  (squares, long dashed),  $1$   $mg\ mL^{-1}$  (triangles, short dashed), and  $0.5$   $mg\ mL^{-1}$  (circles, broken).

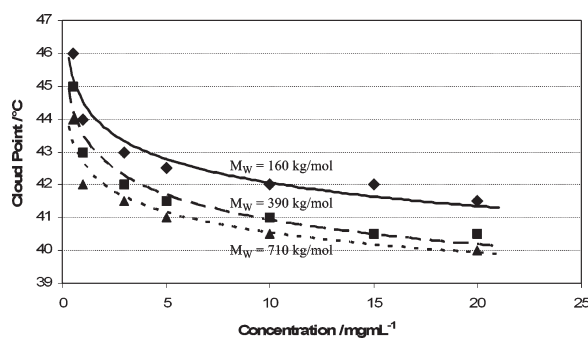


**Figure 6.** Cloud point vs concentration for aqueous PDEVP solutions with different molecular weight:  $160$   $kg\ mol^{-1}$  (diamonds, plain),  $390$   $kg\ mol^{-1}$  (squares, long dashed), and  $710$   $kg\ mol^{-1}$  (triangles, short dashed).

more challenging purification by precipitation of the product (and is only possible for molecular weights above ca.  $30$   $kg\ mol^{-1}$ ).

Being between the two solubility extremes showed by the hydrophilic PDMVP and the rather hydrophobic PDIVP, respectively, it is not surprising that PDEVP shows amphiphilic behavior. It is highly soluble in both water and lighter alcohols, whereas the solubility in other solvents is strongly dependent on the molecular weight: after a distinct swelling (between 10 and 25 mg of solvent per mg of polymer) polymers with a molecular weight below  $\sim 1000$   $kg\ mol^{-1}$  start to dissolve while ultrahigh-molecular-weight polymers stay in the swollen state. Only in hydrophobic solvents such as hexane or pentane no significant solubility or polymer swelling could be observed.

The amphiphilicity of PDEVP is further underlined by the existence of a lower critical solution temperature (LCST) of aqueous PDEVP solutions. Hereby the LCST is close to the physiological range (Figure 5). For further LCST studies this polymer is interesting due to the living character of the polymerization. Thus, narrow molecular weight distributions (sharp LCST) can be achieved, and block copolymer structures are easily accessible.

Previous studies on thermo-responsive PNIPAM and poly(2-oxazoline)s have shown that the cloud point of these systems exhibits a significant dependence on both concentration and molecular weight of the polymer<sup>9</sup> thus enabling the design of materials with a specific LCST. In the case of PDEVP, we found

that a decrease of the concentration leads to a broadening of the transition and to higher cloud points. Both effects are stronger with reduced concentration (Figures 5 and 6).

To determine the influence of the molecular weight on the LCST of PDEVP, aqueous solutions with a polymer concentration of  $5 \text{ mg mL}^{-1}$  ( $M_w$  range of  $39\text{--}1200 \text{ kg mol}^{-1}$ ) were used. Higher concentrations lead to very viscous solutions for high-molecular-weight polymers, and lower concentrations result in broad transitions. As well as for the concentration the cloud point shows a strong dependence on the molecular weight of the polymers. Lower degrees of polymerization result in polymer solutions with a higher LCST, again with an increasing effect the smaller the molecular weight is (Figure 7).

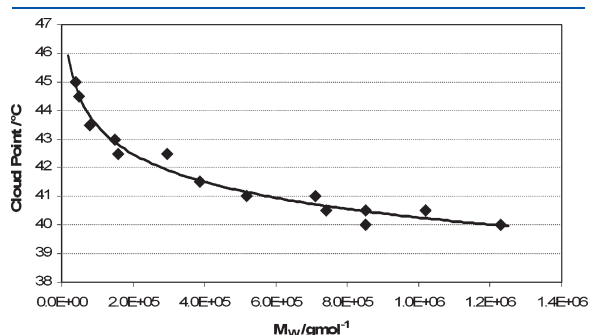
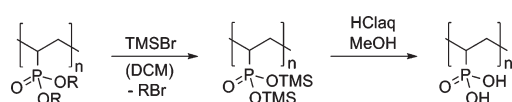


Figure 7. Cloud point vs weight-average  $M_w$  of PDEVP.

**Scheme 2. Transesterification of Poly(dialkyl vinylphosphonate)s to Poly(bis(trimethylsilyl)-vinylphosphonate) and Subsequent Mild Hydrolysis to Poly(vinylphosphonic acid)**



**Polymer Analogous Hydrolysis to Poly(vinylphosphonic acid).** In order to hydrolyze the here-presented esters to their respective acids, a mild method to cleave the alkyl groups is needed in order to avoid polymer degradation. Recently, Wagner et al. presented a hydrolysis of lower molecular weight poly(vinylphosphonate)s ( $M_n < 40 \text{ kDa}$ ) under mild conditions by treatment with trimethylsilyl bromide in refluxing dichloromethane.<sup>3d</sup> We found that this reaction proceeds in a two-step fashion by transesterification and subsequent hydrolysis, similar to the previously described hydrolysis of monomeric phosphonic esters with trimethylsilyl chloride (Scheme 2).<sup>10</sup> The intermediate poly(bis(trimethylsilyl)vinylphosphonate) can be isolated (Figure 8) but proved to be very sensitive to hydrolysis. A direct transformation of this intermediate to other ester functionalities (e.g., poly(dibenzyl vinylphosphonate)) by treatment with TBAF and the corresponding bromide (e.g., benzyl bromide) was possible; however, complete separation of *tert*-butylammonium from the product could not be achieved.

We applied the method described by Wagner et al.<sup>3d</sup> to the obtained high-molecular-weight poly(vinylphosphonate)s ( $M_n > 250 \text{ kDa}$  for both PDEVP and PDIVP, as detailed above PDMVP with  $M_w > 50 \text{ kDa}$  was not accessible) and observed high conversion rates for both PDEVP and PDMVP, as demonstrated by  $^1\text{H}$  NMR spectroscopy (Figure 8 and Figure S5). Using this hydrolysis procedure, it was not possible to achieve a complete cleavage of the ester bonds for high-molecular-weight PDIVP (Figure S6), probably due to a stronger steric hindrance for cleavage of the isopropyl group and to a higher boiling point of the side product 2-bromopropane, which therefore cannot be removed from equilibrium.

In order to verify if the end groups are retained during hydrolysis, we applied the described procedure to oligomeric vinylphosphonates and analyzed the obtained oligomeric vinylphosphonic acids by both ESI and MALDI-ToF MS as well as by  $^1\text{H}$  NMR spectroscopy. In the resulting  $^1\text{H}$  NMR spectrum signals in the region between 5 and 7 ppm were not observed indicating an absence of the expected cyclopentadienyl end group. In MALDI-ToF MS different oligomeric distributions with  $\Delta(m/z) = 108$  (molar mass of vinylphosphonic acid) could be observed in the negative mode, but the corresponding end

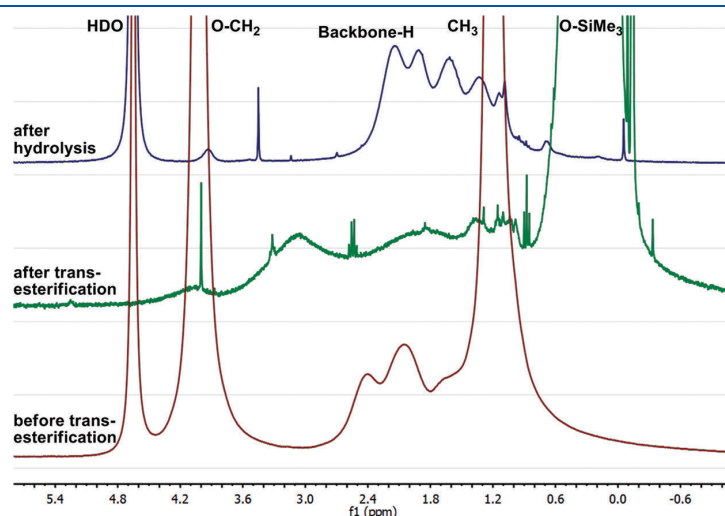
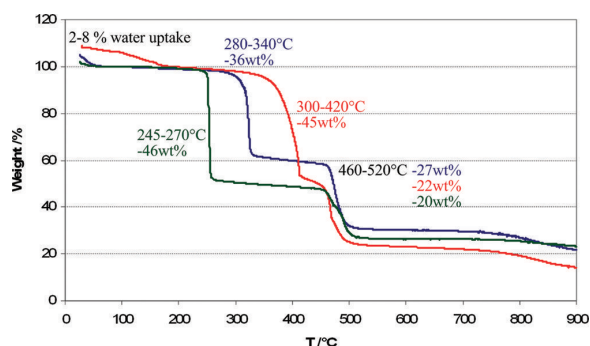
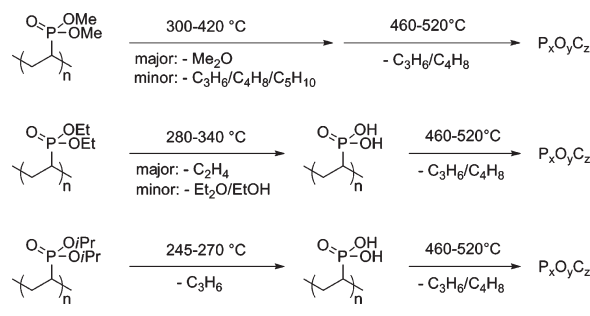


Figure 8.  $^1\text{H}$  NMR spectra of PDEVP before (in  $\text{D}_2\text{O}$ , red) and after (in  $\text{C}_6\text{D}_6$ , green, for easier comparison this spectrum was shifted 0.20 ppm to higher field) transesterification with TMSBr and after hydrolysis (in  $\text{D}_2\text{O}$ , blue).



**Figure 9.** TGA measurements for PDMVP (red), PDEVp (blue), and PDIVP (green); mass losses reported in weight percent (wt %).

### Scheme 3. Proposed Decomposition Processes for Poly(vinylphosphonate)s According to TGA MS



groups could not be identified. Ionization of the oligomers by ESI MS was not possible.

**Thermal Decomposition of Poly(vinylphosphonate)s.** TGA measurements of poly(vinylphosphonate)s revealed a two-step thermal decomposition process for the three evaluated ester side groups (methyl, ethyl, isopropyl). Additionally, water uptake (confirmed by TGA MS) could be observed, which differs according to the hydrophilicity of the polymers (2–8 wt %). In all cases the second decomposition step occurs at the same temperature range (460–520 °C), thus confirming the previous assumption of backbone degradation.<sup>3c</sup> The three polymers differ in the first decomposition step: while for PDIVP a sharp transition is observed at lower temperatures (245–270 °C) relative to PDEVp (280–340 °C), for PDMVP a broader transition at higher temperatures (300–420 °C) is observed (Figure 9). Hereby the mass losses for PDEVp and PDIVP correspond well to cleavage of the ester side chains by elimination: 34 wt % for ethylene cleavage in case of PDEVp (observed: 36 wt %), 44 wt % for propylene cleavage in case of PDIVP (observed: 46 wt %).

In order to understand the decomposition process for PDMVP and to confirm the side-chain cleavage for PDEVp and PDIVP, TGA MS measurements were carried out. For the latter, only propylene ( $m/z = 41/42$ ) could be found as a volatile during the first decomposition step, proving side-group cleavage by elimination. In contrast to the results of Rabe et al.,<sup>3e</sup> for PDEVp not only ethylene ( $m/z = 26/27/28$ , major decomposition compound) and ethanol ( $m/z = 45/46$ , very small amount) could be identified as volatiles, but also diethyl ether ( $m/z = 74/59/45$ , very small amount) (Scheme 3).

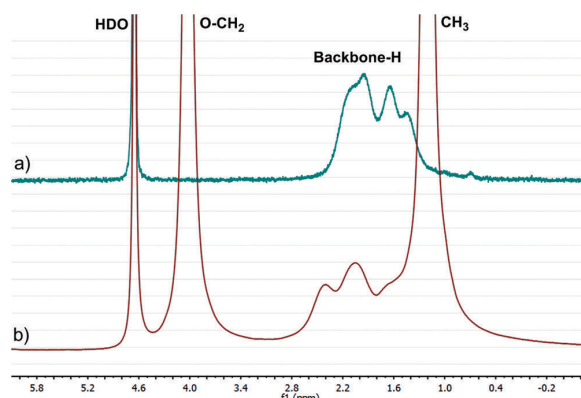


**Figure 10.**  $^1\text{H}$  NMR spectra in  $\text{D}_2\text{O}$  of (a) poly(vinylphosphonic acid) (PVPA) synthesized by thermal treatment (green) of the (b) corresponding poly(diethyl vinylphosphonate) PDEVp (red).

As for PDMVP an elimination reaction as side group cleavage is not possible; only the cleavage of dimethyl ether is observed ( $m/z = 45/46$ ). During this decomposition also partial degradation of the polymer backbone occurs, which can be supported by both the detection of alkenes (propylene  $m/z = 41/42$ , butene  $m/z = 55/56$ , pentene  $m/z = 69/70$ ) as volatile decomposition products as well as by the weight loss (34 wt % for dimethyl ether cleavage, observed: 45 wt %) (Figure 9 and Scheme 3).

For all three polymers during the second degradation step only small amounts of propylene and butene can be observed, indicating main-chain scission. The observed weight loss shows that some volatile phosphorus compounds must be evolving (mass of  $\text{P}_2\text{O}_5$  is much higher than the residual mass), which could though not be observed by MS.

According to these results, poly(vinylphosphonic acid) (PVPA) should be easily accessible by thermal treatment of both PDEVp and PDIVP. This could be confirmed by tempering the corresponding poly(vinylphosphonate)s for 30 min at 350 °C in a nitrogen atmosphere, yielding poly(vinylphosphonic acid) as a gray solid. Full cleavage of the ester side chains was determined by  $^1\text{H}$  NMR spectroscopy (see Figure 10 and Figure S7) and further confirmed by elemental analysis. The molecular weight of the resulting polymer was determined by static light scattering methods in batch, producing Zimm plots. Within the limits of the experimental accuracy, degradation of the polymer backbone could not be observed. Similarly as for the hydrolysis with  $\text{TMSBr}$ , the end groups of obtained oligomeric vinylphosphonic acids could not be identified.

## CONCLUSIONS

Trivalent cyclopentadienyl lanthanide complexes are easily accessible in a one-step reaction and proved to be, in the case of late lanthanides, efficient initiators and highly active catalysts for the group transfer polymerization of various dialkyl vinylphosphonates. For DEVp and DIVP, this living polymerization leads to well-defined polymers with low PDI and a molecular weight close to the initial monomer to catalyst ratio even at elevated temperatures (30–70 °C). The initiation proceeds via nucleophilic transfer of a cyclopentadienyl ligand as shown by mass spectrometric studies. The smaller the metal center (i.e., the higher the Lewis acidity), the higher the initiator efficiency and the normalized catalytic



activity TOF/ $I^*$ . Therefore,  $Cp_2LnX$ -initiated coordinative anionic polymerization of vinylphosphonates with high catalytic activity can only be achieved by using late lanthanide complexes.

Because of the low solubility of PDMVP in suitable solvents, a well-controlled lanthanide-mediated group transfer polymerization of DMVP is not thus far possible. By contrast, due to its high solubility in most common organic solvents, purification of PDIVP by precipitation does not give satisfactory results. Combined with high polymerization activity and easy conversion by both mild hydrolysis or thermal treatment, this makes PDEVPP the ideal basis for well-defined high-molecular weight poly(vinylphosphonic acid) with narrow chain length distribution. Furthermore, aqueous PDEVPP solutions exhibit a lower critical solution temperature (LCST) close to the physiological range, which is strongly dependent on both concentration and molecular weight of the polymer (40–46 °C).

## ■ EXPERIMENTAL SECTION

**General.** All reactions were carried out under an argon atmosphere using standard Schlenk or glovebox techniques. All glassware was heat dried under vacuum prior to use. Unless otherwise stated, all chemicals were purchased from Sigma-Aldrich or Acros Organics and used as received. Toluene was dried using a MBraun SPS-800 solvent purification system. Tetrahydrofuran (THF) was distilled over potassium prior to use. All metal complexes, DEVPP, and DIVPP were prepared according to literature procedures.<sup>4,6</sup> DMVP was purchased from Alpha Aesar. Monomers were dried over calcium hydride and distilled prior to polymerization.

NMR spectra were recorded on a Bruker ARX-300 spectrometer.  $^1H$  NMR spectroscopic chemical shifts  $\delta$  are reported in ppm relative to tetramethylsilane and calibrated to the residual proton signal of the deuterated solvent.  $^{31}P$  NMR spectroscopic chemical shifts are reported in ppm relative to and calibrated to 85%  $H_3PO_4$ . Deuterated solvents were obtained from Deutero Deutschland GmbH and used as received. Elemental analyses were measured at the Laboratory for Microanalytics at the Institute of Inorganic Chemistry at the Technische Universität München. ESI MS analytical measurements were performed with isopropanol solutions on a Varian 500-MS spectrometer, using 70 keV in the positive ionization mode. MALDI-ToF MS measurements were performed on a Bruker Ultraflex ToF/ToF mass spectrometer. All samples were prepared and run in THF solution dithranol doped with sodium trifluoroacetate. TGA was carried out on a Texas Instruments TGA-Q5000 with a heating rate of 10 K  $min^{-1}$ . TGA MS measurements were performed on the same instrument using a heating rate of 25 K  $min^{-1}$ .

**Polymerizations.** Polymerizations were performed in 16 mL of toluene, using a catalyst concentration of 0.625 mg  $mL^{-1}$  (10 mg of catalyst). After dissolving the catalyst in the solvent and thermostating to the desired temperature, the calculated amount of monomer was added. The reaction was stirred at the given temperature for the stated reaction time and then quenched with MeOH (0.5 mL). The polymer was precipitated by addition of the reaction mixture to hexane (150 mL) and decanted from solution. Residual solvents were removed by drying under vacuum at 70 °C overnight.

**Activity Measurements.** For activity measurements 21.7  $\mu mol$  (1 equiv) of the catalyst was dissolved in 20 mL of toluene, and the reaction mixture was thermostated to 30 °C. Then 2.00 mL (2.14 g, 600 equiv) of DEVPP or 2.50 g (600 equiv) of DIVPP was added. During the course of the measurement aliquots (0.5 mL) are taken and quenched by adding to deuterated methanol (0.2 mL). The conversion was determined by  $^{31}P$  NMR spectroscopy. After the stated reaction time a last aliquot was taken, and the reaction was quenched by addition of MeOH (0.5 mL).

Work-up of the polymer was carried out according to the regular polymerizations.

**Molecular Weight Determination.** GPC was carried out on a Varian LC-920 equipped with two PL Polargel columns. As eluent a mixture of 50% THF, 50% water, and 9 g  $L^{-1}$  tetrabutylammonium bromide (TBAB) was used in the case of PDEVPP; for PDIVPP analysis the eluent was THF with 6 g  $L^{-1}$  TBAB. Absolute molecular weights have been determined online by multiangle light scattering (MALS) analysis using a Wyatt Dawn Heleos II in combination with a Wyatt Optilab rEX or the integrated RI detector (356-LC) as concentration source.

**Determination of the LCST.** Turbidity measurements for the determination of the cloud point were carried out with a Cary 50-UV/vis spectrometer from Varian with 4 mL glass cuvettes and aqueous polymer solutions of different concentrations (0.5–20 mg  $mL^{-1}$ ). Using a Peltier thermostat, the samples were heated at a rate of 1 K  $min^{-1}$  followed by a 3 min waiting period to ensure thermal equilibrium. The cloud point was determined by repeated spectrophotometric detection of the changes in transmittance at a wavelength of 550 nm. It was defined as the temperature corresponding to a 15% decrease in optical transmittance. For further evaluation the results of the single experiments are averaged and rounded to 0.5 °C.

**Polymer Analogous Hydrolysis to Poly(vinylphosphonic acid).** Poly(dialkyl vinylphosphonate) was dissolved in dry dichloromethane (10 g  $L^{-1}$ ), 3 equiv of trimethylsilyl bromide (relative to the ester functionalities) was added, and the resulting reaction mixture was refluxed for 24 h. Then the volatiles were removed in vacuo, and the residue was dissolved in a small amount of methanol (~5 equiv) and aqueous HCl (1 M, 4 equiv). After 2 h the reaction mixture was dried in vacuo and purified by aqueous dialysis (100 kDa MWCO).

**Thermal Treatment of Poly(vinylphosphonate)s.** Poly(diethyl vinylphosphonate) (PDEVPP) or poly(diisopropyl vinylphosphonate) (PDIVPP) was heated at a rate of 20 °C  $min^{-1}$  to 350 °C and tempered for 30 min at this temperature. After cooling the corresponding poly(vinylphosphonic acid) was obtained as a gray solid.

Elemental analysis: PVPA: calculated (disregarding end groups): C 22.2%, H 4.66%, P 28.7%; found: from PDEVPP: C 24.5%, H 4.66%, P 29.0%; from PDIVPP: C 24.0%, H 4.28%, P 29.9%.

## ■ ASSOCIATED CONTENT

Supporting Information. ESI and MALDI-ToF MS data of oligomer analysis, DEVPP polymerization results at 70 °C, conversion vs reaction time diagrams for catalysts with low activity, further  $^1H$  NMR spectra for polymer analogous hydrolysis and thermal treatment. This material is available free of charge via the Internet at <http://pubs.acs.org>.

## ■ AUTHOR INFORMATION

### Corresponding Author

\*E-mail [riegler@tum.de](mailto:riegler@tum.de); Tel +49-89-289-13570; Fax +49-89-289-13562.

## ■ ACKNOWLEDGMENT

The authors thank Carly Anderson and Maximilian Lehenmeier for valuable discussions. S.S. is grateful for generous financial support by a scholarship of the Fonds der Chemischen Industrie.

## ■ REFERENCES

- (1) (a) Ellis, J.; Wilson, A. D. *Dent. Mater.* **1992**, *8*, 79–84. (b) Ebdon, J. R.; Price, D.; Hunt, B. J.; Joseph, P.; Gao, F.; Milnes, G. J.;

- Cunliffe, L. K. *Polym. Degrad. Stab.* **2000**, *69*, 267–277. (c) Parvole, J.; Jannasch, P. *Macromolecules* **2008**, *41*, 3893–3903. (d) Price, D.; Pyrah, K.; Hull, T. R.; Milnes, G. J.; Ebdon, J. R.; Hunt, B. J.; Joseph, P. *Polym. Degrad. Stab.* **2002**, *77*, 227–233. (e) Price, D.; Pyrah, K.; Hull, T. R.; Milnes, G. J.; Ebdon, J. R.; Hunt, B. J.; Joseph, P.; Konkel, C. S. *Polym. Degrad. Stab.* **2001**, *74*, 441–447. (f) Steininger, H.; Schuster, M.; Kreuer, K. D.; Kaltbeitzel, A.; Bingoel, B.; Meyer, W. H.; Schauff, S.; Brunklaus, G.; Maier, J.; Spiess, H. W. *Phys. Chem. Chem. Phys.* **2007**, *9*, 1764–1773. (g) Zakikhani, M.; Walker, D. R. E.; Hasling, P. D.; Smith, A. C.; Davis, K. P. Eur. Pat. Appl. 0 780 406 A2, 1997.
- (2) Levin, Y. A.; Fridman, G. B.; Ivanov, B. Y. *Polym. Sci. U.S.S.R.* **1975**, *17*, 971–982.
- (3) (a) Bingoel, B.; Hart-Smith, G.; Barner-Kowollik, C.; Wegner, G. *Macromolecules* **2008**, *41*, 1634–1639. (b) Bingoel, B.; Meyer, W. H.; Wagner, M.; Wegner, G. *Macromol. Rapid Commun.* **2006**, *27*, 1719–1724. (c) Leute, M. In *Polymers with Phosphorus Functionalities*. Ph.D. Thesis, University of Ulm, Ulm, 2007. (d) Wagner, T.; Manhart, A.; Deniz, N.; Kaltbeitzel, A.; Wagner, M.; Brunklaus, G.; Meyer, W. H. *Macromol. Chem. Phys.* **2009**, *210*, 1903–1914. (e) Rabe, G. W.; Komber, H.; Haeussler, L.; Kreger, K.; Lattermann, G. *Macromolecules* **2010**, *43*, 1178–1181.
- (4) Seemann, U. B.; Dengler, J. E.; Rieger, B. *Angew. Chem., Int. Ed.* **2010**, *122*, 3567–3569.
- (5) (a) Yasuda, H.; Yamamoto, H.; Yamashita, M.; Yokota, K.; Nakamura, A.; Miyake, S.; Kai, Y.; Kanehisa, N. *Macromolecules* **1993**, *26*, 7134–7143. (b) Yasuda, H.; Yamamoto, H.; Yokota, K.; Miyake, S.; Nakamura, A. *J. Am. Chem. Soc.* **1992**, *114*, 4908–4910. (c) Chen, E. Y.-X. *Chem. Rev.* **2009**, *109*, 5157–5214.
- (6) Birmingham, J. M.; Wilkinson, G. *J. Am. Chem. Soc.* **1956**, *78*, 42–44.
- (7) Eggers, S. H.; Schultze, H.; Kopf, J.; Fischer, R. D. *Angew. Chem., Int. Ed.* **1986**, *98*, 631–632.
- (8) (a) Evans, W. J.; Perotti, J. M.; Kozimor, S. A.; Champagne, T. M.; Davis, B. L.; Nyce, G. W.; Fujimoto, C. H.; Clark, R. D.; Johnston, M. A.; Ziller, J. W. *Organometallics* **2005**, *24*, 3916–3931. (b) Mueller, T. J.; Nyce, G. W.; Evans, W. J. *Organometallics* **2011**, *30*, 1231–1235.
- (9) (a) Okada, Y.; Tanaka, F. *Macromolecules* **2005**, *38*, 4465–4471. (b) Salzinger, S.; Huber, S.; Jordan, R.; Papadakis, C. M. Poster contribution for the Conference “Frontiers in Polymer Science” in Mainz on June 7th–9th 2009, *Frontiers in Polymer Science* 2009, P2-109.
- (10) Rabinowitz, R. *J. Org. Chem.* **1963**, *28*, 2975–2978.

Reprinted with Permission from Salzinger, S; Seemann, U. B.; Plikhta, A.; Rieger, B. *Macromolecules* **2011**, *44*, 5920. Copyright 2011 American Chemical Society.

## Supporting Information

# Poly(vinylphosphonate)s Synthesized by Trivalent Cyclopentadienyl Lanthanide-Induced Group Transfer Polymerization

*Stephan Salzinger, Uwe B. Seemann, Andriy Plikhta, Bernhard Rieger*

WACKER Lehrstuhl für Makromolekulare Chemie, Technische Universität München,  
Lichtenbergstraße 4, 85748 Garching bei München

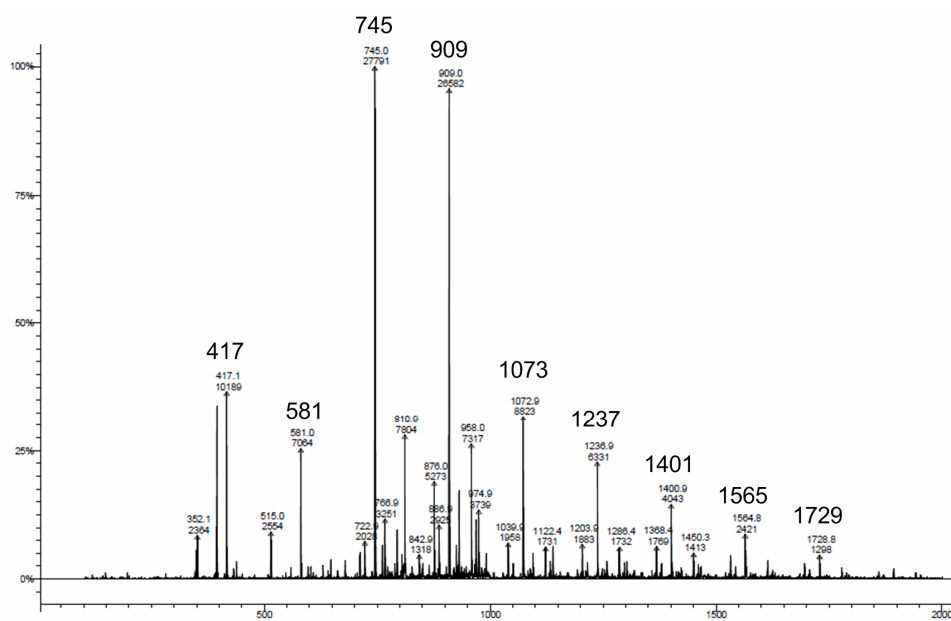


Figure S1: ESI MS analysis of oligomeric PDEVp ( $\text{Cp}_3\text{Yb}$ , toluene, 5 eq DEVp).

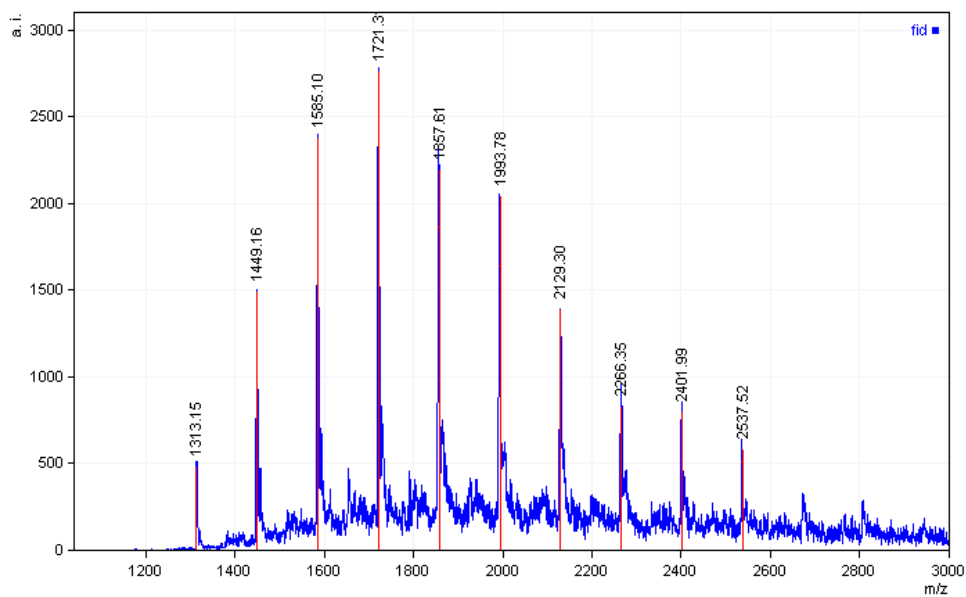


Figure S2: MALDI-ToF MS analysis of oligomeric PDMVP ( $\text{Cp}_3\text{Tm}$ , toluene, 5 eq DMVP).

Table S1: Identified peaks of the ESI MS analysis of PDEVF and the corresponding end groups

Peak $m/z$	Mol. Mass/ $\text{g mol}^{-1}$	Cation <sup>a</sup> / $\text{g mol}^{-1}$	Monomer <sup>b</sup>	Remain/ $\text{g mol}^{-1}$	End group
417	417	23 ( $\text{Na}^+$ )	2	66	CpH
581	581	23 ( $\text{Na}^+$ )	3	66	CpH
745	745	23 ( $\text{Na}^+$ )	4	66	CpH
909	909	23 ( $\text{Na}^+$ )	5	66	CpH
1073	1073	23 ( $\text{Na}^+$ )	6	66	CpH
1237	1237	23 ( $\text{Na}^+$ )	7	66	CpH
1401	1401	23 ( $\text{Na}^+$ )	8	66	CpH
1565	1565	23 ( $\text{Na}^+$ )	9	66	CpH
1729	1729	23 ( $\text{Na}^+$ )	10	66	CpH
876	1752	46 (2 x $\text{Na}^+$ )	10	66	CpH
958	1916	46 (2 x $\text{Na}^+$ )	11	66	CpH
1040	2080	46 (2 x $\text{Na}^+$ )	12	66	CpH
1122	2244	46 (2 x $\text{Na}^+$ )	13	66	CpH
1204	2408	46 (2 x $\text{Na}^+$ )	14	66	CpH
1286	2572	46 (2 x $\text{Na}^+$ )	15	66	CpH
1368	2736	46 (2 x $\text{Na}^+$ )	16	66	CpH
1450	2900	46 (2 x $\text{Na}^+$ )	17	66	CpH

<sup>a</sup> Ionizing cation for mass analysis

<sup>b</sup> Number of DEVF repeating units

Table S2: Identified peaks of the MALDI-ToF MS analysis of PDMVP and the corresponding end groups

Peak $m/z$	Mol. Mass/ $\text{gmol}^{-1}$	Cation <sup>a</sup> / $\text{gmol}^{-1}$	Monomer <sup>b</sup>	Remain / $\text{gmol}^{-1}$	End-group
1313	1313	23 ( $\text{Na}^+$ )	9	66	CpH
1449	1449	23 ( $\text{Na}^+$ )	10	66	CpH
1585	1585	23 ( $\text{Na}^+$ )	11	66	CpH
1721	1721	23 ( $\text{Na}^+$ )	12	66	CpH
1857	1857	23 ( $\text{Na}^+$ )	13	66	CpH
1993	1993	23 ( $\text{Na}^+$ )	14	66	CpH
2129	2129	23 ( $\text{Na}^+$ )	15	66	CpH
2266	2265	23 ( $\text{Na}^+$ )	16	66	CpH
2401	2401	23 ( $\text{Na}^+$ )	17	66	CpH
2537	2537	23 ( $\text{Na}^+$ )	18	66	CpH

<sup>a</sup> Ionizing cation for mass analysis

<sup>b</sup> Number of DMVP repeating units

Table S3: Polymerizations of DEVP ( $Cp_3Ln$ , toluene, 70 °C, monomer to catalyst ratio: 200, reaction time: 1 h)

$Cp_3Ln$	$M_w$ /kDa	$M_n$ /kDa	PDI	$I^*$ <sup>a</sup> /%	Yield <sup>b</sup>
Lu	50	40	1.12	82	96%
Yb	85	75	1.30	44	95%
Tm	240	170	1.40	19	99%
Er	240	170	1.40	19	91%
Ho	260	185	1.41	18	91%
Dy	270	200	1.35	16	98%
Tb	265	200	1.35	- <sup>c</sup>	69%
Gd	230	150	1.53	- <sup>c</sup>	54%

---

<sup>a</sup>  $I^* = M_{exp}/M_n$ ,  $I^*$  = Initiator efficiency,  $M_{exp}$ : Expected molecular weight, based on living polymerization calculation.

<sup>b</sup> Determined by weighing of the components

<sup>c</sup> Not calculable due to incomplete conversion

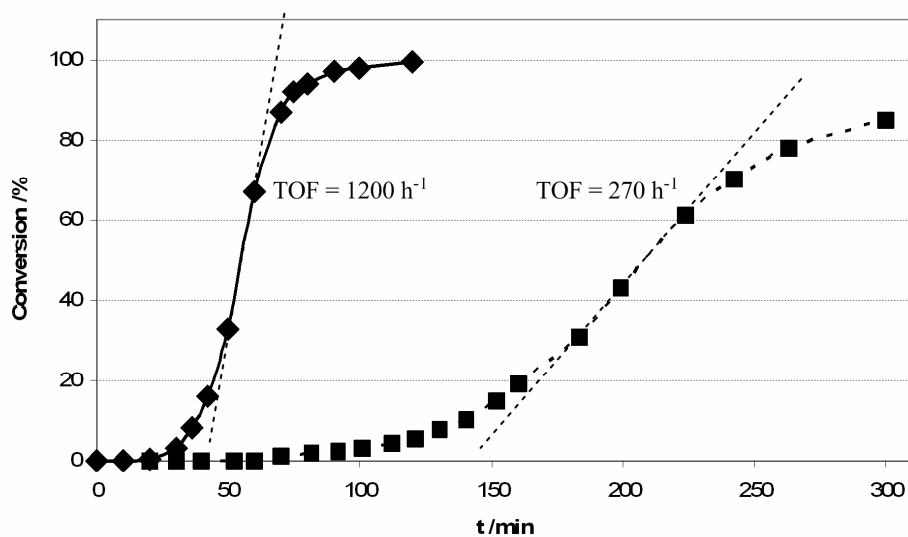


Figure S3: Determination of the catalytic activity of Cp<sub>3</sub>Ho (diamond, plain, TOF = 1200 h<sup>-1</sup>) and Cp<sub>3</sub>Dy (squares, short dashed, TOF = 270 h<sup>-1</sup>) for the polymerization of DEVP (monomer to catalyst ratio: 600).

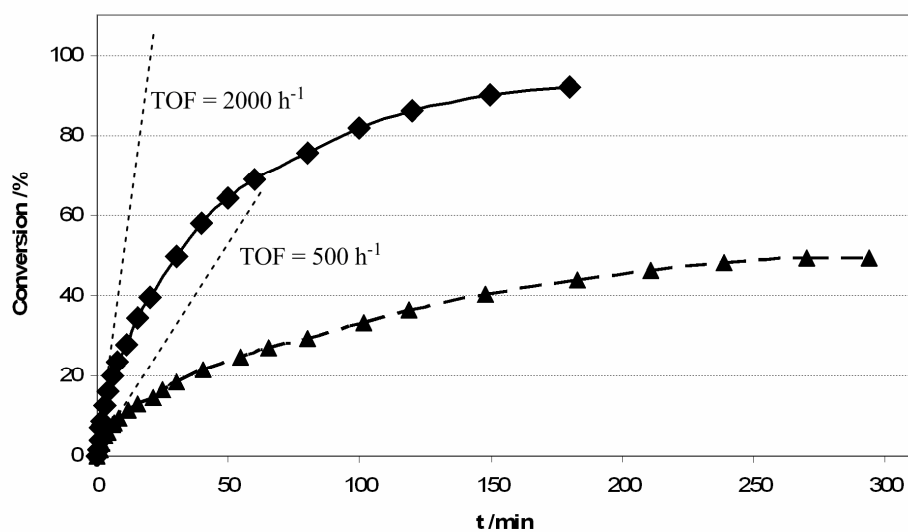


Figure S4: Determination of the catalytic activity of Cp<sub>3</sub>Er (diamond, plain, TOF = 2000 h<sup>-1</sup>) and Cp<sub>3</sub>Ho (triangles, long dashed, TOF = 500 h<sup>-1</sup>) for the polymerization of DIVP (monomer to catalyst ratio: 600).



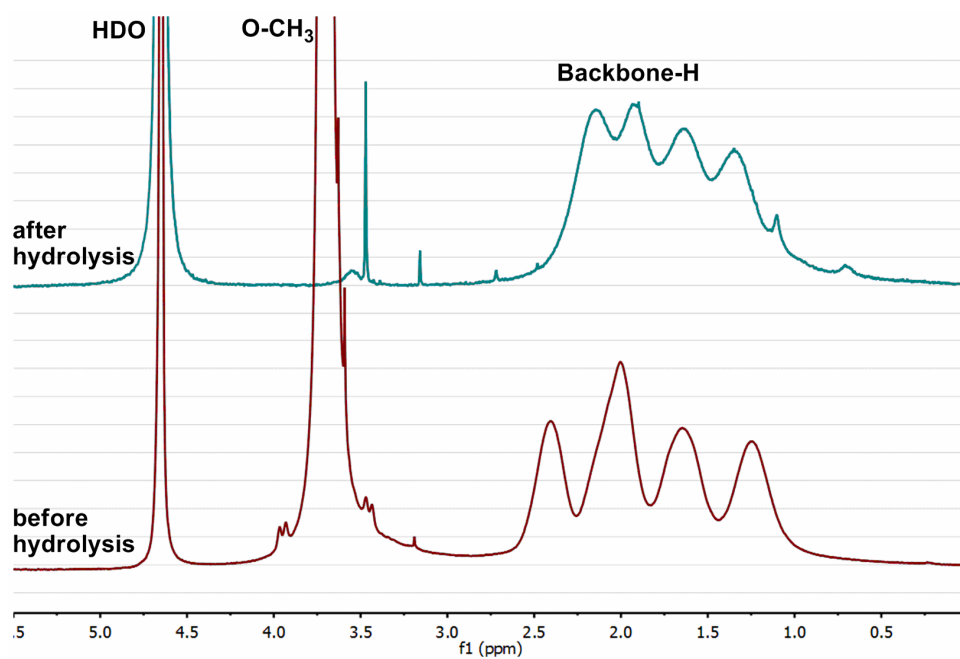


Figure S5: <sup>1</sup>H NMR spectra in D<sub>2</sub>O of PDMVP before (red) and after (green) hydrolysis.

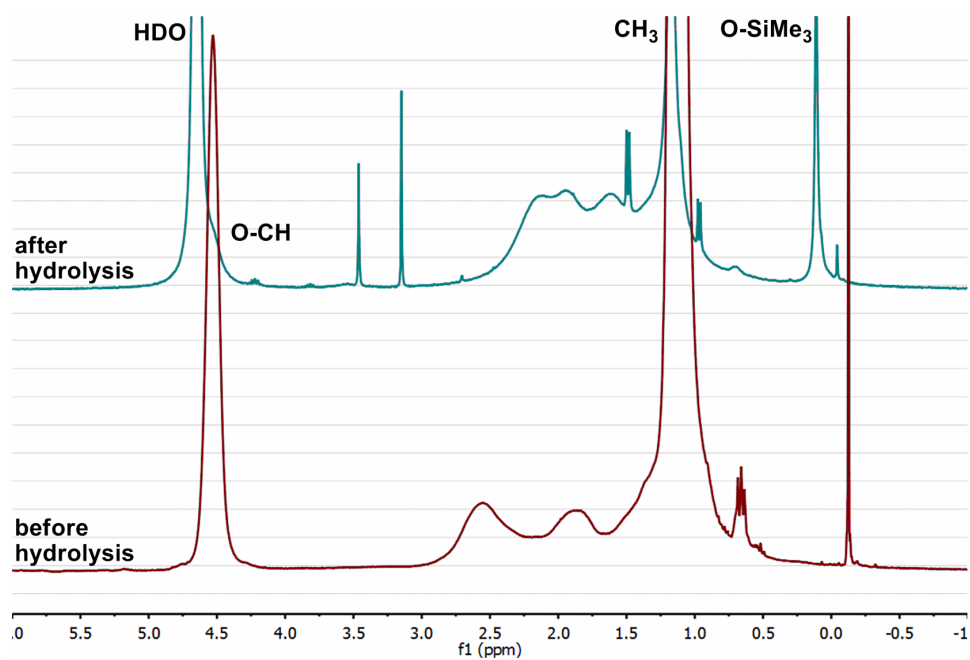


Figure S6: <sup>1</sup>H NMR spectra of PDIVP before (in CDCl<sub>3</sub>, red, for easier comparison this spectrum was shifted 0.15 ppm to higher field) and after (in D<sub>2</sub>O, green) hydrolysis. Both residual isopropyl ( $\delta = 1.1$  and 4.5 ppm) and trimethylsilyl ( $\delta = 0.2$  ppm) side groups are visible.

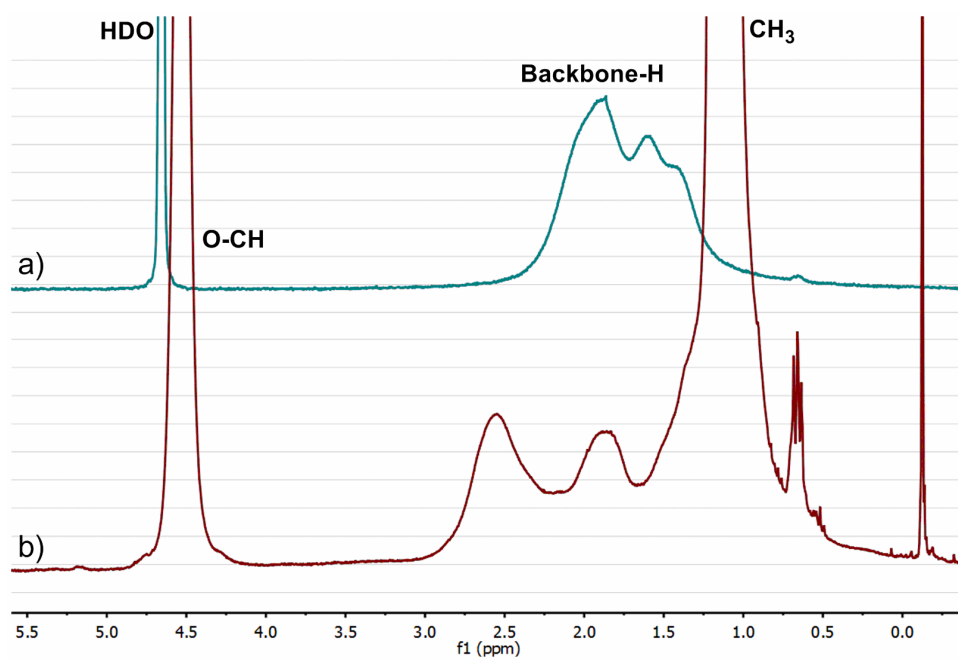
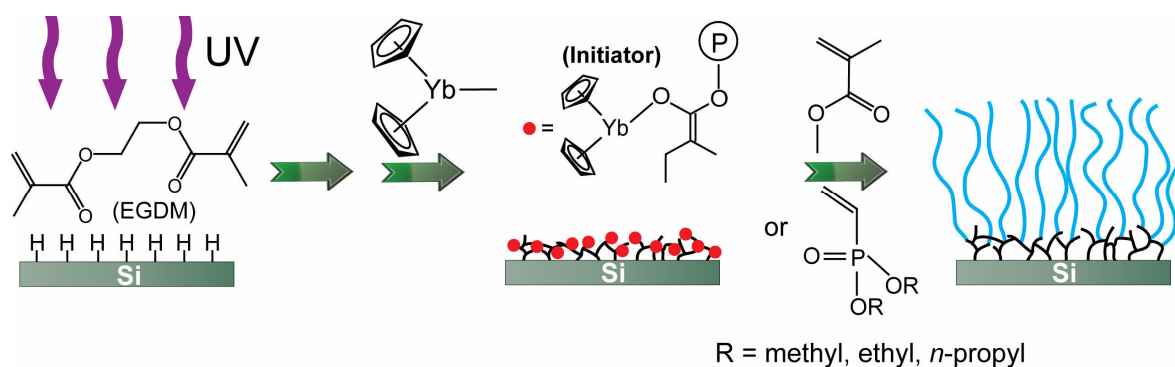


Figure S7:  $^1\text{H}$  NMR spectra of a) poly(vinylphosphonic acid) (PVPA) synthesized by thermal treatment (in  $\text{D}_2\text{O}$ , green) of the b) corresponding poly(diisopropyl vinylphosphonate) PDIVP (in  $\text{CDCl}_3$ , red, for easier comparison this spectrum was shifted 0.15 ppm to higher field).

## CHAPTER 6:

# SURFACE-INITIATED GROUP TRANSFER POLYMERIZATION MEDIATED BY RARE EARTH METAL CATALYSTS



*“Daring ideas are like chessmen moved forward;  
they may be beaten, but they may start a winning game.”*

- Johann Wolfgang von Goethe (1749-1832)



**Status:** Published online: April 12, 2012  
**Journal:** Journal of the American Chemical Society  
Issue 134, 7333-7336  
**Publisher:** ACS Publications  
**Article type:** Communication  
**DOI:** 10.1021/ja3027423  
**Authors:** Ning Zhang, Stephan Salzinger, Frank Deubel, Rainer Jordan,  
Bernhard Rieger

**Content:**

This chapter presents a new possibility for the perfect decoration of surfaces with dense polymer brushes of specific functionality – surface-initiated group transfer polymerization mediated by rare earth metal catalysts. This experimentally facile method allows rapid grafting of polymer brushes with a thickness of more than 150 nm in less than 5 min at room temperature.

SI-GTP follows a two-step method for which the rare earth metal catalyst is first reacted with a pre-formed binding layer containing methacrylate functionalities (or other suitable binding sites), *e.g.* poly(ethylene glycol dimethacrylate), which then serves as an efficient initiator for a subsequent SI-GTP of Michael acceptor-type monomers, *e.g.* MMA or DAVP. SI-GTP is not only suitable to common (meth)acrylic monomers, but also to a variety functional monomers, which cannot be polymerized by other surface-initiated polymerizations. Thus, SI-GTP widens the range of accessible functional polymer brushes, *e.g.* the method gives access to both thermoresponsive PDEVP and proton-conducting PVPA brush layers.



RightsLink®

Home

Create Account

Help



ACS Publications

High quality. High impact.

**Title:** Surface-Initiated Group Transfer Polymerization Mediated by Rare Earth Metal Catalysts**Author:** Ning Zhang, Stephan Salzinger, Frank Deubel, Rainer Jordan, and Bernhard Rieger**Publication:** Journal of the American Chemical Society**Publisher:** American Chemical Society**Date:** May 1, 2012

Copyright © 2012, American Chemical Society

User ID
<input type="text"/>
Password
<input type="text"/>
<input type="checkbox"/> Enable Auto Login
<input type="button" value="LOGIN"/>
<a href="#">Forgot Password/User ID?</a>
<b>If you're a copyright.com user,</b> you can login to RightsLink using your copyright.com credentials. Already a <b>RightsLink user</b> or want to <a href="#">learn more?</a>

**PERMISSION/LICENSE IS GRANTED FOR YOUR ORDER AT NO CHARGE**

This type of permission/license, instead of the standard Terms & Conditions, is sent to you because no fee is being charged for your order. Please note the following:

- Permission is granted for your request in both print and electronic formats, and translations.
- If figures and/or tables were requested, they may be adapted or used in part.
- Please print this page for your records and send a copy of it to your publisher/graduate school.
- Appropriate credit for the requested material should be given as follows: "Reprinted (adapted) with permission from (COMPLETE REFERENCE CITATION). Copyright (YEAR) American Chemical Society." Insert appropriate information in place of the capitalized words.
- One-time permission is granted only for the use specified in your request. No additional uses are granted (such as derivative works or other editions). For any other uses, please submit a new request.

BACK

CLOSE WINDOW

Copyright © 2013 Copyright Clearance Center, Inc. All Rights Reserved. [Privacy statement.](#)  
Comments? We would like to hear from you. E-mail us at [customer@copyright.com](mailto:customer@copyright.com)


Reprinted with Permission from Zhang, N.; Salzinger, S.; Deubel, F.; Jordan, R.; Rieger, B. *J. Am. Chem. Soc.* **2012**, *134*, 7333. Copyright 2012 American Chemical Society.

## Surface-Initiated Group Transfer Polymerization Mediated by Rare Earth Metal Catalysts

Ning Zhang,<sup>†</sup> Stephan Salzinger,<sup>†</sup> Frank Deubel,<sup>†</sup> Rainer Jordan,<sup>†,‡</sup> and Bernhard Rieger<sup>\*,†</sup>

<sup>†</sup>WACKER-Lehrstuhl für Makromolekulare Chemie, Technische Universität München, Lichtenbergstrasse 4, 85747 Garching bei München, Germany

<sup>‡</sup>Professur für Makromolekulare Chemie, Department Chemie, Technische Universität Dresden, Zellescher Weg 19, 01069 Dresden, Germany

 Supporting Information

**ABSTRACT:** We present the first example of a surface-initiated group transfer polymerization (SI-GTP) mediated by rare earth metal catalysts for polymer brush synthesis. The experimentally facile method allows rapid grafting of polymer brushes with a thickness of >150 nm in <5 min at room temperature. We show the preparation of common poly(methacrylate) brushes and demonstrate that SI-GTP is a versatile route for the preparation of novel polymer brushes. The method gives access to both thermoresponsive and proton-conducting brush layers.

Rare-earth-metal-mediated group transfer polymerization (GTP) was first reported by Yasuda et al. in 1992.<sup>1</sup> In view of the polymerization mechanism, it is also referred to as coordinative-anionic addition polymerization.<sup>2</sup> Over the past decades, intensive research has been carried out to optimize the reaction conditions and initiator efficiency and to broaden its use for a variety of monomers, e.g. different (meth)acrylates and (meth)acrylamides.<sup>2,3</sup> Due to its highly living character, rare earth (RE) metal-mediated GTP gives strictly linear polymers with very low dispersity (characterically <1.10), exhibits a linear increase in average molar mass upon monomer conversion, and allows the synthesis of block copolymers as well as the introduction of chain end functionalities.<sup>2,4</sup> Coordination of the growing chain end at the catalyst suppresses side reactions and allows stereospecific polymerization as well as activity optimization by variation of both the metal center and the catalyst ligand sphere.<sup>2,5</sup> RE metal-mediated GTP is applicable to common acrylic monomers as well as to several functional monomers of interest, i.e. dialkyl vinylphosphonates (DAVP) and 2-vinylpyridine.<sup>6,7,37,38</sup> Such monomers are of specific interest for the modification of solids for biomedical applications.

Until now, almost all polymerization types have been transferred to surface-initiated (SI) polymerizations to prepare dense polymer brushes. This spans tolerant free radical polymerization yielding less defined brushes to nontolerant but highly defined living cationic and anionic polymerizations.<sup>8–21</sup> Controlled radical polymerizations have been especially intensively studied in regard to their implementation for surface modification, as they are relatively tolerant toward impurities but allow the synthesis of quite defined polymer brushes.<sup>22</sup> For instance, surface-initiated atom transfer radical

polymerization (SI-ATRP) gained great interest, as it can be performed even at room temperature (rt) in aqueous solution.<sup>23</sup> However, to our knowledge, SI-GTP mediated by RE metals has not been employed yet, although it combines the advantages of both living ionic and coordinative polymerizations and would give access to several new polymer brush coatings that cannot be realized by current techniques. The most intriguing are poly(vinylphosphonate)s and other phosphorus-containing polymers. As coatings, they have attracted interest due to their halogen-free flame retardation and proton-conducting properties.<sup>24–27</sup> Because of the low toxicity,<sup>28</sup> much attention has recently been drawn to their use in biomedical applications such as nonfouling coatings,<sup>29,30</sup> tissue engineering,<sup>31</sup> drug delivery systems,<sup>32</sup> and cell proliferation.<sup>33</sup> However, only RE metal-mediated GTP allows the well-controlled polymerization of vinylphosphonates, as radical and classical anionic approaches result in low yields of polymer with unsatisfying degrees of polymerization.<sup>34–36</sup>

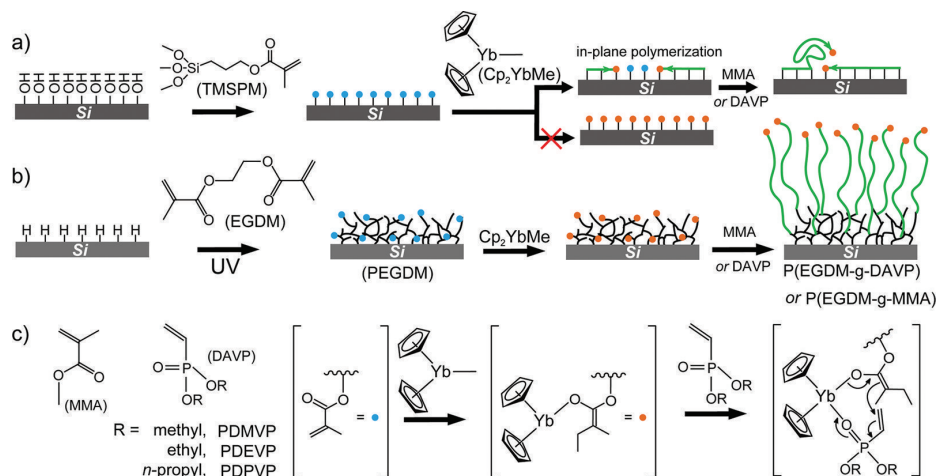
Here, we present the first example of SI-GTP mediated by RE metal catalysts. SI-GTP is applicable to the polymerization of common acrylic monomers such as methyl methacrylate (MMA) as well as special functional monomers such as DAVP. It is experimentally facile and can be performed at rt, and polymer layer thicknesses up to 300 nm can be achieved within a few minutes at rt.

We recently reported on the synthesis of PMMA–poly(diethyl vinylphosphonate) (PDEV) block copolymers using simple ytterbium complexes through a living GTP mechanism.<sup>37</sup> For the translation of GTP to a defined SI-GTP, we first followed the established strategy and employed self-assembled monolayers (SAMs) of 3-(trimethoxysilyl)propyl methacrylate (TMSPM) on oxidized silicon (Scheme 1a). Upon addition of bis(cyclopentadienyl)methyl ytterbium (Cp<sub>2</sub>YbMe), a highly active enolate initiating species is formed (Scheme 1) for SI-GTP with added vinyl monomers. The reaction mechanism for GTP of (meth)acrylates and DAVP has been previously outlined in detail.<sup>1,2,38</sup> In brief, the surface-bound enolate is transferred to a monomer coordinated at the Yb catalyst, and successive chain growth occurs via repeated conjugate addition over an eight-membered-ring intermediate (Scheme 1c).

Received: March 21, 2012

Published: April 12, 2012

**Scheme 1. Preparation of Precoating Layer, Ytterbocene Catalyst Immobilization, and Subsequent SI-GTP of MMA or DAVP from (a) a TMSPM Monolayer and (b) a PEGDM Film on Silicon Wafer; (c) Molecular Structure of MMA and DAVP, and SI-GTP Reaction Mechanism for Initiation and Chain Growth**



However, after attempted SI-GTP with MMA or DAVP and thorough removal of physisorbed polymer and remaining catalyst residues using different solvents under ultrasonication, AFM measurements reveal a relatively rough and inhomogeneous surface topography, indicating insufficient coverage of the substrate by the polymeric layer (Supporting Information). The only partial SI-GTP may be due to the fact that the dense and rigid SAM initiator limits the accessibility of the terminal methacrylate moieties for the bulky  $\text{Cp}_2\text{YbMe}$ . Moreover, the close packing facilitates an in-plane topopolymerization via GTP of the surface-bound methacrylate functionalities in the organized monolayer (Scheme 1a). Hence, the consumption of surface methacrylic moieties does not allow the formation of a reactive monolayer of the enolate initiating species.

To cope with this problem, the precoating layer should offer high surface coverage of the catalyst binding sites, which are prone to in-plane topopolymerization. This can be realized by a thin cross-linked polymer precoating with embedded but isolated (meth)acrylate units. A facile and direct approach for the synthesis of such binding layers is the self-initiated photografting and photopolymerization (SI-PGP) of, e.g., ethylene glycol dimethacrylate (EGDM) on hydrogen-terminated silicon.

First, H-terminated silicon substrates were prepared by means of oxide layer stripping using hydrofluoric acid and subsequently irradiated by UV light [spectral distribution between 300 and 400 nm ( $\lambda_{\text{max}} = 350$  nm) in bulk EGDM]. UV irradiation of  $\sim 350$  nm without oxygen and solvents results in direct grafting of unsaturated compounds by formation of stable Si–C bonds via photoactivated hydrosilylation.<sup>39–42</sup> Moreover, the (meth)acrylate units can also undergo polymerization via the SI-PGP mechanism via H-abstraction from the Si–H surface as well as from C–H moieties of already grafted EGDM.<sup>43–48</sup> Because of the low bond dissociation energy of Si–H,<sup>49</sup> direct grafting is likely by both grafting reaction mechanisms.<sup>44</sup> In any case, surface dangling bonds are created and responsible for efficient surface grafting of EGDM, resulting in a cross-linked PEGDM network film grafted to silicon via Si–C bonds of superior thermal and chemical

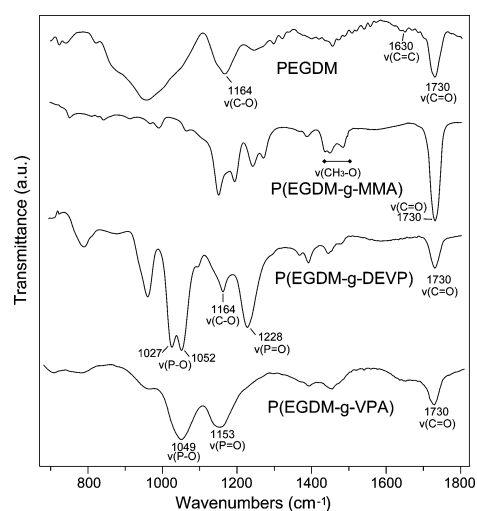


**Figure 1.** IR spectra of poly(ethylene glycol dimethacrylate) [PEGDM], poly(ethylene glycol dimethacrylate-graft-diethyl vinylphosphonate) [P(EGDM-g-DEVP)], poly(ethylene glycol dimethacrylate-graft-vinylphosphonic acid) [P(EGDM-g-VPA)], and poly(ethylene glycol dimethacrylate-graft-methyl methacrylate) [P(EGDM-g-MMA)] brushes on a silicon wafer.

stability.<sup>50</sup> To our knowledge, this is also the first example of direct photografting of polymers onto H-terminated silicon.

After UV irradiation, the substrate was rigorously cleaned (ultrasonication in several solvents with different polarities) to ensure that only chemically grafted polymer remains on the substrate. The successful grafting of PEGDM was confirmed by IR spectroscopy (Figure 1). The strong bands around 1730 and 1164  $\text{cm}^{-1}$  are assigned to the C=O and C–O stretching modes. A weak band at 1630  $\text{cm}^{-1}$  assigned to the C=C stretching mode indicates that some of the methacrylate groups were preserved after photografting, which is crucial for catalyst immobilization.  $\text{Cp}_2\text{YbMe}$  was added to the PEGDM-modified silicon substrate to react with the remaining methacrylate functionalities to give the active initiating species for SI-GTP.



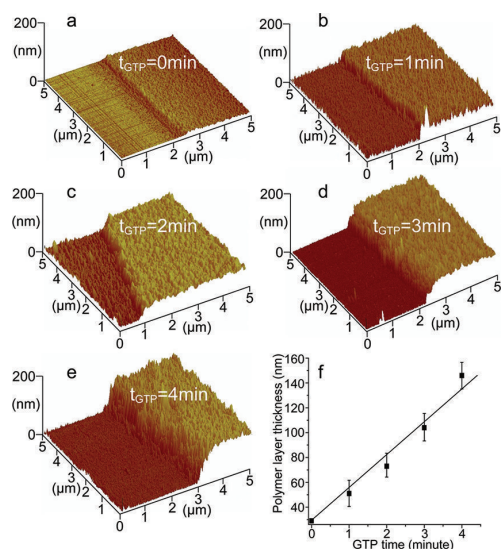


**Figure 2.** Three-dimensional representation of AFM scans of a PEGDM film on a silicon wafer and polymer brushes after SI-GTP of DEVP. (a) SI-GTP of EGDM for 30 min gives a PEGDM film with a thickness of  $29 \pm 6$  nm. (b–e) SI-GTP of DEVP on the same substrate after 1, 2, 3, and 4 min results in  $51 \pm 11$ ,  $73 \pm 9$ ,  $104 \pm 11$ , and  $146 \pm 12$  nm polymer brush layers, respectively. (f) P(EGDM-g-DEVP) layer thickness as a function of SI-GTP time.

Using  $\text{Cp}_2\text{YbMe}$  as the catalyst and silicon coated with a  $29 \pm 6$  nm (after 30 min UV irradiation) PEGDM primer layer, SI-GTP of diethyl vinylphosphonate (DEVP) results in an almost linear layer thickness increase with a constant growth rate of 26.5 nm/min (Figure 2). This rapid, constant growth rate is expected for a living SI-GTP.<sup>37</sup> AFM measurements also revealed homogeneous coverage of the entire substrate. The successful surface polymerization of DEVP was confirmed by IR spectroscopy (Figure 1). The  $1630\text{ cm}^{-1}$  band assigned to the  $\text{C}=\text{C}$  stretching mode disappears completely, and a new intensive band at  $1228\text{ cm}^{-1}$  is observed, characteristic for the  $\text{P}=\text{O}$  stretching mode of poly(vinylphosphonate)s. Formation of the PEGDM layer, immobilization of Yb, and formation of PDEVP brushes were further corroborated by systematic XPS measurements (Supporting Information).

Besides poly(vinylphosphonate)s, the current method is applicable to other monomers polymerizable by GTP. To demonstrate the general applicability of the method, SI-GTP of MMA was performed following the above-described procedure, resulting in very uniform PMMA brushes with a layer thickness of 316 nm within only 5 min at rt (Supporting Information). The remarkably high and constant layer growth rate of 57 nm/min and final layer thickness make SI-GTP an interesting alternative to SI-ATRP. The successful formation of PMMA brushes was confirmed by IR spectroscopy. As shown in Figure 1, upon SI-GTP of MMA on the PEGDM pre-coating layer, a new band arises at  $1485\text{--}1449\text{ cm}^{-1}$ , assignable to the typical  $\text{CH}_3\text{--O}$  stretching mode of PMMA.

So far, we have successfully prepared poly(dimethyl, diethyl, and di-*n*-propyl vinylphosphonate) (PDMVP, PDEVP, and PDPVP, respectively) brushes on H-terminated silicon. The influence of the polymer pendant alkyl chain length on the hydrophilic/hydrophobic character of the polymer layer was investigated by contact angle (CA) measurements (Figure 3).

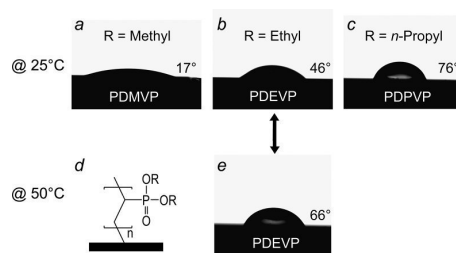


**Figure 3.** Molecular structure of poly(dialkyl vinylphosphonate)s (PDAVP) (d) and static water contact angle (CA) on different PDAVP coatings on silicon substrates at different temperatures. (a–c) CA of PDMVP, PDEVP, and PDPVP brushes at 25 °C. (e) CA of PDEVP brush at 50 °C.

The hydrophilic PDMVP gave a static water CA of  $17 \pm 3^\circ$ , while the more hydrophobic PDPVP displayed a CA of  $76 \pm 2^\circ$ . PDEVP displays a lower critical solution temperature of  $40\text{--}46^\circ\text{C}$ , depending on molar mass and concentration.<sup>38</sup> The PDEVP-modified substrate was found to have a static water CA of  $44 \pm 2^\circ$  at rt that increased to  $66 \pm 2^\circ$  upon heating to  $50^\circ\text{C}$ . The prepared PDMVP, PDPVP, and temperature-responsive PDEVP brushes have potential applications as bacterial, protein, peptide, and cell adhesion mediators and are first candidates for the study of (bio)mineralization in confined geometries.<sup>51</sup>

It was previously reported that poly(vinylphosphonate)s could be converted to poly(vinylphosphonic acid) (PVPA) by hydrolysis under mild conditions.<sup>38</sup> In this work, PVPA brushes were obtained analogously by treatment with trimethylsilyl bromide and successive HCl treatment to cleave the pendant alkyl groups from PDEVP brushes. The formation of PVPA brushes is apparent from the shift of the  $\text{P}=\text{O}$  stretching mode from  $1228$  to  $1153\text{ cm}^{-1}$  (Figure 1) and is in agreement with previous reports.<sup>52,53</sup> The hydrolysis of a 120 nm P(EGDM-g-DEVP) layer resulted in an 88 nm P(EGDM-g-VPA) film (Figure 4). The thickness decrease is ascribed to material loss after cleavage of the alkyl groups.

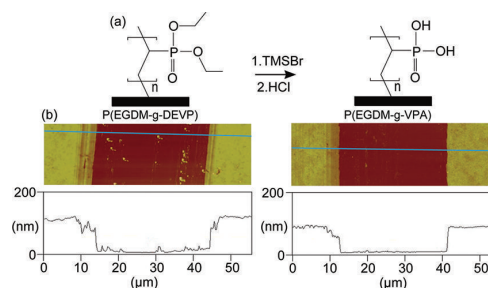


**Figure 4.** (a) Conversion from PDEVP to PVPA brushes by hydrolysis reaction. (b) AFM height images and section views along the indicated lines before and after reaction with TMSBr/HCl.

In summary, we have demonstrated a two-step method to efficiently prepare PMMA and PDAVP brushes using surface-initiated group transfer polymerization mediated by rare earth metal catalysts. First, a PEGDM network is prepared by photohydrolysis/SI-GTP of EGDM directly on hydrogen-terminated silicon. The preserved methacrylate groups can be reacted with bis(cyclopentadienyl)methylterbium, serving as efficient initiators for the successive SI-GTP of (meth)acrylates

or dialkyl vinylphosphonates forming polymer brushes. Remarkably fast and almost constant polymer layer thickness growth rates of 57 and 26.5 nm/min were found for MMA and DEVP, respectively. The method is applicable to functional monomers that cannot be polymerized by other surface-initiated polymerizations and thus widens the range of accessible functional polymer brushes. Moreover, we show the preparation of functional thermoresponsive PDEVF brushes. Poly(vinylphosphonic acid) is now easily accessible under mild conditions. The nontoxic and thermoswitchable surfaces are of great interest for diverse biological and medical applications, including controlled cell growth and cell release from surfaces as well as proton conducting films.

## ■ ASSOCIATED CONTENT

### ☎ Supporting Information

Detailed procedures for chemical reactions and XPS spectra. This material is available free of charge via the Internet at <http://pubs.acs.org>.

## ■ AUTHOR INFORMATION

### Corresponding Author

rieger@tum.de

### Notes

The authors declare no competing financial interest.

## ■ ACKNOWLEDGMENTS

The authors thank Matthias Sachsenhauser for XPS measurement, Dr. Sergei Vagin and Dr. Marin Steenackers for valuable discussions, and Roche Diagnostics GmbH for financial support. S.S. is grateful for a generous scholarship from the Fonds der Chemischen Industrie. F.D. acknowledges Wacker Chemie AG for a stipend within the Institute of Silicon Chemistry. R.J. is thankful for DFG support via the Center for Regenerative Therapies Dresden.

## ■ REFERENCES

- (1) Yasuda, H.; Yamamoto, H.; Yokota, K.; Miyake, S.; Nakamura, A. *J. Am. Chem. Soc.* **1992**, *114*, 4908.
- (2) Chen, E. Y.-X. *Chem. Rev.* **2009**, *109*, 5157.
- (3) Yasuda, H.; Tamai, H. *Prog. Polym. Sci.* **1993**, *18*, 1097.
- (4) Yasuda, H. *Prog. Polym. Sci.* **2000**, *25*, 573.
- (5) Yasuda, H.; Ihara, E. *Adv. Polym. Sci.* **1997**, *133*, 53.
- (6) Kaneko, H.; Nagae, H.; Tsurugi, H.; Mashima, K. *J. Am. Chem. Soc.* **2011**, *133*, 19626.
- (7) Rabe, G. W.; Komber, H.; Haeussler, L.; Kreger, K.; Lattermann, G. *Macromolecules* **2010**, *43*, 1178.
- (8) Advincula, R. C.; Brittain, W. J.; Caster, K. C.; Rühle, J., Eds. *Polymer Brushes*; Wiley-VCH: Weinheim, 2004.
- (9) Jordan, R., Ed. *Surface-initiated Polymerization I & II*; Advances in Polymer Science 197 & 198; Springer-Verlag: Berlin, 2006.
- (10) Jordan, R.; Ulman, A. *J. Am. Chem. Soc.* **1998**, *120*, 243.
- (11) Jordan, R.; Ulman, A.; Kang, J. F.; Rafailovich, M. H.; Sokolov, J. *J. Am. Chem. Soc.* **1999**, *121*, 1016.
- (12) Dronavajjala, K. D.; Rajagopalan, R.; Uppili, S.; Sen, A.; Allara, D. L.; Foley, H. C. *J. Am. Chem. Soc.* **2006**, *128*, 13040.
- (13) Prucker, O.; Rühle, J. *Langmuir* **1998**, *14*, 6893.
- (14) Bao, Z.; Bruening, M. L.; Baker, G. L. *J. Am. Chem. Soc.* **2006**, *128*, 9056.
- (15) Dong, H.; Zhu, M.; Yoon, J. A.; Gao, H.; Jin, R.; Matyjaszewski, K. *J. Am. Chem. Soc.* **2008**, *130*, 12852.
- (16) Husemann, M.; Mecerreyes, D.; Hawker, C. J.; Hedrick, J. L.; Shah, R.; Abbott, N. L. *Angew. Chem., Int. Ed.* **1999**, *38*, 647.
- (17) Ulbricht, M.; Yang, H. *Chem. Mater.* **2005**, *17*, 2622.
- (18) Tria, M. C. R.; Grande, C. D. T.; Ponnappati, R. R.; Advincula, R. C. *Biomacromolecules* **2010**, *11*, 3422.
- (19) Kong, H.; Gao, C.; Yan, D. *J. Am. Chem. Soc.* **2004**, *126*, 412.
- (20) Fan, X.; Lin, L.; Dalsin, J. L.; Messersmith, P. B. *J. Am. Chem. Soc.* **2005**, *127*, 15843.
- (21) Zhou, F.; Huck, W. T. S. *Chem. Commun.* **2005**, 5999.
- (22) Barbey, R.; Lavanant, L.; Paripovic, D.; Schuwer, N.; Sugnaux, C.; Tugulu, S.; Klok, H. A. *Chem. Rev.* **2009**, *109*, 5437.
- (23) Pyun, J.; Kowalewski, T.; Matyjaszewski, K. *Macromol. Rapid Commun.* **2003**, *24*, 1043.
- (24) Price, D.; Pyrah, K.; Hull, T. R.; Milnes, G. J.; Ebdon, J. R.; Hunt, B. J.; Joseph, P. *Polym. Degrad. Stab.* **2002**, *77*, 227.
- (25) Parvole, J.; Jannasch, P. *Macromolecules* **2008**, *41*, 3893.
- (26) Steininger, H.; Schuster, M.; Kreuer, K. D.; Kaltbeitzel, A.; Bingöel, B.; Meyer, W. H.; Schauf, S.; Brunklaus, G.; Maier, J.; Spiess, H. W. *Phys. Chem. Chem. Phys.* **2007**, *9*, 1764.
- (27) Wagner, T.; Manhart, A.; Deniz, N.; Kaltbeitzel, A.; Wagner, M.; Brunklaus, G.; Meyer, W. H. *Macromol. Chem. Phys.* **2009**, *210*, 1903.
- (28) Gemeinhart, R. A.; Bare, C. M.; Haasch, R. T.; Gemeinhart, E. J. *J. Biomed. Mater. Res., Part A* **2006**, *78A*, 433.
- (29) Seo, J. H.; Matsuno, R.; Takai, M.; Ishihara, K. *Biomaterials* **2009**, *30*, 5330.
- (30) Goda, T.; Matsuno, R.; Konno, T.; Takai, M.; Ishihara, K. *J. Biomed. Mater. Res., Part B* **2009**, *89B*, 184.
- (31) Macarie, L.; Ilia, G. *Prog. Polym. Sci.* **2010**, *35*, 1078.
- (32) Georgieva, R.; Tsevi, R.; Kossev, K.; Kusheva, R.; Balgijiska, M.; Petrova, R.; Tenchova, V.; Gitsov, I.; Troev, K. *J. Med. Chem.* **2002**, *45*, 5797.
- (33) Monge, S.; Canniccionni, B.; Graillet, A.; Robin, J. *Biomacromolecules* **2011**, *12*, 1973.
- (34) Bingöel, B.; Hart-Smith, G.; Barner-Kowollik, C.; Wegner, G. *Macromolecules* **2008**, *41*, 1634.
- (35) Bingöel, B.; Meyer, W. H.; Wagner, M.; Wegner, G. *Macromol. Rapid Commun.* **2006**, *27*, 1719.
- (36) Markova, D.; Kumar, A.; Klapper, M.; Muellen, K. *Polymer* **2009**, *50*, 3411.
- (37) Seemann, U. B.; Dengler, J. E.; Rieger, B. *Angew. Chem., Int. Ed.* **2010**, *49*, 3489.
- (38) Salzinger, S.; Seemann, U. B.; Plikhta, A.; Rieger, B. *Macromolecules* **2011**, *44*, 5920.
- (39) Cicero, R. L.; Linford, M. R.; Chidsey, C. E. D. *Langmuir* **2000**, *16*, 5688.
- (40) Stewart, M. P.; J. Buriak, M. *Angew. Chem., Int. Ed.* **1998**, *37*, 3257.
- (41) Stewart, M. P.; Robins, E. G.; Geders, T. W.; Allen, M. J.; Choi, H. C.; Buriak, J. M. *Phys. Status Solidi A* **2000**, *182*, 109.
- (42) Huck, L. A.; Buriak, J. M. *J. Am. Chem. Soc.* **2012**, *134*, 489.
- (43) Deng, J.; Yang, W.; Rånby, B. *Macromol. Rapid Commun.* **2001**, *22*, 535.
- (44) Deubel, F.; Stutzmann, M.; Garrido, J. A.; Jordan, R. Poster presented at Frontiers in Silicon Chemistry, Munich, April 14–15, 2011; PA38.
- (45) Steenackers, M.; Lud, S. Q.; Niedermeier, M.; Bruno, P.; Gruen, D. M.; Feulner, P.; Stutzmann, M.; Garrido, J. A.; Jordan, R. *J. Am. Chem. Soc.* **2007**, *129*, 15655.
- (46) Zhang, N.; Steenackers, M.; Luxenhofer, R.; Jordan, R. *Macromolecules* **2009**, *42*, 5345.
- (47) Steenackers, M.; Küller, A.; Stoycheva, S.; Grunze, M.; Jordan, R. *Langmuir* **2009**, *25*, 2225.
- (48) Chen, T.; Amin, I.; Jordan, R. *Chem. Soc. Rev.* **2012**, *41*, 3280.
- (49) Van de Walle, C. G.; Street, R. A. *Phys. Rev. B* **1994**, *49*, 14766.
- (50) Seival, A. B.; Demirel, A. L.; Nissink, J. W. M.; Linford, M. R.; Van der Maas, J. H.; De Jeu, W. H.; Zuilhof, H.; Sudhölter, E. J. R. *Langmuir* **1998**, *14*, 1759.
- (51) Tugulu, S.; Harms, M.; Fricke, M.; Volkmer, D.; Klok, H. A. *Angew. Chem., Int. Ed.* **2006**, *45*, 7458.
- (52) Ellis, J.; Wilson, A. D. *Polym. Int.* **1991**, *24*, 221.
- (53) Ingrassia, M.; Elomaa, M.; Jannasch, P. *Polym. Chem.* **2010**, *1*, 739.

Reprinted with Permission from Zhang, N.; Salzinger, S.; Deubel, F.; Jordan, R.; Rieger, B. *J. Am. Chem. Soc.* **2012**, *134*, 7333. Copyright 2012 American Chemical Society.

***Supporting Information:***

**Surface-Initiated Group Transfer Polymerization (SI-GTP)  
Mediated by Rare Earth Metal Catalysts**

Ning Zhang,<sup>a</sup> Stephan Salzinger,<sup>a</sup> Frank Deubel,<sup>a</sup> Rainer Jordan,<sup>a,b</sup> and Bernhard Rieger<sup>a,\*</sup>

<sup>a</sup>WACKER-Lehrstuhl für Makromolekulare Chemie, Technische Universität München, Lichtenbergstraße 4, 85747 Garching bei München, Germany. Fax: +49-89-289-13562, E-mail: rieger@tum.de

<sup>b</sup>Professur für Makromolekulare Chemie, Department Chemie, Technische Universität Dresden, Zellescher Weg 19, 01069 Dresden, Germany

## Materials and methods

Chemicals were purchased from Aldrich or Acros and used without further treatment if not otherwise stated. All reactions were carried out under argon atmosphere using standard Schlenk techniques or a *MBraun* glovebox. All glassware was heat-dried under vacuum prior to use. Toluene was dried applying a *MBraun* SPS-800 and used as received. Tetrahydrofuran (THF) was distilled over potassium prior to use.  $\text{Cp}_2\text{YbMe}$ , diethyl- and di-*n*-propyl vinylphosphonates were prepared according to literature.<sup>1,2,3,4</sup> Infrared spectroscopy (IR) was performed using an Vertex 70 Bruker instrument equipped with a diffuse reflectance infrared Fourier transform (DRIFT) setup from SpectraTech and a mercury-cadmium-telluride (MCT) detector. For each spectrum, 100 scans were accumulated with a spectral resolution of  $4\text{ cm}^{-1}$ . Background spectra were recorded on bare silicon substrates. Atomic force microscopy (AFM) scans were obtained with a Nanoscope IIIa scanning probe microscope from Veeco Instruments (Mannheim, Germany). The microscope was operated in tapping mode using Si cantilevers with a resonance frequency of 270 kHz, a driving amplitude of 1.52 V at a scan rate of 0.4 Hz. The water contact angles were determined with a full-automated Krüss DSA 10 Mk2 contact angle goniometer and three points were measured on each surface. The data were obtained with the aid of the Krüss Drop Shape Analysis v3 software package. X-ray Photoelectron Spectroscopy (XPS) measurements were performed under ultrahigh-vacuum conditions ( $5.0 \times 10^{-9}$  mbar) using an Mg  $K\alpha$  radiation and a Specs Phoibos 100 hemispherical analyzer equipped with an MCD-5 detector. All spectra were recorded with a pass energy of 25 eV and a takeoff angle of  $0^\circ$ .

## Synthesis and characterization

**Poly(ethylene glycol dimethacrylate) PEGDM layer.** A silicon wafer piece with a native oxide layer was first cleaned with a Piranha solution ( $\text{H}_2\text{O}_2$  (35wt. %)/ $\text{H}_2\text{SO}_4$  = 1/3). The substrates were placed in a plastic vial with a 5 wt. % HF aqueous solution for 5 min for oxide layer stripping. After thorough rinsing with Millipore water and later ethanol, the substrates were submerged in degassed bulk ethylene glycol dimethacrylate (EGDM) for UV irradiation in a photoreaction tube (Duran). The

reaction was allowed to proceed for maximum 40 min to avoid bulk gelation. The samples were then thoroughly cleaned in different solvents of suitable polarity and under constant ultrasonication to remove unreacted monomer and only physisorbed polymers.

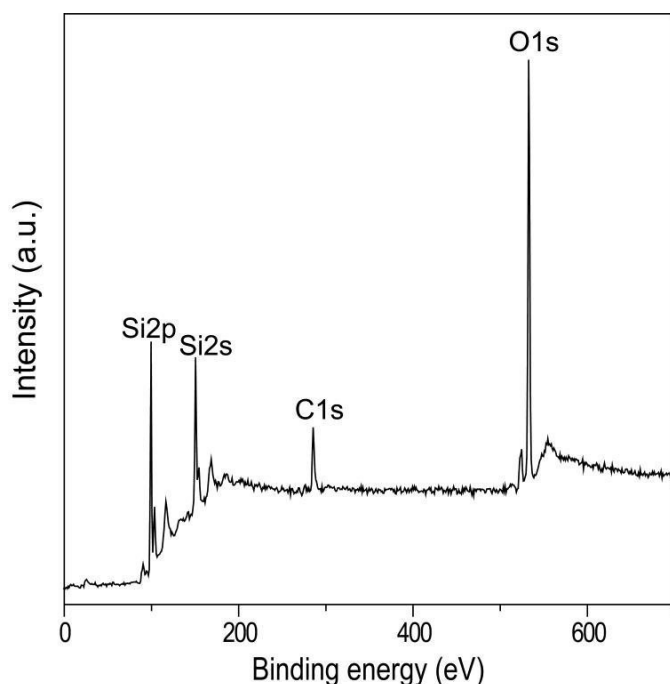


**Figure S1.** XPS survey scan of thin PEGDM network (thickness  $\approx$  5 nm, after 20 min UV grafting polymerization) on hydrogen terminated silicon substrate.

**Poly(ethylene glycol dimethacrylate-graft-methyl methacrylate) P(EGDM-g-MMA) brushes and Poly(ethylene glycol dimethacrylate-graft-dialkyl vinylphosphonate) P(EGDM-g-DAVP).** A PEGDM modified silicon substrate was placed in a solution of 1 mg *bis*(cyclopentadienyl) methyl ytterbium ( $\text{Cp}_2\text{YbMe}$ ) in 3 mL toluene for 1 h at room temperature (**Figure S3**, XPS). Subsequently, 1000 equivalents of methyl methacrylate (MMA) (**Figure S2**, AFM) or dialkyl vinylphosphonate (DAVP) *i.e.* dimethyl vinylphosphonate (DMVP), diethyl vinylphosphonate (DEVP) (**Figure S4**, XPS), and di-*n*-propyl vinylphosphonate (DPVP) were added to perform surface-initiated group transfer polymerization (SI-GTP). The reaction was terminated with an excess of methanol. The samples were removed and thoroughly cleaned by ultrasonication in toluene, ethanol and finally

Millipore water for 2 minutes each to remove monomer, physisorbed polymer and residue.

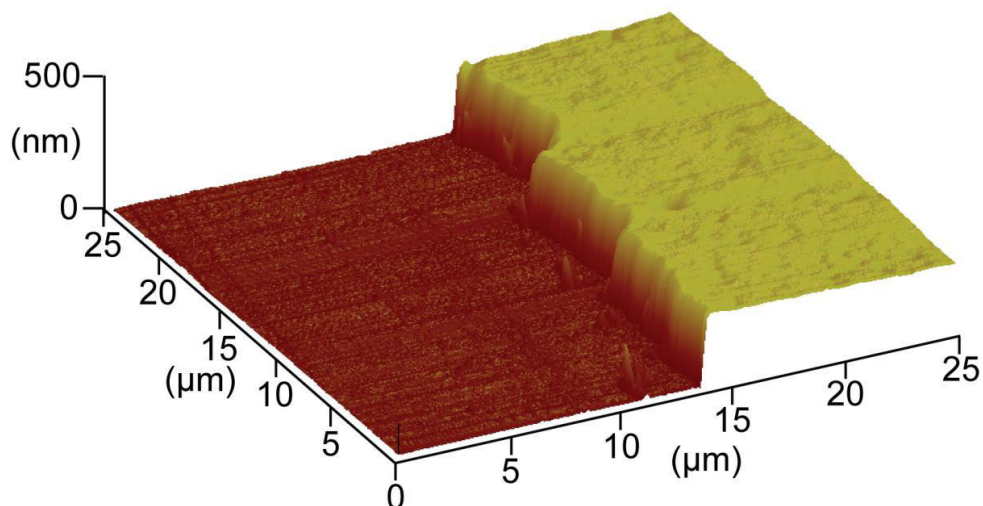


**Figure S2.** a) AFM 3D view of a  $316\pm 13$ nm thick P(EGDM-g-MMA) brush after 5minute GTP of MMA on a 29nm (after 30min UV irradiation) thick PEGDM layer.

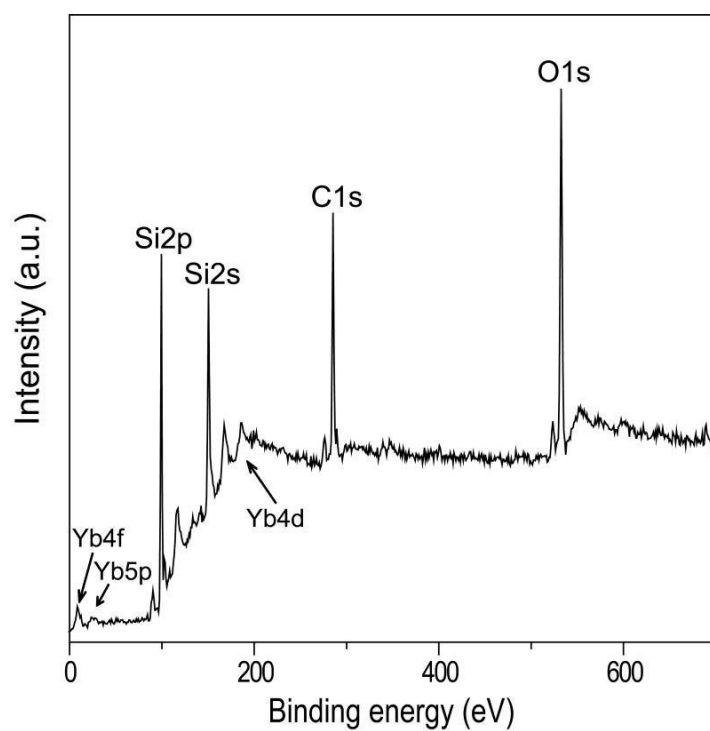


**Figure S3.** XPS survey scan of a 5nm thick PEGDM network on a hydrogen terminated silicon substrate. (after reacted with  $\text{Cp}_2\text{YbMe}$ )

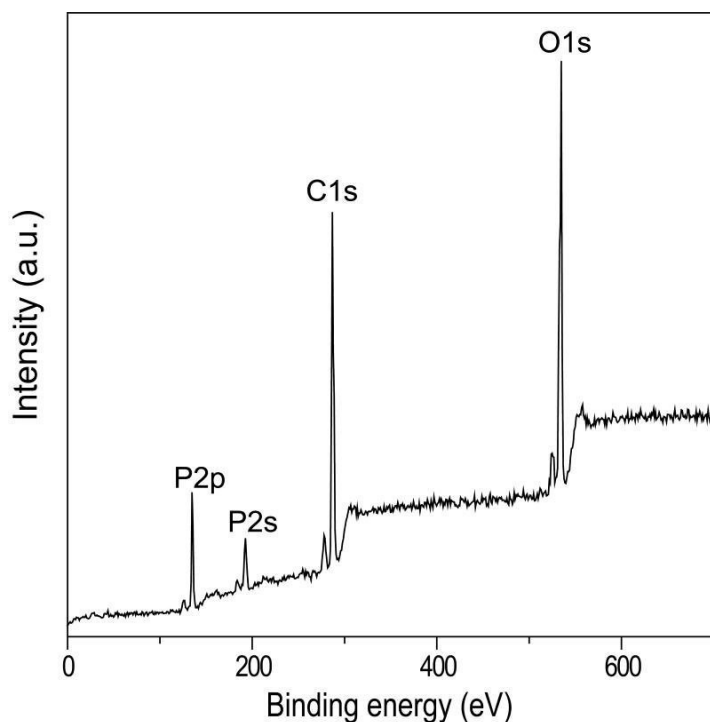


**Figure S4.** XPS survey scan of P(EGDM-g-DEVP) brush (from a 5nm thick PEGDM layer) on hydrogen terminated silicon substrate.

**PDEVP brushes on 3-(trimethoxysilyl) propyl methacrylate (TMSPM) monolayer.** The self-assembled monolayer of 3-(trimethoxysilyl) propyl methacrylate (TMSPM) were prepared by the silanization of TMSPM on the oxidized silicon wafer. Successively,  $\text{Cp}_2\text{YbMe}$  was attached to the surface by reaction with the methacrylate groups, enabling a subsequent surface-initiated polymerization of vinylphosphonate monomers (**Figure S5**).

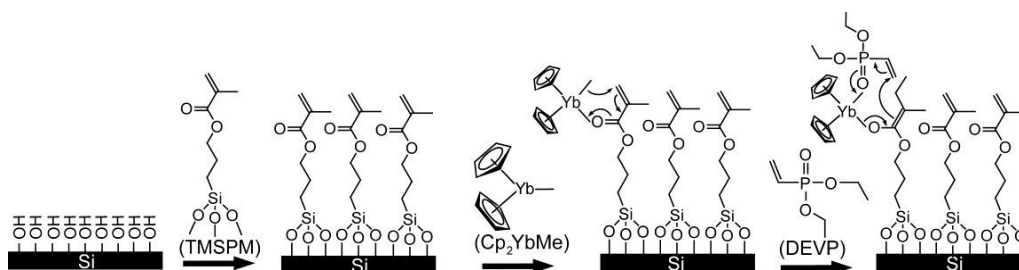


**Figure S5.** Initiation of the  $\text{Cp}_2\text{YbMe}$ -induced polymerization of DEVP on TMSPM self-assembled monolayer on silicon wafer.

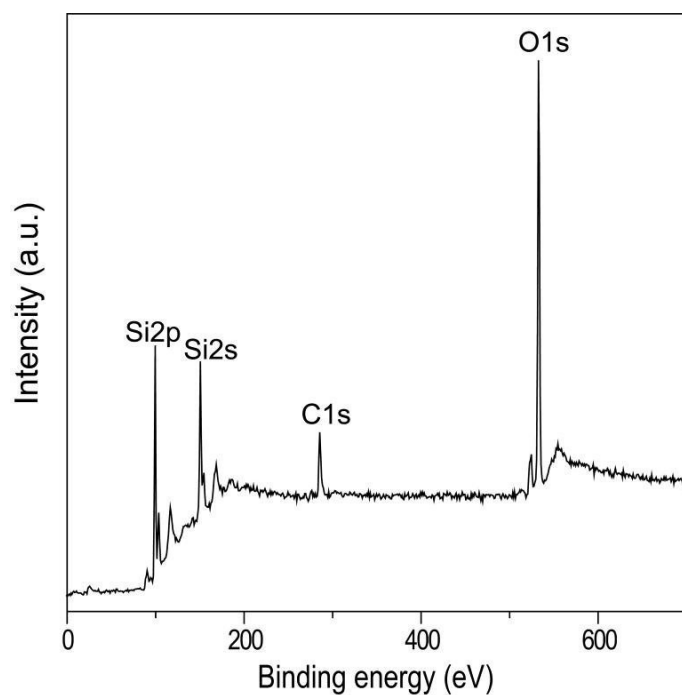


**Figure S6.** XPS survey scan of TMSPM monolayer on a silicon/silicon dioxide substrate.

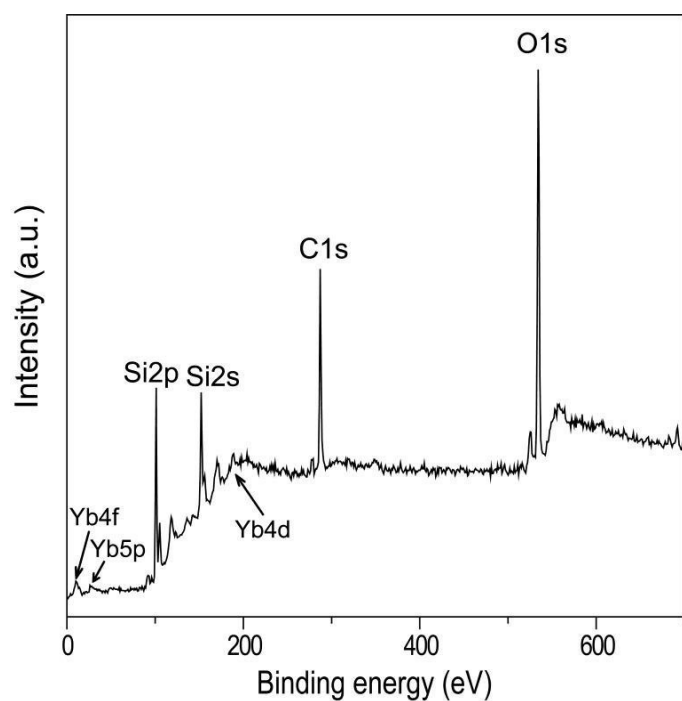


**Figure S7.** XPS survey scan of TMSPM monolayer on a silicon/silicon dioxide substrate after reaction with  $\text{Cp}_2\text{YbMe}$ .



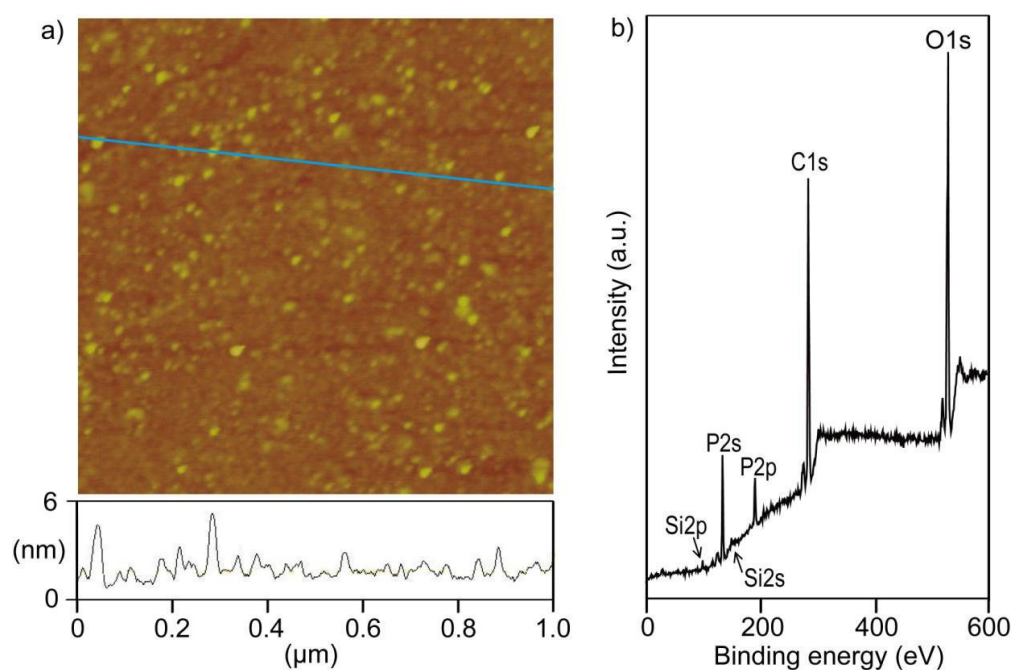


**Figure S8.** a) AFM scan and section view, and b) XPS survey scan of a PDEVP brush on 3-(trimethoxysilyl)propyl methacrylate (TMSPM) modified silicon substrate.

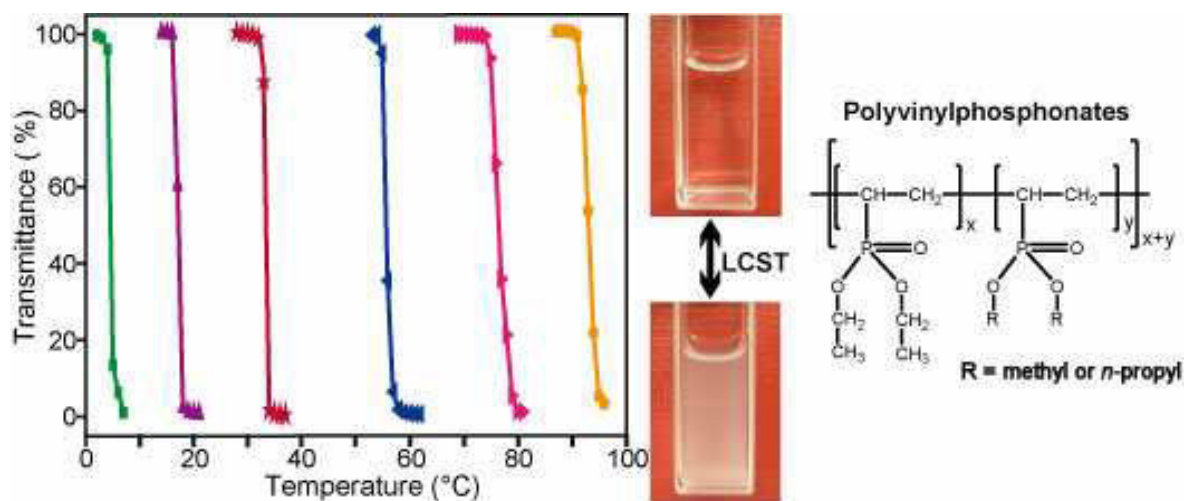
## References

- (1) Seemann, U. B.; Dengler, J. E.; Rieger, B. *Angew. Chem. Int. Ed.* **2010**, *49*, 3489-3491.
- (2) Evans, W. J.; Dominguez, R.; Hanusa, T. P. *Organometallics* **1986**, *5*, 263-270.
- (3) Ely, N. M.; Tsutsui, M. *Inorg. Chem.* **1975**, *14*, 2680-2687.
- (4) Leute, M. PhD Thesis, University of Ulm, **2007**.



## CHAPTER 7:

# POLY(VINYLPHOSPHONATE)S WITH WIDELY TUNEABLE LCST: A PROMISING ALTERNATIVE TO CONVENTIONAL THERMORESPONSIVE POLYMERS



*“Insanity: doing the same thing over and over again and expecting different results.”*

- Albert Einstein (1879-1955)



**Status:** Published online: November 30, 2012  
**Journal:** Macromolecules  
Issue 45, 9751-9758  
**Publisher:** ACS Publications  
**Article type:** Article  
**DOI:** 10.1021/ma3019014  
**Authors:** Ning Zhang, Stephan Salzinger, Bernhard Rieger

**Content:**

This chapter presents a detailed evaluation of statistical rare earth metal-mediated dialkyl vinylphosphonate copolymerizations and of the thermoresponsive behavior of the resulting (co)polymers. Evaluation of the copolymerization parameters from activity measurements have shown the formation of nearly perfectly random copolymers (*i.e.*  $r_1, r_2 \sim 1$ ). In view of the pronounced dependence of the polymerization rate of DAVP homopolymerizations on the phosphonate side chains, this observation indicates that the propagation rate of vinylphosphonate REM-GTP is mainly determined by the steric demand of the growing polymer chain end, not by the added monomer.

The obtained random copolymers of DEVP and dimethyl or di-*n*-propyl vinylphosphonate exhibit thermoresponsive properties, *i.e.* having an LCST which can be tuned in a wide range by controlling the feed ratio of the comonomers. Hereby, the LCST correlates linearly with content of hydrophilic and hydrophobic comonomer. The LCST phase diagram of aqueous PDEVP solutions shows, in combination with DSC analysis, the occurrence of a coil–globule transition mechanism. According to the absence of hydrogen bond donors, a sharp and reversible phase transition was observed, exhibiting a remarkably small dependence of the thermoresponsiveness on additives and polymer concentration. In combination with its biocompatibility, these features make PDAVP an interesting alternative compared to established thermoresponsive polymers.



RightsLink®

Home

Create Account

Help

ACS Publications  
High quality. High impact.

**Title:** Poly(vinylphosphonate)s with Widely Tunable LCST: A Promising Alternative to Conventional Thermoresponsive Polymers

**Author:** Ning Zhang, Stephan Salzinger, and Bernhard Rieger

**Publication:** Macromolecules

**Publisher:** American Chemical Society

**Date:** Dec 1, 2012

Copyright © 2012, American Chemical Society

User ID
<input type="text"/>
Password
<input type="text"/>
<input type="checkbox"/> Enable Auto Login
<input type="button" value="LOGIN"/>
<a href="#">Forgot Password/User ID?</a>
<b>If you're a copyright.com user,</b> you can login to RightsLink using your copyright.com credentials. Already a <b>RightsLink user</b> or want to <a href="#">learn more?</a>

### PERMISSION/LICENSE IS GRANTED FOR YOUR ORDER AT NO CHARGE

This type of permission/license, instead of the standard Terms & Conditions, is sent to you because no fee is being charged for your order. Please note the following:

- Permission is granted for your request in both print and electronic formats, and translations.
- If figures and/or tables were requested, they may be adapted or used in part.
- Please print this page for your records and send a copy of it to your publisher/graduate school.
- Appropriate credit for the requested material should be given as follows: "Reprinted (adapted) with permission from (COMPLETE REFERENCE CITATION). Copyright (YEAR) American Chemical Society." Insert appropriate information in place of the capitalized words.
- One-time permission is granted only for the use specified in your request. No additional uses are granted (such as derivative works or other editions). For any other uses, please submit a new request.

BACK

CLOSE WINDOW

Copyright © 2013 [Copyright Clearance Center, Inc.](#) All Rights Reserved. [Privacy statement.](#)  
Comments? We would like to hear from you. E-mail us at [customer@copyright.com](mailto:customer@copyright.com)

Reprinted with Permission from Zhang, N.; Salzinger S.; Rieger, B. *Macromolecules* **2012**, *45*, 9751. Copyright 2012 American Chemical Society.

## Poly(vinylphosphonate)s with Widely Tunable LCST: A Promising Alternative to Conventional Thermoresponsive Polymers

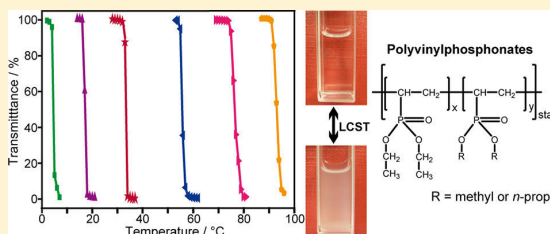
Ning Zhang,<sup>\*,†,‡,§</sup> Stephan Salzinger,<sup>†,§</sup> and Bernhard Rieger<sup>\*,†</sup>

<sup>†</sup>WACKER-Lehrstuhl für Makromolekulare Chemie, Technische Universität München, Lichtenbergstraße 4, 85747 Garching bei München, Germany

<sup>‡</sup>Changchun Institute of Applied Chemistry, Chinese Academy of Sciences, Changchun 130022, China

### Supporting Information

**ABSTRACT:** Novel statistic copolymers of dialkyl vinylphosphonates have been synthesized via rare earth metal-mediated group transfer polymerization using easily accessible tris(cyclopentadienyl)ytterbium. The copolymerization parameters have been determined by activity measurements showing the formation of almost perfectly random copolymers ( $r_1, r_2 \sim 1$ ). Thus, the polymerization rate of vinylphosphonate GTP is mainly limited by the steric demand of growing polymer chain end. The obtained copolymers of diethyl vinylphosphonate and dimethyl or di-*n*-propyl vinylphosphonate show thermoresponsive properties, i.e., exhibit a tunable lower critical solution temperature following a coil-globule transition mechanism, with cloud points between 5 and 92 °C. Hereby, the LCST can be precisely adjusted by varying the comonomer composition and correlates linearly with the content of hydrophilic/hydrophobic comonomer. These thermoresponsive poly(vinylphosphonate)s, exhibiting a sharp and reversible phase transition, and minor environmental effects such as concentration and additives on their cloud point, are promising candidates in biomedical applications.



### INTRODUCTION

During the past decades, phosphorus-containing polymers including poly(phosphate ester)s, poly(phosphazene)s, poly(phosphonic acid)s, and poly(phosphonate)s have received wide interest due to their flame-retardant properties,<sup>1</sup> proton conductivity,<sup>2–4</sup> and commercial use as a binder in bone and dental concrete.<sup>5</sup> Recently, much attention has been drawn to the investigation of these polymers in biomedical applications such as drug and gene delivery,<sup>6</sup> tissue engineering,<sup>7</sup> and temperature-controlled cell growth and release from polymer-coated surfaces.<sup>6</sup> Nevertheless, in spite of the intriguing potential applications, the development of phosphorus-containing polymers is mainly limited by the absence of efficient synthetic strategies; for instance, poly(vinylphosphonate)s prepared by radical and ionic approaches mostly resulted in low yields and degrees of polymerization.<sup>8–10</sup>

Very recently, our group and other researchers found that poly(dialkyl vinylphosphonate)s (PDAVP) with high and defined molar mass as well as low polydispersity can be synthesized, not only in bulk<sup>11–13</sup> but also on silicon substrate,<sup>10,14</sup> in the presence of rare earth metal complexes.

For a variety of applications, polymers that possess reversible and controllable thermoresponsive properties are highly demanded, e.g., for controlled drug delivery,<sup>15</sup> cell growth/release,<sup>16</sup> or thermoresponsive chromatography using a polymer-modified stationary phase.<sup>17–22</sup> This thermal response is expressed by a solubility transition upon changes in temperature. The most prominent representative of these

thermoresponsive polymers, poly(*N*-isopropylacrylamide) (PNIPAM), shows a lower critical solution temperature (LCST) close to body temperature (32 °C) with a relatively small dependence of the cloud point on changes in concentration, pH, or ionic strength.<sup>23,24</sup> Moreover, the LCST can be regulated above and below 37 °C by incorporation of comonomer units rendering PNIPAM-based materials particularly suitable for a variety of bioapplications.<sup>25–27</sup> However, the pronounced hysteresis in its phase transition<sup>28</sup> – due to the formation of inter- and intramolecular hydrogen bonds in the collapsed state delaying the hydration of PNIPAM during cooling<sup>29</sup> – may impair its application, in particular in cases requiring a fast response. Other poly(*N,N*-dialkylacrylamides)<sup>30,31</sup> such as poly(*N,N*-diethylacrylamide) (PDEAM), having a similar monomer molar mass and LCST in comparison to PNIPAM, nevertheless, exhibit no such hysteresis in their phase transition due to the lack of hydrogen bond donors.<sup>32</sup> For poly(ethylene glycol) (PEG), another thermoresponsive polymer widely used in the biomedical field, the cloud point can be adjusted in a wide range by varying the composition, molecular structure, polymer architecture (e.g., main chain or side chain PEG), and copolymerization of (meth)acrylate comonomers bearing PEG chains of different length.<sup>34</sup> In spite of its tunable thermoresponsiveness, large

**Received:** September 11, 2012

**Revised:** November 22, 2012

**Published:** November 30, 2012

success in commercialization, and its biocompatibility, this polymer may lose its biocompatibility in complex biological fluids or in salt water media and can undergo oxidative degradation leading to chain scission.<sup>33–36</sup> Within the past decades, a variety of alternative thermoresponsive polymers such as poly((alkylamino) methacrylate),<sup>37</sup> poly(vinyl alkyl ether),<sup>38</sup> poly(*N*-vinylcaprolactam)s,<sup>39</sup> or poly(2-oxazoline)s<sup>40,57</sup> have been presented. Few of these homopolymers show an LCST satisfactory close to body temperature,<sup>41,42</sup> such as PNIPAM. Copolymerization of monomers with different hydrophilicity is widely adopted in order to obtain a desired LCST, however, often resulting in gradient copolymers, which tend to assemble into complex nanostructures<sup>43</sup> or micelles and therefore exhibit a prolonged or irreversible phase transition.<sup>42,44–46,54,55</sup> Thus, further development of alternative thermoresponsive polymers, which combine biocompatibility, thermoresponsiveness which is less dependent on environmental parameters, a reversible phase transition without hysteresis, and the possibility to synthesize random copolymers, is of substantial importance.

The improved synthetic methodology reported recently and the low toxicity of PDAVP<sup>47</sup> have made this polymer class a promising alternative to conventional PNIPAM and PEG. It was reported by our group that poly(diethyl vinylphosphonate) (PDEV) homopolymer prepared by group transfer polymerization using rare earth metal complexes is amphiphilic, and its aqueous solutions exhibit a cloud point of 40–46 °C, depending on molar mass and concentration.<sup>12</sup>

Herein, we present our recent progress in the efficient synthesis of novel statistic copolymers of dialkyl vinylphosphonates (DAVP) through living rare earth metal-mediated group transfer polymerization (REM-GTP). The REM-GTP kinetics of DAVP copolymerization as well as the thermoresponsiveness of the obtained polymers are investigated.

## ■ EXPERIMENTAL SECTION

**Materials and Methods.** Chemicals were purchased from Sigma-Aldrich or Acros Organics and used without further purification if not otherwise stated. Phosphate buffered saline (PBS) (1.06 mM NaH<sub>2</sub>PO<sub>4</sub>, 5.6 mM Na<sub>2</sub>HPO<sub>4</sub>, and 154 mM NaCl, pH 7.4) was purchased from Lonza Walkersville, Inc. Fetal bovine serum, Qualified, US Origin, was purchased from Invitrogen. All reactions were carried out under an argon atmosphere using standard Schlenk techniques or an MBRAUN glovebox. All glassware was heat-dried under vacuum prior to use. Toluene was dried applying an MBRAUN SPS-800 and used as received. Dimethyl vinylphosphonate (DMVP) was purchased from Alpha-Aesar. NMR spectra were recorded on a Bruker ARX-300 or AV-500C spectrometer. <sup>1</sup>H NMR chemical shifts  $\delta$  are reported in ppm relative to tetramethylsilane and calibrated by the residual proton signal of the deuterated solvent. <sup>31</sup>P NMR chemical shifts are reported relative to and calibrated by the external standard 85% aqueous phosphoric acid. Deuterated solvents were obtained from Deutero Deutschland GmbH or Eurisotop. Energy dispersive X-ray spectroscopy (EDX) analysis was performed on a Hitachi TM-1000 on copper foil. DSC measurements of aqueous poly(vinylphosphonate) solutions were carried out on a TA Instruments DSC-Q2000 with a polymer concentration of 30 wt % and heating rates of 2, 10, and 40 K/min.

**Synthesis.** Tris(cyclopentadienyl)ytterbium, diethyl vinylphosphonate (DEV)P, and di-*n*-propyl vinylphosphonate (DPVP) were prepared according to previous literature.<sup>47–49</sup>

DEV, <sup>1</sup>H NMR (300 MHz, CDCl<sub>3</sub>, 7.26 ppm): 1.09 (t, 6H, –CH<sub>3</sub>), 3.81–3.89 (m, 4H, –CH<sub>2</sub>–O), 5.78–6.10 (m, 3H, CH<sub>2</sub>=CH–). <sup>31</sup>P (202 MHz, MeOD, ppm): 17.72.

DPVP, <sup>1</sup>H NMR (300 MHz, CDCl<sub>3</sub>, 7.26 ppm): 0.95 (t, 6H, –CH<sub>3</sub>), 1.62–1.78 (m, 4H, CH<sub>3</sub>CH<sub>2</sub>CH<sub>2</sub>–O), 3.94–4.01 (q, 4 H,

CH<sub>3</sub>CH<sub>2</sub>CH<sub>2</sub>–O), 6.00–6.31 (m, 3H, CH<sub>2</sub>=CH–). <sup>31</sup>P (202 MHz, MeOD, ppm): 17.82.

**Polymerizations.** All polymerizations have been performed in toluene, using a catalyst concentration of 0.2 mg/mL. After dissolving the catalyst at room temperature (25 °C), the calculated amount of monomer is added. The mixture is stirred for the stated reaction time and the polymerization terminated by addition of 0.5 mL of methanol. The polymer is precipitated by pouring the reaction mixture into 150 mL of hexane and subsequently dried in a vacuum oven at 70 °C. EDX analysis of obtained polymers was performed to verify the presence of residual catalyst, and no Yb signal could be detected.

*Poly(dimethyl vinylphosphonate-co-diethyl vinylphosphonate) (P(DMVP-co-DEV))*. <sup>1</sup>H NMR (300 MHz, D<sub>2</sub>O, 4.79 ppm): 1.36 (b, –CH<sub>2</sub>CH<sub>3</sub> from DEV), 1.98–2.40 (b, –CH<sub>2</sub>CH(CH<sub>2</sub>)–P from backbone), 2.40–2.80 (b, –CH<sub>2</sub>CH(CH<sub>2</sub>)–P– from backbone), 3.82–3.85 (b, –CH<sub>3</sub> from DMVP), 4.18 (b, –CH<sub>2</sub>CH<sub>3</sub> from DEV).

*Poly(diethyl vinylphosphonate-co-di-*n*-propyl vinylphosphonate) (P(DEV-co-DPVP))*. <sup>1</sup>H NMR (300 MHz, D<sub>2</sub>O, 4.79 ppm): 0.99 (b, –CH<sub>2</sub>CH<sub>2</sub>CH<sub>3</sub> from DPVP), 1.38 (b, –CH<sub>2</sub>CH<sub>3</sub> from DEV), 1.74 (b, –CH<sub>2</sub>CH<sub>2</sub>CH<sub>3</sub> from DPVP), 1.98–2.44 (b, –CH<sub>2</sub>CH(CH<sub>2</sub>)–P from backbone), 2.46–2.90 (b, –CH<sub>2</sub>CH(CH<sub>2</sub>)–P– from backbone), 4.09 (b, –CH<sub>2</sub>CH<sub>2</sub>CH<sub>3</sub> from DPVP), 4.21 (b, –CH<sub>2</sub>CH<sub>3</sub> from DEV).

**Activity Measurements.** For activity measurements, 16.3  $\mu$ mol (6 mg) of tris(cyclopentadienyl)ytterbium is dissolved in 30 mL of toluene at room temperature. For homopolymerization, the calculated amount of monomer for a monomer-to-catalyst ratio of 500 (1.109 g of DMVP or 1.337 g of DEV or 1.565 g of DPVP) is added. For copolymerization, the total monomer-to-catalyst ratio is set to 500. During the course of the measurement, aliquots of 0.5 mL are taken and quenched by adding to 0.2 mL of deuterated methanol. The reaction is carried out in an MBRAUN glovebox in order to take samples every 10–30 s at the beginning of the measurement. After the stated reaction time, a last aliquot is taken and the reaction terminated by addition of 0.5 mL of methanol. The (co)monomer conversion is then calculated from <sup>31</sup>P NMR spectra by integration of the phosphorus signals of the respective remaining monomers (17.72 ppm for DEV, 17.82 ppm for DPVP, 20.55 ppm for DMVP) and the overall polymer integration of the region of 32–37 ppm (<sup>31</sup>P NMR spectroscopic chemical shifts of the respective polymers in MeOD: 32.38–34.05 ppm for PDPVP, 32.56–34.25 ppm for PDEV, and 34.91–36.76 ppm for PDMVP).

**Molecular Weight Determination.** GPC was carried out on a Varian LC-920 equipped with two analytical PL Polargel M columns. As eluent, a mixture of 50% THF, 50% water, and 9 g/L tetrabutylammonium bromide was used in the case of PDMVP, PDEV, and copolymers. For analysis of PDPVP, the eluent was a solution made of 100% THF with 6 g/L tetrabutylammonium bromide. Absolute molecular weights have been determined by multiangle light scattering (MALS) analysis using a Wyatt Dawn Heleos II in combination with a Wyatt Optilab rEX as concentration source.

**Determination of the Cloud Points.** Turbidity measurements were carried out on a Cary 50 UV–vis spectrophotometer from Varian. The cloud point was determined by spectrophotometric detection of the changes in transmittance at  $\lambda = 500$  nm of the aqueous polymer solutions. The heating/cooling rate was 1.0 K/min in steps of 1 K followed by a 5 min period of constant temperature to ensure equilibration. For determination of the transition hysteresis, equilibration periods of 3, 1.5, 0.75, 0.5, and 0.25 min or no equilibration period was used. The cloud point was defined as the temperature corresponding to a 10% decrease in optical transmittance.

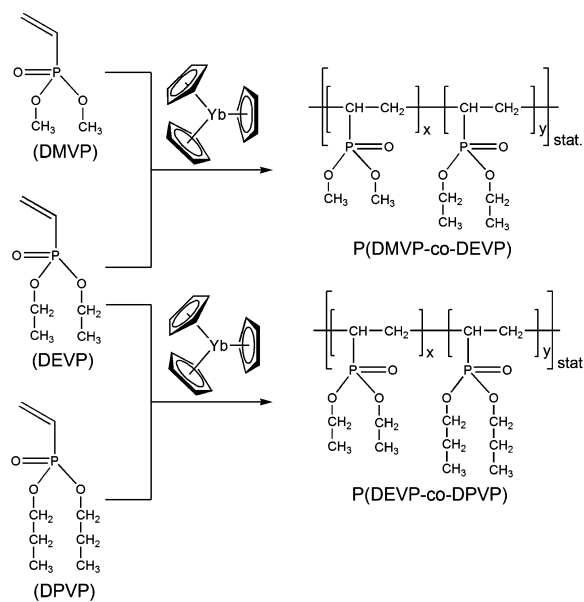
## ■ RESULTS AND DISCUSSION

**Random Copolymerization of Dialkyl Vinylphosphonates.** It was previously reported by our group that dialkyl vinylphosphonates (DAVP, alkyl: methyl, ethyl, *n*-propyl, isopropyl) could be efficiently polymerized in the presence of rare earth metallocenes through a group transfer polymerization



(GTP) mechanism.<sup>12,14</sup> As a living-type polymerization, rare earth metal-mediated GTP allows the synthesis of polymers with narrow polydispersity and a precise control of the molecular weight. In previous work, we have demonstrated the suitability of REM-GTP for the block copolymerization of vinylphosphonates with other monomers suitable for this technique, e.g., methyl methacrylate.<sup>11</sup> In this contribution, efficient and easily accessible tris(cyclopentadienyl)ytterbium ( $\text{Cp}_3\text{Yb}$ ) is used for the homo- and statistical copolymerization of dimethyl, diethyl, and di-*n*-propyl vinylphosphonate (DMVP, DEVP, and DPVP, respectively) (Scheme 1).

**Scheme 1. Molecular Structure of the Dialkyl Vinylphosphonates and Their Conversion to Random Copoly(dialkyl vinylphosphonate)s via  $\text{Cp}_3\text{Yb}$ -Initiated GTP**



Prior to copolymerization experiments, the homopolymerizations of DAVPs initiated by  $\text{Cp}_3\text{Yb}$  were investigated to determine and compare the polymerization rates for these monomers. In accordance with our previous studies, the time-resolved monomer conversion obtained from  $^{31}\text{P}$  NMR spectroscopy revealed that DEVP is polymerized extremely rapid and that conversion reached 100% within 3 min.<sup>12</sup> Assuming propagation to follow first-order kinetics in monomer concentration, the determined turnover frequency (TOF) of  $18\,000\text{ h}^{-1}$  is consistent with earlier activity measurements, for which with approximately triple monomer concentration we observed a TOF of  $59\,400\text{ h}^{-1}$  (Figure 1).<sup>12</sup> The found initiator efficiency  $I^*$  of 39% is, however, in the same range as reported values.<sup>12</sup> We have previously shown that  $\text{Cp}_3\text{Ln}$ -initiated REM-GTP of di-isopropyl vinylphosphonate (DIVP) exhibits both higher initiation and lower propagation rates in comparison to DEVP.<sup>12</sup> Consequently, we found that statistical copolymerization of these two monomers gives rather poor results; only oligomeric materials were obtained. The polymerization of DPVP proceeded slower than for DEVP, giving a comparable TOF of  $3000\text{ h}^{-1}$  to DIVP polymerization and reaching 80% conversion in 30 min (Figure 1). However, both DPVP and DEVP polymerizations show a

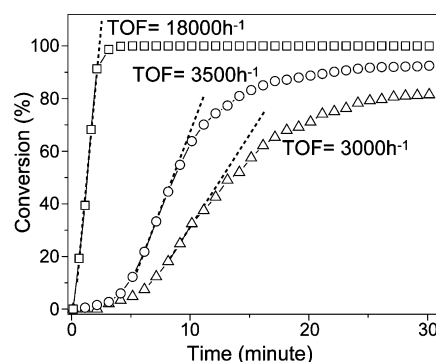


**Figure 1.** Determination of the catalytic activity of  $\text{Cp}_3\text{Yb}$  for the polymerization of DEVP (squares,  $\text{TOF} = 18\,000\text{ h}^{-1}$ ), DPVP (triangles,  $\text{TOF} = 3000\text{ h}^{-1}$ ), and DEVP + DPVP (circles,  $\text{TOF} = 3500\text{ h}^{-1}$ ) ( $[\text{monomer}]:[\text{catalyst}] = 500:1$ ).

distinct initiation period and similar initiator efficiencies  $I^*$  (DPVP, 27%; DEVP, 39%), indicating comparable initiation rates. As a result, the normalized activity  $\text{TOF}/I^*$  is significantly higher for DPVP ( $11\,000\text{ h}^{-1}$ ) in comparison to DIVP ( $5600\text{ h}^{-1}$ ) polymerization.

In spite of the stronger similarity between DEVP and DPVP in comparison to DIVP polymerization, due to the yet significant difference for the propagation rate of DEVP and DPVP, we expected the formation of gradient copolymers. However, as can be observed from  $^{31}\text{P}$  NMR spectroscopic determination of the monomer conversion (Figure 2a) in DEVP/DPVP statistical copolymerizations, both monomers are consumed with very similar rate. The overall monomer conversion rate gives TOFs between  $3500$  and  $11\,500\text{ h}^{-1}$  (initiator efficiency  $I^* = 20\text{--}31\%$ ) (Figure 1 and Figures S1–S4), thus in between the activity for DEVP and DPVP homopolymerization, respectively. For determination of the copolymerization parameters via the Finemann–Ross method,<sup>50</sup> we used

$$\begin{aligned} M_1/M_2 \times \text{TOF}_2/\text{TOF}_1 \times (\text{TOF}_1/\text{TOF}_2 - 1) \\ = (M_1/M_2)^2 \times \text{TOF}_2/\text{TOF}_1 \times r_1 - r_2 \end{aligned} \quad (1)$$

with the residual monomer ratio at the maximum rate  $M_1/M_2$  and the turnover frequencies for both monomers  $\text{TOF}_1$  and  $\text{TOF}_2$  for determination of the copolymerization parameter  $r_1$ , and

$$\begin{aligned} M_2/M_1 \times (\text{TOF}_1/\text{TOF}_2 - 1) = (M_2/M_1)^2 \\ \times (\text{TOF}_1/\text{TOF}_2) \times (-r_2) + r_1 \end{aligned} \quad (2)$$

for determination of the copolymerization parameter  $r_2$ . Using this method for DEVP/DPVP statistical copolymerization, we determined  $r_{\text{DEVP}} = 1.11$  and  $r_{\text{DPVP}} = 0.93$  (Figures S5 and S6), showing the formation of nearly random copolymers (Figure 3a). As both monomers are converted with nearly identical rate, the overall polymerization rate is mainly determined by the growing poly(vinylphosphonate) chain end (DEVP and DPVP, respectively) and not by preference of the addition of one monomer (i.e.,  $r_1, r_2 \sim 1$ ).

It was not possible to determine the homopolymerization activity for the very hydrophilic DMVP. As it was shown in earlier work, DMVP shows high reactivity but formed PDMVP precipitates immediately after the start of the polymerization

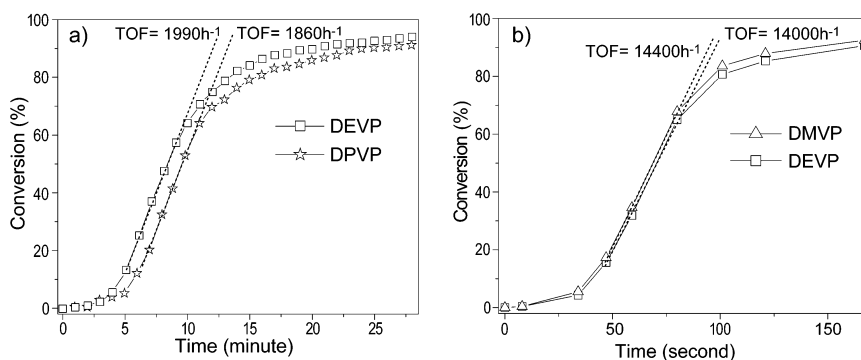


**Figure 2.** Kinetic studies performed by  $^{31}\text{P}$  NMR spectroscopy showing conversion of comonomers during polymerization in toluene. (a) Initial concentration of DEVP  $0.14 \text{ mol L}^{-1}$ , DPVP  $0.14 \text{ mol L}^{-1}$ , catalyst  $0.54 \text{ mmol L}^{-1}$ . (b) Initial concentration of DMVP  $0.14 \text{ mol L}^{-1}$ , DEVP  $0.14 \text{ mol L}^{-1}$ , catalyst  $0.54 \text{ mmol L}^{-1}$ .

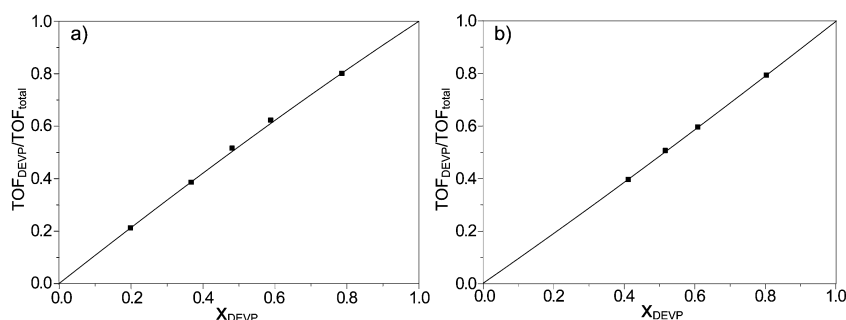


**Figure 3.** Copolymerization diagrams for (a) DEVP/DPVP and (b) DEVP/DMVP copolymerizations. The fit curves are calculated from the copolymerization equation using the copolymerization parameters  $r_1$  and  $r_2$  as determined via the Finemann–Ross method.

from solvents suitable for REM-GTP, causing the polymerization to stop.<sup>12</sup> Therefore, only the copolymerization kinetics of DMVP and DEVP were conducted. Though the polymerization behavior of DMVP in toluene could not be determined in detail, the copolymerization of DMVP and DEVP proceeded smoothly up to DMVP:DEVP ratio of 3:2, due to the higher solubility of the copolymer in toluene. Again, both monomers are converted with similar rate giving overall TOFs between  $14\,900$  and  $36\,000 \text{ h}^{-1}$  and initiator efficiencies  $I^*$  between 31% and 54% (Figure 2b and Figures S7–S9). The copolymerization parameters were determined to be  $r_{\text{DEVP}} = 0.95$  and  $r_{\text{DMVP}} = 1.07$  (Figures S10 and S11), thus showing the formation of even more perfectly random copolymers than observed for DEVP/DPVP copolymerizations (Figure 3b).

NMR spectroscopy did not give insight into the obtained comonomer sequence.  $^1\text{H}$  and  $^{31}\text{P}$  NMR spectroscopic signals are too broad, and no clear assignment can be made for the polymer backbone, whereas no effects on the  $^1\text{H}$  side chains signals can be observed (Figures S12–S18).  $^{13}\text{C}$  spectra are complicated by the  $^{13}\text{C}$ – $^{31}\text{P}$  coupling and thus do not give elemental structure information on the monomer sequence.<sup>13,51,52</sup>

Rare earth metal-mediated (co)polymerization of DAVP is believed to follow a Yasuda-type monometallic group transfer polymerization via repeated conjugate addition over an eight-membered ring intermediate.<sup>9</sup> Assuming the propagation to follow first-order kinetics in monomer concentration (as mentioned above), the rate-limiting step is an associative displacement of the polymer–phosphonate ester at the rare earth center by a vinylphosphonate monomer.<sup>53</sup> All applied

monomers are believed to exhibit similar coordination strength between  $\text{P}=\text{O}$  and  $\text{Yb}$ . Thus, the formation of nearly perfectly random copolymers ( $r_1, r_2 \sim 1$ ) indicates that the polymerization rate of vinylphosphonate GTP is mainly limited by the steric demand of growing polymer chain end, not by the added monomer.<sup>53</sup>

To gain a sharp and reversible phase transition, the observed formation of random copolymers with uniform composition is highly desired as gradient copolymers tend to assemble into complex nanostructures<sup>54</sup> or micelles and therefore often exhibit a prolonged or irreversible phase transition.<sup>55–57</sup>

#### LCST Phase Diagram of Aqueous PDEVP Solutions.

We have previously conducted a first examination of the molecular weight and concentration dependence of the cloud point of aqueous PDEVP homopolymer solutions.<sup>11</sup> However, we only investigated the low concentration regime below 2.0 wt % polymer concentration. In this contribution, in order to determine the full LCST phase diagram of poly(vinylphosphonate)s, we measured the cloud point for a 230 kDa ( $M_w$ ) PDEVP homopolymer at concentrations between 0.04 and 67 wt % (Figure 4). According to our previous study, for low concentrations, the cloud point was found to increase slightly from 42 to 44 °C. In this report, between 0.5 and 10 wt %, phase separation was found to occur continuously at 42 °C. At higher concentrations, a strong increase of the cloud point was observed (up to 71 °C at 67 wt %). In order to evaluate environmental effects on the LCST and to study the adjustment of the LCST by copolymerization with hydrophilic/hydrophobic comonomers, we therefore used 1.0 wt % solutions of the corresponding polymers. At higher concen-

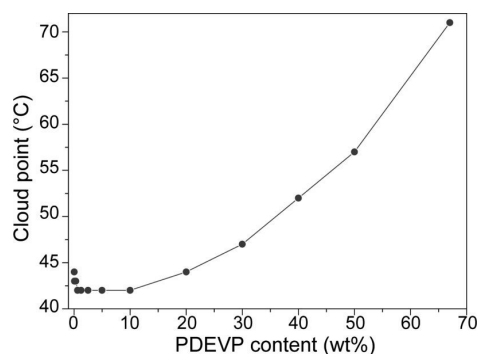


**Figure 4.** LCST phase diagram for PDEVP ( $M_w = 230$  kDa) in deionized water.

trations, particularly between 2.5 and 20 wt %, the polymer coagulates rapidly inhibiting stirring and causing precipitation, which complicates a reliable determination of the cloud point by turbidimetry with the given UV–vis spectrometer setup. The relative independence of the cloud point of aqueous PDEVP solutions on the concentration in the range of 0.1–2 wt % (changes of a few degrees only upon strong dilution) is similar to the behavior observed for PNIPAM and PEG in the same concentration range.<sup>35,58</sup> This indicates PDEVP to follow a coil–globule phase transition mechanism, as it has been previously shown for aqueous PNIPAM and PEG solutions.<sup>35,56</sup>

**Phase Separation Mechanism and Transition Hysteresis of PDEVP.** The obtained LCST phase diagram indicates the occurrence of a coil–globule transition mechanism rather than liquid–liquid phase separation taking place.<sup>25,42,59</sup> To further support this hypothesis, we conducted DSC measurements of a 30 wt % aqueous PDEVP solution at different heating rates. A strongly endothermic process was observed upon heating as a very sharp transition with an onset at 46 °C (Figure 5 and Figures S19 and S20), being in good agreement

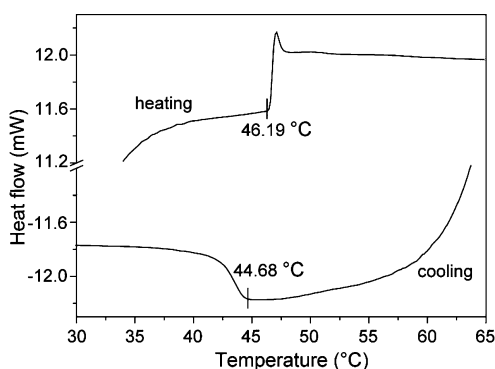


**Figure 5.** DSC experiment for 30 wt % aqueous PDEVP solution (heating/cooling rate: 40 K/min).

with the corresponding cloud point determined by turbidimetry. For a coil–globule transition, the polymer molecules adopt an extended coil conformation below the cloud point. The hydrophobic effect, i.e., the negative mixing entropy upon dissolution of the polymer, a result of the necessary orientation of water molecules around the hydrophobic moieties of the dissolved polymer,<sup>60,61</sup> increases with temperature, promoting

water molecules bonding by hydrogen bonds to detach from the polymer, allowing associative contacts between the newly exposed hydrophobic monomer units.<sup>25,62</sup> Thus, the observation of an endothermic phase separation by DSC analysis reflects this cleavage of the hydrogen bonds between water molecules and the dissolved polymer, clearly revealing the occurrence of a coil–globule transition mechanism.

In the cooling run, a corresponding exothermic process was observed with its onset only slightly shifted to lower temperatures in comparison to the transition upon heating. Even at a heating rate of 40 K/min, the observed hysteresis is only 1.5 °C. As described for a variety of other thermoresponsive polymers, this minor hysteresis can be attributed to the absence of hydrogen bond donors in PDEVP.<sup>30–32</sup>

We also evaluated the transition hysteresis by turbidimetry using faster heating/cooling rates. Independent of the chosen equilibration period, the transition occurred within 1–2 °C upon heating and within 3–4 °C upon cooling, at polymer concentrations of both 1 and 10 wt % (Figures S21 and S22). Hereby, the transition temperature range in the cooling run was found to not be affected by the cooling rate, whereas for the heating cycle, a continuous increase of the cloud point was observed for higher heating rates. This can be attributed to the system setup using a Peltier thermostat, as above room temperature (rt), upon heating, the desired sample temperature is not reached fast enough. For transitions below rt, this effect is reverse and the cooling curve is shifted to lower temperatures. In combination with the results from DSC analysis, the absence of an effect of the heating/cooling rate on the width of the phase transition demonstrates the fast response of aqueous PDEVP solutions, thus exhibiting only a very minor hysteresis.

**Adjustment of the LCST of PDEVP by Copolymerization.** The cloud point of a polymer solution generally depends on the polymer architecture (linear, star, block, etc.), its molar mass, and concentration.<sup>12,63–66</sup> Moreover, the statistic copolymerization of comonomers with different hydrophilicity/hydrophobicity, forming random or gradient copolymers, allows a fine-tuning of the cloud point.<sup>67–69</sup> As a common feature shared by other thermoresponsive polymers, e.g., polyacrylamides<sup>70</sup> and PEGs,<sup>35</sup> the cloud point of a certain thermoresponsive polymer increases/decreases with rising content of introduced hydrophilic/hydrophobic moieties. Thus, this behavior is also expected for PDAMP. Amphiphilic PDEVP shows temperature-dependent solubility like most water-soluble polymers. In order to achieve a wide modulation of the thermoresponsive properties by statistic copolymerization, DMVP was chosen as a comonomer for raising the LCST as it represents the most hydrophilic monomer in the dialkyl vinylphosphonates series. According to the copolymerization studies, which have shown random copolymerization of DEVP and DPVP, we chose DPVP as a hydrophobic comonomer for lowering the LCST.

Copolymers of DEVP and DPVP being polymerized with different feed ratios were obtained using the above detailed procedure. In all cases, the conversion of both monomers exceeded 90%, and comonomer compositions of the formed copolymers as determined by <sup>1</sup>H NMR spectroscopy are close to the feed ratio (Table 1). The degree of polymerization obtained from GPC-MALS indicates rather low initiator efficiency (31–48%); i.e., the determined molar mass is higher than the theoretical value as calculated from the monomer/initiator feed ratio. This incomplete initiation is addressed to the combination of a fast propagation with a rather slow

**Table 1. Results of the Synthesis of Polyvinylphosphonates and Characterization of the Obtained Polymers**

sample	feed <sup>a</sup>	$M_n^b$ ( $10^5$ g/mol)	$I^*c$ (%)	PDI <sup>b</sup>	cloud point <sup>d</sup> (°C)	composition (x:y) <sup>e</sup>
1	DE <sub>0.5</sub> :DP <sub>0.5</sub>	3.59	31	1.20	5	0.51:0.49
2	DE <sub>0.6</sub> :DP <sub>0.4</sub>	3.23	32	1.28	12	0.60:0.40
3	DE <sub>0.7</sub> :DP <sub>0.3</sub>	2.95	34	1.24	17	0.69:0.31
4	DE <sub>0.8</sub> :DP <sub>0.2</sub>	2.78	35	1.25	24	0.77:0.23
5	DE <sub>0.9</sub> :DP <sub>0.1</sub>	2.30	37	1.28	34	0.89:0.11
6	DE <sub>1.0</sub>	2.2	39	1.16	42	1.0:0
7	DE <sub>0.8</sub> :DM <sub>0.2</sub>	2.01	41	1.32	56	0.78:0.22
8	DE <sub>0.6</sub> :DM <sub>0.4</sub>	1.86	43	1.20	76	0.60:0.40
9	DE <sub>0.4</sub> :DM <sub>0.6</sub>	1.6	48	1.12	92	0.41:0.59

<sup>a</sup>By weighing the monomer, total monomer:catalyst = 500:1. <sup>b</sup>Calculated from GPC-MALS. <sup>c</sup> $I^* = M_{exp}/(M_n \times conv)$ ,  $I^*$  = initiator efficiency,  $M_{exp}$  = expected molecular weight, based on living polymerization calculation. <sup>d</sup>Determined by turbidity measurement at a 10% transmittance decrease upon heating. <sup>e</sup>Calculated from <sup>1</sup>H NMR spectroscopy.

initiation reaction and is in agreement with previous studies.<sup>12</sup> However, the molecular weight distributions are appreciably narrow (PDI < 1.3). Similarly, copolymers of DEVP and hydrophilic DMVP at different feed ratios were obtained in high yields (Table 1, entries 7–9).

The thermoresponsive properties of the obtained poly-(dialkyl vinylphosphonate)s (PDAVP) were investigated by turbidity measurements determining the cloud points of 10 mg/mL aqueous polymer solutions. Figures 6 and 7 show the

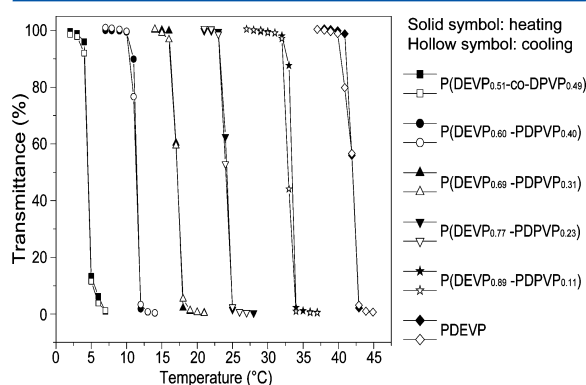


**Figure 6.** Determination of the cloud points of DEVP–DPVP copolymers. The cloud point was determined at 10% decrease of transmittance for a 1.0 wt % aqueous polymer solution.

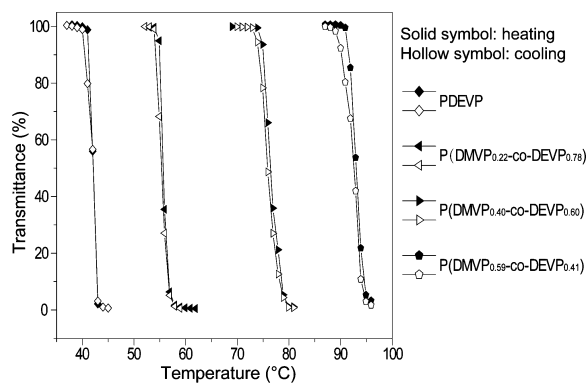


**Figure 7.** Determination of the cloud points of DEVP–DMVP copolymers. The cloud point was determined at 10% decrease of transmittance for a 1.0 wt % aqueous polymer solution.

determination of the cloud point for the DEVP-homopolymers and DAVP-copolymers at different DPVP and DMVP content. The cloud point of the reference PDEVP homopolymer was found to be 42 °C. In order to apply these polymers in polymer therapeutics, poly(vinylphosphonate)s with a cloud point in the physiological interesting temperature region around 37 °C might be attractive. As expected, the random copolymers of DEVP–DPVP show adjustable cloud points ranging from 0 to 42 °C. Most of the transitions occur within 2 °C, which is comparable to or sharper than the phase transition of PNIPAM or PEG systems.<sup>35</sup>

PDMVP is very hydrophilic and does not show a cloud point below 100 °C. Theoretically, the LCST of copolymers of DEVP and DMVP should vary from 42 to 100 °C at different DMVP content. Indeed, we found the copolymers showed a tunable LCST at different monomer compositions. Moreover, the cloud points of DMVP–DEVP copolymers were found to increase linearly with the increasing DMVP molar content, from 42 °C (at 0 mol %) to 92 °C (at 59 mol %) (Figure 8). For DEVP–DPVP copolymers, the cloud points were found to linearly increase with the increasing DEVP content, from 5 °C (at 51 mol %) to 42 °C (at 100 mol %) (Figure 8).

#### Additives Effect on the Thermoresponsive Behavior.

The described novel thermoresponsive copoly(vinylphosphonate)s are very promising for biomedical applications according to the remarkable biocompatibility of polymers containing phosphonate moieties. A first important parameter for biomedical applications is the influence of salts and other

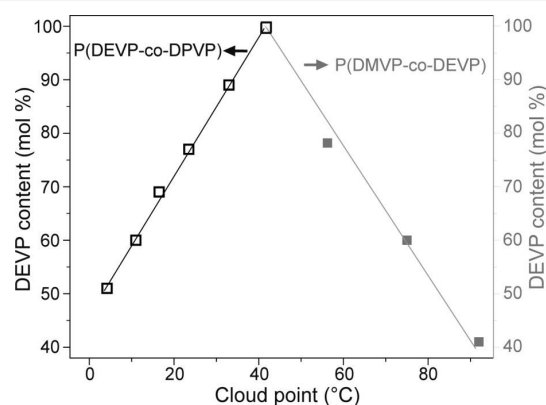


**Figure 8.** Copolymers of DEVP and DPVP/DMVP show linear dependence of the LCST on the comonomer content.

complex media in which biological activities take place on the thermal behavior of the polymers.<sup>18,19</sup> Therefore, the thermoresponsive properties of PDAVP were investigated in the presence of additives such as sodium chloride, calcium chloride, phosphate buffered saline (PBS), and fetal calf serum (FCS). Figure 9 shows cloud points recorded for P(DEVP<sub>0.89</sub>-

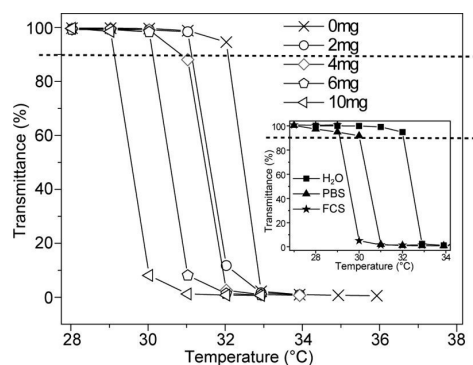


**Figure 9.** Determination of cloud points of P(DEVP<sub>0.89</sub>-co-DPVP<sub>0.11</sub>) in 1.0 wt % aqueous solution at different NaCl concentration upon heating (inset: determination of cloud points of the same polymer in deionized water, PBS, and FCS medium upon heating (polymer concentration = 1.0 wt %)).

co-DPVP<sub>0.11</sub>) in the presence of increasing amounts of sodium chloride. A typical salting-out effect was observed. The presence of sodium chloride leads to a partial dehydration of the macromolecules and consequently to a decrease of the LCST.<sup>35</sup> Nevertheless, the extent of this effect (cloud point shift = 3 °C) is smaller than that for PEG (cloud point shift ≈ 5 °C) and PNIPAM (cloud point shift ≈ 6 °C) systems with comparable degree of polymerization under similar experiment conditions.<sup>35</sup> Because of the presence of phosphonate moieties, the investigation of the calcium salts effect on the cloud point is of specific interest. However, with a decrease of 2 °C at 20 mg/mL CaCl<sub>2</sub>, the dependence of the cloud point on the Ca<sup>2+</sup> concentration is similar to that on the Na<sup>+</sup> concentration (Figure S23). Thus, no effect additionally to the typical salting out has been observed.

P(DEVP<sub>0.89</sub>-co-DPVP<sub>0.11</sub>) behaves similarly in PBS. For a polymer concentration of 10 mg/mL, the cloud point in the buffer solution is roughly 2 °C lower than in pure deionized water, again attributed to a salting-out effect in presence of the phosphate salt in PBS. The cloud point of the same polymer in FCS shifts by 3 °C to 29 °C (Figure 9, inset). The slightly lower cloud points obtained in these physiological media is in good agreement with the cloud point decrease for PNIPAM and PEG for the solvent change from deionized water to tris-buffered saline.<sup>35</sup>

## CONCLUSIONS

In this work, we demonstrated the facile statistic copolymerization of DAVP through REM-GTP, affording copolymers with controlled molecular weights and narrow molecular weight distributions. Evaluation of the copolymerization parameters has shown the formation of nearly perfectly random copolymers ( $r_1, r_2 \sim 1$ ). In view of the pronounced dependence of the polymerization rate of DAVP homopolymerizations on the phosphonate alkyl side chains, these results indicate that the polymerization rate of vinylphosphonate GTP is mainly limited

by the steric demand of growing polymer chain end, not by the added monomer. The obtained co-PDAVPs exhibited thermoresponsive properties, i.e., having an LCST which can be tuned in a wide range by controlling the feed ratio of the comonomers. The LCST phase diagram of aqueous PDEVP solutions has been determined and shows, in combination with DSC analysis, the occurrence of a coil-globule transition mechanism. The observed sharp and reversible phase transition, the small dependence of the thermoresponsiveness on additives and concentration, and its biocompatibility make PDAVP an interesting alternative compared to established thermoresponsive polymers. Such thermoresponsive PDAVPs are promising candidates in biomedical applications, e.g., for controlled cell growth and cell release, which is currently under investigation in our laboratory.

## ASSOCIATED CONTENT

### Supporting Information

Activity measurements and Finemann–Ross evaluation for determination of the copolymerization parameters, <sup>1</sup>H and <sup>31</sup>P NMR spectra of homo- and co-PDAVPs, DSC analyses at 2 and 10 K/min heating/cooling rate, turbidimetric experiments at higher heating/cooling rates, Ca<sup>2+</sup> salt effect on the LCST. This material is available free of charge via the Internet at <http://pubs.acs.org>.

## AUTHOR INFORMATION

### Corresponding Author

\*E-mail: [ning.zhang@ciac.jl.cn](mailto:ning.zhang@ciac.jl.cn) (N.Z.); [rieger@tum.de](mailto:rieger@tum.de) (B.R.).

### Author Contributions

The manuscript was written through contributions of all authors. All authors have given approval to the final version of the manuscript.

### Author Contributions

<sup>§</sup>These authors contributed equally.

### Notes

The authors declare no competing financial interest.

## ACKNOWLEDGMENTS

The authors thank Roche Diagnostics GmbH for financial support. S.S. is grateful for a generous scholarship of the Fonds der Chemischen Industrie. N.Z. thanks Changchun Institute of Applied Chemistry for financial support.

## REFERENCES

- (1) Lu, S. Y.; Hamerton, I. *Prog. Polym. Sci.* **2002**, *27*, 1661–1712.
- (2) Parvole, J.; Jannasch, P. *Macromolecules* **2008**, *41*, 3893–3903.
- (3) Steining, H.; Schuster, M.; Kreuer, K. D.; Kaltbeitzel, A.; Bingöl, B.; Meyer, W. H.; Schauf, S.; Brunklaus, G.; Maier, J.; Spiess, H. W. *Phys. Chem. Chem. Phys.* **2007**, *9*, 1764–1773.
- (4) Wagner, T.; Manhart, A.; Deniz, N.; Kaltbeitzel, A.; Wagner, M.; Brunklaus, G.; Meyer, W. H. *Macromol. Chem. Phys.* **2009**, *210*, 1903–1914.
- (5) Ellis, J.; Wilson, A. D. *Dent. Mater.* **1992**, *8*, 79–84.
- (6) Monge, S.; Canticcioni, B.; Graillet, A.; Robin, J. *Biomacromolecules* **2011**, *12*, 1973–1982.
- (7) Georgieva, R.; Tsevi, R.; Kossev, K.; Kusheva, R.; Balgijiska, M.; Petrova, R.; Tenchova, V.; Gitsov, I.; Troev, K. *J. Med. Chem.* **2002**, *45*, 5797–5801.
- (8) Bingöl, B.; Hart-Smith, G.; Barner-Kowollik, C.; Wegner, G. *Macromolecules* **2008**, *41*, 1634–1639.
- (9) Bingöl, B.; Meyer, W. H.; Wagner, M.; Wegner, G. *Macromol. Rapid Commun.* **2006**, *27*, 1719–1724.

- (10) Salzinger, S.; Rieger, B. *Macromol. Rapid Commun.* **2012**, *33*, 1327–1345.
- (11) Seemann, U. B.; Dengler, J. E.; Rieger, B. *Angew. Chem., Int. Ed.* **2010**, *49*, 3489–3491.
- (12) Salzinger, S.; Seemann, U. B.; Plikhta, A.; Rieger, B. *Macromolecules* **2011**, *44*, 5920–5927.
- (13) Rabe, G. W.; Komber, H.; Haussler, L.; Kreger, K.; Lattermann, G. *Macromolecules* **2010**, *43*, 1178–1181.
- (14) Zhang, N.; Salzinger, S.; Deubel, F.; Jordan, R.; Rieger, B. *J. Am. Chem. Soc.* **2012**, *134*, 7333–7336.
- (15) Chung, J. E.; Yokoyama, M.; Okano, T. *J. Controlled Release* **2000**, *65*, 93–103.
- (16) Stuart, M. A. C.; Huck, W. T. S.; Genzer, J.; Muller, M.; Ober, C.; Stamm, M.; Sukhorukov, G. B.; Szleifer, L.; Tsukruk, V. V.; Urban, M.; Winnik, F.; Zauscher, S.; Luzinov, I.; Minko, S. *Nat. Mater.* **2010**, *9*, 101–113.
- (17) Kanazawa, H.; Yamamoto, K.; Matsushima, Y.; Takai, N.; Kikuchi, A.; Sakurai, Y.; Okano, T. *Anal. Chem.* **1996**, *68*, 100–105.
- (18) Ayano, E.; Kanazawa, H. *J. Sep. Sci.* **2006**, *29*, 738–749.
- (19) Yagi, H.; Yamamoto, K.; Aoyagi, T. *J. Chromatogr., B* **2008**, *876*, 97–102.
- (20) Nagase, K.; Kobayashi, J.; Kikuchi, A.; Akiyama, Y.; Kanazawa, H.; Okano, T. *ACS Appl. Mater. Interfaces* **2012**, *4*, 1998–2008.
- (21) Tan, I.; Roohi, F.; Titirici, M. *Anal. Methods* **2012**, *4*, 34–43.
- (22) Kikuchi, A.; Okano, T. *Prog. Polym. Sci.* **2002**, *27*, 1165–1193.
- (23) Rzaev, Z. M. O.; Dincer, S.; Piskin, E. *Prog. Polym. Sci.* **2007**, *32*, 534–595.
- (24) Aoshima, S.; Kanaoka, S. *Adv. Polym. Sci.* **2008**, *210*, 169–208.
- (25) Schild, H. G. *Prog. Polym. Sci.* **1992**, *17*, 163–249.
- (26) Schmitt, F. J.; Park, C.; Simon, J.; Ringsdorf, H.; Israelachvili, J. *Langmuir* **1998**, *14*, 2838–2845.
- (27) Yamato, M.; Utsumi, M.; Kushida, A.; Konno, C.; Kikuchi, A.; Okano, T. *Tissue Eng.* **2001**, *7*, 473–480.
- (28) Wang, X.; Qiu, X.; Wu, C. *Macromolecules* **1998**, *31*, 2972–2976.
- (29) Cheng, H.; Shen, L.; Wu, C. *Macromolecules* **2006**, *39*, 2325–2329.
- (30) Cao, Y.; Zhao, N.; Wu, K.; Zhu, X. X. *Langmuir* **2009**, *25*, 1699–1704.
- (31) Aseyev, V.; Tenhu, H.; Winnik, F. M. *Adv. Polym. Sci.* **2011**, *242*, 29–89.
- (32) Zhou, K.; Lu, Y.; Li, J.; Shen, L.; Zhang, G.; Xie, Z.; Wu, C. *Macromolecules* **2008**, *41*, 8927–8931.
- (33) Herold, D. A.; Keil, K.; Bruns, D. E. *Biochem. Pharmacol.* **1989**, *38*, 73–76.
- (34) Lutz, J. F. *J. Polym. Sci., Part A: Polym. Chem.* **2008**, *46*, 3459–3470.
- (35) Lutz, J. F.; Akdemir, O.; Hoth, A. *J. Am. Chem. Soc.* **2006**, *128*, 13046–13047.
- (36) Li, L.; Chen, S.; Jiang, S. *J. Biomater. Sci., Polym. Ed.* **2007**, *18*, 1415–1427.
- (37) Yuk, S. H.; Cho, S. H.; Lee, S. H. *Macromolecules* **1997**, *30*, 6856–6859.
- (38) Maeda, Y. *Langmuir* **2001**, *17*, 1737–1742.
- (39) de las Heras Alarcón, C.; Pennadam, S.; Alexander, C. *Chem. Soc. Rev.* **2005**, *34*, 276–285.
- (40) Zhang, N.; Huber, S.; Schulz, A.; Luxenhofer, R.; Jordan, R. *Macromolecules* **2009**, *42*, 2215–2221.
- (41) Yamamoto, K.; Serizawa, T.; Muraoka, Y.; Akashi, M. *Macromolecules* **2001**, *34*, 8014–8020.
- (42) Ajiro, H.; Takahashi, Y.; Akashi, M. *Macromolecules* **2012**, *45*, 2668–2674.
- (43) Blanz, A.; Warren, N. J.; Lewis, A. L.; Armes, S. P.; Ryan, A. J. *Soft Matter* **2011**, *7*, 6399–6403.
- (44) Lambermont Thijs, H. M. L.; Hoogenboom, R.; Fustin, C. A.; Bomal D'Haese, C.; Gohy, J. F.; Schubert, U. S. *J. Polym. Sci., Part A: Polym. Chem.* **2009**, *47*, 515–522.
- (45) Trinh, L. T. T.; Lambermont-Thijs, H. M. L.; Schubert, U. S.; Hoogenboom, R.; Kjoniksen, A. L. *Macromolecules* **2012**, *45*, 4337–4345.
- (46) Salzinger, S.; Huber, S.; Jaksch, S.; Busch, P.; Jordan, R.; Papadakis, C. M. *Colloid Polym. Sci.* **2012**, *290*, 385–400.
- (47) Leute, M. PhD Thesis, University of Ulm, 2007.
- (48) Evans, W. J.; Dominguez, R.; Hanusa, T. P. *Organometallics* **1986**, *5*, 263–270.
- (49) Ely, N. M.; Tsutsui, M. *Inorg. Chem.* **1975**, *14*, 2680–2687.
- (50) Kelen, T.; Tudos, F. *J. Macromol. Sci., Chem.* **1975**, *A9*, 1–27.
- (51) Jakobsen, H. J.; Bundgaard, T.; Hansen, R. S. *Mol. Phys.* **1972**, *23*, 197–201.
- (52) Komber, H.; Steinert, V.; Voit, B. *Macromolecules* **2008**, *41*, 2119–2125.
- (53) Detailed mechanistic studies on the propagation reaction of rare earth metal-mediated GTP of vinylphosphonates are currently underway.
- (54) Blanz, A.; Warren, N. J.; Lewis, A. L.; Armes, S. P.; Ryan, A. J. *Soft Matter* **2011**, *7*, 6399–6403.
- (55) Lambermont Thijs, H. M. L.; Hoogenboom, R.; Fustin, C. A.; Bomal D'Haese, C.; Gohy, J. F.; Schubert, U. S. *J. Polym. Sci., Part A: Polym. Chem.* **2009**, *47*, 515–522.
- (56) Trinh, L. T. T.; Lambermont-Thijs, H. M. L.; Schubert, U. S.; Hoogenboom, R.; Kjoniksen, A. L. *Macromolecules* **2012**, *45*, 4337–4345.
- (57) Salzinger, S.; Huber, S.; Jaksch, S.; Busch, P.; Jordan, R.; Papadakis, C. M. *Colloid Polym. Sci.* **2012**, *290*, 385–400.
- (58) Wu, C.; Wang, X. *Phys. Rev. Lett.* **1998**, *80*, 4092–4094.
- (59) Garcia-Lisbona, M. N.; Galindo, A.; Jackson, G.; Burgess, A. N. *J. Am. Chem. Soc.* **1998**, *120*, 4191–4199.
- (60) Tanford, C. *The Hydrophobic Effect*, 2nd ed.; J. Wiley and Sons: New York, 1973.
- (61) Ben-Naim, A. *Hydrophobic Interactions*; Plenum Press: New York, 1980.
- (62) Widom, B.; Bhimalapuram, B.; Koga, K. *Phys. Chem. Chem. Phys.* **2003**, *5*, 3085–3093.
- (63) Li, W.; Zhang, A.; Feldman, K.; Walde, P.; Schlüter, A. D. *Macromolecules* **2008**, *41*, 3659–3667.
- (64) Furyk, S.; Zhang, Y.; Ortiz-Acosta, D.; Cremer, P. S.; Bergbreiter, D. E. *J. Polym. Sci., Part A: Polym. Chem.* **2006**, *44*, 1492–1501.
- (65) Plamper, F. A.; Ruppel, M.; Schmalz, A.; Borrisov, O.; Ballauff, M.; Müller, A. H. E. *Macromolecules* **2007**, *40*, 8361–8366.
- (66) Zhang, N.; Luxenhofer, R.; Jordan, R. *Macromol. Chem. Phys.* **2012**, *213*, 973–981.
- (67) Yamamoto, S. I.; Pietrasik, J.; Matyjaszewski, K. *J. Polym. Sci., Part A: Polym. Chem.* **2008**, *46*, 194–202.
- (68) Eggenhuisen, T. M.; Becer, C. R.; Fijten, M. W. M.; Eckardt, R.; Hoogenboom, R.; Schubert, U. S. *Macromolecules* **2008**, *41*, 5132–5140.
- (69) Chee, C. K.; Rimmer, S.; Shaw, D. A.; Soutar, I.; Swanson, L. *Macromolecules* **2001**, *34*, 7544–7549.
- (70) Yin, X.; Hoffman, A. S.; Stayton, P. S. *Biomacromolecules* **2006**, *7*, 1381–1385.

## Supporting Information:

### Poly(vinylphosphonate)s with Widely Tuneable LCST: A Promising Alternative to Conventional Thermoresponsive Polymers

Ning Zhang,<sup>\*,†,‡,§</sup> Stephan Salzinger<sup>†#</sup> and Bernhard Rieger<sup>\*,†</sup>

<sup>†</sup>WACKER-Lehrstuhl für Makromolekulare Chemie, Technische Universität München, Lichtenbergstraße 4, 85747 Garching bei München, Germany

<sup>‡</sup>Changchun Institute of Applied Chemistry, Chinese Academy of Sciences, Changchun, 130022, China

#### Copolymerization Kinetics

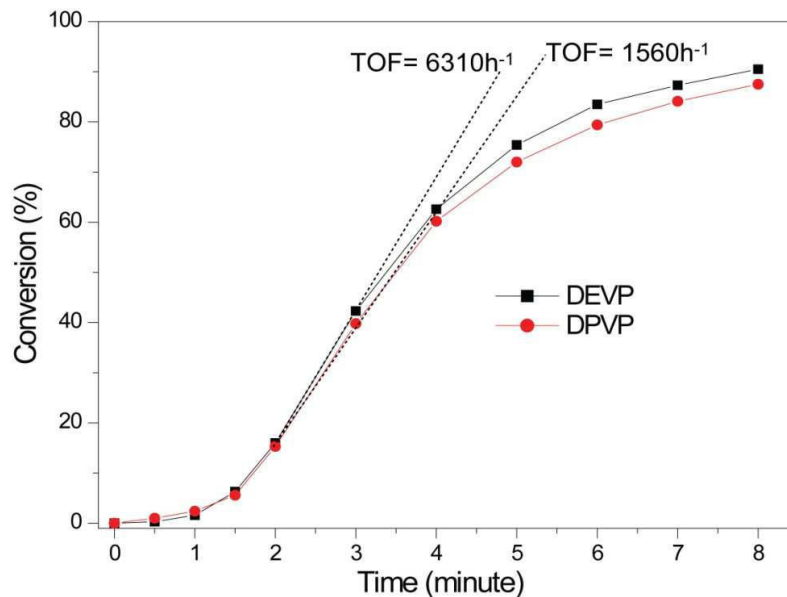


**Figure S1.** Determination of the catalytic activity of  $\text{Cp}_3\text{Yb}$  for the copolymerization of DEVP ( $\text{TOF} = 6310 \text{ h}^{-1}$ ) and DPVP ( $\text{TOF} = 1560 \text{ h}^{-1}$ ) ( $[\text{DEVP}]:[\text{DPVP}]:[\text{catalyst}] = 400:100:1$ ).

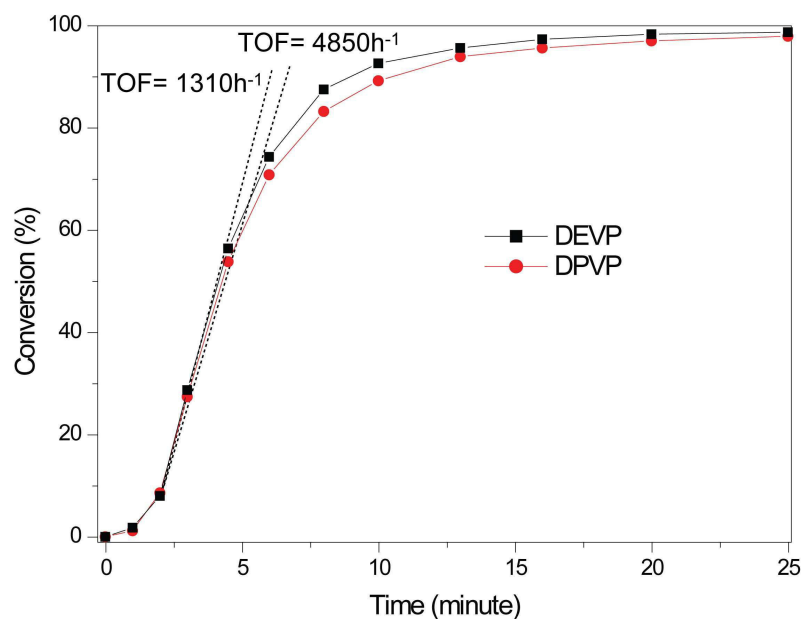


**Figure S2.** Determination of the catalytic activity of  $\text{Cp}_3\text{Yb}$  for the copolymerization of DEVP (TOF =  $1310 \text{ h}^{-1}$ ) and DPVP (TOF =  $4850 \text{ h}^{-1}$ ) ( $[\text{DEVP}]:[\text{DPVP}]:[\text{catalyst}] = 100:400:1$ ).

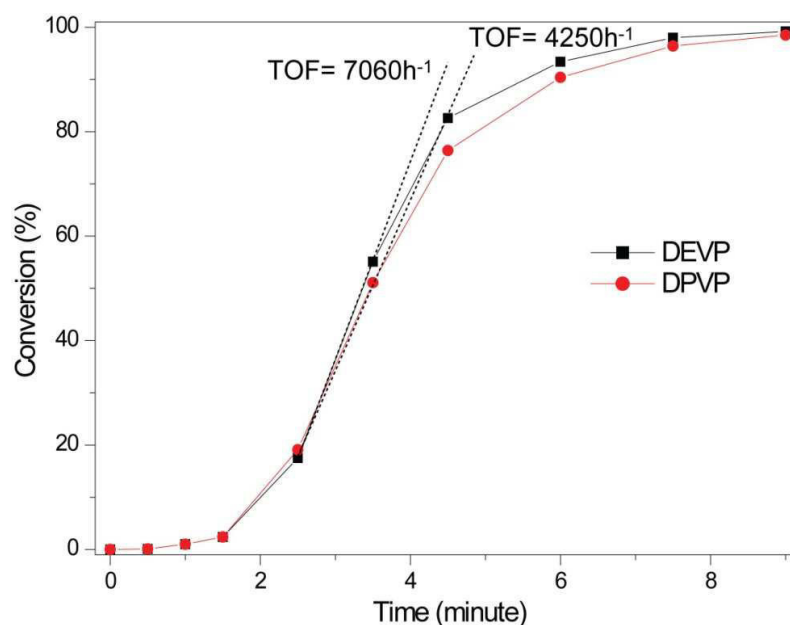


**Figure S3.** Determination of the catalytic activity of  $\text{Cp}_3\text{Yb}$  for the copolymerization of DEVP (TOF =  $7060 \text{ h}^{-1}$ ) and DPVP (TOF =  $4250 \text{ h}^{-1}$ ) ( $[\text{DEVP}]:[\text{DPVP}]:[\text{catalyst}] = 300:200:1$ ).



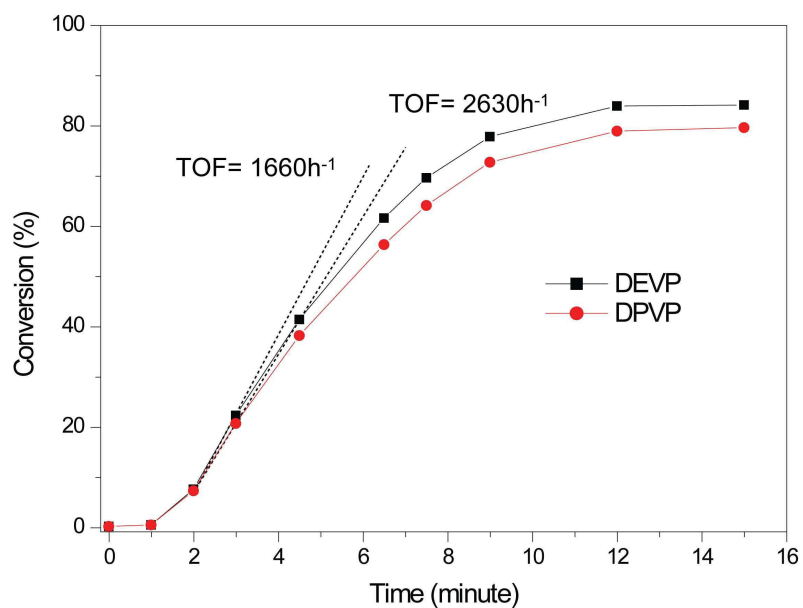


**Figure S4.** Determination of the catalytic activity of  $\text{Cp}_3\text{Yb}$  for the copolymerization of DEVP ( $\text{TOF} = 1660 \text{ h}^{-1}$ ) and DPVP ( $\text{TOF} = 2630 \text{ h}^{-1}$ ) ( $[\text{DEVP}]:[\text{DPVP}]:[\text{catalyst}] = 200:300:1$ ).

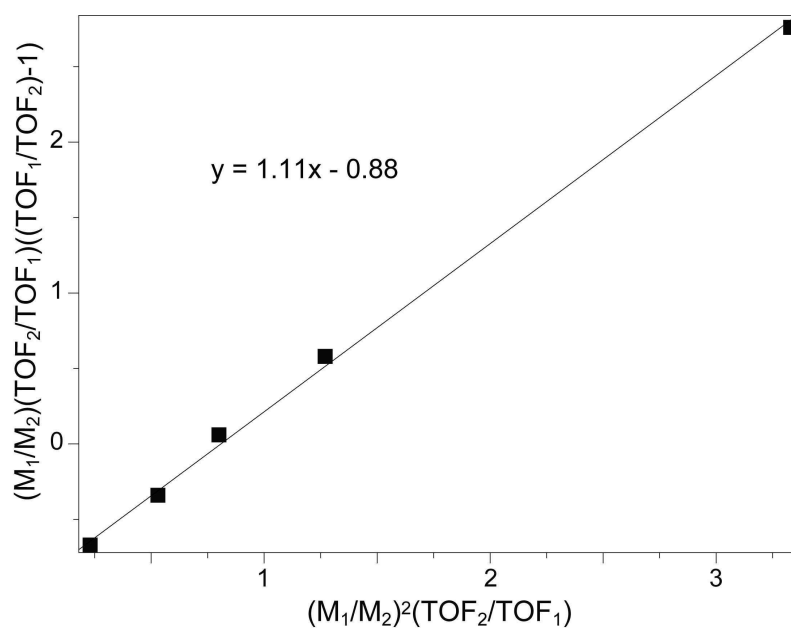


**Figure S5.** Finemann-Ross determination of the copolymerization parameter  $r_{\text{DEVP}}$  for the copolymerization of DEVP and DPVP using  $\text{Cp}_3\text{Yb}$  ( $r_{\text{DEVP}} = 1.11$ ).

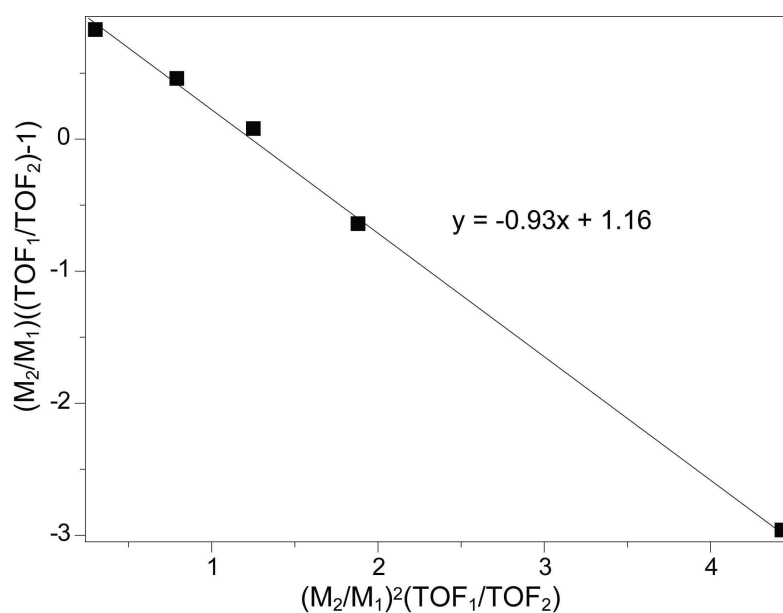


**Figure S6.** Finemann-Ross determination of the copolymerization parameter  $r_{DPVP}$  for the copolymerization of DEVP and DPVP using  $Cp_3Yb$  ( $r_{DPVP} = 0.93$ ).

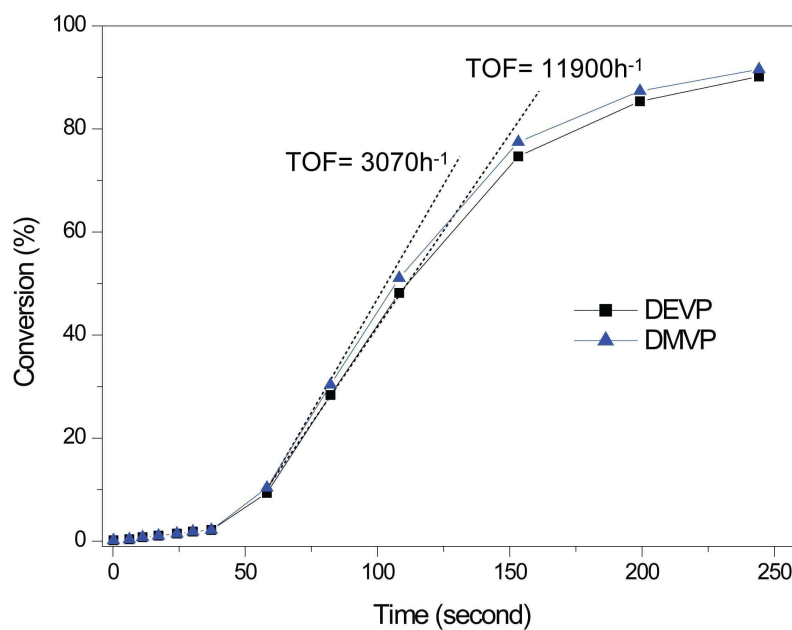


**Figure S7.** Determination of the catalytic activity of  $Cp_3Yb$  for the copolymerization of DEVP (TOF = 11900 h<sup>-1</sup>) and DMVP (TOF = 3080 h<sup>-1</sup>) ([DEVP]:[DMVP]:[catalyst] = 400:100:1).

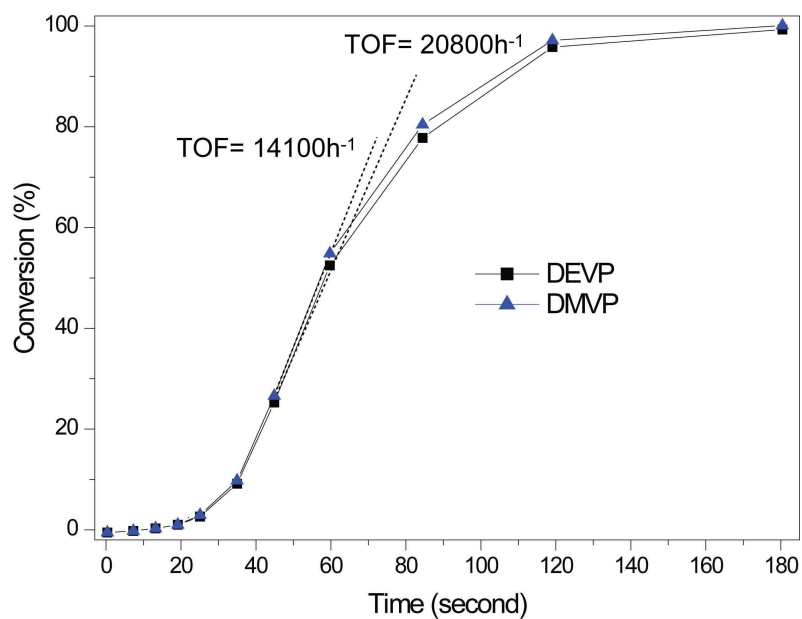


**Figure S8.** Determination of the catalytic activity of  $Cp_3Yb$  for the copolymerization of DEVP (TOF = 20800 h<sup>-1</sup>) and DMVP (TOF = 14100 h<sup>-1</sup>) ([DEVP]:[DMVP]:[catalyst] = 300:200:1).

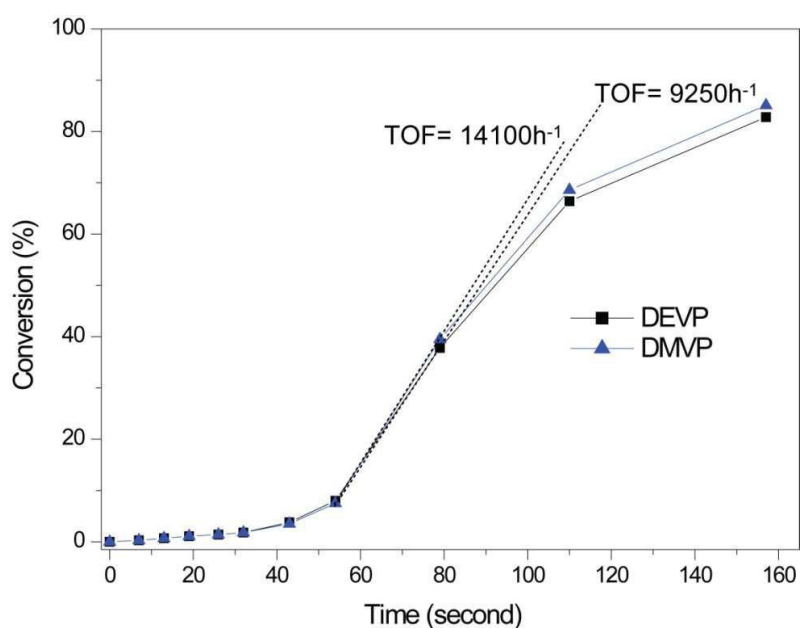


**Figure S9.** Determination of the catalytic activity of  $Cp_3Yb$  for the copolymerization of DEVP (TOF = 9250 h<sup>-1</sup>) and DMVP (TOF = 14100 h<sup>-1</sup>) ([DEVP]:[DMVP]:[catalyst] = 200:300:1).

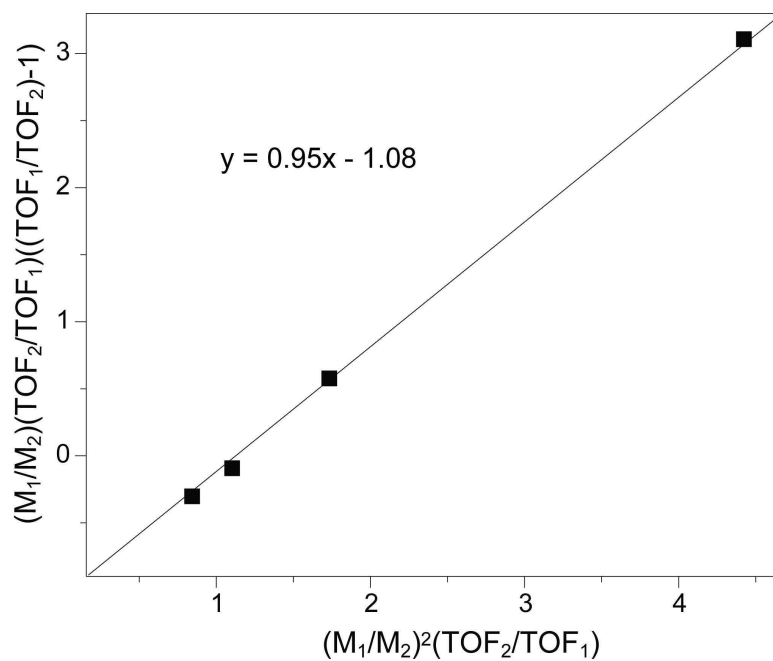


**Figure S10.** Finemann-Ross determination of the copolymerization parameter  $r_{DEVP}$  for the copolymerization of DEVP and DMVP using  $Cp_3Yb$  ( $r_{DEVP} = 0.95$ ).

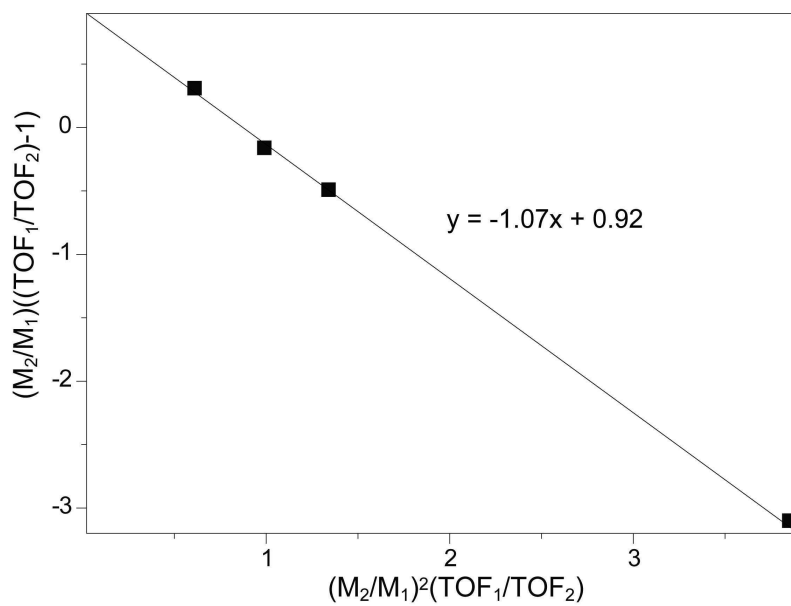


**Figure S11.** Finemann-Ross determination of the copolymerization parameter  $r_{DMVP}$  for the copolymerization of DEVP and DMVP using  $Cp_3Yb$  ( $r_{DMVP} = 1.07$ ).

### <sup>1</sup>H NMR spectra of PDAVP

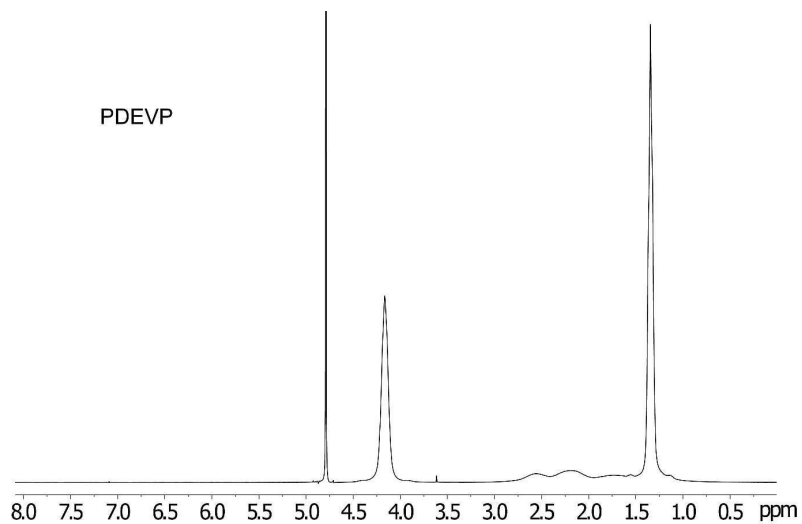


Figure S12. <sup>1</sup>H NMR spectrum of PDEVP in D<sub>2</sub>O.

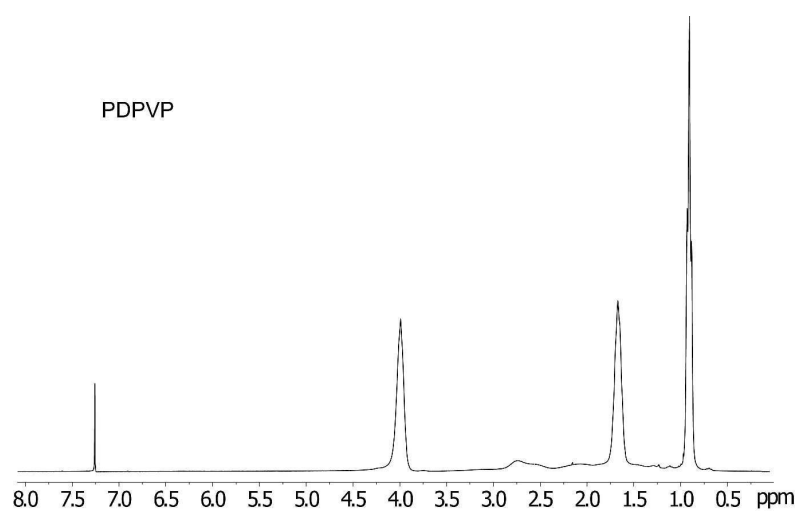
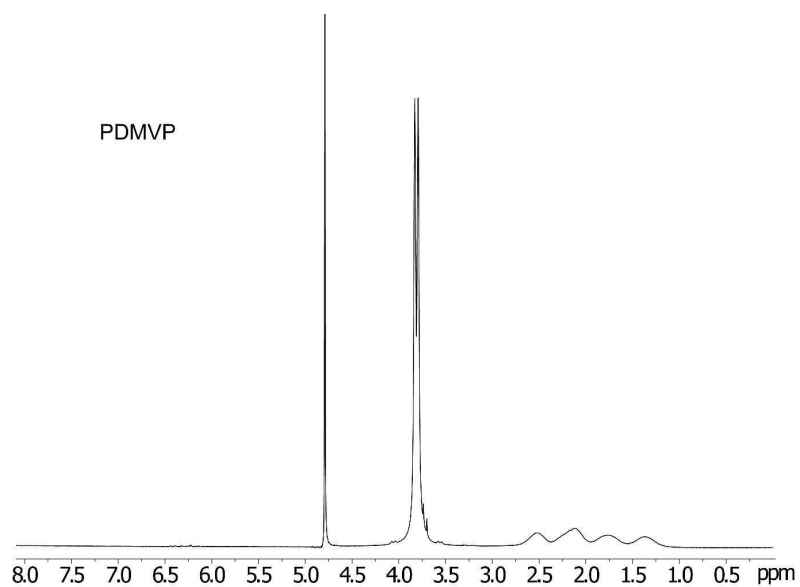
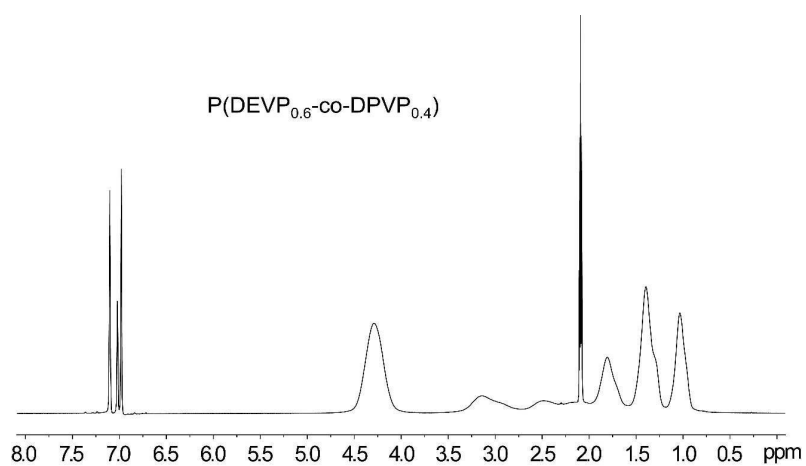


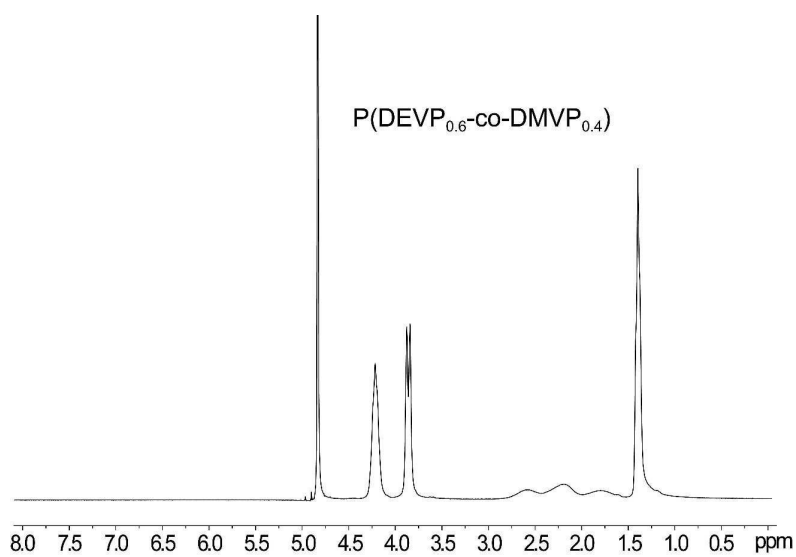
Figure S13. <sup>1</sup>H NMR spectrum of PDPVP in CDCl<sub>3</sub>.



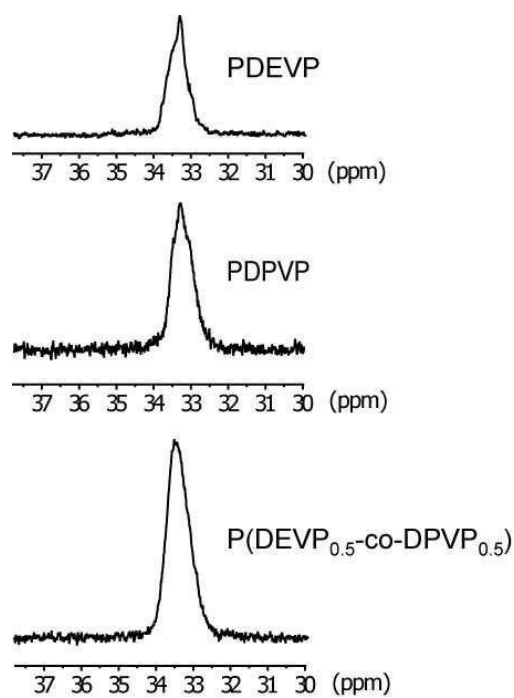
**Figure S14.** <sup>1</sup>H NMR spectrum of PDMVP in D<sub>2</sub>O.



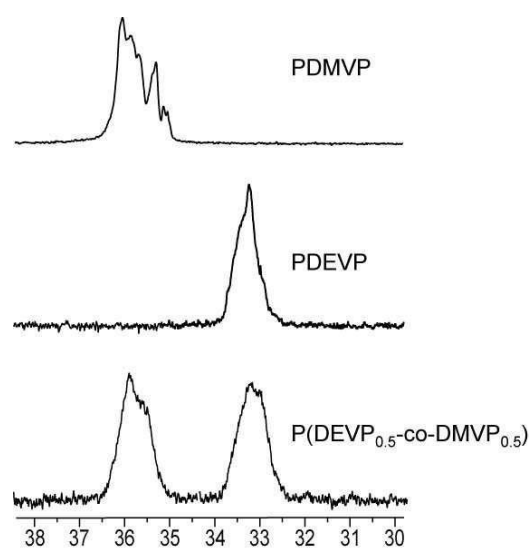
**Figure S15.** <sup>1</sup>H NMR spectrum of P(DEVP<sub>0.6</sub>-co-DPVP<sub>0.4</sub>) in deuterated toluene.



**Figure S16.**  $^1\text{H}$  NMR spectrum of  $\text{P}(\text{DEVP}_{0.6}\text{-co-DMVP}_{0.4})$  in  $\text{D}_2\text{O}$ .

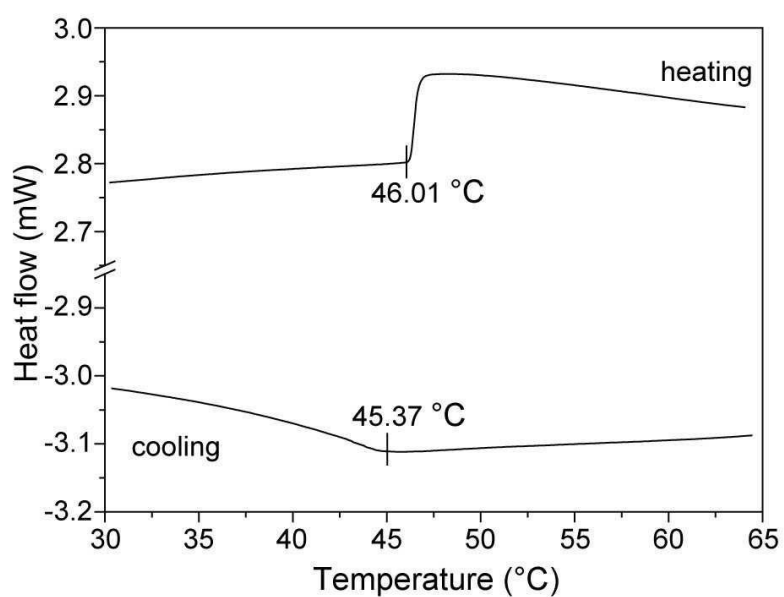


**Figure 17.**  $^{31}\text{P}$  NMR spectra of PDEVP, PDPVP and  $\text{P}(\text{DEVP}_{0.5}\text{-co-DPVP}_{0.5})$ .



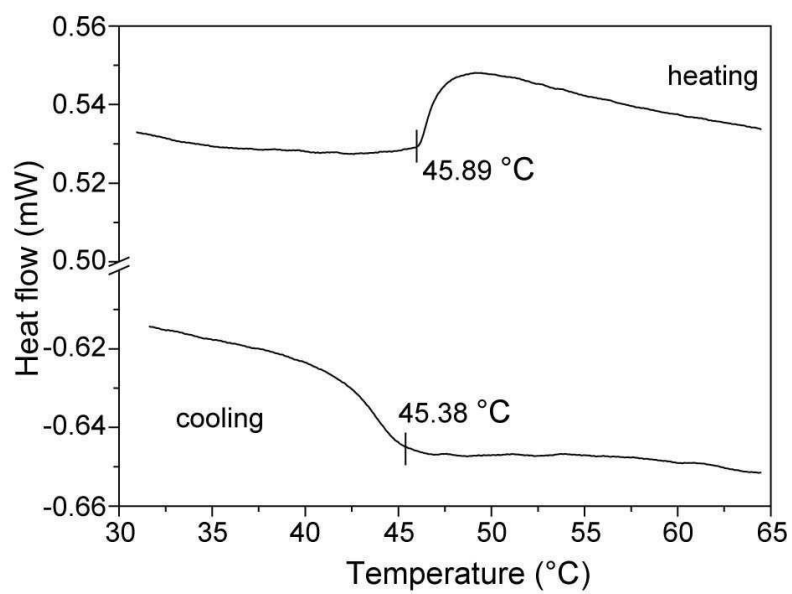
**Figure 18.**  $^{31}\text{P}$  NMR spectra of PDEVP, PDMVP and P(DEVP<sub>0.5</sub>-co-DMVP<sub>0.5</sub>).

### Determination of the Transition hysteresis

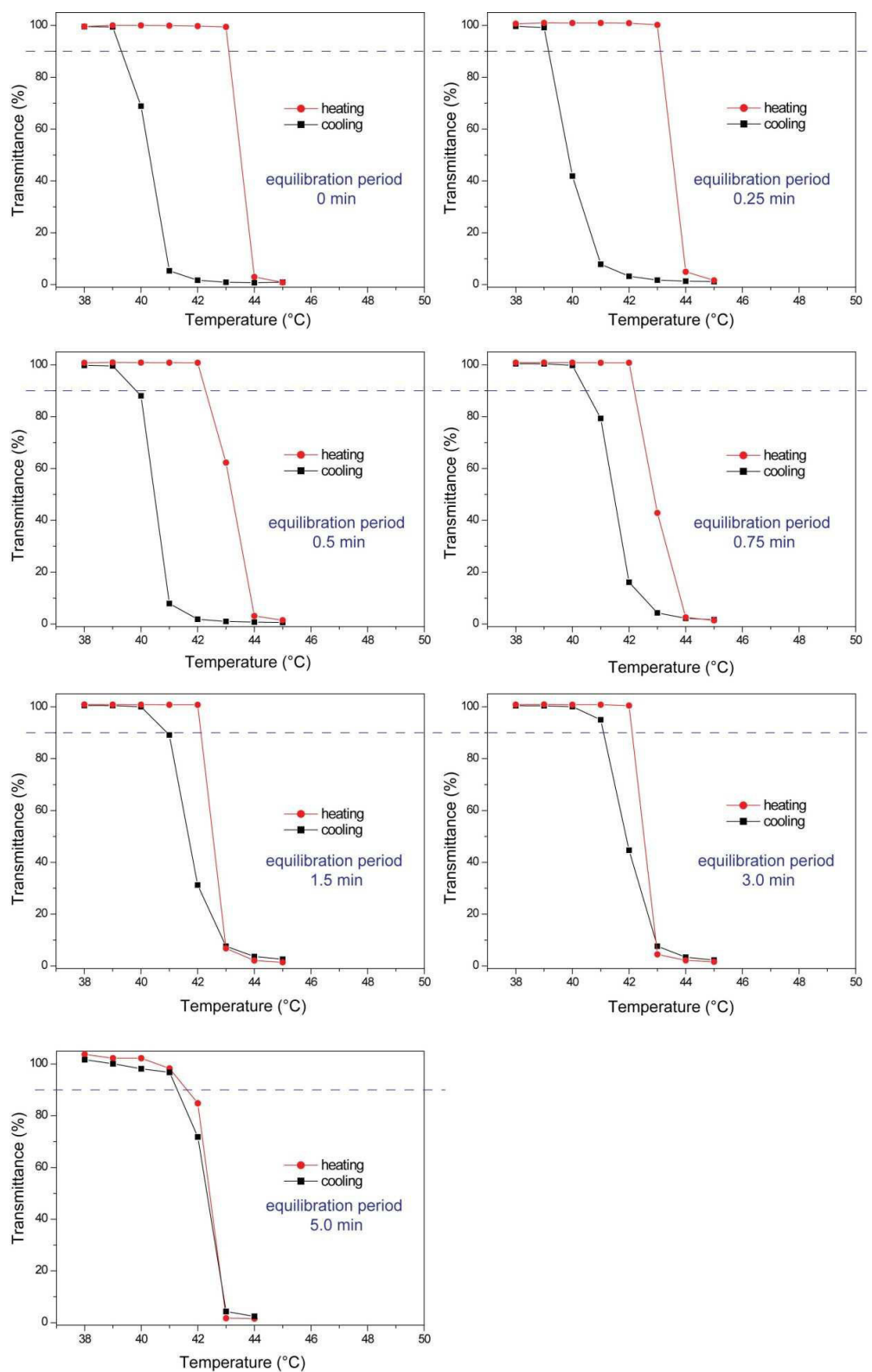


**Figure S19.** DSC analysis of a 30w% aqueous PDEVP solution (heating rate: 10 K/min).

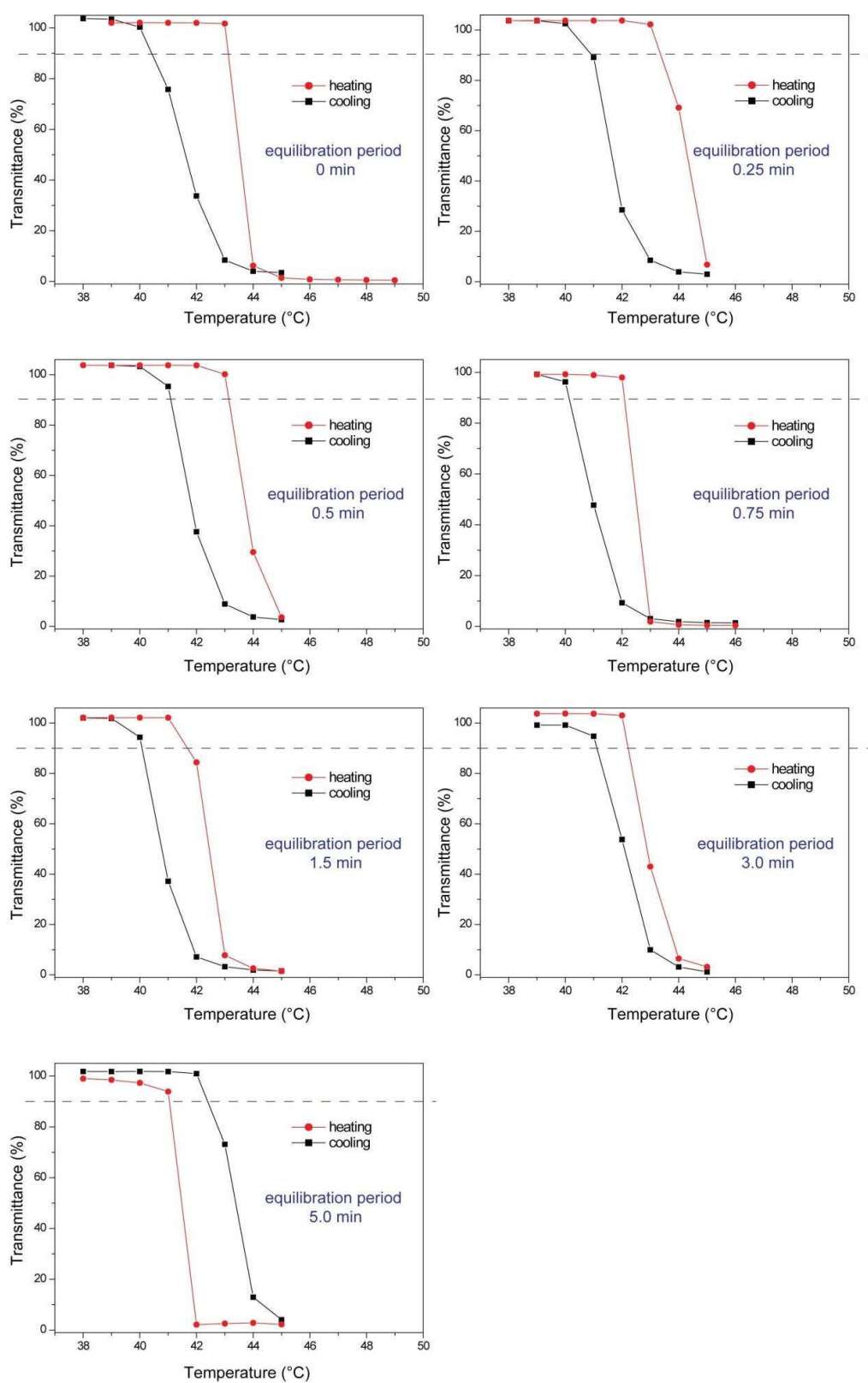




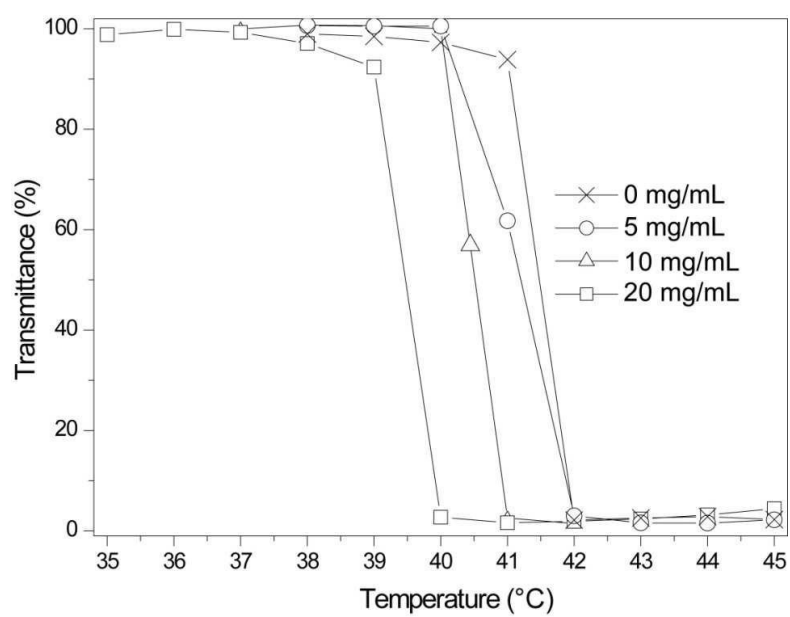
**Figure S20.** DSC analysis of a 30w% aqueous PDEVP solution (heating rate: 2 K/min).



**Figure S21.** Investigation of phase transition hysteresis by turbidimetry using varying equilibration time (10wt% PDEVP aqueous solution).



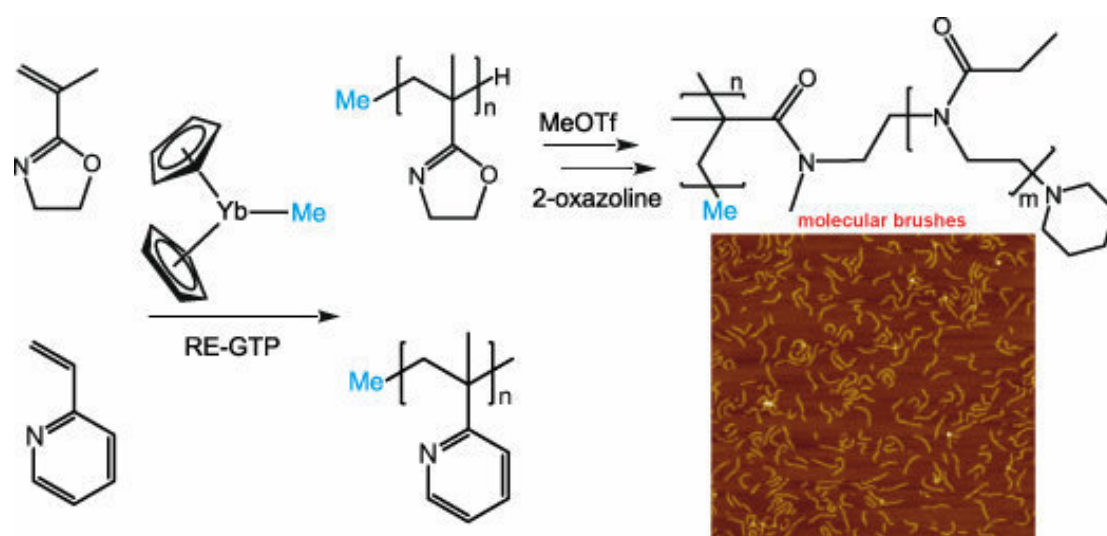
**Figure S22.** Investigation of phase transition hysteresis by turbidimetry using varying equilibration time (1wt% PDEVP aqueous solution).

**Ca<sup>2+</sup> salt effect**

**Figure S23.** Determination of cloud points of PDEVp in 1.0 wt % aqueous solution at different CaCl<sub>2</sub> concentration upon heating.

## CHAPTER 8:

# RARE EARTH METAL-MEDIATED GROUP TRANSFER POLYMERIZATION: FROM DEFINED POLYMER MICROSTRUCTURES TO HIGH PRECISION NANO-SCALED OBJECTS



*“There is a single light of science, and to brighten it anywhere is to brighten it everywhere.”*

- Isaac Asimov (1919-1992)



**Status:** Published online: June 4, 2013  
**Journal:** Journal of the American Chemical Society  
Article ASAP  
**Publisher:** ACS Publications  
**Article type:** Communication  
**DOI:** 10.1021/ja4036175  
**Authors:** Ning Zhang, Stephan Salzinger, Benedikt S. Soller,  
Bernhard Rieger

**Content:**

This chapter reports on the efficient synthesis of poly(2-isopropenyl-2-oxazoline) (PIPOx) and poly(2-vinylpyridine) (P2VP) with high molecular weight and narrow polydispersity *via* rare earth metal-mediated group transfer polymerization as one of the first examples for REM-GTP to proceed *via* N→Ln coordination. Previous REM-GTP copolymerization studies have shown the addition sequence of the comonomers to be critical for monomers with different coordination strength to the metal center, *i.e.* monomers can only be polymerized in order of increasing coordination strength. In order to examine the relative coordination strength of the newly employed N-coordinating monomers IPOx and 2VP, statistical copolymerizations were conducted, establishing a monomer reactivity order for REM-GTP as DEVP > MMA > IPOx > 2VP. Consecutive polymerization of different monomers is hereby only possible in order of increasing coordination strength and restricted to comonomers with similar polarity. In combination with LCROP, PIPOx was converted to molecular brushes with defined backbone and poly(2-oxazoline) side chains using a *grafting-from* method.



RightsLink®

Home

Create Account

Help



ACS Publications

High quality. High impact.

**Title:** Rare Earth Metal-Mediated Group-Transfer Polymerization: From Defined Polymer Microstructures to High-Precision Nano-Scaled Objects

**Author:** Ning Zhang, Stephan Salzinger, Benedikt S. Soller, and Bernhard Rieger

**Publication:** Journal of the American Chemical Society

**Publisher:** American Chemical Society

**Date:** Jun 1, 2013

Copyright © 2013, American Chemical Society

User ID
<input type="text"/>
Password
<input type="text"/>
<input type="checkbox"/> Enable Auto Login
<input type="button" value="LOGIN"/>
<a href="#">Forgot Password/User ID?</a>
<b>If you're a copyright.com user</b> , you can login to RightsLink using your copyright.com credentials. Already a <b>RightsLink user</b> or want to <a href="#">learn more?</a>

### PERMISSION/LICENSE IS GRANTED FOR YOUR ORDER AT NO CHARGE

This type of permission/license, instead of the standard Terms & Conditions, is sent to you because no fee is being charged for your order. Please note the following:

- Permission is granted for your request in both print and electronic formats, and translations.
- If figures and/or tables were requested, they may be adapted or used in part.
- Please print this page for your records and send a copy of it to your publisher/graduate school.
- Appropriate credit for the requested material should be given as follows: "Reprinted (adapted) with permission from (COMPLETE REFERENCE CITATION). Copyright (YEAR) American Chemical Society." Insert appropriate information in place of the capitalized words.
- One-time permission is granted only for the use specified in your request. No additional uses are granted (such as derivative works or other editions). For any other uses, please submit a new request.

BACK

CLOSE WINDOW

Copyright © 2013 [Copyright Clearance Center, Inc.](#) All Rights Reserved. [Privacy statement](#). Comments? We would like to hear from you. E-mail us at [customer@copyright.com](mailto:customer@copyright.com)



Reprinted with Permission from Zhang, N.; Salzinger, S.; Soller, B. S.; Rieger, B. *J. Am. Chem. Soc.*, Article ASAP. Copyright 2013 American Chemical Society.

## Rare Earth Metal-Mediated Group-Transfer Polymerization: From Defined Polymer Microstructures to High-Precision Nano-Scaled Objects

Ning Zhang,<sup>\*,†</sup> Stephan Salzinger,<sup>‡</sup> Benedikt S. Soller,<sup>‡</sup> and Bernhard Rieger<sup>\*,‡</sup>

<sup>†</sup>Changchun Institute of Applied Chemistry, Chinese Academy of Sciences, Changchun 130022, China

<sup>‡</sup>WACKER-Lehrstuhl für Makromolekulare Chemie, Technische Universität München, 85747 Garching bei München, Germany

### Supporting Information

**ABSTRACT:** Poly(2-isopropenyl-2-oxazoline) (PIPOx) and poly(2-vinylpyridine) (P2VP) have been efficiently synthesized using bis(cyclopentadienyl)methyl ytterbium (Cp<sub>2</sub>YbMe) as catalyst. The polymerizations of 2-isopropenyl-2-oxazoline (IPOx) and 2-vinylpyridine (2VP) follow a living group-transfer polymerization (GTP) mechanism, allowing a precise molecular-weight control of both polymers with very narrow molecular-weight distribution. The GTP of IPOx and 2VP occurs via N coordination at the rare earth metal center, which has rarely been reported previously. The relative coordination strength of different monomers at the ytterbium center is determined by copolymerization investigations to be in the order of DEVP > MMA > IPOx > 2VP. In combination with living cationic ring-opening polymerization, PIPOx is converted to molecular brushes with defined backbone and poly(2-oxazoline) side chains using the *grafting-from* method.

Since the first report on rare earth metal-mediated group-transfer polymerization (REM-GTP) by Yasuda et al. in 1992,<sup>1</sup> researchers have devoted their efforts to optimizing reaction conditions and initiator efficiency and extending its utilization for various monomers, e.g., (meth)acrylates and (meth)acrylamides.<sup>2–4</sup> In view of the mechanism, this type of polymerization is recognized as coordinative anionic, and due to its similarity to silyl ketene acetal-initiated GTP, it is also referred to as transition metal-mediated GTP.<sup>4–12</sup> Because of its highly living character, REM-GTP leads to strictly linear polymers with very narrow molecular-weight distribution ( $\bar{M}_w/\bar{M}_n < 1.1$ ), exhibits a linear increase of the average molar mass upon monomer conversion, and allows the synthesis of block copolymers as well as the introduction of chain end functionalities.<sup>2–4,11</sup> Coordination of the growing chain end at the catalyst suppresses side reactions and allows stereospecific polymerization as well as activity optimization by varying both the metal center and the catalyst ligand sphere.<sup>4,11</sup> Accordingly, REM-GTP combines the advantages of living ionic and coordinative polymerizations and thus allows a precise adjustment of the polymer architecture and microstructure.

Recently, our group and other researchers showed that REM-GTP is not restricted to common (meth)acrylates but is also applicable to several other monomer classes of interest, e.g.,

vinylphosphonates and vinylpyridines.<sup>6–8,11,13,14</sup> Moreover, we reported on the development of a surface-initiated group-transfer polymerization (SI-GTP) mediated by rare earth metal catalysts, allowing the perfect decoration of substrates with polymer brushes of specific functionality.<sup>15</sup> Inspired by these recent advances and the high precision offered by REM-GTP, we have made it a major focus of our research to extend the applicability of this method to further monomer classes and to evaluate the utilization of REM-GTP for the production of tailor-made functional polymer-based architectures. In this context, this Communication describes the efficient polymerization of 2-isopropenyl-2-oxazoline (IPOx) and 2-vinylpyridine (2VP) through REM-GTP, occurring via N coordination of the monomer at the rare earth metal center. Copolymerization experiments are conducted to compare the coordination strength of the different monomers to the rare earth metal. Moreover, REM-GTP is combined with living cationic ring-opening polymerization (LCROP), giving the first access to poly(2-oxazoline) molecular brushes with narrow side chain and backbone chain length distribution.

IPOx is a versatile dual-functional monomer comprising an oxazoline and a vinyl moiety. On one hand, it can undergo LCROP of the heterocyclic motif, resulting in defined poly(2-oxazoline)s for a variety of applications in biomedicine.<sup>16–24</sup> On the other hand, radical/anionic polymerization of the vinylidene functionality of IPOx leads to poly(2-isopropenyl-2-oxazoline) (PIPOx) with a broad molecular-weight distribution,<sup>16,25</sup> even though anionic and reversible addition–fragmentation polymerization finitely improves the distribution character.<sup>26,27</sup> Living anionic polymerization, owing to the strict operating conditions and solvent effects,<sup>28</sup> is not a preferred method for the polymerization of IPOx. Moreover, due to a strong complexation of pendant 2-oxazoline units by copper, attempts to polymerize IPOx by atom-transfer radical polymerization (ATRP) were not successful.<sup>25</sup> There seems to be no truly successful method by which PIPOx with controlled molecular weight and narrow  $\bar{M}_w/\bar{M}_n$  ( $\bar{M}_w/\bar{M}_n < 1.1$ ) is accessible. Also for 2VP, another functional monomer comprising a C=C–C=N functionality, there is a continuing demand to seek superior methods for efficient and convenient polymerization. Inspired by the electronic and structural similarity between IPOx/2VP and (meth)acrylates or vinylphosphonates, as well as initial investigations on rare earth metal-

Received: April 11, 2013



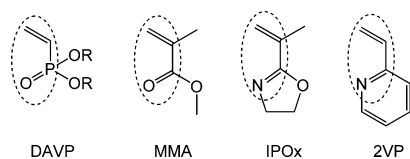


**Figure 1.** Molecular structures of dialkyl vinylphosphonates (DAVP), methyl methacrylate (MMA), 2-isopropenyl-2-oxazoline (IPOx), and 2-vinylpyridine (2VP).

mediated 2VP polymerization,<sup>13</sup> we examined the polymerizability of IPOx/2VP employing rare earth metal complexes as catalysts (Figure 1).

Initially, the polymerization of IPOx was conducted at room temperature in the presence of  $\text{Cp}_2\text{YbCl}$  and  $\text{Cp}_3\text{Yb}$ . In contrast to using MMA and vinylphosphonates,<sup>4,11,29</sup> no polymerization was observed using  $\text{Cp}_2\text{YbCl}$  as initiator. This was attributed to the rather weak coordination strength (*vide infra*) of IPOx at the metal center, inhibiting cleavage of the dimeric complex  $[\text{Cp}_2\text{YbCl}]_2$ . This hypothesis could be confirmed by X-ray structure analysis of single crystals obtained from a mixture of IPOx and  $\text{Cp}_2\text{YbCl}$  in toluene, which were found to be the  $[\text{Cp}_2\text{YbCl}]_2$  starting material. Using  $\text{Cp}_3\text{Yb}$  as catalyst, low yields of polymer could be isolated after several hours of polymerization at room temperature. The poor efficiency of  $\text{Cp}_3\text{Yb}$  for IPOx in contrast to its high reactivity for DEVP polymerization under identical reaction conditions is attributed to the lower steric crowding of the intermediate  $\text{Cp}_3\text{Yb}(\text{IPOx})$  in comparison to  $\text{Cp}_3\text{Yb}(\text{DEVP})$ , leading to an inefficient initiation of IPOx REM-GTP by  $\text{Cp}_3\text{Yb}$ .<sup>7</sup>

Using  $\text{Cp}_2\text{YbMe}$  as initiator, polymerization of IPOx proceeded smoothly at room temperature, exhibiting high reaction velocity; i.e., monomer conversion reached 95% within 2 h at room temperature, as monitored by *in situ*  $^1\text{H}$  NMR (Figure 2). According to MMA, the methyl group was found to be an efficient initiator for IPOx polymerization (Table 1).<sup>4</sup> This

**Table 1. Summary of Different Polymerization of IPOx (Monomer:Initiator = 200:1)**

initiator	$T$ (°C)	TOF <sup>a,b</sup> (h <sup>-1</sup> )	PDI <sup>c</sup>	$M_n^c$ (kDa)	$I^*^d$ (%)	reaction time (h)/conversion <sup>b</sup> (%)
$\text{Cp}_3\text{Yb}$	25	—	—	—	—	10/trace
$\text{Cp}_2\text{YbMe}$	25	380	1.04	21	95	1.5/92
BuLi	25	3100	1.5	40	53	0.2/95
BuLi	-78	18	1.2	2.5	—	2/18
AIBN	60	—	2.0	18	—	8/59

<sup>a</sup>The turnover frequency (TOF) was defined as the maximum slope of the conversion vs reaction time plot. <sup>b</sup>Determined by  $^1\text{H}$  NMR. <sup>c</sup>Determined by GPC-MALS. <sup>d</sup> $I^* = M_{\text{th}}/M_n$ ,  $M_{\text{th}} = 200M_{\text{Mon}} \times \text{conversion} + M_{\text{end group}}$ .

is attributed to the absence of an acidic  $\alpha\text{-CH}$ , as  $\text{Cp}_2\text{YbMe}$  was found to yield a rather inefficient initiation by deprotonation for vinylphosphonate REM-GTP.<sup>29</sup> The obtained PIPOx was characterized by  $^1\text{H}$  NMR (Figure 2). After REM-GTP, the IPOx vinylene proton signals (5.76 and 5.39 ppm) disappear completely, and new peaks at 1.76–2.13 ppm originating from protons of formed methylene groups arise. The 2-oxazoline ring was well preserved after polymerization, as can be seen from  $^1\text{H}$  NMR, with chemical shifts of the oxazoline ring protons slightly shifted from 3.92 and 4.26 ppm to 3.76 and 4.16 ppm, respectively.  $^1\text{H}$  and  $^{13}\text{C}$  NMR spectroscopic analysis (Figure

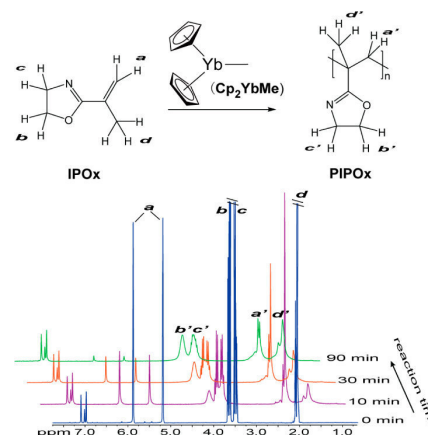


**Figure 2.** Reaction scheme for GTP of IPOx and polymerization kinetics as detected by *in situ*  $^1\text{H}$  NMR and assignment of corresponding signals.

S2) indicates the produced PIPOx to be atactic ( $[\text{mr}] = 35\%$ ), which can be attributed to the rather small steric demand of the Cp ligands, which is insufficient to induce a stereospecific polymerization.

To elucidate the underlying initiation process, oligomers were produced by using an IPOx: $\text{Cp}_2\text{YbMe}$  ratio of 5:1 in toluene and subsequently analyzed by electrospray ionization mass spectrometry (ESI-MS). For all peaks, the molar mass of the corresponding oligomers was found to be  $n \times M_{\text{IPOx}} + 17$  or  $n \times M_{\text{IPOx}} + 39$  g/mol (see Figure 4b and Table S1). The remaining 17 or 39 g/mol corresponds to a methyl group, which initiated chain growth, a  $\text{H}^+$  (or  $\text{Na}^+$ ), and a proton from the termination reaction during methanolic workup. Therefore, transfer of a coordinated ligand ( $\text{CH}_3$ ) to a monomer in the initial step is evident. According to MMA, REM-GTP of IPOx is believed to proceed via an eight-membered ring chelate as shown in Figure 3a, with chain growth occurring by conjugate addition of a coordinated monomer to the covalently bound chain end.<sup>4,11</sup> Attempts to isolate IPOx adducts or the eight-membered intermediate by mixing IPOx and  $\text{Cp}_2\text{YbMe}$  in 1:1 and 2:1

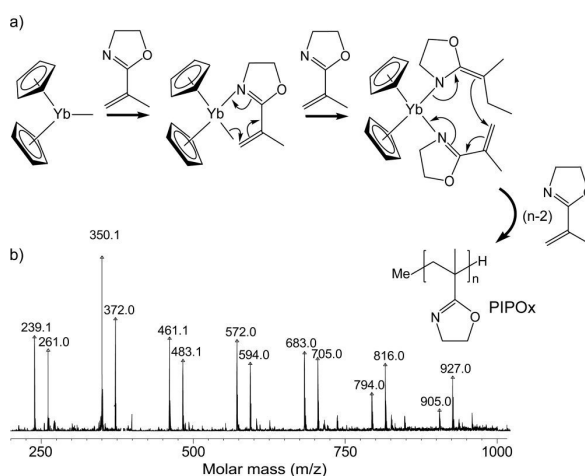


**Figure 3.** (a) Schematic illustration of REM-GTP of IPOx concerning initiation and propagation. (b) Structure of 2-isopropenyl-2-oxazoline oligomer and its ESI-MS spectrum.

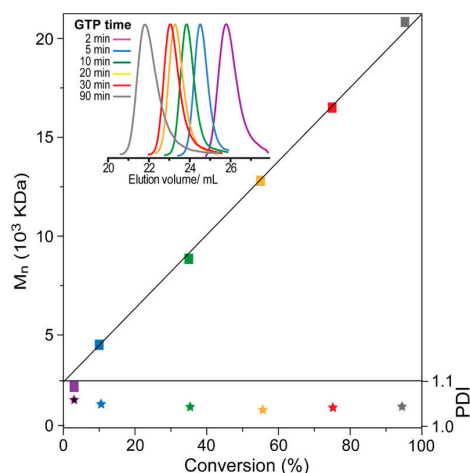


**Figure 4.** Linear growth of the absolute molecular weight ( $M_n$ ) determined by multi-angle laser light scattering as a function of IPOx conversion (determined by  $^1\text{H}$  NMR). Inset: GPC traces as detected by retention volume.

molar ratios at room temperature and  $-35\text{ }^\circ\text{C}$  were unsuccessful, consistently yielding oligomeric PIPOx. However, according to previous literature on rare earth metal oxazoline complexes<sup>30,31</sup> and rare earth metal-mediated 2VP polymerization,<sup>13</sup> we presume the coordination of the eight-membered intermediate as well as the monomer to proceed via the N atom of the oxazoline moiety, thus providing one of the first examples of REM-GTP to proceed via N coordination at the metal center.

To further examine the character of the established REM-GTP of IPOx, aliquots were taken at regular time intervals during the polymerization and analyzed by gel permeation chromatography multi-angle light scattering (GPC-MALS) to estimate the absolute number-averaged molar mass ( $M_n$ ) and the polydispersity index (PDI) of PIPOx. A plot of the  $M_n$  (from  $2.05 \times 10^3$  to  $2.10 \times 10^4$  g/mol) vs monomer (IPOx) conversion (from 2.1% to 95%, respectively) reveals a linear relationship between these two parameters (Figure 4), whereas the PDI remains extremely narrow (PDI < 1.07) for polymers obtained at all conversions. The linear growth of molecular weight against monomer conversion is ascribed to the highly living character of REM-GTP and the observed high initiator efficiency ( $I^* = 95\%$ ).

In order to demonstrate the superiority of REM-GTP in comparison to other polymerization techniques, the polymerization of IPOx initiated by azobisisobutyronitrile (AIBN) and *n*-butyllithium (BuLi) at different temperatures was investigated. As expected, free radical polymerization of IPOx performed at  $60\text{ }^\circ\text{C}$  afforded PIPOx with broad polydispersity (PDI = 2.0, conversion = 59%). Living anionic polymerization of IPOx at  $-78\text{ }^\circ\text{C}$  for 2 h yielded a polymer with improved molar mass distribution (PDI = 1.2) but slow polymer chain growth rate ( $M_n = 2.5$  kDa after 2 h polymerization, conversion = 18%). Anionic polymerization of IPOx at room temperature largely increased the polymerization velocity, however, at the cost of side reactions and loss of control. As a result, the PDI of the obtained polymer increased significantly (PDI = 1.5). The polymerization results for different methods and the used reaction conditions are summarized in Table 1.

In order to verify the versatility of REM-GTP for other monomers, which coordinate to the metal center via an N atom, we subjected another structural similar monomer, i.e. 2VP, to the

REM-GTP reaction conditions. To our delight, the GTP of 2VP occurred and afforded poly(2-vinylpyridine) (P2VP, 43 kDa) in 24 h at room temperature. We found the activity and the initiator efficiency of 2VP REM-GTP to be much lower ( $\text{TOF} = 44\text{ h}^{-1}$ ,  $I^* = 45\%$ ) (Figure S4) than those for IPOx ( $\text{TOF} = 380\text{ h}^{-1}$ ,  $I^* = 95\%$ ) (Figure S1), which may be attributed to the electron delocalization and thus the weak N–Yb coordination. Nevertheless, the PDI of obtained P2VP was narrow (PDI = 1.1) at all monomer conversions (Figure S6). Hence, we attribute the low initiator efficiency to an initial catalyst deactivation by impurities. It was recently shown by Mashima et al. that end-functionalized P2VP could be efficiently obtained by yttrium complex-catalyzed polymerization.<sup>13</sup> Albeit our simple yttrium complex exhibits relatively lower activity in the polymerization of 2VP, the catalyst led to high molar mass P2VP. Therefore, further investigation on the optimization of the catalyst is necessary. It is worth mentioning that ESI-MS investigation of oligomeric P2VP indicates the initiation to occur via a methyl transfer (Figure S5), even though an  $\alpha\text{-CH}$  is present in 2VP. According to the small steric demand of the Cp ligands, as expected, produced P2VP is atactic as indicated from  $^1\text{H}$  and  $^{13}\text{C}$  NMR analysis (Figure S3).

In REM-GTP copolymerizations, the addition sequence of the comonomers is critical for monomers with different coordination strength to the metal center; i.e., monomers can only be polymerized in order of increasing coordination strength.<sup>6,11,32</sup> In order to examine the relative coordination strength of the newly employed N-coordinating monomers IPOx and 2VP, statistical copolymerizations using DEVP, MMA, IPOx, and 2VP were conducted. Consistently, only the corresponding homopolymers of the stronger coordinating comonomer were obtained, as observed via NMR spectroscopy, revealing a monomer coordination strength to the yttrium center in an order of DEVP > MMA > IPOx > 2VP. Accordingly, sequential copolymerization yielded diblock copolymers in sequences of PMMA-*b*-PDEVP, PIPOx-*b*-PMMA, and PIPOx-*b*-PDEVP, as well as P2VP-*b*-PIPOx and P2VP-*b*-PDEVP, while diblock copolymerization in the reverse sequence only afforded homopolymers of PDEVP, PMMA, and PIPOx, respectively (Table S1). However, diblock copolymer synthesis was found to be hindered by a proposed encapsulation of the catalyst during polymerization of the rather hydrophilic IPOx and 2VP. This hypothesis is underlined by precipitation of formed high-molecular-weight PIPOx and P2VP from toluene solution and by ineffective initiation of a second, more hydrophobic comonomer (e.g., MMA) by the PIPOx or P2VP macroinitiator. Moreover, if the degree of polymerization of the first, hydrophilic block is kept low (below 20), an improvement of the PIPOx macroinitiator efficiency could be observed. Chain termination is not a major limitation, as the formation of block copolymers for the more hydrophilic DEVP as second comonomer was feasible (Table S1). Analysis of the molecular weight of the obtained copolymers was complicated due to aggregation, even at the low applied concentration in the GPC-MALS setup (and was verified via analysis of samples with different concentration). A more detailed study on REM-GTP copolymerizations is currently underway.

Some of us have reported previously on the synthesis of molecular brushes with poly(2-oxazoline) side chains and a PIPOx backbone via a *grafting-from* method using LCROP.<sup>25</sup> Since the backbone was prepared by free radical and anionic polymerization, the resulting molecular brushes were of broad molecular mass distribution. Herein, we use REM-GTP-prepared PIPOx as the backbone polymer. After reaction with

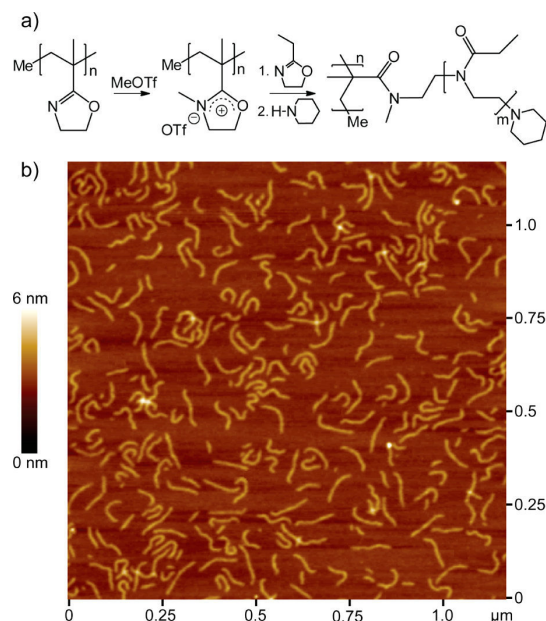


**Figure 5.** AFM scan of the molecular brush P(IPOx-g-EtOx). The polymer was deposited by dip-coating from a dilute chloroform solution onto freshly cleaved mica substrates.

methyl triflate, a polyoxazolium salt is formed as a macro-initiator. Then, molecular brush side chains are formed by LCROP of 2-ethyl-2-oxazoline (EtOx) (Figure 5a). As verified by AFM measurements, all the molecular brushes adopt a stretched conformation due to the repulsion of poly(2-oxazoline) side chains (Figure 5b). Moreover, the contour length distribution is remarkably narrow, which corroborates the narrow molecular mass distribution of the PIPOx backbone. The combination of REM-GTP and LCROP is to our knowledge the first example for the synthesis of well-defined poly(2-oxazoline) molecular brushes with narrow side and backbone chain length distribution.

In conclusion, we have demonstrated an efficient method to prepare poly(2-isopropenyl-2-oxazoline) and poly(2-vinylpyridine) with high molecular weight and very narrow molecular-weight distribution via rare earth metal-mediated GTP. The present study is one of the first examples for REM-GTP to proceed via N-rare earth metal coordination. According to the highly living character of REM-GTP, the molecular weight of PIPOx and P2VP increased linearly with monomer conversion. We established a monomer reactivity order for REM-GTP as DEVP > MMA > IPOx > 2VP, which can be ascribed to the coordination strength of the respective monomers at the rare earth metal center. Consecutive polymerization of different monomers is hereby only possible in order of increasing coordination strength, and restricted to comonomers with similar polarity. Moreover, well-defined molecular brushes could be synthesized via the first combination of REM-GTP of IPOx and successive *grafting-from* LCROP of 2-oxazolines.

## ■ ASSOCIATED CONTENT

### Supporting Information

Detailed procedures and NMR spectra. This material is available free of charge via the Internet at <http://pubs.acs.org>.

## ■ AUTHOR INFORMATION

### Corresponding Author

ning.zhang@ciac.jl.cn; rieger@tum.de

### Notes

The authors declare no competing financial interest.

## ■ ACKNOWLEDGMENTS

N.Z. acknowledges start-up funding from Changchun Institute of Applied Chemistry, Chinese Academy of Sciences, and the National Natural Science Foundation of China. S.S. is grateful for a generous scholarship from the Fonds der Chemischen Industrie.

## ■ REFERENCES

- (1) Yasuda, H.; Yamamoto, H.; Yokota, K.; Miyake, S.; Nakamura, A. *J. Am. Chem. Soc.* **1992**, *114*, 4908.
- (2) Yasuda, H.; Ihara, E. *Adv. Polym. Sci.* **1997**, *133*, 53.
- (3) Yasuda, H. *Prog. Polym. Sci.* **2000**, *25*, 573.
- (4) Chen, E. Y. X. *Chem. Rev.* **2009**, *109*, 5157.
- (5) Webster, O. W. *Adv. Polym. Sci.* **2004**, *167*, 1.
- (6) Seemann, U. B.; Dengler, J. E.; Rieger, B. *Angew. Chem., Int. Ed.* **2010**, *49*, 3489.
- (7) Salzinger, S.; Seemann, U. B.; Plikhta, A.; Rieger, B. *Macromolecules* **2011**, *44*, 5920.
- (8) Zhang, N.; Salzinger, S.; Rieger, B. *Macromolecules* **2012**, *45*, 9751.
- (9) Yasuda, H.; Tamai, H. *Prog. Polym. Sci.* **1993**, *18*, 1097.
- (10) Boffa, L. S.; Novak, B. M. *Chem. Rev.* **2000**, *100*, 1479.
- (11) Salzinger, S.; Rieger, B. *Macromol. Rapid Commun.* **2012**, *33*, 1327.
- (12) Yasuda, H. *J. Polym. Sci., Part A: Polym. Chem.* **2001**, *39*, 1955.
- (13) Kaneko, H.; Nagae, H.; Tsurugi, H.; Mashima, K. *J. Am. Chem. Soc.* **2011**, *133*, 19626.
- (14) Rabe, G. W.; Komber, H.; Haeussler, L.; Kreger, K.; Lattermann, G. *Macromolecules* **2010**, *43*, 1178.
- (15) Zhang, N.; Salzinger, S.; Deubel, F.; Jordan, R.; Rieger, B. *J. Am. Chem. Soc.* **2012**, *134*, 7333.
- (16) Tomalia, D. A.; Thill, B. P.; Fazio, M. J. *Polym. J.* **1980**, *12*, 661.
- (17) Hoogenboom, R. *Angew. Chem., Int. Ed.* **2009**, *48*, 7978.
- (18) Schlaad, H.; Diehl, C.; Gress, A.; Meyer, M.; Demirel, A. L.; Nur, Y.; Bertin, A. *Macromol. Rapid Commun.* **2010**, *31*, 511.
- (19) Luxenhofer, R.; Schulz, A.; Roques, C.; Li, S.; Bronich, T. K.; Batrakova, E. V.; Jordan, R.; Kabanov, A. V. *Biomaterials* **2010**, *31*, 4972.
- (20) Adams, N.; Schubert, U. S. *Adv. Drug Delivery Rev.* **2007**, *59*, 1504.
- (21) Viegas, T. X.; Bentley, M. D.; Harris, J. M.; Fang, Z.; Yoon, K.; Dizman, B.; Weimer, R.; Mero, A.; Pasut, G.; Veronese, F. M. *Bioconjugate Chem.* **2011**, *22*, 976.
- (22) Knop, K.; Hoogenboom, R.; Fischer, D.; Schubert, U. S. *Angew. Chem., Int. Ed.* **2010**, *49*, 6288.
- (23) Luxenhofer, R.; Sahay, G.; Schulz, A.; Alakhova, D.; Bronich, T. K.; Jordan, R.; Kabanov, A. V. *J. Controlled Release* **2011**, *153*, 73.
- (24) Barz, M.; Luxenhofer, R.; Zentel, R.; Vicent, M. J. *Polym. Chem.* **2011**, *2*, 1900.
- (25) Zhang, N.; Huber, S.; Schulz, A.; Luxenhofer, R.; Jordan, R. *Macromolecules* **2009**, *42*, 2215.
- (26) Kagiya, T.; Matsuda, T.; Zushi, K. *J. Macromol. Sci., Chem.* **1972**, *A6*, 1349.
- (27) Weber, C.; Neuwirth, T.; Kempe, K.; Ozkahraman, B.; Tamahkar, E.; Mert, H.; Becer, C. R.; Schubert, U. S. *Macromolecules* **2012**, *45*, 20.
- (28) Odian, G. *Principles of Polymerization*, 4th ed.; John Wiley & Sons, Inc.: New York, 2004.
- (29) Salzinger, S.; Soller, B. S.; Plikhta, A.; Seemann, U. B.; Herdtweck, E.; Rieger, B. *J. Am. Chem. Soc.*, submitted.
- (30) Ward, B. D.; Bellemin-Lapponnaz, S.; Gade, L. H. *Angew. Chem., Int. Ed.* **2005**, *44*, 1668.
- (31) Lukešová, L.; Ward, B. D.; Bellemin-Lapponnaz, S.; Wadepohl, H.; Gade, L. H. *Organometallics* **2007**, *26*, 4652.
- (32) Mariott, W. R.; Chen, E. Y. X. *Macromolecules* **2005**, *38*, 6822.

Reprinted with Permission from Zhang, N.; Salzinger, S.; Soller, B. S.; Rieger, B. *J. Am. Chem. Soc.*, Article ASAP. Copyright 2013 American Chemical Society.

***Supporting Information***

**Rare Earth Metal-Mediated Group Transfer Polymerization:  
From Defined Polymer Microstructures to  
High Precision Nano-Scaled Objects**

Ning Zhang,\* Stephan Salzinger, Benedikt S. Soller, and Bernhard Rieger\*

*Changchun Institute of Applied Chemistry, Chinese Academy of Sciences, Changchun,  
130022, China*

*WACKER-Lehrstuhl für Makromolekulare Chemie, Technische Universität München,  
Lichtenbergstrasse 4, 85747 Garching bei München, Germany*

## Materials and methods

Chemicals were purchased from Sigma-Aldrich or Acros Organics and used without further treatment if not otherwise stated. All reactions were carried out under argon atmosphere using standard Schlenk techniques or an *MBraun* glovebox. All glassware was heat-dried under vacuum prior to use. Toluene was dried applying an *MBraun* SPS-800 and used as received. Tetrahydrofuran (THF) was distilled over potassium prior to use.  $\text{Cp}_2\text{YbMe}$ , diethyl vinylphosphonate were prepared according to literature.<sup>1,2,3,4</sup> Monomers were dried over calcium hydride and distilled prior to polymerization.

NMR spectra were recorded on a *Bruker* ARX-300 spectrometer.  $^1\text{H}$  NMR spectroscopic chemical shifts  $\delta$  are reported in ppm relative to tetramethylsilane and calibrated to the residual proton signal of the deuterated solvent. Deuterated solvents were obtained from Deutero Deutschland GmbH and used as received. ESI MS analytical measurements were performed with methanol solutions on a Varian 500-MS spectrometer, using 70 keV in the positive ionization mode. Atomic force microscopy (AFM) scans were obtained with a Nanoscope IIIa scanning probe microscope from Veeco Instruments (Mannheim, Germany). The microscope was operated in tapping mode using Si cantilevers with a resonance frequency of 270 kHz, a driving amplitude of 1.52 V at a scan rate of 0.6 Hz.

## Oligomerization

5 eq of the monomer were added to 1 eq of catalyst in toluene. The resulting mixture was stirred for 2 hours at room temperature and quenched by addition of MeOH or acidified (37w%  $\text{HCl}_{\text{aq}}$ ) MeOH. Volatiles were removed under reduced pressure and the residue was extracted with MeOH. For end group analysis, ESI MS measurements of the methanolic extract were performed.

## Homo- and statistical copolymerizations

Polymerizations were performed in 30 mL of toluene, using a catalyst concentration of  $0.33 \text{ mg mL}^{-1}$  (10 mg of catalyst). After dissolving the catalyst in the solvent at room temperature, the calculated amount of the monomer (mixture) was added. The reaction was stirred for the stated reaction time and then quenched with MeOH (0.5

mL). The polymer was precipitated by addition of the reaction mixture to hexane (150 mL) and decanted from solution. Residual solvents were removed by drying the polymer under vacuum at 70 °C overnight.

### **Sequential copolymerization**

After dissolving the calculated amount of catalyst in toluene at room temperature, the first monomer was added (monomer concentration 10vol% in toluene). The reaction mixture was stirred for 2 hours (4 hours in case of 2VP) and divided into aliquots. One aliquot was quenched by addition of 0.5 mL MeOH, to each of the other aliquots, the calculated amount of a second monomer was added, the reaction mixtures stirred for another 2 hours at room temperature and quenched by addition of 0.5 mL MeOH. The polymers were precipitated by addition of the reaction mixtures to hexane (150 mL) and decanted from solution. Residual solvents were removed by drying the polymers under vacuum at 70 °C overnight.

### **Molecular weight determination**

GPC was carried out on a Varian LC-920 equipped with two PL Polargel columns. As eluent a mixture of 50% THF, 50% water, and 9 g L<sup>-1</sup> tetrabutylammonium bromide (TBAB) was used in the case of PDEVp, PIPOx, P2VP, P(IPOx-b-DEVp) and P(2VP-b-DEVp); for PMMA, P(MMA-b-DEVp) and P(IPOx-b-MMA) analysis, the eluent was THF with 6 g L<sup>-1</sup> TBAB. Absolute molecular weights have been determined online by multiangle light scattering (MALS) analysis using a Wyatt Dawn Heleos II in combination with a Wyatt Optilab rEX as concentration source.

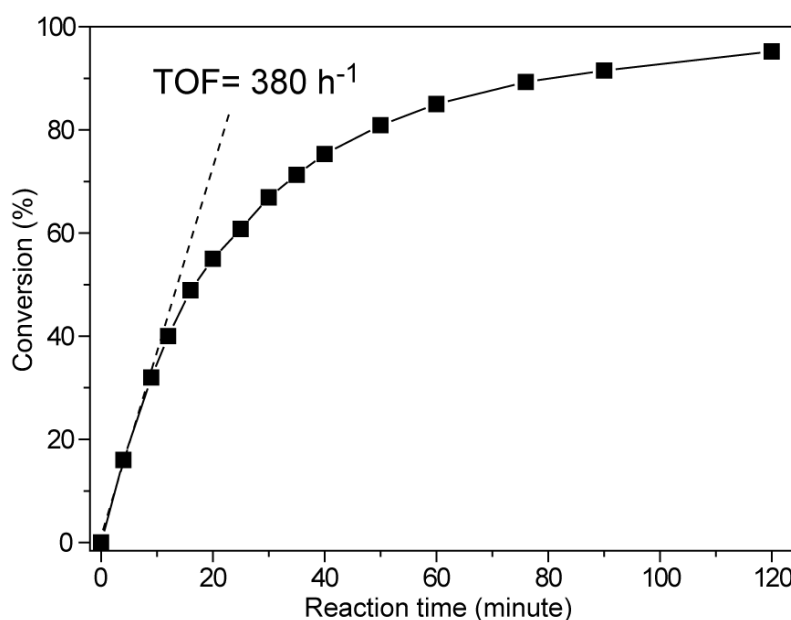
### **Kinetics by *in-situ* <sup>1</sup>H NMR spectroscopy**

*In-situ* NMR measurements were conducted in a sealable NMR tube in toluene-d<sub>8</sub> or C<sub>6</sub>D<sub>6</sub>. After mixing a solution of 1 mg Cp<sub>2</sub>YbMe, 3 mL deuterated solvent and the calculated amount of monomer, 0.6 mL of the reaction solution was immediately transferred to an NMR tube. The NMR spectroscopic measurements were conducted at room temperature.

### Kinetics by aliquots method

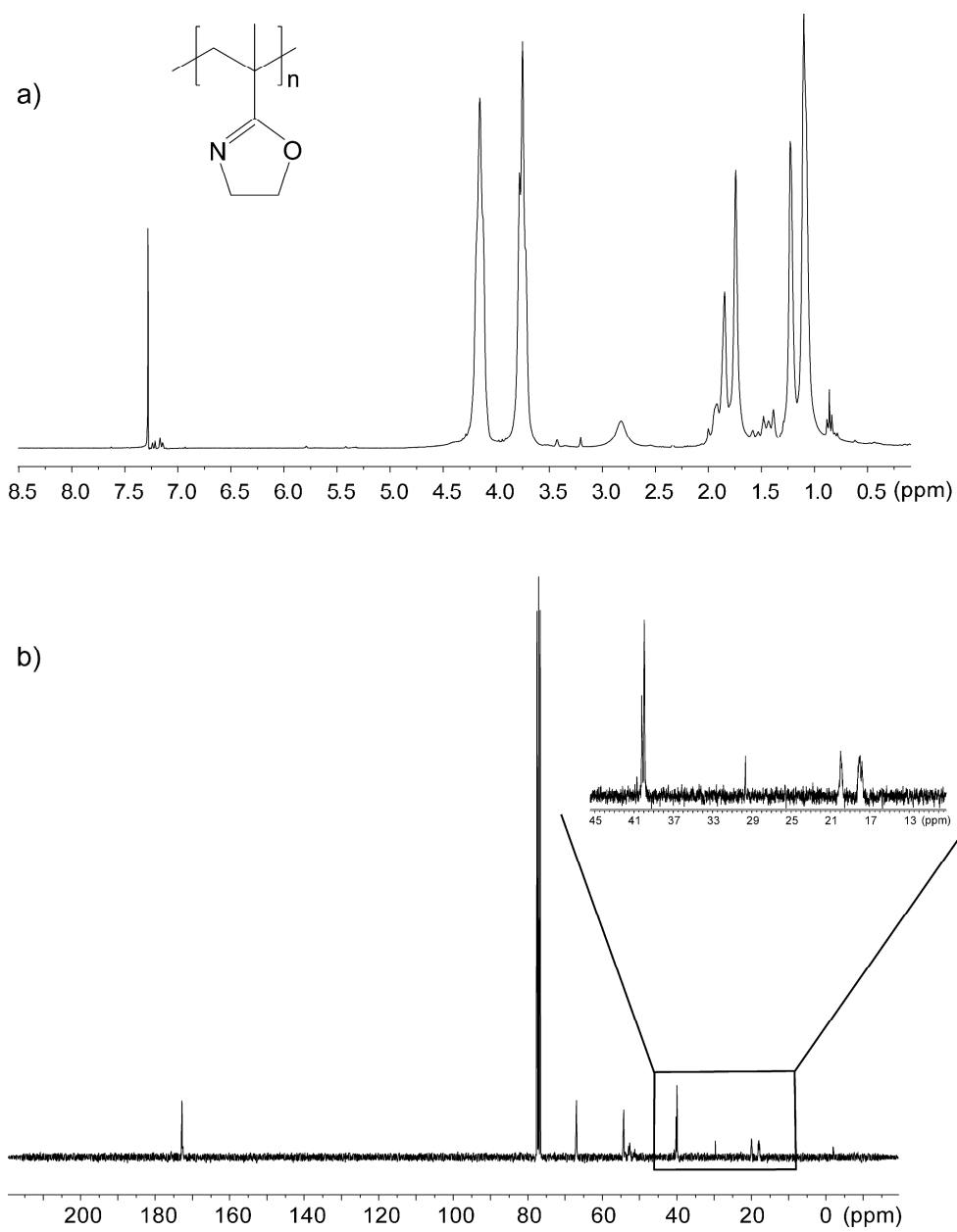
After dissolving 10 mg of  $\text{Cp}_2\text{YbMe}$  in 30mL toluene or toluene- $d_8$  at room temperature, the calculated amount of monomer was added in one injection. Aliquots were taken from the reaction solution at regular time intervals and quenched by addition to (deuterated) MeOH. For each aliquot, the conversion is determined by gravimetry or  $^1\text{H}$  NMR spectroscopy, the molecular weight of the formed polymer by GPC-MALS analysis.

### Reactivity, $^1\text{H}$ NMR, $^{13}\text{C}$ NMR, ESI MS and GPC spectra

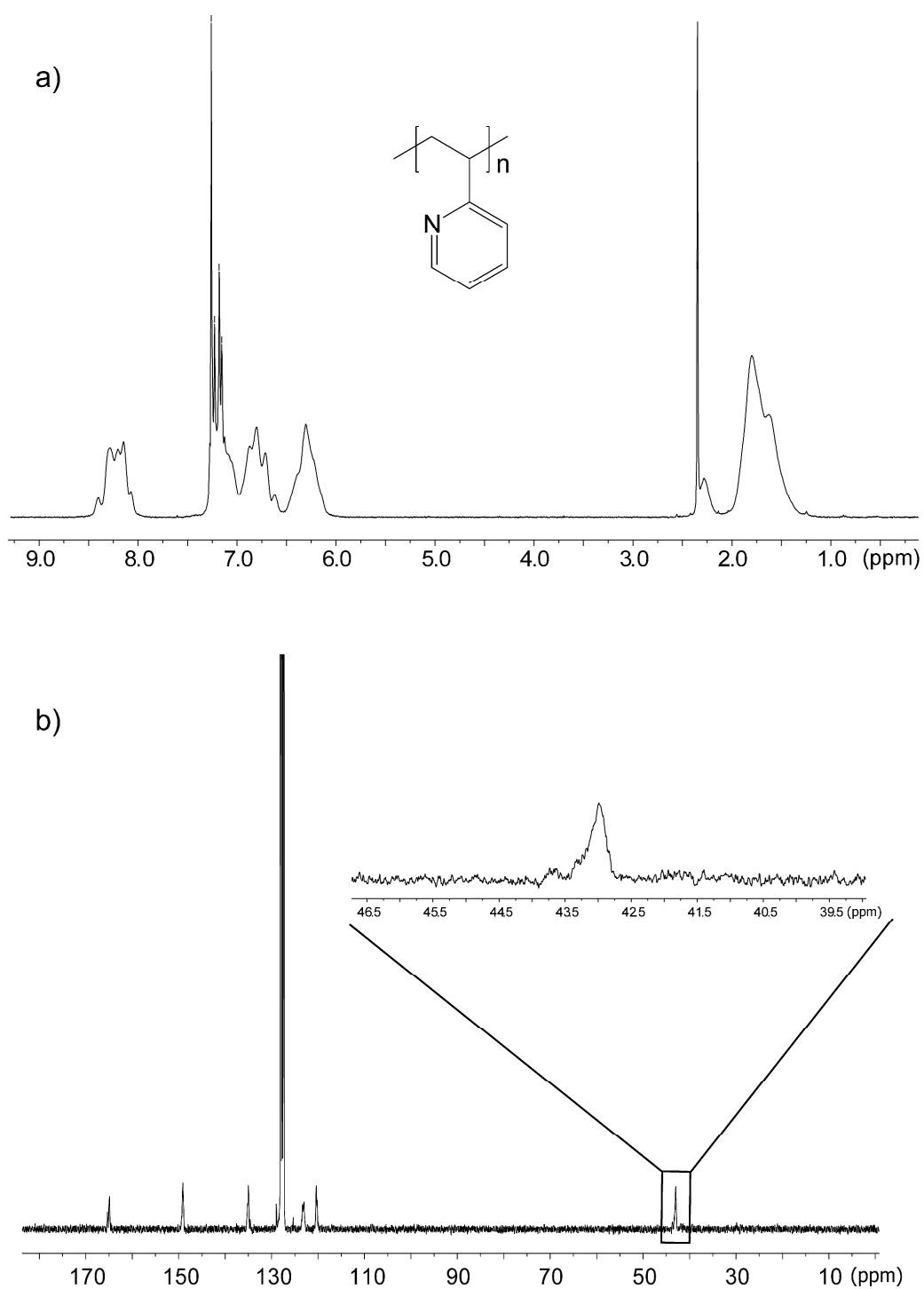


**Figure S1.** Determination of the catalytic activity of  $\text{Cp}_2\text{YbMe}$  for the polymerization of IPOx ( $\text{TOF} = 380 \text{ h}^{-1}$ ) by *in situ*  $^1\text{H}$  NMR spectroscopy (initial  $[\text{IPOx}]:[\text{catalyst}] = 200:1$ ;  $[\text{catalyst}] = 0.33 \text{ mg mL}^{-1}$ ).





**Figure S2.**  $^1\text{H}$  a) and  $^{13}\text{C}$  b) NMR spectra of PIPOx.



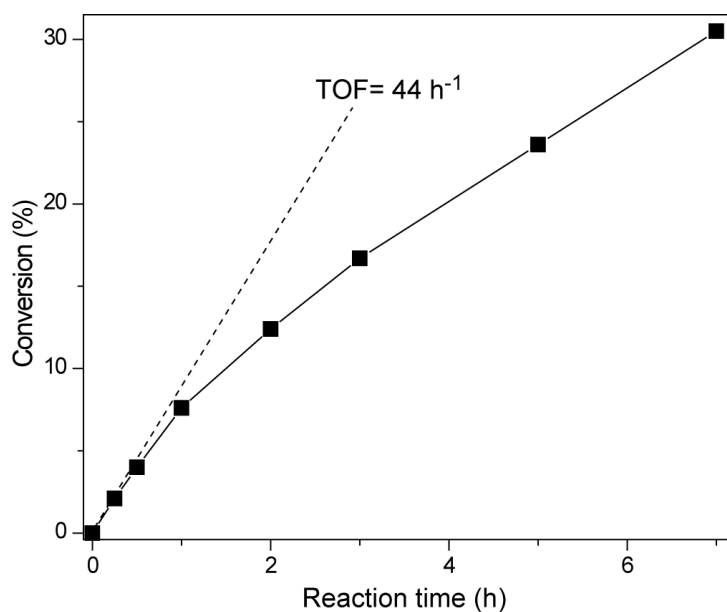


**Figure S4.** Determination of the catalytic activity of  $\text{Cp}_2\text{YbMe}$  for the polymerization of 2VP ( $\text{TOF} = 44 \text{ h}^{-1}$ ) by *in situ*  $^1\text{H}$  NMR spectroscopy (initial  $[\text{2VP}]:[\text{catalyst}] = 500:1$ ;  $[\text{catalyst}] = 0.33 \text{ mg mL}^{-1}$ ).

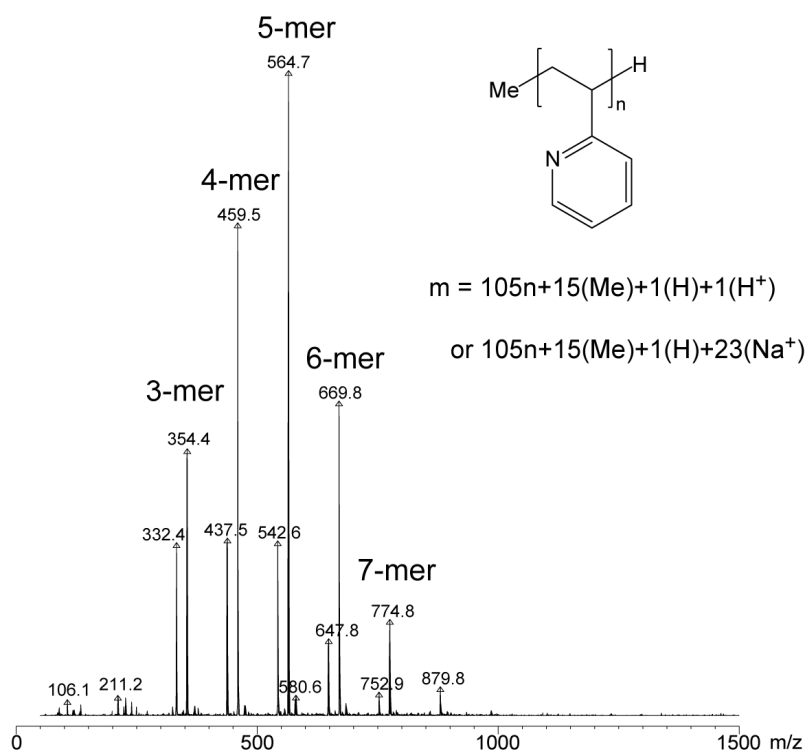


**Figure S5.** Structure of poly(2-vinylpyridine) (P2VP) oligomer and its ESI MS spectrum.

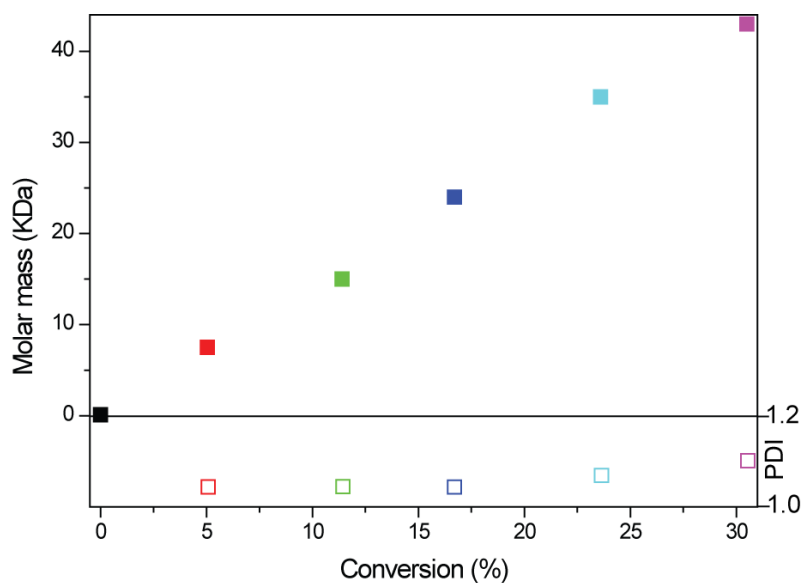


**Figure S6.** Linear growth of the absolute molecular weight ( $M_n$ ) and polydispersity of P2VP determined by multi-angle laser light scattering as a function of 2VP conversion.

**Table S1.** Homo- and block copolymers of 2VP, IPO<sub>x</sub>, MMA and DEVP synthesized by Cp<sub>2</sub>YbMe-initiated REM-GTP.

	$M_n^a$ (kDa)	PDI <sup>a</sup>	$I^{*b}$ (%)	Comonomer ratio A/B <sup>c</sup>	Yield <sup>d</sup> (%)
P2VP <sub>100</sub>	14	1.01	75	—	96
P(2VP <sub>100</sub> -b-IPO <sub>x100</sub> )	29 (14)	1.01 (1.01)	74 (82)	1:1.18	98
P(2VP <sub>100</sub> -b-MMA <sub>100</sub> )	14	1.01	—	1:0	46
P(2VP <sub>100</sub> -b-DEVP <sub>100</sub> )	31	1.04	87	1:1.07	96
P(2VP <sub>20</sub> -b-MMA <sub>80</sub> )	—	—	—	1:0	—
PIPO <sub>x100</sub>	9.1	1.03	120	—	89
P(IPO <sub>x100</sub> -b-MMA <sub>100</sub> )	9.2	1.02	—	1:0	44
P(IPO <sub>x100</sub> -b-DEVP <sub>100</sub> )	1100 (10)	1.40 (1.03)	3 (~1)	1:0.69	62
P(IPO <sub>x20</sub> -b-MMA <sub>80</sub> )	aggregation	—	—	1:1.69	50
P(IPO <sub>x20</sub> -b-DEVP <sub>50</sub> )	390 (2.6)	1.70 (1.12)	3 (2)	1:2.71	62
PMMA <sub>100</sub>	12	1.10	83	—	98
P(MMA <sub>100</sub> -b-DEVP <sub>100</sub> )	22	1.20	120	1.15:1	94

<sup>a</sup>Determined by GPC-MALS, <sup>b</sup> $I^* = M_{th}/M_n$ , number in brackets give the  $I^*$  of the macroinitiator for polymerization of block B (in case of bimodal distributions), <sup>c</sup>determined by <sup>1</sup>H NMR, <sup>d</sup>determined by weighing of the components.

**References**

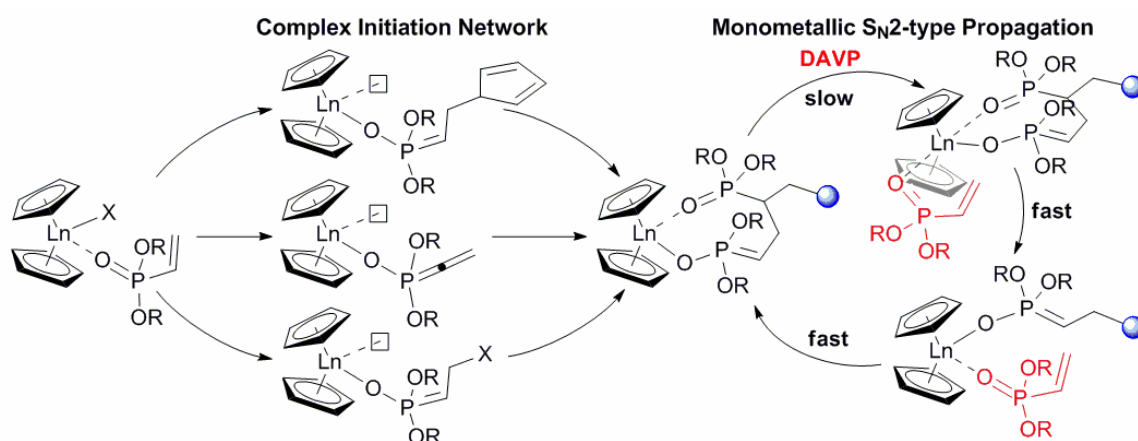
---

- (1) Seemann, U. B.; Dengler, J. E.; Rieger, B. *Angew. Chem. Int. Ed.* **2010**, *49*, 3489-3491.
- (2) Evans, W. J.; Dominguez, R.; Hanusa, T. P. *Organometallics* **1986**, *5*, 263-270.
- (3) Ely, N. M.; Tsutsui, M. *Inorg. Chem.* **1975**, *14*, 2680-2687.
- (4) Leute, M. PhD Thesis, University of Ulm, **2007**.



## CHAPTER 9:

# MECHANISTIC STUDIES ON INITIATION AND PROPAGATION OF RARE EARTH METAL-MEDIATED GROUP TRANSFER POLYMERIZATION OF VINYLPHOSPHONATES



*“We know accurately only when we know little, doubt grows with knowledge.”*

- Johann Wolfgang von Goethe (1749-1832)





**Status:** submitted  
**Journal:** Journal of the American Chemical Society  
**Publisher:** ACS Publications  
**Article type:** Article  
**DOI:** –  
**Authors:** Stephan Salzinger, Benedikt S. Soller, Andriy Plikhta,  
Uwe B. Seemann, Eberhardt Herdtweck, Bernhard Rieger

**Content:**

In this chapter, the first detailed mechanistic studies on both initiation and propagation of rare earth metal-mediated GTP of vinylphosphonates are presented. Isolated DEVP adducts  $\text{Cp}_2\text{LnCl}(\text{DEVP})$  provide first X-ray crystallographic proof for vinylphosphonate coordination at the active site *via* the oxygen of the phosphonate moiety. The reactive  $\alpha$ -CH and the use of unbridged rare earth metallocenes lead to a complex initiation network for vinylphosphonate GTP. Depending on the nature of the initiating ligand, initiation can either proceed *via* abstraction of the acidic  $\alpha$ -CH of the vinylphosphonate, *via* transfer of a nucleophilic ligand to a coordinated monomer or *via* a monomer- (*i.e.* donor-) induced ligand exchange reaction forming  $\text{Cp}_3\text{Ln}$  in equilibrium. Time-resolved analysis of monomer conversion and molecular weights of the formed polymers allows the determination of the initiator efficiency throughout the whole reaction. Using this normalization method, rare earth metal-mediated GTP was shown to follow a monometallic Yasuda-type polymerization mechanism, with an  $\text{S}_{\text{N}}2$ -type associative displacement of the polymer phosphonate ester by a monomer as the rate determining step (RDS). The activation entropy  $\Delta S^\ddagger$  of the RDS is strongly affected by the metal radius and the monomer size, whereas these parameters show only minor influence on the activation enthalpy  $\Delta H^\ddagger$ . Accordingly, the propagation rate of vinylphosphonate REM-GTP is shown to be mainly determined by the change of rotational and vibrational restrictions within the eight-membered metallacycle in the RDS



# Mechanistic Studies on Initiation and Propagation of Rare Earth Metal-Mediated Group Transfer Polymerization of Vinylphosphonates

Stephan Salzinger, Benedikt S. Soller, Andriy Plikhta, Uwe B. Seemann, Eberhardt Herdtweck, Bernhard Rieger\*

WACKER-Lehrstuhl für Makromolekulare Chemie, Technische Universität München, Lichtenbergstraße 4, 85748 Garching b. München

*Catalysis, Coordinative polymerization, Group Transfer Polymerization, Poly(vinylphosphonate)s, Rare Earth Metals*

Supporting Information Placeholder

**ABSTRACT:** Initiation of rare earth metal-mediated vinylphosphonate polymerization with unbridged rare earth metallocenes ( $Cp_2LnX$ ) follows a complex reaction pathway. Depending on the nature of X, initiation can either proceed *via* abstraction of the acidic  $\alpha$ -CH of the vinylphosphonate (*e.g.* for X = Me,  $CH_2TMS$ ), *via* nucleophilic transfer of X to a coordinated monomer (*e.g.* for X = Cp, SR) or *via* a monomer- (*i.e.* donor-) induced ligand exchange reaction forming  $Cp_3Ln$  in equilibrium (*e.g.* for X = Cl, OR), which serves as the active initiating species. As determined by mass spectrometric end group analysis, different initiations may also occur simultaneously (*e.g.* for X =  $N(SiMe_2H)_2$ ). A general differential approach for the kinetic analysis of living polymerizations with fast propagation and comparatively slow initiation is presented. Time-resolved analysis of monomer conversion and molecular weights of the formed polymers allows the determination of the initiator efficiency throughout the whole reaction. Using this normalization method, rare earth metal-mediated vinylphosphonate GTP is shown to follow a Yasuda-type monometallic propagation mechanism, with an  $S_N2$ -type associative displacement of the polymer phosphonate ester by a monomer as the rate determining step. The propagation rate of vinylphosphonate GTP is mainly determined by the activation entropy, *i.e.* the change of rotational and vibrational restrictions within the eight-membered metallacycle in the rate determining step as a function of the steric demand of the metallacycle side chains and the steric crowding at the metal center.

## Introduction

Phosphorus-containing polymers, especially those comprising phosphonate moieties, have gained significant interest due to their potential utilization in a large variety of applications, ranging from polyelectrolytes in batteries and fuel cells over halogen-free flame retardants to diverse uses in the biomedical field.<sup>1-10</sup> However, a straight-forward approach to these polymers *via* polymerization of vinylphosphonates has long been hard to establish, as radical and classical anionic synthesis routes often result in low yields of polymer with unsatisfying degrees of polymerization.<sup>11</sup> Recently, it could be shown that poly(vinylphosphonate)s with high molar mass and low polydispersity can be efficiently prepared in the presence of rare earth metal catalysts,<sup>11-16</sup> presumably following a group transfer polymerization (GTP) mechanism.<sup>11</sup>

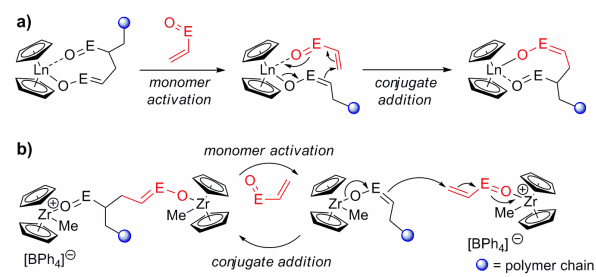
Rare earth metal-mediated GTP (REM-GTP) of acrylic monomers was first reported by Yasuda *et al.*<sup>17</sup> in 1992 and is also referred to as coordinative-anionic or coordination-addition polymerization.<sup>18</sup> Over the past decades, intensive research has been carried out to optimize the reaction conditions, the initiator efficiency and to broaden the use of coordinative-anionic polymerizations for a variety of monomers, *e.g.* different (meth)acrylates and (meth)acrylamides.<sup>18-21</sup> The initiation for this living-type polymerization commonly occurs *via* 1,4-addition of a nucleophilic ligand from the

metal complex to a coordinated monomer, or, in case of divalent lanthanide initiators, *via* redox initiation.<sup>18,22</sup> The propagation proceeds *via* repeated conjugate addition over an eight-membered ring intermediate (Scheme 1a),<sup>18-21,23</sup> which could be isolated and characterized by X-ray crystallography.<sup>17,23</sup> Hereby, the catalyst both stabilizes the anionic chain end and activates the coordinated monomer.<sup>11,18</sup> The coordination of the growing chain end at the catalyst suppresses side reactions and allows stereospecific polymerization as well as activity optimization by variation of both the metal center and the catalyst ligand sphere.<sup>18-21</sup> Besides this monometallic propagation, coordinative-anionic polymerizations may also follow a bimetallic mechanism, for which alternating one metal center activates the monomer while the other stabilizes the growing chain end (*e.g.* for group 4 metal-mediated GTP, Scheme 1b).<sup>24-28</sup>

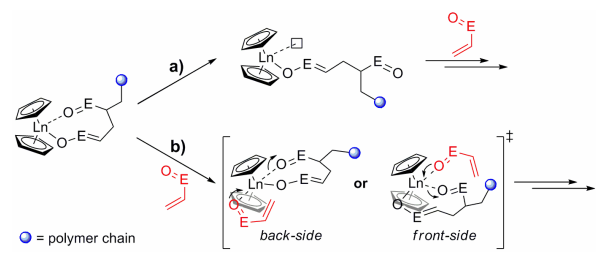
The mechanism taking place and the corresponding rate determining step (RDS) are difficult to predict and were found to be strongly dependent on the ligand architecture, the metal center and the used monomer.<sup>18,25-27,29-36</sup> The influence of mechanism and RDS on the stereoregularity of the polymerization and *vice versa* the mechanistic conclusions drawn from obtained microstructures have been controversially discussed.<sup>20,28-30,33,36-40</sup> Besides the actual conjugate addition, the RDS can be cleavage of the polymer ester

group from the metal center ( $S_N1$ -type reaction, Scheme 2a) or an associative displacement of this ester group by a monomer ( $S_N2$ -type reaction, Scheme 2b).<sup>20,25-30,36,37,40-42</sup> The latter is both described in a back-side manner or *via* an attack at the same site relative to the leaving polymer ester group (front-side), *i.e.* *via* a chain retention or a chain migratory mechanism.<sup>28-30,33,37-40,42</sup> In case of monometallic coordinative-anionic polymerization, depending on the evident RDS, the monomer addition will either occur alternating at both sites of the catalyst or predominantly at only one site *via* site-retention.<sup>29,30,33,36-40,42</sup>

**Scheme 1. Proposed monometallic (a) and bimetallic (b) propagation mechanism for coordinative-anionic polymerization of Michael acceptor-type monomers; E = C(OR), C(NR<sub>2</sub>), P(OR)<sub>2</sub>.**



**Scheme 2. Proposed  $S_N1$ -type (a) and  $S_N2$ -type (b) polymer ester cleavage from/monomer addition to the metal center for REM-GTP, E = C(OR), C(NR<sub>2</sub>), P(OR)<sub>2</sub>.**



Recent publications have shown that REM-GTP is not only applicable to common acrylic monomers, but as well to several other monomer classes, *i.e.* dialkyl vinylphosphonates (DAVP), 2-isopropylene-2-oxazoline and 2-vinylpyridine.<sup>11-16,43,44</sup> In previous work, we have shown that late lanthanide metallocenes are efficient initiators and highly active catalysts for DAVP polymerization.<sup>14,16</sup> Initial investigations have proven the livingness of polymerization and suggest a GTP mechanism taking place,<sup>11,12,14</sup> however, detailed mechanistic studies on both initiation and propagation of REM-GTP of vinylphosphonates have not yet been conducted.

In this article, we show that initiation of vinylphosphonate GTP follows a complex reaction network. We present a general procedure for kinetic analysis of living polymerizations with fast propagation and comparatively slow initiation. A detailed study of the influence of metal radii, steric demand of the monomers and reaction temperature on the polymerization rate gives insight into the mechanism of REM-GTP, both for vinylphosphonates in particular as well as for its general understanding.

## Results and Discussion

We previously reported on the use of *tris*(cyclopentadienyl) lanthanide complexes ( $Cp_3Ln$ ) for the polymerization of diethyl and diisopropyl vinylphosphonate (DEVp and DIVP, respectively).<sup>14</sup> Whereas the rate of initiation was found to be accelerated by both decreasing metal radius and increasing steric demand of the monomer, *i.e.* by higher steric crowding of the intermediate  $Cp_3Ln$ (DAVP), the propagation rate was enhanced by smaller metal radii and decreasing steric demand of the monomer, contradicting to previous work on (meth)acrylate rare earth metal-mediated GTP.<sup>18-20,23,45</sup> Within the frame of this previous work, we could not address the origin of this faster propagation for late lanthanides, *i.e.* for higher Lewis acidity and *higher* steric crowding of the active species, in combination with an increased activity for smaller monomers, *i.e.* *lower* steric crowding of the active species.

In earlier work, we applied *bis*(cyclopentadienyl) chloro, amide and methyl complexes ( $[Cp_2LnCl]_2$ ,  $Cp_2Ln(bdsa)(thf)$  and  $[Cp_2YbMe]_2$ , respectively; *bdsa* = *bis*(dimethylsilyl)amide,  $N(SiMe_2H)_2$ ) for vinylphosphonate polymerization.<sup>11,12,46</sup> For the chloro and amide catalysts, a distinct initiation period was evident. In accordance with their previous use for MMA polymerization, the observed initiator efficiencies were low, however, the activity is considerably higher for vinylphosphonate (Table 1) than for MMA polymerization (TOF = 7 h<sup>-1</sup>).<sup>18,47</sup> According to our study on  $Cp_3Ln$ -initiated vinylphosphonate GTP, the normalized activity TOF/ $T^{14}$  was found to be strongly accelerated for later lanthanides, *e.g.* for  $[Cp_2LnCl]_2$ /DEVp from 1100 h<sup>-1</sup> for Ho to 20500 h<sup>-1</sup> for Lu (Table 1, entry 1-6).<sup>14</sup> At the same time, contradicting the polymerization with  $Cp_3Ln$ , the initiator efficiency was either unaffected by the metal size (Table 1) or found to decrease for smaller metal centers (see Ref. 11), depending on concentration and polymerization temperature. Hereby, all  $Cp_3Ln$  and  $Cp_2LnX$  complexes yielded polymers with the same (essentially) atactic polymer microstructure (Figure 1), indicating the active catalytic species to consistently be a  $Cp_2Ln$ -unit. The normalized activity, however, was found to be strongly different for  $Cp_3Ln$  in comparison to  $[Cp_2LnCl]_2$ ,  $[Cp_2YbMe]_2$  and  $Cp_2Ln(bdsa)(thf)$  (Table 1). In order to explain the observed differences between  $Cp_2LnX$  and  $Cp_3Ln$  complexes and the differences to (meth)acrylate polymerizations, we conducted detailed analysis of both initiation and propagation of vinylphosphonate GTP.

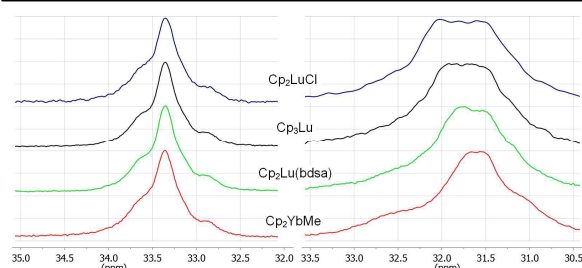


**Figure 1.** <sup>31</sup>P NMR spectra of PDEVp (left, in D<sub>2</sub>O) and PDIVP (right, in CDCl<sub>3</sub>) produced with different catalysts (from top to bottom:  $[Cp_2LuCl]_2$  (blue),  $Cp_3Lu$  (black),  $Cp_2Lu(bdsa)(thf)$  (green) and  $[Cp_2YbMe]_2$  (red)). For all catalysts, polymers with (nearly) identical atactic polymer microstructure are obtained.

**Table 1. DEVP polymerization results for previously applied Cp<sub>2</sub>LnX catalysts (toluene, 30 °C, monomer-to-catalyst ratio 600:1)**

Catalyst	Reaction time	Conversion <sup>a</sup> /%	Init. period <sup>b</sup>	M <sub>n</sub> <sup>c</sup> /kDa	P <sup>c</sup> /%	TOF <sup>a</sup> /P <sup>c</sup> /h <sup>-1</sup>	TOF/P <sup>c</sup> (Cp <sub>3</sub> Ln) <sup>d</sup> /h <sup>-1</sup>
[Cp <sub>2</sub> HoCl] <sub>2</sub>	24 h	76	180 min	810	9.6	1100	8000
[Cp <sub>2</sub> YCl] <sub>2</sub>	6 h	70	100 min	740	9.3	3700	23000
[Cp <sub>2</sub> ErCl] <sub>2</sub>	6 h	79	100 min	780	10.0	2800	28000
[Cp <sub>2</sub> TmCl] <sub>2</sub>	3.5 h	86	90 min	990	8.5	5900	72000
[Cp <sub>2</sub> YbCl] <sub>2</sub>	3 h	81	90 min	890	9.8	8400	185000
[Cp <sub>2</sub> LuCl] <sub>2</sub>	1.5 h	93	7 min	780	11.7	20500	>265000
Cp <sub>2</sub> Y(bdsa)(thf)	3 h	95	15 min	1040	9.0	7200	23000
Cp <sub>2</sub> Lu(bdsa)(thf)	3 h	96	20 min	1350	7.0	21000	>265000
[Cp <sub>2</sub> YbMe] <sub>2</sub>	30 min	99	80 sec	900	10.8	49000	185000

<sup>a</sup>Determined by <sup>31</sup>P NMR spectroscopic measurement, <sup>b</sup>Initiation period, reaction time until 3% conversion is reached, <sup>c</sup>Determined by GPC-MALS,  $P^c = M_{th}/M_n$ ,  $M_{th} = 600 \times M_{Mon} \times \text{conversion}$ , <sup>d</sup>normalized activity for corresponding Cp<sub>3</sub>Ln<sup>14</sup>.

### Initiation mechanism

ESI MS analysis of vinylphosphonate oligomers produced with [Cp<sub>2</sub>YbMe]<sub>2</sub> shows no apparent end group (Figure S1). As methanolic work-up leads to chain termination by a proton, the exclusive observation of signals with  $m/z = n \times M_{Mon} + M_{Na}$  is attributed to an initiation *via* deprotonation yielding CH<sub>2</sub> and an olefinic chain end. Similar to Cp<sub>3</sub>Ln, for [Cp<sub>2</sub>LnCl]<sub>2</sub>, initiation was found to proceed *via* transfer of a cyclopentadienyl ligand to a coordinated monomer (Figure S2, S3).<sup>14,48</sup> These results clearly show that, depending on the ligand's basicity and nucleophilicity, initiation can generally either proceed *via* deprotonation of the acidic α-CH of the vinylphosphonate or *via* nucleophilic transfer (Scheme 3). This is in line with previous observations on classical anionic vinylphosphonate polymerizations.<sup>11,49</sup>

### Scheme 3. Possible initiation reactions for rare earth metal-mediated vinylphosphonate polymerizations.

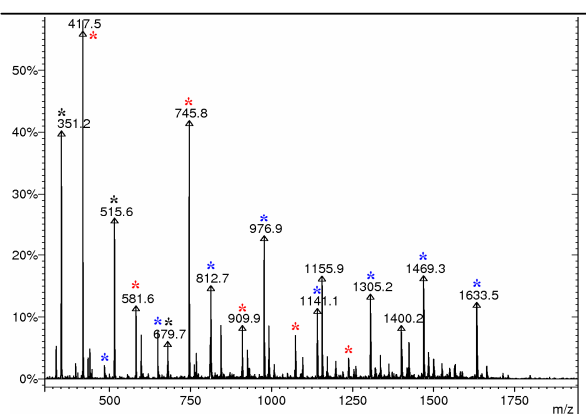
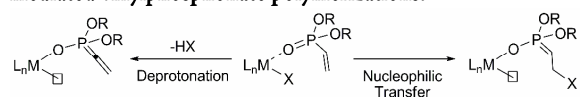
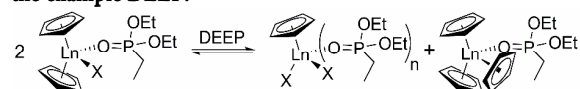


Figure 2. ESI MS spectrum of DEVP oligomers produced with Cp<sub>2</sub>Y(bdsa)(thf). Two major series of peaks are evident:  $m/z = n \times M_{Mon} + 66 + M_{Na}$  (red),  $m/z = n \times M_{Mon} + 133 + M_{Na}$  (blue);  $M_{Mon} = 164$ , end groups:  $M_{Cp} + M_{H} = 66$ ,  $M_{bdsa} + M_{H} = 133$ . Peaks at  $m/z = 351$ ,  $515$  and  $679$  are attributed to fragmentation (black).<sup>48</sup>

For the amide catalysts Cp<sub>2</sub>Ln(bdsa)(thf), on the other hand, two series of peaks were evident in the mass spectrometric end group analysis, one with a bdsa and one with a Cp end group (Figure 2). The ratio of these end groups was found to be strongly dependent on the reaction conditions and frequently, a peak series with olefinic chain ends was observed instead of bdsa end groups (Figure S4, S5). As in some cases, only olefinic chain ends were detected (Figure S5), this observation can be attributed to an elimination of the bdsa end group. Despite the simultaneous occurrence of two different initiation reactions, the obtained polymer shows a monomodal molecular weight distribution, indicating that both types of initiation produce the same active species.

To get deeper insight in the underlying initiation mechanism, an NMR spectroscopic study of phosphonate coordination at the used complexes was conducted. Diethyl ethylphosphonate (DEEP) was used due to its similar steric demand in comparison to DEVP and as it excludes both initiation and subsequent polymerization. Addition of varying amounts of DEEP (0.5, 1, 2 and 5 eq with respect to the metal center, respectively) revealed a monomer- (*i.e.* donor-) induced ligand exchange reaction forming Cp<sub>3</sub>Ln(DEEP) and CpLnX<sub>2</sub>(DEEP)<sub>n</sub> in equilibrium with the adduct Cp<sub>2</sub>LnX(DEEP) (Scheme 4, Figure 3). Line broadening of the DEEP <sup>1</sup>H and <sup>31</sup>P NMR spectroscopic signals indicates a fast exchange (in the NMR timescale) of coordinated and free DEEP (Figure 3). Larger metal centers and higher phosphonate concentration accelerate this exchange reaction and shift the equilibrium to the Cp<sub>3</sub>Ln/CpLnX<sub>2</sub> side. MMA, which is a significantly weaker donor than the applied phosphonates, is believed to induce only a minor extent of this ligand exchange reaction. Additionally, we found that Cp<sub>3</sub>Ln is an inefficient initiator for MMA polymerization, due to the lower steric demand

### Scheme 4. Donor-induced ligand exchange reaction caused by coordination of phosphonates at Cp<sub>2</sub>LnX complexes for the example DEEP.



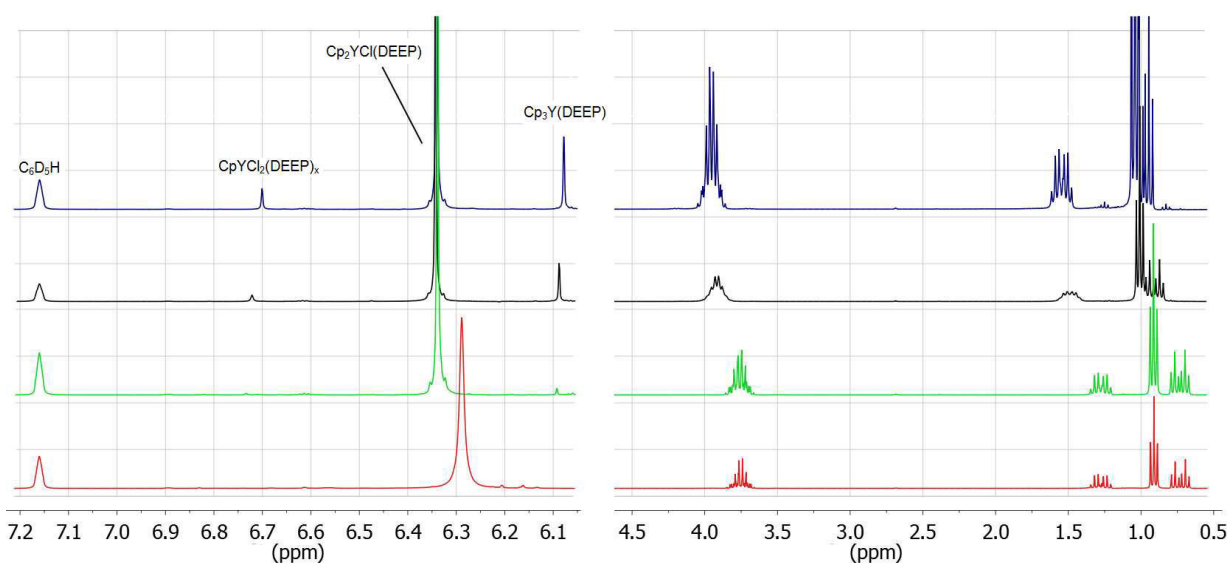


Figure 3.  $^1\text{H}$  NMR spectra of DEEP coordination at the rare earth metal center for addition of 0.5 (red), 1 (green), 2 (black) and 5 eq (blue) of DEEP (in respect to the metal center) to  $[\text{Cp}_2\text{YCl}]_2$  in  $\text{C}_6\text{D}_6$ , respectively. A donor-induced ligand exchange reaction forming  $\text{Cp}_3\text{Y}(\text{DEEP})$  and  $\text{Cp}_2\text{YCl}_2(\text{DEEP})_x$  in equilibrium with the adduct  $\text{Cp}_2\text{YCl}(\text{DEEP})$  is evident. For addition of 2 eq DEEP, line broadening for the DEEP  $^1\text{H}$  NMR spectroscopic signals shows an exchange of free and coordinated DEEP in the  $^1\text{H}$  NMR timescale.

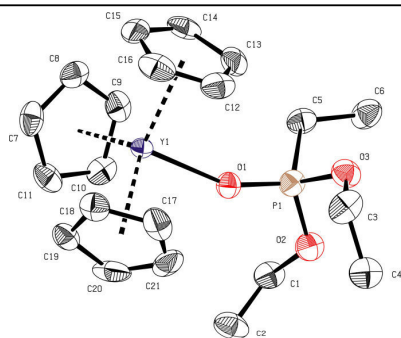


Figure 4. Crystal structure of the adduct  $\text{Cp}_3\text{Y}(\text{DEEP})$  (50% thermal ellipsoids; hydrogen atoms were omitted for clarity). Selected interatomic distances ( $\text{\AA}$ ) and bond angles (deg):  $\text{Y}-\text{O}(1)$ , 2.294;  $\text{P}=\text{O}(1)$ , 1.495;  $\text{Y}-\text{O}(1)=\text{P}$ , 7.24.

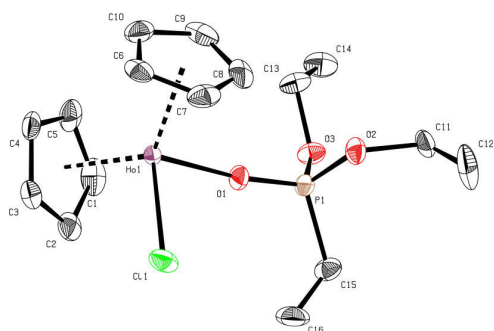


Figure 5. Crystal structure of the adduct  $\text{Cp}_2\text{HoCl}(\text{DEVP})$  (50% thermal ellipsoids; hydrogen atoms were omitted for clarity). Selected interatomic distances ( $\text{\AA}$ ), bond angles (deg) and torsion angles (deg):  $\text{Ho}-\text{Cl}$ , 2.582;  $\text{Ho}-\text{O}(1)$ , 2.227;  $\text{P}=\text{O}(1)$ , 1.485;  $\text{P}-\text{C}(15)$ , 1.779;  $\text{C}(15)=\text{C}(16)$ , 1.314;  $\text{P}=\text{O}(1)-\text{Ho}$ , 167.0;  $\text{O}(1)=\text{P}-\text{C}(15)=\text{C}(16)$ , -10.14.

of MMA in comparison to DAVP.<sup>46</sup> That leads to more stable  $\text{Cp}_3\text{Ln}(\text{MMA})$  adducts thus explaining the very low observed TOFs for MMA polymerization by  $[\text{Cp}_2\text{LnCl}]_2$ .<sup>18,47</sup>

To provide proof of the identity of the  $\text{Cp}_3\text{Ln}(\text{DEEP})$  adduct, the NMR samples of the corresponding Y complex were overlaid with pentane yielding colorless crystals suitable for single crystal X-ray crystallography (Figure 4, S13). In attempts to crystallize a vinylphosphonate adduct, according to the prolonged initiation period, addition of 1 eq of DEVP to a toluene solution of  $[\text{Cp}_2\text{LnCl}]_2$  ( $\text{Ln} = \text{Ho}, \text{Yb}$ ), subsequent overlaying with pentane and cooling to  $-30^\circ\text{C}$  yielded the adduct  $\text{Cp}_2\text{LnCl}(\text{DEVP})$ , as proven by X-ray crystallography. This way, we can provide first crystallographic proof of vinylphosphonate coordination at the active site *via* the oxygen of the phosphonate moiety (Figure 5, S14, S15). Previously, this type of coordination was suggested by  $^1\text{H}$  and  $^{31}\text{P}$  NMR spectroscopies.<sup>13,50</sup> Importantly, the crystal structures show that the Michael system of the coordinated vinylphosphonate is retained in an *S-cis* conformation with a pronounced  $\pi$ -overlap (torsion angles  $\text{O}=\text{P}-\text{C}=\text{C}$  of  $-10.14$  and  $10.47$  deg, Figure 5, S14, S15), a key prerequisite for the polymerizability of a monomer by a repeated conjugate addition polymerization, *i.e.* a GTP.<sup>11,18</sup> When the isolated DEVP adducts are dissolved in toluene, vinylphosphonate oligomers are formed after a few hours at room temperature without the addition of further monomer. This inherent instability of the  $\text{Cp}_2\text{LnCl}(\text{DEVP})$  adducts provides further evidence for the observed ligand exchange reaction.

Different initiators  $\text{Cp}_2\text{LnX}$  were synthesized and tested for their vinylphosphonate polymerization behavior (Table 2). We found that the equilibrium of the ligand exchange is also dependent on the nature of X. However, except for the aryloxy-substituted complexes  $\text{Cp}_2\text{Ln}(\text{OAr})(\text{thf})$ , in all cases, the formation of  $\text{Cp}_3\text{Ln}(\text{DEEP})$  was observed. Similar to  $[\text{Cp}_2\text{LnCl}]_2$ ,

**Table 2. DEVP polymerization results for Cp<sub>2</sub>LnX catalysts (toluene, 30 °C, monomer-to-catalyst ratio 600:1)**

Catalyst	Reaction time	Conversion <sup>a</sup> /%	Init. period <sup>b</sup>	$M_n^c$ /kDa	$I^*$ /%	TOF <sup>d</sup> / $I^*$ /h <sup>-1</sup>	End group <sup>d</sup>	Extent of ligand exchange <sup>e</sup>
[Cp <sub>2</sub> YCl] <sub>2</sub>	6 h	70	100 min	740	9.3	3700	Cp	15%
Cp <sub>2</sub> Y(bdsa)(thf)	3 h	95	15 min	1040	9.0	7200	Cp, bdsa (olefinic) <sup>f</sup>	3%
[Cp <sub>2</sub> Y(O <i>i</i> Pr)] <sub>2</sub>	30 h	26	2.5 h	1070	2.4	2000	Cp	<0.5% (10%) <sup>g</sup>
Cp <sub>2</sub> Y(OAr)(thf)	30 h	-	-	-	-	-	-	<0.5%
[Cp <sub>2</sub> Y(S <i>t</i> Bu)] <sub>2</sub>	3 min	100	5 sec	150	65	69000	S <i>t</i> Bu (olefinic) <sup>f</sup>	4%
Cp <sub>2</sub> Y(CH <sub>2</sub> TMS)(thf)	40 min	88	5 min	510	17	10000	olefinic	5%
[Cp <sub>2</sub> LuCl] <sub>2</sub>	1.5 h	93	7 min	780	11.7	20500	Cp	3%
Cp <sub>2</sub> Lu(bdsa)(thf)	3 h	96	20 min	1350	7.0	21000	Cp, bdsa (olefinic) <sup>f</sup>	1%
[Cp <sub>2</sub> Lu(O <i>i</i> Pr)] <sub>2</sub>	30 h	52	9 h	1270	4.0	600	Cp	<0.5% (<1%) <sup>g</sup>
Cp <sub>2</sub> Lu(OAr)(thf)	30 h	<1	-	-	-	-	-	<0.5%
[Cp <sub>2</sub> Lu(S <i>t</i> Bu)] <sub>2</sub>	1.5 min	100	15 sec	210	47	220000	S <i>t</i> Bu (olefinic) <sup>f</sup>	2%
Cp <sub>2</sub> Lu(CH <sub>2</sub> TMS)(thf)	30 min	92	5 min	1130	8.0	39000	olefinic	1%

<sup>a</sup>Determined by <sup>31</sup>P NMR spectroscopic measurement, <sup>b</sup>Initiation period, reaction time until 3% conversion is reached, <sup>c</sup>Determined by GPC-MALS,  $I^* = M_{th}/M_{ol}$ ,  $M_{th} = 600 \times M_{Mon} \times \text{conversion}$ , <sup>d</sup>determined by ESI MS, <sup>e</sup>conversion of Cp<sub>2</sub>LnX for addition of 5 eq of DEEP, determined from <sup>1</sup>H NMR spectroscopic signals of Cp<sub>2</sub>LnX(DEEP) and Cp<sub>3</sub>Ln(DEEP), <sup>f</sup>olefinic chain ends formed by end group elimination, <sup>g</sup>number in brackets: extent of dimer opening for addition of 5 eq of DEEP, determined from <sup>1</sup>H NMR spectroscopic signals of Cp<sub>2</sub>Ln(O*i*Pr)(DEEP) and DEEP.

the equilibrium is shifted to the formation of Cp<sub>3</sub>Ln for larger metal centers and increasing donor concentration. As previously shown, in case of late lanthanides, Cp<sub>3</sub>Ln(DAVP) serves as an efficient initiator for DAVP polymerization.<sup>14</sup> If neither deprotonation of the acidic  $\alpha$ -CH nor nucleophilic transfer is possible due to insufficient reactivity of the LnX bond (*e.g.* for X = Cl, O(Alk/Ar)), formed Cp<sub>3</sub>Ln(DAVP) will serve as the active initiating species (Scheme 5). This conclusion is corroborated by end group analysis of produced DEVP oligomers as well as by the inability of Cp<sub>2</sub>Ln(OAr)(thf) (which was found to not undergo a ligand exchange reaction, but to decompose upon DEEP addition) and Cp<sub>2</sub>LuCl(thf) (for which formation of Cp<sup>\*</sup><sub>3</sub>Lu and thus a ligand exchange is not possible<sup>51</sup>) to initiate polymerization (Table 2, Figure S6-11).

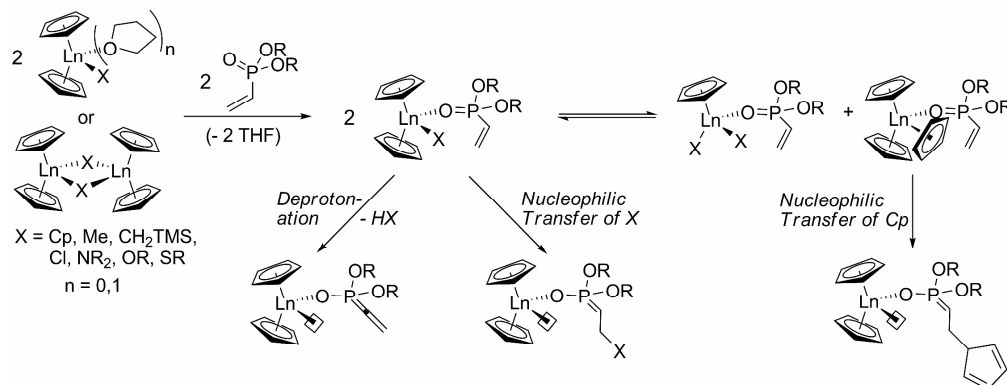
Thiolato complexes [Cp<sub>2</sub>Ln(S*t*Bu)]<sub>2</sub> were found to be well-suited for the initiation of vinylphosphonate GTP. However, for the observed fast transfer of thiolates to a coordinated monomer, the opening of dimers by coordination of a vinylphosphonate becomes rate-limiting (Scheme 5), as underlined by the lengthened initiation period and lower  $I^*$  of the more stable [Cp<sub>2</sub>Lu(S*t*Bu)]<sub>2</sub> dimer in comparison its Y analogue (Table 5, entries 5 and 11). This conclusion is supported by the observation that weaker coordinating monomers, *e.g.* 2-isopropylene-2-oxazoline, may not open *bis*(cyclopentadienyl) chloro- and thiolato-dimers, thus inhibiting polymerization.<sup>43</sup> For the more stable alkoxy dimers (*e.g.* [Cp<sub>2</sub>Ln(O*i*Pr)]<sub>2</sub>), this limitation was observed also for the stronger coordinating vinylphosphonates as an incomplete reaction with DEEP to form Cp<sub>2</sub>Ln(O*i*Pr)(DEEP) (Table 2, entries 3 and 9)).

Similar to bdsa, S*t*Bu end groups were found to be prone to elimination (Figure S8, S9). Even if an acidified work-up procedure is used, olefinic chain ends are still observed. According to the low basicity of the thiolato ligand, a formation of these olefinic chain ends by initial deprotonation of a coordinated vinylphosphonate can be ruled out. Steric repulsion between these bulky end groups and the phosphonate moiety is a major driving force of the elimination reaction, as larger monomers, *e.g.* DIVP, were found to facilitate this reaction, *i.e.* S*t*Bu end groups could not be found in ESI MS analysis of produced PDIVP oligomers (thus also ruling out a formation of olefinic chain ends solely due to fragmentation, Figure S12).

In case of Cp<sub>2</sub>Ln(bdsa)(thf), the observation of different end groups indicates an initiation by both bdsa transfer and a donor-induced ligand exchange. The reaction rates of these two types of initiation show a different dependency on catalyst and monomer concentration, thus explaining the observed strong sensitivity of the obtained ratio of end groups on the reaction conditions. According to [Cp<sub>2</sub>YbMe]<sub>2</sub>, ESI MS analysis of DEVP oligomers produced with strongly basic CH<sub>2</sub>TMS initiators revealed an initiation by deprotonation of the acidic  $\alpha$ -CH of the vinylphosphonate. The low initiator efficiencies of both Me and CH<sub>2</sub>TMS initiators (Table 1 and 2) show that deprotonation of  $\alpha$ -acidic monomers is a slow and thus unsuitable form of initiation for REM-GTP.

The above results clearly show that initiation of vinylphosphonate REM-GTP with unbridged rare earth metallocenes (Cp<sub>2</sub>LnX) follows a complex reaction pathway (Scheme 5). Depending on the nature of X, initiation can either proceed *via* an

**Scheme 5. Initiation of vinylphosphonate GTP using unbridged rare earth metallocenes ( $Cp_2LnX$ ) via deprotonation of the acidic  $\alpha$ -CH, nucleophilic transfer of X or via a monomer-induced ligand exchange reaction forming  $Cp_3Ln(DAVP)$ .**



abstraction of the acidic  $\alpha$ -CH of the vinylphosphonate (e.g. for X = Me, CH<sub>2</sub>TMS), via nucleophilic transfer of X to a coordinated monomer (e.g. for X = Cp, SR) or via a monomer- (i.e. donor-) induced ligand exchange reaction forming  $Cp_3Ln$  in equilibrium (e.g. for X = Cl, OR), which serves as the active initiating and catalytic species. Each of the reaction steps (Scheme 5) can be rate-limiting and different initiations may also occur simultaneously (e.g. for X = N(SiMe<sub>2</sub>H)<sub>2</sub>). However, only nucleophilic transfer ensures a sufficiently fast and thus homogeneous initiation of REM-GTP of fast-polymerizing  $\alpha$ -acidic monomers (e.g. vinylphosphonates). The traditionally used strongly basic methyl, CH<sub>2</sub>TMS or hydride initiators<sup>18-21</sup> are not suitable for these  $\alpha$ -acidic monomers, as the occurring initiation by deprotonation is rather slow. The efficient use of sterically crowded  $Cp_3Ln$  complexes is limited to large monomers and thiolate end groups were found to be prone to elimination, hence, in order to obtain versatile REM-GTP initiators and to open the access to a broad range of chain end functionality, further catalyst development is essential.

### Propagation mechanism

The investigations on the initiation mechanism revealed that  $Cp_2LnX$ -initiated vinylphosphonate polymerizations are generally mediated by a  $Cp_2Ln$ -unit. Nevertheless, the observed normalized activities  $TOF/I^*$  of different *bis*(cyclopentadienyl) complexes with identical metal center are not the same (Table 1, 2). For ideal living polymerizations, i.e. living polymerizations for which the initiation rate is considerably faster than the propagation rate,  $I^*$  is mainly determined by an initial initiator deactivation and does therefore not change during the course of polymerization. REM-GTP of vinylphosphonates is very fast and therefore primarily limited by an inefficient initiation reaction. Thus, the initiator efficiency  $I^*$  is significantly increasing during polymerization. Consequently, for a proper comparison of the catalytic activity,  $I^*$  has to be determined throughout the whole reaction. Better normalization results are yielded, if the initiator efficiency at the maximum rate of monomer conversion  $I^*_i$  is used instead of this efficiency at the end of the reaction (Figure 6).

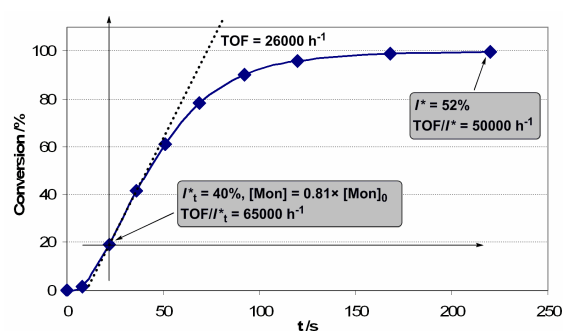


Figure 6. Conversion-reaction time plot for polymerization of DEVP, change of  $I^*_i$  during the reaction and corresponding normalized TOFs (8.6 mg  $[Cp_2Y(S^tBu)]_2$ , 7.5vol% DEVP in toluene (20 mL), 30 °C).

In case of very fast polymerization reactions, as observed e.g. for polymerization of DEVP, the maximum rate is typically observed for a conversion of approximately 15-40% (Figure 6). Thus, temperature (it is not possible to completely remove the reaction heat from the system) and viscosity effects cannot be entirely excluded, especially for high monomer concentrations. As GTP is sensitive to protic impurities and since GPC analysis needs to be performed with the aliquots taken in order to determine  $I^*$ , there is also a lower concentration limit for reliable kinetic analysis. In our study, we found that 2.5 to 10vol% monomer concentration in toluene are ideal.

The general rate law for catalyzed polymerizations reads

$$r = k \times [Cat]^m \times [Mon]^n \quad (1)$$

For a meaningful kinetic analysis, we use the maximum rate of conversion, the present active catalyst concentration  $[Cat^*]$  and the residual monomer concentration  $[Mon]$ . In accordance with a living-type polymerization, we calculate these concentrations following

$$[Cat^*] = [Cat]_0 \times I^*_i \quad (2)$$

and

$$[Mon] = [Mon]_0 \times (1-C) \quad (3)$$



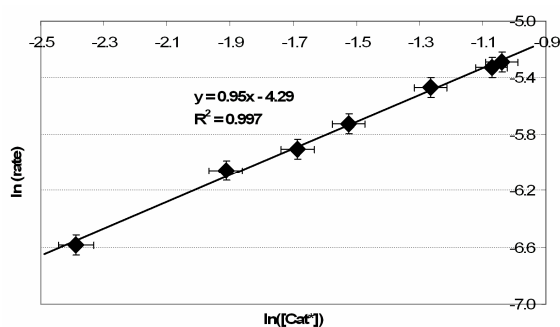


Figure 7. Determination of catalyst order ( $\text{Cp}_3\text{Tm}$ , 5vol% DEVP in toluene, 30 °C).

with the overall catalyst concentration  $[\text{Cat}]_0$ , the initial monomer concentration  $[\text{Mon}]_0$ , the conversion  $C$  and

$$I_t^* = M_{\text{Mon}} \times ([\text{Mon}]_0 / [\text{Cat}]_0) \times C / M_n \quad (4)$$

with the monomer molar mass  $M_{\text{Mon}}$  and the number-averaged molecular weight  $M_n$  at the given reaction time  $t$  as determined *via* absolute analysis using GPC-MALS. This normalization with the initiator efficiency  $I_t^*$  both addresses inefficient initiation and catalyst deactivation due to (protic) impurities.

As the initiator efficiency depends on concentration and monomer-to-catalyst ratio, the active catalyst concentration cannot be exactly predicted. Thus, for the determination of the reaction orders, first, the initial monomer concentration is kept constant to determine the order in catalyst  $m$ . For different concentrations of the same catalyst at otherwise identical reaction conditions, the maximum rate is consistently reached at similar conversion. Therefore, also the residual monomer concentration is assumed to be constant and  $\ln(r)$  is plotted against  $\ln([\text{Cat}^*])$  yielding a reaction order of  $m = 1$  for every evaluated catalyst (Figure 7, S16, Table S1, S2). Consequently, rare earth metal-mediated vinylphosphonate GTP follows a monometallic propagation according to the mechanism previously shown for (meth)acrylic monomers (Scheme 1a).

In order to verify the corresponding RDS, the monomer order  $n$  is determined following

$$r / [\text{Cat}^*] = k \times [\text{Mon}]^n \quad (5)$$

by plotting  $\ln(r / [\text{Cat}^*])$  against  $\ln([\text{Mon}])$ .

The viscosity of the reaction mixture is mainly dependent on molecular weight and concentration of the formed polymer. Consequently, this viscosity is strongly affected by the initial monomer concentration, thus making a reliable determination of the monomer reaction order difficult. Only catalysts with high initiator efficiency  $I_t^*$  allow kinetic analysis of the monomer order, as they both yield lower molecular weight polymers and exhibit their maximum rate for rather low conversions (below 30%). Moreover, an initial heterogeneous polymerization is observed for fast-initiating complexes with poor solubility in toluene, such as  $\text{Cp}_3\text{Ln}$ . Accordingly,  $\text{Cp}_3\text{Tm}$  allows determination of the catalyst order for DEVP polymerization as it dissolves completely during an initiation period of approximately one minute providing initiator efficiencies  $I_t^*$  of 13-21% (Figure 7, Table S1). However, for these low initiator efficiencies, a reliable determination of

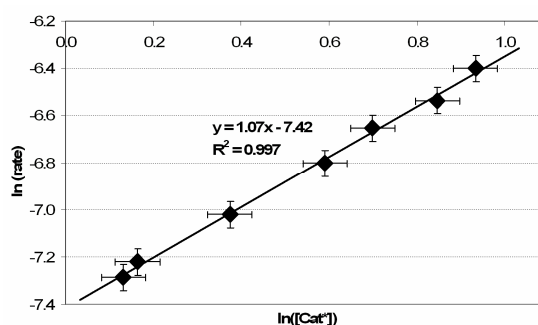


Figure 8. Determination of catalyst order ( $[\text{Cp}_2\text{Y}(\text{SfBu})]_2$ , 12.5vol% DIVP in toluene, 30 °C).

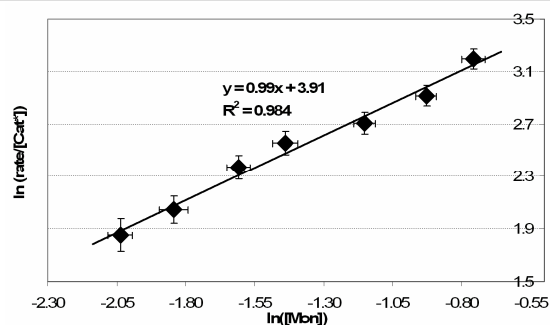


Figure 9. Determination of monomer order ( $[\text{Cp}_2\text{Y}(\text{SfBu})]_2$ , 2.5-10vol% DEVP in toluene, 30 °C).

monomer orders is not possible. In addition, catalyst orders for DIVP polymerization may not be obtained using  $\text{Cp}_3\text{Ln}$  due to an occurring initial heterogeneous polymerization.

For this purpose, a better soluble complex with higher initiator efficiency is necessary.  $[\text{Cp}_2\text{Y}(\text{SfBu})]_2$  was used as it dissolves instantly upon monomer addition and reaches initiator efficiencies  $I_t^*$  of 35-54% and 57-86% in case of DEVP and DIVP polymerization, respectively (Table S2-S5). Using this thiolato yttrocene, the order in catalyst for DIVP polymerization could be determined as  $m = 1$ , showing that further increase of the monomer steric demand does not lead to a change of the polymerization mechanism (Figure 8, Table S3). Determination of the monomer order according to equation (5) yields  $n = 1$  for polymerization of both DEVP and DIVP (Figure 9, S17, Table S4, S5).

These results clearly show that rare earth metal-mediated vinylphosphonate GTP follows a monometallic Yasuda-type polymerization mechanism, with an  $\text{S}_{\text{N}}2$ -type associative displacement of the polymer phosphonate ester by a monomer as the RDS as depicted in Scheme 2b. This conclusion is in line with theoretical calculations from Ziegler *et al.*<sup>28</sup> on REM-GTP of methyl acrylate (MA), which have shown the RDS to be the first transition state for an associative displacement of the metal polymer ester bond by an incoming MA molecule *via* a pentacoordinated intermediate. Whether the addition of vinylphosphonate occurs *via* a back-side or front-side attack, *i.e.* *via* chain-retention or chain migratory mechanism, may not be verified this way. For this purpose, studies on the stereospecificity

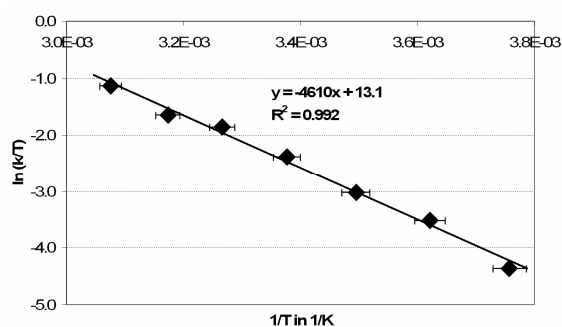


Figure 10. Eyring-plot for  $[\text{Cp}_2\text{Y}(\text{SiBu})_2]$ -initiated DEVP (10vol%) polymerization in toluene ( $-7 - 52^\circ\text{C}$ ,  $\Delta H^\ddagger = 38.3 \text{ kJ mol}^{-1}$ ,  $\Delta S^\ddagger = -88.6 \text{ J (mol K)}^{-1}$ ).

of  $C_s$ - or  $C_1$ -symmetric catalysts and/or theoretical calculations need to be performed. Such studies are currently underway in our laboratories. The coordination strength of 2-isopropylene-oxazoline or methacrylates at the metal center is not sufficient to open the eight-membered ring intermediate by substitution of a coordinated phosphonate. This explains the previously observed unfeasible consecutive polymerization of these monomers after vinylphosphonates.<sup>11,12,43</sup>

Still, these results provide no explanation of the origin of the influence of metal radii and steric demand of monomers on the catalytic activity. For this purpose, temperature-dependent kinetic analysis was performed to determine activation enthalpies  $\Delta H^\ddagger$  and entropies  $\Delta S^\ddagger$  according to the Eyring equation

$$\ln(k/T) = -\Delta H^\ddagger/R \times 1/T + \Delta S^\ddagger/R + \ln(k_B/h) \quad (6)$$

with the rate constant  $k$ , the temperature  $T$ , the gas constant  $R$ , the Boltzmann constant  $k_B$  and the Planck constant  $h$ . Plotting  $\ln(k/T)$  against  $1/T$  yields the activation enthalpy and entropy of the RDS (Figure 10).

These experiments were performed for the metal centers Lu, Tm, Y and Tb (in order of increasing metal ionic radius<sup>52</sup>) as well as for the monomers DEVP and DIVP (Table 3, S6-S12, Figure 10, S18-S23). Contradicting the reactivity order of different rare earth metals for MMA polymerization previously reported by Yasuda *et al.* ( $\text{Sm} > \text{Y} > \text{Yb} > \text{Lu}$ )<sup>23</sup>, vinylphosphonate GTP is accelerated by a decreasing ionic radius of the metal center (see also Ref. 14).

Surprisingly, for both monomers,  $\Delta H^\ddagger$  was found to not be affected by the metal ionic radius (within the limits of experimental accuracy of ca.  $1 - 2 \text{ kJ mol}^{-1}$ ). Thus, enthalpic effects, *e.g.* the  $\text{Ln}-(\text{O}=\text{P})$  bond strength as a function of the Lewis acidity and the metallacycle ring strain as a function of the radius of the metal center, do therefore not determine the activity of different rare earth metals for vinylphosphonate GTP. In fact, different activation barriers  $\Delta G^\ddagger$  were found to be a result of a change of  $-\text{T}\Delta S^\ddagger$ , which was found to decrease linearly with decreasing metal ionic radius (Table 3, Figure 11). Hence, higher activity is caused by a less pronounced loss of degrees of freedom in the RDS for smaller metal centers. The corresponding active centers are sterically more crowded both in the ground as well as in the transition state. The decrease of the activation barrier for smaller metal centers due to  $\Delta S^\ddagger$  shows that the resulting increase

Table 3. Activation enthalpy  $\Delta H^\ddagger$  and entropy  $\Delta S^\ddagger$  dependence on ionic radius and monomer steric demand

metal center	radius /pm <sup>a</sup>	DEVP		DIVP	
		$\Delta H^\ddagger$ /kJ mol <sup>-1</sup>	$\Delta S^\ddagger$ /J (K mol) <sup>-1</sup>	$\Delta H^\ddagger$ /kJ mol <sup>-1</sup>	$\Delta S^\ddagger$ /J (K mol) <sup>-1</sup>
Tb	106.3	38.5	-102	41.3	-124
Y	104.0	38.3	-88.6	40.7	-112
Tm	102.0	39.1	-82.8	-	-
Lu	100.1	38.7	-73.6	42.0	-99.1

<sup>a</sup>Ln<sup>3+</sup> ionic radius<sup>52</sup>.

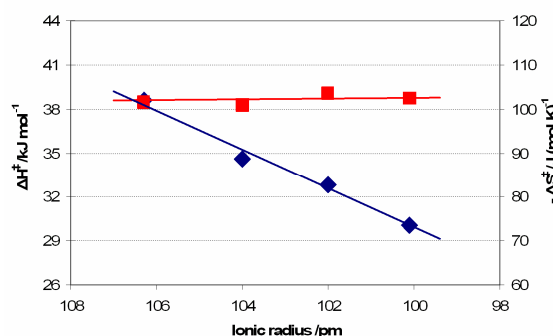


Figure 11. Activation enthalpy (red squares) and entropy (blue diamonds) for DEVP polymerization using  $\text{Cp}_2\text{LnX}$  catalysts in dependence of the metal ionic radius.

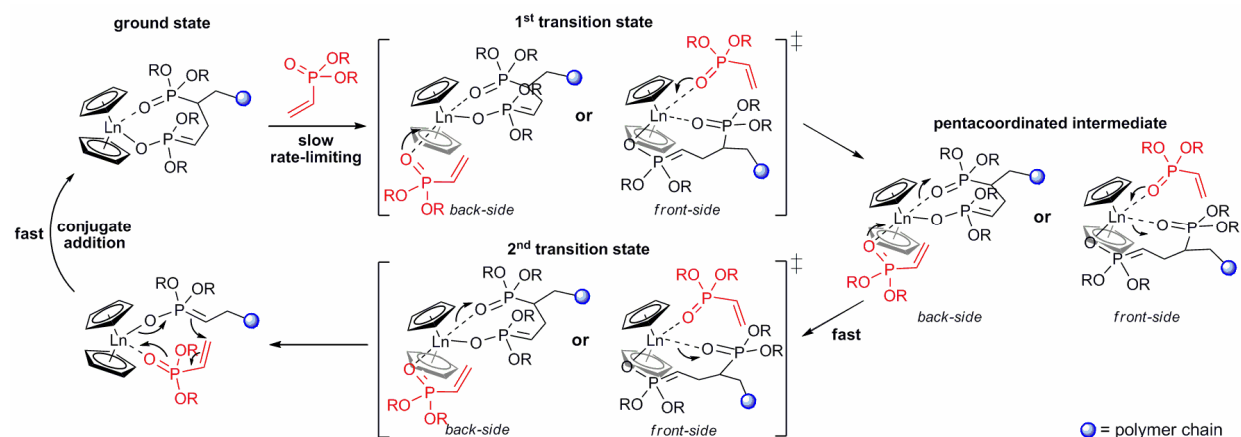
of steric constraints leads to a destabilization of the eight-membered ring polymerization ground state relative to the transition state.

An increase of monomer steric demand leads to an increase of both  $\Delta H^\ddagger$  and  $-\text{T}\Delta S^\ddagger$  (Table 3). Hereby, at room temperature, the change of  $\Delta S^\ddagger$  has a larger effect on the propagation rate ( $\Delta\Delta H^\ddagger \approx 3 \text{ kJ mol}^{-1}$ ,  $-\text{T}\Delta\Delta S^\ddagger \approx 7 \text{ kJ mol}^{-1}$  for DEVP vs DIVP). Hence, increasing steric demand of the monomers leads to relative destabilization of the transition state, which can again be largely attributed to a higher loss of degrees of freedom. The resulting faster propagation for smaller monomers is in agreement with the reactivity order previously determined for methacrylates, but contrary to the one observed for acrylates.<sup>19,23,45</sup>

Importantly, a recent study on statistical copolymerization of different DAVPs revealed that the rate of vinylphosphonate GTP is mainly determined by the steric demand of the growing chain end, not by the added monomer.<sup>16</sup> Taking these considerations into account, the following mechanistic conclusions on rare earth metal-mediated GTP of vinylphosphonates can be drawn:

(1) The steric demand of the incoming monomer only shows minor influence on the propagation rate. Ziegler *et al.*<sup>28</sup> have shown coordinative-anionic polymerization of MA to proceed *via* a pentacoordinated intermediate with its formation by coordination of MA as the RDS. In the corresponding transition state, the metal-(O=C) bond to the incoming monomer is much longer than the metal-(O=C) bond to the polymer ester. In the present case, assuming REM-GTP of DAVP also proceeds over a pentacoordinated intermediate, the longer  $\text{Ln}-(\text{O}=\text{P})$  bond in the

**Scheme 6. Elemental steps of rare earth mediated GTP of vinylphosphonates. The rate-limiting step is an  $S_N2$ -type associative displacement of the polymer phosphonate ester by a vinylphosphonate monomer, presumably *via* a pentacoordinated intermediate.**



corresponding transition state leads to a relatively small steric demand of the added vinylphosphonate (in comparison to the growing chain end). The resulting minor effect of the steric demand of the added monomer on the propagation rate is in accordance with our observations (*vide supra*), thus providing initial evidence for the associative displacement to proceed over two transition states *via* a pentacoordinated intermediate (Scheme 6).

(2) Smaller metal centers destabilize the propagation ground state by a more confined arrangement of the eight-membered metallacycle according to the higher steric constraints caused by shorter Ln–Cp, Ln–(O–P) and Ln–(O=P) bonds. Contradicting to our expectation, the destabilization of the ground state is not of enthalpic (*i.e.* ring strain or the Ln–(O=P) bond strength), but of entropic nature (*i.e.* rotational and vibrational limitations in the eight-membered metallacycle). In the transition state, the Ln–(O=P) polymer phosphonate ester bond is lengthened, thus compensating part of the steric stress induced by the coordination of a vinylphosphonate monomer. This effect is larger for a stronger destabilization of the ground state, *i.e.* for smaller metal centers. Accordingly, we also expect an acceleration of vinylphosphonate REM-GTP by the introduction of sterically more demanding ligand systems (*e.g.* Cp\*<sub>2</sub> instead of Cp<sub>2</sub>). Such studies are currently underway in our laboratories.

(3) Higher steric demand of the growing polymer chain end (*i.e.* sterically more demanding side chains) leads to a relative destabilization of the transition state by both enthalpic and entropic effects, with the latter having the larger impact on the activation barrier. In comparison to the propagation ground state, the incoming monomer increases the steric crowding at the metal center (Scheme 6), leading to higher steric constraints within the eight-membered metallacycle, however, with the actual monomer size playing only a minor role (*vide supra*). In contrast, larger metallacycle side chains induce a stronger increase of rotational and vibrational restrictions in the RDS, thus destabilizing the transition state.

In summary, the propagation rate of vinylphosphonate GTP is mainly determined by the change of rotational and vibrational restrictions within the eight-membered metallacycle in the RDS as a function of the steric demand of the metallacycle side chains and the steric crowding at the metal center. In contrast to (meth)acrylates, the constitution of DAVP is tetrahedral and DAVPs are sterically more demanding. Therefore, rotational limitations (especially of the polymer substituent in the eight-membered metallacycle) and thus entropic effects are believed to have a stronger effect on DAVP than for (meth)acrylate GTP. In previous mechanistic studies on coordinative-anionic polymerization of (meth)acrylates, entropic effects have been largely disregarded,<sup>27,28,32,36-40</sup> even if Eyring-plots were conducted.<sup>37</sup> In case of theoretical studies, the inclusion of entropic effects is computationally extremely expensive.<sup>28,39</sup> However, taking into account the drastic effect of the metal radius and the monomer size on the activation entropy for vinylphosphonate GTP, also for (meth)acrylic monomers, experimental studies on activation entropies and theoretical studies on the free energy surface with a separate investigation of enthalpic and entropic effects may provide useful insight into the mechanism of monometallic rare earth metal-/ group 4 metallocenium cation-mediated GTP.

In case of coordinative-anionic polymerizations, it is well-established that the metal center has to remain easily accessible in order to ensure high activities. The current study and the present activity trend for vinylphosphonate GTP (smaller metal centers yield higher active catalysts) questions the general applicability of this concept. This conclusion is in line with previous observations by Chen *et al.*<sup>40</sup>, which have found an increase of steric crowding at the active site does not only yield higher stereospecificity and a suppression of side reactions, but also an acceleration of the propagation. Hence, in order to obtain high activity, the steric crowding of the catalyst needs to be well-adjusted: high enough to ensure sufficient destabilization of the eight-membered metallacycle ground state and to prohibit unfavored side reactions (*e.g.* site epimerization), small enough to still facilitate an  $S_N2$ -type associative displacement of the polymer ester by an incoming monomer.

## Conclusion

In this manuscript, the first detailed mechanistic studies on both initiation and propagation of rare earth metal-mediated GTP of vinylphosphonates have been presented. During the course of our study, we were able to isolate the DEVP adducts  $\text{Cp}_2\text{LnCl}(\text{DEVP})$ , providing first X-ray crystallographic proof for vinylphosphonate coordination at the active site *via* the oxygen of the phosphonate moiety, and thus further supporting the hypothesis of GTP mechanism taking place. We have shown that the reactive  $\alpha$ -CH and the use of unbridged rare earth metallocenes lead to a complex initiation network for vinylphosphonate GTP. Depending on the nature of the initiating ligand, initiation can either proceed *via* abstraction of the acidic  $\alpha$ -CH of the vinylphosphonate, *via* transfer of a nucleophilic ligand to a coordinated monomer or *via* a monomer- (*i.e.* donor-) induced ligand exchange reaction forming  $\text{Cp}_3\text{Ln}$  in equilibrium, which serves as the active initiating and catalytic species. We found the applied initiators, especially traditionally used strongly basic methyl,  $\text{CH}_2\text{TMS}$  or hydride initiators, to suffer from different limitations, thus restricting their efficient use to selected monomers only. Therefore, rare earth metal-based GTP catalysts still require further development of versatile initiating ligands for an efficient application to a variety of monomers.

A detailed kinetic analysis of DAVP REM-GTP has been complicated by a very fast polymerization reaction in combination with a comparably slow initiation. Thus, the overall reaction rate is influenced by both initiation and propagation. In this manuscript, we have shown a general differential approach to separately analyze the propagation reaction for such living polymerizations. Time-resolved analysis of monomer conversion and molecular weights of the formed polymers allows the determination of the initiator efficiency throughout the whole reaction. Using this normalization method, rare earth metal-mediated GTP was shown to follow a monometallic Yasuda-type polymerization mechanism, with an  $\text{S}_{\text{N}}2$ -type associative displacement of the polymer phosphonate ester by a monomer as the RDS. The activation entropy  $\Delta\text{S}^\ddagger$  of the RDS is strongly affected by the metal radius and the monomer size, whereas these parameters show only minor influence on the activation enthalpy  $\Delta\text{H}^\ddagger$ . As the steric demand of the added monomer shows only a minor influence on the propagation rate, the associative displacement is very likely to proceed over two transition states *via* a pentacoordinated intermediate. In order to support the mechanistic conclusions drawn in this manuscript, further studies with a modified ligand architecture (especially  $\text{C}_1$ - and  $\text{C}_s$ -symmetric complexes) as well as theoretical calculations are currently underway.

The presented results show that the extension of REM-GTP beyond (meth)acrylates allows new insights into the underlying mechanisms, but requires further catalyst development, especially concerning the search for versatile and efficient initiators as well as the regarding the optimization of the steric crowding of the active propagation site.

## Experimental Section

### General

All reactions were carried out under argon atmosphere using standard Schlenk or glovebox techniques. All glassware was heat dried under vacuum prior to use. Unless otherwise stated, all chemicals were purchased from Sigma-Aldrich, Acros Organics or ABCR and used as received. Toluene, THF and pentane were dried using an MBraun SPS-800 solvent purification system. Hexane, isopropanol, *tert*-butylthiol and DEEP were dried over 3Å molecular sieve.  $\text{Cp}_3\text{Ln}$ ,<sup>53</sup>  $[\text{Cp}_2\text{LnCl}]_2$ ,<sup>54</sup>  $[\text{Cp}_2\text{YbMe}]_2$ ,<sup>55</sup>  $\text{Cp}^*\text{LuCl}(\text{thf})$ ,<sup>56</sup>  $\text{NaCp}$ ,<sup>57</sup>  $\text{Li}(\text{bdsa})$ ,<sup>58</sup> the precursor complexes  $\text{Ln}(\text{bdsa})_3(\text{thf})_2$  and  $\text{Ln}(\text{CH}_2\text{TMS})_3(\text{thf})_2$ ,<sup>58,59</sup> as well as the monomers DEVP and DIVP<sup>49</sup> were prepared according to literature procedures. Monomers were dried over calcium hydride and distilled prior to use.

NMR spectra were recorded on a Bruker AV-300 or AV-500C spectrometer.  $^1\text{H}$ ,  $^{13}\text{C}$  and  $^{29}\text{Si}$  NMR spectroscopic chemical shifts  $\delta$  are reported in ppm relative to tetramethylsilane.  $\delta(^1\text{H})$  is calibrated to the residual proton signal,  $\delta(^{13}\text{C})$  to the carbon signal and  $\delta(^{29}\text{Si})$  to the deuterium signal of the solvent.  $^{31}\text{P}$  NMR spectroscopic chemical shifts are reported in ppm relative to and calibrated to 85% aqueous  $\text{H}_3\text{PO}_4$ . Deuterated solvents were obtained from Deutero or Eurisotop and dried over 3Å molecular sieve. Elemental analyses were measured at the Laboratory for Microanalytics at the Institute of Inorganic Chemistry at the Technische Universität München. ESI MS analytical measurements were performed with methanol solutions on a Varian 500-MS spectrometer, using 70 keV in the positive ionization mode. IR spectra were recorded under argon atmosphere on a Bruker Vertex 70 spectrometer with a Bruker Platinum ATR set-up and the integrated MCT detector. Samples were applied as THF solution or  $\text{Et}_2\text{O}$  suspension and measured after evaporation of the solvent.

### Complex Synthesis

**General procedure for synthesis of  $\text{Cp}_2\text{Ln}(\text{bdsa})(\text{thf})$ .** 2 eq of freshly distilled cyclopentadiene are added to a toluene solution of 1 eq of  $\text{Ln}(\text{bdsa})_3(\text{thf})_2$  (ca. 0.25 M). The resulting solution is stirred overnight at 110 °C in a pressure schlenk vessel, the solvent and formed 1,1,3,3-tetramethyldisilazane are removed *in vacuo* and the resulting solid is recrystallized from toluene at -35 °C.

**$\text{Cp}_2\text{Y}(\text{bdsa})(\text{thf})$ :** Yield: 15.5 g colorless crystals (36.8 mmol, 75%).  $^1\text{H}$  NMR ( $\text{C}_6\text{D}_6$ , 298 K, 300 MHz):  $\delta = 0.34$  (d, 12H,  $^3\text{J}(\text{H}-\text{H}) = 3.0$  Hz, Si-CH<sub>3</sub>), 1.15 (m, 4H, THF-H), 3.36 (m, 4H, THF-H<sub>i</sub>), 4.28 (m, 2H, Si-H), 6.13 (s, 10H, Cp-H).  $^{13}\text{C}$  NMR ( $\text{C}_6\text{D}_6$ , 300 K, 125 MHz):  $\delta = 3.4$  (s, Si-CH<sub>3</sub>), 25.2 (s, THF-C), 71.9 (s, THF-C<sub>ii</sub>), 110.7 (s, Cp-C).  $^{29}\text{Si}$  NMR ( $\text{C}_6\text{D}_6$ , 300K, 100 MHz):  $\delta = -25.4$  (s). IR ( $\text{cm}^{-1}$ ): 3674, 3566, 3087, 2974, 2885, 2704, 2083, 2046, 1645, 1458, 1439, 1369, 1346, 1241, 1175, 1059, 1032, 1009, 913, 872, 778, 766, 699. EA: calculated: C 51.05, H 7.62, N 3.31; found: C 50.83, H 7.63, N 3.27.

**$\text{Cp}_2\text{Lu}(\text{bdsa})(\text{thf})$ :** Yield: 9.5 g colorless crystals (18.6 mmol, 78%).  $^1\text{H}$  NMR ( $\text{C}_6\text{D}_6$ , 298 K, 300 MHz):  $\delta = 0.37$  (d, 12H,  $^3\text{J}(\text{Si}-\text{H}) = 3.1$  Hz, Si-CH<sub>3</sub>), 1.23 (m, 4H, THF-H), 3.35 (m, 4H, THF-H<sub>i</sub>), 4.28 (m, 2H, Si-H), 6.11 (s, 10H, Cp-H).  $^{13}\text{C}$  NMR ( $\text{C}_6\text{D}_6$ ,

298 K, 75 MHz):  $\delta = 3.5$  (s, Si-CH<sub>3</sub>), 25.3 (s, THF-C<sub>i</sub>), 72.2 (s, THF-C<sub>ii</sub>), 110.3 (s, Cp-C). <sup>29</sup>Si NMR (C<sub>6</sub>D<sub>6</sub>, 298 K, 60 MHz):  $\delta = -23.7$  (s). IR (cm<sup>-1</sup>): 3561, 3090, 2954, 2707, 2098, 2049, 1438, 1249, 1179, 1011, 906, 875, 779, 735. EA: calculated: C 42.42, H 6.33, N 2.75; found: C 41.90, H 6.29, N 2.91.

**Cp<sub>2</sub>Tb(bdsa)(thf)**: Yield: 1.95 g colorless crystals (3.9 mmol, 70%). IR (cm<sup>-1</sup>): 3666, 3085, 2974, 2886, 2705, 2107, 2045, 1636, 1458, 1439, 1369, 1346, 1243, 1175, 1059, 1033, 1010, 879, 777, 763, 688. EA: calculated: C 43.80, H 6.54, N 2.84; found: C 43.79, H 6.70, N 2.78.

**General procedure for synthesis of Cp<sub>2</sub>Ln(CH<sub>2</sub>TMS)(thf)**. 2 eq of freshly distilled cyclopentadiene are added to a toluene solution of 1 eq of Ln(CH<sub>2</sub>TMS)<sub>3</sub>(thf)<sub>2</sub> (ca. 0.25 M). The resulting solution is stirred overnight at r.t., the solvent and formed tetramethylsilane are removed *in vacuo* and the resulting solid is recrystallized from toluene/hexane at -35 °C.

**Cp<sub>2</sub>Y(CH<sub>2</sub>TMS)(thf)**: Yield: 5.4 g colorless needles (14.3 mmol, 65%). <sup>1</sup>H NMR (C<sub>6</sub>D<sub>6</sub>, 300 K, 500 MHz):  $\delta = -0.67$  (d, 2H, <sup>3</sup>J(Y-H) = 3.5 Hz, Si-CH<sub>3</sub>), 0.43 (s, 9H, Si-CH<sub>3</sub>), 0.92 (m, 4H, THF-H<sub>i</sub>), 2.95 (m, 4H, THF-H<sub>ii</sub>), 6.12 (s, 10H, Cp-H). <sup>13</sup>C NMR (C<sub>6</sub>D<sub>6</sub>, 300 K, 125 MHz):  $\delta = 4.8$  (s, Si-CH<sub>3</sub>), 24.9 (s, THF-C<sub>i</sub>), 25.4 (d, <sup>1</sup>J(Y-C) = 42.5 Hz, Si-CH<sub>2</sub>), 71.2 (s, THF-C<sub>ii</sub>), 110.4 (s, Cp-C). <sup>29</sup>Si NMR (C<sub>6</sub>D<sub>6</sub>, 300K, 100 MHz):  $\delta = -3.0$  (s). IR (cm<sup>-1</sup>): 3674, 3559, 3087, 2955, 2893, 2707, 1638, 1459, 1438, 1422, 1368, 1345, 1287, 1248, 1011, 861, 766, 696. EA: calculated: C 57.13, H 7.72; found: C 57.21, H 7.85.

**Cp<sub>2</sub>Lu(CH<sub>2</sub>TMS)(thf)**: Yield: 5.5 g beige solid (11.9 mmol, 78%). <sup>1</sup>H NMR (C<sub>6</sub>D<sub>6</sub>, 300 K, 500 MHz):  $\delta = -0.76$  (s, 2H, Si-CH<sub>3</sub>), 0.43 (s, 9H, Si-CH<sub>3</sub>), 0.89 (m, 4H, THF-H<sub>i</sub>), 2.91 (m, 4H, THF-H<sub>ii</sub>), 6.06 (s, 10H, Cp-H). <sup>13</sup>C NMR (C<sub>6</sub>D<sub>6</sub>, 300 K, 125 MHz):  $\delta = 5.0$  (s, Si-CH<sub>3</sub>), 24.9 (s, THF-C<sub>i</sub>), 27.3 (s, Si-CH<sub>2</sub>), 71.5 (s, THF-C<sub>ii</sub>), 109.8 (s, Cp-C). <sup>29</sup>Si NMR (C<sub>6</sub>D<sub>6</sub>, 300K, 100 MHz):  $\delta = -0.8$  (s). IR (cm<sup>-1</sup>): 3563, 3091, 2953, 2896, 2710, 1459, 1439, 1420, 1287, 1248, 1122, 1013, 859, 775, 695. EA: calculated: C 46.55, H 6.29; found: C 45.93, H 6.10.

**General procedure for synthesis of Cp<sub>2</sub>LnX**. 1 eq of a stem solution of XH in toluene (ca. 5 w%) is added dropwise to a toluene solution of 1 eq of Cp<sub>2</sub>Ln(bdsa)(thf) (ca. 0.1 M). The resulting mixture is stirred overnight at r.t., the solvent and formed 1,1,3,3-tetramethyldisilazane are removed *in vacuo* yielding pure product in quantitative yield.

**[Cp<sub>2</sub>Y(O<sup>i</sup>Pr)]<sub>2</sub>**: Yield: 230 mg white powder (0.83 mmol). <sup>1</sup>H NMR (THF-d<sub>8</sub>, 298 K, 300 MHz):  $\delta = 1.25$  (d, 6H, <sup>3</sup>J(H-H) = 6.0 Hz, CH<sub>3</sub>), 3.84 (sp, 1H, <sup>3</sup>J(H-H) = 6.0 Hz, O-CH(CH<sub>3</sub>)<sub>2</sub>), 6.20 (s, 10H, Cp-H). <sup>13</sup>C NMR (THF-d<sub>8</sub>, 298 K, 75 MHz):  $\delta = 28.8$  (s, CH<sub>3</sub>), 68.6 (s, O-CH(CH<sub>3</sub>)<sub>2</sub>), 112.1 (s, Cp-C). IR (cm<sup>-1</sup>): 3092, 2960, 2926, 2836, 1653, 1459, 1379, 1368, 1329, 1254, 1157, 1118, 1011, 952, 811, 793, 782, 768, 752. EA: calculated: C 56.13, H 6.16; found: C 55.92, H 5.98.

**[Cp<sub>2</sub>Lu(O<sup>i</sup>Pr)]<sub>2</sub>**: Yield: 150 mg beige powder (0.42 mmol). <sup>1</sup>H NMR (C<sub>6</sub>D<sub>6</sub>, 298 K, 300 MHz):  $\delta = 0.87$  (d, 6H, <sup>3</sup>J(H-H) = 6.1 Hz, CH<sub>3</sub>), 3.49 (sp, 1H, <sup>3</sup>J(H-H) = 6.1 Hz, O-CH(CH<sub>3</sub>)<sub>2</sub>), 6.12 (s, 10H, Cp-H). <sup>13</sup>C NMR (C<sub>6</sub>D<sub>6</sub>, 300 K, 125 MHz):  $\delta = 28.2$  (s, CH<sub>3</sub>), 68.3 (s, O-CH(CH<sub>3</sub>)<sub>2</sub>), 110.8 (s, Cp-C). IR (cm<sup>-1</sup>): 3096, 3071, 2965, 2926, 2842, 1662, 1459, 1381, 1367,

1331, 1257, 1158, 1117, 1010, 951, 818, 796, 786, 754, 676. EA: calculated: C 42.87, H 4.70; found: C 42.17, H 4.50.

**Cp<sub>2</sub>Y(O(C<sub>6</sub>H<sub>2</sub>(CH<sub>3</sub>)<sub>3</sub>)(thf)**: Yield: 200 mg yellow crystals (0.47 mmol). <sup>1</sup>H NMR (C<sub>6</sub>D<sub>6</sub>, 300 K, 500 MHz):  $\delta = 1.06$  (m, 4H, THF-H<sub>i</sub>), 2.29 (s, 6H, ortho-CH<sub>3</sub>), 2.38 (s, 3H, para-CH<sub>3</sub>), 3.24 (m, 4H, THF-H<sub>ii</sub>), 6.13 (s, 10H, Cp-H), 7.03 (s, 2H, Ar-H). <sup>13</sup>C NMR (THF-d<sub>8</sub>, 300 K, 125 MHz):  $\delta = 18.9$  (s, ortho-CH<sub>3</sub>), 21.0 (s, para-CH<sub>3</sub>), 26.7 (s, THF-C<sub>i</sub>), 68.5 (s, THF-C<sub>ii</sub>), 111.2 (s, Cp-C), 123.8 (para-C<sub>Ar</sub>-CH<sub>3</sub>), 125.4 (ortho-C<sub>Ar</sub>-CH<sub>3</sub>), 129.4 (s, C<sub>Ar</sub>H), 161.0 (d, <sup>2</sup>J(Y-C) = 5.2 Hz, C<sub>Ar</sub>-O). IR (cm<sup>-1</sup>): 3086, 2958, 2910, 2854, 1648, 1608, 1478, 1426, 1312, 1266, 1229, 1197, 1160, 1013, 856, 828, 772, 741. EA: calculated: C 64.79, H 6.86; found: C 64.75, H 6.99.

**Cp<sub>2</sub>Lu(O(C<sub>6</sub>H<sub>2</sub>(CH<sub>3</sub>)<sub>3</sub>)(thf)**: Yield: 210 mg yellow crystals (0.42 mmol). <sup>1</sup>H NMR (C<sub>6</sub>D<sub>6</sub>, 298 K, 300 MHz):  $\delta = 1.05$  (m, 4H, THF-H<sub>i</sub>), 2.27 (s, 6H, ortho-CH<sub>3</sub>), 2.39 (s, 3H, para-CH<sub>3</sub>), 3.25 (m, 4H, THF-H<sub>ii</sub>), 6.07 (s, 10H, Cp-H), 7.04 (s, 2H, Ar-H). <sup>13</sup>C NMR (THF-d<sub>8</sub>, 300 K, 125 MHz):  $\delta = 19.0$  (s, ortho-CH<sub>3</sub>), 21.0 (s, para-CH<sub>3</sub>), 26.7 (s, THF-C<sub>i</sub>), 68.5 (s, THF-C<sub>ii</sub>), 110.9 (s, Cp-C), 124.1 (para-C<sub>Ar</sub>-CH<sub>3</sub>), 125.2 (ortho-C<sub>Ar</sub>-CH<sub>3</sub>), 129.5 (s, C<sub>Ar</sub>H), 162.5 (s, C<sub>Ar</sub>-O). IR (cm<sup>-1</sup>): 3089, 2957, 2915, 2857, 1647, 1607, 1479, 1427, 1313, 1267, 1227, 1198, 1160, 1012, 856, 831, 778, 741. EA: calculated: C 53.91, H 5.70; found: C 53.29, H 5.55.

**[Cp<sub>2</sub>Y(S<sup>t</sup>Bu)]<sub>2</sub>**: Yield: 2.92 g white powder (9.45 mmol). <sup>1</sup>H NMR (THF-d<sub>8</sub>, 300 K, 500 MHz):  $\delta = 1.41$  (s, 9H, CH<sub>3</sub>), 6.11 (s, 10H, Cp-H). <sup>13</sup>C NMR (THF-d<sub>8</sub>, 300 K, 125 MHz):  $\delta = 38.8$  (s, CH<sub>3</sub>), 43.3 (s, S-C(CH<sub>3</sub>)<sub>3</sub>), 111.4 (s, Cp-C). IR (cm<sup>-1</sup>): 3088, 2960, 2925, 2853, 1654, 1568, 1452, 1437, 1416, 1360, 1261, 1146, 1093, 1014, 793, 765. EA: calculated: C 54.55, H 6.21, S 10.40; found: C 54.89, H 6.38, S 9.84.

**[Cp<sub>2</sub>Lu(S<sup>t</sup>Bu)]<sub>2</sub>**: Yield: 1.25 g white powder (3.22 mmol). <sup>1</sup>H NMR (THF-d<sub>8</sub>, 300 K, 500 MHz):  $\delta = 1.42$  (s, 9H, CH<sub>3</sub>), 6.06 (s, 10H, Cp-H). <sup>13</sup>C NMR (THF-d<sub>8</sub>, 300 K, 125 MHz):  $\delta = 38.7$  (s, CH<sub>3</sub>), 43.5 (s, S-C(CH<sub>3</sub>)<sub>3</sub>), 110.5 (s, Cp-C). IR (cm<sup>-1</sup>): 3084, 2955, 2924, 2854, 1655, 1577, 1458, 1376, 1360, 1261, 1096, 1013, 795, 768. EA: calculated: C 42.64, H 4.86, S 8.13; found: C 42.79, H 4.93, S 7.75.

**[Cp<sub>2</sub>Tb(S<sup>t</sup>Bu)]<sub>2</sub>**: Yield: 0.45 g bright yellow powder (1.20 mmol). IR (cm<sup>-1</sup>): 3088, 2952, 2924, 2852, 1650, 1579, 1453, 1437, 1416, 1375, 1360, 1256, 1146, 1060, 1010, 806, 765. EA: calculated: C 44.45, H 5.06, S 8.48; found: C 44.21, H 4.94, S 7.95.

#### Single crystal X-ray structure determinations

**Cp<sub>2</sub>Y(DEEP)**: Crystal data: formula: C<sub>21</sub>H<sub>30</sub>O<sub>3</sub>PY; *M<sub>r</sub>* = 450.33; crystal color and shape: colorless fragment, crystal dimensions: 0.18×0.41×0.51 mm; crystal system: monoclinic; space group: *P*2<sub>1</sub>/*n* (no. 14); *a* = 11.5091(4), *b* = 8.2872(3), *c* = 22.6167(8) Å,  $\beta = 101.516(2)^\circ$ ; *V* = 2113.72(13) Å<sup>3</sup>; *Z* = 4;  $\mu(\text{MoK}\alpha) = 2.851 \text{ mm}^{-1}$ ;  $\rho_{\text{calc}} = 1.415 \text{ g cm}^{-3}$ ;  $\theta$ -range = 1.84–25.36°; data collected: 75310; independent data [*I*<sub>o</sub> > 2σ(*I*<sub>o</sub>)]/all data/*R*<sub>int</sub>]: 3531/3849/0.041; data/restraints/parameter: 3849/0/238; *R*1 [*I*<sub>o</sub> > 2σ(*I*<sub>o</sub>)]/all data]: 0.0446/0.0485; *wR*2 [*I*<sub>o</sub> > 2σ(*I*<sub>o</sub>)]/all data]: 0.1182/0.1211; GOF = 1.074;  $\Delta\rho_{\text{max/min}} = 2.98/-0.86 \text{ e}\text{\AA}^{-3}$ .

**Cp<sub>2</sub>HoCl(DEVP)**: Crystal data: formula: C<sub>16</sub>H<sub>23</sub>ClHoO<sub>3</sub>P; *M*<sub>r</sub>=494.69; crystal color and shape: colorless fragment, crystal dimensions: 0.18×0.51×0.64 mm; crystal system: orthorhombic; space group: *Pna*2<sub>1</sub> (no. 33); *a* = 20.7465(6), *b* = 11.7265(4), *c* = 7.8125(3) Å; *V* = 1900.66(11) Å<sup>3</sup>; *Z* = 4;  $\mu(\text{MoK}\alpha)$  = 4.395 mm<sup>-1</sup>;  $\rho_{\text{calc}}$  = 1.729 g cm<sup>-3</sup>;  $\theta$ -range = 1.96–25.42°; data collected: 51428; independent data [*L*<sub>o</sub>>2 $\sigma$ (*L*<sub>o</sub>)/all data/*R*<sub>int</sub>]: 3484/3487/0.044; data/restraints/parameter: 3487/1/202; *R*<sub>1</sub> [*L*<sub>o</sub>>2 $\sigma$ (*L*<sub>o</sub>)/all data]: 0.0144/0.0145; *wR*<sub>2</sub> [*L*<sub>o</sub>>2 $\sigma$ (*L*<sub>o</sub>)/all data]: 0.0369/0.0369; GOF=1.197;  $\Delta\rho_{\text{max/min}}$ : 0.91/-0.73 eÅ<sup>-3</sup>.

**Cp<sub>2</sub>YbCl(DEVP)**: Crystal data: formula: C<sub>16</sub>H<sub>23</sub>ClO<sub>3</sub>PYb; *M*<sub>r</sub>=502.80; crystal color and shape: colorless fragment, crystal dimensions: 0.18×0.51×0.53 mm; crystal system: orthorhombic; space group: *Pna*2<sub>1</sub> (no. 33); *a* = 20.7504(7), *b* = 11.7361(4), *c* = 7.8075(3) Å; *V* = 1901.35(12) Å<sup>3</sup>; *Z* = 4;  $\mu(\text{MoK}\alpha)$  = 5.151 mm<sup>-1</sup>;  $\rho_{\text{calc}}$  = 1.757 g cm<sup>-3</sup>;  $\theta$ -range = 1.96–25.36°; data collected: 46215; independent data [*L*<sub>o</sub>>2 $\sigma$ (*L*<sub>o</sub>)/all data/*R*<sub>int</sub>]: 3449/3461/0.053; data/restraints/parameter: 3461/1/201; *R*<sub>1</sub> [*L*<sub>o</sub>>2 $\sigma$ (*L*<sub>o</sub>)/all data]: 0.0142/0.0143; *wR*<sub>2</sub> [*L*<sub>o</sub>>2 $\sigma$ (*L*<sub>o</sub>)/all data]: 0.0373/0.0374; GOF=1.088;  $\Delta\rho_{\text{max/min}}$ : 0.70/-0.55 eÅ<sup>-3</sup>.

For detailed information, see Supporting Information. CCDC 930675 (**Cp<sub>3</sub>Y(DEEP)**), 930674 (**Cp<sub>2</sub>HoCl(DEVP)**) and 930673 (**Cp<sub>2</sub>YbCl(DEVP)**) contains the supplementary crystallographic data for this compound. This data can be obtained free of charge from The Cambridge Crystallographic Data Centre via [www.ccdc.cam.ac.uk/data\\_request/cif](http://www.ccdc.cam.ac.uk/data_request/cif) or via [https://www.ccdc.cam.ac.uk/services/structure\\_deposit/](https://www.ccdc.cam.ac.uk/services/structure_deposit/).

### Oligomerization

5 eq of DEVP are added to 1 eq of catalyst in toluene. The resulting mixture is stirred for 2 hours at room temperature and quenched by addition of MeOH or acidified (37w% HCl<sub>aq</sub>) MeOH. Volatiles were removed under reduced pressure and the residue was extracted with MeOH. For end group analysis, ESI-MS measurements of the methanolic extract were performed.

### Coordination of DEEP

To a solution/suspension of 1 eq of Cp<sub>2</sub>LnX or Cp<sub>3</sub>Ln in C<sub>6</sub>D<sub>6</sub> 0.5, 1, 2 or 5 eq of a stem solution of DEEP in C<sub>6</sub>D<sub>6</sub> are added, respectively. The resulting mixture is transferred into an NMR tube. <sup>1</sup>H NMR spectroscopic shifts of the formed adducts (signals of Cp and X) are determined for addition of 5 eq of DEEP. <sup>1</sup>H and <sup>31</sup>P NMR spectroscopic shifts of coordinated DEEP for addition of 0.5 eq of DEEP, respectively. The extent of disproportionation (Table 2) is determined from the integral ratio of the <sup>1</sup>H NMR spectroscopic signals of the cyclopentadienyl protons of formed Cp<sub>3</sub>Ln(DEEP) and Cp<sub>2</sub>LnX(DEEP) for addition of 5 eq of DEEP.

**Cp<sub>3</sub>Y(DEEP)**: <sup>1</sup>H NMR (C<sub>6</sub>D<sub>6</sub>, 298 K, 300 MHz):  $\delta$  = 0.78 (dt, 3H, <sup>3</sup>J(P-H) = 20.8 Hz, <sup>3</sup>J(H-H) = 7.7 Hz, P-CH<sub>2</sub>-CH<sub>3</sub>), 0.92 (t, 6H, <sup>3</sup>J(H-H) = 7.1 Hz, P-O-CH<sub>2</sub>-CH<sub>3</sub>), 1.22 (dq, 2H, <sup>2</sup>J(P-H) = 17.6 Hz, <sup>3</sup>J(H-H) = 7.7 Hz, P-CH<sub>2</sub>-CH<sub>3</sub>), 3.68 (m, 4H, P-O-CH<sub>2</sub>-CH<sub>3</sub>), 6.07 (s, 15H, Cp-H). <sup>31</sup>P NMR (C<sub>6</sub>D<sub>6</sub>, 298 K, 121 MHz):  $\delta$  = 35.3 (d, <sup>2</sup>J(Y-P) = 10.4 Hz).

**Cp<sub>3</sub>Lu(DEEP)**: <sup>1</sup>H NMR (C<sub>6</sub>D<sub>6</sub>, 298 K, 300 MHz):  $\delta$  = 0.77 (dt, 3H, <sup>3</sup>J(P-H) = 20.8 Hz, <sup>3</sup>J(H-H) = 7.5 Hz, P-CH<sub>2</sub>-CH<sub>3</sub>), 0.91 (t, 6H, <sup>3</sup>J(H-H) = 7.0 Hz, P-O-CH<sub>2</sub>-CH<sub>3</sub>), 1.23 (dq, 2H, <sup>2</sup>J(P-H) = 17.9 Hz, <sup>3</sup>J(H-H) = 7.7 Hz, P-CH<sub>2</sub>-CH<sub>3</sub>), 3.69 (m, 4H, P-O-CH<sub>2</sub>-CH<sub>3</sub>), 6.05 (s, 15H, Cp-H). <sup>31</sup>P NMR (C<sub>6</sub>D<sub>6</sub>, 298 K, 121 MHz):  $\delta$  = 35.8 (s).

**Cp<sub>2</sub>YCl(DEEP)**: <sup>1</sup>H NMR (C<sub>6</sub>D<sub>6</sub>, 298 K, 300 MHz):  $\delta$  = 0.72 (dt, 3H, <sup>3</sup>J(P-H) = 21.1 Hz, <sup>3</sup>J(H-H) = 7.6 Hz, P-CH<sub>2</sub>-CH<sub>3</sub>), 0.90 (t, 6H, <sup>3</sup>J(H-H) = 7.1 Hz, P-O-CH<sub>2</sub>-CH<sub>3</sub>), 1.27 (dq, 2H, <sup>2</sup>J(P-H) = 18.3 Hz, <sup>3</sup>J(H-H) = 7.6 Hz, P-CH<sub>2</sub>-CH<sub>3</sub>), 3.74 (m, 4H, P-O-CH<sub>2</sub>-CH<sub>3</sub>), 6.33 (s, 10H, Cp-H). <sup>31</sup>P NMR (C<sub>6</sub>D<sub>6</sub>, 298 K, 121 MHz):  $\delta$  = 36.0 (s).

**Cp<sub>2</sub>LuCl(DEEP)**: <sup>1</sup>H NMR (C<sub>6</sub>D<sub>6</sub>, 298 K, 300 MHz):  $\delta$  = 0.70 (dt, 3H, <sup>3</sup>J(P-H) = 21.2 Hz, <sup>3</sup>J(H-H) = 7.7 Hz, P-CH<sub>2</sub>-CH<sub>3</sub>), 0.89 (t, 6H, <sup>3</sup>J(H-H) = 7.1 Hz, P-O-CH<sub>2</sub>-CH<sub>3</sub>), 1.27 (dq, 2H, <sup>2</sup>J(P-H) = 18.3 Hz, <sup>3</sup>J(H-H) = 7.7 Hz, P-CH<sub>2</sub>-CH<sub>3</sub>), 3.75 (m, 4H, P-O-CH<sub>2</sub>-CH<sub>3</sub>), 6.28 (s, 10H, Cp-H). <sup>31</sup>P NMR (C<sub>6</sub>D<sub>6</sub>, 298 K, 121 MHz):  $\delta$  = 36.7 (s).

**Cp<sub>2</sub>Y(bdsa)(DEEP)**: <sup>1</sup>H NMR (C<sub>6</sub>D<sub>6</sub>, 298 K, 300 MHz):  $\delta$  = 0.42 (d, 12H, <sup>3</sup>J(H-H) = 3.0 Hz, Si-CH<sub>3</sub>), 0.76 (dt, 3H, <sup>3</sup>J(P-H) = 20.9 Hz, <sup>3</sup>J(H-H) = 7.6 Hz, P-CH<sub>2</sub>-CH<sub>3</sub>), 0.89 (t, 6H, <sup>3</sup>J(H-H) = 7.1 Hz, P-O-CH<sub>2</sub>-CH<sub>3</sub>), 1.34 (dq, 2H, <sup>2</sup>J(P-H) = 18.1 Hz, <sup>3</sup>J(H-H) = 7.7 Hz, P-CH<sub>2</sub>-CH<sub>3</sub>), 3.72 (m, 4H, P-O-CH<sub>2</sub>-CH<sub>3</sub>), 4.60 (m, 2H, Si-H), 6.28 (s, 10H, Cp-H). <sup>31</sup>P NMR (C<sub>6</sub>D<sub>6</sub>, 298 K, 121 MHz):  $\delta$  = 33.8 (d, <sup>2</sup>J(Y-P) = 11.2 Hz).

**Cp<sub>2</sub>Lu(bdsa)(DEEP)**: <sup>1</sup>H NMR (C<sub>6</sub>D<sub>6</sub>, 298 K, 300 MHz):  $\delta$  = 0.45 (d, 12H, <sup>3</sup>J(H-H) = 2.9 Hz, Si-CH<sub>3</sub>), 0.74 (dt, 3H, <sup>3</sup>J(P-H) = 21.0 Hz, <sup>3</sup>J(H-H) = 7.6 Hz, P-CH<sub>2</sub>-CH<sub>3</sub>), 0.88 (t, 6H, <sup>3</sup>J(H-H) = 7.1 Hz, P-O-CH<sub>2</sub>-CH<sub>3</sub>), 1.33 (dq, 2H, <sup>2</sup>J(P-H) = 18.1 Hz, <sup>3</sup>J(H-H) = 7.6 Hz, P-CH<sub>2</sub>-CH<sub>3</sub>), 3.71 (m, 4H, P-O-CH<sub>2</sub>-CH<sub>3</sub>), 4.66 (m, 2H, Si-H), 6.26 (s, 10H, Cp-H). <sup>31</sup>P NMR (C<sub>6</sub>D<sub>6</sub>, 298 K, 121 MHz):  $\delta$  = 34.8 (s).

**Cp<sub>2</sub>Y(CH<sub>2</sub>TMS)(DEEP)**: <sup>1</sup>H NMR (C<sub>6</sub>D<sub>6</sub>, 300 K, 500 MHz):  $\delta$  = -0.62 (d, 2H, <sup>2</sup>J(Y-H) = 3.4 Hz, Si-CH<sub>2</sub>), 0.48 (s, 9H, Si-CH<sub>3</sub>), 0.63 (dt, 3H, <sup>3</sup>J(P-H) = 21.0 Hz, <sup>3</sup>J(H-H) = 7.7 Hz, P-CH<sub>2</sub>-CH<sub>3</sub>), 0.81 (t, 6H, <sup>3</sup>J(H-H) = 7.1 Hz, P-O-CH<sub>2</sub>-CH<sub>3</sub>), 1.07 (dq, 2H, <sup>2</sup>J(P-H) = 18.1 Hz, <sup>3</sup>J(H-H) = 7.7 Hz, P-CH<sub>2</sub>-CH<sub>3</sub>), 3.51 (m, 4H, P-O-CH<sub>2</sub>-CH<sub>3</sub>), 6.28 (s, 10H, Cp-H). <sup>31</sup>P NMR (C<sub>6</sub>D<sub>6</sub>, 300 K, 202 MHz):  $\delta$  = 34.7 (d, <sup>2</sup>J(Y-P) = 11.0 Hz).

**Cp<sub>2</sub>Lu(CH<sub>2</sub>TMS)(DEEP)**: <sup>1</sup>H NMR (C<sub>6</sub>D<sub>6</sub>, 300 K, 500 MHz):  $\delta$  = -0.72 (s, 2H, Si-CH<sub>2</sub>), 0.50 (s, 9H, Si-CH<sub>3</sub>), 0.63 (dt, 3H, <sup>3</sup>J(P-H) = 21.1 Hz, <sup>3</sup>J(H-H) = 7.6 Hz, P-CH<sub>2</sub>-CH<sub>3</sub>), 0.80 (t, 6H, <sup>3</sup>J(H-H) = 7.1 Hz, P-O-CH<sub>2</sub>-CH<sub>3</sub>), 1.07 (dq, 2H, <sup>2</sup>J(P-H) = 18.1 Hz, <sup>3</sup>J(H-H) = 7.6 Hz, P-CH<sub>2</sub>-CH<sub>3</sub>), 3.51 (m, 4H, P-O-CH<sub>2</sub>-CH<sub>3</sub>), 6.23 (s, 10H, Cp-H). <sup>31</sup>P NMR (C<sub>6</sub>D<sub>6</sub>, 300 K, 202 MHz):  $\delta$  = 35.5 (s).

**Cp<sub>2</sub>Y(O<sup>i</sup>Pr)(DEEP)**: <sup>1</sup>H NMR (C<sub>6</sub>D<sub>6</sub>, 300 K, 500 MHz):  $\delta$  = 1.28 (d, 6H, <sup>3</sup>J(H-H) = 5.9 Hz, CH<sub>3</sub>), 4.28 (m, 1H, O-CH(CH<sub>3</sub>)<sub>2</sub>), 6.32 (s, 10H, Cp-H). Due to incomplete reaction of DEEP with [Cp<sub>2</sub>Y(O<sup>i</sup>Pr)]<sub>2</sub> and exchange of free and coordinated DEEP, <sup>1</sup>H and <sup>31</sup>P NMR spectroscopic signals of coordinated DEEP could not be determined.

For addition of DEEP to [Cp<sub>2</sub>Lu(O<sup>i</sup>Pr)]<sub>2</sub>, no reaction was observed.

**Cp<sub>2</sub>Y(O(C<sub>6</sub>H<sub>2</sub>(CH<sub>3</sub>)<sub>3</sub>)(DEEP)**: <sup>1</sup>H NMR (C<sub>6</sub>D<sub>6</sub>, 300 K, 500 MHz):  $\delta$  = 0.71 (dt, 3H, <sup>3</sup>J(P-H) = 21.0 Hz, <sup>3</sup>J(H-H) = 7.6 Hz, P-

CH<sub>2</sub>-CH<sub>3</sub>), 0.82 (t, 6H, <sup>3</sup>J(H-H) = 7.1 Hz, P-O-CH<sub>2</sub>-CH<sub>3</sub>), 1.18 (dq, 2H, <sup>2</sup>J(P-H) = 17.9 Hz, <sup>3</sup>J(H-H) = 7.6 Hz, P-CH<sub>2</sub>-CH<sub>3</sub>), 2.39 (s, 6H, ortho-CH<sub>3</sub>), 2.41 (s, 3H, para-CH<sub>3</sub>), 3.61 (m, 4H, P-O-CH<sub>2</sub>-CH<sub>3</sub>), 6.28 (s, 10H, Cp-H), 7.07 (s, 2H, Ar-H). <sup>31</sup>P NMR (C<sub>6</sub>D<sub>6</sub>, 300 K, 202 MHz): δ = 35.2 (d, <sup>2</sup>J(Y-P) = 8.1 Hz).

**Cp<sub>2</sub>Lu(O(C<sub>6</sub>H<sub>4</sub>(CH<sub>3</sub>)<sub>2</sub>)(DEEP):** <sup>1</sup>H NMR (C<sub>6</sub>D<sub>6</sub>, 300 K, 500 MHz): δ = 0.73 (dt, 3H, <sup>3</sup>J(P-H) = 20.9 Hz, <sup>3</sup>J(H-H) = 7.6 Hz, P-CH<sub>2</sub>-CH<sub>3</sub>), 0.84 (t, 6H, <sup>3</sup>J(H-H) = 7.1 Hz, P-O-CH<sub>2</sub>-CH<sub>3</sub>), 1.22 (dq, 2H, <sup>2</sup>J(P-H) = 17.9 Hz, <sup>3</sup>J(H-H) = 7.6 Hz, P-CH<sub>2</sub>-CH<sub>3</sub>), 2.39 (s, 6H, ortho-CH<sub>3</sub>), 2.43 (s, 3H, para-CH<sub>3</sub>), 3.65 (m, 4H, P-O-CH<sub>2</sub>-CH<sub>3</sub>), 6.23 (s, 10H, Cp-H), 7.09 (s, 2H, Ar-H). <sup>31</sup>P NMR (C<sub>6</sub>D<sub>6</sub>, 300 K, 202 MHz): δ = 35.9 (s).

**Cp<sub>2</sub>Y(S<sup>t</sup>Bu)(DEEP):** <sup>1</sup>H NMR (C<sub>6</sub>D<sub>6</sub>, 300 K, 500 MHz): δ = 0.74 (dt, 3H, <sup>3</sup>J(P-H) = 20.9 Hz, <sup>3</sup>J(H-H) = 7.7 Hz, P-CH<sub>2</sub>-CH<sub>3</sub>), 0.90 (t, 6H, <sup>3</sup>J(H-H) = 7.1 Hz, P-O-CH<sub>2</sub>-CH<sub>3</sub>), 1.29 (dq, 2H, <sup>2</sup>J(P-H) = 18.1 Hz, <sup>3</sup>J(H-H) = 7.7 Hz, P-CH<sub>2</sub>-CH<sub>3</sub>), 1.81 (s, 9H, CH<sub>3</sub>), 3.77 (m, 4H, P-O-CH<sub>2</sub>-CH<sub>3</sub>), 6.33 (s, 10H, Cp-H). <sup>31</sup>P NMR (C<sub>6</sub>D<sub>6</sub>, 300 K, 202 MHz): δ = 35.1 (s).

**Cp<sub>2</sub>Lu(S<sup>t</sup>Bu)(DEEP):** <sup>1</sup>H NMR (C<sub>6</sub>D<sub>6</sub>, 300 K, 500 MHz): δ = 0.73 (dt, 3H, <sup>3</sup>J(P-H) = 21.1 Hz, <sup>3</sup>J(H-H) = 7.6 Hz, P-CH<sub>2</sub>-CH<sub>3</sub>), 0.89 (t, 6H, <sup>3</sup>J(H-H) = 7.1 Hz, P-O-CH<sub>2</sub>-CH<sub>3</sub>), 1.28 (dq, 2H, <sup>2</sup>J(P-H) = 18.1 Hz, <sup>3</sup>J(H-H) = 7.7 Hz, P-CH<sub>2</sub>-CH<sub>3</sub>), 1.79 (s, 9H, CH<sub>3</sub>), 3.77 (m, 4H, P-O-CH<sub>2</sub>-CH<sub>3</sub>), 6.28 (s, 10H, Cp-H). <sup>31</sup>P NMR (C<sub>6</sub>D<sub>6</sub>, 300 K, 202 MHz): δ = 36.0 (s).

#### Activity measurements and kinetic analysis

For activity measurements, the stated amount of catalyst (15–50 μmol) is dissolved/suspended in 20 mL of toluene, and the reaction mixture is thermostated to the desired temperature. Then, the stated amount of monomer (3.5–13 mmol) is added. During the course of the measurement, the temperature is monitored with a digital thermometer and aliquots (0.5 mL) are taken and quenched by addition to deuterated methanol (0.2 mL). After the stated reaction time, the reaction was quenched by addition of MeOD (0.5 mL). The reaction is carried out in an MBraun Glovebox under argon atmosphere to take aliquots every 6–10 seconds at the beginning of the measurement. For each aliquot, the conversion is determined by <sup>31</sup>P NMR spectroscopy, the molecular weight of the formed polymer by GPC-MALS analysis.

For kinetic analysis, the maximum rate is determined from the maximum slope of the conversion-reaction time plot.  $F^*_t$  is defined as the given initiator efficiency at the inflection point of the conversion-reaction time plot. In case an aliquot was taken at or sufficiently close to the inflection point, the initiator efficiency determined for this aliquot is used as  $F^*_t$ ; if this is not the case,  $F^*_t$  is determined as the average of the initiator efficiencies of the aliquots taken directly before and after this inflection point. The conversion used for calculation of the residual monomer concentration is determined accordingly. Error bars are calculated from the following uncertainties: Δ[Cat]<sub>0</sub> = 0.1 mg, Δ[Mon]<sub>0</sub> = 0.05 mL (in case of DEVP) or 0.05 g (in case of DIVP), ΔC = 3%, ΔT = 2 K, and a 5% relative uncertainty for the determination of the maximum slope and  $F^*_t$ .

#### Molecular weight determination

GPC was carried out on a Varian LC-920 equipped with two analytical PL Polargel M columns. As eluent, a mixture of 50% THF, 50% water, and 9 g L<sup>-1</sup> tetrabutylammonium bromide (TBAB) was used in the case of PDEVPP; for PDIVP analysis, the eluent was THF with 6 g L<sup>-1</sup> TBAB. Absolute molecular weights have been determined online by multiangle light scattering (MALS) analysis using a Wyatt Dawn Heleos II in combination with a Wyatt Optilab rEX as concentration source.

#### ASSOCIATED CONTENT

ESI MS analysis of DAVP oligomers, detailed information for single crystal X-ray structure determination, obtained data from activity measurements and kinetic analysis. This material is available free of charge via the Internet at <http://pubs.acs.org>.

#### AUTHOR INFORMATION

##### Corresponding Author

\* rieger@tum.de

#### ACKNOWLEDGMENT

The authors thank Dr. Sergej Vagin, Dr. Ning Zhang, Markus Hammann and Dominik Lanzinger for valuable discussions. S.S. is grateful for a generous scholarship from the Fonds der Chemischen Industrie.

#### REFERENCES

- (1) Ellis, J.; Wilson, A. D. *Dent. Mater.* **1992**, *8*, 79.
- (2) Ebdon, J. R.; Price, D.; Hunt, B. J.; P. Joseph, Gao, F.; Milnes, G. J.; Cunliffe, L. K. *Polym. Degrad. Stab.* **2000**, *69*, 267.
- (3) Greish, Y. E.; Brown, P. W. *Biomaterials* **2001**, *22*, 807.
- (4) Gemeinhart, R. A.; Bare, C. M.; Haasch, R. T.; Gemeinhart, E. J. *J. Biomed. Mater. Res., Part A* **2006**, *78A*, 433.
- (5) Bock, T.; Möhwald, H.; Mühlhaupt, R. *Macromol. Chem. Phys.* **2007**, *208*, 1324.
- (6) Steininger, H.; Schuster, M.; Kreuer, K. D.; Kaltbeitzel, A.; Bingöel, B.; Meyer, W. H.; Schauf, S.; Brunklaus, G.; Maier, J.; Spiess, H. W. *Phys. Chem. Chem. Phys.* **2007**, *9*, 1764.
- (7) Parvole, J.; Jannasch, P. *Macromolecules* **2008**, *41*, 3893.
- (8) Macarie, L.; Ilia, G. *Prog. Polym. Sci.* **2010**, *35*, 1078.
- (9) Atanasov, V.; Kerres, J. *Macromolecules* **2011**, *44*, 6416.
- (10) Monge, S.; Canniccioni, B.; Graillot, A.; Robin, J. *Biomacromolecules* **2011**, *12*, 1973.
- (11) Salzinger, S.; Rieger, B. *Macromol. Rapid Commun.* **2012**, *33*, 1327.
- (12) Seemann, U. B.; Dengler, J. E.; Rieger, B. *Angew. Chem., Int. Ed.* **2010**, *49*, 3489.
- (13) Rabe, G. W.; Komber, H.; Haeussler, L.; Kreger, K.; Lattermann, G. *Macromolecules* **2010**, *43*, 1178.
- (14) Salzinger, S.; Seemann, U. B.; Plikhta, A.; Rieger, B. *Macromolecules* **2011**, *44*, 5920.
- (15) Zhang, N.; Salzinger, S.; Deubel, F.; Jordan, R.; Rieger, B. *J. Am. Chem. Soc.* **2012**, *134*, 7333.
- (16) Zhang, N.; Salzinger, S.; Rieger, B. *Macromolecules* **2012**, *45*, 9751.
- (17) Yasuda, H.; Yamamoto, H.; Yokota, K.; Miyake, S.; Nakamura, A. *J. Am. Chem. Soc.* **1992**, *114*, 4908.
- (18) Chen, E. Y.-X. *Chem. Rev.* **2009**, *109*, 5157.
- (19) Yasuda, H.; Ihara, E. *Macromol. Chem. Phys.* **1995**, *196*, 2417.
- (20) Yasuda, H.; Ihara, E. *Adv. Polym. Sci.* **1997**, *133*, 53.
- (21) Yasuda, H. *Prog. Polym. Sci.* **2000**, *25*, 573.
- (22) Boffa, L. S.; Novak, B. M. *Macromolecules* **1994**, *27*, 6993.

- (23) Yasuda, H.; Yamamoto, H.; Yamashita, M.; Yokota, K.; Nakamura, A.; Miyake, S.; Kai, Y.; Kanehisa, N. *Macromolecules* **1993**, *26*, 7134.
- (24) Collins, S.; Ward, D. G. *J. Am. Chem. Soc.* **1992**, *114*, 5460.
- (25) Collins, S.; Ward, D. G.; Suddaby, K. H. *Macromolecules* **1994**, *27*, 7222.
- (26) Li, Y.; Ward, D. G.; Reddy, S. S.; Collins, S. *Macromolecules* **1997**, *30*, 1875.
- (27) Sustmann, R.; Sicking, W.; Bandermann, F.; Ferenz, M. *Macromolecules* **1999**, *32*, 4204.
- (28) Tomasi, S.; Weiss, H.; Ziegler, T. *Organometallics* **2006**, *25*, 3619.
- (29) Giardello, M. A.; Yamamoto, Y.; Brard, L.; Marks, T. J. *J. Am. Chem. Soc.* **1995**, *117*, 3276.
- (30) Nguyen, H.; Jarvis, A. P.; Lesley, M. J. G.; Kelly, W. M.; Reddy, S. S.; Taylor, N. J.; Collins, S. *Macromolecules* **2000**, *33*, 1508.
- (31) Cameron, P. A.; Gibson, V. C.; Graham, A. J. *Macromolecules* **2000**, *33*, 4329.
- (32) Hölscher, M.; Keul, H.; Höcker, H. *Macromolecules* **2002**, *35*, 8194.
- (33) Rodriguez-Delgado, A.; Mariott, W. R. ; Chen, E. Y.-X. *Macromolecules* **2004**, *37*, 3092.
- (34) Ning, Y.; Cooney, M. J.; Chen, E. Y.-X. *J. Organomet. Chem.* **2005**, *690*, 6263.
- (35) Rodriguez-Delgado, A.; Mariott, W. R. ; Chen, E. Y.-X. *J. Organomet. Chem.* **2006**, *691*, 3490.
- (36) Ning, Y.; Caporaso, L.; Correa, A.; Gustafson, L. O.; Cavallo, L.; Chen, E. Y.-X. *Macromolecules* **2008**, *41*, 6910.
- (37) Frauenrath, H.; Keul, H.; Höcker, H. *Macromolecules* **2001**, *34*, 14.
- (38) Hölscher, M.; Keul, H.; Höcker, H. *Chem. Eur. J.* **2001**, *7*, 5419.
- (39) Caporaso, L.; Cavallo, L. *Macromolecules* **2008**, *41*, 3439.
- (40) Zhang, Y.; Ning, Y.; Caporaso, L.; Cavallo, L.; Chen, E. Y.-X. *J. Am. Chem. Soc.* **2010**, *132*, 2695.
- (41) Rodriguez-Delgado, A.; Chen, E. Y.-X. *Macromolecules* **2005**, *38*, 2587.
- (42) Ning, Y.; Chen, E. Y.-X. *J. Am. Chem. Soc.* **2008**, *130*, 2463.
- (43) Zhang, N.; Salzinger, S.; Soller, B. S.; Rieger, B. *J. Am. Chem. Soc.*, submitted.
- (44) Kaneko, H.; Nagae, H.; Tsurugi, H.; Mashima, K. *J. Am. Chem. Soc.* **2011**, *133*, 19626.
- (45) Ihara, E.; Morimoto, M.; Yasuda, H. *Macromolecules* **1995**, *28*, 7886.
- (46) Seemann, U. B. *PhD Thesis*, Technische Universität München, Garching bei München, October **2010**.
- (47) Qian, Y.; Bala, M. D.; Yousaf, M.; Zhang, H. Huang, J.; Sun, J.; Liang, C. *J. Organomet. Chem.* **2002**, *188*, 1.
- (48) Observation of lower molecular weight fragments with  $m/z = n \times M_{\text{Mon}} + M_{\text{Na}}$  has been previously observed for initiation with  $\text{Cp}_3\text{Ln}$ , and can be attributed to chain scission during ESI MS analysis as these fragments are not observed for analysis by MALDI-ToF MS.
- (49) Leute, M. *PhD Thesis*, Universität Ulm, **2007**.
- (50) Dengler, J. E. *Diploma Thesis*, Technische Universität München, Garching bei München, August **2007**.
- (51) Demir, S.; Mueller, T. J.; Ziller, J. W.; Evans, W. J. *Angew. Chem., Int. Ed.* **2011**, *50*, 515.
- (52) Hollemann, A.F.; Wiberg, E.; Wiberg, N.; Eds. *Lehrbuch der Anorganischen Chemie*; Walter de Gruyter & Co, Berlin **2007**.
- (53) Birmingham, J. M.; Wilkinson, G. *J. Am. Chem. Soc.* **1956**, *78*, 42.
- (54) Maginn, R. E.; Manastyrskij, S.; Dubeck, M. *J. Am. Chem. Soc.* **1963**, *85*, 672.
- (55) Evans, W. J.; Dominguez, R.; Hanusa, T. P. *Organometallics* **1986**, *5*, 263.
- (56) Tilley, T. D.; Andersen, A. R. *Inorg. Chem.* **1981**, *20*, 3267.
- (57) Panda, T. K.; Gamer, M. T.; Roesky, P. W. *Organometallics* **2003**, *22*, 877.
- (58) Eppinger, J. *PhD Thesis*, Technische Universität München, Garching bei München, May **1999**.
- (59) Hultsch, K. C.; Voth, P.; Beckerle, K.; Spaniol, T. P.; Okuda, J. *Organometallics* **2000**, *19*, 228.



## Supporting Information:

# Mechanistic Studies on Initiation and Propagation of Rare Earth Metal-Mediated Group Transfer Polymerization of Vinylphosphonates

Stephan Salzinger, Benedikt S. Soller, Andriy Plikhta, Uwe B. Seemann, Eberhardt Herdtweck, Bernhard Rieger\*

WACKER-Lehrstuhl für Makromolekulare Chemie, Technische Universität München,  
Lichtenbergstraße 4, 85748 Garching

### Oligomerization Experiments

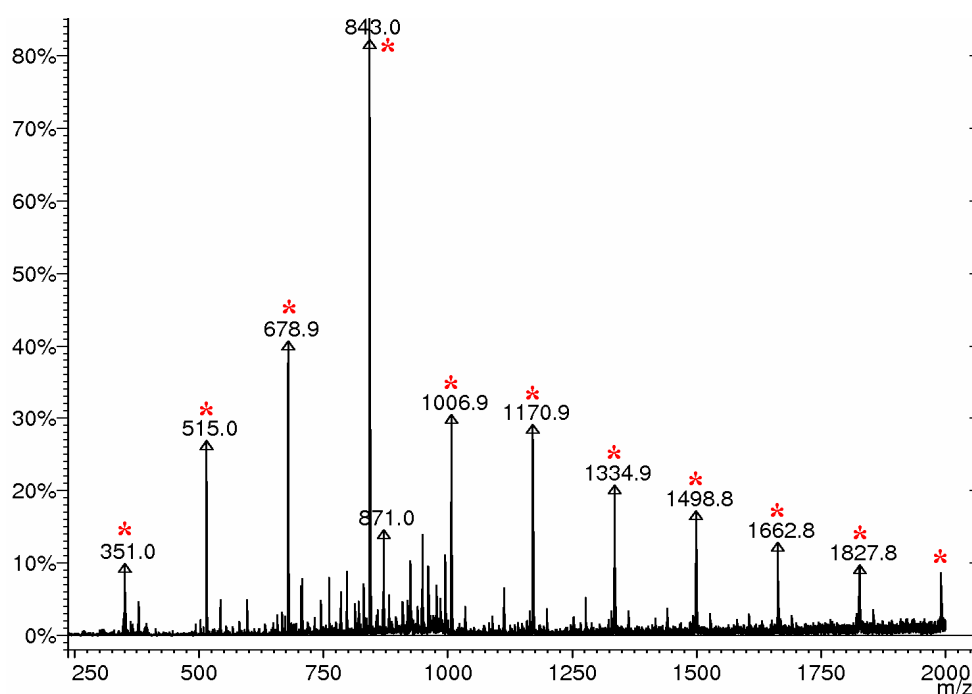


**Figure S1.** ESI MS spectrum of DEVP oligomers produced with  $[\text{Cp}_2\text{YbMe}]_2$ . One major series of peaks is evident:  $m/z = n \times M_{\text{Mon}} + M_{\text{Na}}$  (red);  $M_{\text{Mon}} = 164$ , no apparent end group.

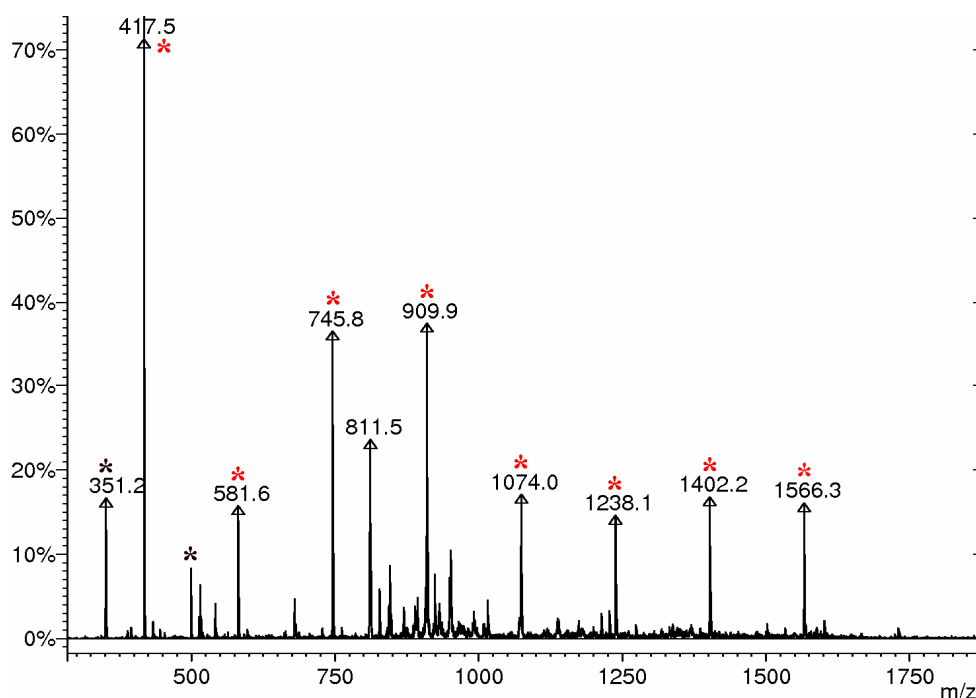


**Figure S2.** ESI MS spectrum of DEVP oligomers produced with  $[\text{Cp}_2\text{YCl}]_2$ . One major series of peaks is evident:  $m/z = n \times M_{\text{Mon}} + 66 + M_{\text{Na}}$  (red);  $M_{\text{Mon}} = 164$ , end groups:  $M_{\text{Cp}} + M_{\text{H}} = 66$ . Peaks at  $m/z = 351$  and  $515$  are attributed to fragmentation (black).

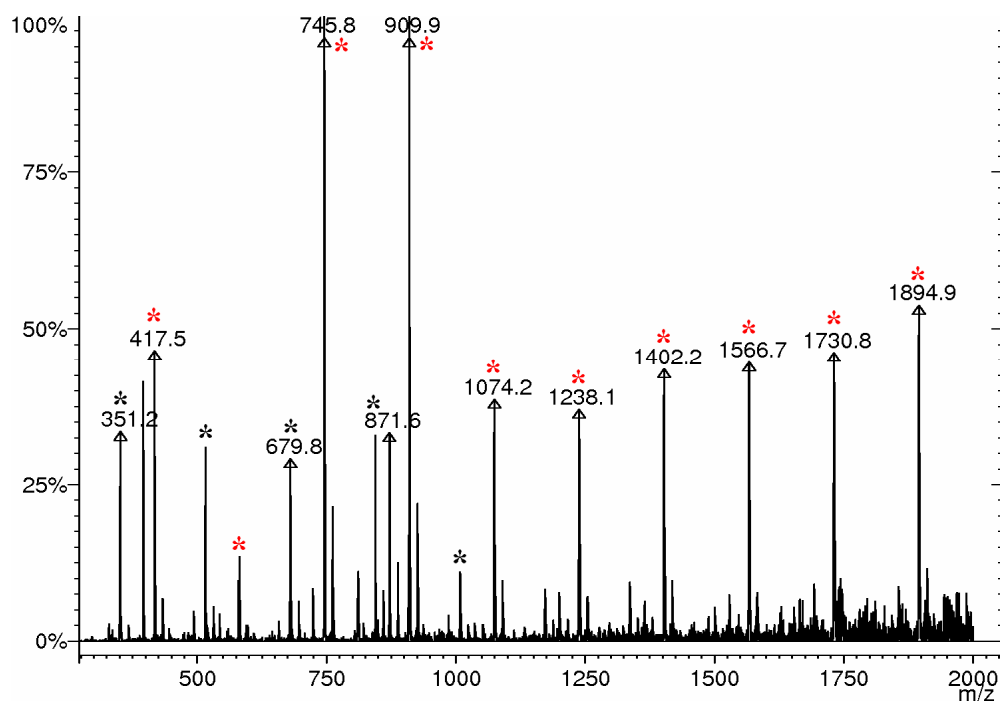


**Figure S3.** ESI MS spectrum of DEVP oligomers produced with  $[\text{Cp}_2\text{LuCl}]_2$ . One major series of peaks is evident:  $m/z = n \times M_{\text{Mon}} + 66 + M_{\text{Na}}$  (red);  $M_{\text{Mon}} = 164$ , end groups:  $M_{\text{Cp}} + M_{\text{H}} = 66$ . Peaks at  $m/z = 351, 515, 679, 843$  and  $1007$  are attributed to fragmentation (black).

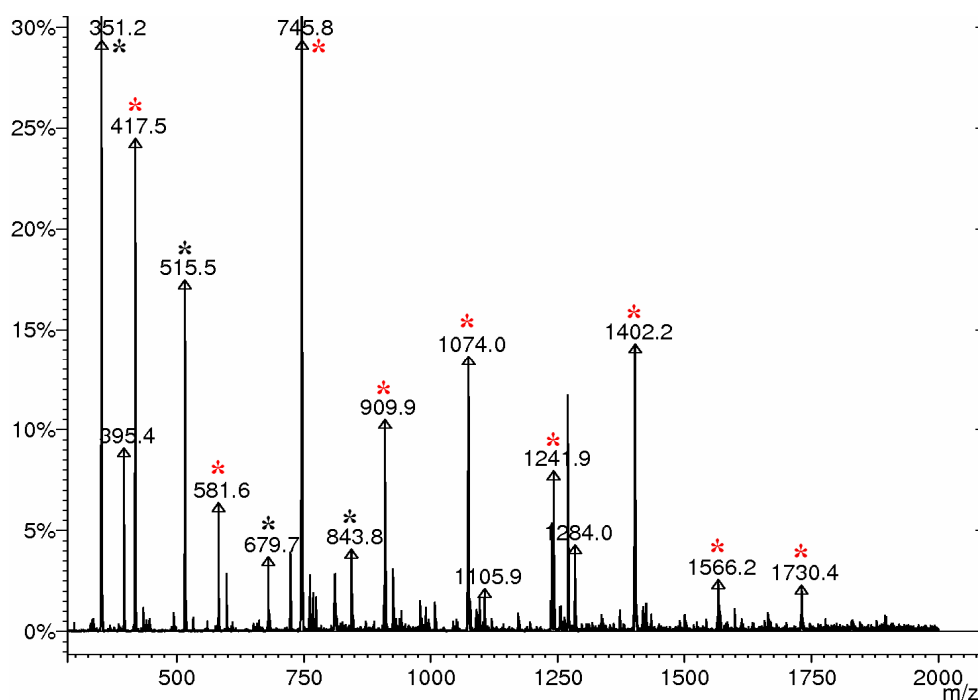


**Figure S4.** ESI MS spectrum of DEVP oligomers produced with  $\text{Cp}_2\text{Lu}(\text{bdsa})(\text{thf})$ . One major series of peaks is evident:  $m/z = n \times M_{\text{Mon}} + 66 + M_{\text{Na}}$  (red);  $M_{\text{Mon}} = 164$ , end groups:  $M_{\text{Cp}} + M_{\text{H}} = 66$ . Peaks at  $m/z = 351, 515, 679$  and  $843$  are attributed to fragmentation (black).

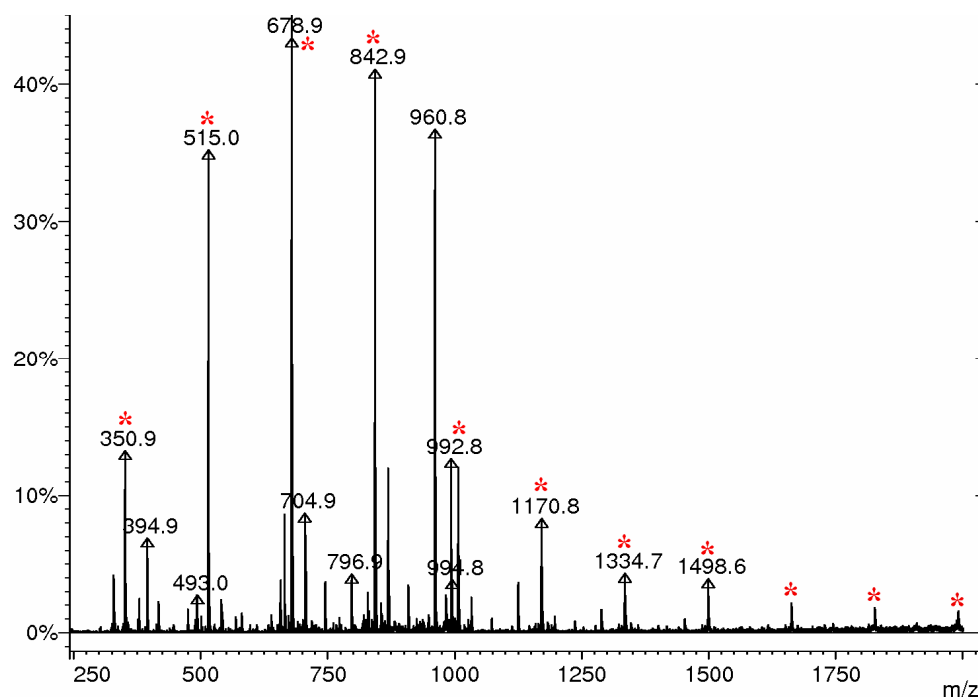


**Figure S5.** ESI MS spectrum of DEVP oligomers produced with  $\text{Cp}_2\text{Lu}(\text{bdsa})(\text{thf})$ . One major series of peaks is evident:  $m/z = n \times M_{\text{Mon}} + M_{\text{Na}}$  (red);  $M_{\text{Mon}} = 164$ , no apparent end groups.

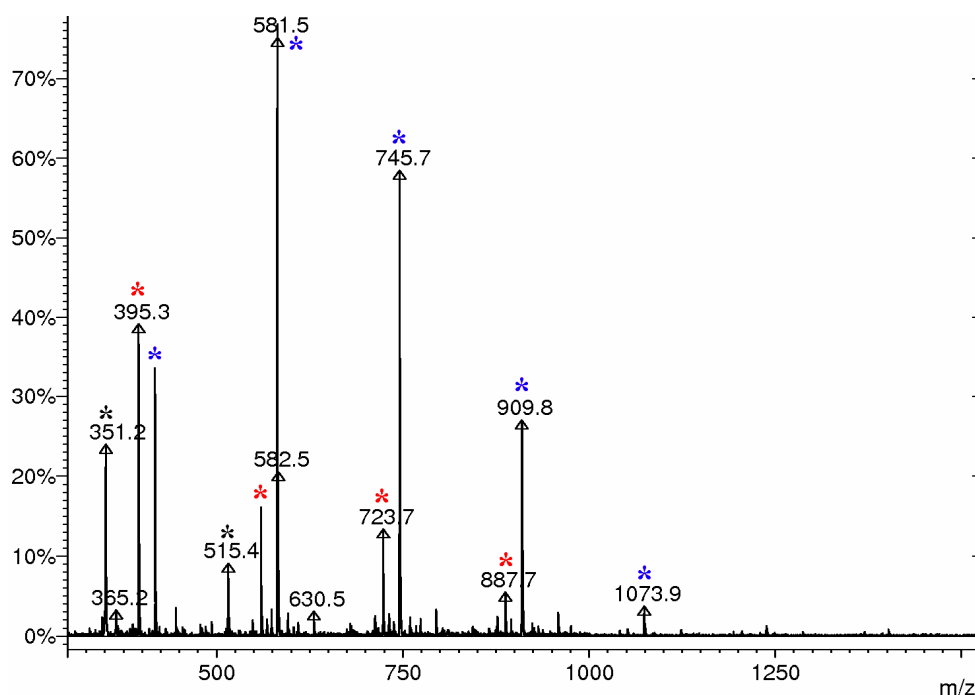


**Figure S6.** ESI MS spectrum of DEVP oligomers produced with  $[\text{Cp}_2\text{Y}(\text{OiPr})]_2$ . Two major series of peaks are evident:  $m/z = n \times M_{\text{Mon}} + 66 + M_{\text{H}}$  (red),  $m/z = n \times M_{\text{Mon}} + 66 + M_{\text{Na}}$  (blue);  $M_{\text{Mon}} = 164$ , end groups:  $M_{\text{Cp}} + M_{\text{H}} = 66$ . Peaks at  $m/z = 351$  and  $515$  are attributed to fragmentation.

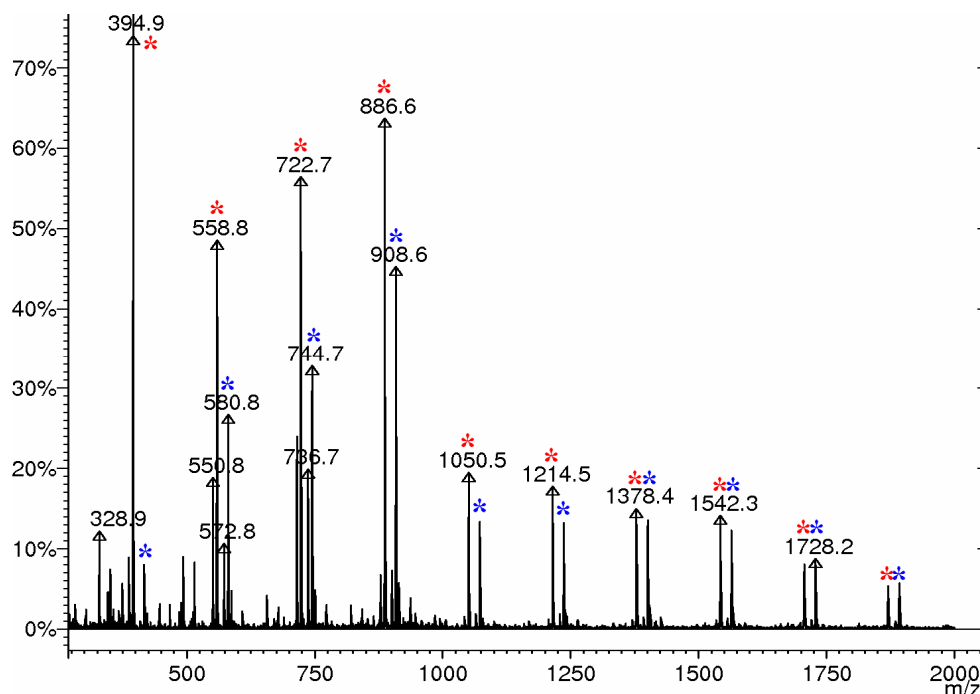


**Figure S7.** ESI MS spectrum of DEVP oligomers produced with  $[\text{Cp}_2\text{Lu}(\text{OiPr})]_2$ . Two major series of peaks are evident:  $m/z = n \times M_{\text{Mon}} + 66 + M_{\text{H}}$  (red),  $m/z = n \times M_{\text{Mon}} + 66 + M_{\text{Na}}$  (blue);  $M_{\text{Mon}} = 164$ , end groups:  $M_{\text{Cp}} + M_{\text{H}} = 66$ .

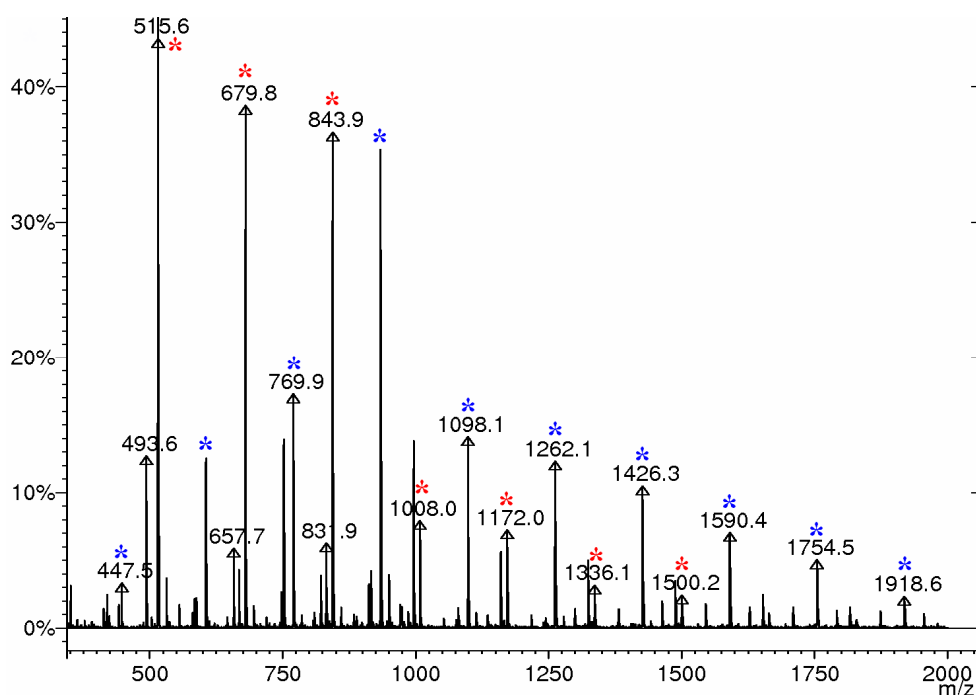


**Figure S8.** ESI MS spectrum of DEVP oligomers produced with  $[\text{Cp}_2\text{YStBu}]_2$ . Two major series of peaks are evident:  $m/z = n \times M_{\text{Mon}} + M_{\text{Na}}$  (red),  $m/z = n \times M_{\text{Mon}} + 90 + M_{\text{Na}}$  (blue);  $M_{\text{Mon}} = 164$ , end groups:  $M_{\text{StBu}} + M_{\text{H}} = 90$ .

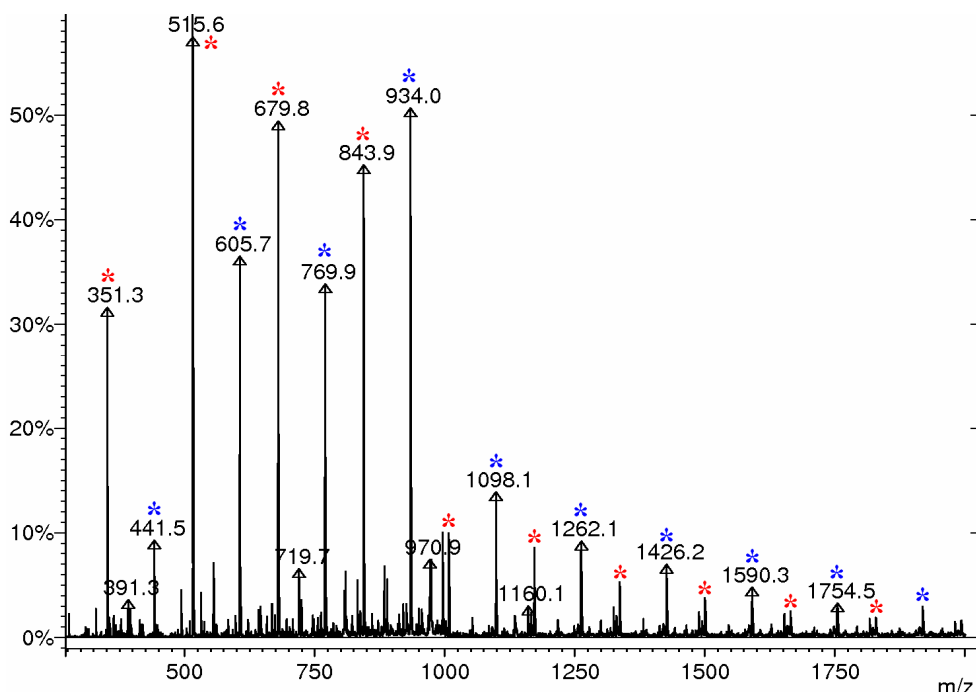


**Figure S9.** ESI MS spectrum of DEVP oligomers produced with  $[\text{Cp}_2\text{LuStBu}]_2$ . Two major series of peaks are evident:  $m/z = n \times M_{\text{Mon}} + M_{\text{Na}}$  (red),  $m/z = n \times M_{\text{Mon}} + 90 + M_{\text{Na}}$  (blue);  $M_{\text{Mon}} = 164$ , end groups:  $M_{\text{StBu}} + M_{\text{H}} = 90$ .

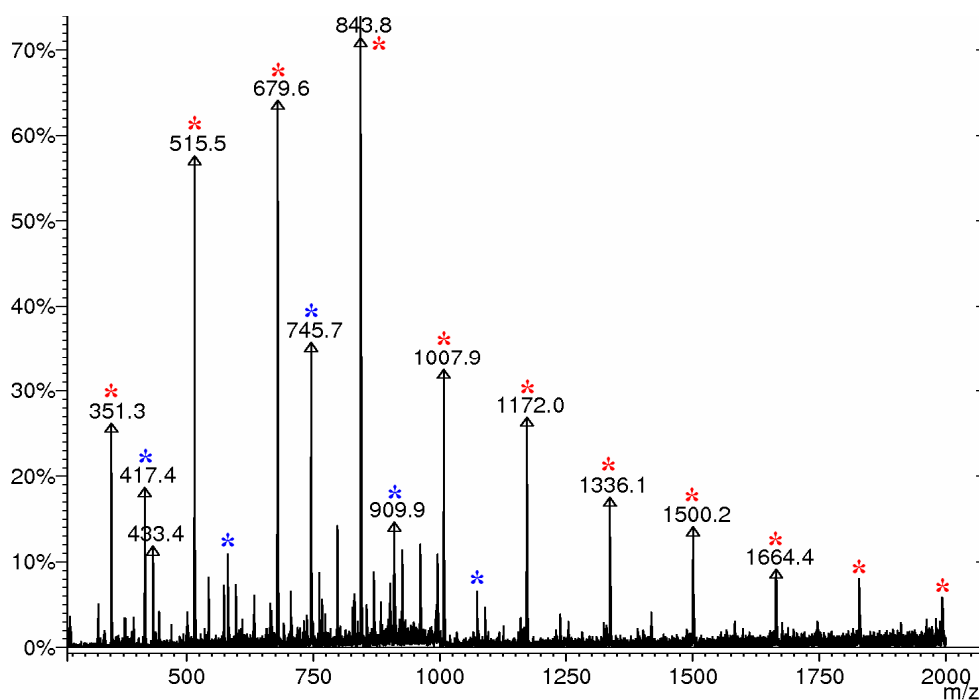


**Figure S10.** ESI MS spectrum of DEVP oligomers produced with  $\text{Cp}_2\text{Y}(\text{CH}_2\text{TMS})(\text{thf})$ . Two major series of peaks are evident:  $m/z = n \times M_{\text{Mon}} + M_{\text{Na}}$  (red),  $m/z = n \times M_{\text{Mon}} + 66 + M_{\text{Na}}$  (blue);  $M_{\text{Mon}} = 164$ , end groups:  $M_{\text{Cp}} + M_{\text{H}} = 66$ .

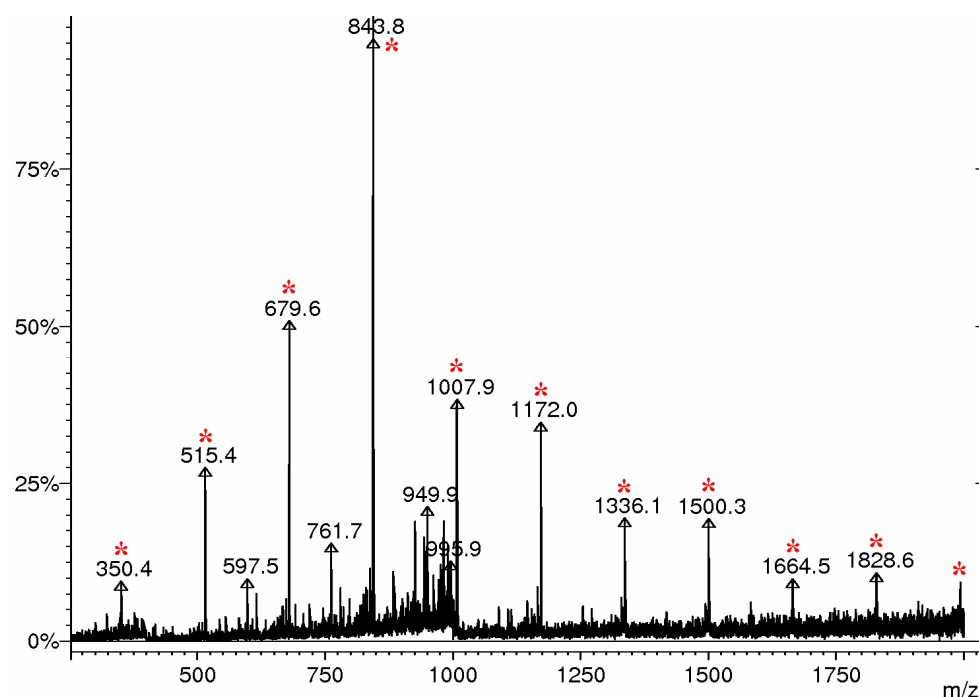


**Figure S11.** ESI MS spectrum of DEVP oligomers produced with  $\text{Cp}_2\text{Lu}(\text{CH}_2\text{TMS})(\text{thf})$ . One major series of peaks is evident:  $m/z = n \times M_{\text{Mon}} + M_{\text{Na}}$  (red);  $M_{\text{Mon}} = 164$ , no apparent end group.

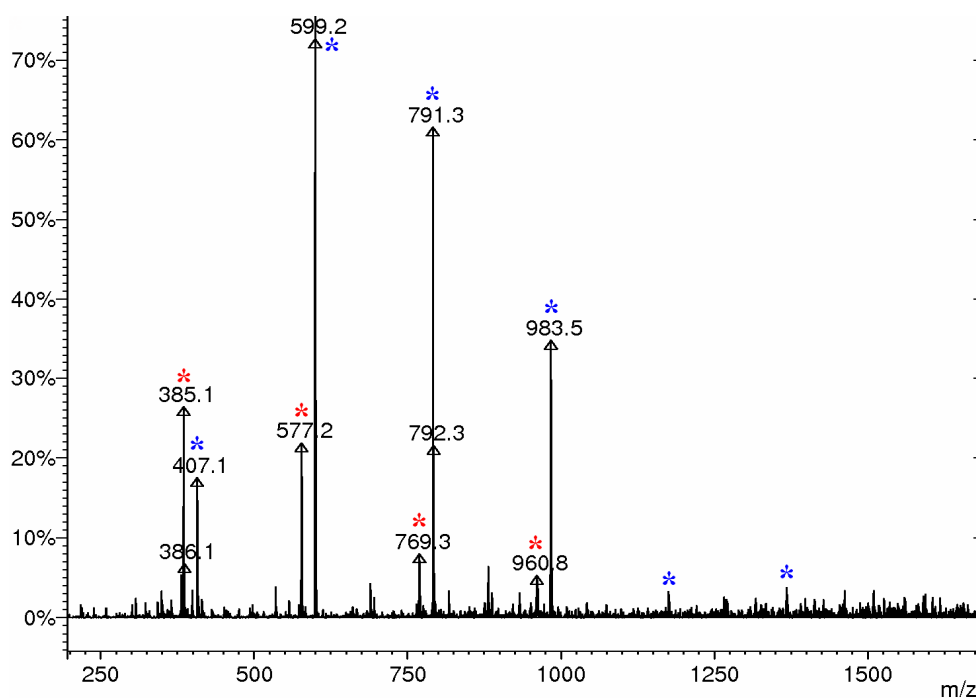


**Figure S12.** ESI MS spectrum of DIVP oligomers produced with  $[\text{Cp}_2\text{YStBu}]_2$ . Two major series of peaks are evident:  $m/z = n \times M_{\text{Mon}} + M_{\text{H}}$  (red),  $m/z = n \times M_{\text{Mon}} + M_{\text{Na}}$  (red);  $M_{\text{Mon}} = 192$ , no apparent end group.

## Single Crystal X-Ray Structure Determination of Compounds $\text{Cp}_3\text{Y}(\text{DEEP})$ , $\text{Cp}_2\text{HoCl}(\text{DEVP})$ , and $\text{Cp}_2\text{YbCl}(\text{DEVP})$

### *General:*

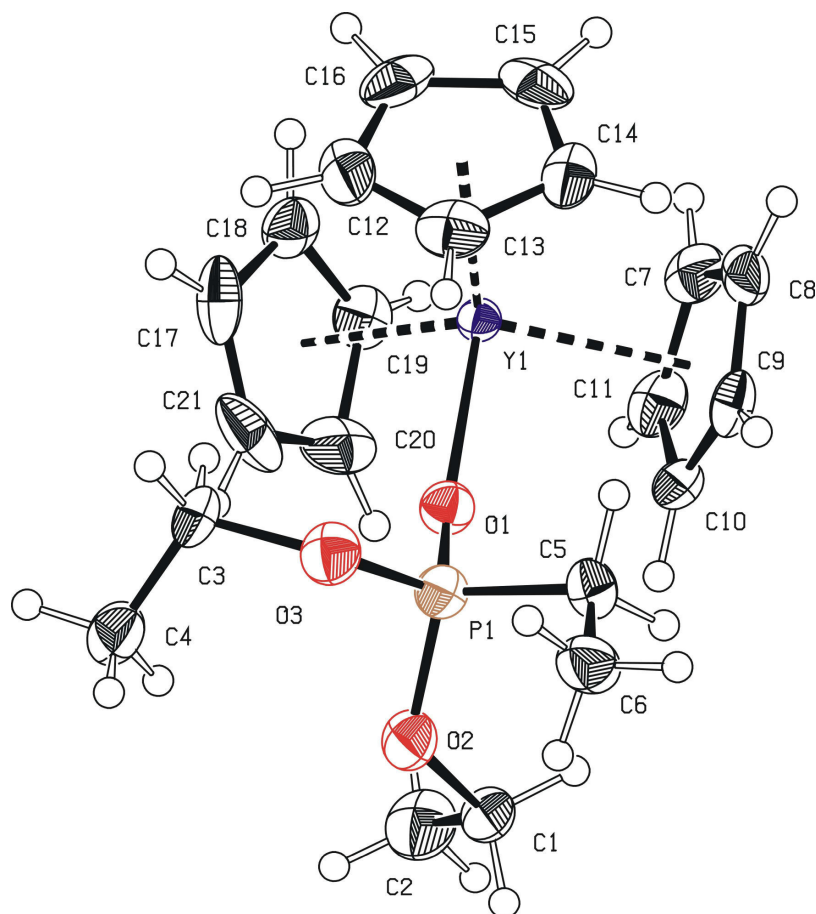
Data were collected on an X-ray single crystal diffractometer equipped with a CCD detector (Bruker APEX II,  $\kappa$ -CCD), a rotating anode (Bruker AXS, FR591) with  $\text{MoK}_\alpha$  radiation ( $\lambda = 0.71073 \text{ \AA}$ ), and a graphite monochromator by using the SMART software package.<sup>1</sup> The measurements were performed on a single crystal coated with perfluorinated ether. The crystal was fixed on the top of a glass fiber and transferred to the diffractometer. The crystal was frozen under a stream of cold nitrogen. A matrix scan was used to determine the initial lattice parameters. Reflections were merged and corrected for Lorenz and polarization effects, scan speed, and background using SAINT.<sup>2</sup> Absorption corrections, including odd and even ordered spherical harmonics were performed using SADABS.<sup>2</sup> Space group assignments were based upon systematic absences,  $E$  statistics, and successful refinement of the structures. Structures were solved by direct methods with the aid of successive difference Fourier maps, and were refined against all data using WinGX<sup>7</sup> based on SIR-92.<sup>3</sup> If not mentioned otherwise, non-hydrogen atoms were refined with anisotropic displacement parameters. Methyl hydrogen atoms were refined as part of rigid rotating groups, with  $\text{C-H} = 0.98 \text{ \AA}$  and  $U_{\text{iso}(\text{H})} = 1.5U_{\text{eq}(\text{C})}$ . Other H atoms were placed in calculated positions and refined using a riding model, with methylene and aromatic C-H distances of 0.99 and 0.95  $\text{ \AA}$ , respectively, and  $U_{\text{iso}(\text{H})} = 1.2 \cdot U_{\text{eq}(\text{C})}$ . Full-matrix least-squares refinements were carried out by minimizing  $\Sigma w(F_o^2 - F_c^2)^2$  with SHELXL-97<sup>5</sup> weighting scheme. Neutral atom scattering factors for all atoms and anomalous dispersion corrections for the non-hydrogen atoms were taken from *International Tables for Crystallography*.<sup>4</sup> Images of the crystal structures were generated by PLATON.<sup>6</sup>

### *Special:*

**$\text{Cp}_2\text{HoCl}(\text{DEVP})$ :** Extinction Correction. The correct enantiomere is proved by Flack's Parameter.

**$\text{Cp}_2\text{YbCl}(\text{DEVP})$ :** The correct enantiomere is proved by Flack's Parameter.

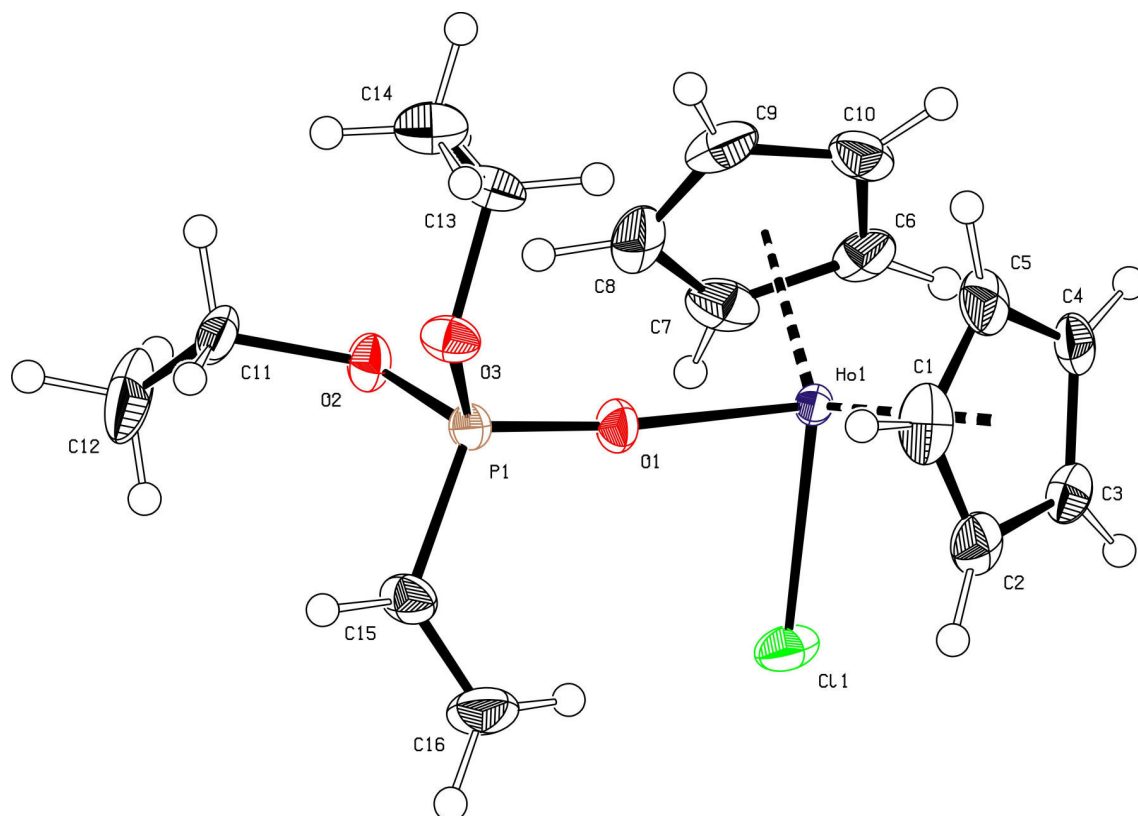


**Cp<sub>3</sub>Y(DEEP)**

**Figure S13.** Ortep drawing drawing of compound Cp<sub>3</sub>Y(DEEP) with 50% ellipsoids.<sup>6</sup>

Operator:	*** Herdtweck ***
Molecular Formula:	C <sub>21</sub> H <sub>30</sub> O <sub>3</sub> P Y
Crystal Color / Shape	Colorless fragment
Crystal Size	Approximate size of crystal fragment used for data collection: 0.18 × 0.41 × 0.51 mm
Molecular Weight:	450.33 a.m.u.
F <sub>000</sub> :	936
Systematic Absences:	h0l: h+l≠2n; 0k0: k≠2n
Space Group:	Monoclinic <i>P</i> 2 <sub>1</sub> / <i>n</i> (I.T.-No.: 14)
Cell Constants:	Least-squares refinement of 9637 reflections with the programs "APEX suite" and "SAINT" [1,2]; theta range 1.84° < θ < 25.36°; Mo(Kα); λ = 71.073 pm a = 1150.91(4) pm b = 828.72(3) pm β = 101.516(2)° c = 2261.67(8) pm V = 2113.72(13) · 10 <sup>6</sup> pm <sup>3</sup> ; Z = 4; D <sub>calc</sub> = 1.415 g cm <sup>-3</sup> ; Mos. = 0.72
Diffractometer:	Kappa APEX II (Area Diffraction System; BRUKER AXS); rotating anode; graphite monochromator; 50 kV; 40 mA; λ = 71.073 pm; Mo(Kα)

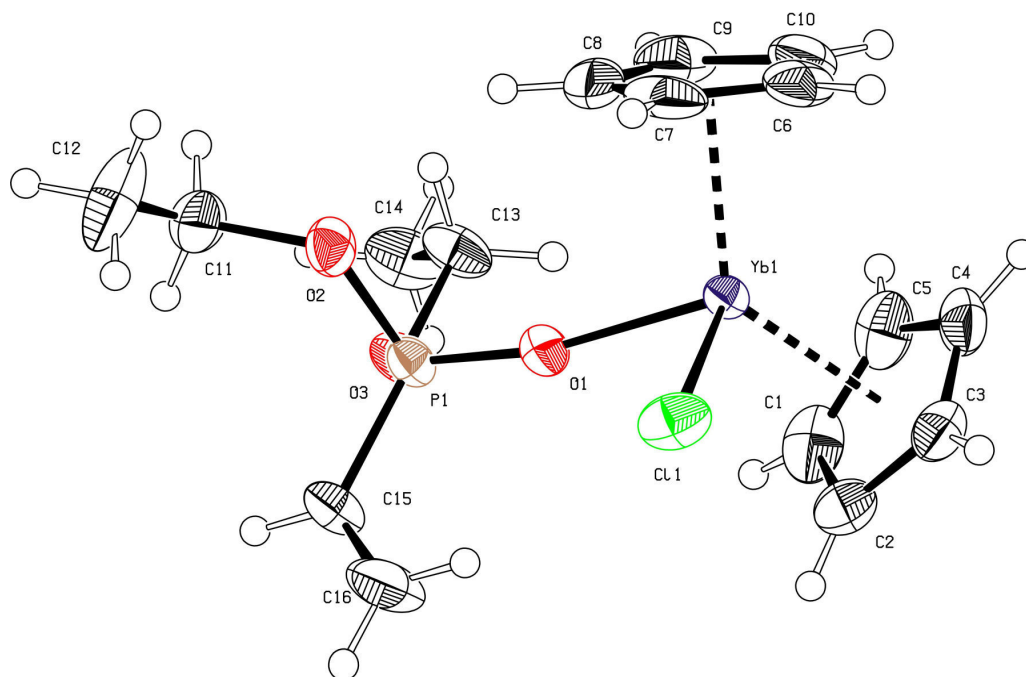
Temperature:	(-150±1) °C;	(123±1) K
Measurement Range:	1.84° < $\theta$ < 25.36°; h: -13/13, k: -9/9, l: -27/27	
Measurement Time:	2 × 5 s per film	
Measurement Mode:	measured: 13 runs; 8565 films / scaled: 13 runs; 8565 films $\varphi$ - and $\omega$ -movement; Increment: $\Delta\varphi/\Delta\omega = 0.50^\circ$ ; dx = 55.0 mm	
LP - Correction:	Yes [2]	
Intensity Correction	No/Yes; during scaling [2]	
Absorption Correction:	Multi-scan; during scaling; $\mu = 2.851 \text{ mm}^{-1}$ [2]	
	Correction Factors:	$T_{\min} = 0.3668$ $T_{\max} = 0.7452$
Reflection Data:	79021	reflections were integrated and scaled
	3711	reflections systematic absent and rejected
	75310	reflections to be merged
	3849	independent reflections
	0.041	$R_{\text{int}}$ : (basis $F_o^2$ )
	3849	independent reflections (all) were used in refinements
	3531	independent reflections with $I_o > 2\sigma(I_o)$
	99.7 %	completeness of the data set
	238	parameter full-matrix refinement
	16.2	reflections per parameter
Solution:	Direct Methods [3]; Difference Fourier syntheses	
Refinement Parameters:	In the asymmetric unit:	
	26	Non-hydrogen atoms with anisotropic displacement parameters
Hydrogen Atoms:	In the difference map(s) calculated from the model containing all non-hydrogen atoms, not all of the hydrogen positions could be determined from the highest peaks. For this reason, the hydrogen atoms were placed in calculated positions ( $d_{\text{C-H}} = 95, 98, 99 \text{ pm}$ ). Isotropic displacement parameters were calculated from the parent carbon atom ( $U_{\text{H}} = 1.2/1.5 U_{\text{C}}$ ). The hydrogen atoms were included in the structure factor calculations but not refined.	
Atomic Form Factors:	For neutral atoms and anomalous dispersion [4]	
Extinction Correction:	no	
Weighting Scheme:	$w^{-1} = \sigma^2(F_o^2) + (a * P)^2 + b * P$ with a: 0.0637; b: 5.8032; P: $[\text{Maximum}(0 \text{ or } F_o^2) + 2 * F_c^2] / 3$	
Shift/Err:	Less than 0.001 in the last cycle of refinement:	
Resid. Electron Density:	+2.98 $e_0/\text{\AA}^3$ ; -0.86 $e_0/\text{\AA}^3$	
R1:	$\Sigma( F_o  -  F_c ) / \Sigma F_o $	
[ $F_o > 4\sigma(F_o)$ ; N=3531]:		= 0.0446
[all reflctns; N=3849]:		= 0.0485
wR2:	$[\Sigma w(F_o^2 - F_c^2)^2 / \Sigma w(F_o^2)^2]^{1/2}$	
[ $F_o > 4\sigma(F_o)$ ; N=3531]:		= 0.1182
[all reflctns; N=3849]:		= 0.1211
Goodness of fit:	$[\Sigma w(F_o^2 - F_c^2)^2 / (\text{NO-NV})]^{1/2}$	= 1.074
Remarks:	Refinement expression $\Sigma w(F_o^2 - F_c^2)^2$	

**Cp<sub>2</sub>HoCl(DEVP)**

**Figure S14.** Ortep drawing drawing of compound Cp<sub>2</sub>HoCl(DEVP) with 50% ellipsoids.<sup>6</sup>

Operator:	*** Herdtweck ***
Molecular Formula:	C <sub>16</sub> H <sub>23</sub> Cl Ho O <sub>3</sub> P
Crystal Color / Shape	Colorless fragment
Crystal Size	Approximate size of crystal fragment used for data collection: 0.18 × 0.51 × 0.64 mm
Molecular Weight:	494.69 a.m.u.
F <sub>000</sub> :	968
Systematic Absences:	0kl: k+l≠2n; h0l: h≠2n; 00l: l≠2n
Space Group:	Orthorhombic <i>P na</i> 2 <sub>1</sub> (I.T.-No.: 33)
Cell Constants:	Least-squares refinement of 9797 reflections with the programs "APEX suite" and "SAINT" [1,2]; theta range 1.96° < θ < 25.42°; Mo(K $\alpha$ ); λ = 71.073 pm a = 2074.65(6) pm b = 1172.65(4) pm c = 781.25(3) pm V = 1900.66(11) · 10 <sup>6</sup> pm <sup>3</sup> ; Z = 4; D <sub>calc</sub> = 1.729 g cm <sup>-3</sup> ; Mos. = 0.70
Diffractometer:	Kappa APEX II (Area Diffraction System; BRUKER AXS); rotating anode; graphite monochromator; 50 kV; 40 mA; λ = 71.073 pm; Mo(K $\alpha$ )
Temperature:	(-150±1) °C; (123±1) K
Measurement Range:	1.96° < θ < 25.42°; h: -24/25, k: -14/14, l: -9/9
Measurement Time:	2 × 5 s per film

Measurement Mode:	measured: 11 runs; 4738 films / scaled: 11 runs; 4738 films $\varphi$ - and $\omega$ -movement; Increment: $\Delta\varphi/\Delta\omega = 0.50^\circ$ ; dx = 45.0 mm	
LP - Correction:	Yes [2]	
Intensity Correction	No/Yes; during scaling [2]	
Absorption Correction:	Multi-scan; during scaling; $\mu = 4.395 \text{ mm}^{-1}$ [2]	
Reflection Data:	Correction Factors:	$T_{\min} = 0.2508$ $T_{\max} = 0.7452$
	53506	reflections were integrated and scaled
	2077	reflections systematic absent and rejected
	1	obvious wrong intensity and rejected
	51428	reflections to be merged
	3487	independent reflections
	0.044	$R_{\text{int}}$ : (basis $F_o^2$ )
	3487	independent reflections (all) were used in refinements
	3484	independent reflections with $I_o > 2\sigma(I_o)$
	99.4 %	completeness of the data set
	202	parameter full-matrix refinement
	17.3	reflections per parameter
Solution:	Direct Methods [3]; Difference Fourier syntheses	
Refinement Parameters:	In the asymmetric unit:	
	22	Non-hydrogen atoms with anisotropic displacement parameters
Hydrogen Atoms:	In the difference map(s) calculated from the model containing all non-hydrogen atoms, not all of the hydrogen positions could be determined from the highest peaks. For this reason, the hydrogen atoms were placed in calculated positions ( $d_{\text{C-H}} = 95, 98, 99 \text{ pm}$ ). Isotropic displacement parameters were calculated from the parent carbon atom ( $U_{\text{H}} = 1.2/1.5 U_{\text{C}}$ ). The hydrogen atoms were included in the structure factor calculations but not refined.	
Atomic Form Factors:	For neutral atoms and anomalous dispersion [4]	
Extinction Correction:	$F_c(\text{korr}) = kF_c[1 + 0.001 \cdot \varepsilon \cdot F_c^2 \cdot \lambda^3/\sin(2\theta)]^{-1/4}$ SHELXL-97 [5] $\varepsilon$ refined to $\varepsilon = 0.0024(2)$	
Weighting Scheme:	$w^{-1} = \sigma^2(F_o^2) + (a \cdot P)^2 + b \cdot P$ with a: 0.0091; b: 1.7395; P: $[\text{Maximum}(0 \text{ or } F_o^2) + 2 \cdot F_c^2]/3$	
Shift/Err:	Less than 0.001 in the last cycle of refinement:	
Resid. Electron Density:	$+0.91 \text{ e}_0/\text{\AA}^3$ ; $-0.73 \text{ e}_0/\text{\AA}^3$	
R1:	$\Sigma( F_o  -  F_c )/\Sigma F_o $	
$[F_o > 4\sigma(F_o)$ ; N=3484]:		= 0.0144
[all reflctns; N=3487]:		= 0.0145
wR2:	$[\Sigma w(F_o^2 - F_c^2)^2 / \Sigma w(F_o^2)^2]^{1/2}$	
$[F_o > 4\sigma(F_o)$ ; N=3484]:		= 0.0369
[all reflctns; N=3487]:		= 0.0369
Goodness of fit:	$[\Sigma w(F_o^2 - F_c^2)^2 / (\text{NO} - \text{NV})]^{1/2}$	= 1.197
Flack's Parameter :	$x = 0.07(1)$	
Remarks:	Refinement expression $\Sigma w(F_o^2 - F_c^2)^2$	

Compound  $\text{Cp}_2\text{YbCl}(\text{DEVP})$ 

**Figure S15.** Ortep drawing drawing of compound  $\text{Cp}_2\text{YbCl}(\text{DEVP})$  with 50% ellipsoids.<sup>6</sup>

Operator:	*** Herdtweck ***
Molecular Formula:	$\text{C}_{16}\text{H}_{23}\text{ClO}_3\text{PYb}$
Crystal Color / Shape	Colorless fragment
Crystal Size	Approximate size of crystal fragment used for data collection: $0.18 \times 0.51 \times 0.53$ mm
Molecular Weight:	502.80 a.m.u.
$F_{000}$ :	980
Systematic Absences:	$0kl: k+l \neq 2n; h0l: h \neq 2n; 00l: l \neq 2n$
Space Group:	Orthorhombic $Pna2_1$ (I.T.-No.: 33)
Cell Constants:	Least-squares refinement of 9735 reflections with the programs "APEX suite" and "SAINT" [1,2]; theta range $1.96^\circ < \theta < 25.36^\circ$ ; $\text{Mo}(\text{K}\alpha)$ ; $\lambda = 71.073$ pm $a = 2075.04(7)$ pm $b = 1173.61(4)$ pm $c = 780.75(3)$ pm $V = 1901.35(12) \cdot 10^6$ pm <sup>3</sup> ; $Z = 4$ ; $D_{\text{calc}} = 1.757$ g cm <sup>-3</sup> ; Mos. = 0.40
Diffractometer:	Kappa APEX II (Area Diffraction System; BRUKER AXS); rotating anode; graphite monochromator; 50 kV; 40 mA; $\lambda = 71.073$ pm; $\text{Mo}(\text{K}\alpha)$
Temperature:	$(-120 \pm 1)^\circ\text{C}$ ; $(153 \pm 1)$ K
Measurement Range:	$1.96^\circ < \theta < 25.36^\circ$ ; h: -24/24, k: -14/14, l: -9/9
Measurement Time:	$2 \times 5$ s per film
Measurement Mode:	measured: 13 runs; 4857 films / scaled: 13 runs; 4857 films $\varphi$ - and $\omega$ -movement; Increment: $\Delta\varphi/\Delta\omega = 0.50^\circ$ ; dx = 45.0 mm
LP - Correction:	Yes [2]
Intensity Correction	No/Yes; during scaling [2]

Absorption Correction:	Multi-scan; during scaling; $\mu = 5.151 \text{ mm}^{-1}$ [2]
Correction Factors:	$T_{\min} = 0.3291$ $T_{\max} = 0.7452$
Reflection Data:	48470 reflections were integrated and scaled
	2255 reflections systematic absent and rejected
	46215 reflections to be merged
	3461 independent reflections
	0.053 $R_{\text{int}}$ : (basis $F_o^2$ )
	3461 independent reflections (all) were used in refinements
	3449 independent reflections with $I_o > 2\sigma(I_o)$
	99.3 % completeness of the data set
	201 parameter full-matrix refinement
	17.2 reflections per parameter
Solution:	Direct Methods [3]; Difference Fourier syntheses
Refinement Parameters:	In the asymmetric unit:
	22 Non-hydrogen atoms with anisotropic displacement parameters
Hydrogen Atoms:	In the difference map(s) calculated from the model containing all non-hydrogen atoms, not all of the hydrogen positions could be determined from the highest peaks. For this reason, the hydrogen atoms were placed in calculated positions ( $d_{\text{C-H}} = 95, 98, 99 \text{ pm}$ ). Isotropic displacement parameters were calculated from the parent carbon atom ( $U_{\text{H}} = 1.2/1.5 U_{\text{C}}$ ). The hydrogen atoms were included in the structure factor calculations but not refined.
Atomic Form Factors:	For neutral atoms and anomalous dispersion [4]
Extinction Correction:	no
Weighting Scheme:	$w^{-1} = \sigma^2(F_o^2) + (a*P)^2 + b*P$ with a: 0.0125; b: 1.2304; P: [Maximum(0 or $F_o^2$ )+2* $F_c^2$ ]/3
Shift/Err:	Less than 0.002 in the last cycle of refinement:
Resid. Electron Density:	+0.70 $e_0/\text{\AA}^3$ ; -0.55 $e_0/\text{\AA}^3$
R1:	$\Sigma( F_o  -  F_c ) / \Sigma F_o $
[ $F_o > 4\sigma(F_o)$ ; N=3449]:	= 0.0142
[all reflctns; N=3461]:	= 0.0143
wR2:	$[\Sigma w(F_o^2 - F_c^2)^2 / \Sigma w(F_o^2)^2]^{1/2}$
[ $F_o > 4\sigma(F_o)$ ; N=3449]:	= 0.0373
[all reflctns; N=3461]:	= 0.0374
Goodness of fit:	$[\Sigma w(F_o^2 - F_c^2)^2 / (\text{NO} - \text{NV})]^{1/2}$ = 1.088
Flack's Parameter :	$x = 0.08(1)$
Remarks:	Refinement expression $\Sigma w(F_o^2 - F_c^2)^2$

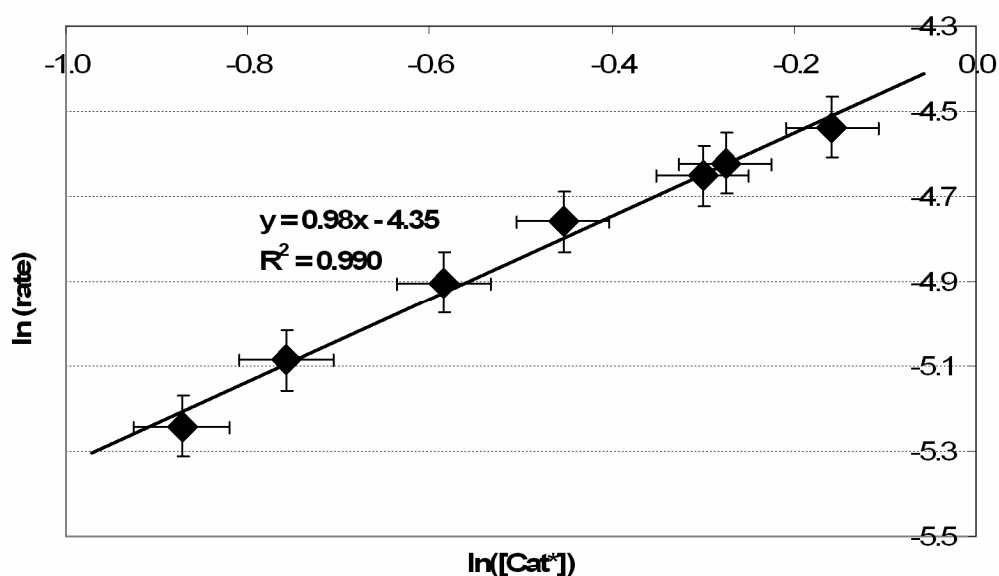
## Kinetic Studies

**Table S1.** Determination of catalyst order ( $\text{Cp}_3\text{Tm}$ , 5vol% DEVP, toluene, 30 °C)

[Cat] /mmol L <sup>-1</sup>	TOF /h <sup>-1</sup>	$I_t^*$ /%	TOF/ $I_t^*$ /h <sup>-1</sup>	ln([Cat*])	rate /mol L <sup>-1</sup> s <sup>-1</sup>	ln(rate)
0.54	9100	17	54000	-2.39	1.38E-03	-6.59
0.82	10000	18	56000	-1.91	2.34E-03	-6.06
1.09	9000	17	53000	-1.69	2.73E-03	-5.90
1.36	8600	16	54000	-1.53	3.26E-03	-5.73
1.63	11000	21	52000	-1.07	4.87E-03	-5.32
2.17	7000	13	54000	-1.27	4.22E-03	-5.47
2.72	6700	13	52000	-1.04	5.04E-03	-5.29

**Table S2.** Determination of catalyst order ( $[\text{Cp}_2\text{Y}(\text{StBu})]_2$ , 5vol% DEVP, toluene, 30 °C)

[Cat] /mmol L <sup>-1</sup>	TOF /h <sup>-1</sup>	$I_t^*$ /%	TOF/ $I_t^*$ /h <sup>-1</sup>	ln([Cat*])	rate /mol L <sup>-1</sup> s <sup>-1</sup>	ln(rate)
0.95	19900	44	45000	-0.87	5.29E-03	-5.24
1.09	20600	43	48000	-0.76	6.18E-03	-5.09
1.36	19700	41	48000	-0.58	7.43E-03	-4.90
1.63	19000	39	49000	-0.45	8.58E-03	-4.76
1.90	18000	39	46000	-0.30	9.55E-03	-4.65
2.17	16400	35	47000	-0.28	9.84E-03	-4.62
2.44	15400	35	44000	-0.16	1.07E-02	-4.54

**Figure S16.** Determination of catalyst order ( $[\text{Cp}_2\text{Y}(\text{StBu})]_2$ , 5vol% DEVP, toluene, 30 °C).

**Table S3.** Determination of catalyst order ( $[\text{Cp}_2\text{Y}(\text{StBu})]_2$ , 12.5vol% DIVP, toluene, 30 °C)

[Cat] /mmol L <sup>-1</sup>	TOF /h <sup>-1</sup>	$I_t^*$ /%	TOF/ $I_t^*$ /h <sup>-1</sup>	ln([Cat*])	rate /mol L <sup>-1</sup> s <sup>-1</sup>	ln(rate)
1.63	1520	70	2170	0.13	6.85E-04	-7.29
1.90	1380	62	2230	0.16	7.31E-04	-7.22
2.17	1480	67	2210	0.37	8.93E-04	-7.02
2.44	1640	74	2220	0.59	1.11E-03	-6.80
2.72	1710	74	2310	0.70	1.29E-03	-6.65
2.99	1760	78	2260	0.85	1.45E-03	-6.54
3.26	1840	78	2360	0.93	1.66E-03	-6.40

**Table S4.** Determination of monomer order ( $[\text{Cp}_2\text{Y}(\text{StBu})]_2$ , DEVP, toluene, 30 °C)

[Mon] <sub>0</sub> /mol L <sup>-1</sup>	[Cat] /mmol L <sup>-1</sup>	TOF /h <sup>-1</sup>	$I_t^*$ /%	TOF/ $I_t^*$ /h <sup>-1</sup>	Conversion at max. rate /%	ln([Mon])	rate /mol L <sup>-1</sup> s <sup>-1</sup>	ln(rate/[Cat*])
0.163	1.09	8300	36	23000	20	0.130	2.50E-03	1.85
0.223	1.09	12900	45	29000	29	0.158	3.79E-03	2.04
0.260	1.09	14700	38	39000	23	0.200	4.43E-03	2.37
0.325	1.09	20600	44	47000	27	0.237	6.18E-03	2.56
0.390	1.09	32000	54	60000	19	0.316	8.80E-03	2.70
0.488	1.09	26700	40	67000	19	0.395	8.05E-03	2.92
0.651	1.09	45000	51	88000	28	0.469	1.36E-02	3.20

**Table S5.** Determination of monomer order ( $[\text{Cp}_2\text{Y}(\text{StBu})]_2$ , DIVP, toluene, 30 °C)

[Mon] <sub>0</sub> /mol L <sup>-1</sup>	[Cat] /mmol L <sup>-1</sup>	TOF /h <sup>-1</sup>	$I_t^*$ /%	TOF/ $I_t^*$ /h <sup>-1</sup>	Conversion at max. rate /%	ln([Mon])	rate /mol L <sup>-1</sup> s <sup>-1</sup>	ln(rate/[Cat*])
0.195	1.09	610	86	710	12.8	0.170	1.82E-04	-1.64
0.260	1.09	660	76	870	10.2	0.233	1.99E-04	-1.43
0.325	1.39	950	79	1200	12.3	0.285	3.66E-04	-1.10
0.390	1.09	760	57	1330	5.5	0.369	2.29E-04	-1.00
0.480	2.17	1230	68	1810	8.7	0.438	7.47E-04	-0.68
0.520	2.17	1230	69	1780	7.9	0.479	7.39E-04	-0.71
0.650	2.72	1710	74	2310	12.0	0.572	1.29E-03	-0.44



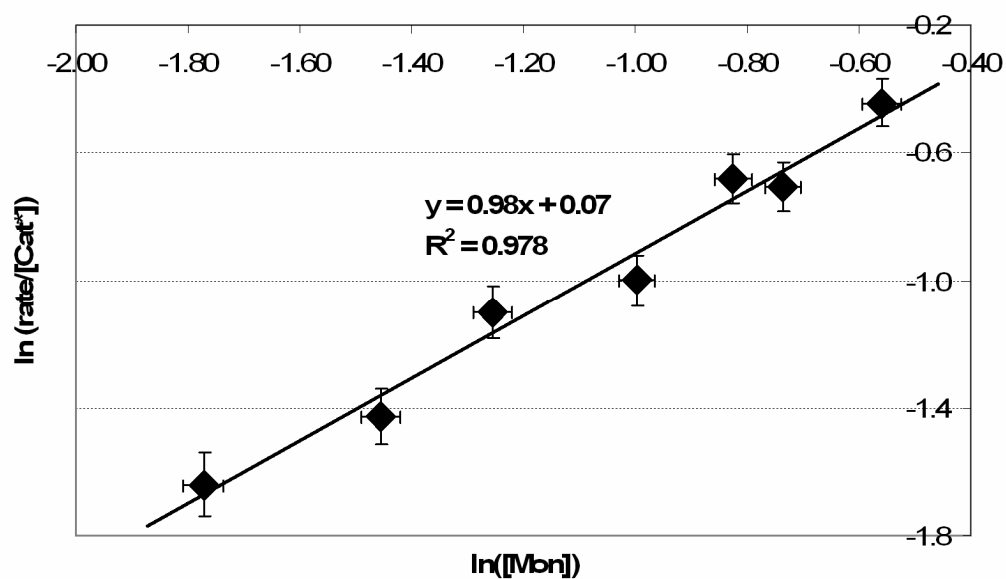


**Figure S17.** Determination of monomer order ( $[\text{Cp}_2\text{Y}(\text{StBu})]_2$ , 3-12.5vol% DIVP, toluene, 30 °C).

**Table S6.** Temperature-dependent kinetics for  $\text{Cp}_2\text{Y}$ -catalyzed DEVP polymerization (1.09 mmol L<sup>-1</sup>  $[\text{Cp}_2\text{Y}(\text{StBu})]_2$ , 0.651 mol L<sup>-1</sup> DEVP, toluene)

T / °C	TOF / h <sup>-1</sup>	$I_t^*$ / %	TOF/ $I_t^*$ / h <sup>-1</sup>	Conversion at max. rate / %	rate / mol L <sup>-1</sup> s <sup>-1</sup>	1/T / K <sup>-1</sup>	ln(k/T)
-7	3400	64	5300	34	1.02E-03	3.76E-03	-4.36
3	8950	67	13400	32	2.67E-03	3.62E-03	-3.51
13	14500	58	25000	24	4.37E-03	3.49E-03	-3.02
23	25900	54	48000	26	7.80E-03	3.38E-03	-2.38
33	44000	54	81000	28	1.33E-02	3.27E-03	-1.85
42	53000	47	110000	21	1.59E-02	3.17E-03	-1.65
52	90000	49	180000	25	2.72E-02	3.08E-03	-1.14

**Table S7.** Temperature-dependent kinetics for Cp<sub>2</sub>Tb-catalyzed DEVP polymerization (1.09 mmol L<sup>-1</sup> [Cp<sub>2</sub>Y(S*t*Bu)]<sub>2</sub>, 0.325 mol L<sup>-1</sup> DEVP, toluene)

T /°C	TOF /h <sup>-1</sup>	I* <sub>t</sub> /%	TOF/I* <sub>t</sub> /h <sup>-1</sup>	Conversion at max. rate /%	rate /mol L <sup>-1</sup> s <sup>-1</sup>	1/T /K <sup>-1</sup>	ln(k/T)
21	1640	40	4100	10	5.00E-04	3.40E-03	-4.32
33	6000	70	8570	18	1.81E-03	3.27E-03	-3.54
40	7920	61	13000	13	2.38E-03	3.19E-03	-3.21
51	12600	61	20700	12	3.78E-03	3.08E-03	-2.79
62	19600	69	28000	22	5.89E-03	2.98E-03	-2.38
71	26000	69	37700	36	7.83E-03	2.91E-03	-1.93

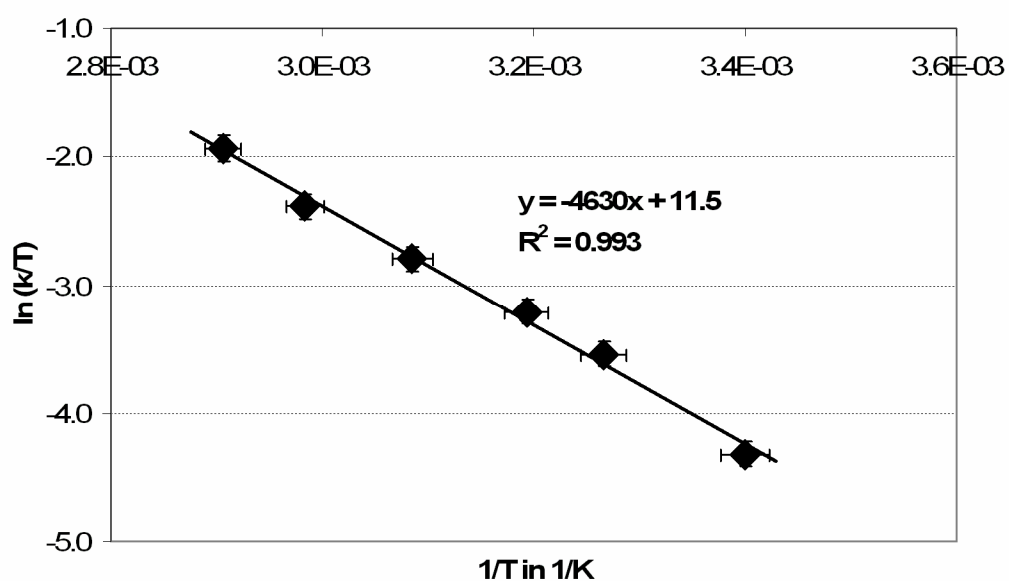


**Figure S18.** Eyring-plot for [Cp<sub>2</sub>Tb(S*t*Bu)]<sub>2</sub>-initiated DEVP (5vol%) polymerization in toluene (21 – 70 °C,  $\Delta H^\ddagger = 38.0 \text{ kJ mol}^{-1}$ ,  $\Delta S^\ddagger = -104 \text{ J (mol K)}^{-1}$ ).

**Table S8.** Temperature-dependent kinetics for Cp<sub>2</sub>Tm-catalyzed DEVP polymerization (1.09 mmol L<sup>-1</sup> Cp<sub>3</sub>Tm, 0.325 mol L<sup>-1</sup> DEVP, toluene)

T /°C	TOF /h <sup>-1</sup>	I* <sub>t</sub> /%	TOF/I* <sub>t</sub> /h <sup>-1</sup>	Conversion at max. rate /%	rate /mol L <sup>-1</sup> s <sup>-1</sup>	1/T /K <sup>-1</sup>	ln(k/T)
-1	730	13	5600	41	2.21E-04	3.67E-03	-3.51
10	1900	15	13600	37	5.65E-04	3.53E-03	-2.82
21	4500	18	25000	34	1.34E-03	3.40E-03	-2.22
32	9000	19	47000	38	2.72E-03	3.28E-03	-1.54
42	15800	20	79000	40	4.75E-03	3.17E-03	-1.04
55	26400	26	100000	48	7.94E-03	3.05E-03	-0.68
61	51000	27	190000	39	1.53E-02	2.99E-03	-0.24

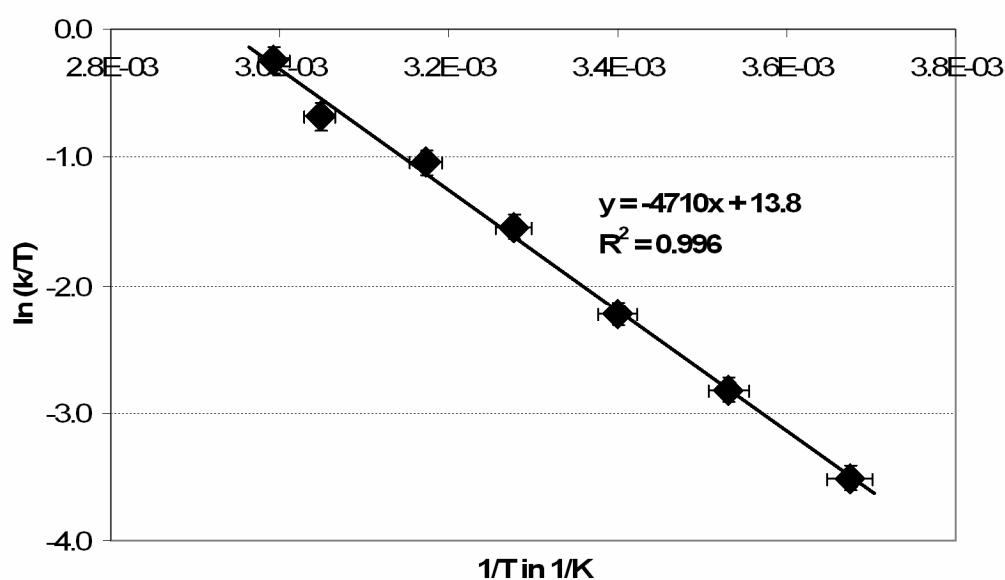


**Figure S19.** Eyring-plot for Cp<sub>3</sub>Tm-initiated DEVP (5vol%) polymerization in toluene (-1 – 61 °C,  $\Delta H^\ddagger = 39.1 \text{ kJ mol}^{-1}$ ,  $\Delta S^\ddagger = -82.8 \text{ J (mol K)}^{-1}$ ).

**Table S9.** Temperature-dependent kinetics for Cp<sub>2</sub>Lu-catalyzed DEVP polymerization (1.09 mmol L<sup>-1</sup> [Cp<sub>2</sub>Lu(*St*Bu)]<sub>2</sub>, 0.325 mol L<sup>-1</sup> DEVP, toluene)

T /°C	TOF /h <sup>-1</sup>	I* <sub>t</sub> /%	TOF/I* <sub>t</sub> /h <sup>-1</sup>	Conversion at max. rate /%	rate /mol L <sup>-1</sup> s <sup>-1</sup>	1/T /K <sup>-1</sup>	ln(k/T)
14	8500	15	61000	37	2.55E-03	3.48E-03	-1.33
23	16600	17	98000	29	4.99E-03	3.38E-03	-0.93
33	33000	19	165000	29	9.85E-03	3.27E-03	-0.40
43	67000	22	300000	30	2.02E-02	3.16E-03	0.16
53	84000	24	350000	49	2.53E-02	3.07E-03	0.58
63	141000	23	600000	42	4.25E-02	2.97E-03	0.98

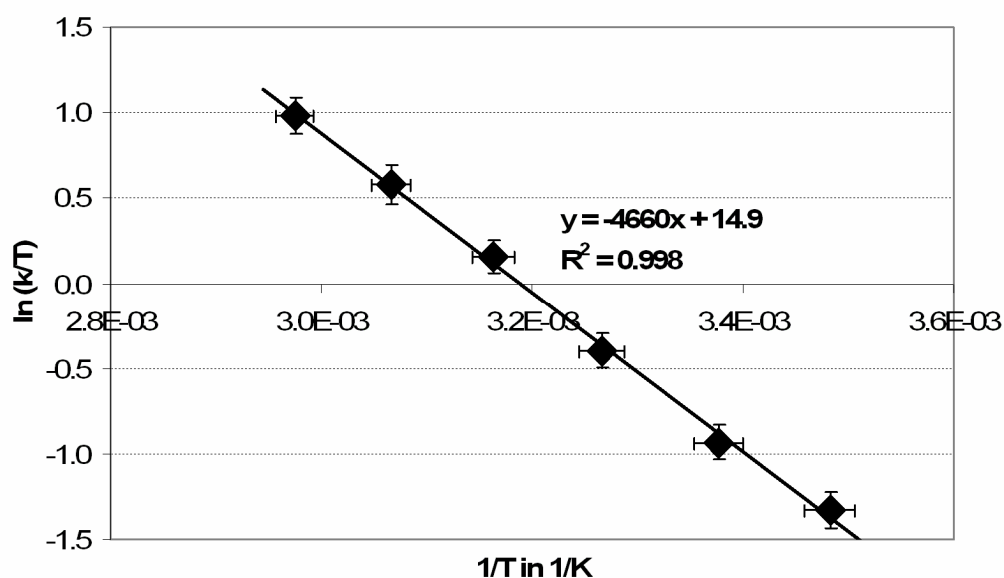


**Figure S20.** Eyring-plot for [Cp<sub>2</sub>Lu(*St*Bu)]<sub>2</sub>-initiated DEVP (5vol%) polymerization in toluene (14 – 63 °C,  $\Delta H^\ddagger = 38.7$  kJ mol<sup>-1</sup>,  $\Delta S^\ddagger = -73.6$  J (mol K)<sup>-1</sup>).

**Table S9.** Temperature-dependent kinetics for Cp<sub>2</sub>Lu-catalyzed DEVP polymerization (1.09 mmol L<sup>-1</sup> [Cp<sub>2</sub>Lu(*St*Bu)]<sub>2</sub>, 0.325 mol L<sup>-1</sup> DEVP, toluene)

T /°C	TOF /h <sup>-1</sup>	I* <sub>t</sub> /%	TOF/I* <sub>t</sub> /h <sup>-1</sup>	Conversion at max. rate /%	rate /mol L <sup>-1</sup> s <sup>-1</sup>	1/T /K <sup>-1</sup>	ln(k/T)
14	8500	15	61000	37	2.55E-03	3.48E-03	-1.33
23	16600	17	98000	29	4.99E-03	3.38E-03	-0.93
33	33000	19	165000	29	9.85E-03	3.27E-03	-0.40
43	67000	22	300000	30	2.02E-02	3.16E-03	0.16
53	84000	24	350000	49	2.53E-02	3.07E-03	0.58
63	141000	23	600000	42	4.25E-02	2.97E-03	0.98

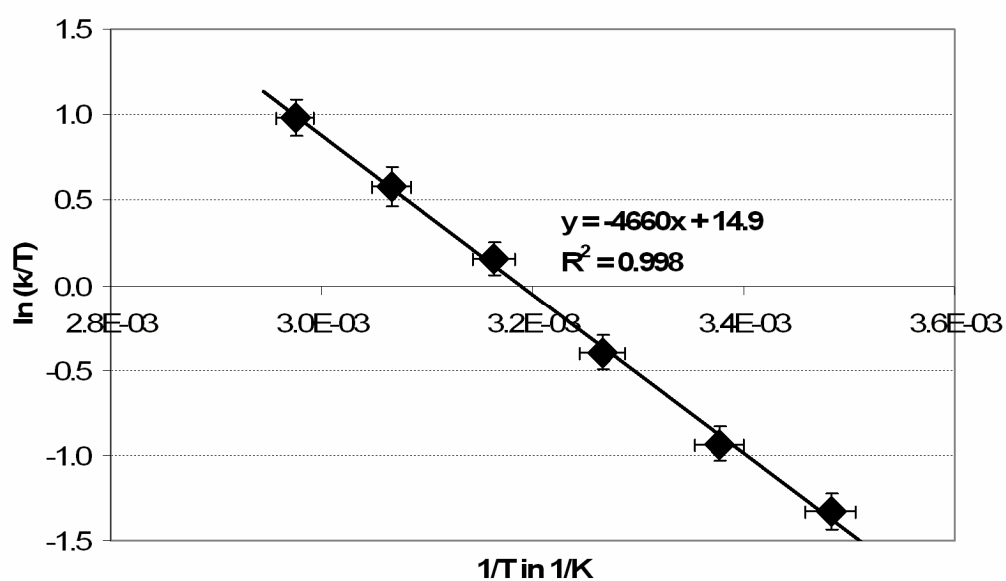


**Figure S20.** Eyring-plot for [Cp<sub>2</sub>Lu(*St*Bu)]<sub>2</sub>-initiated DEVP (5vol%) polymerization in toluene (14 – 63 °C,  $\Delta H^\ddagger = 38.7$  kJ mol<sup>-1</sup>,  $\Delta S^\ddagger = -73.6$  J (mol K)<sup>-1</sup>).

**Table S11.** Temperature-dependent kinetics for Cp<sub>2</sub>Y-catalyzed DIVP polymerization (2.17 mmol L<sup>-1</sup> [Cp<sub>2</sub>Y(S*t*Bu)]<sub>2</sub>, 0.651 mol L<sup>-1</sup> DIVP, toluene)

T /°C	TOF /h <sup>-1</sup>	I* <sub>t</sub> /%	TOF/I* <sub>t</sub> /h <sup>-1</sup>	Conversion at max. rate /%	rate /mol L <sup>-1</sup> s <sup>-1</sup>	1/T /K <sup>-1</sup>	ln(k/T)
10	350	65	530	9.9	2.09E-04	3.53E-03	-7.02
21	760	67	1130	8.2	4.59E-04	3.40E-03	-6.32
30	1460	71	2060	8.0	8.79E-04	3.30E-03	-5.76
41	2460	71	3460	9.4	1.48E-03	3.18E-03	-5.26
50	3530	73	4840	8.5	2.13E-03	3.09E-03	-4.96
59	5600	74	7570	11.9	3.36E-03	3.01E-03	-4.51
69	10600	74	14300	11.8	6.37E-03	2.92E-03	-3.90

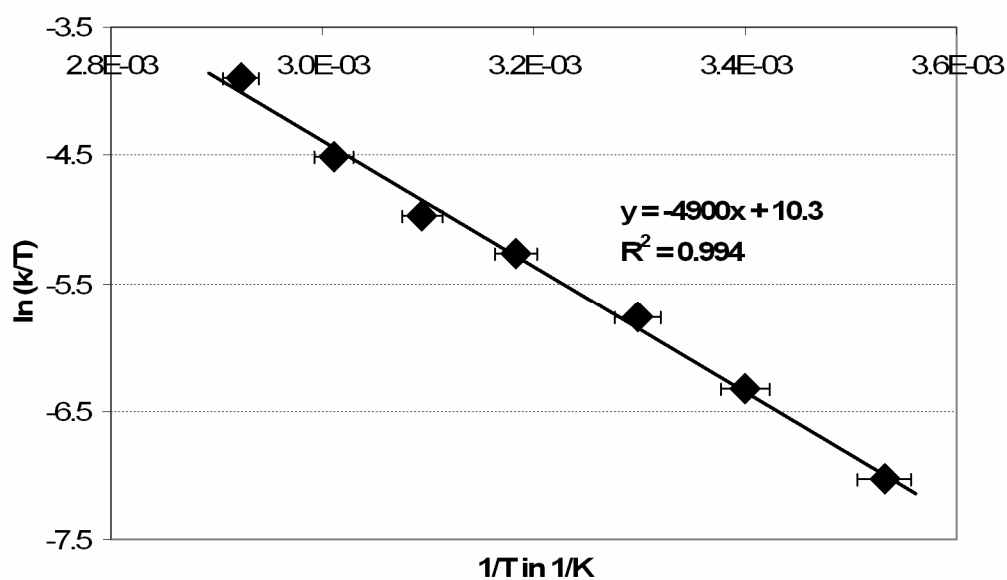


**Figure S22.** Eyring-plot for [Cp<sub>2</sub>Y(S*t*Bu)]<sub>2</sub>-initiated DIVP (12.5vol%) polymerization in toluene (10 – 69 °C,  $\Delta H^\ddagger = 40.7 \text{ kJ mol}^{-1}$ ,  $\Delta S^\ddagger = -112 \text{ J (mol K)}^{-1}$ ).

**Table S12.** Temperature-dependent kinetics for Cp<sub>2</sub>Lu-catalyzed DIVP polymerization (1.09 mmol L<sup>-1</sup> [Cp<sub>2</sub>Y(*St*Bu)]<sub>2</sub>, 0.325 mol L<sup>-1</sup> DIVP, toluene)

T /°C	TOF /h <sup>-1</sup>	I* <sub>t</sub> /%	TOF/I* <sub>t</sub> /h <sup>-1</sup>	Conversion at max. rate /%	rate /mol L <sup>-1</sup> s <sup>-1</sup>	1/T /K <sup>-1</sup>	ln(k/T)
11	350	57	610	28	1.05E-04	3.52E-03	-5.97
21	560	46	1220	24	1.69E-04	3.40E-03	-5.38
32	2000	86	2330	25	6.01E-04	3.28E-03	-4.75
42	3100	65	4770	23	9.46E-04	3.17E-03	-4.08
51	4500	70	6430	23	1.34E-03	3.08E-03	-3.83
59	8400	89	9400	23	2.54E-03	3.01E-03	-3.46
70	14800	82	18000	21	4.45E-03	2.91E-03	-2.87

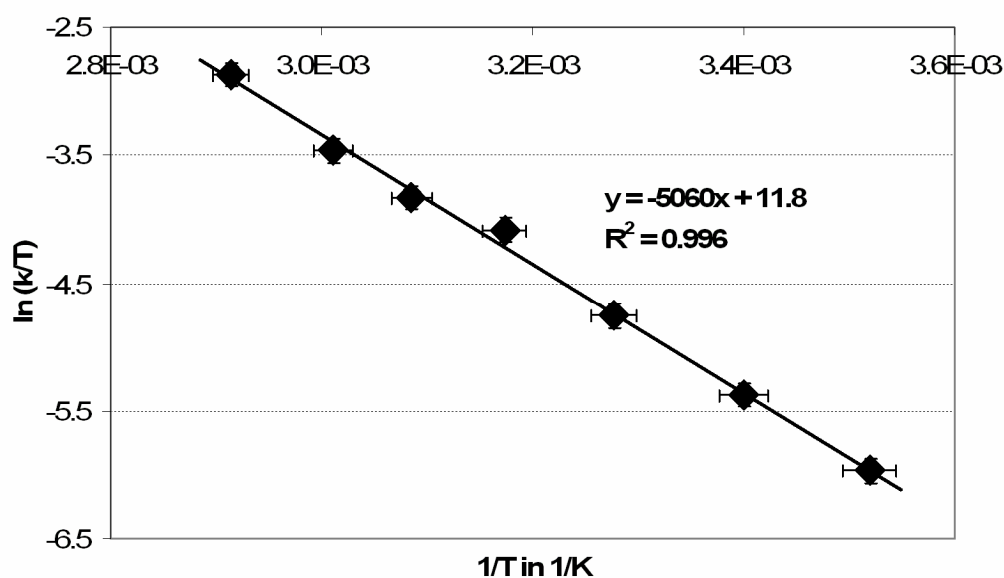


**Figure S23.** Eyring-plot for [Cp<sub>2</sub>Lu(*St*Bu)]<sub>2</sub>-initiated DIVP (6.25vol%) polymerization in toluene (11 – 70 °C,  $\Delta H^\ddagger = 42.0 \text{ kJ mol}^{-1}$ ,  $\Delta S^\ddagger = -99.1 \text{ J (mol K)}^{-1}$ ).

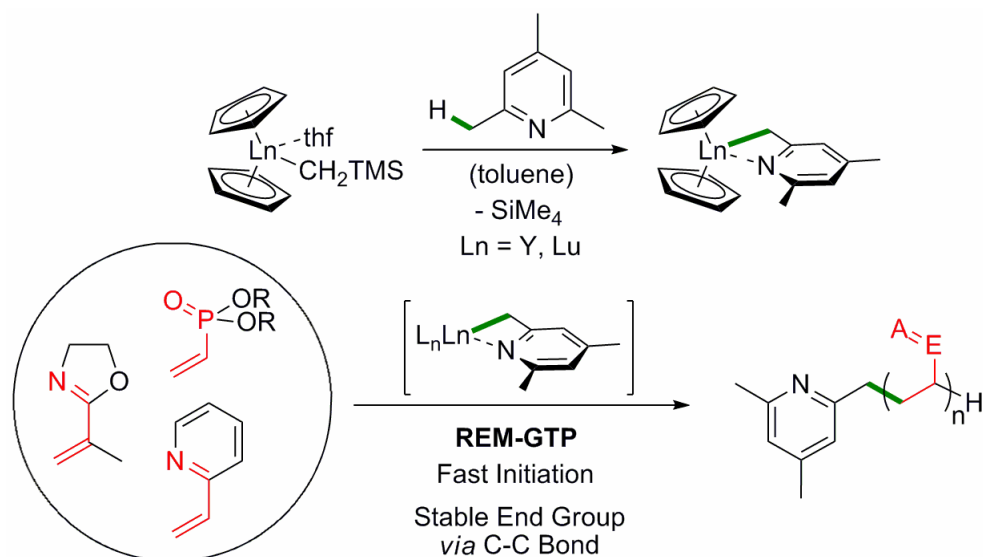
**References:**

- (1) APEX suite of crystallographic software. APEX 2 Version 2008.4. Bruker AXS Inc., Madison, Wisconsin, USA (2008).
- (2) SAINT, Version 7.56a and SADABS Version 2008/1. Bruker AXS Inc., Madison, Wisconsin, USA (2008).
- (3) Altomare, A.; Cascarano, G.; Giacovazzo, C.; Guagliardi, A.; Burla, M. C.; Polidori, G.; Camalli M. "**SIR92**", *J. Appl. Cryst.* **1994**, *27*, 435-436.
- (4) International Tables for Crystallography, Vol. C, Tables 6.1.1.4 (pp. 500-502), 4.2.6.8 (pp. 219-222), and 4.2.4.2 (pp. 193-199), Wilson, A. J. C., Ed., Kluwer Academic Publishers, Dordrecht, The Netherlands, 1992.
- (5) Sheldrick, G. M. "**SHELXL-97**", University of Göttingen, Göttingen, Germany, (1998).
- (6) Spek, A. L. "**PLATON**", A Multipurpose Crystallographic Tool, Utrecht University, Utrecht, The Netherlands, (2010).
- (7) L. J. Farrugia, "**WinGX** (Version 1.70.01 January 2005) ", *J. Appl. Cryst.* **1999**, *32*, 837-838.



## CHAPTER 10:

# C–H BOND ACTIVATION BY $\sigma$ -BOND METATHESIS AS A VERSATILE ROUTE TOWARDS HIGHLY EFFICIENT INITIATORS FOR RARE EARTH METAL-MEDIATED GROUP TRANSFER POLYMERIZATION



*“The great tragedy of science – the slaying of a beautiful hypothesis by an ugly fact.”*

- Thomas Henry Huxley (1825-1895)



**Status:** Preliminary Study  
**Journal:** designed for Organometallics  
**Publisher:** ACS Publications  
**Article type:** Note  
**DOI:** –  
**Authors:** Stephan Salzinger, Benedikt S. Soller, Bernhard Rieger

**Content:**

Within the scope of this chapter, it will be shown that C–H bond activation by protonolysis of classical  $\alpha$ -CH-acidic substrates is not a suitable alternative for the synthesis of rare earth metal enolates in comparison to the inconvenient established synthetic routes. On the contrary, C–H bond activation of non-classical CH-acidic substrates by  $\sigma$ -bond metathesis is a versatile route towards highly efficient and versatile initiators for REM-GTP. Accordingly, 2,4,6-trimethylpyridyl *bis*(cyclopentadienyl) rare earth metal complexes exhibit unprecedented initiation rates for rare earth metal-mediated dialkyl vinylphosphonate polymerization and facilitate an efficient initiation for a broad scope of Michael acceptor-type monomers. The further development of this synthetic route and the evaluation of the resulting REM-GTP initiators are of major importance for the expansion of REM-GTP to new monomers. Within the frame of this chapter, certain points are raised which need to be addressed before the corresponding manuscript is ready for submission.



# C-H Bond Activation by $\sigma$ -Bond Metathesis as a Versatile Route towards Highly Efficient Initiators for Rare Earth Metal-Mediated Group Transfer Polymerization

Stephan Salzinger, Benedikt S. Soller, Bernhard Rieger\*

WACKER-Lehrstuhl für Makromolekulare Chemie, Technische Universität München, Lichtenbergstraße 4, 85747 Garching bei München, Germany

## Supporting Information Placeholder

**ABSTRACT:** The use of C–H bond activation by alkylttrium-mediated  $\sigma$ -bond metathesis for the introduction of chain end functionalization in 2-vinylpyridine polymerization has been recently published. In this work, we demonstrate the suitability of this synthetic approach to rare earth metallocenes and show the applicability of the resulting complexes as highly efficient initiators for rare earth metal-mediated group transfer polymerization. 2,4,6-trimethylpyridyl *bis*(cyclopentadienyl) complexes exhibit unprecedented initiation rates for rare earth metal-mediated dialkyl vinylphosphonate polymerization and facilitate an efficient initiation for a broad scope of Michael acceptor-type monomers.

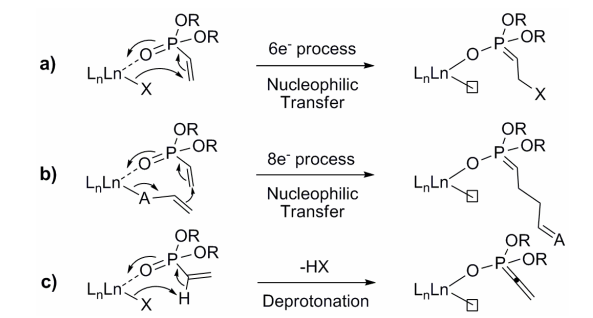
Since the first reports on living polymerizations of acrylic monomers using early transition metal initiators by Collins, Ward<sup>1</sup> and Yasuda *et al.*<sup>2</sup> in 1992, researchers have devoted their efforts in the optimization of reaction conditions and initiator efficiency and the extension of this method to a variety of (meth)acrylates and (meth)acrylamides.<sup>3–6</sup> In view of the propagation mechanism, this type of polymerization is recognized as coordinative-anionic or coordination-addition polymerization, and due to its similarity to silyl ketene acetal-initiated group transfer polymerization, it is also referred to as transition metal-mediated GTP.<sup>6–8</sup> Rare earth metal-mediated group transfer polymerization (REM-GTP) is of particular interest, as recent publications have shown that its applicability is not limited to common acrylic monomers, but that REM-GTP also facilitates the polymerization of several other monomer classes, *i.e.* dialkyl vinylphosphonates (DAVP), 2-isopropylene-2-oxazoline (IPOx) and 2-vinylpyridine (2VP).<sup>8–15</sup> Moreover, our group recently reported on the development of a surface-initiated group transfer polymerization (SI-GTP) mediated by rare earth metal catalysts allowing the perfect decoration of substrates with polymer brushes of specific functionality.<sup>16</sup>

The applicability of REM-GTP to these new monomers opens the access to a variety of tailor-made functional materials, as this polymerization method combines the advantages of both living ionic and coordinative polymerizations. According to its highly living character, REM-GTP leads to strictly linear polymers with

very narrow molecular weight distribution ( $PDI < 1.1$ ), exhibits linear increase of the average molar mass upon monomer conversion and allows the synthesis of block copolymers as well as the introduction of chain end functionalities.<sup>3–6</sup> The coordination of the growing chain end at the catalyst suppresses side reactions and allows stereospecific polymerization as well as activity optimization by variation of both the metal center and the catalyst ligand sphere.<sup>3–6,8</sup>

REM-GTP initiation usually proceeds *via* nucleophilic transfer of a strongly basic ligand, *e.g.* hydride, methyl or  $\text{CH}_2\text{TMS}$ , to a coordinated monomer (Scheme 1a, this is not the case for divalent rare earth metal centers, for which redox initiation occurs).<sup>6,17</sup> This stands in large contrast to group 4 metal-mediated GTP, for which these initiators often lead to a slow and non-uniform initiation.<sup>6</sup> Accordingly, for these systems, a variety of strategies for the synthesis of enolate initiators, which follow a faster initiation mechanism over an eight electron process (Scheme 1b), has been presented.<sup>6</sup> Surprisingly and supposedly attributed to the suitability of more simple initiators, only little efforts were devoted to the development of new initiating species for rare earth metal-based catalysts, which would in turn allow the introduction of a large range of chain end functionalities.

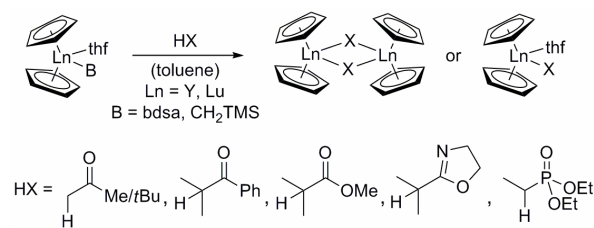
**Scheme 1. Possible initiation reactions for REM-GTP of DAVP: nucleophilic transfer *via* a (a)  $6e^-$  or (b)  $8e^-$  process and (c) deprotonation of the acidic  $\alpha$ -CH.**



In previous work, we have shown that late lanthanide metallocenes are highly active catalysts for DAVP polymerization.<sup>11</sup> However, in detailed mechanistic studies we found that the traditionally used strongly basic methyl and CH<sub>2</sub>TMS initiators lead to an inefficient, slow initiation by deprotonation of the acidic  $\alpha$ -CH (Scheme 1c).<sup>18</sup> Sterically crowded Cp<sub>3</sub>Ln complexes and thiolato complexes [Cp<sub>2</sub>Ln(S*t*Bu)]<sub>2</sub> were found to efficiently initiate DAVP polymerization, however, further development of Cp<sub>3</sub>Ln complexes is limited and thiolate end groups were found to be prone to elimination.<sup>18</sup> Moreover, these complexes are not suitable initiators for sterically less demanding or weaker coordinating monomers such as IPOx or 2VP.<sup>15,18</sup>

Accordingly, the development of new initiators for REM-GTP, which facilitate an efficient initiation for a broad scope of monomers and which lead to a stable end group functionalization *via* a C–C bond, is still of current interest. Inspired by the use of enolate-type initiators in zirconium-mediated GTP our group focused on the development enolate or enamide initiators (Scheme 2) in order to facilitate an initiation over an eight electron process also for rare earth metal-based systems.

**Scheme 2. Attempted synthesis of enolate and enamide rare earth metallocene initiators *via* C–H bond activation of classical  $\alpha$ -CH-acidic substrates.**



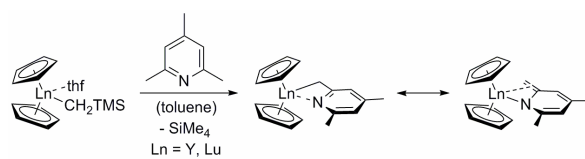
As synthetic routes *via* salt metathesis from lithium enolates and rare earth metal chlorides and *via* thermolysis of alkyl complexes in presence of tetrahydrofuran are restricted to selected systems only,<sup>19</sup> we decided to investigate the accessibility of rare earth enolates *via*  $\alpha$ -CH-activation of the respective carbonyls (or oxazoline/phosphonate) by amide and alkyl precursors Cp<sub>2</sub>Ln(bdsa)(thf) and Cp<sub>2</sub>Ln(CH<sub>2</sub>TMS)(thf) (bdsa = *bis*(dimethylsilylamide), N(SiMe<sub>2</sub>H)<sub>2</sub>).

The rather low basicity of the bdsa precursor (pK<sub>a</sub>(bdsaH) = 22.8<sup>20</sup>) limits its suitable spectrum of  $\alpha$ -acidic substrates to ketones and aldehydes. Accordingly, we first evaluated the reaction between Cp<sub>2</sub>Ln(bdsa)(thf) and acetone resulting in the quantitative formation of Cp<sub>2</sub>Ln(N(SiMe<sub>2</sub>O*t*Pr)(SiMe<sub>2</sub>H)) by hydrosilylation of the carbonyl moiety. Addition of a second equivalent of acetone leads to decomposition. Nevertheless, the isolated complex was tested towards DAVP polymerization, exhibiting similar efficiency and activity as the precursor complex. Attempts to preclude a hydrosilylation reaction by the use of a more sterically demanding ketone, *i.e.* *tert*-butyl methyl ketone, were unsuccessful. In contrast to the reaction with acetone, a statistic mixture between starting material, single and double hydrosilylated product is formed for addition of 1 equivalent of ketone.

Surprisingly, the more reactive Cp<sub>2</sub>Ln(CH<sub>2</sub>TMS)(thf) precursor lead to no reaction with a large variety of substrates up to elevated reaction temperatures, at which decomposition was observed, revealing a pronounced kinetic limitation for the protonolysis reaction. Only with *iso*-butyrophenone, a defined reaction product could be isolated. However, instead of deprotonation of the acidic  $\alpha$ -CH, a nucleophilic attack of the CH<sub>2</sub>TMS ligand at the carbonyl moiety under the formation of the corresponding alkoxide was observed.

Despite numerous attempts and the use of a different precursor complexes and substrates, the formation of enolate rare earth complexes by protonolysis of classical  $\alpha$ -CH-acidic substrates could not be facilitated. Only recently, Mashima *et al.* reported on the introduction of chain end functionality for 2VP polymerization by initial C–H bond activation of non-classical CH-acidic substrates *via* alkylttrium-mediated  $\sigma$ -bond metathesis.<sup>12</sup> In order to evaluate the applicability of this approach to rare earth metallocenes, we reacted Cp<sub>2</sub>Ln(CH<sub>2</sub>TMS)(thf) with 2,4,6-trimethylpyridine in toluene solution yielding the desired Cp<sub>2</sub>Ln(CH<sub>2</sub>((C<sub>5</sub>N)H<sub>2</sub>Me<sub>2</sub>)) after stirring at room temperature for 30 min or 6 h for Ln = Y or Lu, respectively (Scheme 3).

**Scheme 3. Synthesis of Cp<sub>2</sub>Ln(CH<sub>2</sub>((C<sub>5</sub>N)H<sub>2</sub>Me<sub>2</sub>)) *via* C–H bond activation by  $\sigma$ -bond metathesis and coordination as carbanion or enamide to the metal center.**



In order to verify the suitability of these complexes as initiators for REM-GTP, we carried out polymerization experiments with DEVP and IPOx. Hereby, for the first time using a Cp<sub>2</sub>LnX initiator, polymerization of DEVP could be facilitated without observation of an initiation period (Figure 1, Table 1). Activity measurements revealed a linear increase of the number-averaged molecular weight upon conversion, narrow polydispersity throughout the whole reaction and activities comparable to those observed for the corresponding “state-of-the-art” thiolato complexes (Figure 2, Table 1).<sup>18</sup> Intriguingly, in contrast to the previously applied thiolato complexes,<sup>18</sup> the initiator efficiency of the Y complex remains constant throughout the whole polymerization (Figure 1), indicating the initiator efficiency of 52% to be a result of an initial deactivation by impurities only. Moreover, these complexes also initiated the polymerization of IPOx, even though only materials with a rather broad polydispersity could be obtained, indicating a slow and non-uniform initiation (Table 1). Detailed investigations on IPOx polymerization using the presented catalysts need to be performed still. Nevertheless, the described complexes are the first systems exhibiting high initiator efficiencies for both DAVP and IPOx polymerization.

**Table 1. Comparison of  $\text{Cp}_2\text{Ln}(\text{CH}_2(\text{C}_5\text{N})\text{H}_2\text{Me}_2)$  with “state-of-the-art” catalysts<sup>15,18</sup> (toluene, 30 °C)**

Catalyst	Monomer	$[\text{Mon}]_0/[\text{Cat}]_0$	Init. period <sup>a</sup>	$M_n^b$ /kDa	PDI <sup>b</sup>	$I_t^b$ /%	$I^b$ /%	TOF <sup>c</sup> /h <sup>-1</sup>	TOF/ $I_t$ /h <sup>-1</sup>
$\text{Cp}_2\text{Y}(\text{CH}_2(\text{C}_5\text{N})\text{H}_2\text{Me}_2)$	DEVP	600	-	190	1.11	54	52	43,000	80,000
$[\text{Cp}_2\text{Y}(\text{S}t\text{Bu})_2]$	DEVP	600	5 sec	150	1.18	54	65	44,000	81,000
$\text{Cp}_2\text{Lu}(\text{CH}_2(\text{C}_5\text{N})\text{H}_2\text{Me}_2)$	DEVP	600	-	500	1.41	14	20	31,000	220,000
$[\text{Cp}_2\text{Lu}(\text{S}t\text{Bu})_2]$	DEVP	600	15 sec	210	1.35	30	47	103,000	340,000
$\text{Cp}_2\text{Y}(\text{CH}_2(\text{C}_5\text{N})\text{H}_2\text{Me}_2)$	IPOx	300	-	23	1.6	- <sup>d</sup>	n.d. <sup>e</sup>	- <sup>d</sup>	- <sup>d</sup>
$\text{Cp}_2\text{Lu}(\text{CH}_2(\text{C}_5\text{N})\text{H}_2\text{Me}_2)$	IPOx	300	-	21	1.5	- <sup>d</sup>	n.d. <sup>e</sup>	- <sup>d</sup>	- <sup>d</sup>
$[\text{Cp}_2\text{YbMe}_2]$	IPOx	200	-	21	1.04	95	95	380	400

<sup>a</sup>Initiation period, reaction time until 3% conversion is reached, <sup>b</sup>determined by GPC-MALS,  $I_t^b = M_h/M_n$ ,  $M_h = [\text{Mon}]_0/[\text{Cat}]_0 \times M_{\text{Mon}} \times \text{conversion}$  ( $I_t^b$  at the maximum rate,  $I^b$  at the end of the reaction), <sup>c</sup>determined by <sup>31</sup>P (DEVP) or <sup>1</sup>H (IPOx) NMR spectroscopic measurement, <sup>d</sup>activity measurements still need to be performed, <sup>e</sup>not determined due to incomplete conversion.

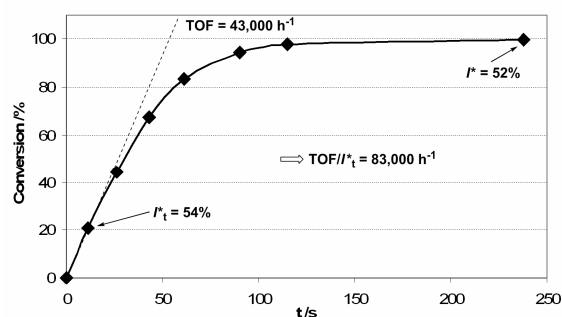


Figure 1. Conversion-reaction time plot for polymerization of DEVP using  $\text{Cp}_2\text{Y}(\text{CH}_2(\text{C}_5\text{N})\text{H}_2\text{Me}_2)$ , showing constant  $I^*$  during the complete reaction (7.4 mg catalyst, 10vol% DEVP in 20 mL toluene, 30 °C).

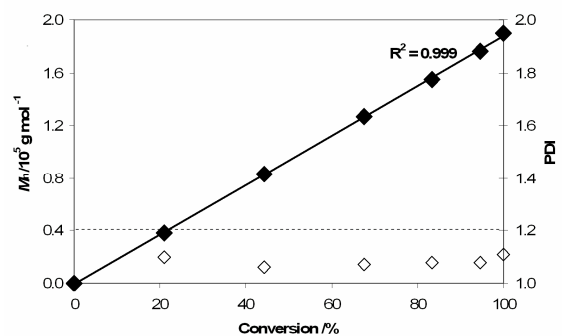


Figure 2. Linear increase of the number-averaged molecular weight during DEVP polymerization using  $\text{Cp}_2\text{Y}(\text{CH}_2(\text{C}_5\text{N})\text{H}_2\text{Me}_2)$ , and corresponding polydispersity (7.4 mg catalyst, 10vol% DEVP in 20 mL toluene, 30 °C).

The (4,6-dimethylpyridin-2-yl)methyl ligand can coordinate to the metal center both in form of a carbanion or in form of an enamide (Scheme 2). Accordingly, initiation of DAVP polymerization could occur *via* all three routes presented in Scheme 1. ESI MS analysis of produced DEVP oligomers shows a chain end

functionalization by (4,6-dimethylpyridin-2-yl)methyl and does not provide any evidence for initial deprotonation (Figure 3), which is in accordance with the observed high initiation rates. Consequently, initiation by nucleophilic transfer is evident; if it proceeds *via* a 6 or 8 electron process may not be revealed by an experimental approach and requires a further theoretical study.

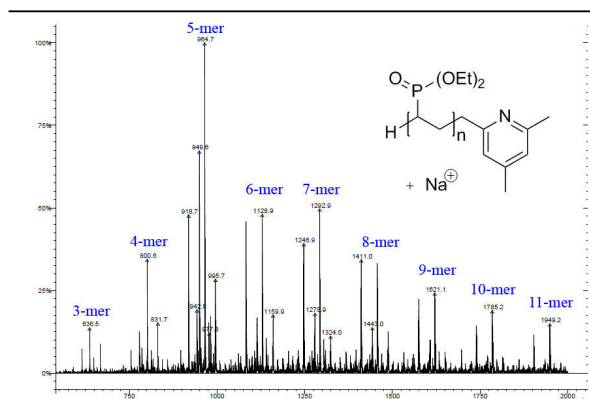
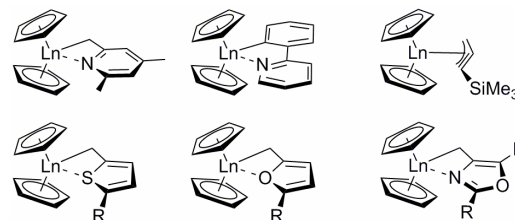


Figure 3. ESI MS spectrum of DEVP oligomers produced with  $\text{Cp}_2\text{Y}(\text{CH}_2(\text{C}_5\text{N})\text{H}_2\text{Me}_2)$ .

#### Chart 1. Examples for REM-GTP initiators accessible by rare earth metal-mediated $\sigma$ -bond metathesis.



In summary, we have shown that C–H bond activation by protonolysis of classical  $\alpha$ -CH-acidic substrates is not a suitable synthetic route towards rare earth metal enolates. On the contrary, C–H bond activation of non-classical CH-acidic substrates by  $\sigma$ -

bond metathesis, as previously presented by Teuben *et al.*<sup>21-23</sup> and Mashima *et al.*,<sup>12</sup> is a versatile route towards highly efficient and versatile initiators for REM-GTP of a variety of Michael acceptor-type monomers.

Before this manuscript is ready for submission, the following points should be addressed: first, a broader variety of initiators needs to be synthesized by  $\sigma$ -bond metathesis and tested for REM-GTP (for examples, see Chart 1). The initiators need to be isolated and fully characterized. Second, polymerization and oligomerization experiments should be conducted for DEVP, MMA, IPOx and 2VP as examples for every important monomer class currently known to be susceptible to REM-GTP. According to the original protocol by Mashima *et al.*<sup>12</sup>, these polymerization experiments should be conducted with both isolated complexes and by *in situ*  $\sigma$ -bond metathesis. From these polymerization data, the versatility of the applied initiators concerning their application to different monomer classes needs to be evaluated. Rare earth metal-mediated  $\sigma$ -bond metathesis allows the introduction of a vast variety of chain end functionality,<sup>12</sup> hence, in combination with the observed fast and simultaneous initiation, this approach is very promising for a further development of new binding layers for SI-GTP. Accordingly, as a third major point, the applicability of these new initiators for SI-GTP should be evaluated. After addressing these points, in respect of the length of the final manuscript, change of the article format from a note to an article may be necessary.

## ASSOCIATED CONTENT

### Supporting Information

Detailed procedures for complex synthesis, polymerization and oligomerization reactions. This material is available free of charge via the Internet at <http://pubs.acs.org>.

## AUTHOR INFORMATION

### Corresponding Author

\*rieger@tum.de.

## ACKNOWLEDGMENT

The authors thank Dr. Ning Zhang for valuable discussions. S.S. is grateful for a generous scholarship from the Fonds der Chemischen Industrie.

## REFERENCES

- (1) Collins, S.; Ward, D. G. *J. Am. Chem. Soc.* **1992**, *114*, 5460.
- (2) Yasuda, H.; Yamamoto, H.; Yokota, K.; Miyake, S.; Nakamura, A. *J. Am. Chem. Soc.* **1992**, *114*, 4908.
- (3) Yasuda, H.; Ihara, E. *Macromol. Chem. Phys.* **1995**, *196*, 2417.
- (4) Yasuda, H.; Ihara, E. *Adv. Polym. Sci.* **1997**, *133*, 53.
- (5) Yasuda, H. *Prog. Polym. Sci.* **2000**, *25*, 573.
- (6) Chen, E. Y.-X. *Chem. Rev.* **2009**, *109*, 5157.
- (7) Webster, O. W. *Adv. Polym. Sci.* **2004**, *167*, 1.
- (8) Salzinger, S.; Rieger, B. *Macromol. Rapid Commun.* **2012**, *33*, 1327.
- (9) Seemann, U. B.; Dengler, J. E.; Rieger, B. *Angew. Chem., Int. Ed.* **2010**, *49*, 3489.
- (10) Rabe, G. W.; Komber, H.; Haeussler, L.; Kreger, K.; Lattermann, G. *Macromolecules* **2010**, *43*, 1178.
- (11) Salzinger, S.; Seemann, U. B.; Plikhta, A.; Rieger, B. *Macromolecules* **2011**, *44*, 5920.
- (12) Kaneko, H.; Nagae, H.; Tsurugi, H.; Mashima, K. *J. Am. Chem. Soc.* **2011**, *133*, 19626.
- (13) Zhang, N.; Salzinger, S.; Rieger, B. *Macromolecules* **2012**, *45*, 9751.
- (14) Zhang, N.; Salzinger, S.; Soller, B. S.; Rieger, B. *in preparation*.
- (15) Zhang, N.; Salzinger, S.; Deubel, F.; Jordan, R.; Rieger, B. *J. Am. Chem. Soc.* **2012**, *134*, 7333.
- (16) Boffa, L. S.; Novak, B. M. *Macromolecules* **1994**, *27*, 6993.
- (17) Salzinger, S.; Soller, B. S.; Plikhta, A.; Seemann, U. B.; Herdtweck, E.; Rieger, B. *in preparation*.
- (18) Evans, W. J.; Dominguez, R.; Hanusa, T. P. *Organometallics* **1986**, *5*, 1291.
- (19) Eppinger, J.; Spiegler, M.; Hieringer, W.; Herrmann, W. A.; Anwander, R. *J. Am. Chem. Soc.* **2000**, *122*, 3080.
- (20) Duchateau, R.; van Wee, C. T.; Teuben, J. H. *Organometallics* **1996**, *15*, 2291.
- (21) Duchateau, R.; Brusse, E. A. C.; Meetsma, A.; Teuben, J. H. *Organometallics* **1997**, *16*, 5506.
- (22) Norambuena, V. F. Q.; Heeres, A.; Heeres, H. J.; Meetsma, A.; Teuben, J. H.; Hessen, B. *Organometallics* **2008**, *27*, 5672.



## *Supporting Information:*

# **C–H Bond Activation by $\sigma$ -Bond Metathesis as a Versatile Route towards Highly Efficient Initiators for Rare Earth Metal-Mediated Group Transfer Polymerization**

*Stephan Salzinger, Benedikt S. Soller, Bernhard Rieger\**

WACKER-Lehrstuhl für Makromolekulare Chemie, Technische Universität München,  
Lichtenbergstraße 4, 85748 Garching

### **Material and Methods**

All reactions were carried out under argon atmosphere using standard Schlenk or glovebox techniques. All glassware was heat dried under vacuum prior to use. Unless otherwise stated, all chemicals were purchased from Sigma-Aldrich, Acros Organics or ABCR and used as received. Toluene, THF and pentane were dried using an MBraun SPS-800 solvent purification system. Hexane was dried over 3Å molecular sieve. Li(bdsa),<sup>1</sup> the precursor complexes Ln(bdsa)<sub>3</sub>(thf)<sub>2</sub>,<sup>1</sup> Ln(CH<sub>2</sub>TMS)<sub>3</sub>(thf)<sub>2</sub>,<sup>2</sup> Cp<sub>2</sub>Ln(bdsa)(thf)<sup>3</sup> and Cp<sub>2</sub>Ln(CH<sub>2</sub>TMS)(thf)<sup>3</sup> as well as DEVP<sup>4</sup> were prepared according to literature procedures. Monomers were dried over calcium hydride and distilled prior to use.

NMR spectra were recorded on a Bruker AV-300 or AV-500C spectrometer. <sup>1</sup>H, <sup>13</sup>C and <sup>29</sup>Si NMR spectroscopic chemical shifts  $\delta$  are reported in ppm relative to tetramethylsilane.  $\delta(^1\text{H})$  is calibrated to the residual proton signal,  $\delta(^{13}\text{C})$  to the carbon signal and  $\delta(^{29}\text{Si})$  to the deuterium signal of the solvent. <sup>31</sup>P NMR spectroscopic chemical shifts are reported in ppm relative to and calibrated to 85% aqueous H<sub>3</sub>PO<sub>4</sub>. Deuterated solvents were obtained from Deutero or Eurisotop and dried over 3Å molecular sieve. Elemental analyses were measured at the Laboratory for Microanalytics at the Institute of Inorganic Chemistry at the Technische Universität München. ESI MS analytical measurements were performed with methanol solutions on a Varian 500-MS spectrometer, using 70 keV in the positive ionization mode.

## Complex Synthesis

### General procedure for the synthesis of $\text{Cp}_2\text{LnX}$ :

1 eq of a stem solution of XH in toluene (ca. 5 w%) is added dropwise to a toluene solution of 1 eq of  $\text{Cp}_2\text{Ln}(\text{bdsa})(\text{thf})$  or  $\text{Cp}_2\text{Ln}(\text{CH}_2\text{TMS})$  (ca. 0.1 M) at room temperature. The resulting mixture is stirred for the stated reaction time, the solvent and formed 1,1,3,3-tetramethyldisilazane/ $\text{SiMe}_4$  are removed *in vacuo* and the resulting solid is washed with pentane.

**$\text{Cp}_2\text{Lu}(\text{N}(\text{SiMe}_2\text{O}i\text{Pr})(\text{SiMe}_2\text{H}))$ :** Yield: 190 mg white powder (0.39 mmol, quantitative).  $^1\text{H}$  NMR ( $\text{C}_6\text{D}_6$ , 300 K, 500 MHz):  $\delta = 0.08$  (s, 6H,  $\text{Si}(\text{O}i\text{Pr})(\text{CH}_3)_2$ ), 0.27 (d, 6H,  $^3J(\text{H}-\text{H}) = 3.0$  Hz,  $\text{SiH}(\text{CH}_3)_2$ ), 0.73 (d, 6H,  $^3J(\text{H}-\text{H}) = 6.2$  Hz,  $\text{CH}(\text{CH}_3)_2$ ), 3.50 (sp, 1H,  $^3J(\text{H}-\text{H}) = 6.2$  Hz,  $\text{O}-\text{CH}(\text{CH}_3)_2$ ), 4.89 (sp, 1H,  $^3J(\text{H}-\text{H}) = 3.0$  Hz,  $\text{Si}-\text{H}$ ), 6.15 (s, 10H,  $\text{Cp}-\text{H}$ ).  $^{13}\text{C}$  NMR ( $\text{C}_6\text{D}_6$ , 300 K, 125 MHz):  $\delta = 2.5$  (s,  $\text{Si}(\text{CH}_3)_2$ ), 3.2 (s,  $\text{Si}(\text{CH}_3)_2$ ), 24.9 (s,  $\text{CH}(\text{CH}_3)_2$ ), 68.7 (s,  $\text{O}-\text{CH}(\text{CH}_3)_2$ ), 111.6 (s,  $\text{Cp}-\text{C}$ ).  $^{29}\text{Si}$  NMR ( $\text{C}_6\text{D}_6$ , 300K, 100 MHz):  $\delta = 24.5$  (s), 45.7 (s).

**$\text{Cp}_2\text{Lu}(\text{CH}_2((\text{C}_5\text{N})\text{H}_2\text{Me}_2))$ :** Yield: 270 mg yellow powder (0.64 mmol, 82%).  $^1\text{H}$  NMR ( $\text{THF}-d_8$ , 298 K, 300 MHz):  $\delta = 1.78$  (s, 2H,  $\text{CH}_2$ ), 2.11 (s, 3H,  $\text{CH}_3$ ), 2.33 (s, 3H,  $\text{CH}_3$ ), 5.75 (s, 10H,  $\text{Cp}-\text{H}$ ), 5.95 (s, 1H,  $\text{Pyr}-\text{CH}$ ), 6.18 (s, 1H,  $\text{Pyr}-\text{CH}$ ).  $^{13}\text{C}$  NMR ( $\text{C}_6\text{D}_6$ , 298 K, 75 MHz):  $\delta = 21.1$  (s,  $\text{CH}_3$ ), 23.5 (s,  $\text{CH}_3$ ), 36.7 (s,  $\text{CH}_2$ ), 109.0 (s,  $\text{Cp}-\text{C}$ ), 113.4 (s,  $\text{Pyr}-\text{CH}$ ), 116.6 (s,  $\text{Pyr}-\text{CH}$ ), 148.4 (s,  $\text{Pyr}-\text{C}_{\text{qu}}$ ), 157.5 (s,  $\text{Pyr}-\text{C}_{\text{qu}}$ ), 170.0 (s,  $\text{Pyr}-\text{C}_{\text{qu}}$ ). Product contains 2,4,6-trimethylpyridine.

**$\text{Cp}_2\text{Y}(\text{CH}_2((\text{C}_5\text{N})\text{H}_2\text{Me}_2))$ :** Yield: 380 mg yellow powder (1.1 mmol, 77%).  $^1\text{H}$  NMR ( $\text{THF}-d_8$ , 298 K, 300 MHz):  $\delta = 1.89$  (s, 2H,  $\text{CH}_2$ ), 2.09 (s, 3H,  $\text{CH}_3$ ), 2.32 (s, 3H,  $\text{CH}_3$ ), 5.84 (s, 10H,  $\text{Cp}-\text{H}$ ), 5.98 (s, 1H,  $\text{Pyr}-\text{CH}$ ), 6.15 (s, 1H,  $\text{Pyr}-\text{CH}$ ).  $^{13}\text{C}$  NMR ( $\text{C}_6\text{D}_6$ , 298 K, 75 MHz):  $\delta = 21.1$  (s,  $\text{CH}_3$ ), 23.8 (s,  $\text{CH}_3$ ), 41.4 (s,  $\text{CH}_2$ ), 109.8 (s,  $\text{Cp}-\text{C}$ ), 111.1 (s,  $\text{Pyr}-\text{CH}$ ), 115.6 (s,  $\text{Pyr}-\text{CH}$ ), 147.1 (s,  $\text{Pyr}-\text{C}_{\text{qu}}$ ), 157.3 (s,  $\text{Pyr}-\text{C}_{\text{qu}}$ ), 167.7 (s,  $\text{Pyr}-\text{C}_{\text{qu}}$ ). Product contains 2,4,6-trimethylpyridine.

## Oligomerization

5 eq of the respective monomer are added to 1 eq of catalyst in toluene. The resulting mixture is stirred for 2 hours at room temperature and quenched by addition of MeOH. Volatiles were removed under reduced pressure and the residue is extracted with MeOH. For end group analysis, ESI-MS measurements of the methanolic extract are performed.

### Activity measurements

For activity measurements, the stated amount of catalyst (15-50  $\mu\text{mol}$ ) is dissolved in 20 mL of toluene (DEVP polymerization) or toluene-d8 (IPOx polymerization), and the reaction mixture is thermostated to the desired temperature. Then, the stated amount of monomer (3.5-13 mmol) is added. During the course of the measurement, the temperature is monitored with a digital thermometer and aliquots (0.5 mL) are taken and quenched by addition to deuterated methanol (0.2 mL). After the stated reaction time, the reaction is quenched by addition of MeOD (0.5 mL). The reaction is carried out in an MBraun Glovebox under argon atmosphere to take aliquots every 6-10 seconds at the beginning of the measurement. For each aliquot, the conversion is determined by  $^1\text{H}$  (IPOx) or  $^{31}\text{P}$  (DEVP) NMR spectroscopy, the molecular weight of the formed polymer by GPC-MALS analysis.

### Molecular Weight Determination

GPC was carried out on a Varian LC-920 equipped with two PL Polargel columns. As eluent a mixture of 50% THF, 50% water, and 9 g L<sup>-1</sup> tetrabutylammonium bromide (TBAB) was used. Absolute molecular weights have been determined online by multiangle light scattering (MALS) analysis using a Wyatt Dawn Heleos II in combination with a Wyatt Optilab rEX as concentration source.

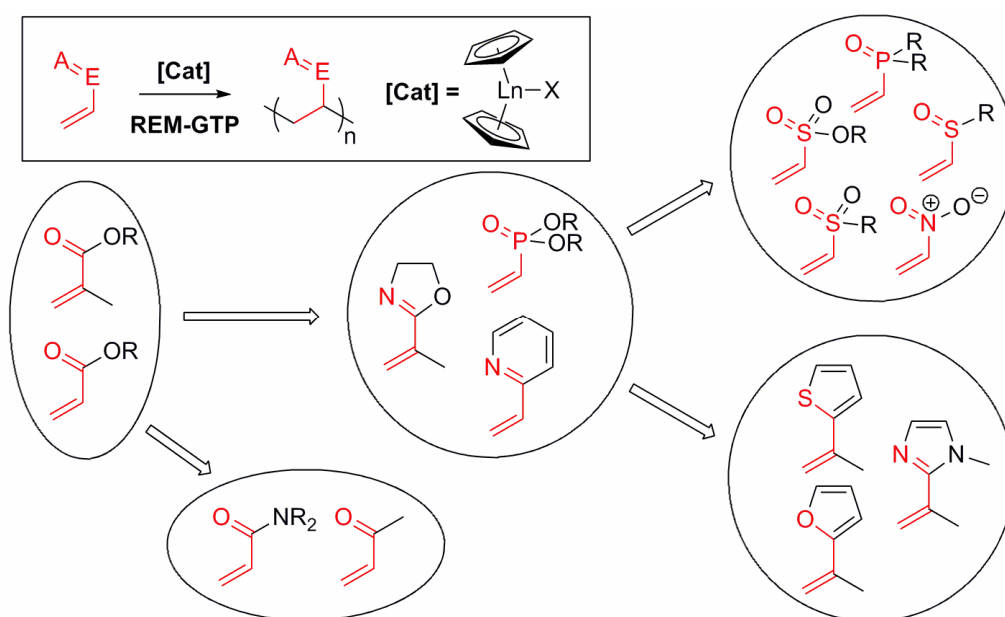
### References

- [1] Eppinger, J. *PhD Thesis*, Technische Universität München, Garching bei München, May 1999.
- [2] Hultsch, K. C.; Voth, P.; Beckerle, K.; Spaniol, T. P.; Okuda, J. *Organometallics* **2000**, 19, 228.
- [3] Salzinger, S.; Soller, B. S.; Plikhta, A.; Seemann, U. B.; Herdtweck, E.; Rieger, B. *in preparation*.
- [4] Leute, M. *PhD Thesis*, Universität Ulm, **2007**.



## CHAPTER 11:

# APPLICATION OF RARE EARTH METAL-MEDIATED GROUP TRANSFER POLYMERIZATION TO NEW MONOMER CLASSES



*“If knowledge can create problems, it is not through ignorance that we can solve them.”*

- Isaac Asimov (1919-1992)



<b>Status:</b>	Concept & Initial Investigations
<b>Journal:</b>	designed for Macromolecules
<b>Publisher:</b>	ACS Publications
<b>Article type:</b>	Article
<b>DOI:</b>	–
<b>Authors:</b>	Stephan Salzinger, Benedikt S. Soller, Bernhard Rieger

**Content:**

Within this chapter, the suitability of REM-GTP for the polymerization of monomer classes with functional groups, which have not yet been tested for REM-GTP, is evaluated, including monomers comprising heteroatom-centered functionalities, *e.g.* phosphineoxide, sulfoxide, sulfone and sulfonate, as well as a variety of heteroaromatic monomers. The previously established monomer reactivity order is expanded to acrylamides, revealing coordination strength to the rare earth metal center comparable to vinylphosphonates. Accordingly, both statistical and block copolymers of *N,N*-dimethyl acrylamide (DMAA) and diethyl vinylphosphonate (DEVP) could be synthesized. A versatile synthetic route towards dialkylvinylphosphineoxides is presented; however, requiring further optimization of the synthesis protocol. A conceptual approach to verify the polymerizability of the described monomers by means of REM-GTP is illustrated, allowing the development of a deeper understanding of the prerequisites monomers need to possess in order to be susceptible to REM-GTP. Furthermore, experiments are suggested to expand the established monomer reactivity order to the new monomers and to analyze and overcome limitations caused by the pronounced polarity of some applied monomers and the corresponding polymers.





# Application of Rare Earth Metal-Mediated Group Transfer Polymerization to New Monomer Classes

Stephan Salzinger, Benedikt S. Soller, Bernhard Rieger\*

WACKER-Lehrstuhl für Makromolekulare Chemie, Technische Universität München, Lichtenbergstraße 4, 85748 Garching b. München

*Catalysis, Copolymerization, Coordinative polymerization, Group Transfer Polymerization, Rare Earth Metals*

Supporting Information Placeholder

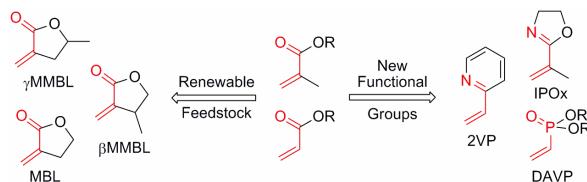
**ABSTRACT:** In this work, we evaluate the suitability of REM-GTP for the polymerization of monomer classes with functional groups, which have not yet been tested for REM-GTP, including monomers comprising heteroatom-centered functionalities, *e.g.* phosphineoxide, sulfoxide, sulfone and sulfonate, as well as a variety of heteroaromatic monomers. The previously established monomer reactivity order could be expanded to acrylamides, revealing coordination strength to the rare earth metal center comparable to vinylphosphonates. A versatile synthetic route towards dialkylvinylphosphineoxides is presented. We propose a conceptual approach to verify the polymerizability of these monomers, allowing the development of a deeper understanding of the prerequisites monomers need to possess in order to be susceptible to REM-GTP. We furthermore suggest experiments to expand the established monomer reactivity order to the new monomers and to analyze and overcome limitations caused by the pronounced polarity of some applied monomers and the corresponding polymers.

## Introduction

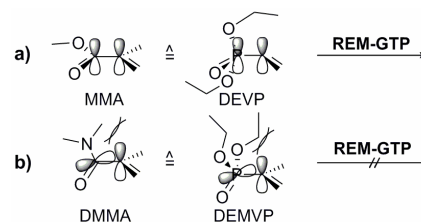
Rare earth metal-mediated group transfer polymerization (REM-GTP) of acrylic monomers was first reported by Yasuda *et al.*<sup>1</sup> in 1992; in view of the polymerization mechanism, it is also referred to as coordinative-anionic or coordination-addition polymerization.<sup>2</sup> REM-GTP combines the advantages of both living ionic and coordinative polymerizations. According to its highly living character, it leads to strictly linear polymers with very narrow molecular weight distribution (PDI < 1.1), exhibits linear increase of the average molar mass upon monomer conversion and allows the synthesis of block copolymers as well as the introduction of chain end functionalities.<sup>2-6</sup> The coordination of the growing chain end at the catalyst suppresses side reactions and allows stereospecific polymerization as well as activity optimization by variation of both the metal center and the catalyst ligand sphere.<sup>2-6</sup>

Over the past decades, intensive research has been carried out to optimize the reaction conditions as well as the initiator efficiency and activity of the applied catalysts.<sup>2-5</sup> Recently, our group reported on the development of a surface-initiated group transfer polymerization (SI-GTP) mediated by rare earth metal catalysts allowing the perfect decoration of substrates with polymer brushes of specific functionality.<sup>7</sup> Despite the advantages combined by REM-GTP, which make this method a versatile tool for the synthesis of tailor-made functional materials, its application has long been restricted to common (meth)acrylates. Recent publications have shown that REM-GTP is also applicable to monomers originating from renewable feedstocks, *i.e.*  $\alpha$ -methylene- $\gamma$ -(methyl)butyrolactones (MBL,  $\beta$ MMBL,  $\gamma$ MMBL),<sup>8-11</sup> as well as to several other monomer classes, *i.e.* dialkyl vinylphosphonates (DAVP), 2-isopropenyl-2-oxazoline (IPOx) and 2-vinylpyridine (2VP) (Scheme 1).<sup>6,7,12-18</sup>

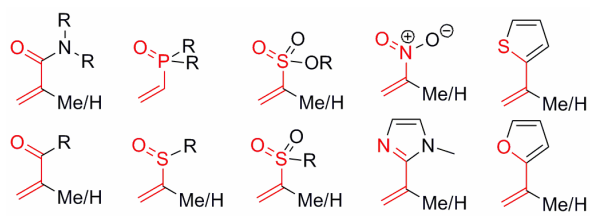
## Scheme 1. Recent expansion of REM-GTP to acrylic monomers from renewable feedstocks and to new monomer classes.



## Scheme 2. (a) Sufficient $\pi$ -overlap of the double bonds as a prerequisite for monomers susceptible to REM-GTP, *e.g.* MMA, DEVP; (b) monomers with disturbed planarity of the Michael system (*e.g.* DMMA, DEMVP) cannot be polymerized by REM-GTP.



This expansion of REM-GTP shows that monomers suitable for this polymerization type need to exhibit Michael acceptor-type behavior and a sufficient  $\pi$ -overlap of the double bonds in an S-cis conformation (Scheme 2a). Accordingly, monomers for which steric repulsion disturbs the planarity of the Michael system, *e.g.* *N,N*-dimethyl methacrylamide (DMMA) or diethyl 1-methylvinylphosphonate (DEMVP), were found to not be susceptible to coordination-addition polymerizations (Scheme 2b).<sup>2,6,19</sup>

**Chart 1. New monomer classes tested for REM-GTP.**

Inspired by its recent expansion, in order to further increase the range of functional materials accessible by REM-GTP, we are currently conducting a detailed investigation on the polymerizability of Michael acceptor-type monomers with other functional groups (Chart 1) by rare earth metal catalysts. For monomers found non-polymerizable by means of REM-GTP, evaluations are performed whether limitations occur according to an unfeasible initiation or propagation or as a result of readily occurring termination reactions (e.g. as observed for methyl acrylate<sup>20,21</sup>). Using this approach, we attempt to develop a deeper understanding of the prerequisites monomers need to possess in order to be susceptible to REM-GTP.

Previous REM-GTP copolymerization studies have shown the addition sequence of the comonomers to be critical for monomers with different coordination strength to the metal center, *i.e.* monomers can only be polymerized in order of increasing coordination strength.<sup>6,12,17,22</sup> Within the frame of this work, the established reactivity order of different monomer classes, *i.e.* DEVP > MMA > IPOx > 2VP,<sup>17</sup> should be expanded to the new monomers found susceptible to REM-GTP. Within our previous study, we observed that consecutive polymerization of comonomers is not only restricted to an order of increasing coordination strength, but also to comonomers with similar polarity.<sup>17</sup> Further verification of the proposed underlying encapsulation of the catalyst during polymerization of rather hydrophilic monomers, *e.g.* IPOx or 2VP, needs to be performed.

In this manuscript, we present first preliminary results in the expansion of REM-GTP to further monomer classes and describe our conceptual approach to address the above detailed inquiries, *i.e.* the verification of necessary monomer prerequisites, the expansion of the monomer reactivity order and how to analyze and overcome limitations caused by the pronounced polarity of some applied monomers and the corresponding polymers.

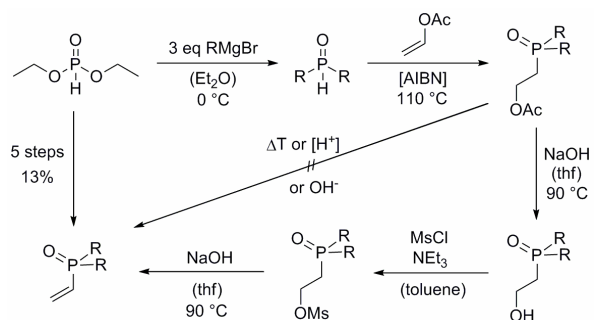
## Results and Discussion

Recently, our group and others reported on rare earth metal-mediated polymerization of DAVP, IPOx and 2VP.<sup>6,7,12-18</sup> Inspired by this recent expansion to new monomer classes, we were interested in increasing the versatility of REM-GTP by evaluating its application to further Michael acceptor-type monomers. Particularly, this includes monomers comprising heteroatom-centered functionalities, *e.g.* phosphineoxide, sulfoxide, sulfone and sulfonate, as well as a variety of heteroaromatic monomers (Chart 1). Surprisingly, to the best of our knowledge, there are also no reports on successful rare earth metal-mediated polymerizations of vinyl and isopropenyl ketones as well as (meth)acrylamides.

Chen *et al.*<sup>2,19,22-24</sup> reported on highly stereospecific polymerizations of acryl- and methacrylamides mediated by group 4 metallocenium cations, however, there are no reports on the polymerization of these monomers by isoelectronic rare earth metal-based systems. In a 1997 review, Yasuda and Ihara stated that silyl ketene acetal-mediated GTP has some advantages in synthesizing *poly(N,N-dimethylacrylamide)*, which [*is*] hardly produced with conventional organolanthanide initiators.<sup>4</sup> In contrast to this statement, we found that common rare earth metal initiators, *i.e.* [Cp<sub>2</sub>YbMe]<sub>2</sub>, Cp<sub>2</sub>Y(CH<sub>2</sub>TMS)(thf) and [Cp<sub>2</sub>Y(S*t*Bu)]<sub>2</sub> readily polymerize *N,N*-dimethyl acrylamide (DMAA) in toluene solution at room temperature. Complete conversion was observed within a couple of seconds; however, formed polymer immediately precipitated as it has been previously reported for group 4 metallocenium-mediated GTP,<sup>23</sup> resulting in low initiator efficiencies (*I*\* < 30%) and inhomogeneous chain growth yielding rather broad polydispersities (PDI < 2.5). Copolymerization studies have shown a relative coordination strength to the rare earth metal center of DMAA > MMA, identical to isoelectronic zirconocenium cation-mediated GTP.<sup>22</sup> Intriguingly, DEVP-DMAA copolymerization studies revealed similar coordination strengths to the metal center for the comonomers, as both statistical and sequential copolymerizations (in both directions) could be facilitated. Statistical DEVP-DMAA copolymers did not immediately precipitate from toluene solution; accordingly, narrower molecular weight distributions were yielded. Detailed investigations on REM-GTP of (meth)acrylamides should include the polymerization of other (more hydrophobic, to preclude precipitation) monomers, the polymerization in DCM<sup>22,23</sup> or polar donor solvents (*vide infra*) and the determination of copolymerization parameters for vinylphosphonate-(meth)acrylamide copolymerizations.

Polymerization of methyl vinyl ketone (MVK) has been reported by both classical anionic polymerization as well as in presence of zirconocenes, however, there are no reports on the polymerization of vinyl or isopropenyl ketones by organo-rare earth metal initiators.<sup>2</sup> In initial attempts to polymerize MVK with the common rare earth metal initiators [Cp<sub>2</sub>YbMe]<sub>2</sub>, Cp<sub>2</sub>Y(CH<sub>2</sub>TMS)(thf) and [Cp<sub>2</sub>Y(S*t*Bu)]<sub>2</sub>, no monomer conversion was observed. More detailed investigations on the polymerizability of vinyl or isopropenyl ketones by rare earth metal complexes according to the conceptual approach presented below are necessary.

Inspired by the exclusive suitability of REM-GTP for the polymerization of DAVP, we investigated the polymerization of vinylphosphineoxides by rare earth metal catalysts. Polymerization of diphenylvinylphosphineoxide (DPVPO) by [Cp<sub>2</sub>YbMe]<sub>2</sub>, Cp<sub>3</sub>Yb and Cp<sub>2</sub>Lu(bdsa)(thf) (bdsa = *bis*(dimethylsilyl)amide) lead to the formation of oligomers only.<sup>25</sup> The polymerization was proposed to be limited by the poor solubility of both monomer and formed PDPVPO in toluene, inhibiting complete conversion.<sup>25</sup> In order to evaluate the suitability of rare earth metal catalysts for a larger variety of vinylphosphineoxides, we investigated a general synthetic approach for the synthesis of dialkylvinylphosphineoxides (DAVPO) in a 5-step procedure starting from commercially available diethyl phosphonate (Scheme 3). The corresponding dialkylphosphineoxide was formed by treatment of the starting material with 2 eq of alkyl grignard reagent (it is better to use 3 eq in order to ensure complete conversion). According to an original procedure invented by Hoechst researchers,<sup>26</sup> the phosphineoxide

**Scheme 3. Synthesis of DAVPO in 5 steps from diethyl phosphonate.**

is reacted in substance at 110 °C by dropwise addition of vinyl acetate and azoisobutyronitrile (AIBN), forming ( $\beta$ -acetoxyethyl)-dialkylphosphineoxide as the main coupling product. After ester hydrolysis and reaction of the hydroxyl function with mesyl chloride, elimination of MsOH under basic condition yields the desired DAVPO. Direct elimination of AcOH by thermal treatment as described in the original synthesis protocol<sup>27</sup> as well as under acidic or basic conditions could not be observed. The presented synthetic approach provides a versatile route to a large variety of DAVPOs, however, optimization of each reaction step is necessary in order to increase the rather poor overall yield of 13%. Synthesized di-*n*-butylvinylphosphineoxide (DBVPO) was not tested for polymerization yet; accordingly, detailed investigations on the applicability of REM-GTP to vinylphosphineoxides still need to be performed.

In order to evaluate the suitability of sulfur-centered moieties, methyl vinyl sulfoxide (MVSO),<sup>28,29</sup> methyl vinyl sulfone (MVSN)<sup>28,30</sup> and ethyl vinylsulfonate (EVS)<sup>31</sup> were synthesized according to literature procedures. For the corresponding isopropenyl monomers (corresponding to methacrylates), no convenient synthesis protocol could be found in literature. In first experiments, rare earth metal-initiated polymerization of EVS could not be observed.<sup>25</sup> Initial theoretical calculations indicate a higher electron density on the oxygen of the S=O moiety which is not part of the Michael system, suggesting a coordination to the metal center *via* this S=O moiety. Accordingly, activation of the Michael system would not be induced and a coordination-addition polymerization is not feasible. Alternatively, also irreversible  $\eta^2$ -coordination over both S=O moieties or formation of coordination oligomers *via* Ln-O=S=O-Ln bridges seems possible, again inhibiting polymerization. Nevertheless, a more detailed theoretical study needs to be performed and supported by experimental data. A corresponding limitation may also be observed for coordination-addition polymerization of vinyl sulfones; however, REM-GTP of vinyl sulfoxides and vinyl sulfones has not been evaluated yet.

Nitroethylene (NE) is readily accessible by dehydration of 2-nitroethanol with phthalic anhydride.<sup>32</sup> REM-GTP could be facilitated, however, analysis of the obtained polymeric material was complicated by poor solubility and intense coloring, inhibiting a reliable determination of the molecular weight *via* static light scattering. Accordingly, an improved synthetic procedure and a more detailed investigation on REM-GTP of NE and 2-nitropropylene (NP) are necessary.

2-isopropenyl-1-methyl imidazole (2IMI),<sup>33</sup> -thiophene (2IT)<sup>34</sup> and -furan (2IF)<sup>34</sup> were synthesized according to literature procedures. However, in our initial investigations we did not observe polymerization of these monomers by any of the applied rare earth metal catalysts. A detailed investigation on the polymerizability of heteroaromatic isopropenyl and especially vinyl monomers is still missing.

Concerning the recently presented rare earth metal-mediated polymerization of  $\alpha$ -methylene- $\gamma$ -(methyl)butyrolactones, an evaluation of the relative coordination strength of these cyclic acrylates to the rare earth metal center should be performed in the context of this work. Particularly, this includes the determination of copolymerization parameters for the statistical copolymerization with other monomer classes.

In order to verify the applicability of REM-GTP to the above detailed monomers, further investigations need to be performed. After proper purification and drying of the respective monomers, homopolymerizations need to be conducted or repeated with selected catalysts. Particularly, this selection should include a variation of the metal center (to adjust the activation barrier for the propagation reaction) and the initiating ligand (*e.g.* CH<sub>2</sub>TMS, Cp,<sup>14</sup> thiolate<sup>18</sup>). If a polymer product cannot be isolated, oligomerization experiments should be performed with the same catalysts. Mass spectrometric analysis should be used in order to verify if oligomers are produced and whether the initiating ligand L is transferred to a coordinated monomer or not (occurrence of  $m/z = M_{Mon} + M_L + M_{H/Na}$ ). Critical evaluation of the end groups should be conducted, in order to exclude an oligomerization *via* radical processes. If formation of oligomers is observed and can clearly be addressed to an initiation by the rare earth metal complex, the polymerization is either limited by a very slow propagation or due to readily occurring chain termination, *e.g.* *via* backbiting as observed for the polymerization of acrylates.<sup>21</sup> The existence of a limitation by chain termination can be verified by determination of the lifetime of the active chain ends<sup>20</sup> (*vide infra*) and by mass spectrometric end group analysis of produced oligomers.<sup>21</sup>

If homopolymerization of a certain monomer A cannot be facilitated by any of the applied catalysts, statistical and sequential copolymerizations should be performed with different comonomers B which are known to undergo REM-GTP and which exhibit (assumed) similar coordination strength to the metal center. If polymerization occurs, it should be verified whether A is incorporated into the formed polymers. If incorporation is observed, it should be verified by change of the feed ratio and kinetic analysis, whether the polymerization stops when B is completely converted. In this case, homopropagation of A is impossible; if polymerization continues, limitations arise according to an unfeasible initiation of A by the applied initiators. If copolymerization with no other monomer B can be facilitated, homopolymerization of B should be conducted with an addition of A before complete conversion of B. If polymerization stops at this point, A cannot be polymerized *and* serves as an inhibitor for REM-GTP.

For monomers which can undergo homopolymerization initiated by rare earth metal complexes, the lifetime of the active species needs to be evaluated. This particularly includes the previously applied monomers DAVP, IPOx and 2VP. According to previous literature,<sup>20</sup> for this purpose, a certain amount of monomer, *e.g.*

100 eq in respect to the initiator, is polymerized at a given temperature until complete conversion. After dividing this reaction mixture into aliquots, one aliquot is quenched by addition of MeOH (as a reference) and each other aliquot is stirred for a different defined period, after which more monomer is added, *e.g.* another 100 eq. Hereby, the reaction temperature is maintained throughout the whole measurement. From the obtained (bimodal) molecular weight distributions of each aliquot, the initiator efficiency of the formed macroinitiator at the second monomer addition can be evaluated in dependency of the incubation period. This way, the lifetime of the active chain ends can be determined in dependency of solvent and temperature.

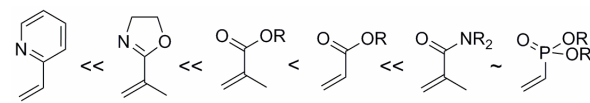
For all monomers susceptible to REM-GTP, statistic copolymerization should be conducted in order to verify the relative coordination strength of the monomers to the metal center. For those comonomers which exhibit similar coordination strength to the metal center and can thus undergo a statistical copolymerization, the copolymerization parameters need to be determined, *e.g.* from activity measurements *via* the Fineman-Ross method.<sup>16</sup> The resulting reactivity order should be confirmed by sequential copolymerizations. These experiments should include a verification of the previously described limitation by encapsulation of the catalyst during polymerization of rather hydrophilic monomers, *e.g.* IPOx or 2VP.<sup>17</sup> For this purpose, copolymerization experiments should be repeated using a more hydrophobic specimen of the same monomer class, resulting in a better solubility of the formed polymer in toluene.

As an alternative solution to overcome limitations which arise due to the pronounced polarity of some of the applied monomers, homo- and copolymerizations should also be performed in different solvents, *e.g.* DCM or polar donor solvents such as THF, dioxane, cyclic propylene carbonate, DMF or DMSO. This approach has already been adopted previously and emphasizes a great advantage of rare earth metal-based systems in comparison to their group 4 metallocenium cation pendants, as REM-GTP is known to be more tolerant to polar media.<sup>11</sup> If polymerization in these solvents is possible, the influence of the solvent on the polymerization behavior, *e.g.* catalyst activity or active chain end lifetime, should be determined.

## Conclusion

In this work, we have demonstrated the suitability of REM-GTP for the polymerization of acrylamides, *e.g.* DMAA, and NE. The previously established monomer reactivity order could be expanded to acrylamides, which interestingly show comparable coordination strength to the metal center as vinylphosphonates (Scheme 4). Accordingly, both statistical and block copolymers of DMAA and DEVP could be synthesized. We furthermore presented a variety of monomer classes with functional groups, which have not yet been tested for REM-GTP, including monomers comprising heteroatom-centered functionalities, *e.g.* phosphineoxide, sulfoxide, sulfone and sulfonate, as well as a variety of heteroaromatic monomers. We have shown a versatile synthetic route towards DAVPOs; however, requiring further optimization of the synthesis protocol.

## Scheme 4. Expanded reactivity order of Michael acceptor-type monomers towards REM-GTP.



We proposed a conceptual approach to verify the polymerizability of the described monomers by means of REM-GTP, allowing the development of a deeper understanding of the prerequisites monomers need to possess in order to be susceptible to REM-GTP. We furthermore suggested experiments to expand the established monomer reactivity order to the new monomers and to analyze and overcome limitations caused by the pronounced polarity of some applied monomers and the corresponding polymers.

## Experimental Part

### General

All reactions were carried out under argon atmosphere using standard Schlenk or glovebox techniques. All glassware was heat dried under vacuum prior to use. Unless otherwise stated, all chemicals were purchased from Sigma-Aldrich, Acros Organics or ABCR and used as received. Toluene, Et<sub>2</sub>O, THF and pentane were dried using an MBraun SPS-800 solvent purification system. Hexane and *tert*-butylthiol were dried over 3Å molecular sieve. Cp<sub>3</sub>Ln,<sup>35</sup> [Cp<sub>2</sub>LnCl]<sub>2</sub>,<sup>36</sup> [Cp<sub>2</sub>YbMe]<sub>2</sub>,<sup>37</sup> [Cp<sub>2</sub>Y(S*t*Bu)]<sub>2</sub>,<sup>18</sup> Cp<sub>2</sub>Lu(bdsa)(thf),<sup>18</sup> Cp<sub>2</sub>Y(CH<sub>2</sub>TMS)(thf)<sup>18</sup> and NaCp,<sup>38</sup> Li(bdsa),<sup>39</sup> the precursor complexes Ln(bdsa)<sub>3</sub>(thf)<sub>2</sub><sup>39</sup> and Ln(CH<sub>2</sub>TMS)<sub>3</sub>(thf)<sub>2</sub>,<sup>40</sup> as well as the monomers DEVP,<sup>41</sup> DPVPO,<sup>41</sup> MVSO,<sup>28,29</sup> MVSN,<sup>28,30</sup> EVS,<sup>31</sup> NE,<sup>32</sup> 2IMI,<sup>33</sup> 2IT<sup>34</sup> and 2IF<sup>34</sup> were prepared according to literature procedures. Monomers were dried over calcium hydride and distilled prior to use.

NMR spectra were recorded on a Bruker AV-300 or AV-500C spectrometer. <sup>1</sup>H, <sup>13</sup>C and <sup>29</sup>Si NMR spectroscopic chemical shifts δ are reported in ppm relative to tetramethylsilane. δ(<sup>1</sup>H) is calibrated to the residual proton signal, δ(<sup>13</sup>C) to the carbon signal and δ(<sup>29</sup>Si) to the deuterium signal of the solvent. <sup>31</sup>P NMR spectroscopic chemical shifts are reported in ppm relative to and calibrated to 85% aqueous H<sub>3</sub>PO<sub>4</sub>. Deuterated solvents were obtained from Deutero or Eurisotop and dried over 3Å molecular sieve. Elemental analyses were measured at the Laboratory for Microanalytics at the Institute of Inorganic Chemistry at the Technische Universität München. ESI MS analytical measurements were performed with methanol solutions on a Varian 500-MS spectrometer, using 70 keV in the positive ionization mode.

### Synthesis of DBVPO

**Di-*n*-butylphosphineoxide:** A solution of 98.4 g (0.72 mol, 2 eq) 1-butylbromide in 150 mL Et<sub>2</sub>O is added dropwise to 17.5 g (0.72 mol, 2 eq) magnesium turnings suspended in 150 mL Et<sub>2</sub>O. After complete conversion of the magnesium turnings, the reaction mixture is cooled to 0 °C and a solution of 49.5 g (0.36 mol, 1 eq) diethyl phosphonate in 150 mL Et<sub>2</sub>O is added dropwise. After addi-

tion is complete, the reaction mixture is stirred for two hours, 200 mL of THF are added and the reaction is quenched by addition of diluted aqueous HCl. The organic phase is washed twice with water and the combined aqueous phases are extracted two times with DCM. The combined organic phases are dried with Na<sub>2</sub>SO<sub>4</sub>, concentrated *in vacuo* and the residue is dissolved in hexane. Crystallization at -30 °C yields 28.1 g (0.17 mol, 47%) of di-*n*-butylphosphineoxide in form of colorless crystals. <sup>1</sup>H NMR (CDCl<sub>3</sub>, 298 K, 300 MHz): δ = 0.96 (t, 6H, <sup>3</sup>J(H-H) = 7.2 Hz, CH<sub>3</sub>), 1.45 (m, 4H, CH<sub>2</sub>-CH<sub>3</sub>), 1.66 (m, 4H, CH<sub>2</sub>-CH<sub>2</sub>-CH<sub>3</sub>), 1.89 (m, 4H, P-CH<sub>2</sub>), 6.89 (d, 1H, <sup>1</sup>J(P-H) = 447 Hz, P-H).

**(β-Acetoxyethyl)di-*n*-butylphosphineoxide:** A mixture of 7.58 g (88 mmol, 1 eq) vinyl acetate and 88 mg (0.54 mmol) AIBN is added to dropwise to 14.3 g (88 mmol, 1 eq) molten di-*n*-butylphosphineoxide at 110 °C. After complete addition, the reaction mixture is stirred for further 1.5 h at this temperature yielding 19.4 g (82 mmol, 93%) of crude product, which is used without further purification. <sup>1</sup>H NMR (CDCl<sub>3</sub>, 298 K, 300 MHz): δ = 0.95 (t, 6H, <sup>3</sup>J(H-H) = 7.1 Hz, CH<sub>2</sub>-CH<sub>3</sub>), 1.44 (m, 4H, CH<sub>2</sub>-CH<sub>3</sub>), 1.57 (m, 4H, CH<sub>2</sub>-CH<sub>2</sub>-CH<sub>3</sub>), 1.76 (m, 4H, P-CH<sub>2</sub>-CH<sub>2</sub>-CH<sub>2</sub>), 2.07 (s, 3H, CO-CH<sub>3</sub>), 2.11 (dt, 2H, <sup>2</sup>J(P-H) = 11.4 Hz, <sup>3</sup>J(H-H) = 7.2 Hz, P-CH<sub>2</sub>-CH<sub>2</sub>OAc), 4.39 (dt, 2H, <sup>3</sup>J(P-H) = 12.1 Hz, <sup>3</sup>J(H-H) = 7.2 Hz, CH<sub>2</sub>-OAc).

**Di-*n*-butyl(β-hydroxyethyl)phosphineoxide:** A mixture of 20 mL water, 20 mL THF, 19.7 g (0.49 mol, 6 eq) NaOH and 19.4 g (82 mmol, 1 eq) (β-acetoxyethyl)di-*n*-butylphosphineoxide is refluxed for 3 h. After removal of THF under reduced pressure and addition of diluted aqueous HCl, the resulting aqueous phase is extracted three times with DCM. The combined organic phases are dried with Na<sub>2</sub>SO<sub>4</sub>, concentrated *in vacuo* yielding 14.0 g (68 mmol, 83%) crude product in form of a pale brown liquid, which is used without further purification. <sup>1</sup>H NMR (CDCl<sub>3</sub>, 298 K, 300 MHz): δ = 0.95 (t, 6H, <sup>3</sup>J(H-H) = 7.2 Hz, CH<sub>3</sub>), 1.44 (m, 4H, CH<sub>2</sub>-CH<sub>3</sub>), 1.56 (m, 4H, CH<sub>2</sub>-CH<sub>2</sub>-CH<sub>3</sub>), 1.77 (m, 4H, P-CH<sub>2</sub>-CH<sub>2</sub>-CH<sub>2</sub>), 1.98 (dt, 2H, <sup>2</sup>J(P-H) = 9.4 Hz, <sup>3</sup>J(H-H) = 6.1 Hz, P-CH<sub>2</sub>-CH<sub>2</sub>OH), 4.03 (dt, 2H, <sup>3</sup>J(P-H) = 17.0 Hz, <sup>3</sup>J(H-H) = 6.1 Hz, CH<sub>2</sub>-OH).

**Di-*n*-butyl(β-mesyloxyethyl)phosphineoxide:** 10.13 g (88 mmol, 1.3 eq) methanesulfonyl chloride are added slowly to a toluene solution of 14.0 g (68 mmol, 1 eq) di-*n*-butyl(β-hydroxyethyl)phosphineoxide and 26.8 g (0.27 mol, 3.9 eq) triethylamine. The reaction mixture is stirred for three hours, filtered and the filtrate concentrated *in vacuo* yielding 13.0 g (49 mmol, 72%) crude product in form of a brown liquid, which is used without further purification. <sup>1</sup>H NMR (CDCl<sub>3</sub>, 298 K, 300 MHz): δ = 0.96 (t, 6H, <sup>3</sup>J(H-H) = 7.2 Hz, CH<sub>2</sub>-CH<sub>3</sub>), 1.45 (m, 4H, CH<sub>2</sub>-CH<sub>3</sub>), 1.58 (m, 4H, CH<sub>2</sub>-CH<sub>2</sub>-CH<sub>3</sub>), 1.76 (m, 4H, P-CH<sub>2</sub>-CH<sub>2</sub>-CH<sub>2</sub>), 2.21 (dt, 2H, <sup>2</sup>J(P-H) = 10.3 Hz, <sup>3</sup>J(H-H) = 7.1 Hz, P-CH<sub>2</sub>-CH<sub>2</sub>OMs), 3.08 (s, 3H, SO<sub>2</sub>-CH<sub>3</sub>), 4.58 (dt, 2H, <sup>3</sup>J(P-H) = 11.1 Hz, <sup>3</sup>J(H-H) = 7.1 Hz, CH<sub>2</sub>-OMs).

**Di-*n*-butylvinylphosphineoxide (DBVPO):** A mixture of 20 mL water, 20 mL thf, 11.9 g (0.30 mol, 6 eq) NaOH and 13.0 g (49 mmol, 1 eq) di-*n*-butyl (β-mesyloxyethyl)phosphineoxide is refluxed for 3 h. After removal of THF under reduced pressure and addition of diluted aqueous HCl, the resulting aqueous phase is extracted three times with DCM. The combined organic phases are dried with Na<sub>2</sub>SO<sub>4</sub> and concentrated *in vacuo*. The orange residue

is recrystallized from hexane yielding 4.65 g (25 mmol, 51%) DBVPO in form of colorless crystals. <sup>1</sup>H NMR (CDCl<sub>3</sub>, 298 K, 300 MHz): δ = 0.91 (t, 6H, <sup>3</sup>J(H-H) = 7.2 Hz, CH<sub>3</sub>), 1.41 (m, 4H, CH<sub>2</sub>-CH<sub>3</sub>), 1.58 (m, 4H, CH<sub>2</sub>-CH<sub>2</sub>-CH<sub>3</sub>), 1.73 (m, 4H, P-CH<sub>2</sub>-CH<sub>2</sub>-CH<sub>2</sub>), 6.03-6.37 (m, 3H, CH=CCH<sub>2</sub>).

### Oligomerization

5 eq of the monomer are added to 1 eq of catalyst in toluene. The resulting mixture is stirred for 2 hours at room temperature and quenched by addition of MeOH or acidified (37w% HCl<sub>aq</sub>) MeOH. Volatiles are removed under reduced pressure and the residue is extracted with MeOH. For end group analysis, ESI MS measurements of the methanolic extract are performed.

### Homo- and statistical copolymerization

After dissolving/suspending the catalyst in the solvent at room temperature, the calculated amount of the monomer (mixture) is added (overall monomer concentration 10vol%). The polymer is precipitated by addition of the reaction mixture to hexane (150 mL) and decanted from solution. Residual solvents are removed by drying the polymers under vacuum at 70 °C overnight.

### Sequential Copolymerization

After dissolving/suspending the calculated amount of catalyst in the solvent at room temperature, the first monomer is added (monomer concentration 10vol%). The reaction mixture is stirred until complete conversion of the monomer and divided into aliquots. One aliquot is quenched by addition of 0.5 mL MeOH, to each of the other aliquots, the calculated amount of a second monomer is added, the reaction mixtures stirred for another 2 hours at room temperature and quenched by addition of 0.5 mL MeOH. The polymers are precipitated by addition of the reaction mixtures to hexane (150 mL) and decanted from solution. Residual solvents are removed by drying the polymers under vacuum at 70 °C overnight.

### Activity measurements

For activity measurements, the 21.7 μmol of catalyst is dissolved/suspended in 20mL of (deuterated) solvent, and the reaction mixture is thermostated to the desired temperature. Then, the calculated amount of monomer is added. During the course of the measurement, the temperature is monitored with a digital thermometer and aliquots (0.5 mL) are taken and quenched by addition to deuterated methanol (0.2 mL). After the stated reaction time, the reaction is quenched by addition of MeOD (0.5 mL). The reaction is carried out in an MBraun Glovebox under argon atmosphere to take aliquots every 6-10 seconds at the beginning of the measurement. For each aliquot, the conversion is determined by <sup>1</sup>H or <sup>31</sup>P NMR spectroscopy, the molecular weight of the formed polymer by GPC-MALS analysis.

### Molecular weight determination

GPC was carried out on a Varian LC-920 equipped with two analytical PL Polargel M columns. As eluent, THF with 6 g L<sup>-1</sup> tetrabu-

tylammonium bromide (TBAB) or a mixture of 50% THF, 50% water, and 9 g L<sup>-1</sup> TBAB was used. Absolute molecular weights have been determined online by multiangle light scattering (MALS) analysis using a Wyatt Dawn Heleos II in combination with a Wyatt Optilab rEX as concentration source.

## AUTHOR INFORMATION

### Corresponding Author

\*rieger@tum.de.

## ACKNOWLEDGMENT

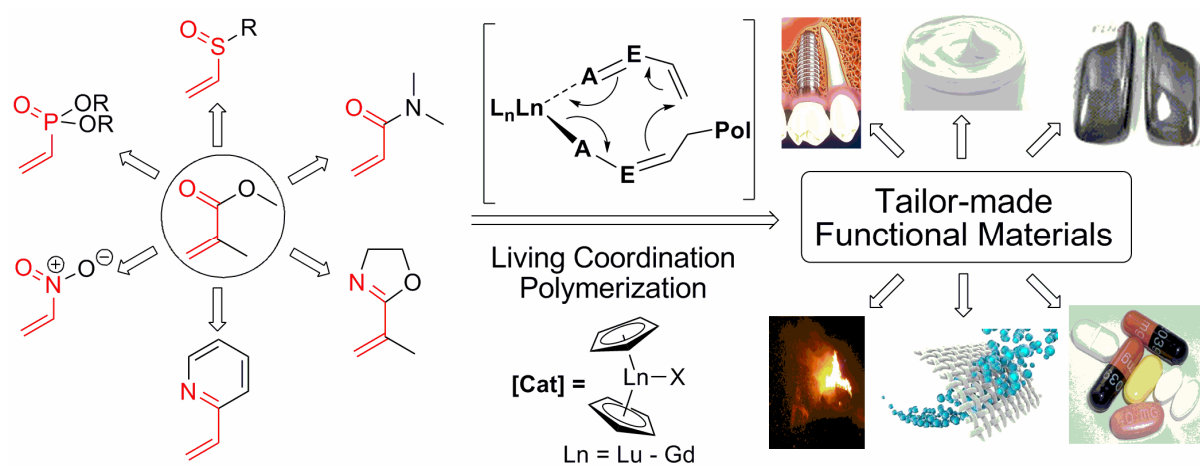
The authors thank Dr. Ning Zhang for valuable discussions. S.S. is grateful for a generous scholarship from the Fonds der Chemischen Industrie.

## REFERENCES

- (1) Yasuda, H.; Yamamoto, H.; Yokota, K.; Miyake, S.; Nakamura, A. *J. Am. Chem. Soc.* **1992**, *114*, 4908.
- (2) Chen, E. Y.-X. *Chem. Rev.* **2009**, *109*, 5157.
- (3) Yasuda, H.; Ihara, E. *Macromol. Chem. Phys.* **1995**, *196*, 2417.
- (4) Yasuda, H.; Ihara, E. *Adv. Polym. Sci.* **1997**, *133*, 53.
- (5) Yasuda, H. *Prog. Polym. Sci.* **2000**, *25*, 573.
- (6) Salzinger, S.; Rieger, B. *Macromol. Rapid Commun.* **2012**, *33*, 1327.
- (7) Zhang, N.; Salzinger, S.; Deubel, F.; Jordan, R.; Rieger, B. *J. Am. Chem. Soc.* **2012**, *134*, 7333.
- (8) Miyake, G. M.; Newton, S. E.; Mariott, W. R.; Chen, E. Y.-X. *Dalton Trans.* **2010**, *39*, 6710.
- (9) Hu, Y.; Xu, X.; Zhang, Y.; Chen, Y.; Chen, E. Y.-X. *Macromolecules* **2010**, *43*, 9328.
- (10) Hu, Y.; Miyake, G. M.; Wang, B.; Cui, D.; Chen, E. Y.-X. *Chem. Eur. J.* **2012**, *18*, 3345.
- (11) Hu, Y.; Wang, X.; Chen, Y.; Caporaso, L.; Cavallo, L.; Chen, E. Y.-X. *Organometallics* **2013**, *32*, 1459.
- (12) Seemann, U. B.; Dengler, J. E.; Rieger, B. *Angew. Chem., Int. Ed.* **2010**, *49*, 3489.
- (13) Rabe, G. W.; Komber, H.; Haeussler, L.; Kreger, K.; Lattermann, G. *Macromolecules* **2010**, *43*, 1178.
- (14) Salzinger, S.; Seemann, U. B.; Plikhta, A.; Rieger, B. *Macromolecules* **2011**, *44*, 5920.
- (15) Kaneko, H.; Nagae, H.; Tsurugi, H.; Mashima, K. *J. Am. Chem. Soc.* **2011**, *133*, 19626.
- (16) Zhang, N.; Salzinger, S.; Rieger, B. *Macromolecules* **2012**, *45*, 9751.
- (17) Zhang, N.; Salzinger, S.; Soller, B. S.; Rieger, B. *in preparation*.
- (18) Salzinger, S.; Soller, B. S.; Plikhta, A.; Seemann, U. B.; Herdtweck, E.; Rieger, B. *in preparation*.
- (19) Miyake, G.; Caporaso, L.; Cavallo, L.; Chen, E. Y.-X. *Macromolecules* **2009**, *42*, 1462.
- (20) Ihara, E.; Morimoto, M.; Yasuda, H. *Macromolecules* **1995**, *28*, 7886.
- (21) Mariott, W. R.; Rodriguez-Delgado, A.; Chen, E. Y.-X. *Macromolecules* **2006**, *39*, 1318.
- (22) Mariott, W. R.; Chen, E. Y.-X. *Macromolecules* **2005**, *38*, 6822.
- (23) Mariott, W. R.; Chen, E. Y.-X. *Macromolecules* **2004**, *37*, 4741.
- (24) Miyake, G.; Mariott, W. R.; Chen, E. Y.-X. *J. Am. Chem. Soc.* **2007**, *129*, 6724.
- (25) Seemann, U. B. *PhD Thesis*, Technische Universität München, Garching bei München, October **2010**.
- (26) Kleiner, H.-J. *Justus Liebigs Ann. Chem.* **1974**, 751.
- (27) Sander, J.; Kleiner, H.-J.; Finke, M. *Angew. Chem.* **1982**, *94*, 561.
- (28) Price, C. C.; Gillis, R. G. *J. Am. Chem. Soc.* **1953**, *75*, 4750.
- (29) Cubbage, J. W.; Guo, Y.; McCulla, R. D.; Jenks, W. S. *J. Org. Chem.* **2001**, *66*, 8722.
- (30) Gilman, H.; Esmay, D. L. *J. Am. Chem. Soc.* **1952**, *74*, 2021.
- (31) Chudasama, V.; Fitzmaurice, R. J.; Ahern, J. M.; Caddick, S. *Chem. Commun.* **2010**, *46*, 133.
- (32) Ranganathan, D.; Rao, C. B.; Ranganathan, S.; Mehrotra, A. K.; Iyengar, R. *J. Org. Chem.* **1980**, *45*, 1185.
- (33) Ohta, S.; Matsukawa, M.; Ohashi, N.; Nagayama, K. *Synthesis* **1990**, 78.
- (34) Gupta, I.; Fröhlich, R.; Ravikanth, M. *Eur. J. Org. Chem.* **2008**, 1895.
- (35) Birmingham, J. M.; Wilkinson, G. *J. Am. Chem. Soc.* **1956**, *78*, 42.
- (36) Maginn, R. E.; Manastyrskyj, S.; Dubeck, M. *J. Am. Chem. Soc.* **1963**, *85*, 672.
- (37) Evans, W. J.; Dominguez, R.; Hanusa, T. P. *Organometallics* **1986**, *5*, 263.
- (38) Panda, T. K.; Gamer, M. T.; Roesky, P. W. *Organometallics* **2003**, *22*, 877.
- (39) Eppinger, J. *PhD Thesis*, Technische Universität München, Garching bei München, May **1999**.
- (40) Hultsch, K. C.; Voth, P.; Beckerle, K.; Spaniol, T. P.; Okuda, J. *Organometallics* **2000**, *19*, 228.
- (41) Leute, M. *PhD Thesis*, Universität Ulm, **2007**.

## CHAPTER 12:

## CONCLUSION AND OUTLOOK



*“Education's purpose is to replace an empty mind with an open one.”*

- Malcolm Stevenson Forbes (1919-1990)



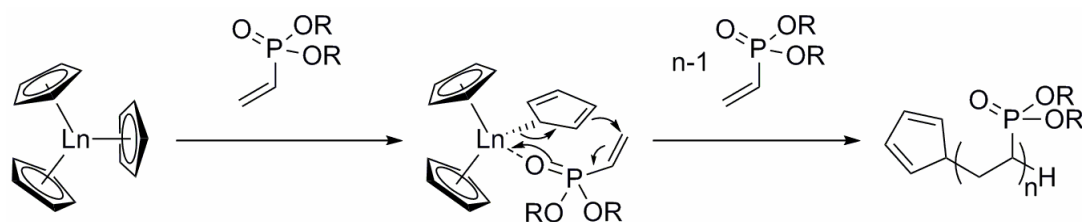


Within the last decades, the need for new materials with designed properties has been a main driving force in polymer research. Coordination polymerization of functional monomers enables a precise adjustment of the polymer structure and thus of the material properties, making this approach a very promising option for the production of such tailor-made functional materials. Organo-rare earth metal catalysts are particularly well-suited tools for the synthesis of functional high value polymers as they facilitate the polymerization of a broad variety of monomers following different polymerization mechanisms. Rare earth metal-mediated group transfer polymerization (REM-GTP) of polar-modified olefins combines the advantages of living ionic and coordination polymerizations; however, according to the restricted utilization for (meth)acrylic monomers only, the interest in REM-GTP has continuously decreased in the first decade of the 21<sup>st</sup> century. Nevertheless, recent publications have shown the suitability of REM-GTP to a variety of other monomer classes, particularly poly(vinylphosphonate)s, a material class which is not satisfactorily accessible *via* other polymerization methods.

Inspired by its recent expansion, in order to further increase the range of accessible functional materials, a major focus of this work was the expansion of REM-GTP to Michael acceptor-type monomers with functional groups which have not yet been tested for REM-GTP. Initial investigations on rare earth metal-mediated vinylphosphonate polymerization have proven the livingness of polymerization and suggest a GTP mechanism taking place, however, other typical characteristics of REM-GTP were found to be strongly altered for its application to vinylphosphonates. Consequently, in order to expand the efficient utilization of REM-GTP towards a broader scope of monomers, a deeper understanding of the underlying initiation and propagation mechanism is inevitable. Therefore, it was a major scope of this thesis to conduct detailed mechanistic studies in order to verify the origin of unexpected polymerization behavior and to allow a prediction of this behavior for other monomers of interest.

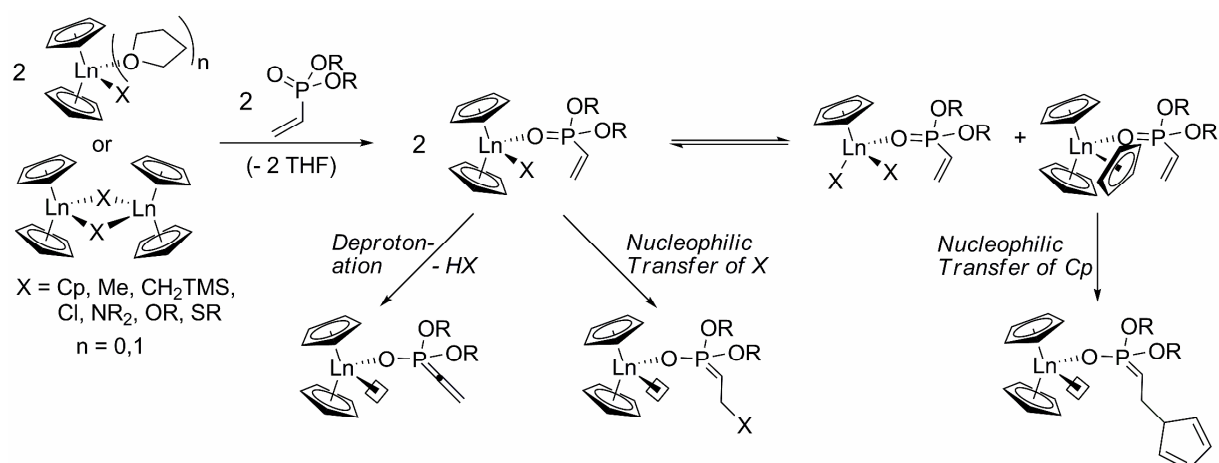
Rare earth metal-mediated polymerization of vinylphosphonates was found to be limited by an inefficient initiation by traditionally used strongly basic carbanion initiators, *e.g.* methyl complexes. Accordingly, a reliable kinetic analysis of vinylphosphonate REM-GTP was found to be hampered by very fast propagation with a comparatively slow initiation. In view of that, both the synthesis of catalysts exhibiting lower activity and faster initiation, as well as a (differential) method for the kinetic analysis of living polymerizations with comparable initiation and propagation rates needed to be developed.

A major improvement of vinylphosphonate REM-GTP has been the first application of *tris*(cyclopentadienyl) rare earth metal complexes ( $\text{Cp}_3\text{Ln}$ ) for REM-GTP. These trivalent cyclopentadienyl rare earth metal complexes are easily accessible in a one-step reaction and proved to be, in case of late lanthanides, efficient initiators and highly active catalysts for REM-GTP of various dialkyl vinylphosphonates, yielding well-defined polymers with low PDI and a molecular weight close to the initial monomer to catalyst ratio even at elevated temperatures (30–70 °C). The initiation for these unusual catalysts was found to proceed *via* nucleophilic transfer of a cyclopentadienyl ligand to a coordinated monomer (Scheme 12.1). For the  $\text{Cp}_3\text{Ln}$  series, for the first time, a detailed dependency of efficiency and activity of the applied complexes towards vinylphosphonate polymerization on the rare earth metal radius could be observed, *i.e.* the smaller the metal center, the higher the initiator efficiency and the normalized catalytic activity.



**Scheme 12.1:** Initiation of  $\text{Cp}_3\text{Ln}$ -initiated REM-GTP of vinylphosphonates.

In order to develop a deeper understanding of both initiation and propagation of vinylphosphonate REM-GTP, a variety of different trivalent *bis*(cyclopentadienyl) rare earth metal complexes ( $\text{Cp}_2\text{LnX}$ ) has been synthesized and tested for vinylphosphonate polymerization. ESI MS analysis of produced oligomers, in combination with *in situ* NMR spectroscopy of phosphonate coordination at the rare earth metal center revealed a complex reaction network for the initiation of vinylphosphonate REM-GTP (Scheme 12.2). Depending on the nature of X, initiation can either proceed *via* abstraction of the acidic  $\alpha$ -CH of the vinylphosphonate (*e.g.* for X = Me,  $\text{CH}_2\text{TMS}$ ), *via* nucleophilic transfer of X to a coordinated monomer (*e.g.* for X = Cp, SR) or *via* a monomer- (*i.e.* donor-) induced ligand exchange reaction forming  $\text{Cp}_3\text{Ln}$  in equilibrium (*e.g.* for X = Cl, OR), which serves as the active initiating and catalytic species. These results were further corroborated by single X-ray crystallography of phosphonate adducts at the rare earth metal center, providing first crystallographic proof of vinylphosphonate coordination at the active site *via* the oxygen of the phosphonate moiety.



**Scheme 12.2:** Initiation of vinylphosphonate GTP using unbridged rare earth metallocenes ( $\text{Cp}_2\text{LnX}$ ) via deprotonation of the acidic  $\alpha$ -CH, nucleophilic transfer of X or via a monomer-induced ligand exchange reaction forming  $\text{Cp}_3\text{Ln}(\text{DAVP})$ .

For ideal living polymerizations, *i.e.* living polymerizations for which the initiation rate is considerably faster than the propagation rate, the initiator efficiency  $I^*$  is mainly determined by initiator deactivation and does therefore not change during the course of polymerization. Rare earth metal-mediated GTP of vinylphosphonates is very fast and therefore primarily limited by an inefficient initiation reaction. Thus,  $I^*$  is increasing significantly during polymerization (Figure 12.1).

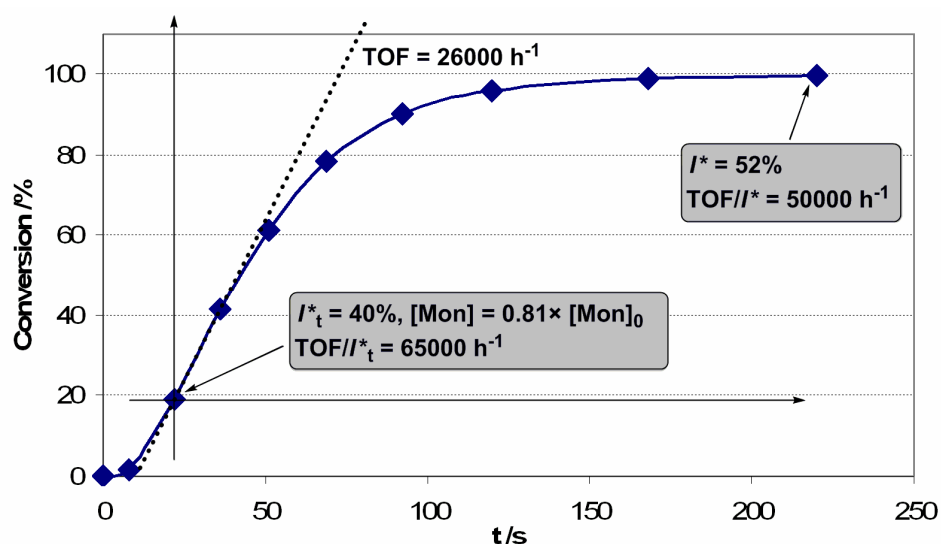
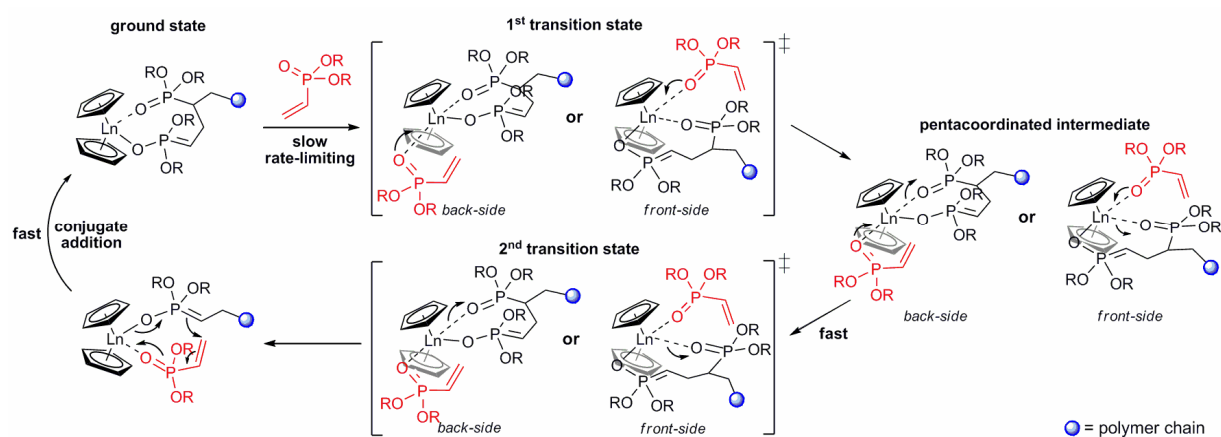


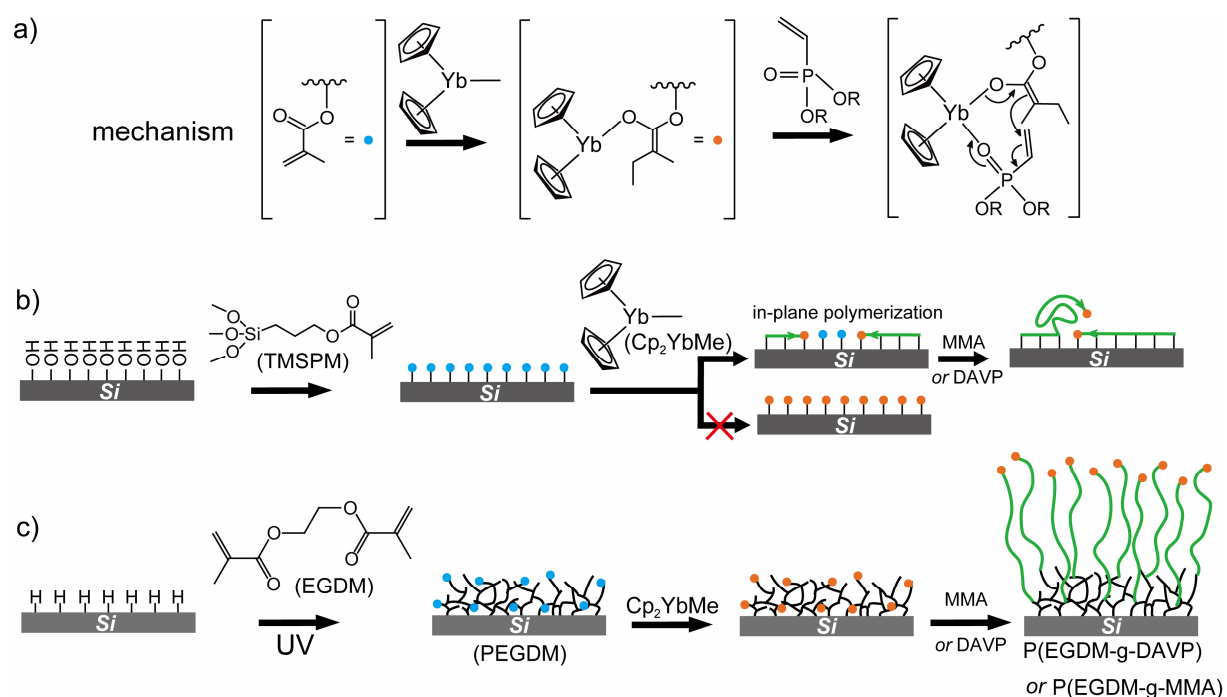
**Figure 12.1:** Conversion-reaction time plot for polymerization of DEVP, change of  $I_t^*$  during the reaction and corresponding normalized TOFs (8.6 mg  $[\text{Cp}_2\text{Y}(\text{StBu})_2]$ , 7.5vol% DEVP in toluene (20 mL), 30 °C).

Time-resolved analysis of monomer conversion and molecular weights of the formed polymers allows the determination of the initiator efficiency throughout the whole reaction. Using this normalization method, REM-GTP of vinylphosphonates was shown to follow a monometallic Yasuda-type polymerization mechanism, with an  $S_N2$ -type associative displacement of the polymer phosphonate ester by a monomer as the RDS. Surprisingly, the activation entropy  $\Delta S^\ddagger$  of the RDS is strongly affected by the metal radius and the monomer size, whereas these parameters show only minor influence on the activation enthalpy  $\Delta H^\ddagger$ . Accordingly, the propagation rate of rare earth metal-mediated vinylphosphonate GTP is mainly determined by the change of rotational and vibrational restrictions within the eight-membered metallacycle in the RDS. This result stands in large contrast to previous measurements on (meth)acrylate REM-GTP and explains the reverse correlation between activity and the radius of the metal center. As the activation entropy was shown to exhibit large influence on the propagation of coordinative-anionic polymerizations, it should be properly addressed in future mechanistic studies. As the steric demand of the added monomer (in contrast to the steric demand of the growing polymer chain end) was shown to exhibit only minor influence on the propagation rate (*i.e.* copolymerization parameters for vinylphosphonate copolymerization were shown to be  $r_1, r_2 \sim 1$ ), the associative displacement is very likely to proceed over two transition states *via* a pentacoordinated intermediate (Scheme 12.3).



**Scheme 12.3: Elemental steps of rare earth mediated GTP of vinylphosphonates. The rate-limiting step is an  $S_N2$ -type associative displacement of the polymer phosphonate ester by a vinylphosphonate monomer, presumably *via* a pentacoordinated intermediate.**

Within the scope of this work, the first example of a surface-initiated group transfer polymerization (SI-GTP) mediated by rare earth metal catalysts could be developed. The experimentally facile method allows a fast grafting of polymer brushes with a thickness of more than 150 nm in less than 5 minutes at room temperature. On basis of the previously reported consecutive copolymerization of MMA and DEVP, *bis*(cyclopentadienyl) methyl ytterbium was reacted with surface-bound methacrylate moieties, forming highly efficient enolate initiators for the successive SI-GTP (Scheme 12.4a). In order to preclude an in-plane polymerization of catalyst binding sites leading to low catalyst loading and thus to an inhomogeneous coverage after SI-GTP (Scheme 12.4b), a binding layer with embedded, but isolated methacrylate moieties needed to be used (Scheme 12.4c). SI-GTP was shown to be a powerful tool for the preparation of common poly(methacrylate) brushes and novel thermo-responsive poly(diethyl vinylphosphonate) and proton-conducting poly(vinylphosphonic acid) brush layers.



**Scheme 12.4:** a) Formation of enolate initiating species during catalyst impregnation by reaction of  $\text{Cp}_2\text{YbMe}$  with surface-bound methacrylates and subsequent initiation of SI-GTP; b) in-plane polymerization of catalyst binding sites leads to inhomogeneous coverage after SI-GTP on a TMSPM monolayer; c) a crosslinked PEGDM network with embedded, but isolated methacrylate moieties leads to high catalyst loading and thus to an efficient SI-GTP.

The use of highly efficient enolate initiators is of substantial importance to facilitate a homogeneous polymer brush growth for SI-GTP. Whereas the reaction with embedded, but isolated methacrylate moieties provides an elegant approach for the synthesis of such enolate initiators on surfaces, there is no convenient synthesis protocol for the production of rare earth enolates in solution. Within the scope of this work, it could be shown that C–H bond activation by protonolysis of classical  $\alpha$ -CH-acidic substrates is not a suitable alternative to the inconvenient established routes. Another approach to highly efficient initiators is the use of substituted, sterically more crowded *tris*(cyclopentadienyl) rare earth metal complexes ( $\text{Cp}^{\text{R}}_3\text{Ln}$ , Figure 12.2). The increased steric constraints in comparison to unsubstituted  $\text{Cp}_3\text{Ln}$  are supposed to lead to a stronger destabilization of the reaction intermediate  $\text{Cp}^{\text{R}}_3\text{Ln}(\text{Mon})$ , and according to the mechanistic studies on vinylphosphonate propagation, to an increase of the propagation rate by a higher steric crowding of the active species. Indeed, initial investigations using *tris*(methylcyclopentadienyl)yttrium ( $\text{Cp}^{\text{Me}}_3\text{Y}$ ) have shown higher activity and drastically increased initiator efficiency in comparison to  $\text{Cp}_3\text{Y}$ . So far, the efficient use of *tris*(cyclopentadienyl) rare earth metal complexes has been limited to vinylphosphonates, however, the higher steric crowding of  $\text{Cp}^{\text{R}}_3\text{Ln}$  may also facilitate an efficient initiation of sterically less demanding monomers. Accordingly, further development of these initiators is a promising route for further catalyst optimization and should be investigated in future work.

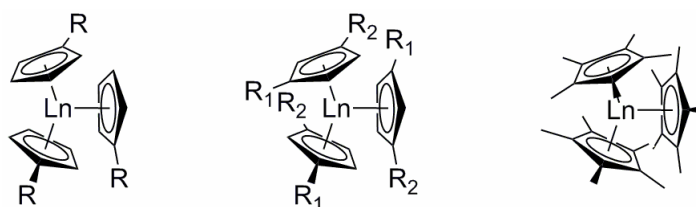
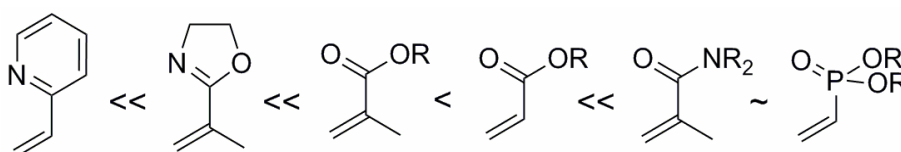


**Figure 12.2:** Optimization of *tris*(cyclopentadienyl) rare earth metal initiators by increase of the steric crowding *via* the use of substituted cyclopentadienyl ligands ( $\text{R}$ ,  $\text{R}_1$ ,  $\text{R}_2 = \text{Me}$ , TMS).

As detailed above, traditionally used strongly basic methyl and  $\text{CH}_2\text{TMS}$  initiators lead to an inefficient, slow initiation of vinylphosphonate polymerization by deprotonation of the acidic  $\alpha$ -CH. Sterically crowded  $\text{Cp}_3\text{Ln}$  complexes and thiolato complexes  $[\text{Cp}_2\text{Ln}(\text{S}t\text{Bu})]_2$  were found to efficiently initiate DAVP polymerization, however, further development of  $\text{Cp}_3\text{Ln}$  complexes is limited and thiolate end groups were found to be prone to elimination. Moreover, these complexes are not suitable initiators for sterically less demanding or weaker coordinating monomers such as IPOx or 2VP. Accordingly, the development of new initiators for REM-GTP, which facilitate an efficient initiation for a broad scope of monomers and

which lead to a stable end group functionalization *via* a C–C bond, is still of current interest. Contrary to C–H bond activation by protonolysis of classical  $\alpha$ -CH-acidic substrates, C–H bond activation of non-classical CH-acidic substrates by  $\sigma$ -bond metathesis has been shown to be a versatile route towards highly efficient and versatile initiators for REM-GTP of a variety of Michael acceptor-type monomers. The further development of this synthetic route and the evaluation of the resulting REM-GTP initiators are of major importance for the expansion of REM-GTP to new monomers.

Within the scope of this work, the first report on facile and efficient REM-GTP of the versatile dual-functional monomer 2-isopropenyl-2-oxazoline (IPOx) was presented, yielding high molecular weight PIPOx with unprecedented low polydispersity (PDI < 1.05). REM-GTP was also found to be applicable to 2-vinylpyridine (2VP), giving access to P2VP of defined molar mass and narrow molecular weight distribution. REM-GTP of IPOx and 2VP occurs *via* N-coordination at the rare earth metal center, which has rarely been reported previously. Furthermore, the suitability of REM-GTP for the polymerization of acrylamides and nitroethylene could be demonstrated. Copolymerization studies established a reactivity order of these new monomers and other established comonomers for REM-GTP as DEVP ~ DMAA >> MA > MMA >> IPOx >> 2VP (Scheme 12.5), which can be ascribed to the coordination strength of the respective monomers at the rare earth metal center (the relative coordination strength of nitroethylene has not been evaluated yet). Consecutive polymerization of different monomers is hereby only possible in order of increasing coordination strength, and restricted to comonomers with similar polarity.



**Scheme 12.5:** Reactivity order of Michael acceptor-type monomers towards REM-GTP.

A variety of further monomer classes were presented, comprising functional groups, which have not yet been tested for REM-GTP, including heteroatom-centered functionalities, *e.g.* phosphineoxide, sulfoxide, sulfone and sulfonate, as well as a variety of heteroaromatic monomers. A conceptual approach to verify the polymerizability of the described monomers by means of REM-GTP was illustrated, allowing the development of a deeper understanding of the prerequisites monomers need to possess in order to be susceptible to REM-GTP.

A detailed investigation on the thermosensitivity of aqueous PDEVP solutions revealed the occurrence of a coil-globule transition mechanism and has shown the possibility to adjust the LCST by statistic copolymerization of DEVP with more hydrophobic and hydrophilic DAVPs. The obtained co-PDAVPs exhibited thermoresponsive properties, which can be tuned in a wide range by controlling the feed ratio of the comonomers. The observed sharp and reversible phase transition, the small dependence of the thermoresponsiveness on additives and concentration as well as its biocompatibility make PDAVP an interesting alternative compared to established thermoresponsive polymers. Intriguingly, the thermal response of PDEVP was well preserved when anchored to the surface by SI-GTP, thus, REM-GTP gives easy access to thermoresponsive polymer brushes.

In order to further increase the scope of functional materials accessible by REM-GTP, polymer-analogous transformations of the introduced new functionalities were evaluated. Accordingly, transformation of poly(vinylphosphonate)s to poly(vinylphosphonic acid) by both mild hydrolysis and thermal treatment could be established, with the latter providing a possibility of converting PDAVP to PVPA in an economic and clean fashion, without the use of solvents or reagents. PVPA synthesis by mild hydrolysis of surface-bound PDAVP was shown to yield PVPA brushes without cleavage from the substrate, thus opening the access to proton-conducting brush layers. As a further polymer-analogous transformation, living cationic ring-opening polymerization (LCROP) of 2-ethyl-2-oxazoline *via* grafting from a PIPO<sub>x</sub> backbone yields well-defined molecular brushes. The combination of REM-GTP and LCROP is the first example for the synthesis of poly(2-oxazoline) molecular brushes with narrow side *and* backbone chain length distribution. Further polymer-analogous transformations, *e.g.* the reduction of phosphineoxides to phosphines or nitro moieties to amino groups, still needs to be evaluated.

One of the major advantages of REM-GTP is its possibility to induce a stereocontrolled polymerization by variation of the catalyst coordination sphere. However, this thesis was mainly concerned with the variation of the metal center and the initiating ligand in order to optimize both initiator efficiency and catalytic activity as well as to provide a deeper mechanistic understanding of REM-GTP. Nevertheless, the evaluation of a variation of the ligand sphere of the active site is still of major interest, as it may provide the first access to highly stereoregular poly(vinylphosphonate)s, poly(2-isopropenyl-2-oxazoline) and other polymers which are not accessible by other coordination polymerizations. These investigations should include the development of a deeper understanding of the correlation between catalyst and monomer structure and the stereospecificity of the polymerization as it has



been previously shown for a variety of (meth)acrylic monomers, particularly comprising an evaluation of the effects that occur for the change from a planar (*e.g.* MMA) to a tetrahedral (*e.g.* DAVP) monomer structure. The use of  $C_5$ - and  $C_1$ -symmetric complexes, in combination with theoretical investigations, would further allow a verification whether the rate determining step of the propagation proceeds *via* a front- or back-side attack of the incoming monomer (or *via* both pathways). According to their rigidity, *ansa*-rare earth metallocenes are the catalysts of choice for a detailed investigation on the influence of the catalyst ligand sphere on REM-GTP of the newly employed monomer classes. A variety of target catalyst structures with different symmetry and steric crowding is summarized in Figure 12.3.

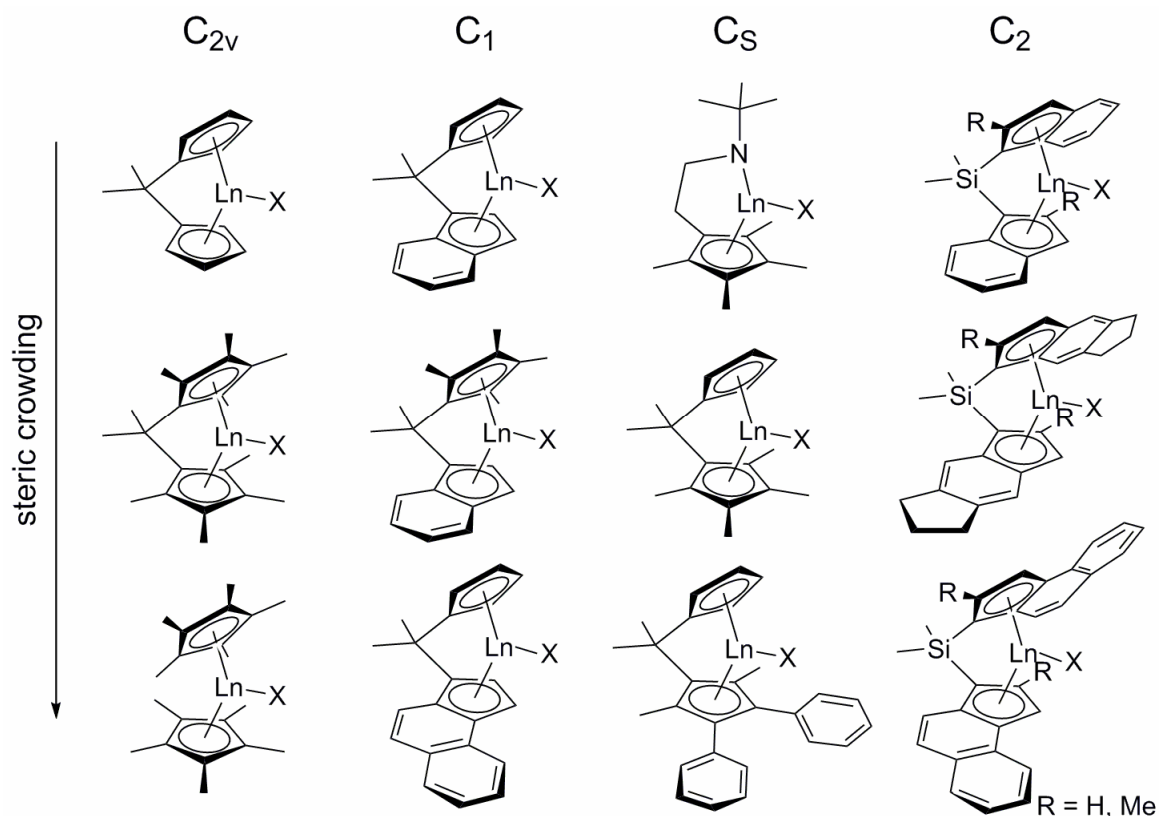
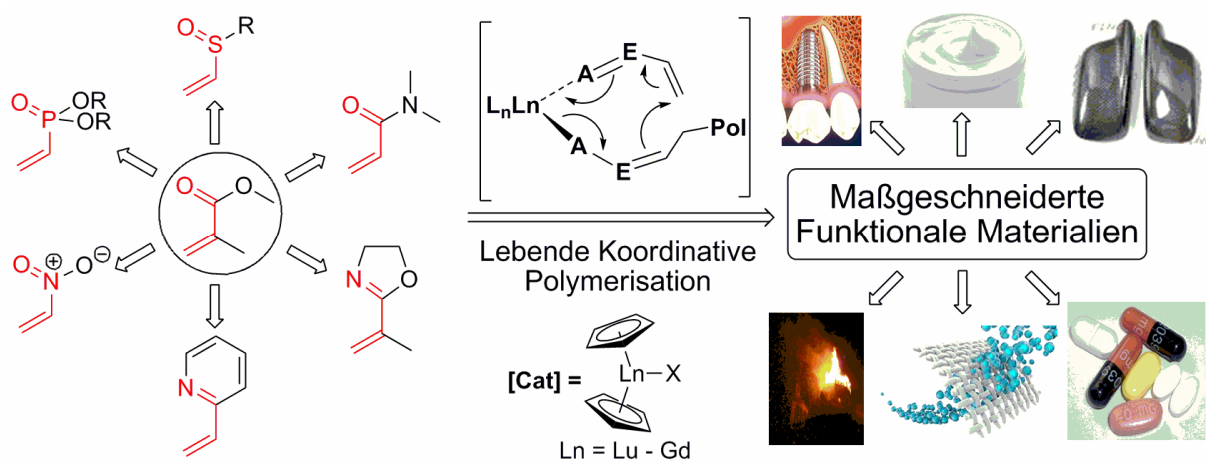


**Figure 12.3:** Rare earth metallocene complexes with different symmetry and steric crowding for a detailed investigation on the influence of the catalyst ligand sphere on REM-GTP of the newly employed monomer classes.



# CHAPTER 13:

## ZUSAMMENFASSUNG UND AUSBLICK



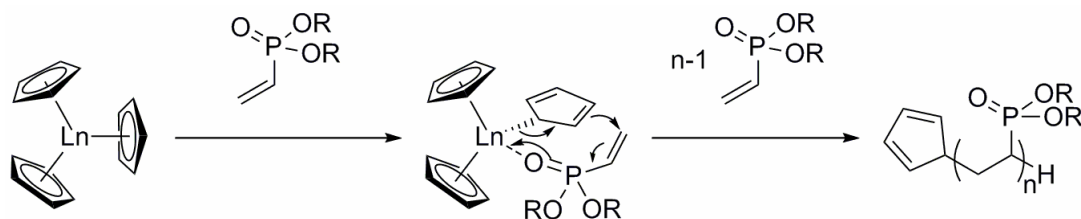
*“Der Zweck der Bildung ist einen leeren Geist durch einem offenen zu ersetzen.”*

- Malcolm Stevenson Forbes (1919-1990)



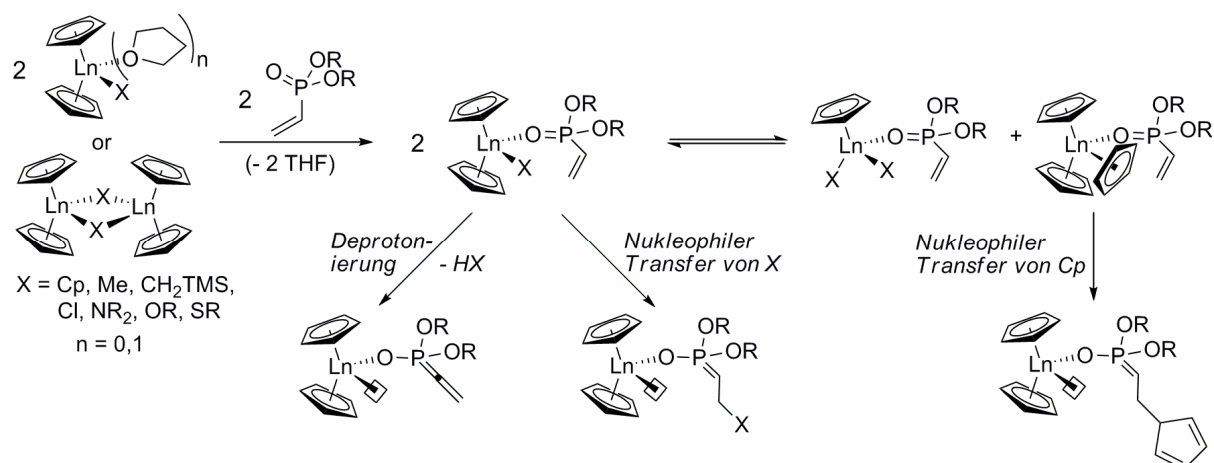
Der Bedarf nach neuen Materialien mit maßgeschneiderten Eigenschaften stellte im Verlauf der letzten Jahrzehnte eine der maßgebenden Triebkräfte in der Polymerforschung dar. Die koordinative Polymerisation von funktionalen Monomeren ermöglicht die präzise Einstellung von Polymerstruktur und Materialeigenschaften und bietet daher einen viel versprechenden Ansatz zur Herstellung solcher funktionaler Materialien. Organo-Seltenerdmetallkatalysatoren eignen sich besonders für die Synthese hochwertiger Kunststoffe, da sie die Polymerisation einer Vielzahl an Monomeren unter Ablauf verschiedener Mechanismen induzieren. Die Seltenerdmetall-medierte Gruppentransferpolymerisation (REM-GTP) von polar-modifizierten Olefinen kombiniert die Vorteile lebender ionischer und koordinativer Polymerisationen. Aufgrund der Beschränkung der Anwendbarkeit auf (Meth)Acrylate hat das Interesse an der REM-GTP innerhalb des letzten Jahrzehnts kontinuierlich abgenommen. Neuere Veröffentlichungen zeigten jedoch die Eignung der REM-GTP für die Polymerisation weiterer Monomerklassen. Dies sind im Besonderen die Poly(vinylphosphonate), eine Materialklasse, die nur unzureichend über andere Polymerisationsmethoden zugänglich ist. Inspiriert durch diese jüngsten Ergebnisse war es das zentrale Ziel dieser Arbeit, durch eine Erweiterung der REM-GTP auf Michael-Akzeptor Monomere mit funktionellen Gruppen, die noch nicht für eine REM-GTP untersucht wurden, die Bandbreite an zugänglichen funktionalen Materialien zu erweitern. Voruntersuchungen der Seltenerdmetall-medierten Polymerisation von Vinylphosphonaten zeigten den lebenden Charakter der Polymerisation und weisen auf das Vorliegen eines GTP-Mechanismus hin, andere Charakteristika der REM-GTP zeigten sich jedoch bei ihrer Anwendung auf Vinylphosphonate stark verändert. Um die effiziente Nutzung der REM-GTP für ein breiteres Spektrum an Monomeren zu etablieren, ist es nötig, ein tieferes Verständnis der zugrunde liegenden Initiations- und Propagationsmechanismen zu entwickeln. Es war daher ein wichtiges Ziel dieser Arbeit, mit Hilfe detaillierter mechanistischer Studien die Ursachen für unerwartetes Polymerisationsverhalten zu ermitteln und somit eine Vorhersage des Polymerisationsverhaltens anderer Monomere zu ermöglichen. Traditionell verwendete stark basische Carbanion-Initiatoren, z.B. Methylkomplexe, führen zu einer ineffizienten Initiation der REM-GTP von Vinylphosphonaten. Entsprechend ist eine verlässliche kinetische Analyse durch eine sehr schnelle Propagation in Kombination mit einer vergleichsweise langsamen Initiation gehindert. Diesbezüglich waren die Synthese von Katalysatoren, die eine geringere Aktivität bei höherer Initiationsrate aufweisen, sowie die Entwicklung eines (differentiellen) Ansatzes zur kinetischen Analyse von lebenden Polymerisationen mit vergleichbaren Initiations- und Propagationsraten weitere Ziele dieser Arbeit.

Eine zentrale Weiterentwicklung der REM-GTP von Vinylphosphonaten ist die Verwendung von *Tris*(cyclopentadienyl) Seltenerdmetallkomplexen ( $\text{Cp}_3\text{Ln}$ ). Diese trivalenten Cyclopentadienylkomplexe sind synthetisch einfach über eine einstufige Reaktion zugänglich und haben sich, im Falle der späten Lanthanide, als effiziente Initiatoren und hochaktive Katalysatoren für die REM-GTP von verschiedenen Dialkylvinylphosphonaten erwiesen, wobei selbst bei höheren Temperaturen (30-70 °C) Polymere mit geringer Polydispersität und definiertem Molekulargewicht erhalten werden. Die Initiation durch diese eher ungewöhnlichen Katalysatoren erfolgt hierbei durch nukleophilen Übertrag eines Cyclopentadienylliganden auf ein koordiniertes Monomer (Schema 13.1). Für die Reihe der  $\text{Cp}_3\text{Ln}$  Komplexe konnte darüber hinaus erstmals ein detaillierter Zusammenhang zwischen Effizienz und Aktivität der verwendeten Komplexe für die Polymerisation von Vinylphosphonaten und dem Radius des Seltenerdmetallzentrums beobachtet werden. Hierbei gilt, je kleiner das Zentralmetall, desto höher sind die Initiatoreffektivität und die normalisierte Aktivität der Komplexe.



**Schema 13.1:** Initiation der  $\text{Cp}_3\text{Ln}$ -initiierten REM-GTP von Vinylphosphonaten.

Um ein tieferes Verständnis von Initiation und Propagation der REM-GTP von Vinylphosphonaten zu entwickeln, wurden verschiedene trivalente *Bis*(cyclopentadienyl) Seltenerdmetallkomplexe ( $\text{Cp}_2\text{LnX}$ ) synthetisiert und bezüglich der Polymerisation von Vinylphosphonaten getestet. ESI-MS Analyse erzeugter Oligomere und *in situ* NMR Spektroskopie der Phosphonat-Koordination am Seltenerdmetallzentrum haben ein komplexes Reaktionsnetzwerk für die Initiation von Vinylphosphonat-REM-GTP aufgedeckt (Schema 13.2). In Abhängigkeit von X kann die Initiation über Abstraktion des aciden  $\alpha$ -CH des Vinylphosphonats (z.B. für  $\text{X} = \text{Me}, \text{CH}_2\text{TMS}$ ), über nukleophilen Transfer von X auf ein koordiniertes Monomer (z.B. für  $\text{X} = \text{Cp}, \text{SR}$ ) oder über einen Monomer- (Donor-)induzierten Ligandenaustausch unter Bildung von  $\text{Cp}_3\text{Ln}$  im Gleichgewicht erfolgen. Im letzteren Fall fungiert  $\text{Cp}_3\text{Ln}$  als aktive initiiierende und katalytische Spezies. Einkristallröntgenstrukturanalyse von Phosphonat-Addukten der Seltenerdmetallkomplexe bestätigte das postulierte Reaktionsnetzwerk und eine Vinylphosphonat-Koordination am aktiven Zentrum über den Sauerstoff der Phosphonatgruppe.



**Schema 13.2:** Initiation der GTP von Vinylphosphonaten durch unverbrückte Seltenerdmetallocene ( $\text{Cp}_2\text{LnX}$ ) via Deprotonierung des aciden  $\alpha\text{-CH}$ , nukleophilen Transfer von X oder via einen Monomer-induzierten Ligandenaustausch unter Bildung von  $\text{Cp}_3\text{Ln(DAVP)}$ .

Im Falle ideal lebender Polymerisationen, d.h. lebender Polymerisationen mit erheblich schnellerer Initiations- als Propagationsrate, wird die Initiatoreffektivität  $I^*$  nur durch eine anfängliche Initiatordeaktivierung bestimmt und bleibt daher im Verlauf der Polymerisation unverändert. Die REM-GTP von Vinylphosphonaten verläuft außerordentlich schnell und ist daher primär durch eine ineffiziente Initiation limitiert. Daher nimmt  $I^*$  im Verlauf der Polymerisation merklich zu (Abbildung 13.1).

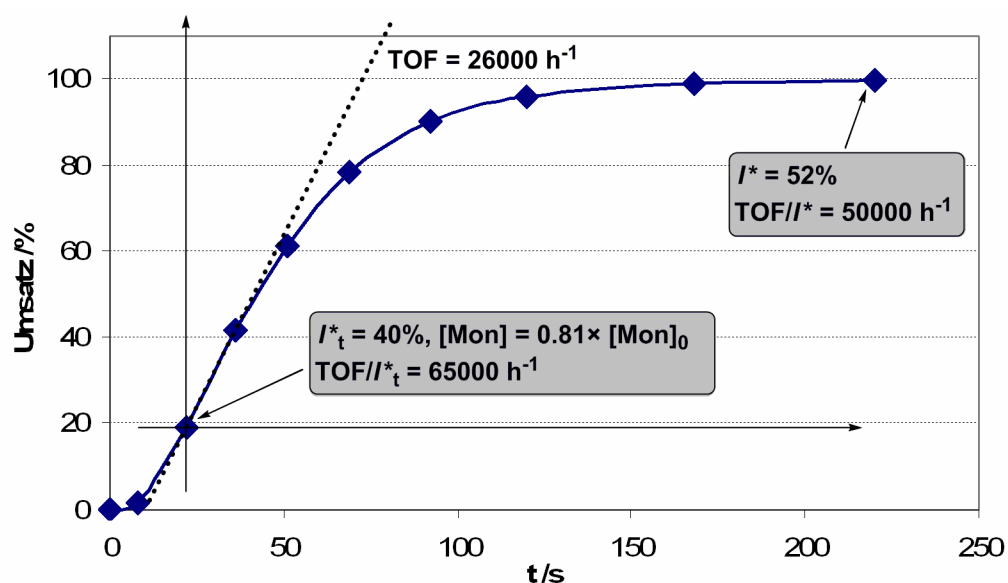
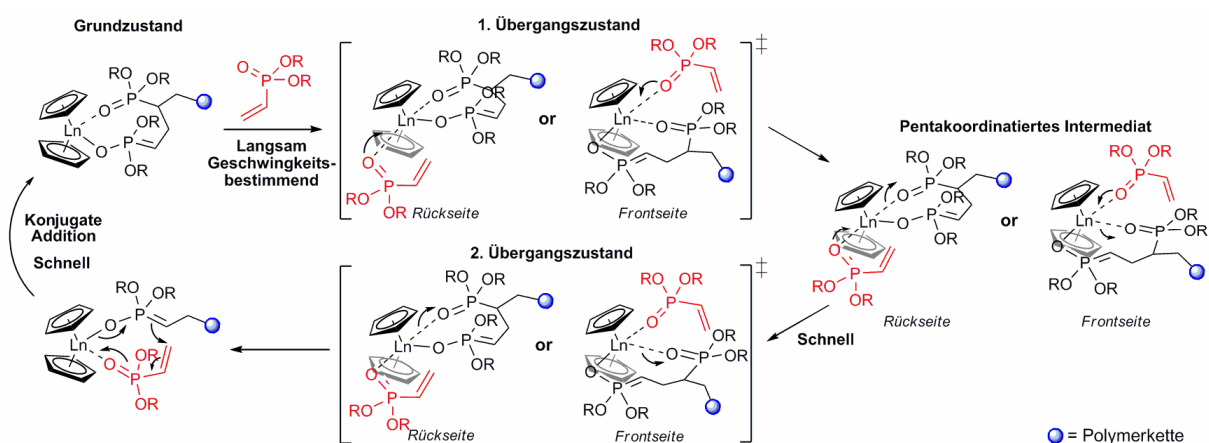


**Abbildung 13.1:** Umsatz-Reaktionszeit-Diagramm für die Polymerisation von DEVP, Änderung von  $I^*_t$  im Verlauf der Reaktion und entsprechende normierte TOFs (8.6 mg  $[\text{Cp}_2\text{Y}(\text{StBu})_2]$ , 7.5vol% DEVP in Toluol (20 mL), 30 °C).

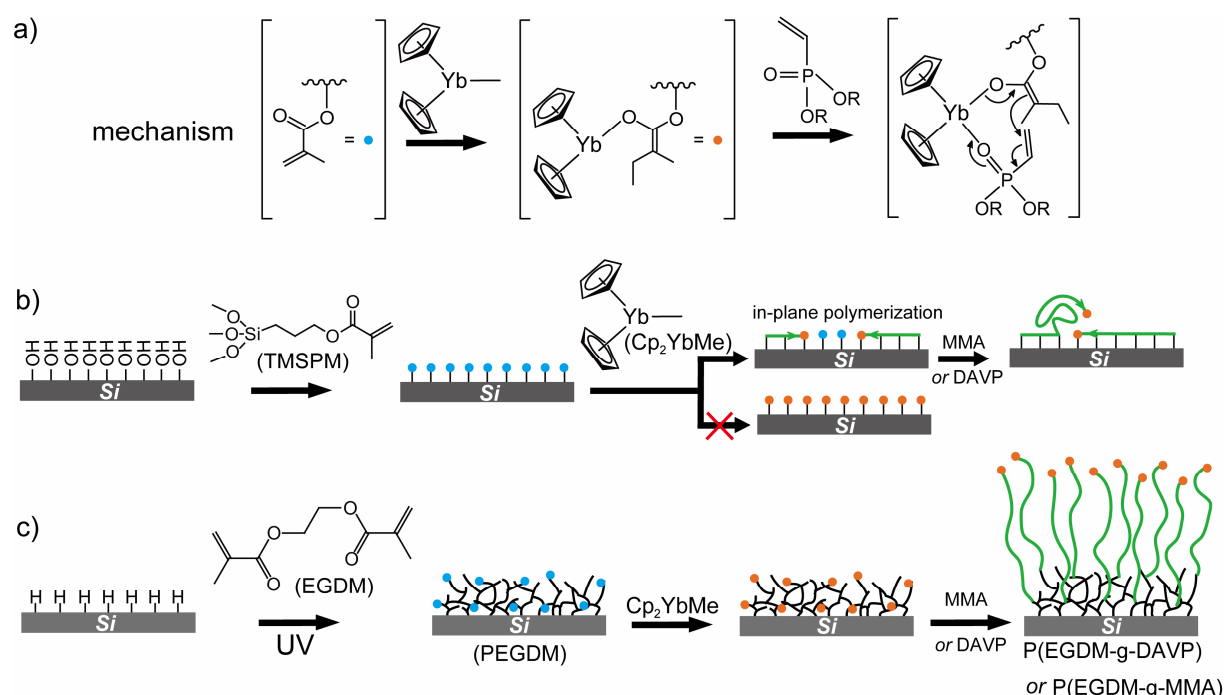
Eine zeitaufgelöste Analyse des Monomerumsatzes und des Molekulargewichts der gebildeten Polymere erlaubt die Bestimmung der Initiatoreffektivität während des gesamten Verlaufs der Reaktion. Mithilfe dieser Normierung konnte gezeigt werden, dass die REM-GTP von Vinylphosphonaten einem monometallischen, von Yasuda vorgeschlagenen Mechanismus folgt, mit einem  $S_N2$ -artigen assoziativen Austausch des Polymer-Phosphonat-Esters durch ein Monomer als geschwindigkeitsbestimmender Schritt (RDS). Überraschenderweise wird die Aktivierungsentropie  $\Delta S^\ddagger$  des RDS stark durch den Metallradius und die Größe des Monomers beeinflusst, wohingegen diese Parameter nur einen geringfügigen Einfluss auf die Aktivierungsenthalpie  $\Delta H^\ddagger$  aufweisen. Folglich wird die Propagationsrate der REM-GTP von Vinylphosphonaten hauptsächlich durch die Änderung von Rotations- und Vibrationsfreiheitsgraden innerhalb des achtgliedrigen Metallazyklus im RDS bestimmt. Dieses Ergebnis steht im Gegensatz zu vorangehenden Untersuchungen der REM-GTP von (Meth)Acrylaten und erklärt die beobachtete gegensätzliche Korrelation zwischen Katalysatoraktivität und Metallradius. Da die Aktivierungsentropie einen derart großen Einfluss auf die Propagation der koordinativ-anionischen Polymerisation aufweisen kann, sollte sie in zukünftigen mechanistischen Studien ausführlicher berücksichtigt werden. Da der sterische Anspruch des addierten Monomers (im Gegensatz zum sterischen Anspruch des wachsenden Kettenendes) nur einen geringfügigen Einfluss auf die Propagationsrate aufweist (d.h. Copolymerisationsparameter für Vinylphosphonat-Copolymerisation wurden zu  $r_1, r_2 \sim 1$  bestimmt), ist es sehr wahrscheinlich, dass der assoziative Austausch über zwei Übergangszustände und ein pentakoordiniertes Intermediat verläuft (Schema 13.3).



**Schema 13.3: Elementarschritte der REM-GTP von Vinylphosphonaten. Der geschwindigkeitsbestimmende Schritt ist ein  $S_N2$ -artiger assoziativer Austausch des Polymer-Phosphonat-Esters durch ein Vinylphosphonat-Monomer über ein pentakoordiniertes Intermediat.**



Im Rahmen dieser Arbeit konnte das erste Beispiel einer Seltenerdmetall-medierten Oberflächen-initiierten Gruppentransferpolymerisation (SI-GTP) entwickelt werden. Diese experimentell einfache Methode erlaubt ein schnelles Grafting von Polymerbürsten mit einer Dicke von mehr als 150 nm in weniger als 5 Minuten bei Raumtemperatur. Auf Basis der bereits veröffentlichten konsekutiven Polymerisation von MMA und DEVP wurde hierzu *Bis*(cyclopentadienyl)methyl Ytterbium mit Oberflächen-gebundenen Methacrylat-Einheiten unter Bildung von hocheffizienten Enolat-Initiatoren für die folgende SI-GTP umgesetzt (Schema 13.4a). Um eine Topopolymerisation der Katalysatorbindestellen und eine damit verbundene geringe Katalysatorbeladung mit folgender inhomogener Schichtbildung zu vermeiden (Schema 13.4b), wurde eine Bindschicht mit eingebetteten, aber isolierten Methacrylat-Einheiten verwendet (Schema 13.4c). SI-GTP stellt eine leistungsfähige Methode zur Herstellung von gewöhnlichen Poly(methacrylat)- sowie neuartigen thermosensitiven Poly(diethylvinylphosphonat)- und protonenleitenden Poly(vinylphosphonsäure)-Bürsten dar.



**Schema 13.4:** a) Bildung von Enolat-Initiatoren während der Katalysatorimpregnierung durch Reaktion von  $\text{Cp}_2\text{YbMe}$  mit Oberflächen-gebundenen Methacrylaten und anschließende Initiation der SI-GTP; b) Topopolymerisation der Katalysatorbindestellen führt zu einer inhomogenen Beschichtung durch SI-GTP; c) ein quervernetztes PEGDM Netzwerk mit eingebetteten, aber isolierten Methacrylat-Einheiten führt zu einer hohen Katalysatorbeladung und somit zu einer effizienten SI-GTP.

Die Verwendung hocheffizienter Enolat-Initiatoren ist essentiell um ein homogenes Polymerbürstenwachstum durch SI-GTP zu gewährleisten. Wohingegen die Reaktion mit eingebetteten, aber isolierten Methacrylat-Einheiten einen eleganten Ansatz für die Synthese von Enolat-Initiatoren auf Oberflächen darstellt, gibt es keine zufrieden stellende Synthesevorschrift für die Herstellung von Seltenerdmetallenolaten in Lösung. Im Rahmen dieser Arbeit konnte gezeigt werden, dass eine C–H-Bindungsaktivierung durch Protonolyse klassischer  $\alpha$ -CH-acider Substrate keine erfolgreiche Alternative zu den wenig geeigneten, etablierten Syntheserouten bietet. Ein weiterer Ansatz zur Entwicklung hocheffizienter Initiatoren ist die Verwendung substituierter, enorm sterisch überfrachteter *Tris*(cyclopentadienyl) Seltenerdmetallkomplexe ( $\text{Cp}^{\text{R}}_3\text{Ln}$ , Abbildung 13.2). Es ist anzunehmen, dass die im Vergleich zu unsubstituiertem  $\text{Cp}_3\text{Ln}$  größere sterische Überfrachtung eine stärkere Destabilisierung des  $\text{Cp}^{\text{R}}_3\text{Ln}(\text{Mon})$  Intermediats und, gemäß der mechanistischen Untersuchung zur Propagationsreaktion der Vinylphosphonate, die damit verbundene größere sterische Überfrachtung des aktiven Zentrums auch eine Erhöhung der Propagationsrate hervorruft. Tatsächlich zeigten erste Untersuchungen der Vinylphosphonat-Polymerisation mit *Tris*(methylcyclopentadienyl)yttrium ( $\text{Cp}^{\text{Me}}_3\text{Y}$ ) eine höhere Aktivität und eine drastische Erhöhung der Initiatoreffektivität im Vergleich zu  $\text{Cp}_3\text{Y}$ . Bislang war die effiziente Nutzung von *Tris*(cyclopentadienyl) Seltenerdmetallkomplexen auf die Polymerisation von Vinylphosphonaten beschränkt; die größere sterische Überfrachtung der  $\text{Cp}^{\text{R}}_3\text{Ln}$ -Komplexe könnte jedoch auch die effiziente Initiation sterisch weniger anspruchsvoller Monomere ermöglichen. Demgemäß ist die Weiterentwicklung dieser Initiatoren ein viel versprechender Ansatz zur Katalysatoroptimierung und sollte in zukünftigen Arbeiten berücksichtigt werden.

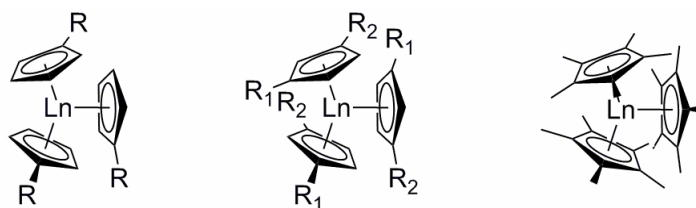
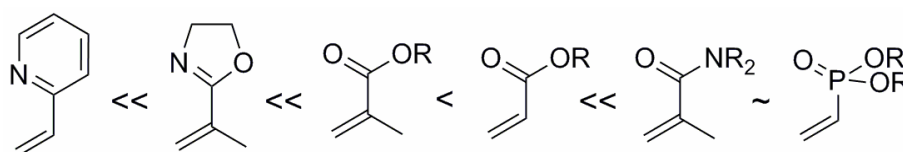


**Abbildung 13.2: Optimierung von *Tris*(cyclopentadienyl) Seltenerdmetallinitiatoren durch Erhöhung der sterischen Überfrachtung mittels Verwendung substituierter Cyclopentadienylliganden ( $\text{R}$ ,  $\text{R}_1$ ,  $\text{R}_2 = \text{Me}$ , TMS).**

Wie bereits näher erläutert führt die Verwendung herkömmlicher stark basischer Methyl- und  $\text{CH}_2\text{TMS}$ -Initiatoren zu einer langsamen, ineffizienten Initiation der Polymerisation von Vinylphosphonaten durch Deprotonierung des aciden  $\alpha$ -CH. Sterisch überfrachtete  $\text{Cp}_3\text{Ln}$  sowie Thiolato-Komplexe  $[\text{Cp}_2\text{Ln}(\text{StBu})]_2$  führen zu einer effizienten Initiation der REM-

GTP von DAVP, die Weiterentwicklung von  $Cp_3Ln$ -Komplexen ist jedoch stark eingeschränkt und für Thiolato-Endgruppen wurde häufig eine Eliminierung beobachtet. Darüber hinaus sind diese Komplexe nicht für die Polymerisation sterisch weniger anspruchsvoller oder schwächer koordinierender Monomere, wie z.B. IPOx oder 2VP, geeignet. Dementsprechend ist die Entwicklung neuartiger Initiatoren für die REM-GTP, die eine effiziente Initiation für ein breites Spektrum an Monomern ermöglichen und zu einer stabilen Endgruppenfunktionalisierung über C–C-Bindungen führen, weiterhin von großem Interesse. Im Gegensatz zur C–H-Bindungsaktivierung durch Protonolyse klassischer  $\alpha$ -CH-acider Substrate konnte gezeigt werden, dass eine C–H-Bindungsaktivierung nicht-klassischer CH-acider Substrate durch  $\sigma$ -Bindungsmetathese eine vielseitige Methode zur Herstellung hocheffizienter und vielseitiger Initiatoren für die REM-GTP einer Vielzahl an Michael-Akzeptor Monomeren darstellt. Die Weiterentwicklung dieser Syntheseroute und die Evaluierung der resultierenden REM-GTP-Initiatoren sind von großer Bedeutung für die Erweiterung der REM-GTP auf neue Monomere.

Im Rahmen dieser Arbeit konnte erstmals über die einfache und effiziente REM-GTP des vielseitigen bifunktionalen Monomers 2-Isopropenyl-2-oxazolin (IPOx) berichtet werden, wobei hochmolekulares PIPOx mit extrem geringer Polydispersität ( $PDI < 1.05$ ) erhalten wurde. Darüber hinaus ist REM-GTP von 2-Vinylpyridine (2VP) eine geeignete Methode zur Bildung von P2VP mit definierter Molmasse und schmaler Molekulargewichtsverteilung. Die Polymerisation von IPOx und 2VP stellt eines der ersten Beispiele für eine REM-GTP über N-Koordination zum Seltenerdmetall dar. Des Weiteren konnte die Eignung von REM-GTP zur Polymerisation von Acrylamiden und Nitroethylen gezeigt werden. Copolymerisationsexperimente ergaben eine Reihenfolge für die Reaktivität dieser neuartigen sowie etablierter Comonomere gemäß  $DEVP \sim DMAA \gg MA > MMA \gg IPOx \gg 2VP$  (Schema 13.5), was auf die relative Koordinationsstärke der Monomere zum Seltenerdmetall zurückgeführt werden kann (die relative Koordinationsstärke von Nitroethylen wurde noch nicht ermittelt). Eine konsekutive Polymerisation verschiedener Monomere ist hierbei nur in der Reihenfolge zunehmender Koordinationsstärke möglich und auf Comonomere mit vergleichbarer Polarität limitiert.



**Schema 13.5: Reaktivitätsreihenfolge von Michael-Akzeptor Monomeren für REM-GTP.**

Ein Spektrum an Monomerklassen mit funktionellen Gruppen, die noch nicht für eine REM-GTP getestet wurden, insbesondere Heteroatom-zentrierte Funktionalitäten, z.B. Phosphinoxid, Sulfoxid, Sulfon oder Sulfonat, sowie einige heteroaromatische Monomere, wurden im Rahmen dieser Arbeit vorgestellt. Ein allgemeiner konzeptioneller Ansatz zur Verifikation der Polymerisierbarkeit dieser Monomere durch REM-GTP wurde veranschaulicht und soll zur Entwicklung eines tieferen Verständnisses der Voraussetzungen, die ein Monomer für eine Eignung zur REM-GTP aufweisen muss, beitragen.

Eine detaillierte Untersuchung der Thermosensitivität von wässrigen PDEVp-Lösungen zeigte das Auftreten eines *coil-globule transition* Mechanismus und die Möglichkeit zur Feineinstellung des LCST durch statistische Copolymerisation von DEVp mit hydrophileren und hydrophoberen DAVp. Die erhaltenen co-PDAVP zeigten thermosensitives Verhalten, das in einem breiten Rahmen durch Einstellung des Feedverhältnisses der Comonomere eingestellt werden konnte. Der beobachtete scharfe und reversible Phasenübergang, die geringe Abhängigkeit der Thermosensitivität von Additiven und Konzentration sowie die Biokompatibilität machen PDAVP zu einer viel versprechenden Alternative im Vergleich zu etablierten thermosensitiven Polymeren. Darüber hinaus konnte gezeigt werden, dass die Thermosensitivität von PDEVp auch bei kovalenter Anbindung an eine Oberfläche erhalten bleibt, wodurch SI-GTP einen einfachen Zugang zu thermosensitiven Beschichtungen ermöglicht.

Um das durch REM-GTP zugängliche Spektrum an funktionalen Materialien weiter zu vergrößern, wurden polymeranaloge Umsetzungen der neu eingeführten Funktionalitäten evaluiert. So konnte eine Umsetzung von Poly(vinylphosphonat)en zu Poly(vinylphosphonsäure) sowohl durch milde Hydrolyse sowie durch thermische Behandlung ermöglicht werden, wobei die letztere eine wirtschaftliche und saubere Methode ohne die Verwendung von Lösungsmitteln oder Reagenzien darstellt. Die Synthese von PVPA durch milde Hydrolyse konnte auch für Oberflächen-gebundenes PDAVP ohne Abspaltung der Beschichtung angewendet werden und gibt somit einen einfachen Zugang zu protonenleitenden Polymerbeschichtungen. Als weitere polymeranaloge Umsetzung konnten durch lebende kationische Ringöffnungspolymerisation (LCROP) von 2-Ethyl-2-oxazolin auf einem PIPOx-Rückgrat definierte molekulare Bürsten erhalten werden. Die Kombination von REM-GTP und LCROP stellt das erste Beispiel für die Synthese von molekularen Poly(2-oxazolin)bürsten mit enger Molekulargewichtsverteilung der Seitenketten *und* des Polymerrückgrades dar. Die Evaluierung weiterer polymeranaloger Umsetzungen, z.B. die

Reduktion von Phosphinoxiden zu Phosphinen oder von Nitro- zu Aminofunktionen, ist noch durchzuführen.

Einer der zentralen Vorteile der REM-GTP ist die Möglichkeit der Einführung einer stereokontrollierten Polymerisation durch Variation der Ligandensphäre des Katalysators. Diese Arbeit beschäftigte sich jedoch vornehmlich mit der Variation des Metallzentrums und des initiierenden Liganden um sowohl die Initiatoreffektivität und die Aktivität der Komplexe zu optimieren sowie um ein tieferes mechanistisches Verständnis der REM-GTP zu entwickeln. Nichtsdestotrotz ist die Evaluierung der Variation der Ligandensphäre des aktiven Zentrums weiterhin von großem Interesse, da dies erstmals den Zugang zu hoch stereoregularen Poly(vinylphosphonat)en, Poly(2-isopropenyl-2-oxazolin) sowie weiteren Polymeren, die nicht durch andere koordinative Polymerisationen zugänglich sind, ermöglicht. Diese Untersuchungen sollten die Entwicklung eines tieferen Verständnisses der Korrelation zwischen Monomer- und Katalysatorstruktur und der Stereospezifität der Polymerisation beinhalten, so wie dies bereits für einige (Meth)Acrylate gezeigt wurde. Insbesondere sollte dabei eine Evaluierung der Effekte, die durch den Wechsel von einer planaren (z.B. MMA) zu einer tetraedrischen (z.B. DAVP) Monomerstruktur entstehen, erfolgen. Die Verwendung  $C_S$ - und  $C_1$ -symmetrischer Komplexe sollte in Kombination mit theoretischen Berechnungen herangezogen werden, um festzustellen, ob der geschwindigkeitsbestimmende Schritt der Propagation über einen Front- oder Rückseitenangriff des Monomers erfolgt (oder über beide Reaktionswege). Entsprechend ihrer Rigidität sind *ansa*-Seltenerdmetallocene die Katalysatoren der Wahl für eine detaillierte Untersuchung des Einflusses der Ligandensphäre des Katalysators auf die REM-GTP der neu verwendeten Monomerklassen. Eine Auswahl an Katalysator-Zielstrukturen mit unterschiedlicher Symmetrie und sterischer Überfrachtung ist in Abbildung 13.3 zusammengefasst.

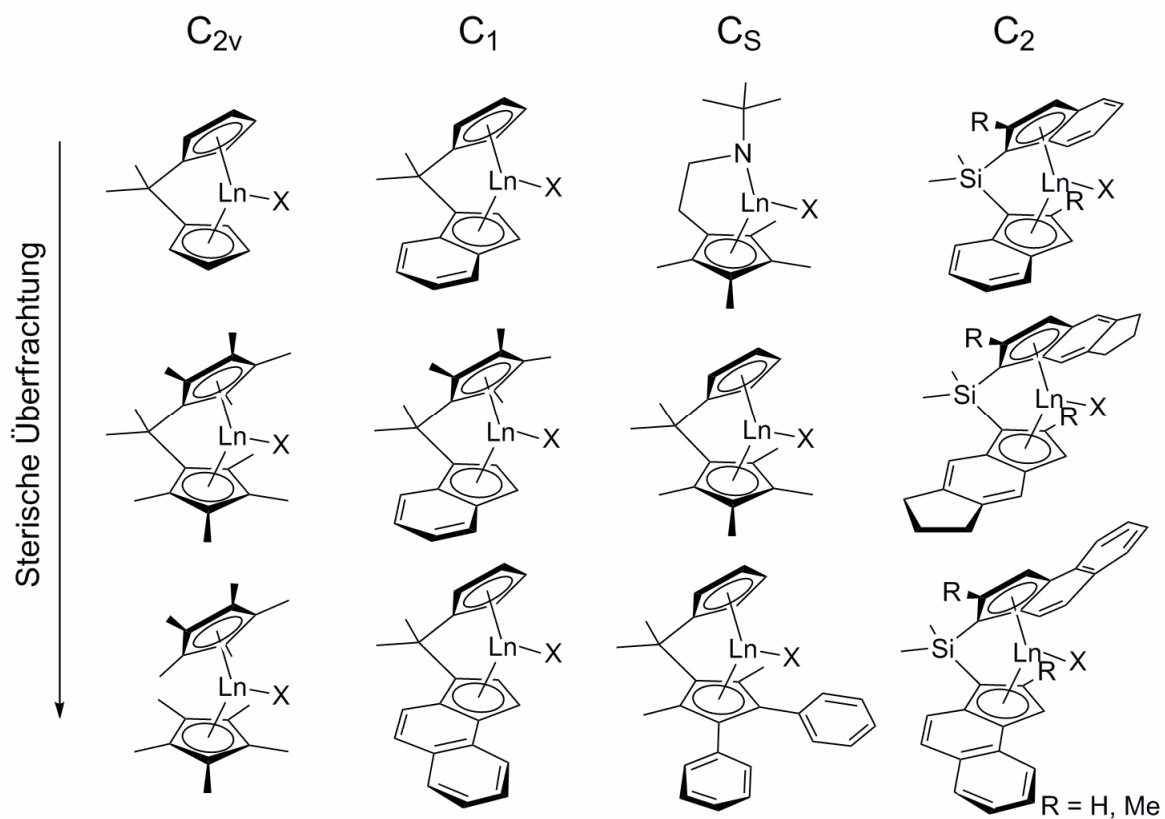
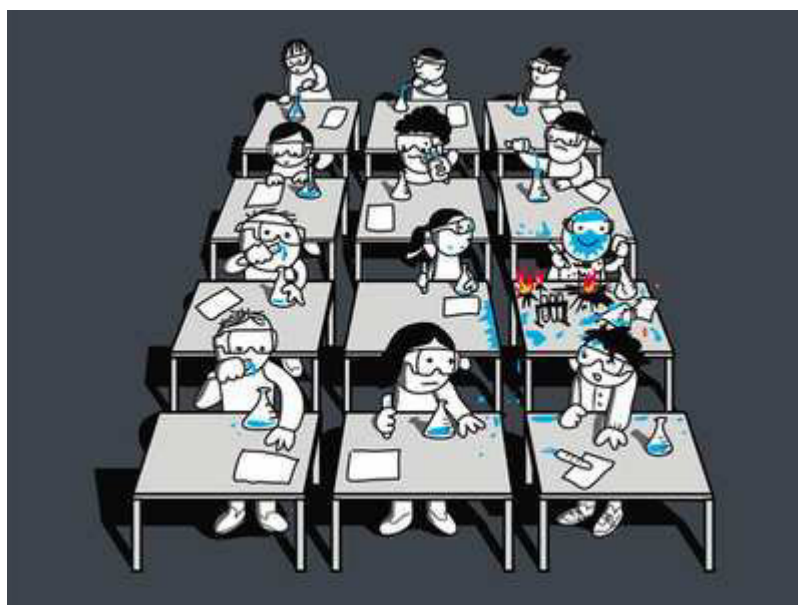


Abbildung 13.3: Seltenerdmetallocene mit unterschiedlicher Symmetrie und sterischer Überfrachtung für eine detaillierte Untersuchung des Einflusses der Ligandensphäre des Katalysators auf die REM-GTP der neu verwendeten Monomerklassen.

## CHAPTER 14:

## APPENDIX



(Title: The Chemist)

*“A Chemist is a person who develops a general theory from a string of diverse formulae derived from micromatic precision from vague assumptions based on debatable tables of results extracted from inconclusive experiments carried out with inaccurate equipment of doubtful reliability and questionably mentality.”*

- W. Brostow, 1979





## Posters and Presentations

### Phosphorus-Containing Polymers by Rare Earth Metal-Mediated Group Transfer Polymerization

**Type:** Poster Contribution  
**Conference:** Makromolekulares Colloquium 2011, Freiburg  
Heidelberg Forum for Molecular Catalysis 2011, Heidelberg  
**Authors:** Stephan Salzinger, Uwe B. Seemann Andriy Plihkta,  
Bernhard Rieger

#### Abstract:

Recent studies have shown that diethyl vinylphosphonate can be converted to high molecular weight polymers by rare earth metal-initiated Group Transfer Polymerization. Here we present a further development of the catalytic species, rare earth metal-based tricyclopentadienyl complexes ( $\text{Cp}_3\text{Ln}$ ,  $\text{Ln} = \text{Gd} - \text{Lu}$ ), which have been used to polymerize different dialkyl vinylphosphonates (alkyl: methyl, ethyl, isopropyl) in toluene. Additionally the thermosensitive behavior of the obtained polymers was characterized. A series of independently performed reactions showed high activities and initiator efficiencies for these complexes for the homopolymerization of the applied monomers. Polymeric materials of high molecular weight with a previously unknown low polydispersity index ( $\text{PD} < 1.05$ ) have been determined by GPC-MALS (Multi Angle Light Scattering) methods. The reaction shows a linear  $M_w$  vs. consumption plot, proving a living type polymerization. The initiation of the reaction has been investigated by end-group analysis with different mass spectrometric analytical methods such as MALDI-TOF and ESI. A new and interesting chain end functionalization of the achieved polymer chains has been detected over the course of the mass spectrometric analytical studies. The so far unreported LCST (Lower Critical Solution Temperature) of polyvinylphosphonate in water has been evaluated and the correlation between the molecular weight of the material with this temperature has been determined.

## Mechanistic Studies on Initiation and Propagation of Rare Earth Metal-Mediated Group Transfer Polymerization of Vinylphosphonates

**Type:** Presentation  
**Conference:** ACS National Meeting 2012, San Diego  
**Authors:** Stephan Salzinger, Bernhard Rieger

### Abstract:

Recent studies have shown that poly(vinylphosphonate)s are readily accessible by rare earth metal-mediated Group Transfer Polymerization (GTP). Late lanthanide metallocenes proved to be efficient initiators and highly active catalysts for vinylphosphonate polymerization yielding polymers of precise molecular weight and low polydispersity. Despite the proof of a living polymerization mechanism, an exact understanding of both initiation and propagation of rare earth metal-mediated GTP of vinylphosphonates is still lacking.

Within our latest studies we observed a complex reaction pathway for the initiation with unbridged rare earth metallocenes ( $\text{Cp}_2\text{LnX}$ ,  $\text{X} = \text{Cp}, \text{Cl}, \text{Me}, \text{NR}_2, \text{OR}, \text{SR}$ ). Depending on the nature of X, initiation can either proceed *via* deprotonation of the acidic  $\alpha$ -CH of the vinylphosphonate (*e.g.* for  $\text{X} = \text{Me}, \text{NR}_2$ ), *via* nucleophilic transfer of X to a coordinated monomer (*e.g.* for  $\text{X} = \text{Cp}, \text{SR}$ ) or *via* a monomer- (*i.e.* donor) induced ligand exchange reaction forming  $\text{Cp}_3\text{Ln}$  in equilibrium (*e.g.* for  $\text{X} = \text{Cl}, \text{OR}$ ), which serves as the active initiating and catalytic species. As observed by mass spectrometric end group analysis, different initiations may also occur simultaneously (*e.g.* for  $\text{X} = \text{N}(\text{SiMe}_2\text{H})_2$ ). These findings could be confirmed by  $^1\text{H}$  and  $^{31}\text{P}$  NMR spectroscopic measurements of phosphonate coordination at the corresponding Lu and Y centers, and are further supported by kinetic investigations as well as by X-ray crystallography.

For a better understanding of the chain propagation, kinetic  $^{31}\text{P}$  NMR spectroscopic studies were carried out, which were significantly complicated by three factors; the relatively slow initiation step (in comparison to the rate of chain growth), the high viscosity of the polymerization reaction mixture and the moisture sensitivity of the rare earth catalysts. However, it could be proven that propagation proceeds in a monometallic fashion and the rate determining step of chain growth could be identified.

## Publications beyond the Scope of this Thesis

### Aggregation behavior of thermo-responsive poly(2-oxazoline)s at the cloud point investigated by FCS and SANS

<b>Status:</b>	Published online: December 27, 2011
<b>Journal:</b>	Colloid and Polymer Science Issue 290, 385-400
<b>Publisher:</b>	Springer
<b>Article type:</b>	Original Contribution
<b>DOI:</b>	10.1007/s00396-011-2564-z
<b>Authors:</b>	Stephan Salzinger, Stephan Huber, Sebastian Jaksch, Peter Busch, Rainer Jordan, Christine M. Papadakis

#### Abstract:

We have studied different thermo-responsive poly(2-oxazoline)s with iso-propyl (iPrOx) and n-propyl (nPrOx) pendant groups in aqueous solutions, where they exhibit lower critical solution temperature behavior. This paper focuses on the effect of the degree of polymerization,  $n$ , the concentration,  $c$ , in the dilute regime, and the presence of hydrophobic moieties. The cloud points were investigated as a function of the degree of polymerization,  $n$ , and of the polymer concentration,  $c$ . The aggregation behavior near the cloud point was studied by temperature-resolved small-angle neutron scattering and fluorescence correlation spectroscopy, i.e., a combination of ensemble and single molecule methods. We found that at the cloud points, large aggregates are formed and that the cloud points depend strongly on both,  $n$  and  $c$ . Diblock copolymers from iPrOx and nPrOx form large aggregates already at the cloud point of PnPrOx, and, unexpectedly, no micelles are observed between the cloud points of the two blocks. Gradient copolymers from iPrOx and n-nonyl-2-oxazoline (NOx) display a complex aggregation behavior resulting from the interplay between intra- and intermolecular association mediated by the hydrophobic NOx blocks. Above the cloud point, an intermediate temperature regime with a width of a few Kelvin was found with small but stable polymer aggregates. Only at higher temperatures, larger aggregates are found in significant number.

## Organic-Inorganic Hybrid Nanoparticles via Photoinduced Micellation and Siloxane Core Cross-Linking of Stimuli-Reponsive Copolymers

**Status:** Published online: January 15, 2013  
**Journal:** ACS Macro Letters  
Issue 2, 121-124  
**Publisher:** ACS Publications  
**Article type:** Letter  
**DOI:** 10.1021/mz3006439  
**Authors:** Christian Anger, Frank Deubel, Stephan Salzinger,  
Jürgen Stohrer, Tobias Halbach, Rainer Jordan,  
Jonathan G. C. Veinot, Bernhard Rieger

### Abstract:

Photoacid-induced siloxane cross-linking of stimuli-responsive copolymer micelles allows the synthesis of well-defined organic–inorganic hybrid nanoparticles. Two conceptually different synthetic approaches are presented, both via photoinduced crosslinking of poly(4-hydroxystyrene-block-styrene) micelles and via one-pot photoacid-catalyzed micelle formation and siloxane cross-linking of poly(4-tert-butoxystyrene-block-styrene). The multistep synthetic route showed intermicellar cross-linking leading to agglomerates. In contrast to this, the formation of the nanoparticles via the one-pot synthesis yielded well-defined structures. The use of different siloxane crosslinking agents and their effects on the properties of the cross-linked micellar structures have been evaluated. Scanning electron microscopy and differential scanning calorimetry indicate rigid core cross-linked nanoparticles. Their size, molar mass, and swelling behavior were analyzed by dynamic and static light scattering. Cyclic siloxane cross-linking agents lead to residual C=C double bonds within the nanoparticle core that allow postsynthetic modification by, e.g., thiol–ene click reactions.

## Synthesis of Cyclic $\gamma$ -Amino Acids for Foldamers and Peptide Nanotubes

**Status:** Accepted  
**Journal:** European Journal of Organic Chemistry  
**Publisher:** Wiley VCH  
**Article type:** Full Paper  
**DOI:** 10.1002/ejoc.201201565  
**Authors:** Nuria Rodríguez-Vázquez, Stephan Salzinger, Luis F. Silva, Manuel Amorín, Juan R. Granja

### Abstract:

Cyclic  $\gamma$ -amino acids are molecular building blocks of great interest in peptide and foldamer chemistry, as they allow the preparation of new structures that are not found in Nature. In this paper, we describe the synthesis of cyclic  $\gamma$ -amino acids that have a *cis* relationship between the amino and the carboxylic acid groups. This arrangement, in most cases, induces the resulting peptides to adopt a flat conformation, which makes them appropriate for the design of foldamers that adopt  $\beta$ -sheet-type structures.